frontiers | Research Topics

The role of imaging in gynecological malignancies

Edited by
Kathy Han and Alessio G. Morganti

Published in
Frontiers in Oncology

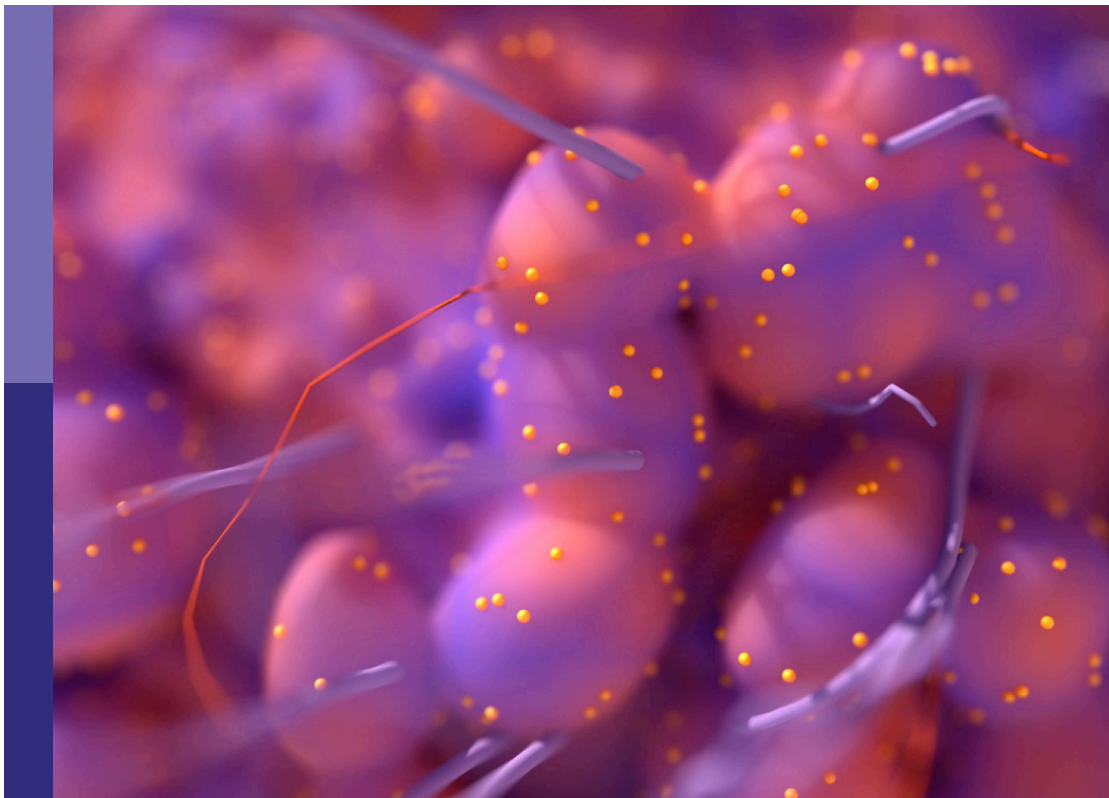

ISSN 1664-8714
ISBN 978-2-8325-2929-4
DOI 10.3389/978-2-8325-2929-4

About Frontiers

Frontiers is more than just an open access publisher of scholarly articles: it is a pioneering approach to the world of academia, radically improving the way scholarly research is managed. The grand vision of Frontiers is a world where all people have an equal opportunity to seek, share and generate knowledge. Frontiers provides immediate and permanent online open access to all its publications, but this alone is not enough to realize our grand goals.

Frontiers journal series

The Frontiers journal series is a multi-tier and interdisciplinary set of open-access, online journals, promising a paradigm shift from the current review, selection and dissemination processes in academic publishing. All Frontiers journals are driven by researchers for researchers; therefore, they constitute a service to the scholarly community. At the same time, the *Frontiers journal series* operates on a revolutionary invention, the tiered publishing system, initially addressing specific communities of scholars, and gradually climbing up to broader public understanding, thus serving the interests of the lay society, too.

Dedication to quality

Each Frontiers article is a landmark of the highest quality, thanks to genuinely collaborative interactions between authors and review editors, who include some of the world's best academicians. Research must be certified by peers before entering a stream of knowledge that may eventually reach the public - and shape society; therefore, Frontiers only applies the most rigorous and unbiased reviews. Frontiers revolutionizes research publishing by freely delivering the most outstanding research, evaluated with no bias from both the academic and social point of view. By applying the most advanced information technologies, Frontiers is catapulting scholarly publishing into a new generation.

What are Frontiers Research Topics?

Frontiers Research Topics are very popular trademarks of the *Frontiers journals series*: they are collections of at least ten articles, all centered on a particular subject. With their unique mix of varied contributions from Original Research to Review Articles, Frontiers Research Topics unify the most influential researchers, the latest key findings and historical advances in a hot research area.

Find out more on how to host your own Frontiers Research Topic or contribute to one as an author by contacting the Frontiers editorial office: frontiersin.org/about/contact

The role of imaging in gynecological malignancies

Topic editors

Kathy Han — University Health Network, Canada

Alessio G. Morganti — University of Bologna, Italy

Citation

Han, K., Morganti, A. G., eds. (2023). *The role of imaging in gynecological malignancies*. Lausanne: Frontiers Media SA. doi: 10.3389/978-2-8325-2929-4

Table of contents

frontiers | Frontiers in Oncology

TYPE Editorial
PUBLISHED 22 June 2023
DOI 10.3389/fonc.2023.1238537

OPEN ACCESS

EDITED AND REVIEWED BY
Sophia George,
University of Miami, United States

*CORRESPONDENCE
Kathy Han
Kathy.han@rmp.uhn.ca

RECEIVED 11 June 2023
ACCEPTED 12 June 2023
PUBLISHED 22 June 2023

CITATION
Han K and Morganti AG (2023) Editorial: The role of imaging in gynecological malignancies. *Front. Oncol.* 13:1238537. doi: 10.3389/fonc.2023.1238537

Editorial: The role of imaging in gynecological malignancies

Kathy Han[1]* and Alessio G. Morganti[2,3]

[1]Department of Radiation Oncology, Princess Margaret Cancer Centre, University Health Network, University of Toronto, Toronto, ON, Canada, [2]Radiation Oncology, IRCCS Azienda Ospedaliero-Universitaria di Bologna, Bologna, Italy, [3]Radiation Oncology, Department of Medical and Surgical Sciences (DIMEC), Alma Mater Studiorum - Bologna University, Bologna, Italy

KEYWORDS

editorial, gynecological neoplasms, imaging, cervical cancer, MRI

Editorial on the Research Topic
The role of imaging in gynecological malignancies

Despite the improvements recorded in the last decades, the outcome of patients with gynecological cancer is still unfavorable, in particular for some tumors and for some risk groups. At the same time, the evolution of imaging techniques in oncology is progressively accelerating, with the growing importance of topics such as the application of artificial intelligence and the study of body composition. The papers included in this Research Topic present an interesting summary of novel and still controversial aspects in the field of imaging of gynecological tumors (Scepanovic et al.; Hu et al.; Wang et al.; Matsuura et al.; Zhu et al.; Rizzo et al.; Cordoba et al.; Matani et al.; deSouza et al.; Su et al.; Wang et al.; Ciulla et al.; Jeon et al.; Ambrosio et al.; Wang et al.; Bi et al.; Shao et al.; Han et al.; Turco et al.). As evidence of the evolving scenario, it is particularly interesting to note, in this Research Topic, the lack of "classic" studies based on the evaluation of the diagnostic performance of single methods or on the comparison between different imaging methods.

Some studies evaluated the accuracy of imaging in the non-invasive prediction of malignancy in suspicious lesions of the female reproductive organs. In particular, it has been observed that: i) diffusion-weighted MRI (Scepanovic et al.) and multi-parametric (mp) MRI-based radiomic image analysis (Bi et al.) are able to effectively differentiate benign endometrial masses from malignant ones; ii) the US-based ADNEX model can differentiate benign adnexal masses from malignant or borderline ones (Hu et al.); iii) mpMRI can distinguish uterine sarcomas from leiomyomas and atypical leiomyomas (Wang et al.); IV) 3T MRI can predict histological type and grading in cervical carcinomas (Shao et al.). Conversely, mpMRI was unable to predict grading in endometrial tumors (Scepanovic et al.).

In terms of imaging-based prediction of tumor response, one study showed that superb microvascular imaging (an US image processing method) predicts response to chemoradiation in patients with locally advanced cervical cancer (Zhu et al.), while a literature review achieved similar conclusions regarding MRI in the same setting (Matani et al.). Other studies reported the possibility of predicting outcome by imaging in gynecological malignancies. In particular, it has been observed that radiomics analysis of CT and MRI images can predict recurrences in locally advanced cervical cancer (Wang et al.) and that similar results can be achieved, in the same patients, through MRI-based tumor monitoring during treatment (Cordoba et al.), as confirmed by a literature review on

the role of MRI in cervical cancers (Matani et al.). Also, the increase in abdominal fat in sarcopenic patients (assessed by CT) during treatment is correlated with a greater risk of recurrences (Han et al.). Conversely, tumor size estimation by US did not correlate with prognosis in endometrial carcinomas (Ambrosio et al.).

Other studies reported on imaging assessments of tumor biology. In particular, it was demonstrated that DCE-MRI is able to effectively evaluate the degree of proliferation (Ki-67) in cervical tumors (Wang et al.), while a literature review analyzed the role of imaging in evaluating the degree of hypoxia in endometrial tumors (deSouza et al.). Interestingly, two papers reported on the role of imaging in predicting or analyzing anticancer drug toxicity. In particular, a systematic review found variable association of body composition by imaging and chemo-induced toxicity in ovarian tumors (Rizzo et al.) while, in a case report, the authors observed that MRI can help distinguish, between two drugs, which one is responsible for the neurological toxicity (Matsuura et al.).

Instead, other studies evaluated the results of integrating different imaging methods. One paper reported a higher sensitivity and specificity, in discriminating adnexal masses, in case of combination of ADNEX model (US) and MRI (Hu et al.), while another study showed better results in the differential diagnosis between uterine sarcomas and benign lesions with the combination of conventional MRI and diffusion-weighted MRI (Wang et al.). In addition, a paper reported effective risk stratification, in patients with cervical cancer, by radiomics analysis based on CT and MRI (Wang et al.). Finally, one study showed that, compared to a single method, the combined CT-based assessment of both waist skeletal muscle volume using an AI-based tool and waist fat gained during treatment improves the prediction of outcomes (Han et al.).

Other studies reported on dynamic imaging assessments. A paper reported reliable prediction of tumor response with US-based superb microvascular imaging monitoring in patients with locally advanced cervical cancer treated with chemoradiation (Zhu et al.). Furthermore, in the same setting, a study showed that tumor monitoring by MRI allows an effective prediction of disease-free survival and overall survival (Cordoba et al.), as confirmed by a review of the literature (Matani et al.). Finally, another literature review on advanced cervical cancer discussed the role of different imaging methods (spectroscopy, PET-MRI, radiomics) in tumor monitoring during radiotherapy and in assessing clinical response (Ciulla et al.).

As further evidence of the growing importance of imaging in the clinical management of patients with gynecological cancers, we must underline the importance of a study evaluating the impact of ^{18}FDG-PET-CT in 4167 patients with IB-IVA cervical cancer treated with radiotherapy or chemoradiation. The study, which categorized patients (propensity score-matching) based on whether or not ^{18}FDG-PET-CT was performed, showed, regardless of tumor stage, a significant improvement in overall survival in patients undergoing PET (HR: 0.88; $_{95\%}$CI: 0.80-0.97; p=0.01) (Su et al.).

We sincerely hope that the papers contained in this Research Topic (Scepanovic et al.; Hu et al.; Wang et al.; Matsuura et al.; Zhu et al.; Rizzo et al.; Cordoba et al.; Matani et al.; deSouza et al.; Su et al.; Wang et al.; Ciulla et al.; Jeon et al.; Ambrosio et al.; Wang et al.; Bi et al.; Shao et al.; Han et al.; Turco et al.) represent a useful update for researchers and health professionals involved in gynecological cancers. Furthermore, we hope that these papers will be a starting point and a stimulus for the design and conduct of further clinical studies in this field. Finally, the growing role of imaging not only in the diagnosis and staging of gynecological cancers, but also in the prediction of the prognosis or even in its refinement, suggest the need for an ever greater integration of imaging in the multidisciplinary management of these neoplasms.

Author contributions

Both authors have made a substantial, direct and intellectual contribution to the work, and approved it for publication.

Conflict of interest

The authors declare that the research was conducted in the absence of any commercial or financial relationships that could be construed as a potential conflict of interest.

Publisher's note

frontiers in Oncology

ORIGINAL RESEARCH
published: 24 September 2021
doi: 10.3389/fonc.2021.741071

Impact of Computed Tomography-Based, Artificial Intelligence-Driven Volumetric Sarcopenia on Survival Outcomes in Early Cervical Cancer

Qingling Han[1†], Se Ik Kim[1†], Soon Ho Yoon[2,3], Taek Min Kim[3], Hyun-Cheol Kang[4], Hak Jae Kim[4], Jeong Yeon Cho[3] and Jae-Weon Kim[1]*

[1] Department of Obstetrics and Gynecology, Seoul National University College of Medicine, Seoul, South Korea, [2] Department of Radiology, UMass Memorial Medical Center, Worcester, MA, United States, [3] Department of Radiology, Seoul National University College of Medicine, Seoul, South Korea, [4] Department of Radiation Oncology, Seoul National University College of Medicine, Seoul, South Korea

OPEN ACCESS

Edited by:
Jitti Hanprasertpong,
Prince of Songkla University, Thailand

Reviewed by:
Jie Lee,
MacKay Memorial Hospital, Taiwan
Lilia Castillo-Martinez,
Instituto Nacional de Ciencias Médicas y Nutrición Salvador Zubirán (INCMNSZ), Mexico
Lingying Wu,
Chinese Academy of Medical Sciences and Peking Union Medical College, China

***Correspondence:**
Jae-Weon Kim
kjwksh@snu.ac.kr

[†]These authors have contributed equally to this work and share first authorship

Specialty section:
This article was submitted to Gynecological Oncology, a section of the journal Frontiers in Oncology

Received: 14 July 2021
Accepted: 03 September 2021
Published: 24 September 2021

Citation:
Han Q, Kim SI, Yoon SH, Kim TM, Kang H-C, Kim HJ, Cho JY and Kim J-W (2021) Impact of Computed Tomography-Based, Artificial Intelligence-Driven Volumetric Sarcopenia on Survival Outcomes in Early Cervical Cancer. Front. Oncol. 11:741071. doi: 10.3389/fonc.2021.741071

The purpose of this study was to investigate the impact of sarcopenia and body composition change during primary treatment on survival outcomes in patients with early cervical cancer. We retrospectively identified patients diagnosed with 2009 International Federation of Gynecology and Obstetrics stage IB1-IIA2 cervical cancer who underwent primary radical hysterectomy between 2007 and 2019. From pre-treatment CT scans (n = 306), the skeletal muscle area at the third lumbar vertebra (L3) and the waist skeletal muscle volume were measured using an artificial intelligence-based tool. These values were converted to the L3 and volumetric skeletal muscle indices by normalization. We defined L3 and volumetric sarcopenia using 39.0 cm^2/m^2 and the first quartile (Q1) value, respectively. From pre- and post-treatment CT scan images (n = 192), changes (%) in waist skeletal muscle and fat volumes were assessed. With the use of Cox regression models, factors associated with progression-free survival (PFS) and overall survival (OS) were analyzed. Between the L3 sarcopenia and non-sarcopenia groups, no differences in PFS and OS were observed. In contrast, volumetric sarcopenia was identified as a poor prognostic factor for PFS (adjusted hazard ratio [aHR], 1.874; 95% confidence interval [CI], 1.028–3.416; $p = 0.040$) and OS (aHR, 3.001; 95% CI, 1.016–8.869; $p = 0.047$). During primary treatment, significant decreases in waist skeletal muscle (median, –3.9%; $p < 0.001$) and total fat (median, –5.3%; $p < 0.001$) were observed. Of the two components, multivariate analysis revealed that the waist fat gain was associated with worse PFS (aHR, 2.007; 95% CI, 1.009–3.993; $p = 0.047$). The coexistence of baseline volumetric sarcopenia and waist fat gain further deteriorated PFS (aHR, 2.853; 95% CI, 1.257–6.474; $p = 0.012$). In conclusion, baseline volumetric sarcopenia might be associated with poor survival outcomes in patients with early cervical cancer undergoing primary RH. Furthermore, sarcopenia patients who gained waist fat during primary treatment were at a high risk of disease recurrence.

Keywords: uterine cervical neoplasms, body composition, sarcopenia, muscles, abdominal fat, prognosis, survival

INTRODUCTION

Cervical cancer is a major health problem, as it ranks the fourth highest incidence and mortality rates among cancers in women worldwide (1). The incidence of cervical cancer shows a geographical difference. Age-standardized incidence rate of cervical cancer is higher in Korea than in the United States and other Western countries (2, 3). However, owing to the effective cervical cancer screening program, more than half (55.8%) of cervical cancer cases are diagnosed at a localized disease in Korea (4, 5). For early cervical cancer, primary radical hysterectomy (RH) is recommended as one of the standard treatment options (6, 7).

Body composition analysis refers to quantifying different body compartments, such as fat and muscle, and assessing their relative ratio in an individual. Researchers have mainly focused on excessive fat accumulation, so-called obesity, and they investigated the relationship between obesity and risk of developing cancer (8, 9) and the role of obesity in cancer survival and recurrence (10, 11). Sarcopenia, characterized by the loss of skeletal muscle mass and function, recently emerged in the cancer research field, as it was associated with higher recurrence and mortality rates, surgical complications, and treatment-related toxicity (12–15). In cervical cancer, only few studies have investigated prognostic role of pre-treatment sarcopenia, resulting in conflicting results (16–18). Moreover, all these previous studies included patients who underwent primary concurrent chemoradiation therapy (CCRT) or radiation therapy (RT), rather than primary RH.

For body composition analysis, computed tomography (CT) is widely used because it can quantify the body composition components. Researchers have measured individuals' area of skeletal muscle and adipose tissue at the third lumbar vertebral body (L3)-level cross-sectional image of CT scans, which is known to reflect amounts of total body muscle and adipose tissue well (19, 20). In addition, the latest high-throughput technology allows automated and fast volumetric measurements of each component from CT scans (21, 22). With the use of such an advanced tool, tracking the volumetric change of specific body composition components is feasible (23), which has not yet been investigated in early cervical cancer.

Thus, we aimed to investigate the impact of pre-treatment sarcopenia determined by two different measurements (L3 level skeletal muscle area and waist skeletal muscle volume) on survival outcomes in Korean patients with early-stage cervical cancer who underwent primary RH. Additionally, we traced the change of body composition during primary treatment and investigated their prognostic roles.

MATERIALS AND METHODS

Study Population

From the institution's cervical cancer cohort database, we identified and collected patients who met the following conditions: 1) patients aged 20 years or older at the time of diagnosis; 2) patients diagnosed with 2009 International Federation of Gynecology and Obstetrics (FIGO) stage IB1 to IIA2 cervical cancer who were treated at Seoul National University Hospital between January 2007 and December 2019; 3) patients who underwent primary type B-C RH, according to Querleu–Morrow classification (24), and pelvic lymphadenectomy by faculty who finished gynecologic oncology fellowship; and 4) those whose pre-treatment CT scans, performed less than a month before the primary surgery, were stored in the Picture Archiving and Communication System.

Meanwhile, patients with the following conditions were excluded: 1) those who received neoadjuvant chemotherapy prior to RH; 2) those whose tumor had histologic types other than squamous cell carcinoma, usual type adenocarcinoma, and adenosquamous carcinoma; 3) those who were diagnosed with other cancers before and/or at the time of cervical cancer diagnosis; 3) those with insufficient clinicopathologic data; 4) those lost to follow-up before completion of primary treatment; and 5) those for whom we were unable to obtain pre-treatment CT scans.

In total, 306 patients were included in this analysis (study population I). To assess changes in body composition components, we further identified 192 patients whose post-treatment CT scans were available (study population II). For the patients who did not undergo adjuvant treatment, we referred to CT scans obtained 3 months after the surgery. For the patients who received adjuvant RT or CCRT, we used CT scans obtained within a month after the completion of RT (**Figure 1**).

Data Collection

We collected patients' clinicopathologic features, such as age at diagnosis, FIGO stage, surgical approach, histologic type, radicality of hysterectomy, para-aortic lymphadenectomy, pathologic risk factors, risk group, and adjuvant treatment. Based on pre-treatment body mass index (BMI), patients were divided into four groups, according to the WHO's recommendation for Asian population (25): <18.5 kg/m^2 (underweight), 18.5–22.9 kg/m^2 (normal), 23.0–24.9 kg/m^2 (overweight), and ≥25.0 kg/m^2 (obese). Clinical cervical tumor size was determined by either colposcopic examination or pre-treatment magnetic resonance imaging (MRI).

During pre-treatment workup, advanced imaging modalities, such as MRI and whole-body ^{18}F-FDG positron emission tomography (PET)/CT imaging, have been frequently conducted at this institution. While we measure the cervical tumor size and evaluate parametrium involvement using MRI, we evaluate distant site metastasis using CT scans and PET/CT imaging. Pelvic and para-aortic lymph node status is assessed from all the available imaging modalities. Among the study population (n = 306), 15 (4.9%) received pre-treatment CT scans only, while 36 (11.8%) and 63 (20.6%) received CT scans plus MRI and CT scans plus PET/CT imaging, respectively. The other 192 (62.7%) patients received all three imaging modalities.

After surgery, patients who had lymph node metastasis, positive resection margins, or parametrium involvement were classified as the high-risk group. According to the Sedlis criteria, we classified patients with various combinations of the three

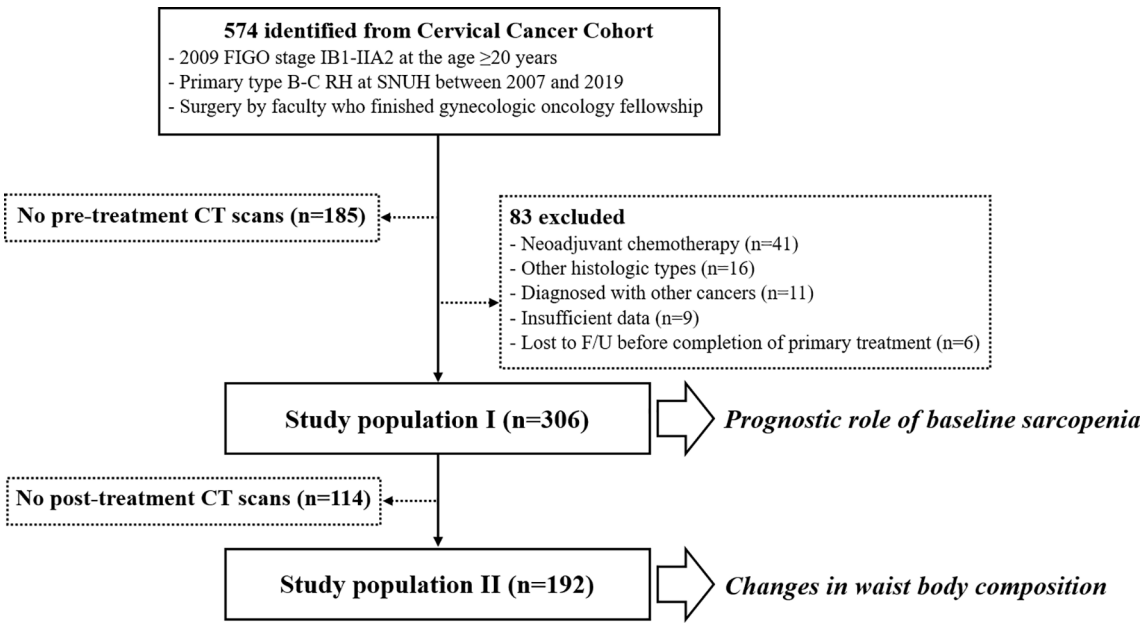

FIGURE 1 | Flow diagram depicting selection of study population.

factors (tumor size, depth of invasion, and lymphovascular space invasion) as the intermediate-risk group (26). High-risk and intermediate-risk patients received adjuvant CCRT or RT after RH.

Adjuvant RT consisted of a combination of external beam RT (EBRT) with/without high-dose-rate intracavitary radiotherapy (HDR-ICR). With regard to RT planning, our institution had used 3D conformal RT before November 2015 and adopted intensity-modulated RT (IMRT) since then. The prescribed dose fractionation schedule for pelvic EBRT was 50.4 Gy in 28 fractions. For patients with pathologically confirmed para-aortic lymph node metastasis, extended field RT consisting of an additional boost dose of 9–10 Gy in five fractions to the para-aortic lymphatics was delivered. HDR-ICR was implemented with the dose fractionation schedule of 15 Gy in three fractions. The treatment duration of RT usually took 5–6 weeks. As the most common regimen for CCRT, 40 mg/m^2 of cisplatin was administered weekly for 4–6 cycles during EBRT.

From the patients' medical records, we also collected gastrointestinal toxicities that occurred during adjuvant RT. Because of the retrospective study design, it was challenging to identify the exact grade according to the Common Terminology Criteria for Adverse Events version 5.0 (27). Instead, we checked the presence or absence of any grade gastrointestinal toxicities.

Surveillance frequency for symptom review and examination depended on FIGO stage, pathologic risk factors, and adjuvant therapy (6, 7). In general, patients who completed the initial treatment (hysterectomy and adjuvant treatment) consulted a physician every 3 months in the first 2 years, and every 6 months for the next 3 years. Thereafter, patients visited the clinic every year.

We determined the progression or recurrence of the disease from imaging studies based on the Response Evaluation Criteria in Solid Tumors version 1.1 (28). Progression-free survival (PFS) refers to the time interval between the beginning of treatment and disease progression. Overall survival (OS) was defined as the time interval between the date of diagnosis and the date of cancer-related death or the last visit.

Imaging Analysis

Imaging analysis methods for this study were the same as our previous study on patients with epithelial ovarian cancer (23), including the use of the same commercially available, artificial intelligence-based software (DEEPCATCH v1.0.0.0; MEDICALIP Co. Ltd., Seoul, Korea). In brief, we used this deep neural network-based software for automatic volumetric segmentation of body composition (skeletal muscle, abdominal visceral fat, and subcutaneous fat) from anonymized, precontrast CT images in DICOM format. According to the previous validation study, the software's average segmentation accuracy was reported as 97% compared with manual segmentation (21). After segmentation, the abdominal waist was automatically labeled based on WHO's waist definition (29): between the lower end of the thoracic ribs and the upper end of the iliac crest. One expert radiologist (SHY) confirmed the results of automatic segmentation and labeling. Subsequently, the waist volume (cm^3) of skeletal muscle and total fat (sum of abdominal visceral fat and subcutaneous fat) were quantified and normalized to the height (m^3), generating the volumetric skeletal muscle index (SMI) and total fat index. This software also automatically measured skeletal muscle area (cm^2) from the single cross-sectional CT image at the L3 level. The skeletal

muscle area was normalized to the height (m^2) and reported as the L3 SMI (**Supplementary Figure 1**).

Statistical Analysis

L3 sarcopenia was defined as an individual's L3 SMI <39.0 cm^2/m^2, per the cutoff value proposed by an international consensus of cancer cachexia (30). This value was also used in our previous study, which investigated the impact of sarcopenia on survival outcomes in patients with advanced-stage high-grade serous ovarian cancer (31). Because there is no study of volumetric SMI, we used the Q1 value and divided patients into volumetric sarcopenia and non-sarcopenia groups accordingly.

Differences in the pre- and post-treatment waist volume of body compositions components were evaluated using the paired t-test. Change (%) in a specific component was calculated as follows:

$$\frac{x_{Post-treatment} - x_{Pre-treatment}}{x_{Pre-treatment}} \times 100$$

We regarded a negative value as a loss during treatment. The extent of changes in body composition components between the two groups was compared using Student's t-test, while that among the three or more groups were compared using one-way ANOVA.

The characteristics and survival outcomes were compared between the two groups, such as volumetric sarcopenia *versus* non-sarcopenia groups. We used Student's t-test or Mann–Whitney U test to compare continuous variables, and Pearson's chi-square test or Fisher's exact test to compare categorical variables. Pearson's correlation coefficient test was used to calculate the correlation value. Kaplan–Meier methods and log-rank tests were used for the survival analysis. In multivariate analysis, we used the Cox proportional hazards model to calculate adjusted hazard ratios (aHRs) and 95% confidence intervals (CIs). IBM SPSS software (version 25.0; IBM Corp., Armonk, NY, USA) was used for statistical analysis. We considered a p-value <0.05 as statistically significant.

Ethics Statement

This study was approved by the Institutional Review Board of Seoul National University Hospital (No. H-2012-061-117) and performed according to the principles of the Declaration of Helsinki. The requirement for informed consent was waived.

RESULTS

Patients' Characteristics

Table 1 describes the clinicopathologic features of the study population I (n = 306). Squamous cell carcinoma was the most common histological type (74.2%), and 64.1% of the patients had 2009 FIGO stage IB1. The median clinical cervical tumor size was 26.5 mm (interquartile range [IQR], 10.0–40.1). After RH, 119 (38.9%) did not undergo adjuvant treatment, while 30 (9.8%) and 157 (51.3%) underwent adjuvant RT and CCRT, respectively.

Of 187 patients with (CC)RT, 154 (82.4%) and 33 (17.6%) received EBRT and EBRT plus HDR-ICR, respectively (**Supplementary Table 1**). For RT planning, 3D conformal RT was conducted in 116 (62.0%), whereas IMRT was conducted in 71 (38.0%). Extended field RT was administered in nine (4.8%) patients. Five patients refused RT due to poor general condition (early termination of RT). During RT, more than a half (55.1%) experienced nausea. Other common gastrointestinal toxicities were as follows: diarrhea (45.5%), constipation (31.6%), anorexia (22.5%), abdominal pain (20.3%), and vomiting (19.3%) (in the order of frequency).

In terms of baseline body composition, the median values for L3 SMI and volumetric SMI were 39.4 cm^2/m^2 (IQR, 34.0–44.3) and 206.5 cm^3/m^3 (IQR, 181.5–236.2), respectively. As shown in **Supplementary Figure 2**, baseline BMI was weakly correlated with L3 SMI (Pearson's correlation coefficient r = 0.249; $p < 0.001$) and volumetric SMI (r = 0.423; $p < 0.001$). The L3 SMI and volumetric SMI also showed a very weak positive correlation (r = 0.176; $p = 0.002$).

During a median observation period of 55.2 months, 50 (16.3%) patients experienced disease recurrence, and 14 (4.6%) patients died.

Prognostic Role of Baseline Sarcopenia

With the use of the well-known cutoff value (39.0 cm^2/m^2) of L3 SMI, 141 (46.1%) and 165 (53.9%) patients were assigned to the L3 sarcopenia and non-sarcopenia groups, respectively. Patients in the L3 sarcopenia group had a significantly lower BMI (mean, 22.1 *vs.* 24.8 kg/m^2; $p < 0.001$), than had the L3 non-sarcopenia group. However, other clinicopathologic characteristics were similar between the two groups (**Supplementary Table 2**). In survival analysis, the L3 sarcopenia and non-sarcopenia groups showed similar PFS ($p = 0.415$) and OS ($p = 0.743$) (**Figures 2A, B**).

With the use of the Q1 value (181.5 cm^3/m^3) of volumetric SMI, 76 (24.8%) and 230 (75.2%) were identified as the volumetric sarcopenia and non-sarcopenia groups, respectively. The volumetric sarcopenia group had a significantly lower BMI (22.1 *vs.* 23.9 kg/m^2; $p < 0.001$) than the volumetric non-sarcopenia group, while other baseline clinicopathologic characteristics were similar between the two groups (**Table 1**).

Among the patients who received (CC)RT (n = 187), the proportions of patients who received HDR-ICR (12.8% *vs.* 19.3%; $p = 0.310$) and extended field EBRT (2.1% *vs.* 5.7%; $p = 0.454$) were also similar between the volumetric sarcopenia and non-sarcopenia groups (**Supplementary Table 1**). However, IMRT was less frequently used in the volumetric sarcopenia group (21.3% *vs.* 43.6%; $p = 0.006$). Regarding incidences of gastrointestinal toxicities during RT, patients in the volumetric sarcopenia group experienced diarrhea (59.6% vs. 40.7%; $p = 0.025$) and vomiting (29.8% *vs.* 15.7%; $p = 0.034$) more frequently, but similar other gastrointestinal toxicities.

In survival analysis, the volumetric sarcopenia group showed significantly worse PFS (3-year PFS rate, 78.3% *vs.* 88.7%; $p = 0.039$) and OS (5-year OS rate, 90.0% *vs.* 97.6%; $p = 0.031$), than the volumetric non-sarcopenia group (**Figures 2C, D**). In multivariate analysis that adjusted for clinicopathologic factors, volumetric sarcopenia was identified as a poor prognostic factor for PFS (aHR, 1.874; 95% CI, 1.028–3.416; $p = 0.040$) and OS (aHR, 3.001; 95% CI, 1.016–8.869; $p = 0.047$) (**Table 2**).

TABLE 1 | Clinicopathologic characteristics of volumetric sarcopenia and non-sarcopenia groups.

Characteristics	All (n = 306, %)	Volumetric sarcopenia (n = 76, %)	Volumetric non-sarcopenia (n = 230, %)	*p*
Age, years				
Mean ± SD	51.5 ± 11.3	52.6 ± 11.0	51.1 ± 11.4	0.295
BMI, kg/m^2				
Median (IQR)	23.4 (21.2–25.9)	22.1 (20.2–24.7)	23.9 (21.7–26.4)	<0.001
Underweight (<18.5)	12 (3.9)	6 (7.9)	6 (2.6)	0.001
Normal (18.5–22.9)	132 (43.1)	42 (55.3)	90 (39.1)	
Overweight (23.0–24.9)	58 (19.0)	15 (19.7)	43 (18.7)	
Obesity (≥25.0)	104 (34.0)	13 (17.1)	91 (39.6)	
Surgical approach				0.914
Open	143 (46.7)	37 (48.7)	106 (46.1)	
Laparoscopy	131 (42.8)	31 (40.8)	100 (43.5)	
Robot-assisted surgery	32 (10.5)	8 (10.5)	24 (10.4)	
Conization	88 (28.8)	17 (22.4)	71 (30.9)	0.156
Histologic type				0.209
Squamous cell carcinoma	227 (74.2)	62 (81.6)	165 (71.7)	
Adenocarcinoma	66 (21.6)	11 (14.5)	55 (23.9)	
Adenosquamous carcinoma	13 (4.2)	3 (3.9)	10 (4.3)	
2009 FIGO stage				0.293
IB1	196 (64.1)	47 (61.8)	149 (64.8)	
IB2	49 (16.0)	9 (11.8)	40 (17.4)	
IIA1	21 (6.9)	8 (10.5)	13 (5.7)	
IIA2	40 (13.1)	12 (15.8)	28 (12.2)	
Radicality of hysterectomy				0.285
Type B	27 (8.8)	9 (11.8)	18 (7.8)	
Type C	279 (91.2)	67 (88.2)	212 (92.2)	
Para-aortic lymphadenectomy				0.916
No	220 (71.9)	55 (72.4)	165 (71.7)	
Sampling/dissection	86 (28.1)	21 (27.6)	65 (28.3)	
Clinical cervical tumor size*, mm				
Median (IQR)	26.5 (10.0–40.1)	26.5 (13.5–26.5)	26.5 (10.0–40.0)	0.839
<20	109 (35.6)	26 (34.2)	83 (36.1)	0.897
≥20 and <40	110 (35.9)	29 (38.2)	81 (35.2)	
≥40	87 (28.4)	21 (27.6)	66 (28.7)	
Pathologic risk factors				
Parametrial invasion	62 (20.3)	18 (23.7)	44 (19.1)	0.392
Lymph node metastasis	85 (27.8)	21 (27.6)	64 (27.8)	0.974
Resection margin involvement	30 (9.8)	7 (9.2)	23 (10.0)	0.841
LVSI	154 (50.3)	36 (47.4)	118 (51.3)	0.552
Deep one-third stromal invasion	161 (52.6)	39 (51.3)	122 (53.0)	0.794
Risk group				0.735
Low risk	119 (8.9)	30 (39.5)	89 (38.7)	
Intermediate risk	70 (22.9)	15 (19.7)	55 (23.9)	
High risk	117 (38.2)	31 (40.8)	86 (37.4)	
Adjuvant treatment				0.788
No	119 (38.9)	29 (38.2)	90 (39.1)	
RT only	30 (9.8)	9 (11.8)	21 (9.1)	
CCRT	157 (51.3)	38 (50.0)	119 (51.7)	

BMI, body mass index; CCRT, concurrent chemoradiation therapy; FIGO, International Federation of Gynecology and Obstetrics; IQR, interquartile range; LVSI, lymphovascular space invasion; RT, radiation, therapy; SD, standard deviation.

**Measured by either colposcopic examination or pre-treatment magnetic resonance imaging.*

Changes in Waist Body Composition

From the study population I, 114 patients were excluded owing to the absence of post-treatment CT scans. Compared with the study population II (n = 192), these 114 patients had significantly smaller clinical cervical tumor size (median, 20.0 *vs.* 30.0 mm; $p = 0.026$) and less frequent lymph node metastasis (20.2% *vs.* 32.3%; $p = 0.022$) and, therefore, omitted adjuvant treatment more frequently (46.5% *vs.* 34.4%; $p = 0.036$) (**Supplementary Table 3**).

Next, we evaluated changes in body composition components among 192 patients in the study population II. **Supplementary Figure 3** depicts the distribution of the patients by extent of changes in body composition components during the treatment: while 65.1% of the patients experienced loss of waist skeletal muscle volume, 61.5% experienced loss of waist total fat volume. There were significant changes in waist skeletal muscle ($p < 0.001$) and total fat ($p < 0.001$) volumes with median values of −3.9% (IQR, −11.0 to 3.7) and −5.3% (IQR, −17.6 to 8.0), respectively. Correlation analyses revealed that there were no correlations between baseline BMI and changes in waist skeletal muscle and total fat volumes (**Supplementary Figures 4A, B**). In contrast, a

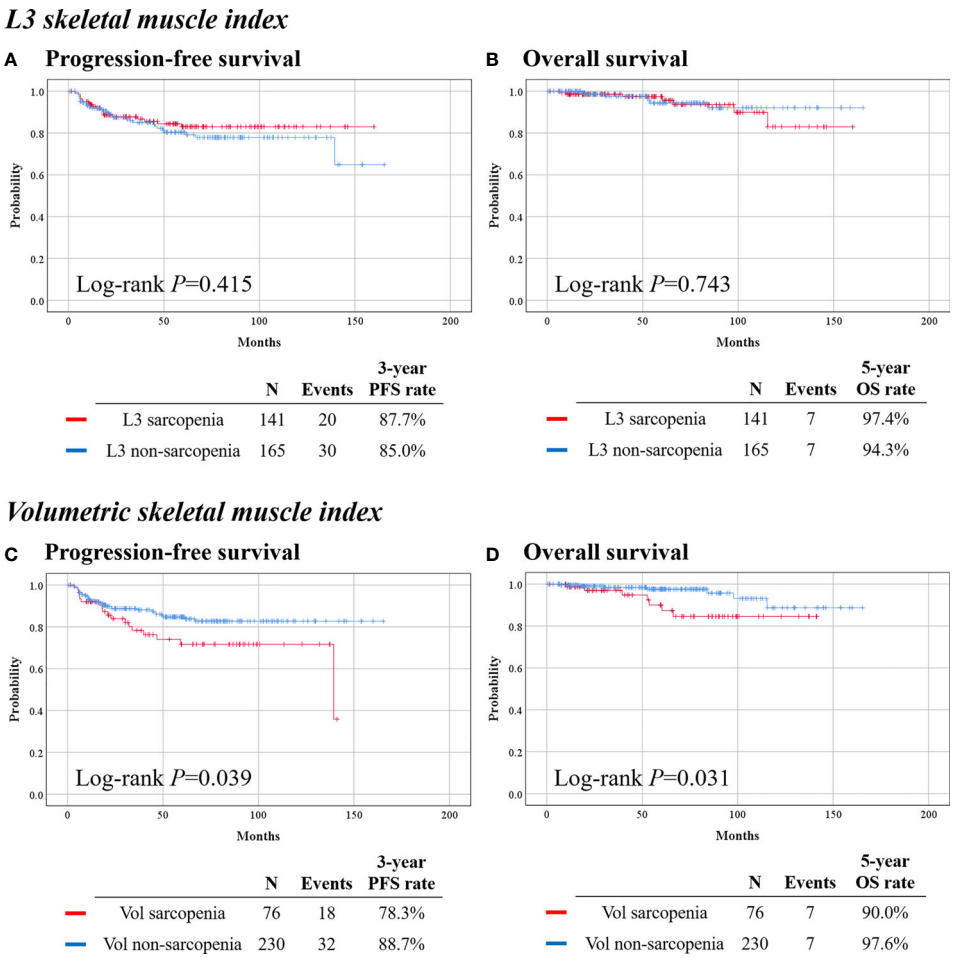

FIGURE 2 | Survival outcomes of patients by skeletal muscle index. (Top) Calculated from L3 level cross-sectional image. (Bottom) Calculated from volumetric measurement of the waist. **(A, C)** Progression-free survival. **(B, D)** Overall survival.

positive, moderate relationship was observed between the extent of skeletal muscle volume change and that of total fat volume change (r = 0.556; $p < 0.001$) (**Supplementary Figure 4C**).

The extent of skeletal muscle volume change was not associated with patients' FIGO stage, pathologic risk group, adjuvant treatment, and baseline BMI classification (**Supplementary Table 4**). Meanwhile, the extent of total fat volume change was associated with patients' FIGO stage ($p = 0.002$) and administration of (CC)RT, rather than no adjuvant treatment (median, −6.1% *vs.* −2.3%; $p = 0.034$). Patients without baseline volumetric sarcopenia showed significantly greater loss of skeletal muscle (median, −4.5% *vs.* 1.2%; $p = 0.003$) and total fat (median, −6.7% *vs.* 6.0%; $p = 0.011$) volumes, than did those with baseline volumetric sarcopenia. Patients who received open RH, rather than minimally invasive RH, also showed significantly greater loss of skeletal muscle (median, −7.5% *vs.* −1.7%; $p = 0.001$) and total fat (median, −12.9% *vs.* 0.2%; $p < 0.001$) volumes.

Among the patients who received (CC)RT (n = 126), the use of IMRT, HDR-ICR, and extended field EBRT was not associated with the extent of changes in skeletal muscle and total fat volumes (**Supplementary Table 5**). Among the various gastrointestinal toxicities during RT, none was associated with the extent of body composition changes in body composition components, except vomiting: patients who experienced vomiting showed significantly greater loss of total fat volume than those who did not (median, −17.1% *vs.* −5.6%; $p = 0.049$).

Next, we focused on prognostic implications of fat gain or loss during cervical cancer treatment. As shown in **Supplementary Table 6**, patients who gained waist total fat volume (n = 74) and those who lost (n = 118) had similar clinicopathologic characteristics, except for surgical approach and para-aortic lymphadenectomy. Patients in the total fat gain group received minimally invasive RH more frequently (66.2% *vs.* 40.7%; $p = 0.001$) and para-aortic lymphadenectomy less frequently (18.9% *vs.* 41.5%; $p = 0.001$), than did those in the total fat loss group.

During a median observation period of 55.6 months, no differences in PFS (3-year PFS rate, 79.3% *vs.* 87.0%; $p = 0.071$) and OS (5-year OS rate, 91.6% *vs.* 99.1%; $p = 0.148$) were observed between the total fat gain and loss groups (**Figure 3**).

TABLE 2 | Factors associated with patients' survival outcomes.

Characteristics		Progression-free survival						Overall survival					
		Univariate analysis			Multivariate analysis			Univariate analysis			Multivariate analysis		
		HR	95% CI	p	aHR	95% CI	p	HR	95% CI	p	aHR	95% CI	p
Age	≥50 *vs.* <50 years	1.159	0.662–2.027	0.606				1.266	0.439–3.654	0.663			
BMI	Continuous	1.010	0.938–1.087	0.789	1.034	0.958–1.117	0.387	0.996	0.859–1.154	0.953			
2009 FIGO stage	IIA *vs.* IB	1.418	0.764–2.632	0.268				2.599	0.898–7.517	0.078			
Histologic type	Non-SCC *vs.* SCC	1.096	0.591–2.032	0.771	1.737	0.903–3.340	0.098	1.084	0.339–3.462	0.892	2.147	0.612–7.533	0.233
Risk group	High *vs.* low intermediate	3.600	1.986–6.522	<0.001	3.882	2.103–7.168	<0.001	4.282	1.340–13.683	0.014	4.739	1.397–16.072	0.013
Adjuvant treatment	Yes *vs.* no	3.934	1.769–8.745	0.001				3.996	0.891–17.923	0.070			
Surgical approach	MIS *vs.* open	1.005	0.575–1.758	0.985				0.729	0.238–2.239	0.581			
Volumetric sarcopenia	Yes *vs.* no	1.823	1.023–3.248	0.042	1.874	1.028–3.416	0.040	3.004	1.052–8.574	0.040	3.001	1.016–8.869	0.047

aHR, adjusted hazard ratio; BMI, body mass index; CI, confidence interval; FIGO, International Federation of Gynecology and Obstetrics; HR, hazard ratio; MIS, minimally invasive surgery; SCC, squamous cell carcinoma.

However, in multivariate analyses adjusting for clinicopathologic factors, total fat volume gain was identified as an independent poor prognostic factor for PFS (aHR, 2.007; 95% CI, 1.009–3.993; $p = 0.047$) (**Table 3**). Owing to the small events, we could not conduct further analysis for OS.

Lastly, we classified patients by the combinations of baseline volumetric sarcopenia and waist total fat change during primary treatment. The baseline volumetric sarcopenia patients who gained total fat (n = 22) showed significantly worse PFS (3-year PFS rate, 64.8% *vs.* 86.6%; $p = 0.014$) than others (n = 170); however, no difference in OS was observed (5-year OS rate, 86.6% *vs.* 97.8%; $p = 0.050$) (**Figure 3**). The two groups had similar clinicopathologic characteristics (**Supplementary Table 7**). Multivariate analyses revealed that initial volumetric sarcopenia with total fat gain during primary treatment was associated with worse PFS (aHR, 2.853; 95% CI, 1.257–6.474; $p = 0.012$) (**Table 3**).

DISCUSSION

In this study, we found that the pre-treatment or baseline L3 sarcopenia did not affect survival outcomes in patients with early cervical cancer who underwent primary RH. However, patients with volumetric sarcopenia showed significantly higher disease recurrence and mortality, than did those with volumetric non-sarcopenia. Regarding changes in body composition components during primary treatment, the volumetric total fat gain was identified as a poor prognostic factor for PFS.

CT-determined L3 sarcopenia was reported as a poor prognostic factor for many malignancies despite the cutoff values varying among the studies. According to a Korean retrospective study, sarcopenia, defined as L3 SMI ≤31 cm^2/m^2 for women and ≤49 cm^2/m^2 for men, was an independent poor prognostic factor for OS in patients with advanced gastric cancer (15). Defining sarcopenia as L3 SMI <29.9 cm^2/m^2 for women and <49.5 cm^2/m^2 for men, Xie et al. reported that baseline sarcopenia was closely related to the risk of recurrence, postoperative complications, and long-term prognosis in Chinese elderly colorectal cancer patients (32).

In contrast, studies conducted in cervical cancer have reported inconsistent results. Yoshikawa et al. measured L3 psoas muscle index (PMI) of Japanese patients with metastatic cervical cancer (n = 40) and identified L3 PMI ≤3.72 cm^2/m^2 as an independent poor prognostic factor for OS (16). In contrast, Lee et al. (17) and Matsuoka et al. (18) observed no association between baseline sarcopenia and survival in patients with locally advanced cervical cancer who underwent primary CCRT or RT, similar to our results. However, these two studies differed from our study in terms of ethnicity (Taiwanese *vs.* Japanese *vs.* Korean) and sarcopenia definition (L3 SMI, <41.0 *vs.* <36.55 *vs.* <39.0 cm^2/m^2), besides the stage and primary treatment methods.

We recognize that the analysis of a single cross-sectional CT image at the L3 level is a well-established, standard method for body composition analysis. However, this method has limitations. Due to the displacement of the gastrointestinal tract, the abdominal muscle and visceral fat may be measured inaccurately on a single abdominal

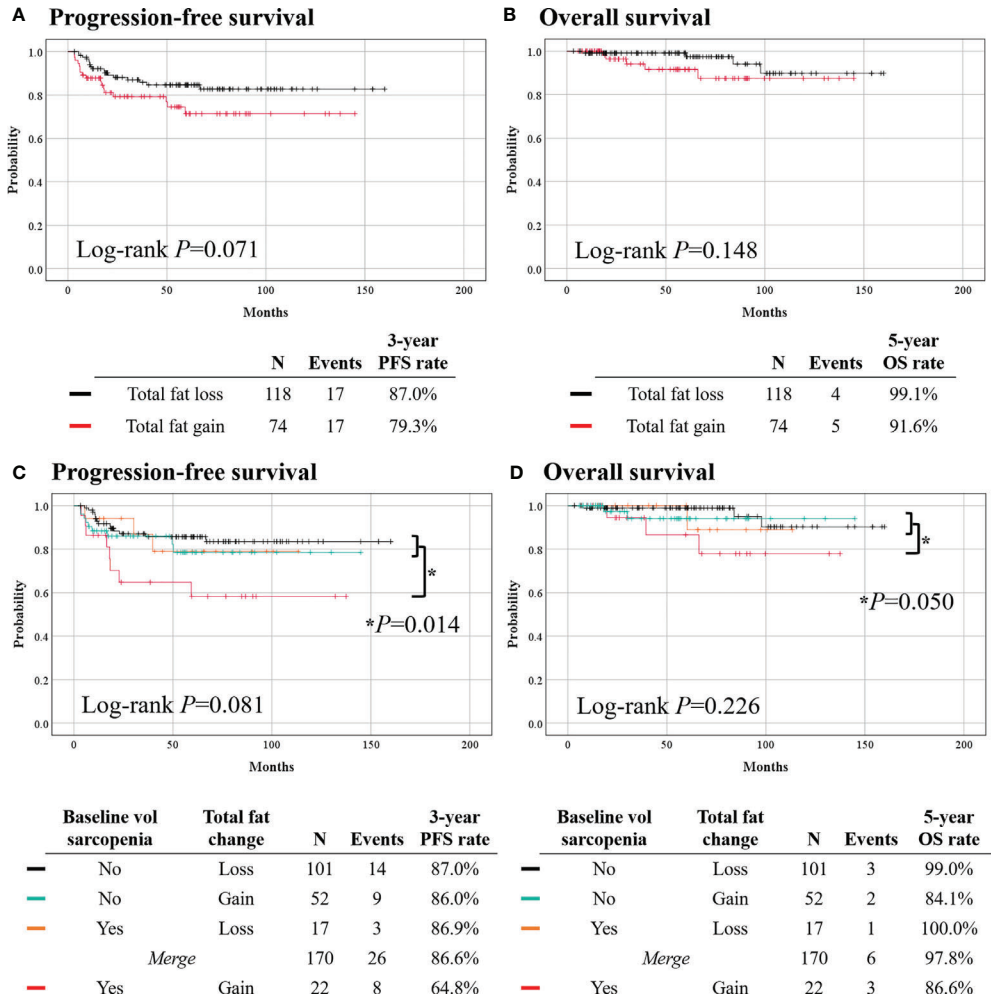

	N	Events	3-year PFS rate
Total fat loss	118	17	87.0%
Total fat gain	74	17	79.3%

	N	Events	5-year OS rate
Total fat loss	118	4	99.1%
Total fat gain	74	5	91.6%

Baseline vol sarcopenia	Total fat change	N	Events	3-year PFS rate
No	Loss	101	14	87.0%
No	Gain	52	9	86.0%
Yes	Loss	17	3	86.9%
Merge		170	26	86.6%
Yes	Gain	22	8	64.8%

Baseline vol sarcopenia	Total fat change	N	Events	5-year OS rate
No	Loss	101	3	99.0%
No	Gain	52	2	84.1%
Yes	Loss	17	1	100.0%
Merge		170	6	97.8%
Yes	Gain	22	3	86.6%

FIGURE 3 | Comparisons of survival outcomes according to changes in total fat volume (top) and combinations of baseline volumetric sarcopenia and waist total fat change (bottom). **(A, C)** Progression-free survival. **(B, D)** Overall survival.

CT image; the distribution of muscle and visceral fat may vary as high as twice the true value (33). Therefore, a volumetric measurement might be a more accurate method than a single areal measurement. Some might argue that ascites, bowel obstruction, or huge abdominal mass might interfere with accurate volumetric measurement (22). However, such cases were not identified in our study population, as we included only those with early-stage disease.

Compared with L3 SMI, waist volumetric SMI is a relatively new concept; thus, there is no established cutoff value for the volumetric sarcopenia. In this study, we classified patients with volumetric sarcopenia using the Q1 value of the waist volumetric SMI, considering that many early studies on sarcopenia defined cutoff values based on sex-specific, lowest 20% of the study group (34), and recent studies on sarcopenia also use Q1 or quartiles to investigate their impact on cancer prognosis or other health outcomes, such as metabolic syndrome (35, 36). Further population-based studies are warranted to determine an optimal cutoff value for the presence of volumetric sarcopenia.

There are many reasons for decreased skeletal muscle in cancer patients (37). To date, studies on sarcopenia in cancer patients have been conducted in the context of cancer cachexia (38). Patients with cancer cachexia, especially those with enlarging tumor masses, suffer metabolic dysfunction towards catabolism. Considering that the current study population had early-stage disease, influence of cancer cachexia on the pre-treatment sarcopenia seems to be minimal. However, we also admit that even among patients with early cervical cancer, some might already have cancer cachexia at the time of diagnosis. As patients with volumetric sarcopenia were at high risk of disease recurrence in our study, physicians may consider routine baseline body composition analysis to screen for volumetric sarcopenia.

According to the sarcopenia working groups, early recognition and intervention are key to proper management of sarcopenia (34, 39). If the same methodology of the current study is applied to the CT scans, obtained during diagnostic workup, patients with volumetric sarcopenia can be identified easily in the

TABLE 3 | Changes in waist body composition and survival outcomes.

Characteristics		Progression-free survival								
		Univariate analysis			Multivariate analysis			Multivariate analysis		
		HR	95% CI	p	aHR	95% CI	p	aHR	95% CI	p
Age	≥50 *vs.* <50 years	1.318	0.665–2.612	0.429						
BMI	Continuous	0.969	0.879–1.069	0.534						
2009 FIGO stage	IIA *vs.* IB	0.951	0.430–2.101	0.900						
Histologic type	Non-SCC *vs.* SCC	2.106	1.053–4.212	0.035	2.699	1.322–5.510	0.006	2.933	1.409–6.104	0.004
Risk group	High *vs.* low intermediate	2.278	1.127–4.603	0.022	2.973	1.415–6.249	0.004	2.773	1.322–5.821	0.007
Adjuvant treatment	Yes *vs.* no	2.462	1.019–5.947	0.045						
Surgical approach	MIS *vs.* open	1.252	0.638–2.459	0.514	1.461	0.715–2.984	0.299	1.556	0.774–3.127	0.214
Total fat change	Gain *vs.* loss	1.840	0.939–3.607	0.076	2.007	1.009–3.993	0.047			
Baseline volumetric sarcopenia and total fat change	Sarcopenia plus fat gain *vs.* others	2.613	1.182–5.776	0.018				2.853	1.257–6.474	0.012

aHR, adjusted hazard ratio; BMI, body mass index; CI, confidence interval; FIGO, International Federation of Gynecology and Obstetrics; HR, hazard ratio; MIS, minimally invasive surgery; SCC, squamous cell carcinoma.

early phase of the treatment. For those, further muscle loss should be prevented by providing individualized consultation with a nutritional expert, adequate nutritional supplementation, and interventions with physical exercise, consisting of aerobic and resistance exercises during the course of primary treatment (40, 41).

To our knowledge, the current study is the first to report volumetric changes in both skeletal muscle and fat during primary treatment in patients with early cervical cancer. While significant decreases in waist skeletal muscle (median, −3.9%; $p < 0.001$) and total fat (median, −5.3%; $p < 0.001$) were observed in our volumetric measurement study, L3 SMI did not decrease significantly in the Taiwanese longitudinal study on locally advanced cervical cancer (17). Nevertheless, that study identified SMI loss >10% as an independent poor prognostic factor for OS. Among the treatment-related factors, we identified open RH, rather than minimally invasive RH, as an aggravating factor for the loss of skeletal muscle and total fat volumes. Compared with no adjuvant treatment, adjuvant (CC)RT was associated with the greater loss of total fat volume. In the study of Matsuoka et al. (18), anorexia and reduced food intake were frequently observed during postoperative care and at the time of adjuvant CCRT or RT (18). Similarly, we also observed high incidence of gastrointestinal toxicities during adjuvant (CC)RT. Especially, the presence of vomiting was significantly associated with the loss of total fat volume. Considering that gastrointestinal toxicities during adjuvant (CC)RT hinder patients' food intake, such toxicities should be relieved by using antiemetics, antidiarrheal agents, and other drugs adequate to maintain body compositions (42, 43). Persistent or recurrent bowel obstruction, which might further aggravate malnutrition and loss of body weight, should be also managed properly (44).

Interestingly, 38.5% of the study population experienced gain of waist total fat volume, which was identified as a poor prognostic factor for PFS. While we conducted a volumetric approach, most previous studies have measured BMI and body weight change during cancer treatment. For example, Kroenke et al. reported relationship between weight gain after diagnosis and higher recurrence and mortality in breast cancer (45). Current evidence suggests that excessive visceral fat accumulation, also known as visceral obesity, is associated with adverse metabolic consequences, systemic inflammation, and cancer development and progression (46). In the current study, the patients who were initially volumetric sarcopenia and gained total fat during primary treatment were identified to have higher risk of disease recurrence than the others. Similar results were also observed in previous studies on ovarian cancer (31) and colorectal cancer (47). Worse PFS from the coexistence of sarcopenia and fat gain might be explained by the concept, sarcopenic obesity, known to affect the survival outcome of patients, which is equal to or greater than the sum of the respective risks of obesity and sarcopenia (48). As a possible explanation, researchers have indicated adipose stem cells from visceral and subcutaneous fat may promote the growth and migration of cancer cells (49). Therefore, initial sarcopenia patients should be cautious of excessive fat gain by avoiding

excessive intake and lack of physical exercise (50, 51). It might be necessary to monitor body composition changes during the treatment courses.

Our study had several limitations. First, selection bias is one of the most problematic issues originating from the retrospective study design. For example, among the original study population, we further excluded patients who did not receive post-treatment CT scans to investigate the impact of changes in waist body composition on survival outcomes. We recognize that the excluded patients tended to belong to a favorable risk group, thus omitting adjuvant treatment after surgery. Second, the small sample size is also problematic. Owing to the small number of intraoperative and postoperative complications, the relationship between sarcopenia and complications related to surgery has not been reported. Further subgroup analyses by the administration of adjuvant treatment and detailed radiation methods were not performed because of the small number of recurrent and death cases. Third, we could not obtain BMI data after treatment or conduct further analysis based on the changes in BMI. Lastly, the precise underlying mechanisms for poor survival outcomes from volumetric sarcopenia and total fat gain could not be elucidated from the current study. Therefore, further cell line or animal level proof-of-concept studies are warranted.

CONCLUSION

In conclusion, our study results demonstrate that waist volumetric SMI might be a prognostic biomarker for early cervical cancer. In particular, initial sarcopenia patients who gained body fat during primary treatment were at a high risk of disease recurrence. It is feasible to measure the waist volume of each body component and their longitudinal changes using the artificial intelligence-based volumetric tool. Further validation studies verifying our findings are warranted.

DATA AVAILABILITY STATEMENT

The raw data supporting the conclusions of this article will be made available by the authors, without undue reservation.

ETHICS STATEMENT

The studies involving human participants were reviewed and approved by Institutional Review Board of Seoul National University Hospital (No. H-2012-061-117). Written informed consent for participation was not required for this study in accordance with the national legislation and the institutional requirements.

AUTHOR CONTRIBUTIONS

QH: investigation, data curation, formal analysis, and writing–original draft. SIK: methodology, investigation, data curation, formal analysis, and writing–original draft. SHY: resources, methodology, investigation, formal analysis, and writing–review and editing. TMK and JYC: investigation, validation, and writing–review and editing. H-CK and HJK: investigation, validation, and writing–review and editing. J-WK: conceptualization, resources, methodology, investigation, formal analysis, validation, supervision, and writing–review and editing. All authors contributed to the article and approved the submitted version.

SUPPLEMENTARY MATERIAL

The Supplementary Material for this article can be found online at: https://www.frontiersin.org/articles/10.3389/fonc.2021.741071/full#supplementary-material

REFERENCES

1. Sung H, Ferlay J, Siegel RL, Laversanne M, Soerjomataram I, Jemal A, et al. Global Cancer Statistics 2020: GLOBOCAN Estimates of Incidence and Mortality Worldwide for 36 Cancers in 185 Countries. *CA Cancer J Clin* (2021) 71(3):209–49. doi: 10.3322/caac.21660
2. Jung KW, Won YJ, Hong S, Kong HJ, Im JS, Seo HG. Prediction of Cancer Incidence and Mortality in Korea, 2021. *Cancer Res Treat* (2021) 53(2):316–22. doi: 10.4143/crt.2021.290
3. Siegel RL, Miller KD, Fuchs HE, Jemal A. Cancer Statistics, 2021. *CA Cancer J Clin* (2021) 71(1):7–33. doi: 10.3322/caac.21654
4. Lim MC, Won YJ, Ko MJ, Kim M, Shim SH, Suh DH, et al. Incidence of Cervical, Endometrial, and Ovarian Cancer in Korea During 1999-2015. *J Gynecol Oncol* (2019) 30(1):e38. doi: 10.3802/jgo.2019.30.e38
5. Hong S, Won YJ, Lee JJ, Jung KW, Kong HJ, Im JS, et al. Cancer Statistics in Korea: Incidence, Mortality, Survival, and Prevalence in 2018. *Cancer Res Treat* (2021) 53(2):301–15. doi: 10.4143/crt.2021.291
6. National Comprehensive Cancer Network. *Cervical Cancer (Version 1.2021)*. Available at: http://www.nccn.org/professionals/physician_gls/pdf/cervical.pdf (Accessed on: April 1, 2021).
7. Marth C, Landoni F, Mahner S, McCormack M, Gonzalez-Martin A, Colombo N. Cervical Cancer: ESMO Clinical Practice Guidelines for Diagnosis, Treatment and Follow-Up. *Ann Oncol* (2017) 28(suppl_4):iv72–83. doi: 10.1093/annonc/mdx220
8. Lauby-Secretan B, Scoccianti C, Loomis D, Grosse Y, Bianchini F, Straif K. Body Fatness and Cancer–Viewpoint of the IARC Working Group. *New Engl J Med* (2016) 375(8):794–8. doi: 10.1056/NEJMsr1606602
9. Bhaskaran K, Douglas I, Forbes H, dos-Santos-Silva I, Leon DA, Smeeth L. Body-Mass Index and Risk of 22 Specific Cancers: A Population-Based Cohort Study of 5·24 Million UK Adults. *Lancet* (2014) 384(9945):755–65. doi: 10.1016/S0140-6736(14)60892-8
10. Demark-Wahnefried W, Platz EA, Ligibel JA, Blair CK, Courneya KS, Meyerhardt JA, et al. The Role of Obesity in Cancer Survival and Recurrence. *Cancer Epidemiol Biomarkers Prev* (2012) 21(8):1244–59. doi: 10.1158/1055-9965.EPI-12-0485
11. Petrelli F, Cortellini A, Indini A, Tomasello G, Ghidini M, Nigro O, et al. Association of Obesity With Survival Outcomes in Patients With Cancer: A Systematic Review and Meta-Analysis. *JAMA Netw Open* (2021) 4(3):e213520. doi: 10.1001/jamanetworkopen.2021.3520
12. Caan BJ, Cespedes Feliciano EM, Prado CM, Alexeeff S, Kroenke CH, Bradshaw P, et al. Association of Muscle and Adiposity Measured by Computed Tomography With Survival in Patients With Nonmetastatic Breast Cancer. *JAMA Oncol* (2018) 4(6):798–804. doi: 10.1001/jamaoncol.2018.0137
13. Song EJ, Lee CW, Jung SY, Kim BN, Lee KS, Lee S, et al. Prognostic Impact of Skeletal Muscle Volume Derived From Cross-Sectional Computed Tomography Images in Breast Cancer. *Breast Cancer Res Treat* (2018) 172 (2):425–36. doi: 10.1007/s10549-018-4915-7

14. Kim EY, Kim YS, Park I, Ahn HK, Cho EK, Jeong YM. Prognostic Significance of CT-Determined Sarcopenia in Patients With Small-Cell Lung Cancer. *J Thorac Oncol* (2015) 10(12):1795–9. doi: 10.1097/JTO.0000000000000690
15. Lee JS, Kim YS, Kim EY, Jin W. Prognostic Significance of CT-Determined Sarcopenia in Patients With Advanced Gastric Cancer. *PloS One* (2018) 13(8): e0202700. doi: 10.1371/journal.pone.0202700
16. Yoshikawa N, Shirakawa A, Yoshida K, Tamauchi S, Suzuki S, Kikkawa F, et al. Sarcopenia as a Predictor of Survival Among Patients With Organ Metastatic Cervical Cancer. *Nutr Clin Pract* (2020) 35(6):1041–6. doi: 10.1002/ncp.10482
17. Lee J, Chang CL, Lin JB, Wu MH, Sun FJ, Jan YT, et al. Skeletal Muscle Loss Is an Imaging Biomarker of Outcome After Definitive Chemoradiotherapy for Locally Advanced Cervical Cancer. *Clin Cancer Res* (2018) 24(20):5028–36. doi: 10.1158/1078-0432.CCR-18-0788
18. Matsuoka H, Nakamura K, Matsubara Y, Ida N, Nishida T, Ogawa C, et al. Sarcopenia Is Not a Prognostic Factor of Outcome in Patients With Cervical Cancer Undergoing Concurrent Chemoradiotherapy or Radiotherapy. *Anticancer Res* (2019) 39(2):933–9. doi: 10.21873/anticanres.13196
19. Mourtzakis M, Prado CM, Lieffers JR, Reiman T, McCargar LJ, Baracos VE. A Practical and Precise Approach to Quantification of Body Composition in Cancer Patients Using Computed Tomography Images Acquired During Routine Care. *Appl Physiol Nutr Metab* (2008) 33(5):997–1006. doi: 10.1139/H08-075
20. Lee K, Shin Y, Huh J, Sung YS, Lee IS, Yoon KH, et al. Recent Issues on Body Composition Imaging for Sarcopenia Evaluation. *Korean J Radiol* (2019) 20 (2):205–17. doi: 10.3348/kjr.2018.0479
21. Lee YS, Hong N, Witanto JN, Choi YR, Park J, Decazes P, et al. Deep Neural Network for Automatic Volumetric Segmentation of Whole-Body CT Images for Body Composition Assessment. *Clin Nutr* (2021) 40(8):5038–46. doi: 10.1016/j.clnu.2021.06.025
22. Nowak S, Faron A, Luetkens JA, Geißler HL, Praktiknjo M, Block W, et al. Fully Automated Segmentation of Connective Tissue Compartments for CT-Based Body Composition Analysis: A Deep Learning Approach. *Invest Radiol* (2020) 55(6):357–66. doi: 10.1097/RLI.0000000000000647
23. Kim SI, Yoon S, Kim TM, Cho JY, Chung HH, Song YS. Prognostic Implications of Body Composition Change During Primary Treatment in Patients With Ovarian Cancer: A Retrospective Study Using an Artificial Intelligence-Based Volumetric Technique. *Gynecol Oncol* (2021) 162(1):72–9. doi: 10.1016/j.ygyno.2021.05.004
24. Querleu D, Cibula D, Abu-Rustum NR. Update on the Querleu-Morrow Classification of Radical Hysterectomy. *Ann Surg Oncol* (20172017) 24 (11):3406–12. doi: 10.1245/s10434-017-6031-z
25. WHO Expert Consultation. Appropriate Body-Mass Index for Asian Populations and Its Implications for Policy and Intervention Strategies. *Lancet* (2004) 363 (9403):157–63. doi: 10.1016/S0140-6736(03)15268-3
26. Sedlis A, Bundy BN, Rotman MZ, Lentz SS, Muderspach LI, Zaino RJ. A Randomized Trial of Pelvic Radiation Therapy *Versus* No Further Therapy in Selected Patients With Stage IB Carcinoma of the Cervix After Radical Hysterectomy and Pelvic Lymphadenectomy: A Gynecologic Oncology Group Study. *Gynecol Oncol* (1999) 73(2):177–83. doi: 10.1006/gyno.1999.5387
27. National Cancer Institute. *Common Terminology Criteria for Adverse Events (CTCAE) Version 5.0*. Available at: https://ctep.cancer.gov/protocoldevelopment/electronic_applications/ctc.htm#ctc_50 (Accessed on: August 1, 2021).
28. Eisenhauer EA, Therasse P, Bogaerts J, Schwartz LH, Sargent D, Ford R, et al. New Response Evaluation Criteria in Solid Tumours: Revised RECIST Guideline (Version 1.1). *Eur J Cancer* (2009) 45(2):228–47. doi: 10.1016/j.ejca.2008.10.026
29. Ross R, Neeland IJ, Yamashita S, Shai I, Seidell J, Magni P, et al. Waist Circumference as a Vital Sign in Clinical Practice: A Consensus Statement From the IAS and ICCR Working Group on Visceral Obesity. *Nat Rev Endocrinol* (2020) 16(3):177–89. doi: 10.1038/s41574-019-0310-7
30. Fearon K, Strasser F, Anker SD, Bosaeus I, Bruera E, Fainsinger RL, et al. Definition and Classification of Cancer Cachexia: An International Consensus. *Lancet Oncol* (2011) 12(5):489–95. doi: 10.1016/S1470-2045(10)70218-7
31. Kim SI, Kim TM, Lee M, Kim HS, Chung HH, Cho JY, et al. Impact of CT-Determined Sarcopenia and Body Composition on Survival Outcome in Patients With Advanced-Stage High-Grade Serous Ovarian Carcinoma. *Cancers (Basel)* (2020) 12(3):559. doi: 10.3390/cancers12030559
32. Xie H, Gong Y, Kuang J, Yan L, Ruan G, Tang S, et al. Computed Tomography-Determined Sarcopenia Is a Useful Imaging Biomarker for Predicting Postoperative Outcomes in Elderly Colorectal Cancer Patients. *Cancer Res Treat* (2020) 52(3):957–72. doi: 10.4143/crt.2019.695
33. Weston AD, Korfiatis P, Kline TL, Philbrick KA, Kostandy P, Sakinis T, et al. Automated Abdominal Segmentation of CT Scans for Body Composition Analysis Using Deep Learning. *Radiology* (2019) 290(3):669–79. doi: 10.1148/radiol.2018181432
34. Cruz-Jentoft AJ, Baeyens JP, Bauer JM, Boirie Y, Cederholm T, Landi F, et al. Sarcopenia: European Consensus on Definition and Diagnosis: Report of the European Working Group on Sarcopenia in Older People. *Age Ageing* (2010) 39(4):412–23. doi: 10.1093/ageing/afq034
35. Wang S, Xie H, Gong Y, Kuang J, Yan L, Ruan G, et al. The Value of L3 Skeletal Muscle Index in Evaluating Preoperative Nutritional Risk and Long-Term Prognosis in Colorectal Cancer Patients. *Sci Rep* (2020) 10(1):8153. doi: 10.1038/s41598-020-65091-0
36. Kim SH, Jeong JB, Kang J, Ahn DW, Kim JW, Kim BG, et al. Association Between Sarcopenia Level and Metabolic Syndrome. *PloS One* (2021) 16(3): e0248856. doi: 10.1371/journal.pone.0248856
37. Aversa Z, Costelli P, Muscaritoli M. Cancer-Induced Muscle Wasting: Latest Findings in Prevention and Treatment. *Ther Adv Med Oncol* (2017) 9(5):369–82. doi: 10.1177/1758834017698643
38. Rausch V, Sala V, Penna F, Porporato PE, Ghigo A. Understanding the Common Mechanisms of Heart and Skeletal Muscle Wasting in Cancer Cachexia. *Oncogenesis* (2021) 10(1):1. doi: 10.1038/s41389-020-00288-6
39. Chen LK, Woo J, Assantachai P, Auyeung TW, Chou MY, Iijima K, et al. Asian Working Group for Sarcopenia: 2019 Consensus Update on Sarcopenia Diagnosis and Treatment. *J Am Med Dir Assoc* (2020) 21(3):300–7.e2. doi: 10.1016/j.jamda.2019.12.012
40. Dent E, Morley JE, Cruz-Jentoft AJ, Arai H, Kritchevsky SB, Guralnik J, et al. International Clinical Practice Guidelines for Sarcopenia (ICFSR): Screening, Diagnosis and Management. *J Nutr Health Aging* (2018) 22(10):1148–61. doi: 10.1007/s12603-018-1139-9
41. Burton LA, Sumukadas D. Optimal Management of Sarcopenia. *Clin Interv Aging* (2010) 5:217–28. doi: 10.2147/cia.s11473
42. Beaudart C, McCloskey E, Bruyère O, Cesari M, Rolland Y, Rizzoli R, et al. Sarcopenia in Daily Practice: Assessment and Management. *BMC Geriatr* (2016) 16(1):170. doi: 10.1186/s12877-016-0349-4
43. Seol A, Kim SI, Song YS. Sarcopenia: Clinical Implications in Ovarian Cancer, Diagnosis, Etiology, and Management. *Sports Med Health Sci* (2020) 2(4):202–10. doi: 10.1016/j.smhs.2020.10.001
44. Gadducci A, Cosio S, Fanucchi A, Genazzani AR. Malnutrition and Cachexia in Ovarian Cancer Patients: Pathophysiology and Management. *Anticancer Res* (2001) 21(4b):2941–7.
45. Kroenke CH, Chen WY, Rosner B, Holmes MD. Weight, Weight Gain, and Survival After Breast Cancer Diagnosis. *J Clin Oncol* (2005) 23(7):1370–8. doi: 10.1200/JCO.2005.01.079
46. Donohoe CL, Doyle SL, Reynolds JV. Visceral Adiposity, Insulin Resistance and Cancer Risk. *Diabetol Metab Syndr* (2011) 3:12. doi: 10.1186/1758-5996-3-12
47. Malietzis G, Currie AC, Athanasiou T, Johns N, Anyamene N, Glynne-Jones R, et al. Influence of Body Composition Profile on Outcomes Following Colorectal Cancer Surgery. *Br J Surg* (2016) 103(5):572–80. doi: 10.1002/bjs.10075
48. Baracos VE, Arribas L. Sarcopenic Obesity: Hidden Muscle Wasting and its Impact for Survival and Complications of Cancer Therapy. *Ann Oncol* (2018) 29(suppl_2):ii1–9. doi: 10.1093/annonc/mdx810
49. Kim B, Kim HS, Kim S, Haegeman G, Tsang BK, Dhanasekaran DN, et al. Adipose Stromal Cells From Visceral and Subcutaneous Fat Facilitate Migration of Ovarian Cancer Cells *via* IL-6/JAK2/STAT3 Pathway. *Cancer Res Treat* (2017) 49(2):338–49. doi: 10.4143/crt.2016.175
50. Stenholm S, Harris TB, Rantanen T, Visser M, Kritchevsky SB, Ferrucci L. Sarcopenic Obesity: Definition, Cause and Consequences. *Curr Opin Clin Nutr Metab Care* (2008) 11(6):693–700. doi: 10.1097/MCO.0b013e328312c37d

51. Sakuma K, Yamaguchi A. Sarcopenic Obesity and Endocrinal Adaptation With Age. *Int J Endocrinol* (2013) 2013:204164. doi: 10.1155/2013/204164

Conflict of Interest: SHY works in the MEDICALIP as a chief medical officer.

The remaining authors declare that the research was conducted in the absence of any commercial or financial relationships that could be construed as a potential conflict of interest.

Publisher's Note: All claims expressed in this article are solely those of the authors and do not necessarily represent those of their affiliated organizations, or those of the publisher, the editors and the reviewers. Any product that may be evaluated in this article, or claim that may be made by its manufacturer, is not guaranteed or endorsed by the publisher.

frontiers in Oncology

ORIGINAL RESEARCH
published: 15 November 2021
doi: 10.3389/fonc.2021.737938

Near-Infrared Imaging With Indocyanine Green for the Treatment of Endometriosis: Results From the Gre-Endo Trial

Luigi Carlo Turco[1], Giuseppe Vizzielli[1], Virginia Vargiu[2], Salvatore Gueli Alletti[1], Maria De Ninno[3], Gabriella Ferrandina[1,4], Luigi Pedone Anchora[1], Giovanni Scambia[1,4] and Francesco Cosentino[2,5]*

[1] Department of Women's and Children's Health, Fondazione Policlinico Universitario A. Gemelli IRCCS, Rome, Italy, [2] Department of Gynecologic Oncology, Gemelli Molise, Campobasso, Italy, [3] Department of Pathology, Gemelli Molise, Campobasso, Italy, [4] Università Cattolica del Sacro Cuore, Rome, Italy, [5] Department of Medicine and Health Sciences "Vincenzo Tiberio", Università degli Studi del Molise, Campobasso, Italy

OPEN ACCESS

Edited by:
Alessandro Lucidi,
Asl Lanciano Vasto Chieti, Italy

Reviewed by:
Silvia De Rocco,
Università G. d'Annunzio di Chieti e Pescara, Italy
Stefano Cosma,
University Hospital of the City of Health and Science of Turin, Italy
Stefano Restaino,
Ospedale Santa Maria della Misericordia di Udine, Italy

***Correspondence:**
Virginia Vargiu
virginia.vargiu@gmail.com

Specialty section:
This article was submitted to Gynecological Oncology, a section of the journal Frontiers in Oncology

Received: 07 July 2021
Accepted: 21 October 2021
Published: 15 November 2021

Citation:
Turco LC, Vizzielli G, Vargiu V, Gueli Alletti S, De Ninno M, Ferrandina G, Pedone Anchora L, Scambia G and Cosentino F (2021) Near-Infrared Imaging With Indocyanine Green for the Treatment of Endometriosis: Results From the Gre-Endo Trial. Front. Oncol. 11:737938. doi: 10.3389/fonc.2021.737938

Introduction: A current challenge for endometriosis surgery is to correctly identify the localizations of disease, especially when small or hidden (occult endometriosis), and to exactly define their real extension. The use of near-infrared radiation imaging (NIR) after injection of indocyanine green (ICG) represents one of the most encouraging method. The aim of this study is to assess the diagnostic value of NIR-ICG imaging in the surgical treatment of endometriosis compared with the standard of treatment.

Material and Methods: The Gre-Endo trial is a prospective, single-arm study (NCT03332004). After exploring the operatory field using the white light (WL) mode, patients were injected with ICG and then observed in NIR mode. All suspected areas were classified and chronicled according to lesions visualized only in WL, NIR-ICG, or in the combination of both. Lesion not visualized in WL was considered as suspect occult lesion (s-OcL). In addition, a random control biopsy from an apparent negative peritoneum visualized in WL and NIR-ICG imaging was taken for all patients (control cases). All lesions removed were considered "suspect endometriosis" until pathology.

Results: Fifty-one patients were enrolled between January 2016 and October 2019. A total of 240 suspected lesions have been identified with both methods (WL + NIR-ICG). Two hundred and seven (86.2%) lesions out of the overall 240 were visualized with WL imaging, and 200 were confirmed to be pathologic (true positive for WL). The remaining 33/240 (13.75%) (false negative for WL) lesions were identified only with NIR-ICG imaging and collected as s-OcL. All 33 s-OcLs removed were confirmed to be pathologic (c-OcL = 100%). NIR-ICG vision showed PPV of 98.5%, NPV of 87.1%, Se of 87%, and Sp of 98.5%, confirming that this kind of imaging is an excellent diagnostic and screening test (p = 0.001 and p = 0.835, according to McNemar's and Cohen's kappa tests, respectively).

Conclusions: The use of NIR-ICG vision alone and combined with WL showed good results in intraoperative detection rate and fluorescence-guided surgery of endometriosis. Furthermore, NIR-ICG allowed surgeons to remove occult lesions that otherwise would remain, leading to possible greater postoperative pain and a higher risk of persistence and relapse.

Keywords: near-infrared imaging, indocyanine green, deep infiltrating endometriosis, personalized medicine, gynecological surgery

INTRODUCTION

Endometriosis is considered a public health problem compromising the social, employment, financial, and reproductive quality of life of the patients (1). When pharmacologic treatment fails, surgical treatment can improve quality of life and fertility by radically removing extra-ovarian endometriosis localizations using the best minimally invasive techniques such as laparoscopy, the current gold standard of treatment (2–4).

Early technical difficulties have been overcome by surgeon experience and the refinement of techniques; a frequent current challenge involves identifying endometriosis localizations, especially when small or hidden (occult endometriosis) (5–9), to not leave out disease and determine a possible "undertreatment" and/or to predispose patients to possible recurrences.

Indeed, there is evidence that postoperative recurrence of endometriosis may be due to incomplete resection during the primary surgery (8).

Furthermore, eradicating surgery for endometriosis presents the risk of "overtreatment" as well, since the surgeon usually may remove lesions suspected of being endometriosis that are not pathologically confirmed to be endometriosis from 16% to 53% of cases (8). The excessive dissection and resection of heathy tissues surrounding the diseased, moreover, could determine postoperative surgical and functional morbidity (10–13).

Indocyanine green (ICG) is nowadays increasingly used in gynecological surgery, both in oncological and benign fields (14–16). It is frequently used in the identification of lymphatic tissue (17, 18), but if injected intravenously, it binds to plasma proteins and persists in the vascular system, helping in the definition of the vascular network (19).

Given the typical neovascularization of endometriosis, related to chronic inflammation, the visualization of abnormal areas of peritoneal vascularization could be useful to better identify and define the endometriosis lesions in their real extension and to visualize the lesions even when not obvious, as in puckered peritoneal lesions (8–11, 20). For all of this, several methods have been proposed to improve the intraoperative treatment of endometriosis through enhancing the human vision power, with encouraging results (21–23).

The use of cameras with near-infrared radiation imaging (NIR) after injection of ICG represents one of the most encouraging methods in this experimental scenario, demonstrating a good profile of safety and accuracy as an intraoperative diagnostic method (9–11, 24).

The aim of this study is to assess the diagnostic value of NIR-ICG imaging in the surgical treatment of endometriosis compared with the standard of treatment, that is laparoscopy in white light (WL), and the standard diagnostic method, that is pathologic finding.

MATERIALS AND METHODS

The Gre-Endo trial is a prospective, single-arm study (ClinicalTrials.gov Identifier: NCT03332004) carried on at the Fondazione Policlinico Universitario "A. Gemelli"—IRCCS, Rome, Italy, and Gemelli-Molise, Campobasso, Italy. The local ethics committee approved the experimentation (Prot.sf. A.287/C.E./2013).

Materials

The NIR-ICG camera system adopted for the study was the Olympus ICG Imaging System Prototype based on the VISERA Pro System (custom camera head, modified light source, and modified camera control unit; Olympus Europa Holding GmbH, Hamburg, Germany), the merchandized camera head CH-S200-XZ-EB connected to VISERA ELITE II system with NIR filter (Olympus Europa Holding GmbH, Hamburg, Germany), and the IMAGE1 S^{TM} Rubina imaging technology from KARL STORZ.

The ICG adopted for intravenous injection during the procedures was Pulsion (PULSION Medical Systems SE, Feldkirchen, Germany) and VerDye (Diagnostic Green GmbH, Aschheim-Dornach, Germany).

Patients

Inclusion criteria were suspected endometriosis with surgical indication for treatment needing laparoscopic and pathologic confirmation. Patients were triaged to surgery according with the common indications for endometriosis (25). Exclusion criteria were age <18 and >47 years at the time of surgery. Other exclusion criteria were a history of allergic reactions attributed to compounds of similar chemical or biologic composition to ICG; pregnancy or breastfeeding period; active participation of the patient to other drug, biologic, and/or device study; the presence of medical conditions contraindicating general anesthesia or standard surgical approaches; and any contraindicating medical condition, according to the discretion of the investigator, that made the subject a poor candidate for the investigational procedure.

Patients with ovarian endometriosis and/or endometriosis of the fallopian tubes were excluded from the study because of the intraoperative lack of fluorescence of the ovaries and the diffuse fluorescence of the tubes because of physiological vascular web density at preliminary pilot surgeries.

After obtaining informed consent, patients were included in the study and they could withdraw from the study at any time without impacting treatment. Patient demographic features and preoperative pain were scored using the visual analog scale (VAS) (26), and the intraoperative classification of endometriosis severity scheduled according to the revised American Fertility Society (rAFS) (27). All data were prospectively collected.

Method and Surgical Procedure

All the procedures were performed by a team of three well-trained surgeons with >10 years of experience in minimally invasive techniques for endometriosis.

During surgery, the abdomen and pelvis were visually inspected using direct laparoscope visualization under WL conditions. The surgeon prepared the operating field by adhesion lysis exposing the *torus uteri* and the *ovarian fossa* and freeing the bowel from eventual retrocervical nodule attachment. All suspected areas were classified as either peritoneal superficial endometriosis (PE) or deep infiltrating endometriosis (DIE). All suspected PE was classified as white, black, and red lesions and documented with their anatomic location in the surgical record under WL condition. Similarly, all suspected DIE lesions were also recorded with their anatomic location in the surgical record (retrocervical, vaginal, rectosigmoid, bladder lesions, etc.) (8) under WL condition. The patient was then administered with 0.25 mg/kg of ICG intravenously. After an interval of time from a minimum of 5 min, NIR-ICG imaging was activated and the whole surgical field inspected with this filter (**Figure 1**). It was necessary to wait to permit blood flow washout of ICG and its accumulation in the third space of neovascularized areas. All suspected lesions for endometriosis (PE and DIE) were tabulated and chronicled according to lesions visualized only in WL, only in NIR-ICG, or in the combination of both. In addition, a random control biopsy from an apparent negative peritoneum visualized in WL and NIR-ICG imaging was taken for all patients (control cases). Every specimen resected during surgery was considered as "suspect lesion" for endometriosis when visualized with WL and/or with NIR-ICG until pathology confirmation. If a suspect lesion had been visualized with NIR-ICG and not in WL or, conversely, only with WL, it was named "suspect occult lesion" (s-OcL), and only after conformation by pathology, it has been considered "confirmed occult lesion" (c-OcL).

All specimens resected were analyzed by a dedicated pathologist that, even when facing with macroscopically negative tissue samples, embedded in paraffin the specimens *in toto* and analyzed them at multiple levels. A surgical specimen was considered as "pathologic" when containing endometriosis *foci* (stroma and/or gland and/or hemosiderin) and/or acute or chronic sclerosing inflammatory infiltrate (28, 29).

Perioperative complications have been reported with the extended Clavien–Dindo classification (30).

Statistical Analysis

The primary objective of the study was to assess the feasibility of NIR-ICG to identify endometriosis lesions and distinguish the surrounding tissue in comparison with WL. The secondary objective was to assess the power of identifying OcL and the power of the test combining the two methods of visualization (WL plus NIR-ICG).

Normally, WL is the intraoperative gold standard imaging technique for detecting endometriosis, while pathology the definitive confirmation test.

We tested the null hypothesis that the possibility of correctly identifying endometriosis could improve from 85% with WL visualization to 100% when assessed together with NIR-ICG. The sample size was calculated according to the Simon two-stage design (31) using an alpha error of 0.01 and a beta error of 0.90. Considering a patient dropout of approximately 10%, the study was planned to enroll at least 47 women.

Because the control biopsy was achieved from a negative peritoneum using WL and NIR-ICG imaging for all women, the true-negative lesions were defined as the negative lesions for endometriosis that were correctly identified as negative by WL or NIR-ICG imaging; the false-negative lesions were defined as not correctly identified by WL or NIR-ICG imaging. The true-positive lesions were the positive lesions for endometriosis that were correctly identified by WL or NIR-ICG imaging; the false-positive lesions were the lesions identified as positive for endometriosis by WL or NIR-ICG imaging that were not pathologically identified as endometriosis. Sensitivity, specificity, positive predictive value (PPV), negative predictive value (NPV), and overall accuracy were calculated for each visualization. Sensitivity (Se) was defined as the number of positive lesions for endometriosis that were correctly identified (true positives) divided by the total number of positive lesions for endometriosis (true positives + false negatives). Specificity (Sp) was defined as the number of negative lesions for endometriosis that were correctly identified (true negatives) divided by the total number of negative lesions (true negatives + false positives). PPV was calculated as the number of true positives divided by the total number of positive results (true positives + false positives), and NPV was defined as the number of true negatives divided by the total number of negative results (true negatives + false negatives). Accuracy was calculated as the number of true positives plus true negatives (total correct number) divided by the total number of patients studied. Sensitivity, specificity, and accuracy were compared using McNemar's and Cohen's kappa tests. The diagnostic performances of WL and NIR-ICG imaging were calculated per patient as well as per lesion. Statistical calculations were performed using the Statistical Package for Social Sciences (Version 17.0; SPSS Inc., Chicago, IL, USA).

The receiver operating characteristic (ROC) curve was designed to assess the diagnostic performance of WL and NIR-ICG for identifying pathologic lesions compared to pathology. The statistical significance was set at p-values <0.05.

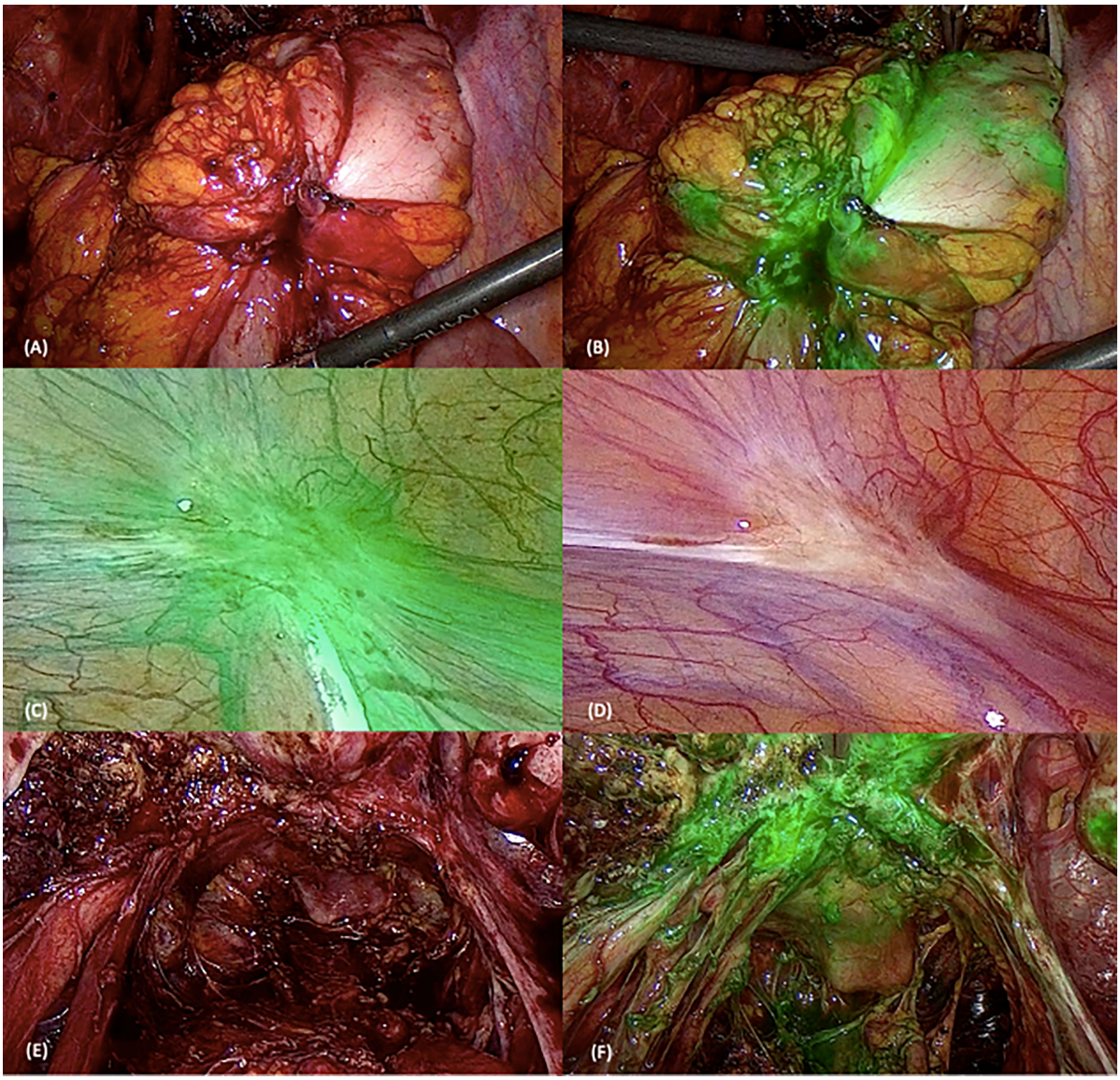

FIGURE 1 | Surgical images using white light (WL) and near-infrared indocyanine green (NIR-ICG) mode. The first two pictures represent a rectosigmoid nodule using WL **(A)** and NIR-ICG mode **(B)**. **(C, D)** Superficial peritoneal lesion in WL **(D)** and NIR-ICG **(C)**. The last two pictures show retrocervical lesions with uterosacral ligament involvement using the two vision systems [WL in **(E)** and NIR-ICG in **(F)**].

RESULTS

General Results

A total of 135 patients with symptomatic endometriosis were screened and 51 were enrolled between January 2016 and October 2019 (**Figure 2**). All patient demographics are listed in **Table 1**. Patients were in premenopausal age between 26 and 47 years old (median age = 35 years) with a median body mass index of 20.5. Nineteen (35%) women had already undergone previous surgery for endometriosis. All patients suffered from severe symptoms referred at the VAS scale. Forty-five patients had an intraoperative assignment to III/IV stage by the rAFS.

All patients underwent laparoscopic surgery, and no laparotomy conversions were recorded. The most performed surgery was uterosacral ligament (USL) nodule removal in 80% of the patients, while retrocervical nodule resection was performed in 78% of the cases. Overall, segmental colorectal resection represented 28% of the cases.

Table 2 reports the surgical procedures performed and the perioperative outcomes observed. There was no increase in operating times because of the use of NIR-ICG imaging because injection of the ICG dye occurred during the preparation of the operating field. ICG median dose injected was 15 mg (range 10.25–24).

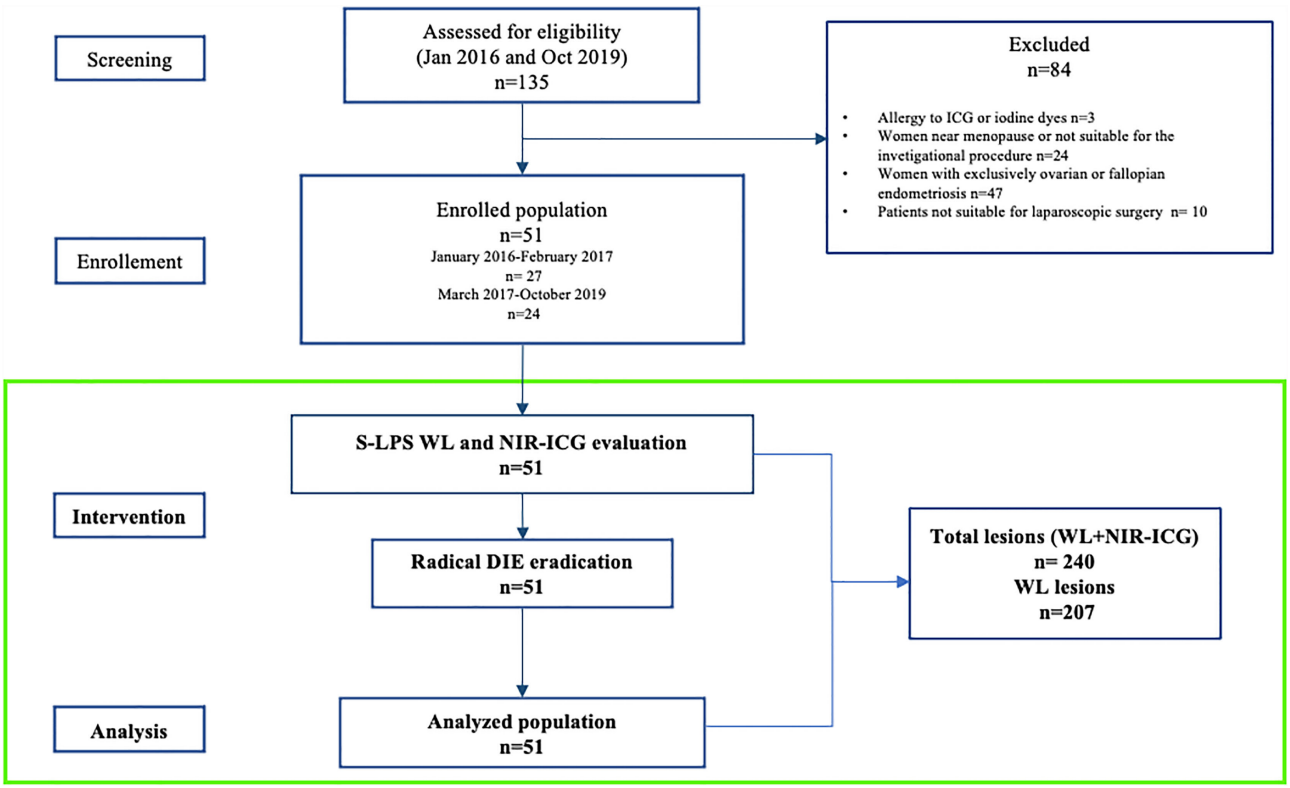

FIGURE 2 | Study flow diagram.

No hemorrhages, allergic reactions, and/or any type of intraoperative complications were reported. Postoperative complications affected nine (17.6%) patients and were not directly associated to the ICG infusion or to the experimental plan. In particular, only *early* complications were registered: among grade I, one case of urinary retention and one case of fever; among grade II, one case of postoperative bleeding of colorectal anastomosis in postoperative day 2 was noted and controlled by hospitalization and the administration of 500 mg tranexamic acid orally every 8 h for 3 days, three cases of fever needing for antibiotic infusion, and one case of anemia needing red cell-concentrated unit transfusion; among grade III, one case of colorectal anastomosis dehiscence then subjected to resuturing and loop ileostomy creation and one case of vaginal fornix dehiscence after a posterior wall nodule resection needing to be resutured.

Study Protocol Results

Fifty patients administered with ICG presented tissue fluorescence, except one woman that was completely negative even after a second repeated dose.

A total of 240 suspected lesions have been identified with both methods (WL + NIR-ICG). Two hundred and seven (86.2%) lesions out of the overall 240 ones were visualized with WL imaging, and 200 were confirmed to be pathologic (true positive for WL). The remaining 33 out of 240 (13.75%) (false negative for WL) lesions were identified only with NIR-ICG imaging and collected as s-OcL (**Table 3** and **Figure 3**). The s-OcLs were so distributed: 3 (9%) white lesions for PE, while 7 (21%) as retrocervical, 3 (9%) as USL, 11 (33%) as periureteral/ovarian fossa, 4 (12%) as rectal, and 5 (15%) as prevesical/vesical localizations for DIE (**Table 3**). All 33 s-OcLs removed were confirmed to be pathologic (c-OcL = 100%): in particular, 25 (76%) lesions out of 33 harbored occult endometrioses, while 8 (24%) harbored severe sclerosing inflammatory infiltrate. Moreover, 30 (15%) lesions out of the 200 confirmed lesions identified by WL have not visualized by NIR-ICG.

Table 4 reports the specific results obtained using NIR-ICG. With NIR-ICG imaging, 206 suspected lesions were identified; 173 of them were already visualized in WL. Two hundred and three suspected lesions out of 206 (98.5%) had pathologic confirmation (true positive for NIR-ICG), while 3 lesions were not confirmed as pathologic (false positive for NIR-ICG). As reported above, 33 lesions further than conventional WL were identified and confirmed at pathology (c-OcL) thanks to NIR-ICG (**Figure 3**).

Regarding WL vision, the overall PPV and NPV were 96.6% and 86.3%, while Se and Sp were 85.8% and 96.7% (**Table 5**). NIR-ICG vision showed PPV of 98.5%, NPV of 87.1%, Se of 87%, and Sp of 98.5% (**Table 5**), confirming that this kind of imaging

TABLE 1 | Characteristics of the patients.

Variables	Value	Percentage
All cases	51	100%
Age, years (range)	35 (26–47)	–
Body mass index (range)	20.5 (14–33)	–
ASA class		
1	35	69%
2	16	31%
3	0	–
Previous delivery	18	35%
Prior surgery for endometriosis	19	37%
Preoperative symptoms (VAS)[a]		
Dysmenorrhea	9 (3–10)	86%
Dyschezia	7 (2–10)	59%
Dysuria	7 (4–10)	18%
Dyspaurenia	8 (1–10)	67%
Chronic pelvic pain	6 (2–10)	69%
Stage[b]		
Stage I (minimal)	0	–
Stage II (mild)	6	12%
Stage III (moderate)	19	37%
Stage IV (severe)	26	51%

Data are shown as median/range for the referred positive VAS. Percentage refers to the number of patients according to symptoms.
[a]*Pain is valued with the visual analog scale (VAS) for symptomatic patients.*
[b]*According to the rAFS classification.*

is an excellent diagnostic and screening test (p = 0.001 and p = 0.835, according to McNemar's and Cohen's kappa tests, respectively).

As far as PE is concerned, NIR-ICG demonstrated higher values of PPV and specificity than WL, while NPV and sensitivity were lower. The accuracy of the NIR-ICG was lower than WL regarding white lesion (40% *vs*. 46.7%); conversely, it was superior in recognizing black lesion (60% *vs*. 50%).

As far as DIE is concerned, the two visualization approaches demonstrated superimposable values of Sp, while Se and accuracy resulted higher for NIR-ICG for the visualization of periureteral/ovarian fossas and colorectal nodules (McNemar's test: p = 0.002 and 0.768 and Cohen's kappa test: p = 0.01 and 0.876). Conversely, WL demonstrated superiority than NIR-ICG in the recognition of prevesical/vesical lesions (McNemar's test: p = 0.001, Cohen's kappa test: p = 0.705).

The overall accuracy of both methods was 46% with McNemar's (p = 0.001) and Cohen's kappa tests (p = 0.83), revealing that both methods, regardless of the operator, should always be integrated to ensure complete eradication of endometriotic lesions (**Table 5**).

Figure 4 details the ROC curves of the two approaches. The areas under the curves (AUCs) were >0.8, and the diagnostic powers of the two methods were not statistically different (p = 0.31).

DISCUSSION

Results in the Context of Published Literature

The role of surgery in endometriosis is to remove the affected tissues to obtain pain relief, to improve fertility, and to abate not only the persistence of disease but also the risk of recurrence that occurs from 20% up to 50% of women at 2 and 5 years after treatment (9, 32, 33).

On the other hand, endometriosis is not cancer, so the excessive search for surgical radicality can imply an increase in perioperative morbidity and can cause serious functional damage, especially if the resection of tissues affected by

TABLE 2 | Surgical procedures and perioperative data.

Surgical procedure	Value	Percentage
Ovarian cyst removal	26	51%
Peritoneal removal	36	70%
Retrocervical nodule removal	40	78%
Vaginal nodule removal	14	27%
Uterosacral ligament nodule removal	41	80%
Rectal nodule shaving	12	23%
Segmental resection and anastomosis of sigma-rectum	10	20%
Segmental resection and anastomosis of sigma-rectum plus ileostomy	4	8%
Other procedures (appendectomy, salpingectomy, ureteral stent placement)	14	27%
Operative time (min)[a]	142 (65–375)	–
Dose of ICG injected[a]	15 (10.25–24)	–
Intraoperative complications	0	–
Estimated blood loss (ml)[a]	100 (0–350)	–
Postoperative complications[b]		
Early	9	17.6%
I	2	–
II	5	–
III	2	–
IV	0	–
Late	0	
Hospital stay (no. of days)[a]	2 (1–13)	–

[a]*Data are shown as median/range.*
[b]*According to Clavien–Dindo classification.*

TABLE 3 | Intraoperative and pathologic data collection resulting from WL vision and the combination of the two techniques (WL plus NIR-ICG).

Variables	WL visualization	Overall visualization (WL plus NIR-ICG)	Pathology for WL	Overall pathology (WL plus NIR-ICG)	True positive for WL	False positive for WL	True negative for WL[a]	False negative for WL (s-OcL)	c-OcL
Peritoneal endometriosis									
White lesion	21	24	17	20	17	4	21	3	3
Black lesion	16	16	15	15	15	1	16	0	0
Deep infiltrating endometriosis									
Retrocervical nodule	35	42	34	41	34	1	35	7	7
USL nodule	62	65	61	64	61	1	62	3	3
Periureteral/ ovarian fossa nodule	20	31	20	31	20	0	20	11	11
Vaginal nodule	11	11	11	11	11	0	11	0	0
Sigma-rectum nodule	26	30	26	30	26	0	26	4	4
Prevesical/vesical nodule	16	21	16	21	16	0	16	5	5
Overall endometriosis									
Total (PE and DIE)	207	240	200	233	200	7	207	33	33

WL, white light visualization mode/expert surgeon eye; c-OcL, confirmed occult endometriosis lesion at WL (=FN); PE, superficial peritoneal endometriosis; DIE, deep infiltrating endometriosis.

[a]*True negative for WL = 51 control biopsies performed in WL.*

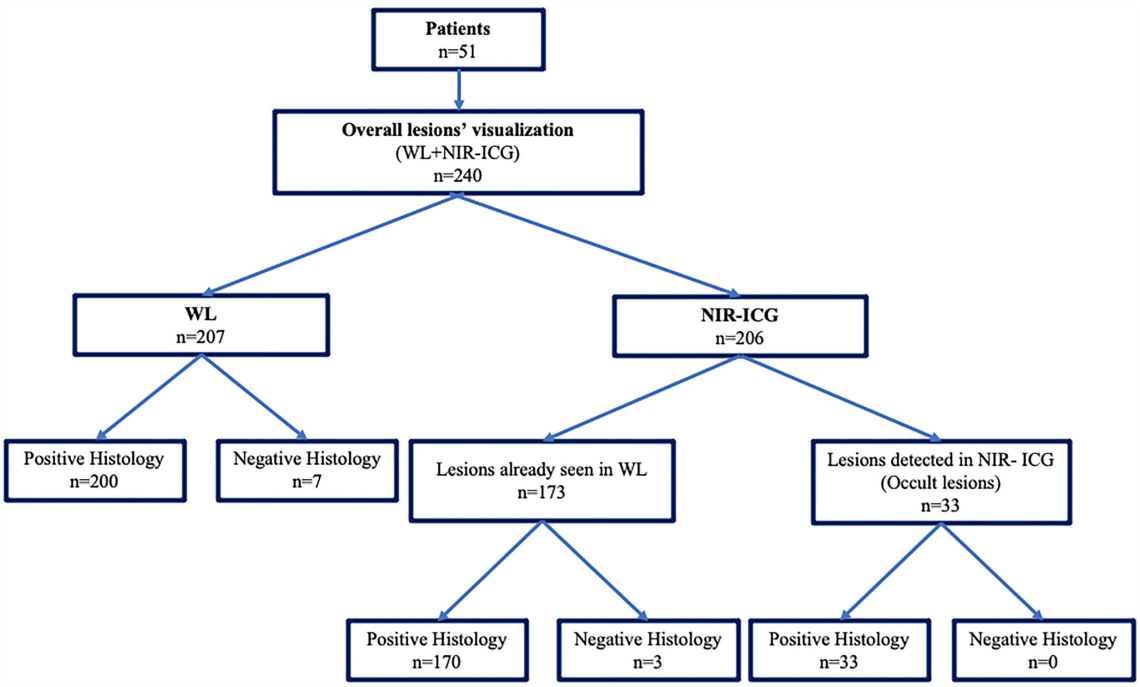

FIGURE 3 | Graphical representation of the collection of intraoperative and pathological data derived from WL vision and the combination of the two techniques (WL plus NIR-ICG).

endometriosis is associated with the removal of healthy tissues surrounding the diseased or mimicking them (10, 34–43).

Furthermore, the sensory perception of the surgeon, albeit an expert one, in identifying intraoperatively suspect lesions for endometriosis based on location, color, size, and depth has obtained well-known limits. Indeed, Stegmann et al. found that the PPV of using only the impression of an experienced surgeon to identify histologically positive lesions was 64.0%, and the NPV was 88%, while the Se and Sp of using this method were 98% and 21%, respectively (34).

TABLE 4 | Intraoperative and pathologic data collection resulting from NIR-ICG.

Variables	Overall NIR-ICG visualization	NIR-ICG visualization already seen in WL	Pathology for NIR-ICG	True positive for NIR-ICG	False positive for NIR-ICG	True negative for NIR-ICG[a]	False negative for NIR-ICG	c-OcL
Peritoneal endometriosis								
White lesion	14	11	13	13	1	14	7	7
Black lesion	9	9	9	9	0	9	6	6
Deep infiltrating endometriosis								
Retrocervical nodule	41	34	40	40	1	40	1	1
USL nodule	61	58	57	57	1	58	4	4
Periureteral/ovarian fossa nodule	29	18	29	29	0	29	2	2
Vaginal nodule	10	10	10	10	0	10	1	1
Sigma-rectum nodule	27	23	27	27	0	27	3	3
Prevesical/vesical nodule	15	10	15	15	0	15	6	6
Overall endometriosis								
Total (PE and DIE)	206	173	203	203	3	206	30	33

NIR-ICG, near-infrared visualization mode with indocyanine green; c-OcL, confirmed occult lesion at NIR-IGC (=FN at WL); PE, superficial peritoneal endometriosis; DIE, deep infiltrating endometriosis.

[a]*Number of control biopsies performed in NIR-ICG + TN of PE and DIE.*

TABLE 5 | Comparison between the NIR-ICG and WL for each surgical site in the whole population.

Variable	Vision	PPV (%)	NPV (%)	Sensitivity (%)	Specificity (%)	Accuracy (%)	McNemar's test	Cohen's kappa
Peritoneal endometriosis								
White lesion	WL	81.0	87.5	85.0	84.0	46.7	0.301	0.667
	NIR-ICG	92.9	66.7	65.0	93.3	40.0		
Black lesion	WL	93.8	100	100	94.1	50.0	0.125	0.751
	NIR-ICG	100	60.0	60.0	100	60.0		
Deep infiltrating endometriosis								
Retrocervical nodule	WL	97.1	83.3	82.9	97.2	45.4	0.109	0.874
	NIR-ICG	97.6	97.6	97.6	97.6	50.0		
USL nodule	WL	98.4	95.4	95.3	98.4	48.8	0.179	0.927
	NIR-ICG	98.3	93.5	93.4	98.3	48.3		
Periureteral/ovarian fossa nodule	WL	100	64.5	64.5	100	39.2	**0.002**	0.768
	NIR-ICG	100	93.5	93.5	100	48.3		
Vaginal nodule	WL	100	100	100	100	50.0	1.0	0.960
	NIR-ICG	100	90.9	90.9	100	47.6		
Sigma-rectum nodule	WL	100	86.7	86.7	100	46.4	**0.01**	0.876
	NIR-ICG	100	90.0	90.0	100	47.3		
Prevesical/vesical nodule	WL	100	76.2	76.2	100	43.2	**0.001**	0.705
	NIR-ICG	100	71.4	71.4	100	41.6		
Overall endometriosis								
Total (PE and DIE)	WL	96.6	86.3	85.8	96.7	46.3	**0.001**	0.835
	NIR-ICG	98.5	87.1	87.0	98.5	46.5		

NIR-ICG, near-infrared visualization vision with indocyanine green; WL, white light vision; PPV, positive predictive value; NPV, negative predictive value; PE, superficial peritoneal endometriosis; DIE, deep infiltrating endometriosis.

The bold style means that the values reported are statistic significant.

Furthermore, the possibility of not recognizing outbreaks of endometriosis that is not visible because it is microscopic or hidden (occult endometriosis) in 6%–13% of the cases may further worsen the effectiveness of surgical clearance (6, 9, 44).

For these reasons, different approaches to increase the potential for intraoperative recognition of endometriosis (enhanced vision) have been investigated using different dyes or technologies such as 3D robotic vision, with different efficacy and safety profiles (9–11, 21–24, 45–47). The results of the Gre-Endo trial seem to answer to the need of an "enhanced vision" and the utility of an intraoperative screening test.

Moreover, in association with the intraoperative diagnostic role of NIR-ICG, a challenging additional advantage seems to be the capability of distinguishing the diseased tissue from the surrounding healthy ones and to evaluate the residual vascularization of noble organs subjected to dissection and/or eradicating surgery such as the rectum and ureter (10, 11, 48, 49).

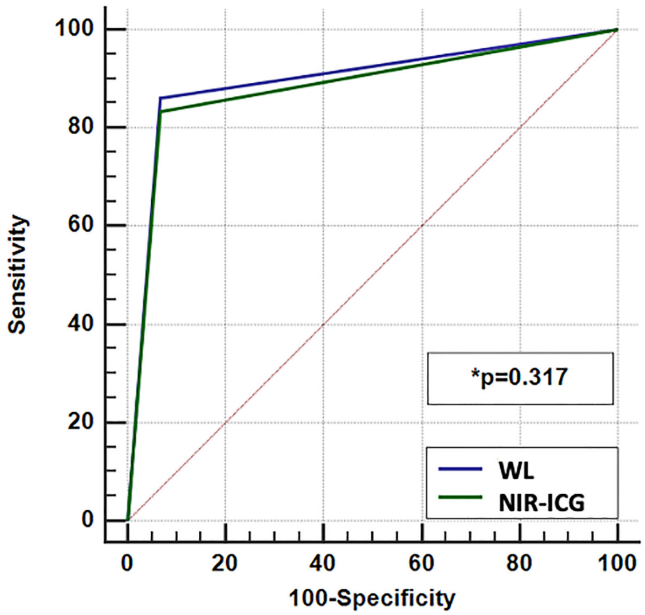

FIGURE 4 | ROC curves of the two approaches (white light and near-infrared indocyanine green).

In this study, we confirmed what was already found in recent literature about the identification of lesion and the definition of the extent and limitation of lesions from healthy tissues (9–11, 21–25, 45, 48, 49). In addition, we defined the diagnostic power of the method, which was not systematically investigated before.

In this cohort, NIR-ICG showed higher values of Se and Sp compared with the standard WL (87% *vs.* 85.8% and 98.5% *vs.* 96.7%, respectively). Moreover, the overall values registered at McNemar's (p = 0.001) and Cohen's kappa (p = 0.83) tests showed that NIR-ICG is an excellent screening and diagnostic confirmation test compared with WL. Cohen's kappa is higher than 0.4 for all types of lesion observed: it means that the evaluation of the two tests is good and independent from the observer.

In McNemar's test, on the other hand, we noticed the statistical significance in the overall results, in the USL lesions, and on the rectum and bladder localization: it means that NIR-ICG and WL should always be integrated to provide the most complete eradication of endometriosis, in particular in the sites described above.

Finally, the AUC of ROC curves for WL and NIR-ICG resulted in values >0.8 that in association with the K Cohen results >0.4 encountered, represents a positive evaluation of the diagnostic tests with excellent diagnostic powers.

Subsequently, we could sustain that the two approaches should be used sequentially during the same surgery to compare the lack and the gains of one against the other.

Moreover, in this series, the diagnostic power of NIR-ICG imaging seems also maintained in two situations of vascularization impairment, i.e., i) in patients with previous surgery and ii) after surgical dissection and tissue cruentation (data not shown). However, considering the few cases analyzed, further prospective studies are needed to confirm the excellent result for this subset of patients.

Finally, it is necessary to underline, thanks to NIR-ICG, that 33 lesions (c-OcL), which otherwise would not have been removed with standard approaches, had been resected, with a gain of 16.5% in the count of lesions removed only by WL and a gain of 14.16% in the overall count of lesions resected by the combination of the methods.

Interestingly, no iatrogenic opening of the bowel during conservative eradication procedures nor intraoperative ureteral lesions or postoperative fistulas occurred; moreover, the postoperative urinary retention observed was only 2%, lower than the rate reported in the literature (36). These interesting low rates of perioperative complications may be possible, thanks to the already noticed benefits of fluorescence-guided surgery (10, 48–50). Only one case of anastomotic colorectal dehiscence occurred, but the anastomotic vascularization (48) was not investigated because of the washout of ICG employed at the beginning of the surgery for the study purpose. Further studies focused on complication rate with adequate population are needed to confirm these results.

To our knowledge, this is the first prospective trial with the most consistent population subjected to the same homogeneous procedure (surgery, ICG dose of injection, time of observation, dedicated pathologist) (51).

Recently, Siegenthaler et al. (11) found that NIR-ICG resulted as useful for identifying the extent of lesions, allowing for the resection of nodules and the preservation of healthy tissue surrounding the diseased, but the results were not satisfactory regarding detection rate. In fact, in this study, the PPV reported

for WL, NIR-ICG, and the combination of the two methods were 89.8%, 68.8%, and 86.7%, respectively, while in our cohort, the values noticed were 96.6%, 98.5%, and 97.6%, respectively. Moreover, s-OcLs for NIR-ICG in Siegenthaler et al. (11) were at least 22%, but only one lesion was a c-OCL (4.5%). Those results may differ from our results for several factors, identifiable in the different selection of population for the rAFS stage: different times of intraoperative observation for a subset of the population [only 35 (55.6%) patients of that cohort received a comparable observation time with the Gre-Endo trial] and different doses of ICG adopted. Moreover, another difference was the fact that we considered as pathologic not only endometriosis per se but also lesions characterized by acute or chronic sclerosing inflammatory infiltrate (28, 29, 51).

Strengths and Limitations of the Study

The strengths of this study are the single-center prospective design, the considerable population enrolled subjected to the same experimental procedure and the standardized surgery by a limited team of high-volume surgeons, and a dedicated pathologist (51).

The limitations of the present study include the exclusion by the investigation of the adnexal endometriosis and the higher percentage (~89%) of advanced endometriosis stage (stages III and IV for rAFS) that could represent a bias of selection.

However, this type of population enrolment could be explained by the fact that our hospital is a third referral center to triage treatment of women with endometriosis who may be suffering from an advanced stage that cannot be treated elsewhere. Moreover, according to recent literature, the enrolment of higher stage of disease may have worsened the detection rate results of the present study (11). These limitations could be partially solved by the fact that in our institutions, surgical care and laparoscopic evaluation are standardized and there is the ability to partially overcome differences such as preoperative patient selection, surgical strategies, and intraoperative visualization.

Future Perspectives

This type of approach has recently been associated with a promising improvement in the quality of life (25), but further studies are needed to establish the real benefit in terms of pain relief, recurrence rate, and fertility rate resulting from the strengthening of the eradication power found. In addition, another direction in which research should be directed should be its use in a population that includes all stages of disease and, therefore, also focuses on the lower stages of disease.

Conclusions

The use of NIR-ICG alone and above all combined with WL during laparoscopy for endometriosis showed good results in intraoperative detection rate and fluorescence-guided surgery. Furthermore, NIR-ICG allowed surgeons to remove occult lesions that otherwise would remain, leading to possible greater postoperative pain and a higher risk of persistence and relapse.

Further prospective studies that overcome the possible biases of this study are warranted to validate and confirm these results and permit a diffusion of fluorescence-guided endometriosis surgery as a useful aid for a more effective and safe surgery.

DATA AVAILABILITY STATEMENT

The raw data supporting the conclusions of this article will be made available by the authors, without undue reservation.

ETHICS STATEMENT

The studies involving human participants were reviewed and approved by Ethics Committee of Fondazione Policlinico Universitario "A. Gemelli"—IRCCS, Rome, Italy (Prot.sf. A.287/C.E./2013). The patients/participants provided their written informed consent to participate in this study.

AUTHOR CONTRIBUTIONS

Study concepts: LT, VV, GV, and FC. Study design: LT, GV, and GF. Data acquisition: VV, LT, and MN. Quality control of data and algorithms: GS, FC, and SG. Data analysis and interpretation: GV, LT, GF, and LP. Statistical analysis: GV, LP, and GF. Manuscript preparation: LCT, GV, and SG. Manuscript editing: LT, VV, GS, and GV. Manuscript review: all authors. All authors contributed to the article and approved the submitted version.

ACKNOWLEDGMENTS

The authors thank Richard H. Renston, M.D., Ph.D., for his important contribution in revising the form and the English language of this article.

REFERENCES

1. Caruso S, Iraci M, Cianci S, Fava V, Casella E, Cianci A. Comparative, Open-Label Prospective Study on the Quality of Life and Sexual Function of Women Affected by Endometriosis-Associated Pelvic Pain on 2 Mg Dienogest/30 G Ethinyl Estradiol Continuous or 21/7 Regimen Oral Contraceptive. *J Endocrinol Invest* (2016) 39:923–31. doi: 10.1007/s40618-016-0460-6
2. Duffy JM, Arambage K, Correa FJ, Olive D, Farquhar C, Garry R, et al. Laparoscopic Surgery for Endometriosis. *Cochrane Database Syst Rev* (2014) 4:CD011031. doi: 10.1002/14651858.CD011031.pub2
3. Caruso S, Cianci A, Iraci M, Fava V, Di Pasqua S, Cianci S. Does Nomegestrol Acetate Plus 17β-Estradiol Oral Contraceptive Improve Endometriosis-Associated Chronic Pelvic Pain in Women? *J Womens Health (Larchmt)* (2020) 29(9):1184–91. doi: 10.1089/jwh.2020.8291
4. Caruso S, Iraci M, Cianci S, Casella E, Fava V, Cianci A. Quality of Life and Sexual Function of Women Affected by Endometriosis-Associated Pelvic Pain When Treated With Dienogest. *J Endocrinol Invest* (2015) 38(11):1211–8. doi: 10.1007/s40618-015-0383-7
5. Greene R, Stratton P, Cleary SD, Ballweg ML, Sinaii N. Diagnostic Experience Among 4,334 Women Reporting Surgically Diagnosed Endometriosis. *Fertil Steril* (2009) 91:32–9. doi: 10.1016/j.fertnstert.2007.11.020

6. Khan KN, Fujishita A, Kitajima M, Hiraki K, Nakashima M, Masuzaki H. Occult Microscopic Endometriosis: Undetectable by Laparoscopy in Normal Peritoneum. *Hum Reprod* (2014) 29(3):462–72. doi: 10.1093/humrep/det438
7. Levey KA. Use of Fluorescence Imaging Technology to Identify Peritoneal Endometriosis: A Case Report of New Technology. *Surg Laparosc Endosc Percutan Tech* (2014) 24:e63–5. doi: 10.1097/SLE.0b013e31828fa28d
8. Taylor E, Williams C. Surgical Treatment of Endometriosis: Location and Patterns of Disease at Reoperation. *Fertil Steril* (2010) 93:57–61. doi: 10.1016/j.fertnstert.2008.09.085
9. Cosentino F, Vizzielli G, Turco LC, Fagotti A, Cianci S, Vargiu V, et al. Near-Infrared Imaging With Indocyanine Green for Detection of Endometriosis Lesions (Gre-Endo Trial): A Pilot Study. *J Minim Invasive Gynecol* (2018) 25(7):1249–54. doi: 10.1016/j.jmig.2018.02.023
10. De Neef A, Cadière G-B, Bourgeois P, Barbieux R, Dapri G, Fastrez M. Fluorescence of Deep Infiltrating Endometriosis During Laparoscopic Surgery: A Preliminary Report on 6 Cases. *Surg Innov* (2018) 25:450–4. doi: 10.1177/1553350618785486
11. Siegenthaler F, Knabben L, Mohr S, Nirgianakis K, Imboden S, Mueller MD. Visualization of Endometriosis With Laparoscopy and Near-Infrared Optics With Indocyanine Green. *Acta Obstet Gynecol Scand* (2020) 99(5):591–7. doi: 10.1111/aogs.13803
12. Turco LC, Scaldaferri F, Chiantera V, Cianci S, Ercoli A, Fagotti A, et al. Long-Term Evaluation of Quality of Life and Gastrointestinal Well-Being After Segmental Colo-Rectal Resection for Deep Infiltrating Endometriosis (ENDO-RESECT QoL). *Arch Gynecol Obstet* (2020) 301(1):217–28. doi: 10.1007/s00404-019-05382-8
13. Turco LC, Tortorella L, Tuscano A, Palumbo MA, Fagotti A, Uccella S, et al. Surgery-Related Complications and Long-Term Functional Morbidity After Segmental Colo-Rectal Resection for Deep Infiltrating Endometriosis (ENDO-RESECT Morb). *Arch Gynecol Obstet* (2020) 302(4):983–93. doi: 10.1007/s00404-020-05694-0
14. Sozzi G, Fanfani F, Berretta R, Capozzi VA, Uccella S, Buono N, et al. Laparoscopic Sentinel Node Mapping With Intracervical Indocyanine Green Injection for Endometrial Cancer: The SENTIFAIL Study - A Multicentric Analysis of Predictors of Failed Mapping. *Int J Gynecol Cancer* (2020) 30(11):1713–8. doi: 10.1136/ijgc-2020-001724
15. Capozzi VA, Sozzi G, Uccella S, Ceni V, Cianciolo A, Gambino G, et al. Novel Preoperative Predictive Score to Evaluate Lymphovascular Space Involvement in Endometrial Cancer: An Aid to the Sentinel Lymph Node Algorithm. *Int J Gynecol Cancer* (2020) 30(6):806–12. doi: 10.1136/ijgc-2019-001016
16. Uccella S, Zorzato PC, Lanzo G, Fagotti A, Cianci S, Gallina D, et al. The Role of Sentinel Node in Early Ovarian Cancer: A Systematic Review. *Minerva Med* (2019) 110(4):358–66. doi: 10.23736/S0026-4806.19.06145-7
17. Capozzi VA, Riemma G, Rosati A, Vargiu V, Granese R, Ercoli A, et al. Surgical Complications Occurring During Minimally Invasive Sentinel Lymph Node Detection in Endometrial Cancer Patients. A Systematic Review of the Literature and Metanalysis. *Eur J Surg Oncol* (2021) 47(8):2142–9. doi: 10.1016/j.ejso.2021.03.253
18. Zorzato PC, Bosco M, Franchi MP, Mariani A, Cianci S, Garzon S, et al. Sentinel Lymph Node for Endometrial Cancer Treatment: Review of the Literature. *Minerva Med* (2021) 112(1):70–80. doi: 10.23736/S0026-4806.20.07117-7
19. Capozzi VA, Ceni V, Sozzi G, Cianciolo A, Gambino G, Pugliese M, et al. Endoscopic Near Infrared and Indocyanine Green to Verify the Viability of the Subcutaneous Flap for Vulvar Cancer. *Gynecol Oncol* (2019) 154(3):653–4. doi: 10.1016/j.ygyno.2019.06.018
20. Asante A, Taylor RN. Endometriosis: The Role of Neuroangiogenesis. *Annu Rev Physiol* (2011) 73:163–82. doi: 10.1146/annurev-physiol-012110-142158
21. Vlek SL, Lier M, Ankersmit M, Ket JC, Dekker JJ, Mijatovic V, et al. Laparoscopic Imaging Techniques in Endometriosis Therapy: A Systematic Review. *J Minim Invasive Gynecol* (2016) 23:886–92. doi: 10.1016/j.jmig.2016.06.019
22. Al-Taher M, Hsien S, Schols RM, Hanegem NV, Bouvy ND, Dunselman GAJ, et al. Intraoperative Enhanced Imaging for Detection of Endometriosis: A Systematic Review of the Literature. *Eur J Obstet Gynecol Reprod Biol* (2018) 224:108–16. doi: 10.1016/j.ejogrb.2018.03.020
23. Maheux-Lacroix S, Belanger M, Pinard L, Lemyre M, Laberge P, Boutin A. Diagnostic Accuracy of Intraoperative Tools for Detecting Endometriosis: A Systematic Review and Meta-Analysis. *J Minim Invasive Gynecol* (2020) 27(2):433–40.e1. doi: 10.1016/j.jmig.2019.11.010
24. Jayakumaran J, Pavlovic Z, Fuhrich D, Wiercinski K, Buffington C, Caceres A. Robotic Single-Site Endometriosis Resection Using Near-Infrared Fluorescence Imaging With Indocyanine Green: A Prospective Case Series and Review of Literature. *J Robot Surg* (2020) 14(1):145–54. doi: 10.1007/s11701-019-00951-0
25. Keckstein J, Becker CM, Canis M, Feki A, Grimbizis GF, Hummelshoj L, et al. Recommendations for the Surgical Treatment of Endometriosis. Part 2: Deep Endometriosis. *Hum Reprod Open* (2020) 2020(1):hoaa002. doi: 10.1093/hropen/hoaa002
26. Bourdel N, Alves J, Pickering G, Ramilo I, Roman H, Canis M. Systematic Review of Endometriosis Pain Assessment: How to Choose a Scale? *Hum Reprod Update* (2015) 21(1):136–52. doi: 10.1093/humupd/dmu046
27. Revised American Fertility Society Classification of Endometriosis: 1985. *Fertil Steril* (1985) 43(3):351–2. doi: 10.1016/s0015-0282(16)48430-x
28. Riccio LDGC, Santulli P, Marcellin L, Abrão MS, Batteux F, Chapron C. Immunology of Endometriosis. *Best Pract Res Clin Obstet Gynaecol* (2018) 50:39–49. doi: 10.1016/j.bpobgyn.2018.01.010
29. Moen MH, Halvorsen TB. Histologic Confirmation of Endometriosis in Different Peritoneal Lesions. *Acta Obstet Gynecol Scand* (1992) 71(5):337–42. doi: 10.3109/00016349209021069
30. Katayama H, Kurokawa Y, Nakamura K, Ito H, Kanemitsu Y, Masuda N, et al. Extended Clavien Dindo Classification of Surgical Complications: Japan Clinical Oncology Group Postoperative Complications Criteria. *Surg Today* (2016) 46(6):668–85. doi: 10.1007/s00595-015-1236-x
31. Simon R. Optimal Two Stage Design for Phase II Clinical Trials. *Control Clin Trials* (1989) 10:1–10. doi: 10.1016/0197-2456(89)90015-9
32. Guo SW. Recurrence of Endometriosis and Its Control. *Hum Reprod Update* (2009) 15:441–61. doi: 10.1093/humupd/dmp007
33. Di Donato N, Montanari G, Benfenati A, Leonardi D, Bertoldo V, Monti G, et al. Prevalence of Adenomyosis in Women Undergoing Surgery for Endometriosis. *Eur J Obstet Gynecol Reprod Biol* (2014) 181:289–93. doi: 10.1016/j.ejogrb.2014.08.016
34. Stegmann BJ, Sinaii N, Liu S, Segars J, Merino M, Nieman LK, et al. Using Location, Color, Size, and Depth to Characterize and Identify Endometriosis Lesions in a Cohort of 133 Women. *Fertil Steril* (2008) 89(6):1632–6. doi: 10.1016/j.fertnstert.2007.05.042
35. Uccella S, Marconi N, Casarin J, Ceccaroni M, Boni L, Sturla D, et al. Impact of Endometriosis on Surgical Outcomes and Complications of Total Laparoscopic Hysterectomy. *Arch Gynecol Obstet* (2016) 294(4):771–8. doi: 10.1007/s00404-016-4115-9
36. Serati M, Cattoni E, Braga A, Uccella S, Cromi A, Ghezzi F. Deep Endometriosis and Bladder and Detrusor Functions in Women Without Urinary Symptoms: A Pilot Study Through an Unexplored World. *Fertil Steril* (2013) 100(5):1332–6. doi: 10.1016/j.fertnstert.2013.06.044
37. Di Donato N, Montanari G, Benfenati A, Monti G, Leonardi D, Bertoldo V, et al. Sexual Function in Women Undergoing Surgery for Deep Infiltrating Endometriosis: A Comparison With Healthy Women. *J Fam Plann Reprod Health Care* (2015) 41(4):278–83. doi: 10.1136/jfprhc-2014-100993
38. Spagnolo E, Zannoni L, Raimondo D, Ferrini G, Mabrouk M, Benfenati A, et al. Urodynamic Evaluation and Anorectal Manometry Pre- and Post-Operative Bowel Shaving Surgical Procedure for Posterior Deep Infiltrating Endometriosis: A Pilot Study. *J Minim Invasive Gynecol* (2014) 21(6):1080–5. doi: 10.1016/j.jmig.2014.05.012
39. Uccella S, Capozzi VA, Ricco' M, Perrone E, Zanello M, Ferrari S, et al. Sexual Function Following Laparoscopic Versus Transvaginal Closure of the Vaginal Vault After Laparoscopic Hysterectomy: Secondary Analysis of a Randomized Trial by the Italian Society of Gynecological Endoscopy Using a Validated Questionnaire. *J Minim Invasive Gynecol* (2020) 27(1):186–94. doi: 10.1016/j.jmig.2019.03.018
40. Cianci S, Tarascio M, Rosati A, Caruso S, Uccella S, Cosentino F, et al. Sexual Function and Quality of Life of Patients Affected by Ovarian Cancer. *Minerva Med* (2019) 110(4):320–9. doi: 10.23736/S0026-4806.19.06080-4
41. Caruso S, Cianci S, Malandrino C, Cicero C, Lo Presti L, Cianci A. Quality of Sexual Life of Women Using the Contraceptive Vaginal Ring in Extended Cycles: Preliminary Report. *Eur J Contracept Reprod Health Care* (2014) 19(4):307–14. doi: 10.3109/13625187.2014.914488

42. Caruso S, Agnello C, Malandrino C, Lo Presti L, Cicero C, Cianci S. Do Hormones Influence Women's Sex? Sexual Activity Over the Menstrual Cycle. *J Sex Med* (2014) 11(1):211–21. doi: 10.1111/jsm.12348
43. Caruso S, Iraci M, Cianci S, Vitale SG, Fava V, Cianci A. Effects of Long-Term Treatment With Dienogest on the Quality of Life and Sexual Function of Women Affected by Endometriosis-Associated Pelvic Pain. *J Pain Res* (2019) 12:2371–8. doi: 10.2147/JPR.S207599
44. Buck Louis GM, Hediger ML, Peterson CM, Croughan M, Sundaram R, Stanford J, et al. Incidence of Endometriosis by Study Population and Diagnostic Method: The ENDO Study. *Fertil Steril* (2011) 96:360–5. doi: 10.1016/j.fertnstert.2011.05.087
45. Vizzielli G, Cosentino F, Raimondo D, Turco LC, Vargiu V, Iodice R, et al. Real 3D Approach *vs* 2D Camera With and Without Real-Time Near-Infrared Imaging With Indocyanine Green for Detection of Endometriosis: A Case-Control Study. *Acta Obstet Gynecol Scand* (2020) 99(10):1330–8. doi: 10.1111/aogs.13866
46. Capozzi VA, Armano G, Rosati A, Tropea A, Biondi A. The Robotic Single-Port Platform for Gynecologic Surgery: A Systematic Review of the Literature and Meta-Analysis. *Updates Surg* (2020) 73(3):1155–67. doi: 10.1007/s13304-020-00812-8
47. Raimondo D, Turco LC, Cosentino F, Mabrouk M, Mastronardi M, Borghese G, et al. Feasibility and Safety of Two Different Surgical Routes for the Eradication of Recto-Vaginal Endometriosis With Vaginal Mucosa Infiltration (Endo-Vag-R Study). *Acta Obstet Gynecol Scand* (2020) 99 (8):1050–6. doi: 10.1111/aogs.13824
48. Seracchioli R, Raimondo D, Arena A, Zanello M, Mabrouk M. Clinical Use of Endovenous Indocyanine Green During Rectosigmoid Segmental Resection for Endometriosis. *Fertil Steril* (2018) 109(6):1135. doi: 10.1016/j.fertnstert.2018.02.122
49. Raimondo D, Borghese G, Mabrouk M, Arena A, Ambrosio M, Del Forno S, et al. Use of Indocyanine Green for Intraoperative Perfusion Assessment in Women With Ureteral Endometriosis: A Preliminary Study. *J Minim Invasive Gynecol* (2020) 28(1):42–9. doi: 10.1016/j.jmig.2020.04.004
50. Bar-Shavit Y, Jaillet L, Chauvet P, Canis M, Bourdel N. Use of Indocyanine Green in Endometriosis Surgery. *Fertil Steril* (2018) 109(6):1136–7. doi: 10.1016/j.fertnstert.2018.02.113
51. Turco LC, Vizzielli G, De Ninno M, Scambia G, Cosentino F. Value of Indocyanine Green and Laparoscopic Near-Infrared Technology in the Surgical Management of Endometriosis: What is the Evidence? *Acta Obstet Gynecol Scand* (2020) 99(10):1417–8. doi: 10.1111/aogs.13864

Conflict of Interest: The authors declare that the research was conducted in the absence of any commercial or financial relationships that could be construed as a potential conflict of interest.

frontiers | Frontiers in Oncology

ORIGINAL RESEARCH
published: 05 April 2022
doi: 10.3389/fonc.2022.851677

Cervical Carcinoma: Evaluation Using Diffusion MRI With a Fractional Order Calculus Model and its Correlation With Histopathologic Findings

Xian Shao[1†], Li An[1†], Hui Liu[2], Hui Feng[2], Liyun Zheng[3], Yongming Dai[3], Bin Yu[4] and Jin Zhang[1*]*

[1] Department of Anesthesiology, The Fourth Hospital of Shijiazhuang, Shijiazhuang, China, [2] Department of Radiology, The Fourth Hospital of Hebei Medical University, Shijiazhuang, China, [3] MR Collaboration, Central Research Institute, United Imaging Healthcare, Shanghai, China, [4] Department of Emergency, The Fourth Hospital of Hebei Medical University, Shijiazhuang, China

OPEN ACCESS

Edited by:
Alessio G. Morganti, University of Bologna, Italy

Reviewed by:
Muge Karaman, University of Illinois at Chicago, United States
Xiaohong Joe Zhou, University of Illinois at Chicago, United States

***Correspondence:**
Bin Yu
yubin_hb@126.com
Jin Zhang
2270532832@qq.com

[†]These authors have contributed equally to this work

Specialty section:
This article was submitted to Gynecological Oncology, a section of the journal Frontiers in Oncology

Received: *10 January 2022*
Accepted: *03 March 2022*
Published: *05 April 2022*

Citation:
Shao X, An L, Liu H, Feng H, Zheng L, Dai Y, Yu B and Zhang J (2022) Cervical Carcinoma: Evaluation Using Diffusion MRI With a Fractional Order Calculus Model and its Correlation With Histopathologic Findings. Front. Oncol. 12:851677. doi: 10.3389/fonc.2022.851677

Objective: The objective of the study is to investigate the feasibility of using the fractional order calculus (FROC) model to reflect tumor subtypes and histological grades of cervical carcinoma.

Methods: Sixty patients with untreated cervical carcinoma underwent multi-b-value diffusion-weighted imaging (DWI) at 3.0T magnetic resonance imaging (MRI). The mono-exponential and the FROC models were fitted. The differences in the histological subtypes and grades were evaluated by the Mann–Whitney U test. Receiver operating characteristic (ROC) analyses were performed to assess the diagnostic performance and to determine the best predictor for both univariate analysis and multivariate analysis. Differences between ROC curves were tested using the Hanley and McNeil test, while the sensitivity, specificity, and accuracy were compared using the McNemar test. *P*-value <0.05 was considered as significant difference. The Bonferroni corrections were applied to reduce problems associated with multiple comparisons.

Results: Only the parameter β, derived from the FROC model could differentiate cervical carcinoma subtypes ($P = 0.03$) and the squamous cell carcinoma (SCC) lesions exhibited significantly lower β than that in the adenocarcinoma (ACA) lesions. All the individual parameters, namely, ADC, β, *D*, and μ derived from the FROC model, could differentiate low-grade cervical carcinomas from high-grade ones ($P = 0.022$, 0.009, 0.004, and 0.015, respectively). The combination of all the FROC parameters showed the best overall performance, providing the highest sensitivity (81.2%) and AUC (0.829).

Conclusion: The parameters derived from the FROC model were able to differentiate the subtypes and grades of cervical carcinoma.

Keywords: magnetic resonance imaging, diffusion-weighted imaging, cervical carcinoma, cervical squamous cell carcinoma, cervical adenocarcinoma

INTRODUCTION

Cervical cancer is the fourth most common cancer in women worldwide (1). In developing countries, probably due to the poor access to the screening programs, most of the new cases present advanced stages and remain poor prognosis. Both histological subtypes and grades are the most common prognostic factors of cervical cancer. The two main histological subtypes, squamous cell carcinoma (SCC) and adenocarcinoma (ACA), account for approximately 70 and 25% of all cervical cancers, respectively (1). According to a previous study, the different cell types probably have different patterns of failure and survival (2). The aggressiveness of tumors represented by histological grade can also provide critical information for selecting treatment plans. Therefore, the clear insights into tumor subtypes and histological grades are essential in cervical carcinoma diagnosis and management. Despite biopsy being currently performed for the assessment of cervical carcinoma and is considered as a gold standard for patients presenting with advantage stages, it is an invasive procedure associated with certain risks of bleeding and infection, and sampling bias may occur especially for larger tumors (3, 4).

Magnetic resonance imaging (MRI) emerged as a powerful noninvasive diagnostic tool in oncology. Among MRI techniques, diffusion-weighted imaging (DWI) probes tissue microenvironment based on its sensitivity to water molecular diffusion that can be quantified using apparent diffusion coefficient (ADC) derived from the Gaussian diffusion model. Previous studies reported the potential use of ADC to evaluate cervical carcinoma subtypes and grades (5–7). However, this conventional mono-exponential diffusion model lacks specific parameters to reflect tumor microstructures, which are essential for assessing tumor subtypes and grades. According to the previous studies, the differentiation of cervical carcinoma histological grades based on ADC alone was reported to be difficult as the overlapped ADC values among different histological grades would act as a confounder (8, 9). Similarly, some overlap in ADC values were found between SCC and ACA (6).

Recently, the fractional order calculus (FROC) model was suggested to evaluate the microstructural and heterogeneity changes in tumor tissues. The FROC model provides a new set of parameters, including an anomalous diffusion coefficient D, an intravoxel diffusion heterogeneity parameter β, and a spatial parameter μ (10). Collectively, these parameters offer a multi-faceted characterization of cancerous tissues and can be used as a new class of biomarker in tumor diagnosis (11–14). Prior research proved that the FROC model could better reflect the complexity and heterogeneity of tissue microstructure than conventional diffusion model in gastric adenocarcinoma (15) and prostate lesions (16).

This study aimed to investigate whether the parameters derived from the FROC model can be used for imaging-based assessment of histological subtypes and grades of cervical carcinoma. Furthermore, the diagnostic performance results of ADC and the FROC parameters were compared to find the best predictor.

MATERIALS AND METHODS

Study Population

This prospective study was approved by our institutional review board and written informed consents were obtained from all participants. The inclusion criteria were as follows: (1) no previous treatment for cervical carcinoma prior to the MR examination; (2) no contraindications to the MR examination; (3) clinically and radiologically suspected cervical carcinoma patients. Exclusion criteria were as follows: (1) poor image quality; (2) rare histological subtypes; (3) lack of subtype classification and/or grade information through pathological evaluation. With these criteria, one patient with poor image quality, two patients with adenosquamous carcinoma, and two patients without pathological evaluation were excluded. Finally, between January 2021 to November 2021, sixty patients (mean age, 53.0 years ± 10.1 [standard deviation]) were enrolled.

All cases involved in this study were confirmed to have cervical carcinoma by the biopsy, which were further analyzed and reconfirmed by an experienced pathologist specialized in gynecological malignancies. Histological subtypes were separated into an SCC group and an ACA group. Besides, all the cases were classified into a high-grade group (poorly differentiated tumor) and a low-grade group (well- or moderately differentiated tumor).

MR Imaging

All the MRI examinations were performed on a 3.0T MR scanner (uMR 780, United Imaging Healthcare, Shanghai, China) with a commercial 12-channel body phased array coil. MR sequences included: 1) axial T1-weighted (T1W) fast spin echo (FSE) sequence; 2) axial T2-weighted (T2W) FSE sequence; 3) coronal fat-suppressed T2W FSE sequence; 4) sagittal T2W FSE sequence; and 5) diffusion-weighted imaging with a series of b-value 0, 20, 40, 80, 160, 200, 500, 1,000, and 2,000 s/mm^2. **Table 1** presents all the detailed protocols.

Image Analysis

The conventional mono-exponential diffusion model was applied to estimate ADC based on the images with two b-values, 0 and 1,000 s/mm^2.

The FROC model was set up following the equation (17, 18)

$$S = S_0 \exp[-D\mu^{2(\beta-1)}(\gamma G_d \delta)^{2\beta}(\Delta - \frac{2\beta-1}{2\beta+1}\delta)] \quad (1)$$

where S_0 is the signal intensity without diffusion weighting, G_d is the diffusion gradient amplitude, D is the anomalous diffusion coefficient, β is the intravoxel diffusion heterogeneity parameter, and μ is the spatial parameter.

Two experienced radiologists with 8 and 19 years of experience in gynecological imaging delineated the volumes of the interest (VOIs) using a 3D slicer (19). The VOIs were placed on the solid regions of tumors to avoid confounding effects caused by other tissue compositions, such as necrosis, mucinous

TABLE 1 | MRI protocols.

Parameters	Sequences				
	Axial T1W FSE	Axial T2W FSE	Coronal fat-suppressed T2W FSE	Sagittal T2W FSE	EPI-DWI
TR (ms)	586	2,268	4,139	2,103	6,152
TE (ms)	11.38	98.28	79.52	71.88	82.7
Flip angle (°)	130	105	105	105	90
FOV (cm)	22 × 22	22 × 22	22 × 22	22 × 22	30 × 26
Matrix	432 × 432	432 × 432	456 × 456	456 × 456	256 × 222
Slice Thickness (mm)	4	4	4	4	5
Intersection gap (mm)	0	0	0	0	0
Bandwidth (Hz/pixel)	200	220	200	180	2,120
Number of slices	30	30	23	23	25
b-value (s/mm^2)	/	/	/	/	0, 20, 40, 80, 160, 200, 500, 1,000, 2,000

T1W, T1-weighted; T2W, T2-weighted; FSE, fast spin echo; EPI, echo-planar imaging; DWI, diffusion weighted imaging; TR, repetition time; TE, echo time; FOV, field of view.

lake, and calcification. The VOIs were first determined on the diffusion-weighted images with b = 0, and then propagated to the corresponding *D*, β, μ, and ADC map. The mean values of *D*, β, μ, and ADC were recorded.

Statistics

Statistical analyses were performed with the SPSS software (Version 26, SPSS Inc., Chicago, IL, USA) and MedCalc (Version 20; MedCalc Software, Ostend, Belgium). The Mann–Whitney U tests were utilized to determine the statistical significance in mean parametric differences between the cervical carcinoma subtypes and differentiation grades. With the histopathological results as a gold standard, the receiver operating characteristic (ROC) analyses were performed on individual FROC parameters and ADC for the differentiation between a) SCC and ACA, and b) high-grade tumor and low-grade tumor. Then, the significant predictors were selected. Logistic regression analysis was performed to determine the optimal linear combination of these significant predictors in a model. The Youden index was exploited to determine the cutoff value for both univariate analysis and multivariate analysis, along with the area under the curve (AUC), sensitivity, specificity, and accuracy. Differences between ROC curves were tested using the Hanley and McNeil test (20), while the sensitivity, specificity, and accuracy were compared using the McNemar test. *P*-value <0.05 was considered as statistically significant. Bonferroni corrections were applied to reduce problems associated with multiple comparisons.

RESULTS

Patient demographics and tumor characteristics are given for all patients in **Table 2**. Of the 60 patients, 47 (78.3%) were SCC patients and 13 (21.7%) were ACA patients. Besides, there were 28 (46.7%) patients with low-grade tumors, while 32 (53.3%) patients with high-grade ones.

Comparative Analysis of ADC and the FROC Parameters in Cervical Carcinoma Subtypes

Figure 1 shows a set of representative anatomic images and corresponding β, *D* and μ maps for a 70-year-old patient with SCC and a 56-year-old patient with ACA. The descriptive statistics of ADC and the FROC model parameters from each patient group are summarized in **Table 3**. As shown in **Figure 2**, no significant result was found for ADC, *D* and μ in differentiation SCC lesions from ACA lesions. However, β derived from the FROC model could differentiate cervical carcinoma subtypes (P = 0.031 <0.05) and the SCC lesions exhibited significantly lower β than that in the ACA lesions. For the ROC analysis, β proved to be the significant predictor with the best cut-off value 0.697 (AUC = 0.697, 95% confidence

TABLE 2 | Summary of the demographic and clinical features of the patients.

Variables	Patients
Number (n)	60
Age, y (mean ± SD)	53.0 ± 10.1
Histological Subtypes, n (%)	
SCC	47 (78.3%)
ACA	13 (21.7%)
Tumor grade, n (%)	
Well-differentiated	15 (25.0%)
Moderately-differentiated	13 (21.7%)
Poorly differentiated	32 (53.3%)

SD, standard deviation; SCC, cervical squamous cell carcinoma; ACA, cervical adenocarcinoma.

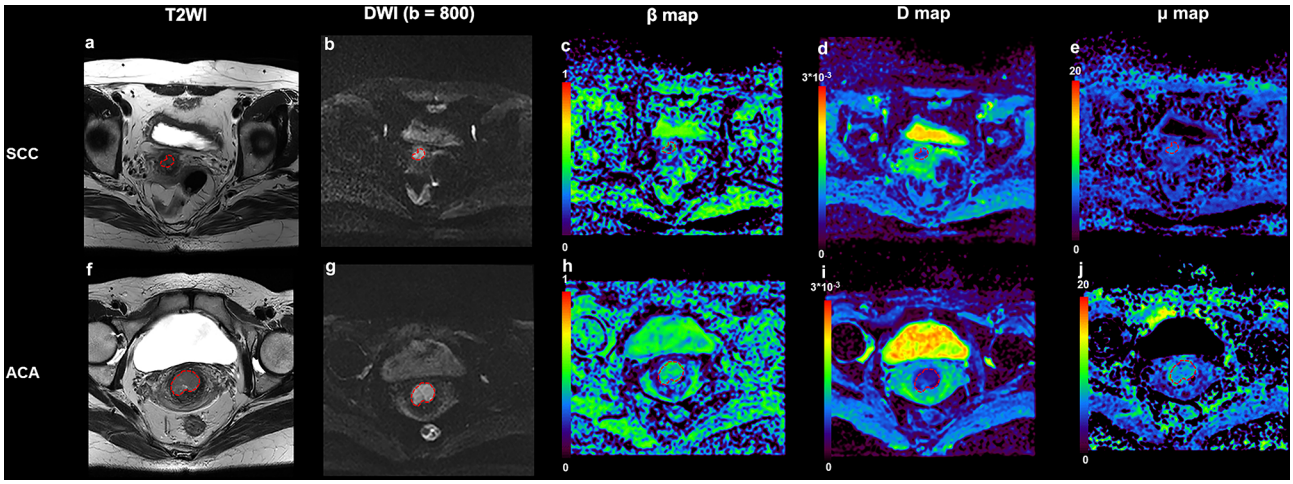

FIGURE 1 | An example of SCC from a 70-year-old patient and ACA from a 56-year-old patient. **(A)** Transverse T2 image for patient with SCC; **(B)** DWI image (b = 800 s/mm^2) for patient with SCC; **(C)** β map for patient with SCC; **(D)** *D* map for patient with SCC; **(E)** μ map for patient with SCC; **(F)** Transverse T2 image for patient with ACA; **(G)** DWI image (b = 800 s/mm^2) for patient with ACA; **(H)** β map for patient with ACA; **(I)** *D* map for patient with SCC; **(J)** μ map for patient with SCC. SCC, cervical squamous cell carcinoma; ACA, cervical adenocarcinoma; DWI, diffusion-weighted imaging.

interval 0.565 to 0.809; sensitivity = 63.8%, specificity = 84.6%, accuracy = 68.3%).

Comparative Analysis of ADC and the FROC Parameters in Cervical Carcinoma Grade

Figure 3 shows a set of β, *D*, μ and ADC maps for a 53-year-old patient with low-grade cervical carcinoma and a 64-year-old patient with high-grade one. As shown in **Figures 4A–D**, all the individual parameters, namely, ADC, β, *D* and μ, could differentiate low-grade cervical carcinoma from high-grade ones (P = 0.022, 0.009, 0.004, and 0.015, respectively). The high-grade lesions exhibited significantly lower ADC, β, *D* and μ than those in the low-grade lesions. **Figure 5A** and associated **Table 4** show the results from the ROC analysis. Among all the parameters, exhibited the best overall performance and outperformed ADC in AUC *D* (0.714 vs. 0.673), sensitivity (68.7% vs. 59.4%), and accuracy (73.3% vs. 70.0%). However, the differences between sensitivities, specificities, accuracies, and AUC values were not significant among all these individual parameters.

The combinations of the FROC parameters further improved the differentiation of low-grade tumors from high-grade ones. All the combinations, namely, D + β, D+ μ, β + μ, and D+ β + μ, yielded significant differences (P <0.05). As shown in **Figure 5B** and associated **Table 5**, the combination of all the FROC parameters D + β + μ showed the best overall performance, producing the highest sensitivity (81.2%) and AUC (0.829). Significantly higher sensitivity (P = 0.016) and AUC (P = 0.043) were observed in the combination D + β + μ than in ADC. The combination of *D* and β showed the highest specificity (89.3%) and accuracy (80.0%). Though D + β had no significant differences from ADC in specificity (P = 0.500), its accuracy was significantly higher than ADC (P = 0.031).

DISCUSSION

In this study, the feasibility of using the FROC model to classify cervical carcinoma subtypes and histological grades was investigated. The results demonstrated that only β derived from the FROC model could differentiate SCC from ACA. The

TABLE 3 | The descriptive statistics of ADC and FROC model parameters from different groups.

	ADC	β	*D*	μ
SCC	0.92 ± 0.17 (0.90, 0.36)	0.67 ± 0.05 (0.68, 0.18)	0.77 ± 0.12 (0.74, 0.32)	8.19 ± 0.80 (8.28, 0.91)
ACA	1.00 ± 0.27 (1.04, 0.85)	0.71 ± 0.08 (0.72, 0.26)	0.80 ± 0.20 (0.83, 0.63)	8.40 ± 0.31 (8.50, 0.82)
P	0.286	0.031	0.673	0.110
Low-grade	0.98 ± 0.19 (0.96, 0.49)	0.73 ± 0.06 (0.72, 0.18)	0.82 ± 0.13 (0.80, 0.28)	8.27 ± 0.93 (8.48, 1.19)
High-grade	0.90 ± 0.20 (0.86, 0.65)	0.68 ± 0.08 (0.68, 0.23)	0.74 ± 0.14 (0.72, 0.47)	8.26 ± 0.36 (8.27, 0.53)
P	0.022	0.009	0.004	0.015

Values are given as mean ± SD (median, range). β is unitless; ADC and D with unit (×10^{-3} mm^2/s); μ with unit (μm).
P-values are statistical comparisons between different tumor subtypes and histological grades.
ADC, apparent diffusion coefficient; FROC, fractional order calculus; SCC, cervical squamous cell carcinoma; ACA, cervical adenocarcinoma.

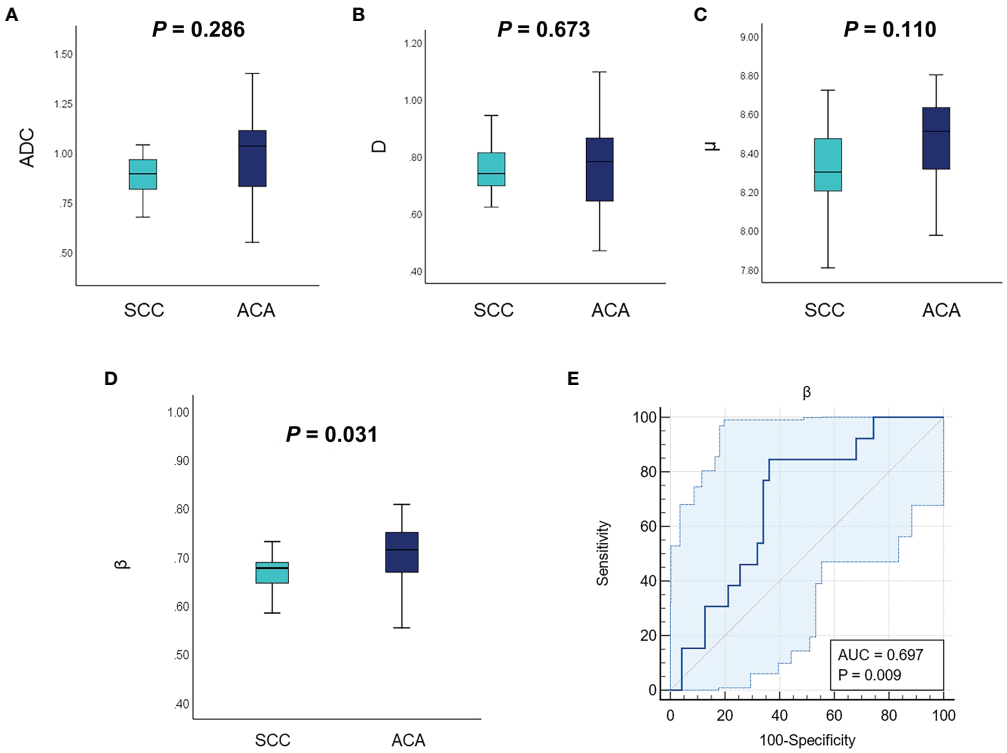

FIGURE 2 | Comparison of the mean ADC **(A)**, *D* **(B)**, μ **(C)**, and β **(D)** between different tumor subtypes using the Mann–Whitney U test. **(E)** The ROC curve of using β for classification of SCC and ACA. ADC, apparent diffusion coefficient; ROC, receiver operating characteristic; SCC, cervical squamous cell carcinoma; ACA, cervical adenocarcinoma.

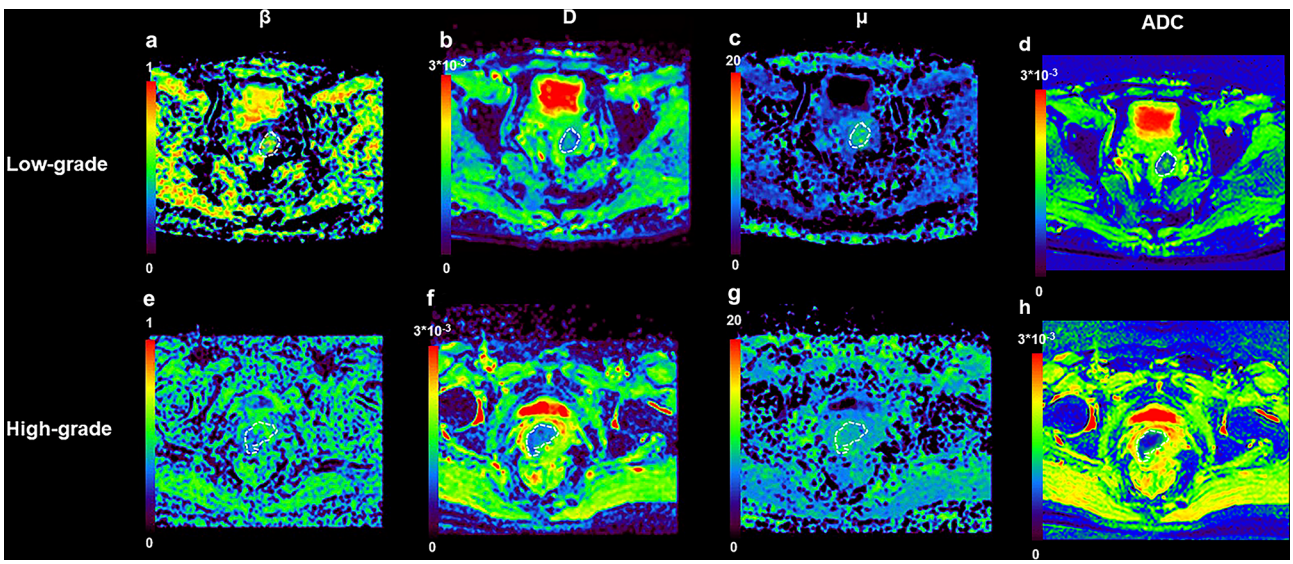

FIGURE 3 | An example of low-grade tumor from a 53-year-old patient and high-grade from a 64-year-old patient. **(A)** β map for patient with low-grade tumor; **(B)** *D* map for patient with low-grade tumor; **(C)** μ map for patient with low-grade tumor; **(D)** ADC map for patient with low-grade tumor; **(E)** β map for patient with high-grade tumor; **(F)** *D* map for patient with high-grade tumor; **(G)** μ map for patient with high-grade tumor; **(H)** ADC map for patient with high-grade tumor.

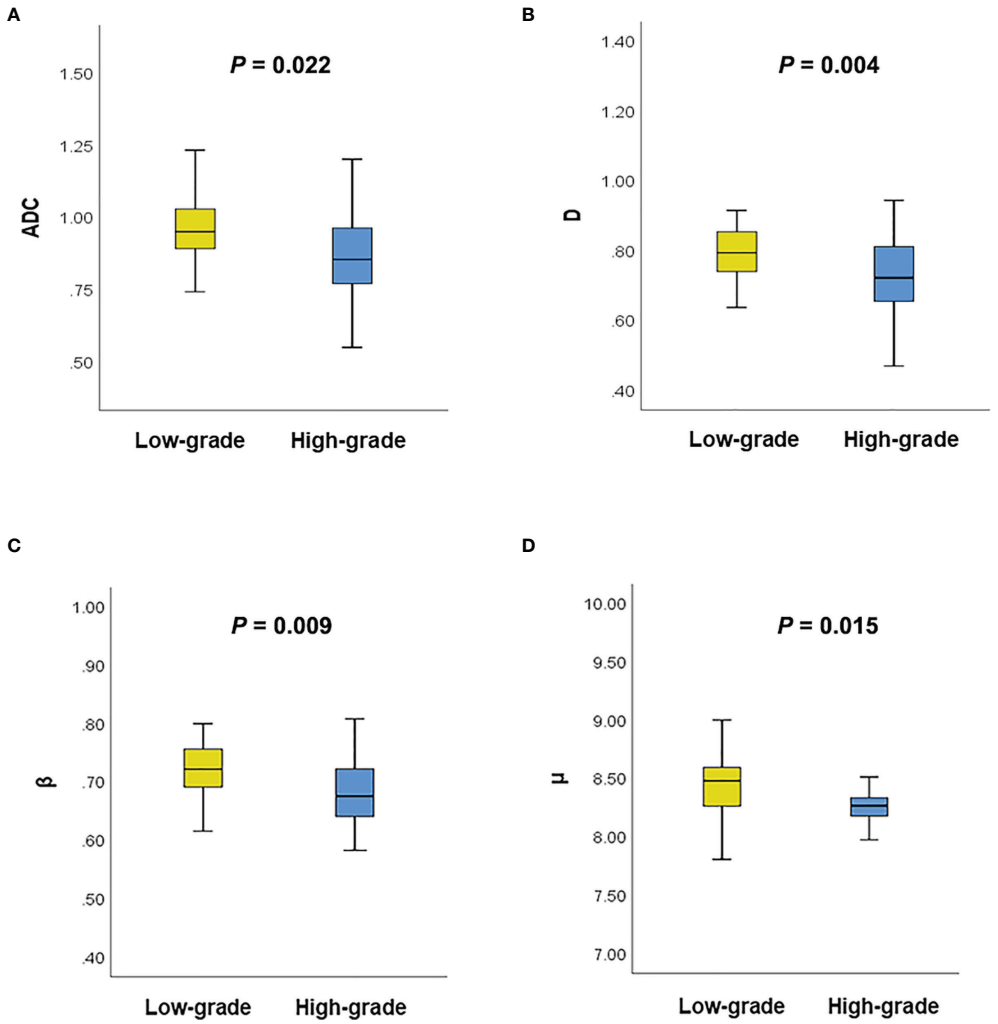

FIGURE 4 | **(A)** Comparison of the ADC between different tumor grades using the Mann–Whitney U test; **(B)** Comparison of the *D* between different tumor grades using the Mann–Whitney U test; **(C)** Comparison of the β between different tumor grades using the Mann–Whitney U test; **(D)** Comparison of the μ between different tumor grades using the Mann–Whitney U test.

combination of all the FROC parameters provided the highest overall performance in identifying high-grade tumors from low-grade ones, demonstrating 0.829 AUC, 81.2% sensitivity, 75.0% specificity, and 78.3% accuracy. Significantly higher sensitivity (P = 0.016) and AUC (P = 0.043) were observed in the combination D+ β + μ than in ADC.

Prior studies suggested that different cervical carcinoma subtypes had different treatment outcome and prognosis. Hopkins et al. demonstrated that ACA had a worse 5-year overall survival rate of 15–30% compared to SCC in all stages (21). Katanyoo et al. reported that ACA had more radio resistance than SCC. ACA in locally advanced cervical cancer had poorer response rate from radiation therapy and concurrent chemoradiation and also took a longer time to achieve complete response than SCC (22). Consequently, differentiation between SCC and ACA in an early time is critical for treatment decision and patient management. With its sensitivity to tissue structural and functional alterations, DWI has been routinely used in conjunction with T2-weighted imaging for tumor detection. In cervical cancer, the lower ADC in tumors compared with non-tumor epithelium provides excellent tumor-to-normal-tissue contrast (23, 24). However, the potential of ADC values to differentiate the cervical carcinoma subtypes remains controversial. Some studies reported that the ADC values of SCC were significantly lower than those of ACA (6, 25), whereas Winfield et al. showed that ADC values could not differentiate SCC from ACA (26). In the present study, no significant difference was found for ADC between the tumor subtypes, while β was significantly lower for the SCC lesions than ACA ones. The diffusion heterogeneity parameter in the FROC model has been increasingly focused in recent literatures. Unlike all previous studies on cervical carcinoma using conventional DWI

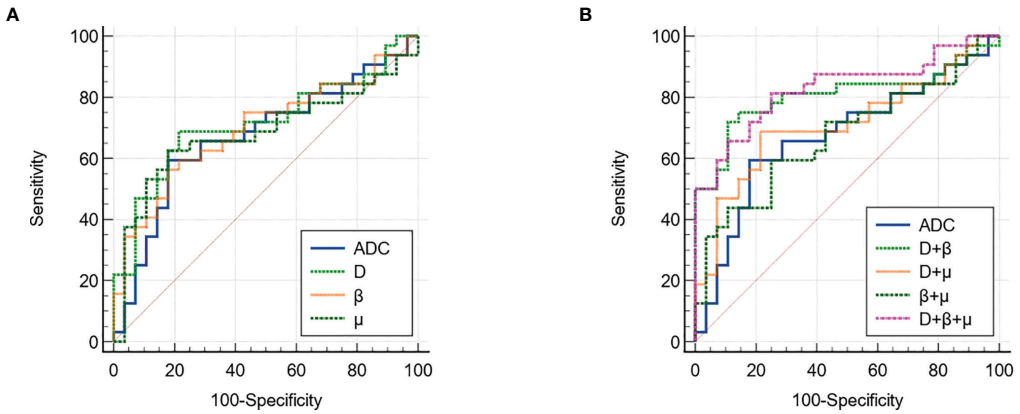

FIGURE 5 | The ROC curves of using **(A)** individual and **(B)** different combinations of FROC parameters for differentiation of low-grade tumor and high-grade tumor. ROC, receiver operating characteristic; FROC, fractional order calculus.

model, the FROC model is able to probe the tissue microstructural information with high b-values and increase the diagnostic performance to some extent. Prior research suggested that *D* reflected intrinsic diffusivity, μ was related to mean free length of diffusion, and β had a significant negative correlation with increased intravoxel tissue heterogeneity (11, 17, 27, 28). This study suggested a significant increase of tissue heterogeneity of SCC compared to ACA, which agreed with the findings in previous conventional DWI and diffusion kurtosis imaging (DKI) studies in cervical carcinoma. For instance, Wang et al. reported that mean diffusivity (MD) in SCC was significantly lower than that in ACA, and the lower MD in cervical carcinoma was likely related to the restriction of free water diffusion in more cellular packed tumor environment (29).

Aside from differentiation of the subtypes, cervical cancer grading also relies on invasive biopsy, which introduces the location bias. Therefore, developing non-invasive imaging biomarkers to assist tumor grading on the basis of MR images holds clinical significance. Previous studies reported that the FROC parameters could effectively distinguish tumor grades in glioma (30), pediatric brain tumor (28), and prostate cancer (16). In this study, the high-grade lesions exhibited significantly lower ADC, β, *D*, and *μ* than those in the low-grade ones and *D* derived from the FROC model provided the best individual parameter performance in grading the tumors compared with the other parameters. Similarly, prior studies found that ADC was negatively correlated with tumor grades of cervical carcinoma, indicating the aggressiveness of cervical carcinoma (31, 32). Related literatures suggested that the high-grade tumor resulted in increased cellular density, enlarged nuclei, and higher nuclear-to-cytoplasmic ratio with a more heterogeneous microenvironment (32, 33). However, the considerable overlap of ADC values among different tumor grades may limit the value of conventional DWI in diagnosis (8, 9). Furthermore, the high-grade tumors can have a higher degree of tissue heterogeneity, a characteristic that may not be adequately captured in a simple ADC value obtained from a mono-exponential diffusion model (34, 35).

It should be noted that β was found to be the only parameter which showed significance among the different cervical cancer subtypes; however, it is the one with the lowest diagnostic accuracy in differentiation among the low- and high-grade cervical carcinoma. These results may be attributed to the complex network of tumor microenvironment. The mechanism of differentiation of tumor subtype probably different from the differentiation of tumor grade. Results were also mixed in previous DWI-related studies. For instance, according to Wang et al., MD derived from DKI model and conventional ADC were significantly lower in squamous cell carcinoma than in adenocarcinoma, while no difference was observed in different tumor grade (29). Besides, Winfield showed that α from the stretched exponential model, K from the kurtosis model, and f and D* from the bi-exponential model were significantly different between types of tumor, while ADC from the mono-exponential model, DDC from the stretched exponential model, DK from the kurtosis model, Ds' from the statistical model and D

TABLE 4 | The ROC analysis results of using ADC and individual FROC model parameters to differentiate low-grade tumor from high-grade tumor.

	ADC	β	*D*	μ
Sensitivity	59.4%	56.2%	68.7%	62.5%
Specificity	82.1%	82.1%	78.6%	82.1%
Accuracy	70.0%	68.3%	73.3%	71.7%
AUC*	0.673 (0.540–0.789)	0.696 (0.564–0.809)	0.714 (0.583–0.824)	0.683 (0.550–0.797)

ROC, receiver operating characteristic; ADC, apparent diffusion coefficient; FROC, fractional order calculus; AUC, are under the curve.
**Data in parenthesis are 95% confidence intervals.*

TABLE 5 | The ROC analysis results of using ADC and the combinations of the FROC model parameters to differentiate low-grade tumor from high-grade tumor.

	ADC	$D + \beta$	$D + \mu$	$\beta + \mu$	$D + \beta + \mu$
Sensitivity	59.4%	71.9%	68.7%	59.4%	81.2%
Specificity	82.1%	89.3%	78.6%	75.0%	75.0%
Accuracy	70.0%	80.0%	73.3%	66.7%	78.3%
AUC*	0.673 (0.540–0.789)	0.807 (0.685–0.897)	0.711 (0.579–0.821)	0.672 (0.539–0.788)	0.829 (0.710–0.914)

ROC, receiver operating characteristic; ADC, apparent diffusion coefficient; FROC, fractional order calculus; AUC, are under the curve.
**Data in parenthesis are 95% confidence intervals.*

from the bi-exponential model were significantly different between tumor grades (26).

Compared to the conventional mono-exponential diffusion model that is limited to the single parameter ADC, the FROC model has the preponderance of the ability of combining multiple parameters, which greatly improved the diagnostic performance. This combination approach suggests that multiple tissue properties, namely, cellularity, microstructures, and heterogeneity, can complement each other and contribute to the diagnosis and prognosis of tumors simultaneously. In the present study, the combination of all the FROC parameters showed the best overall performance in grading the cervical carcinoma, producing the highest sensitivity (81.2%) and AUC (0.829). The $D + \beta$ showed the highest specificity (89.3%) and accuracy (80.0%). These multivariate analysis results further suggested that a noninvasive DWI-based classifier which reflected tumor grade of cervical carcinoma could be developed.

This study has several limitations. First, this is a single-site study with relatively small sample size and only 13 cases of ACA were included, which could reduce the accuracy of results. Further study with more patients would be needed. Second, due to the limited cases of ACA, we did not evaluate the tumor grade separately based on different tumor subtypes, which may lead to the potential bias and decrease the specificity of results. Third, rare histological subtypes, especially adenosquamous carcinoma, were excluded from this study. However, these rare tumor subtypes tend to have a poorer prognosis and remain difficulty in imaging diagnosis (36). Further investigation with more such cases should be conducted to validate this preliminary result and provide more robust support for clinical decision making. Finally, in order to take full advantage of the FROC model, b-values must be sufficiently high to accentuate non-Gaussian diffusion behaviors. Nevertheless, in this study, the maximal b-value was limited to 2,000 s/mm^2, and the higher b-values were more sparsely sampled than the lower b-values due to the efficiency considerations. The effect of the selection of b-value on the FROC model needs to be investigated in future study.

In conclusion, this study demonstrated the feasibility of using non-Gaussian diffusion FROC model to differentiate the tumor subtypes and histological grades of cervical carcinoma. In particular, the FROC model provided a set of novel diffusion parameters and the combination of these parameters contributed to the best diagnostic performance in differentiation between low-grade and high-grade cervical carcinoma. This advanced diffusion approach could be a noninvasive and *in vivo* diagnostic technique in cervical carcinoma, which is conducive to treatment decision and patient management.

DATA AVAILABILITY STATEMENT

The datasets generated for this study are available on request to the corresponding authors.

ETHICS STATEMENT

The studies involving human participants were reviewed and approved by The Fourth Hospital of Hebei Medical University. The patients/participants provided their written informed consent to participate in this study.

AUTHOR CONTRIBUTIONS

XS: Writing—original draft, Investigation. LA: Writing—original draft, Formal analysis. HL: Visualization, Data curation. HF: Resources, Data curation. LZ: Software, Validation. YD: Methodology. JZ: Writing—review & editing, Project administration. BY: Writing—review & editing, Supervision. All authors listed have made a substantial, direct, and intellectual contribution to the work and approved it for publication.

REFERENCES

1. de Juan A, Redondo A, Rubio M, García Y, Cueva J, Gaba L, et al. SEOM Clinical Guidelines for Cervical Cancer (2019). *Clin Trans Oncol* (2020) 22 (2):270–8. doi: 10.1007/s12094-019-02271-z
2. Hong J, Tsai C, Wang C, Lai C, Chen W, Lee S, et al. Comparison of Clinical Behaviors and Responses to Radiation Between Squamous Cell Carcinomas and Adenocarcinomas/Adenosquamous Carcinomas of the Cervix. *Chang Gung Med J* (2000) 23(7):396–404.
3. Moukarzel LA, Angarita AM, VandenBussche C, Rositch A, Thompson CB, Fader AN, et al. Preinvasive and Invasive Cervical Adenocarcinoma: Preceding Low-Risk or Negative Pap Result Increases Time to Diagnosis. *J Low Genit Tract Dis* (2017) 21(2):91. doi: 10.1097/LGT.0000000000000286
4. Fan A, Zhang L, Wang C, Wang Y, Han A, Xue F. Analysis of Clinical Factors Correlated With the Accuracy of Colposcopically Directed Biopsy. *Arch Gynecol Obstet* (2017) 296(5):965–72. doi: 10.1007/s00404-017-4500-z
5. Exner M, Kuehn A, Stumpp P, Hoeckel M, Horn L-C, Kahn T, et al. Value of Diffusion-Weighted MRI in Diagnosis of Uterine Cervical Cancer: A

Prospective Study Evaluating the Benefits of DWI Compared to Conventional MR Sequences in a 3T Environment. *Acta Radiol* (2016) 57(7):869–77. doi: 10.1177/0284185115602146
6. Kuang F, Ren J, Zhong Q, Liyuan F, Huan Y, Chen Z. The Value of Apparent Diffusion Coefficient in the Assessment of Cervical Cancer. *Eur Radiol* (2013) 23(4):1050–8. doi: 10.1007/s00330-012-2681-1
7. Karunya RJ, Tharani P, John S, Kumar RM, Das S. Role of Functional Magnetic Resonance Imaging Derived Parameters as Imaging Biomarkers and Correlation With Clinicopathological Features in Carcinoma of Uterine Cervix. *J Clin Diagn Res: JCDR* (2017) 11(8):XC06. doi: 10.7860/JCDR/2017/29165.10426
8. Kundu S, Chopra S, Verma S, Mahantshetty U, Engineer R, Shrivastava SK. Functional Magnetic Resonance Imaging in Cervical Cancer: Current Evidence and Future Directions. *J Cancer Res Ther* (2012) 8(1):11. doi: 10.4103/0973-1482.95167
9. Liu Y, Ye Z, Sun H, Bai R. Grading of Uterine Cervical Cancer by Using the ADC Difference Value and its Correlation With Microvascular Density and Vascular Endothelial Growth Factor. *Eur Radiol* (2013) 23(3):757–65. doi: 10.1007/s00330-012-2657-1
10. Tang L, Zhou XJ. Diffusion MRI of Cancer: From Low to High B-Values. *J Magn Reson Imaging* (2019) 49(1):23–40. doi: 10.1002/jmri.26293
11. Bickelhaupt S, Steudle F, Paech D, Mlynarska A, Kuder TA, Lederer W, et al. On a Fractional Order Calculus Model in Diffusion Weighted Breast Imaging to Differentiate Between Malignant and Benign Breast Lesions Detected on X-Ray Screening Mammography. *PloS One* (2017) 12(4):e0176077. doi: 10.1371/journal.pone.0176077
12. Chen J, Guo Y, Guo Y, Jiang M, Zhang Y, Dai Y, et al. Preoperative Assessment of Microvascular Invasion of Hepatocellular Carcinoma Using non-Gaussian Diffusion-Weighted Imaging With a Fractional Order Calculus Model: A Pilot Study. *Magn Reson Imaging* (2021). doi: 10.1016/j.mri.2021.09.003
13. Feng C, Wang Y, Dan G, Zhong Z, Karaman MM, Li Z, et al. Evaluation of a Fractional-Order Calculus Diffusion Model and Bi-Parametric VI-RADS for Staging and Grading Bladder Urothelial Carcinoma. *Eur Radiol* (2021) p:1–11. doi: 10.1007/s00330-021-08203-2
14. Tang L, Sui Y, Zhong Z, Damen FC, Li J, Shen L, et al. Non-Gaussian Diffusion Imaging With a Fractional Order Calculus Model to Predict Response of Gastrointestinal Stromal Tumor to Second-Line Sunitinib Therapy. *Magn Reson Med* (2018) 79(3):1399–406. doi: 10.1002/mrm.26798
15. Karaman MM, Tang L, Li Z, Sun Y, Li J-Z, Zhou XJ. In Vivo Assessment of Lauren Classification for Gastric Adenocarcinoma Using Diffusion MRI With a Fractional Order Calculus Model. *Eur Radiol* (2021) p:1–10. doi: 10.1007/s00330-021-07694-3
16. Liu G, Lu Y, Dai Y, Xue K, Yi Y, Xu J, et al. Comparison of Mono-Exponential, Bi-Exponential, Kurtosis, and Fractional-Order Calculus Models of Diffusion-Weighted Imaging in Characterizing Prostate Lesions in Transition Zone. *Abdom Radiol* (2021) 1–11. doi: 10.1007/s00261-020-02903-x
17. Zhou XJ, Gao Q, Abdullah O, Magin RL. Studies of Anomalous Diffusion in the Human Brain Using Fractional Order Calculus. *Magn Reson Med* (2010) 63(3):562–9. doi: 10.1002/mrm.22285
18. Magin RL, Abdullah O, Baleanu D, Zhou XJ. Anomalous Diffusion Expressed Through Fractional Order Differential Operators in the Bloch–Torrey Equation. *J Magn Reson* (2008) 190(2):255–70. doi: 10.1016/j.jmr.2007.11.007
19. Fedorov A, Beichel R, Kalpathy-Cramer J, Finet J, Fillion-Robin J-C, Pujol S, et al. 3D Slicer as an Image Computing Platform for the Quantitative Imaging Network. *Magn Reson Imaging* (2012) 30(9):1323–41. doi: 10.1016/j.mri.2012.05.001
20. McNeil BJ, Hanley JA. Statistical Approaches to the Analysis of Receiver Operating Characteristic (ROC) Curves. *Med Decis Making* (1984) 4(2):137–50. doi: 10.1177/0272989X8400400203
21. Hopkins MP, Morley GW. A Comparison of Adenocarcinoma and Squamous Cell Carcinoma of the Cervix. *Obstet Gynecol* (1991) 77(6):912–7. doi: 10.1016/0020-7292(92)90065-Q
22. Katanyoo K, Sanguanrungsirikul S, Manusirivithaya S. Comparison of Treatment Outcomes Between Squamous Cell Carcinoma and Adenocarcinoma in Locally Advanced Cervical Cancer. *Gynecol Oncol* (2012) 125(2):292–6. doi: 10.1016/j.ygyno.2012.01.034
23. Charles-Edwards EM, Messiou C, Morgan VA, De Silva SS, McWhinney NA, Katesmark M, et al. Diffusion-Weighted Imaging in Cervical Cancer With an Endovaginal Technique: Potential Value for Improving Tumor Detection in Stage Ia and Ib1 Disease. *Radiology* (2008) 249(2):541–50. doi: 10.1148/radiol.2491072165
24. Downey K, Attygalle AD, Morgan VA, Giles SL, MacDonald A, Davis M, et al. Comparison of Optimised Endovaginal vs External Array Coil T2-Weighted and Diffusion-Weighted Imaging Techniques for Detecting Suspected Early Stage (IA/IB1) Uterine Cervical Cancer. *Eur Radiol* (2016) 26(4):941–50. doi: 10.1007/s00330-015-3899-5
25. Wang M, Perucho JA, Tse KY, Chu MM, Ip P, Lee EY. MRI Texture Features Differentiate Clinicopathological Characteristics of Cervical Carcinoma. *Eur Radiol* (2020) 30(10):5384–91. doi: 10.1007/s00330-020-06913-7
26. Winfield JM, Orton MR, Collins DJ, Ind TE, Attygalle A, Hazell S, et al. Separation of Type and Grade in Cervical Tumours Using Non-Mono-Exponential Models of Diffusion-Weighted MRI. *Eur Radiol* (2017) 27 (2):627–36. doi: 10.1007/s00330-016-4417-0
27. Karaman MM, Wang H, Sui Y, Engelhard HH, Li Y, Zhou XJ. A Fractional Motion Diffusion Model for Grading Pediatric Brain Tumors. *NeuroImage: Clin* (2016) 12:707–14. doi: 10.1016/j.nicl.2016.10.003
28. Sui Y, Wang H, Liu G, Damen FW, Wanamaker C, Li Y, et al. Differentiation of Low-and High-Grade Pediatric Brain Tumors With High B-Value Diffusion-Weighted MR Imaging and a Fractional Order Calculus Model. *Radiology* (2015) 277(2):489–96. doi: 10.1148/radiol.2015142156
29. Wang M, Perucho JA, Chan Q, Sun J, Ip P, Tse KY, et al. Diffusion Kurtosis Imaging in the Assessment of Cervical Carcinoma. *Acad Radiol* (2020) 27(5): e94–e101. doi: 10.1016/j.acra.2019.06.022
30. Sui Y, Xiong Y, Jiang J, Karaman MM, Xie KL, Zhu W, et al. Differentiation of Low-and High-Grade Gliomas Using High B-Value Diffusion Imaging With a non-Gaussian Diffusion Model. *Am J Neuroradiol* (2016) 37(9):1643–9. doi: 10.3174/ajnr.A4836
31. Liu Y, Bai R, Sun H, Liu H, Wang D. Diffusion-Weighted Magnetic Resonance Imaging of Uterine Cervical Cancer. *J Comput Assisted Tomogr* (2009) 33 (6):858–62. doi: 10.1097/RCT.0b013e31819e93af
32. Liu Y, Ye Z, Sun H, Bai R. Clinical Application of Diffusion-Weighted Magnetic Resonance Imaging in Uterine Cervical Cancer. *Int J Gynecologic Cancer* (2015) 25(6):1073–8. doi: 10.1097/IGC.0000000000000472
33. Lin M, Yu X, Chen Y, Ouyang H, Wu B, Zheng D, et al. Contribution of Mono-Exponential, Bi-Exponential and Stretched Exponential Model-Based Diffusion-Weighted MR Imaging in the Diagnosis and Differentiation of Uterine Cervical Carcinoma. *Eur Radiol* (2017) 27(6):2400–10. doi: 10.1007/s00330-016-4596-8
34. Zhang Q, Yu X, Ouyang H, Zhang J, Chen S, Xie L, et al. Whole-Tumor Texture Model Based on Diffusion Kurtosis Imaging for Assessing Cervical Cancer: A Preliminary Study. *Eur Radiol* (2021) 1–10. doi: 10.1007/s00330-020-07612-z
35. Halle MK, Ojesina AI, Engerud H, Woie K, Tangen IL, Holst F, et al. Clinicopathologic and Molecular Markers in Cervical Carcinoma: A Prospective Cohort Study. *Am J Obstet Gynecol* (2017) 217(4):432.e1–432.e17. doi: 10.1016/j.ajog.2017.05.068
36. Farley JH, Hickey KW, Carlson JW, Rose GS, Kost ER, Harrison TA. Adenosquamous Histology Predicts a Poor Outcome for Patients With Advanced-Stage, But Not Early-Stage, Cervical Carcinoma. *Cancer: Interdiscip Int J Am Cancer Soc* (2003) 97(9):2196–202. doi: 10.1002/cncr.11371

Conflict of Interest: Authors LZ and YD were employed by United Imaging Healthcare.

The remaining authors declare that the research was conducted in the absence of any commercial or financial relationships that could be construed as a potential conflict of interest.

frontiers | Frontiers in Oncology

TYPE Original Research
PUBLISHED 05 August 2022
DOI 10.3389/fonc.2022.939930

OPEN ACCESS

EDITED BY
Alessio G. Morganti,
University of Bologna, Italy

REVIEWED BY
Tao Yu,
China Medical University, China
Komsun Suwannarurk,
Thammasat University, Thailand

*CORRESPONDENCE
Kunhua Wu
khcgz@sina.com

†These authors have contributed equally to this work and share first authorship

SPECIALTY SECTION
This article was submitted to Gynecological Oncology, a section of the journal Frontiers in Oncology

RECEIVED 09 May 2022
ACCEPTED 12 July 2022
PUBLISHED 05 August 2022

CITATION
Bi Q, Wang Y, Deng Y, Liu Y, Pan Y, Song Y, Wu Y and Wu K (2022) Different multiparametric MRI-based radiomics models for differentiating stage IA endometrial cancer from benign endometrial lesions: A multicenter study.
Front. Oncol. 12:939930.
doi: 10.3389/fonc.2022.939930

Different multiparametric MRI-based radiomics models for differentiating stage IA endometrial cancer from benign endometrial lesions: A multicenter study

Qiu Bi[1†], Yaoxin Wang[1†], Yuchen Deng[1], Yang Liu[2], Yuanrui Pan[3], Yang Song[4], Yunzhu Wu[4] and Kunhua Wu[1*]

[1]Department of MRI, The First People's Hospital of Yunnan Province, The Affiliated Hospital of Kunming University of Science and Technology, Kunming, China, [2]Department of Radiology, The First Affiliated Hospital of Chongqing Medical University, Chongqing, China, [3]State Key Laboratory of Ultrasound in Medicine and Engineering, College of Biomedical Engineering, Chongqing Medical University, Chongqing, China, [4]MR Scientific Marketing, Siemens Healthineers, Shanghai, China

Purpose: The aim of this study was to evaluate the value of different multiparametric MRI-based radiomics models in differentiating stage IA endometrial cancer (EC) from benign endometrial lesions.

Methods: The data of patients with endometrial lesions from two centers were collected. The radiomics features were extracted from T2-weighted imaging (T2WI), diffusion-weighted imaging (DWI), apparent diffusion coefficient (ADC) map, and late contrast-enhanced T1-weighted imaging (LCE-T1WI). After data dimension reduction and feature selection, nine machine learning algorithms were conducted to determine which was the optimal radiomics model for differential diagnosis. The univariate analyses and logistic regression (LR) were performed to reduce valueless clinical parameters and to develop the clinical model. A nomogram using the radscores combined with clinical parameters was developed. Two integrated models were obtained respectively by the ensemble strategy and stacking algorithm based on the clinical model and optimal radiomics model. The area under the curve (AUC), clinical decisive curve (CDC), net reclassification index (NRI), and integrated discrimination index (IDI) were used to evaluate the performance and clinical benefits of the models.

Results: A total of 371 patients were incorporated. The LR model was the optimal radiomics model with the highest average AUC (0.854) and accuracy (0.802) in the internal and external validation groups (AUC = 0.910 and 0.798, respectively), and outperformed the clinical model (AUC = 0.739 and 0.592, respectively) or the radiologist (AUC = 0.768 and 0.628, respectively). The nomogram (AUC = 0.917 and 0.802, respectively) achieved better discrimination performance than the optimal radiomics model in two validation groups. The stacking model (AUC = 0.915) and ensemble model

(AUC = 0.918) had a similar performance compared with the nomogram in the internal validation group, whereas the AUCs of the stacking model (AUC = 0.792) and ensemble model (AUC = 0.794) were lower than those of the nomogram and radiomics model in the external validation group. According to the CDC, NRI, and IDI, the optimal radiomics model, nomogram, stacking model, and ensemble model achieved good net benefits.

Conclusions: Multiparametric MRI-based radiomics models can non-invasively differentiate stage IA EC from benign endometrial lesions, and LR is the best machine learning algorithm. The nomogram presents excellent and stable diagnostic efficiency.

KEYWORDS

endometrial cancer, magnetic resonance imaging, radiomics, nomogram, benign endometrial lesions

Introduction

Endometrial cancer (EC) and endometrial hyperplasia and polyps are the most common malignant and benign uterine endometrial cavity lesions, respectively (1). In order to avoid insufficient curing or excessive treatment and to protect the patient's fertility, it is necessary to accurately identify benign and malignant endometrial lesions before operation. Although endometrial samplings such as dilatation and curettage, endometrial cytology, and biopsy can preoperatively identify some endometrial lesions (2), they do not always provide a definitive diagnosis. Because these procedures are often performed in a blind manner, they may be subject to sampling error and cannot properly diagnose focal endometrial lesions (3). Furthermore, they are difficult to perform in patients with pelvic organ prolapse and vaginal or cervical stenosis (4). In addition, endometrial sampling procedures are invasive with some complications including pain, discomfort, and bleeding. Hence, it is important to find a noninvasive method to distinguish benign and malignant uterine lesions.

Magnetic resonance imaging (MRI) with excellent soft tissue contrast resolution plays an important role in the preoperative diagnosis and staging of EC in situations where it is difficult to obtain histologic samples, and is more sensitive than transvaginal sonography for diagnosing endometrial lesions (1, 5). Multiparametric MRI, including T2-weighted imaging (T2WI), contrast-enhanced MRI (CE-MRI), diffusion-weighted imaging (DWI), and apparent diffusion coefficient (ADC) are increasingly being applied for diagnosing various endometrial lesions (1). However, conventional imaging evaluation of the uterine cavity lesions may present many challenges to the radiologist. The endometrium structure is susceptible to age, menopausal status, menstrual cycle, and hormonal replacement therapy (6). There are a variety of appearances and overlapping imaging features of early-stage EC and benign mimickers (7). Moreover, the experience of the radiologist usually contributes to high interobserver variation. All of these factors lead to inaccurate diagnoses.

Radiomics is an emerging field of application of artificial intelligence in medical imaging by extracting high-throughput quantitative image features and is a problem-solving tool when there is a dilemma in conventional imaging diagnosis (8). Recently, MRI-based radiomics has been gradually applied in the evaluation of EC including risk stratification (9–11), lymph node metastasis (12–14), myometrial invasion (15–17), prognosis and recurrence (18–20), and histological characteristics (21–23). Chen et al. (24) had confirmed that MRI-based radiomics was a valuable tool for distinguishing EC from benign mimics. However, they included stage IB to IV ECs that were easily distinguishable from benign uterine lesions, and only one machine learning algorithm model was studied. Therefore, this study aims to compare the performance of various multiparametric MRI-based machine learning radiomics models in differentiating stage IA EC from benign endometrial lesions, and further assess the potential utility of diverse integrated models utilizing clinical parameters and radiomics features.

Materials and methods

Study population

Ethical approval was obtained for this retrospective study, and written informed consent was waived. Between January 2017 and

June 2021, consecutive patients with endometrial lesions from center A and center B were collected. Inclusion criteria were as follows: (1) patients with stage IA EC, endometrial hyperplasia, or endometrial polyps confirmed by histopathology; (2) underwent MR examination including T2WI, DWI, and dynamic contrast-enhanced (DCE-MRI) within 2 weeks prior to treatment; and (3) complete clinical data. Exclusion criteria were as follows: (1) MRI quality did not meet the requirement of analysis; (2) received treatment before the MR examination; (3) the maximum diameter of the lesion was less than 1 cm; and (4) patients with other pelvic diseases. Patients from center A were randomly allocated into the training group and the internal validation group at a ratio of 3:1. All patients from center B served as the external validation group. Clinical and histological characteristics of all patients, including histological subtypes, age, menopause, clinical manifestation, metabolic syndrome, body mass index (BMI), actual treatment options, and CA125 and CA199 level, and immunohistochemical findings such as estrogen receptor (ER), progesterone receptor (PR), P53, and Ki-67 were collected.

Imaging acquisition and lesion segmentation

All MR examinations were performed using 1.5/3.0-T scanners (GE Signa HDXt, Siemens Prisma, and Siemens Aera) with eight-channel phased-array abdominal coils. Each patient underwent preoperative MR scanning using the standard protocol. In the study, uterus-axial T2WI, DWI (b-value = 1,000 s/mm^2), ADC map, and late contrast-enhanced T1-weighted imaging (LCE-T1WI) were acquired for lesion segmentation. Parameter details are shown in Table 1. Some parameters would be adjusted according to the individual differences of patients. The ADC map was automatically reconstructed and generated after scanning DWI by the Siemens MRI scanners, or manually reconstructed on the Functool Software (ADW 4.7 Workstation) by the GE MRI scanner. CE-T1WI was performed immediately after administering a standard dose (0.1 mmol/kg) of gadopentetate dimeglumine (Magnevist; Bayer Healthcare Pharmaceuticals, Germany) at approximately 2 ml/s *via* the elbow vein. Uterus-axial LCE-T1WI was obtained at 240 s into the examination after the contrast agent injection.

The original MR images of uterus-axial T2WI, DWI, ADC map, and LCE-T1WI in Digital Imaging and Communications in Medicine (DICOM) format were loaded into 3D Slicer 4.11.0 software (https://www.slicer.org/). Region of interest (ROI) of the lesion was manually delineated layer by layer to form three-dimensional (3D) volume of interest (VOI) by two radiologists (reader 1 and reader 2, with 3 years and 7 years of experience in pelvic MRI, respectively), with unknown clinical information and pathological diagnosis. Reader 1 delineated the boundary of all lesions on uterus-axial T2WI, DWI, and LCE-T1WI, respectively. After 2 months, reader 1 and reader 2 randomly selected the same 50 patients to outline. Care was taken to avoid including endometrial cavity fluid and hematocele and nearby normal myometrium, but necrotic, bleeding, and cystic areas inside the tumor can be included.

Feature extraction and selection

The open-source Python package Pyradiomics (https://pypi.org/project/pyradiomics/) was used to extract radiomics features from the VOI of each patient at the 3D Slicer platform. To obtain isotropic voxels, the VOIs were resampled to 3 × 3 × 3 mm, then cubic spline interpolation was performed. In order to reduce the imaging differences among different MRI scanners, image normalization was performed so that all gray-level values in the images were distributed in the range of 0–600. A fixed bin width of 1 was selected to ensure better comparability of MRI

TABLE 1 The parameter details of primary sequences.

		Repetition time (ms)	Echo time (ms)	Field of view (mm^2)	Matrix	Slice thickness (mm)	Slice gap (mm)
Siemens Prisma 3.0 T	T2WI	3,200	90	200 × 200	320 × 320	3	3.6
	DWI	6,300	75	250 × 134	72 × 134	3	3.6
	LCE-T1WI	2.9	1.19	220 × 200	288 × 262	3	0
GE Signa HDXt 3.0T	T2WI	3,500	104	200 × 200	240 × 240	3	1.5
	DWI	4,250	70	200 × 200	240 × 240	3	1
	LCE-T1WI	3.26	1.6	240 × 240	350 × 350	3	1.5
Siemens Aera 1.5 T	T2WI	3,900	90	320 × 320	512 × 512	3	1.5
	DWI	5,600	90	200 × 200	256 × 256	4	1
	LCE-T1WI	3.41	1.3	240 × 240	320 × 320	2	1.5

T2WI, T2-weighted imaging; DWI, diffusion-weighted imaging; LCE-T1WI, late contrast-enhanced T1-weighted imaging.

gray values as suggested in a previous study (12). Before feature extraction, several built-in filters such as gradient, exponent, logarithm, square, square root, wavelet, and Laplacian of Gaussian (LOG) filters were applied on the normalized MR images, and derived images were achieved. The extracted features were divided into the following categories (25): first-order features, two-dimensional features, gray-level co-occurrence matrix (GLCM), gray-level dependence matrix (GLDM), gray-level size-zone matrix (GLSZM), gray-level run-length matrix (GLRLM), and neighboring gray tone difference matrix (NGTDM). A total of 1,781 radiomics features were extracted from each MRI modality, resulting in 7,124 radiomics features for each patient in total. All the above features were standardized by the *Z* score.

The datasets of the patients with stage IA EC and benign endometrial lesions were balanced by using the synthetic minority oversampling technique in the training group. To ensure repeatability and avoid the subjective difference in lesion segmentation, the intraclass correlation coefficient (ICC) of each feature was calculated. Only features with ICC values ≥ 0.75 between observers and within observers were retained. Pearson correlation coefficients were calculated for identifying redundant features. If the correlation coefficient of two features was ≥ 0.9, the feature with the largest mean absolute correlation was deleted. Whereafter, least absolute shrinkage and selection operator (LASSO) was used to select the most representative features and 10-fold cross-validation was performed (26).

Model building

On the construction of the clinical model, firstly, univariate analysis was conducted to compare the clinical characteristics of benign and malignant endometrial lesions in the training group, and find out the clinical parameters with statistically significant difference. Secondly, the individual predictors of stage IA EC were chosen according to the univariate logistic regression (LR) analysis. Finally, the clinical model was constructed based on the multivariate LR, and the efficient clinical predictive parameters were selected.

Different radiomics models were developed and tested respectively to predict stage IA endometrial cancer based on the following nine machine learning classification algorithms: LR, support vector machine (SVM), stochastic gradient descent (SGD), K nearest neighbor (KNN), decision tree (DT), random forest (RF), extremely randomized trees (ET), eXtreme Gradient Boosting (XGBoost), and Light Gradient Boosting Machine (LightGBM). A fivefold cross-validation strategy was applied to tune and optimize the model parameter, and assess the performance of the models. Referring to a recently published study (27), the machine learning algorithm with the highest average area under the receiver operating characteristic (ROC) curve (AUC) of the internal and external validation group was used to construct the optimal radiomics model. Then, the radiomics score (radscore) was calculated. A nomogram based on the multivariate LR analysis was developed by using the combination of clinical predictive parameters and radscore in the training group.

The stacking model is an integrated learning technology, which can combine the predictions of learned classifiers in order to create prediction of new instances to improve overall performance (28). In the study, a two-tier stacking model was conducted; the first tier was the above clinical model and the optimal radiomics model, and the second tier used the output of the first tier as the input of the multivariate LR. The ensemble algorithm is developed using superlearner (29), and belongs to an integrated strategy. According to the accuracy weight, the predictions obtained from the foregoing clinical model and radiomics model were calculated by the weighted average method and the new output as the final results.

Through the nomogram, stacking model, or ensemble model, the clinical and radiomics features were combined, so as to achieve model fusion. All model building was implemented in Python (https://www.python.org/getit/), and the detailed process of model building is shown in Figure 1. The AUC, accuracy, sensitivity, specificity, and calibration curve were used as metrics to assess the performance and goodness of fit of the models.

Clinical application of the models

One radiologist (reader 3, with 30 years of experience in pelvic MRI) who was blind to the clinicopathological information of the patient independently reviewed the MR images to diagnose stage IA EC and benign uterine disease in the training and validation groups. The AUC, accuracy, sensitivity, and specificity of the radiologist were calculated. Clinical decisive curve (CDC), net reclassification index (NRI), and integrated discrimination index (IDI) were performed to estimate the clinical usefulness and net benefit of different models and the radiologist by comparing the actual treatment options of patients.

Correlations between radiomics features and immunohistochemical findings

In order to explore the correlation between radiomics information and histological characteristics, Spearman correlation coefficients were used to evaluate the correlations between the selected radiomics features and immunohistochemical findings.

Statistical analysis

All statistical tests were performed using SPSS 26.0 (IBM, New York, USA), R software 4.1.2 (https://www.r-project.org/),

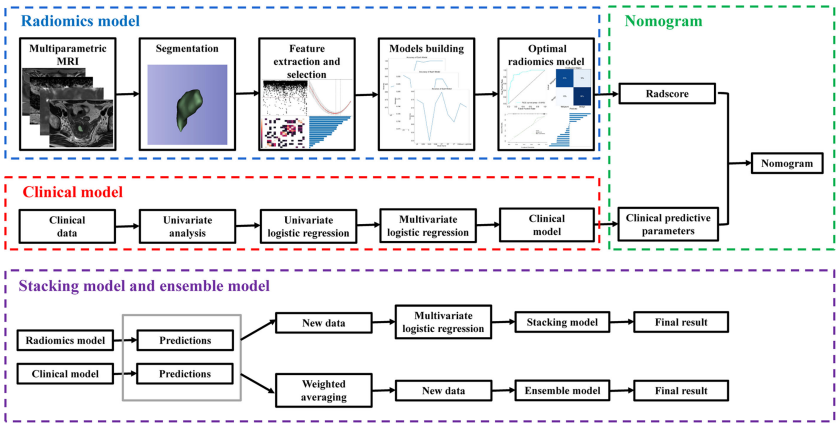

FIGURE 1
The overall workflow of this study.

and Python 3.9.7 (https://www.python.org/). Continuous variables and categorical variables were respectively expressed as mean value ± standard deviation and counts. The Kolmogorov–Smirnov test was used to check the normality of the continuous data distribution. Continuous variables were analyzed using one-way ANOVA, Mann–Whitney *U* test, or Kruskal–Wallis test. Categorical variables were compared using the Chi-square test or Fisher's exact test. Univariate and multivariate LR analyses were used to filtrate the clinical predictors and model building. A *p*-value less than 0.05 was considered statistically significant. Pearson correlation analyses were performed to assess correlations between continuous variables, and Spearman correlation analyses were used to evaluate the correlations between continuous variables and ranked data. If $p < 0.05$, there were correlations between the variables.

Results

Clinical parameters

A total of 371 patients were divided into the training group (245 patients from center A), the internal validation group (82 patients from center A), and the external validation group (44 patients from centers B). The clinicopathological characteristics of incorporated patients are listed in Table 2. The 371 patients included 234 patients with stage IA EC and 137 patients with benign endometrial lesions. Three hundred and twenty patients were treated following the protocol for EC and 51 patients for benign endometrial disease. A total of 112 (30.2%) patients received inappropriate treatment, including 13 (3.5%) patients with stage IA EC who were undertreated and 99 (26.7%) patients with benign endometrial lesions who were overtreated. Univariate analysis showed that the mean age of patients with stage IA EC (51.65 ± 7.94) was significantly older than that of patients with benign uterine lesions (48.12 ± 8.35) in the training group ($p = 0.001$). Compared with benign endometrial lesions, there were more patients with irregular vaginal bleeding and menopause in stage IA EC ($p < 0.05$). No significant differences in metabolic syndrome, BMI, CA125, and CA199 between patients with stage IA EC and benign endometrial lesions were shown ($p > 0.05$). According to the univariate and multivariate LR analysis, age and irregular vaginal bleeding were the valid predictive parameters.

Feature selection and optimal machine learning algorithm

Among all the extracted features, 3,356 features were excluded because the ICC values between observers or within observers were <0.75. There were 847 features retained after the Pearson correlation analysis. Finally, the LASSO classifier selected 18 features as shown in Figure 2.

The AUC and accuracy of radiomics models constructed by nine machine learning algorithms are shown in Table 3, and the broken line graphs of accuracy for different algorithms in the training group, internal validation group, and external validation group are presented in Figures 3A–C. The LR algorithm showed the highest average AUC (0.854) in the validation groups, and also had the highest average accuracy (0.802). Therefore, LR was considered to be the optimal machine learning algorithm for radiomics model building. The radscore was calculated based on the coefficients and intercepts obtained from the LR model. The selected features and weights are shown in Figure 3D. The top four features that contribute most to the radiomics model were CE_original_shape_flatness, T2_exponential_GLSZM_zone

TABLE 2 Clinical and histological characteristics for patients.

	Training group	Internal validation group	External validation group	*p*
Total number	245	82	44	
Patients				
Stage IA endometrial cancer	155	53	26	0.824
Benign endometrial lesions	90	29	18	
Histological subtypes				
Endometrioid adenocarcinoma	155	53	26	0.673
Endometrial hyperplasia	60	21	13	
Endometrial polyp	17	5	5	
Endometrial hyperplasia+polyp	13	3	0	
Age at diagnosis (years)	50.36 ± 8.26	50.52 ± 9.80	54.32 ± 9.34	0.136
Menopause (yes/no)	106/139	33/49	24/20	0.286
Irregular vaginal bleeding (yes/no)	135/110	34/48	36/8	<0.001
Metabolic syndrome (yes/no)	66/179	17/65	13/31	0.468
BMI (kg/m^2)	25.11 ± 4.38	24.44 ± 3.54	24.80 ± 4.03	0.485
CA125 (U/ml)	37.29 ± 72.77	34.63 ± 64.67	29.52 ± 27.10	0.292
CA199 (U/ml)	23.86 ± 63.44	26.53 ± 46.34	28.39 ± 45.58	0.037

BMI, body mass index.

percentage, DWI_LOG-sigma-6-0-mm-3D_first order_root mean squared, and ADC_LOG-sigma-2-0-mm-3D_first order_median, respectively.

Performance and clinical application of different models

A nomogram was constructed by using the clinical predictive parameters (age and irregular vaginal bleeding) and the radscore (Figure 3E). The diagnostic performance of each model and radiologist is displayed in Table 4. Figure 4 shows ROC curves and calibration curves of different models. In the training group, the AUCs of the clinical model, radiomics model, nomogram, stacking model, ensemble model, and radiologist were 0.760, 0.921, 0.922, 0.925, 0.916, and 0.769, respectively. In the internal validation group, they were 0.739, 0.910, 0.917, 0.915, 0.918, and 0.768, respectively. In the external validation group, they were 0.592, 0.798, 0.802, 0.792, 0.794, and 0.628, respectively. According to the calibration curves, the Brier scores of the clinical model, radiomics model, nomogram, stacking model, and ensemble model were 0.200, 0.114, 0.114, 0.113, and 0.129, respectively in the training group. They were 0.206, 0.123, 0.118, 0.119, and 0.129, respectively, in the internal validation

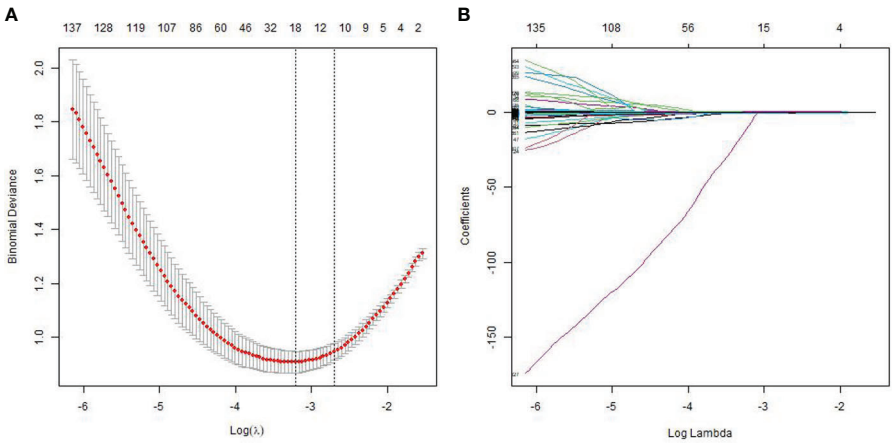

FIGURE 2
Feature selection using the least absolute shrinkage and selection operator (LASSO) regression model. The cross-validation plot **(A)** and the coefficient profile plot **(B)**.

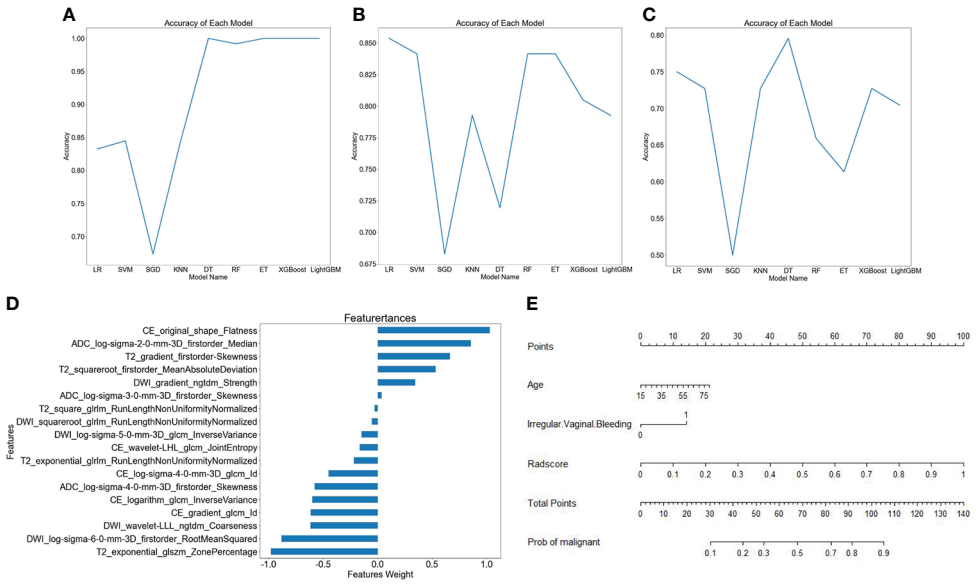

FIGURE 3
Different model building. Broken line graphs of accuracy for different machine learning algorithms in the training group **(A)**, the internal validation group **(B)**, and the external validation group **(C)**. Bar chart of feature weight for the logistic regression model **(D)**. Nomogram of the training group **(E)**.

group, and they were 0.274, 0.188, 0.184, 0.182, and 0.184, respectively, in the external validation group. The radiomics model, nomogram, stacking model, and ensemble model demonstrated good goodness of fit due to their Brier scores being <0.25.

The CDCs of the different models and the radiologist are presented in Figure 5, and the NRI and IDI are shown in Table 3. The results showed that the radiomics model, nomogram, stacking model, and ensemble model for predicting stage IA EC added benefit and performed better than the actual treatment options in the training and validation groups ($p < 0.05$). In the training group, the NRI and IDI of the clinical model, radiomics model, nomogram, stacking model, ensemble model, and radiologist were 0.130 and 0.023, 0.414 and 0.393, 0.429 and 0.396, 0.451 and 0.498, 0.410 and 0.397, and 0.319 and 0.242, respectively. In the internal validation group, they were −0.163 and −0.034, 0.307 and 0.341, 0.395 and 0.362, 0.395 and 0.356, 0.395 and 0.366, and 0.216 and 0.137, respectively. In the external validation group, they were −0.068 and −0.004, 0.423 and 0.272, 0.368 and 0.234, 0.423 and 0.255, 0.368 and 0.241, and 0.188 and 0.099, respectively.

TABLE 3 The performance of various machine learning algorithms.

	Training group		Internal validation group		External validation group		Validation groups	
	AUC	Accuracy	AUC	Accuracy	AUC	Accuracy	Average AUC	Average Accuracy
LR	0.921	0.832	0.910	0.853	0.798	0.750	0.854	0.802
SVM	0.919	0.844	0.902	0.841	0.796	0.727	0.804	0.784
SGD	0.887	0.804	0.854	0.792	0.705	0.636	0.780	0.714
KNN	0.923	0.844	0.881	0.792	0.757	0.727	0.819	0.760
DT	1	1	0.720	0.719	0.795	0.795	0.758	0.757
RF	1	0.991	0.867	0.841	0.700	0.659	0.784	0.750
ET	1	1	0.905	0.841	0.675	0.613	0.790	0.727
XGBoost	1	1	0.889	0.804	0.813	0.727	0.851	0.766
LightGBM	1	1	0.884	0.792	0.795	0.704	0.840	0.748

AUC, area under the curve; LR, logistic regression; SVM, support vector machine; SGD, stochastic gradient descent; KNN, K nearest neighbor; DT, decision tree; RF, random forest; ET, extremely randomized trees; XGBoost, eXtreme Gradient Boosting; LightGBM, Light Gradient Boosting Machine.

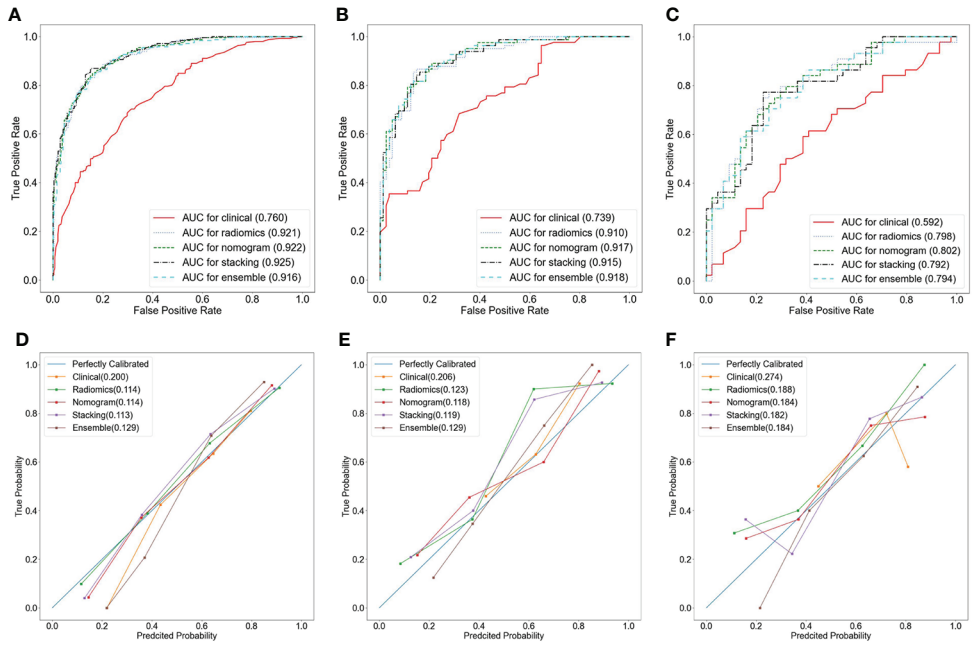

FIGURE 4
Receiver operator characteristic (ROC) curves **(A–C)** and calibration curves **(D–F)** of different models in the training group **(A, D)**, the internal validation group **(B, E)**, and the external validation group **(C, F)**.

Correlations between radiomics features and immunohistochemical findings

A heatmap (Figure 6) showed that the selected radiomics features were not correlated with immunohistochemical findings (ER, PR, P53, and Ki-67) (all $p > 0.05$). The selected sequences for lesion segmentation and pathological and immunohistochemical pictures are presented in Figure 7.

Discussion

In the study, age and irregular vaginal bleeding were the valid predictive parameters in the clinical model. On the basis of several common machine learning algorithms, the diverse multiparametric MRI-based radiomics models were developed to differentiate stage IA EC from benign endometrial lesions, and the LR algorithm model was selected as the optimal radiomics

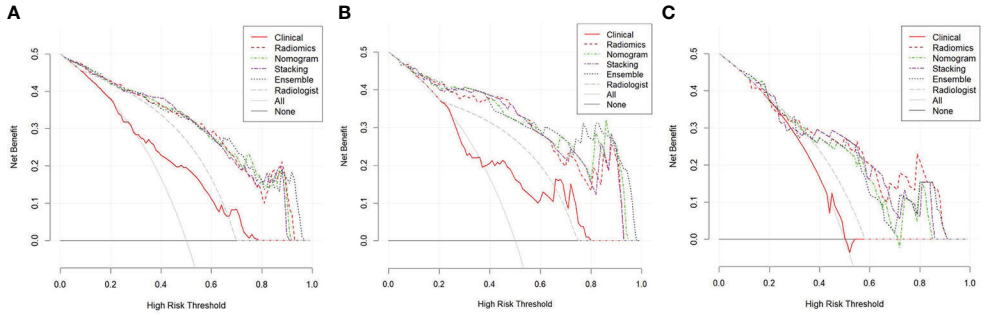

FIGURE 5
Clinical decision curves (CDCs) of different models and the radiologist in the training group **(A)**, the internal validation group **(B)**, and the external validation group **(C)**.

model with the highest AUC and accuracy. Compared with the clinical model and the radiologist, the optimal radiomics model and the compositive models combining clinical parameters with radiomics features, like the nomogram, stacking model, and ensemble model, showed better diagnostic performance and achieved good clinical net benefits. The nomogram had a higher AUC than the optimal radiomics model, and revealed more stable discrimination efficiency and better generalization ability than stacking and ensemble models.

The standard surgery of early-stage EC is total hysterectomy with bilateral salpingo-oophorectomy with or without lymphadenectomy/radiotherapy/chemotherapy (30), while the treatment for benign endometrial lesions is a minimally invasive approach compared to hysterectomy, such as hysteroscopic resection or conservative treatment (31, 32). In this study, 3.5% of patients with stage IA EC had undergone inadequate surgery and 26.7% of patients with benign endometrial lesions had undergone overtreatment. As a consequence, the rationalization of treatment options is crucial for patients with stage IA EC and benign mimickers. The most common symptom of EC is irregular vaginal bleeding, which often occurs in the early stage, and the American Cancer Society recommended that all women older than 65 years should be advised to seek risk evaluation of EC if bleeding occurs (33). Therefore, age and irregular vaginal bleeding could be used as effective clinical predictors of stage IA EC. Benign endometrial lesions, such as endometrial hyperplasia and polyps, are highly prevalent in postmenopausal women; symptoms include abnormal uterine bleeding (31, 32). Due to the overlapping clinical features of benign endometrial lesions and EC, the AUC and the diagnostic accuracy of clinical model on the training group and validation groups were low.

In radiomics, the digital medical images that hold information of tumor pathophysiology are transformed into quantitative high-dimensional data to improve medical decision-making, and are gaining importance in cancer research (8). In this study, the radiomics models had high diagnostic performance, which was consistent with the research of Chen et al. (24). The models with high efficiency and reliability are fundamental factors driving the success of radiomics (34), and the recognition of optimal machine learning methods for radiomics models is crucial (35); thus, multiple machine learning algorithms should be employed. We trained nine common classification algorithms, namely, LR, SVM, SGD, KNN, DT, RF, ET, XGBoost, and LightGBM, in model establishment. LR performed best among all classifiers, and the reason might be that complex models required more training samples (36). The optimal radiomics model modeled by LR had higher AUCs and diagnostic accuracies than those of the clinical model and the radiologist in this study. This result further confirmed that radiomics could be a problem-solving tool when there is a dilemma in clinical diagnosis and the observation of conventional imaging (8).

Unlike the study of Chen et al. (24), CE-MRI was included and extracted features in our study. The top four vital features in the optimal radiomics model were from CE-MRI, T2WI, DWI, and the ADC map, respectively. Due to the differences in vascular permeability and microvessel density between EC and benign lesions, most ECs showed early maximal enhancement and late gradual washout, and frequently showed lower signal

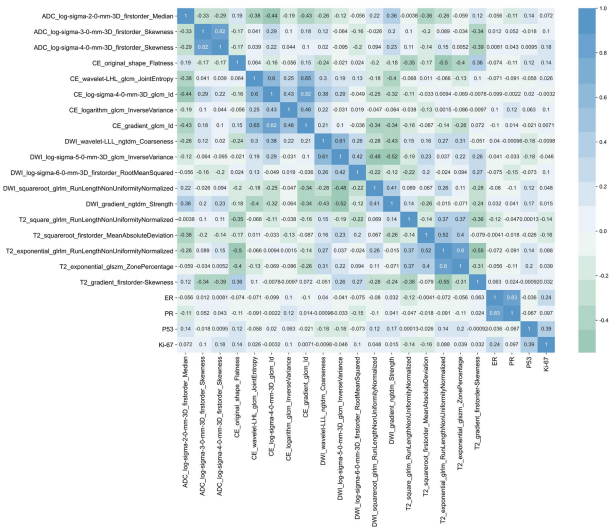

FIGURE 6
Heatmap of the correlations between the selected radiomics features and ER, PR, P53, and Ki-67.

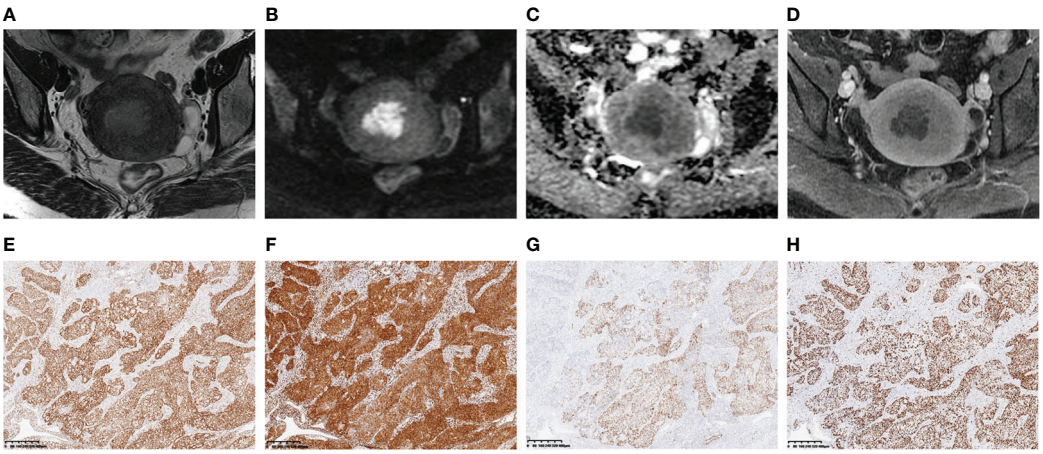

FIGURE 7
A 46-year-old woman with stage IA endometrial cancer (EC) whose main clinical complication was irregular vaginal bleeding for 3 months. The selected MR images for lesion segmentation included uterus-axial T2-weighted imaging (T2WI) **(A)**, diffusion-weighted imaging (DWI) **(B)**, apparent diffusion coefficient (ADC) map **(C)**, and late contrast-enhanced T1-weighted imaging (LCE-T1WI) **(D)**. The estrogen receptor (ER) **(E)**, progesterone receptor (PR) **(F)**, P53 **(G)**, and Ki-67 **(H)** immunohistochemical staining (40×) showed 90%, 90%, focal, and 80% positive cells, respectively.

intensity than the myometrium on LCE-MRI. In contrast, benign lesions showed delayed persistent enhancement pattern, and tended to show higher signal intensity than the myometrium on LCE-MRI (37). The shape of benign and malignant endometrial lesions might be more clearly shown on LCE-MRI. Flatness shows the relationship between the largest and smallest principal components in the ROI shape (8). In consequence, CE_original_shape_flatness was the most contributing feature. Endometrial polyp and hyperplasia are rich in fibrous stromal structures and endometrial glands (1). Specific MRI findings such as a fibrous tissue (hypointensity on T2WI) and intratumoral cysts (hyperintensity on T2WI) might be useful to differentiate benign endometrial lesions from EC (1). Additionally, the zone percentage of GLSZM features

TABLE 4 Diagnostic efficiency and clinical benefit of different models.

	Models	AUC	Accuracy	Sensitivity	Specificity	NRI (*p*)	IDI (*p*)
Training group	Clinical model	0.760	0.694	0.690	0.700	0.130 (0.082)	0.023 (<0.001)
	Radiomics model	0.921	0.833	0.838	0.833	0.414 (<0.001)	0.393 (<0.001)
	Nomogram	0.922	0.841	0.877	0.800	0.429 (<0.001)	0.396 (<0.001)
	Stacking model	0.925	0.853	0.903	0.800	0.451 (<0.001)	0.498 (<0.001)
	Ensemble model	0.916	0.837	0.832	0.833	0.410 (<0.001)	0.397 (<0.001)
	Radiologist	0.769	0.816	0.948	0.589	0.319 (<0.001)	0.242 (<0.001)
Internal validation group	Clinical model	0.739	0.683	0.528	0.896	−0.163 (0.251)	−0.034 (0.523)
	Radiomics model	0.910	0.854	0.868	0.862	0.307 (0.011)	0.341 (<0.001)
	Nomogram	0.917	0.817	0.887	0.827	0.395 (0.001)	0.362 (<0.001)
	Stacking model	0.915	0.841	0.887	0.828	0.395 (0.001)	0.356 (<0.001)
	Ensemble model	0.918	0.817	0.887	0.828	0.395 (0.001)	0.366 (<0.001)
	Radiologist	0.768	0.780	0.811	0.724	0.216 (0.065)	0.137 (0.018)
External validation group	Clinical model	0.592	0.591	0.500	0.611	−0.068 (0.572)	−0.004 (0.780)
	Radiomics model	0.798	0.750	0.731	0.833	0.423 (0.024)	0.272 (<0.001)
	Nomogram	0.802	0.727	0.731	0.778	0.368 (0.049)	0.234 (0.001)
	Stacking model	0.792	0.773	0.769	0.778	0.423 (0.024)	0.255 (<0.001)
	Ensemble model	0.794	0.705	0.769	0.778	0.368 (0.049)	0.241 (0.001)
	Radiologist	0.628	0.682	0.923	0.333	0.188 (0.220)	0.099 (0.054)

AUC, area under the curve; NRI, net reclassification index; IDI, integrated discrimination index.

represents the coarseness of the texture, and can better reflect the heterogeneity of different tumors (8). Thus T2_exponential_GLSZM_zone percentage was also an important feature. A previous study had suggested that DWI with ADC values were a potential quantitative and qualitative tool for differentiating between early-stage EC and benign mimickers (38). On DWI, benign endometrial lesions showed low signal intensity, which was an important point in differentiating them from EC that showed high signal intensity due to relatively high cellularity (39). Nevertheless, the top two important features were not derived from DWI and the ADC map in this study. The possible reason was that DWI was acquired in different scanners, which might lead to inconsistency in image quality and ADC estimation across vendors, although the models remained effective after cross-validation in datasets from scanners with different manufacturers or with different Tesla. Another possible reason was that benign uterine lesions rich in cystic areas and mucus might increase DWI signal intensity due to the influence of the T2-penetration effect, and hemorrhagic areas and mucous components could reduce the signal intensity of the ADC map, which would lead to a slight difference between DWI and ADC maps of benign and malignant endometrial lesions, thus resulting in the reduction of the weight of their features.

Gatenby et al. (40) believed that radiomics features could offer information on the phenotype and microenvironment of tumors, which was complementary to other data like clinical parameters. Radiomics features combined with clinical parameters and other pertinent data can produce accurate robust evidence-based clinical-decision support systems (8). In this study, according to ROCs, CDCs, NRI, and IDI, the compositive models modeled by clinical parameters and radiomics features, such as the nomogram, stacking, and ensemble models, showed better diagnostic performance and achieved better clinical net benefits than the clinical model and the radiologist. Compared with the radiomics model, the nomogram had a higher AUC. Yan et al. (11) developed an MRI- and clinical-based radiomics nomogram to preoperatively assess high-risk EC, and obtained a similar result to this study, which was the prediction efficiency of nomogram was better than that of the radiomics model. The advantage of the ensemble strategy was that it can reduce the variance and bias of the model by a powerful process of majority vote or group averaging, and it improves the robustness and generalizability of the model in prediction and classification (27). A recent study had confirmed that the two-tier stacking model could further improve the generalization ability of the radiomics model compared with the single model (41). In the present study, the diagnostic performance of the stacking model and ensemble model was similar with that of the nomogram and better than that of the radiomics model in the internal validation group, whereas the AUCs of the stacking model and ensemble model were lower than those of the nomogram and radiomics model in the external validation group. Therefore, the nomogram presented more excellent and stable differential diagnostic efficiency than stacking and ensemble models with good reproducibility and reliability.

There were some limitations in the study. First, this study only collected patients from two centers. Patients from more centers need to be included to improve the universality of the model in clinical application. Second, the MRI systems and scanning parameters were not uniform, and it may influence the models' results, especially in the external validation group. Third, only traditional radiomics features were extracted; the deep-learning-based features were not investigated. In the future, we will conduct in-depth learning combined with traditional radiomics to build models. Last, manual lesion segmentation is time-consuming and is easily affected by the experience of readers; automatic or semiautomatic methods that delineate lesions more accurately need to be explored in the future.

Conclusions

The multiparametric MRI-based radiomics models can be conveniently used for preoperative identification of patients with stage IA EC and benign endometrial lesions, and the model established by the LR algorithm has the highest accuracy. Incorporating radiomics and clinical parameters (age and irregular vaginal bleeding) into a combined model to estimate patients was more accurate than the clinical model and the radiologist. This study is beneficial in noninvasively identifying benign and malignant endometrial lesions that are difficult to determine by clinicians and radiologists before surgery, avoiding misdiagnosis and missed diagnosis, and providing a basis for the patient protocol of individualized diagnosis and treatment.

Data availability statement

The raw data supporting the conclusions of this article will be made available by the authors, without undue reservation.

Ethics statement

The studies involving human participants were reviewed and approved by Medical Ethics review committee of the First People's Hospital of Yunnan Province. Written informed consent for participation was not required for this study in accordance with the national legislation and the institutional requirements.

Author contributions

QB designed the study, performed the statistical analysis, and wrote the manuscript. YXW collected the data and performed the statistical analysis. YD, YL, and YP collected the data. YS and YZW revised the manuscript. KW guaranteed the integrity of the entire study. All authors approved the submitted version of the manuscript.

Acknowledgments

We sincerely thank Programmer Guanghong Yang and Platform Onekey AI for Code consultation of the study.

Conflict of interest

Authors YS and YW were employed by Siemens Healthineers.

The remaining authors declare that the research was conducted in the absence of any commercial or financial relationships that could be construed as a potential conflict of interest.

Publisher's note

References

1. Lee Y, Kim KA, Song MJ, Park YS, Lee J, Choi JW, et al. Multiparametric magnetic resonance imaging of endometrial polypoid lesions. *Abdom Radiol (NY)* (2020) 45(11):3869–81. doi: 10.1007/s00261-020-02567-7

2. Koh WJ, Abu-Rustum NR, Bean S, Bradley K, Campos SM, Cho KR, et al. Uterine neoplasms, version 1.2018, NCCN clinical practice guidelines in oncology. *J Natl Compr Canc Netw* (2018) 16(2):170–99. doi: 10.6004/jnccn.2018.0006

3. Svirsky R, Smorgick N, Rozowski U, Sagiv R, Feingold M, Halperin R, et al. Can we rely on blind endometrial biopsy for detection of focal intrauterine pathology? *Am J Obstet Gynecol* (2008) 199(2):111–5. doi: 10.1016/j.ajog.2008.02.015

4. Narice BF, Delaney B, Dickson JM. Endometrial sampling in low-risk patients with abnormal uterine bleeding: A systematic review and meta-synthesis. *BMC Fam Pract* (2018) 19(1):135. doi: 10.1186/s12875-018-0817-3

5. Bi Q, Chen Y, Wu K, Wang J, Zhao Y, Wang B, et al. The diagnostic value of MRI for preoperative staging in patients with endometrial cancer: A meta-analysis. *Acad Radiol* (2020) 27(7):960–8. doi: 10.1016/j.acra.2019.09.018

6. Nalaboff KM, Pellerito JS, Ben-Levi E. Imaging the endometrium: Disease and normal variants. *Radiographics* (2001) 21(6):1409–24. doi: 10.1148/radiographics.21.6.g01nv211409

7. Kierans AS, Bennett GL, Haghighi M, Rosenkrantz AB. Utility of conventional and diffusion-weighted MRI features in distinguishing benign from malignant endometrial lesions. *Eur J Radiol* (2014) 83(4):726–32. doi: 10.1016/j.ejrad.2013.11.030

8. Lambin P, Leijenaar R, Deist TM, Peerlings J, de Jong E, van Timmeren J, et al. Radiomics: The bridge between medical imaging and personalized medicine. *Nat Rev Clin Oncol* (2017) 14(12):749–62. doi: 10.1038/nrclinonc.2017.141

9. Zhang K, Zhang Y, Fang X, Fang M, Shi B, Dong J, et al. Nomograms of combining apparent diffusion coefficient value and radiomics for preoperative risk evaluation in endometrial carcinoma. *Front Oncol* (2021) 11:705456. doi: 10.3389/fonc.2021.705456

10. Chen J, Gu H, Fan W, Wang Y, Chen S, Chen X, et al. MRI-Based radiomic model for preoperative risk stratification in stage I endometrial cancer. *J Cancer* (2021) 12(3):726–34. doi: 10.7150/jca.50872

11. Yan BC, Li Y, Ma FH, Feng F, Sun MH, Lin GW, et al. Preoperative assessment for high-risk endometrial cancer by developing an MRI- and clinical-based radiomics nomogram: A multicenter study. *J Magn Reson Imaging* (2020) 52(6):1872–82. doi: 10.1002/jmri.27289

12. Yan BC, Li Y, Ma FH, Zhang GF, Feng F, Sun MH, et al. Radiologists with MRI-based radiomics aids to predict the pelvic lymph node metastasis in endometrial cancer: A multicenter study. *Eur Radiol* (2021) 31(1):411–22. doi: 10.1007/s00330-020-07099-8

13. Yang LY, Siow TY, Lin YC, Wu RC, Lu HY, Chiang HJ, et al. Computer-aided segmentation and machine learning of integrated clinical and diffusion-weighted imaging parameters for predicting lymph node metastasis in endometrial cancer. *Cancers (Basel)* (2021) 13(6):1406. doi: 10.3390/cancers13061406

14. Xu X, Li H, Wang S, Fang M, Zhong L, Fan W, et al. Multiplanar MRI-based predictive model for preoperative assessment of lymph node metastasis in endometrial cancer. *Front Oncol* (2019) 9:1007. doi: 10.3389/fonc.2019.01007

15. Zhu X, Ying J, Yang H, Fu L, Li B, Jiang B. Detection of deep myometrial invasion in endometrial cancer MR imaging based on multi-feature fusion and probabilistic support vector machine ensemble. *Comput Biol Med* (2021) 134:104487. doi: 10.1016/j.compbiomed.2021.104487

16. Rodriguez-Ortega A, Alegre A, Lago V, Carot-Sierra JM, Ten-Esteve A, Montoliu G, et al. Machine learning-based integration of prognostic magnetic resonance imaging biomarkers for myometrial invasion stratification in endometrial cancer. *J Magn Reson Imaging* (2021) 54(3):987–95. doi: 10.1002/jmri.27625

17. Stanzione A, Cuocolo R, Del GR, Nardiello A, Romeo V, Travaglino A, et al. Deep myometrial infiltration of endometrial cancer on MRI: A radiomics-powered machine learning pilot study. *Acad Radiol* (2021) 28(5):737–44. doi: 10.1016/j.acra.2020.02.028

18. Jacob H, Dybvik JA, Ytre-Hauge S, Fasmer KE, Hoivik EA, Trovik J, et al. An MRI-based radiomic prognostic index predicts poor outcome and specific genetic alterations in endometrial cancer. *J Clin Med* (2021) 10(3):538. doi: 10.3390/jcm10030538

19. Hoivik EA, Hodneland E, Dybvik JA, Wagner-Larsen KS, Fasmer KE, Berg HF, et al. A radiogenomics application for prognostic profiling of endometrial cancer. *Commun Biol* (2021) 4(1):1363. doi: 10.1038/s42003-021-02894-5

20. Zhang K, Zhang Y, Fang X, Dong J, Qian L. MRI-Based radiomics and ADC values are related to recurrence of endometrial carcinoma: A preliminary analysis. *BMC Cancer* (2021) 21(1):1266. doi: 10.1186/s12885-021-08988-x

21. Zheng T, Yang L, Du J, Dong Y, Wu S, Shi Q, et al. Combination analysis of a radiomics-based predictive model with clinical indicators for the preoperative assessment of histological grade in endometrial carcinoma. *Front Oncol* (2021) 11:582495. doi: 10.3389/fonc.2021.582495

22. Yan BC, Ma XL, Li Y, Duan SF, Zhang GF, Qiang JW. MRI-Based radiomics nomogram for selecting ovarian preservation treatment in patients with early-stage endometrial cancer. *Front Oncol* (2021) 11:730281. doi: 10.3389/fonc.2021.730281

23. Luo Y, Mei D, Gong J, Zuo M, Guo X. Multiparametric MRI-based radiomics nomogram for predicting lymphovascular space invasion in endometrial carcinoma. *J Magn Reson Imaging* (2020) 52(4):1257–62. doi: 10.1002/jmri.27142

24. Chen X, Wang X, Gan M, Li L, Chen F, Pan J, et al. MRI-Based radiomics model for distinguishing endometrial carcinoma from benign mimics: A multicenter study. *Eur J Radiol* (2022) 146:110072. doi: 10.1016/j.ejrad.2021.110072

25. van Griethuysen J, Fedorov A, Parmar C, Hosny A, Aucoin N, Narayan V, et al. Computational radiomics system to decode the radiographic phenotype. *Cancer Res* (2017) 77(21):e104–7. doi: 10.1158/0008-5472.CAN-17-0339

26. Sauerbrei W, Royston P, Binder H. Selection of important variables and determination of functional form for continuous predictors in multivariable model building. *Stat Med* (2007) 26(30):5512–28. doi: 10.1002/sim.3148

27. Rui W, Qiao N, Wu Y, Zhang Y, Aili A, Zhang Z, et al. Radiomics analysis allows for precise prediction of silent corticotroph adenoma among non-functioning pituitary adenomas. *Eur Radiol* (2022) 32(3):1570–8. doi: 10.1007/s00330-021-08361-3

28. Naimi AI, Balzer LB. Stacked generalization: An introduction to super learning. *Eur J Epidemiol* (2018) 33(5):459–64. doi: 10.1007/s10654-018-0390-z

29. Schuler MS, Rose S. Targeted maximum likelihood estimation for causal inference in observational studies. *Am J Epidemiol* (2017) 185(1):65–73. doi: 10.1093/aje/kww165

30. Concin N, Matias-Guiu X, Vergote I, Cibula D, Mirza MR, Marnitz S, et al. ESGO/ESTRO/ESP guidelines for the management of patients with endometrial carcinoma. *Radiother Oncol* (2021) 154:327–53. doi: 10.1016/j.radonc.2020.11.018

31. Auclair MH, Yong PJ, Salvador S, Thurston J, Colgan T, Sebastianelli A. Guideline no. 390-classification and management of endometrial hyperplasia. *J Obstet Gynaecol Can* (2019) 41(12):1789–800. doi: 10.1016/j.jogc.2019.03.025

32. Wolfman W. No. 249-asymptomatic endometrial thickening. *J Obstet Gynaecol Can* (2018) 40(5):e367–77. doi: 10.1016/j.jogc.2018.03.005

33. Braun MM, Overbeek-Wager EA, Grumbo RJ. Diagnosis and management of endometrial cancer. *Am Fam Physician* (2016) 93(6):468–74. Available at: https://www.aafp.org/pubs/afp/issues/2016/0315/p468.html

34. Gillies RJ, Kinahan PE, Hricak H. Radiomics: Images are more than pictures, they are data. *Radiology* (2016) 278(2):563–77. doi: 10.1148/radiol.2015151169

35. Parmar C, Grossmann P, Bussink J, Lambin P, Aerts H. Machine learning methods for quantitative radiomic biomarkers. *Sci Rep* (2015) 5:13087. doi: 10.1038/srep13087

36. Mao B, Ma J, Duan S, Xia Y, Tao Y, Zhang L. Preoperative classification of primary and metastatic liver cancer *Via* machine learning-based ultrasound radiomics. *Eur Radiol* (2021) 31(7):4576–86. doi: 10.1007/s00330-020-07562-6

37. Park BK, Kim B, Park JM, Ryu JA, Kim MS, Bae DS, et al. Differentiation of the various lesions causing an abnormality of the endometrial cavity using MR imaging: Emphasis on enhancement patterns on dynamic studies and late contrast-enhanced T1-weighted images. *Eur Radiol* (2006) 16(7):1591–8. doi: 10.1007/s00330-005-0085-1

38. Wang X, Zhao Y, Hu Y, Zhou Y, Ye X, Liu K, et al. Evaluation and validation of the diagnostic value of the apparent diffusion coefficient for differentiating early-stage endometrial carcinomas from benign mimickers at 3T MRI. *Oncotarget* (2017) 8(28):46390–7. doi: 10.18632/oncotarget.18553

39. Bakir B, Sanli S, Bakir VL, Ayas S, Yildiz SO, Iyibozkurt AC, et al. Role of diffusion weighted MRI in the differential diagnosis of endometrial cancer, polyp, hyperplasia, and physiological thickening. *Clin Imaging* (2017) 41:86–94. doi: 10.1016/j.clinimag.2016.10.016

40. Gatenby RA, Grove O, Gillies RJ. Quantitative imaging in cancer evolution and ecology. *Radiology* (2013) 269(1):8–15. doi: 10.1148/radiol.13122697

41. Dai H, Wang Y, Fu R, Ye S, He X, Luo S, et al. Radiomics and stacking regression model for measuring bone mineral density using abdominal computed tomography. *Acta Radiol* (2021), 200323829. doi: 10.1177/02841851211068149

frontiers | Frontiers in Oncology

TYPE Original Research
PUBLISHED 23 September 2022
DOI 10.3389/fonc.2022.993629

OPEN ACCESS

EDITED BY
Kathy Han,
University Health Network, Canada

REVIEWED BY
Roberto Berretta,
University Hospital of Parma, Italy
Roberto Montera,
Campus Bio-Medico University, Italy

*CORRESPONDENCE
Antonio Raffone
anton.raffone@gmail.com;
antonio.raffone2@unibo.it
Diego Raimondo
die.raimondo@gmail.com;
diego.raimondo@aosp.bo.it

SPECIALTY SECTION
This article was submitted to Gynecological Oncology, a section of the journal Frontiers in Oncology

RECEIVED 13 July 2022
ACCEPTED 12 September 2022
PUBLISHED 23 September 2022

CITATION
Ambrosio M, Raffone A, Alletto A, Cini C, Filipponi F, Neola D, Fabbri M, Arena A, Raimondo D, Salucci P, Guerrini M, Travaglino A, Paradisi R, Mollo A, Seracchioli R and Casadio P (2022) Is preoperative ultrasound tumor size a prognostic factor in endometrial carcinoma patients? *Front. Oncol.* 12:993629. doi: 10.3389/fonc.2022.993629

Is preoperative ultrasound tumor size a prognostic factor in endometrial carcinoma patients?

Marco Ambrosio[1], Antonio Raffone[2,3]*, Andrea Alletto[3], Chiara Cini[3], Francesco Filipponi[3], Daniele Neola[4], Matilde Fabbri[3], Alessandro Arena[2,3], Diego Raimondo[2]*, Paolo Salucci[3], Manuela Guerrini[2], Antonio Travaglino[5], Roberto Paradisi[3], Antonio Mollo[6], Renato Seracchioli[2,3] and Paolo Casadio[2]

[1]Mother-Child Department, Ospedale Maggiore, Azienda Unità Sanitaria Locale di Bologna, Bologna, Italy, [2]Division of Gynaecology and Human Reproduction Physiopathology, IRCCS Azienda Ospedaliero-Universitaria di Bologna, Bologna, Italy, [3]Department of Medical and Surgical Sciences, University of Bologna, Bologna, Italy, [4]Gynecology and Obstetrics Unit, Department of Neuroscience, Reproductive Sciences and Densitry, School of Medicine, University of Naples Federico II, Naples, Italy, [5]Gynecopathology and Breast Pathology Unit, Department of Woman's Health Science, Agostino Gemelli University Polyclinic, Rome, Italy, [6]Gynecology and Obstetrics Unit, Department of Medicine, Surgery and Dentistry "Schola Medica Salernitana", University of Salerno, Baronissi, Italy

Objective: We aimed to assess the prognostic value of preoperative ultrasound tumor size in EC through a single center, observational, retrospective, cohort study.

Methods: Medical records and electronic clinical databases were searched for all consecutive patients with EC, preoperative ultrasound scans available to *ad hoc* estimate tumor size, and a follow-up of at least 2-year, at our Institution from January 2010 to June 2018. Patients were divided into two groups based on different dimensional cut-offs for the maximum tumor diameter: 2, 3 and 4 cm. Differences in overall survival (OS), disease specific survival (DSS) and progression-free survival (PFS) were assessed among the groups by using the Kaplan–Meier estimator and the log-rank test.

Results: 108 patients were included in the study. OS, DSS and PFS did not significantly differ between the groups based on the different tumor diameter cut-offs. No significant differences were found among the groups sub-stratified by age, BMI, FIGO stage, FIGO grade, lymphovascular space invasion status, myometrial invasion, lymph nodal involvement, histotype, and adjuvant treatment.

Conclusions: Preoperative ultrasound tumor size does not appear as a prognostic factor in EC women.

KEYWORDS
risk assessment, cancer, tumor, prognosis, death, recurrence, relapse

Highlights

Preoperative ultrasound assessment of tumor size in women with endometrial cancer does not seem to be a prognostic factor for OS, DSS or PFS.

Introduction

Endometrial carcinoma (EC) is the most common gynecologic malignancy in western countries (1). In the last two decades, it has shown an increase in number of deaths even higher than that in incidence, because of an inaccurate risk stratification (1, 2).

In 2020, in order to improve such an inaccurate risk assessment, the ESGO-ESTRO-ESP guidelines for the management of EC patients recommended to integrate The Cancer Genome ATLAS (TCGA) molecular signature and conventional histological factors (3). In particular, EC patients are assigned to a risk group and therefore to a type of adjuvant treatment based on the International Federation of Gynecology and Obstetrics (FIGO) stage, histotype, FIGO grade, lymphonodal status, myometrial invasion depth, lymphovascular space invasion (LVSI) and molecular signature (i.e., DNA polymerase epsilon mutations, p53 abnormal expression and mismatch repair deficient expression) (3).

In accordance with the principles of the precision medicine, an increasingly tailored approach is recommended to improve survival in cancer patients (4–6), highlighting the need for adding new prognostic factors and integrating them with the current ones (3). In EC patients, the tumor size appears as one of the histological prognostic factors remained to be further investigated. In fact, although it has shown prognostic significance in several malignancies (7, 8), its value is unclear in EC patients. On the one hand, some studies suggested a prognostic value as it could affect the risk of lymph node metastasis (9–12). In particular, Schink et al. observed that tumors larger than 2 cm were associated with an increased risk of lymph node involvement (13). On the other hand, some studies reported that tumor size was not an independent prognostic factor as the rate of lymph node involvement was similar regardless of the size of the lesion (14–16).

The aim of this study was to assess the prognostic value of preoperative ultrasound tumor size in EC patients.

Materials and methods

Study protocol and patient selection

The study was carried out according to an *a priori* defined protocol, and was designed as a single center, observational, retrospective, cohort study.

The Strengthening the Reporting of Observational Studies in Epidemiology (STROBE) guidelines and checklist were followed for study reporting (17).

Medical records and electronic clinical databases were searched for all consecutive patients with histological diagnosis of EC after definitive surgery at our Institution from January 2010 to June 2018. Inclusion criteria were: patients with EC diagnosis; availability of stored preoperative ultrasound scans performed by an expert sonographer (i.e. sonographers with at least 5 years of experience in onco-gynecological ultrasound) to *ad hoc* estimate tumor size; follow-up of at least 2-year. Patients who did not undergo definitive surgery were excluded. No selection was made based on EC histological prognostic factors, FIGO stage or adjuvant treatment.

Based on the data available in the Literature, although the most common cut off used for the tumor diameter in EC patients was 2.0 cm (12, 13, 15, 18), some authors used greater cut-offs (11, 14, 19). Therefore, we divided our population into two groups according to different dimensional cut-offs for the maximum tumor diameter: 2.0, 3.0 and 4.0 cm. Differences in survival outcomes were assessed among the groups.

Main outcome measures

The primary outcome measure was the difference in overall survival (OS) between patients with tumor ≥ and < 2 cm.

Secondary outcome measures were the difference in OS, disease specific survival (DSS) and progression-free survival (PFS) among the groups according to the different tumor diameter cut-offs.

The time of origin for patient survival was set as the date of surgery. In particular, OS was defined as time from surgery until death of any cause, DSS as time from surgery until death due to EC, and PFS as time from surgery until there was evidence of recurrent or progressive disease (diagnosed through either clinic or imaging). In case of unknown event status at last follow-up

date, data were considered missing. Patients died of an intercurrent disease or an unspecified reason were not considered in DSS analyses.

Ultrasound

All transvaginal ultrasound examinations were performed using a Voluson™ E6 (GE Healthcare, Chicago, Illinois, United States) equipped with a multifrequency endovaginal probe (4.0 to 9.0 MHz). The probe was introduced into the posterior vaginal fornix, and the uterus was studied in sagittal and transversal section. The tumor was evaluated by two-dimensional gray-scale ultrasound. The three maximum orthogonal diameters of the tumor were recorded and the maximum diameter was used for analysis.

Data collection

Collected data included patient age, menopausal status, body mass index (BMI), history of abnormal uterine bleeding (AUB), hypertension, diabetes, previous use of tamoxifen, FIGO stage, grade, histotype, LVSI, myometrial invasion, lymph nodes involvement and adjuvant treatment.

Statistical analysis

Numerical and categorical variables were summarized as median [range] and as frequencies and percentages, respectively.

Differences in the distribution of classic prognostic factors (i.e. age >70 years, myometrial invasion, cervical stromal invasion, LVSI, and lymph node involvement) between groups of patients based on tumor diameter were evaluated using the chi-squared test or Fisher's exact test, where appropriate. We used the Kaplan–Meier estimator to display OS, DSS and PFS in the two groups; the equality of survivor functions was assessed using the log-rank test. The same analysis was repeated according to age (≤70, >70 years), BMI (<25, 25–29.9,≥30 kg/m^2), FIGO stage, FIGO grade (1-2; 3), LVSI status (LVS no, LVS yes), myometrial invasion (<50%, >50%), lymph nodal involvement (no, yes), histotype (endometrioid, non-endometrioid), adjuvant treatment (no, yes).

If an association was found between tumor size and survival outcomes, a Cox proportional hazards model including the propensity score of belonging to one of the two groups given the set of baseline potential confounders was planned to analyze the adjusted association between tumor size and survival. Effect sizes were expressed as hazard ratios (HRs) and 95% confidence intervals (CIs).

All analyses were carried out using Stata software, version 15 (StataCorp, 2017, Stata Statistical Software: Release 15, College Station, Texas, USA: StataCorp LP). The significance level was set at 5%.

Ethical statement

The study received approval by the Institutional Review Board of the IRCCS Azienda Ospedaliero-Universitaria di Bologna, S. Orsola Hospital, University of Bologna, Italy (No.: 429/2021/Oss/AOUBo) and was carried out according to the principles of the Declaration of Helsinki. All patients signed a written informed consent, and all data were anonymized.

Results

Study population

A total of 108 patients meeting selection criteria were included in the study. Characteristics of the study population are summarized in Table 1, while the distribution of histological prognostic factors both overall and by tumor size, is shown in Table 2.

All patients were diagnosed with EC by hysteroscopic endometrial biopsy. Regarding surgical treatment, 78 patients (72.2%) underwent laparoscopic surgery, while 30 patients (27.8%) underwent laparotomic surgery. Systematic lymphadenectomy was performed in 60 patients (55.6%), respectively 47 patients (78.3%) underwent pelvic lymphadenectomy and 13 patients (21.7%) pelvic and lombo-aortic lymphadenectomy. Lymph node metastasis were reported in 29 cases (26.9%). Sentinel lymph node biopsy was performed in 48 (44.4%) cases and metastasis were found in 4 (3.7%) patients (Table 1).

According to the tumor size, 26 patients (24.1%) were included in the group with <2 cm tumor, 82 (75.9%) in ≥2 cm group, 43 (39.8%) in <3 cm group, 65 (60.2%) in ≥3 cm group, 83 (76.8%) in <4 cm group and 25 (23.2%) in ≥4 cm group. Among classic prognostic factors, LVSI was significantly more frequent in ≥2, ≥3 and ≥4 cm groups compared to <2, <3 and <4 cm groups, respectively (Table 2).

Survival analyses

The cumulative incidence was 18.5% for death of any cause, 6.5% for death due to EC and 14.8% for disease recurrence. The incidence density rates were 5.1×100, 1.8×100 and 4.3×100 person-years, respectively. Eighty-eight patients were alive at the time of this analysis, with a median follow-up of 50 months (47 months if extended to the whole sample).

OS, DSS and PFS did not significantly differ between the groups based on the different tumor diameter cut-offs

10.3389/fonc.2022.993629

TABLE 1 Characteristics of the study population (n = 108).

Characteristic	
Age, years	68 [35-90]
Body mass index, kg/m^2	27.0 [19.5-49.0]
Presence of Abnormal Uterine Bleeding	99 (91.7)
Diabetes	17 (15.7)
Hypertension	61 (56.5)
FIGO stage	
IA	61 (56.5)
IB	16 (14.8)
II	2 (1.9)
IIIA	0 (0.0)
IIIB	0 (0.0)
IIIC1	16 (14.8)
IIIC2	13 (12.0)
Grade	
Grade 1	21 (19.5)
Grade 2	74 (68.5)
Grade 3	13 (12.0)
Histotype	
Endometrioid	102 (94.4)
Non-endometrioid	6 (5.6)
Mean tumor size	3.3 cm
Type of surgery (Total Hysterectomy with BSO)	
Laparoscopic	78 (72.2)
Abdominal	30 (27.8)
Evaluation of LN status during surgery	
Sentinel LN	48 (44.4)
Systematic Lymphadenectomy	60 (55.6)
Pelvic	47 (78.3)
Pelvic and Lombo-Aortic	13 (21.7)

Data are presented as median [range] for continuous variables and as n (%) for categorical variables. FIGO, International Federation of Gynecology and Obstetrics; BSO, bilateral salpingo-oophorectomy; LN, lymph node.

(Figures 1–3). No significant differences in OS, DSS and PFS were found among the groups sub-stratified by age, BMI, FIGO stage, FIGO grade, LVSI status, myometrial invasion, lymph nodal involvement, histotype, and adjuvant treatment (Supplementary Figures 1–9).

Discussion

Main findings and interpretation

This study shows that preoperative ultrasound tumor size does not appear as a prognostic factor for death of any cause, death due to EC and recurrence in EC patients. Moreover, no significant differences in survival analyses were found among the groups sub-stratified by other prognostic factors.

In accordance with the principles of the precision medicine (4–6) and even more after the increase in number of deaths per year reported in the last decades in EC patients (20), an increasingly tailored and accurate risk assessment appears crucial. New prognostic factors to be investigated may be useful to refine the current risk stratification system. Beyond the TCGA molecular advances, the tumor size remains the only prognostic factor to be further assessed among the histological ones.

Tumor size has shown prognostic significance in several malignancies, such as lung, breast and ovarian granulosa cell tumors (7, 8, 21). However, its value is unclear in EC patients. In particular, while some authors found a significant association between tumor size and some histological prognostic factors, its impact on survival outcomes was uncertain (9, 10, 13, 22). Berretta et al. found a significant difference in size between FIGO stage IA (mean diameter 2,9 cm) and stage IB (mean diameter 4,4 cm) ECs, showing an increased risk of deep myometrial invasion and LVSI in tumor greater than 3 cm (10). On the other hand, Laufer et al. showed that even tumors greater than 2 cm were associated with an increased risk of deep myometrial invasion, low FIGO grade and LVSI (21). Furthermore, tumor size has also been associated with lymph node involvement. Boyraz et al. reported that a tumor size greater than 2 cm might be considered an independent predictor of lymph node metastasis in patients with low-risk EC (9). Mariani et al. reported no lymph node metastases among patients with primary tumor diameter ≤2 cm (12). A similar conclusion was reached by Vargas et al. assessing data from the National Cancer Institute's Surveillance, Epidemiology, and End Results Program (SEER) registry. In particular, they found that

TABLE 2 Distribution of histological prognostic factors in the study population, overall and by tumor size.

Prognostic factor	All (n = 108)	Tumor size								
		<2 cm (n = 26)	≥2 cm (n = 82)	p	<3 cm (n = 43)	≥3 cm (n = 65)	p	<4 cm (n = 83)	≥4 cm (n = 25)	p
Age >70 y	45 (41.7%)	10 (38.5%)	35 (42.7%)	0.704	17 (39.5%)	28 (43.1%)	0.715	34 (41.0%)	11 (44.0%)	0.787
Deep myometrial invasion	100 (92.6%)	22 (84.6%)	78 (95.1%)	0.093	38 (88.4%)	62 (95.4%)	0.261	76 (91.6%)	24 (96.0%)	0.678
Cervical stromal invasion	11 (10.2%)	0 (0.0%)	11 (13.4%)	0.063	1 (2.3%)	10 (15.4%)	0.047*	6 (7.2%)	5 (20.0%)	0.123
Lymph-vascular space invasion	57 (52.8%)	9 (34.6%)	48 (58.5%)	0.033*	15 (34.9%)	42 (64.6%)	0.002*	39 (47.0%)	18 (72.0%)	0.028*
Lymph node involvement	29 (26.9%)	5 (19.2%)	24 (29.3%)	0.314	8 (18.6%)	21 (32.3%)	0.116	19 (22.9%)	10 (40.0%)	0.091

*P value ≤0.05.

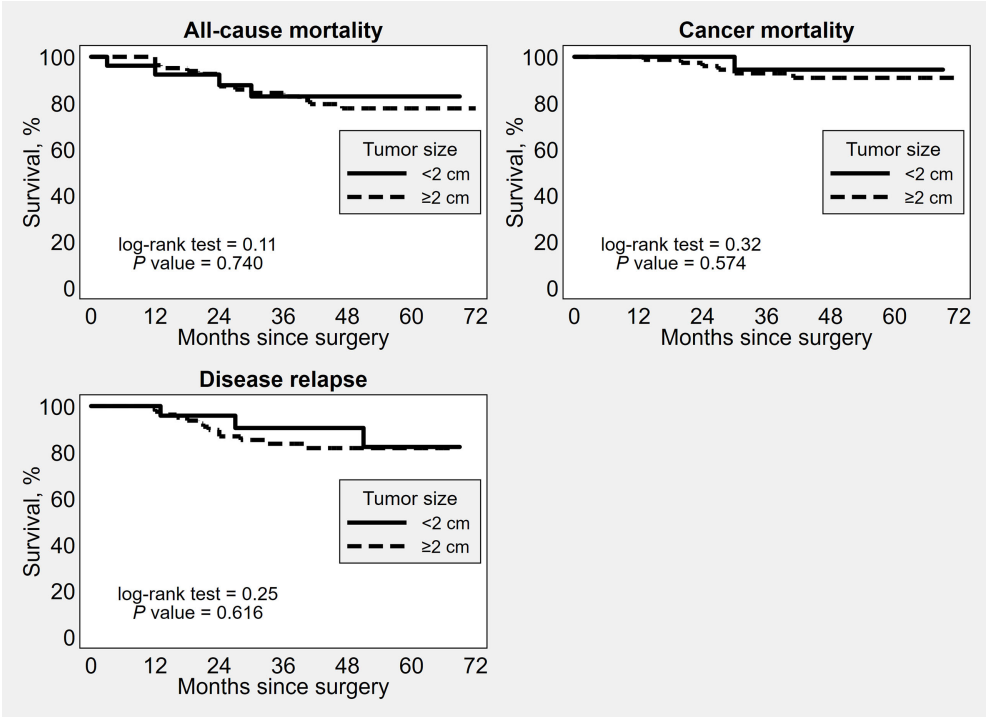

FIGURE 1
Kaplan–Meier survival estimates of time to all-cause mortality, cancer mortality and disease recurrence after surgery, by 2 cm tumor diameter cut-off.

lymph node involvement rate increased from 1.3% in grade 1 and 3.8% in grade 2 tumors ≤2 cm to 12.7% in grade 1 and 23% in grade 2 tumors ≥ 5 cm, independently of myometrial invasion. The increased risk of node metastasis was also confirmed at multivariate analysis (23). In another study Cox-Bauer et al. reported that a cut-off of 5 cm was significantly more predictive of nodal involvement than a tumor diameter of 2 cm (11).

Concerning the impact of tumor size on survival outcomes, conflicting results have been reported in the Literature. Some Authors reported tumor size as an independent prognostic factor for recurrence alone (19, 24) or for recurrence and death due to EC (25); other Authors did not confirm an independent association between tumor size and recurrence (14, 15, 26). In particular, Chattopadhyay S. et al. found that a tumor size cut-off of 3.75 cm could be considered a significant independent prognostic factor of death due to EC and recurrence in FIGO Stage I EC patients who did not undergo lymphadenectomy (25). Senol T. et al. showed that the same cut-off was a predictor for recurrence, but not for death of any cause ($p > 0.05$) (19). The association between tumor size and recurrence was found even with a smaller cut-off (i.e. 2.5 cm) in low-risk EC patients according to the European Society of Medical Oncology-European Society of Gynecological Oncology-European Society for Radiotherapy and Oncology classification (24). On the contrary, other studies showed that, although there was an increased risk of nodal metastasis in patients with tumors >2 cm, tumor size did not appear as an independent predictor of recurrence (15, 26). In another study, the association with recurrence was not confirmed neither considering a cut-off of 3.5 cm (14).

Beyond the conflicting findings, previous studies have focused on tumor size at histological examination. In our study, conversely, we focused on the tumor diameter at ultrasound. In fact, this could improve the preoperative risk stratification of EC patients. Although preoperative ultrasound tumor size was associated with LVSI, we found that it was not a prognostic factor for death of any cause, death due to EC and recurrence in EC patients. These findings were confirmed even adopting different tumor diameter cut-offs (i.e. 2, 3 and 4 cm). Our results suggest that ultrasound tumor size does not appear as an additional prognostic factor to further refine the preoperative risk stratification of EC patients. However, further studies are needed to confirm these findings.

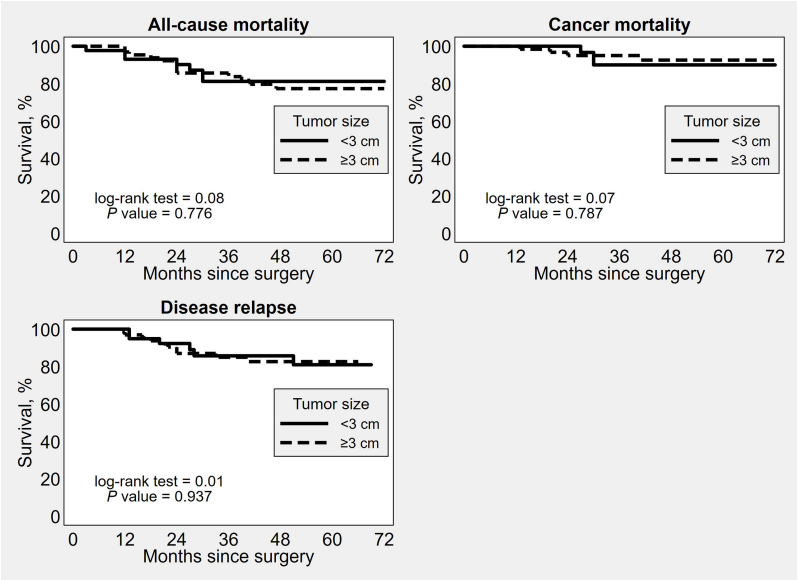

FIGURE 2
Kaplan–Meier survival estimates of time to all-cause mortality, cancer mortality and disease recurrence after surgery, by 3 cm tumor diameter cut-off.

Strengths and limitations

To our knowledge, our study may be the first study to assess the prognostic value of tumor size in EC patients at preoperative ultrasound. In fact, the impact of tumor size on cancer outcomes has been mainly assessed at postoperative histological examination so far, with only few studies assessing its prognostic role preoperatively on magnetic resonance imaging

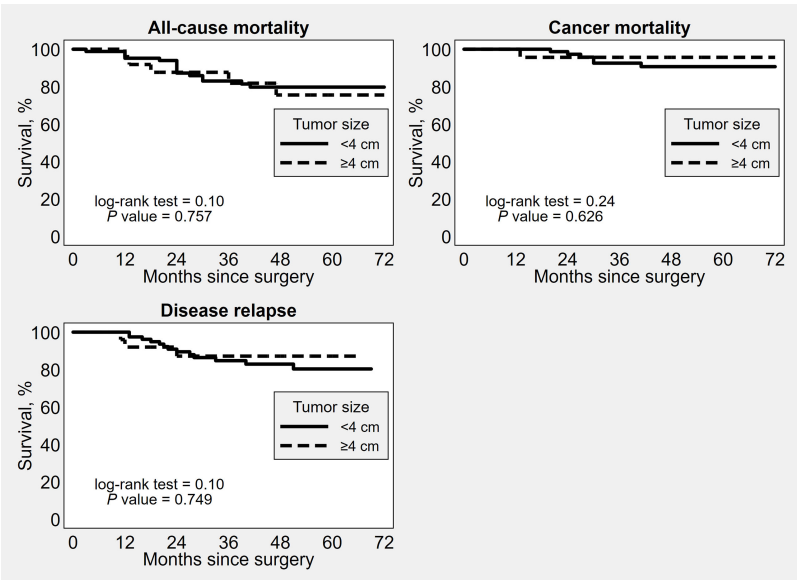

FIGURE 3
Kaplan–Meier survival estimates of time to all-cause mortality, cancer mortality and disease recurrence after surgery, by 4 cm tumor diameter cut-off.

(27, 28). Having an additional preoperative prognostic factor might help plan surgical staging and further refine risk stratification and management of EC patients.

A major limitation of our study underlies in the retrospective design which affects data availability. However, missing data from medical records and clinical electronic databases did not affect our main analyses. Moreover, the inclusion of patients from a single center minimized the biases arising from different patient management and data collection. Another important limitation of our study may be that we didn't assess postoperative pathological tumor size in addition to preoperative ultrasound tumor size. Anyway, transvaginal ultrasound has been established as an effective tool to evaluate endometrial pathology (29–31). Lastly, as a further limitation, we were unable to assess tumor size as a prognostic factor in each TCGA molecular group. In fact, like other histological factors (32–36), it might have a prognostic role only in selected TCGA groups.

Conclusions

Preoperative ultrasound tumor size does not appear as a prognostic factor for death of any cause, death due to EC and recurrence in EC women. Its assessment does not seem to be useful to further refine the preoperative risk stratification of patients. Further studies are needed to confirm these findings.

Data availability statement

The raw data supporting the conclusions of this article will be made available by the authors, without undue reservation.

Ethics statement

The studies involving human participants were reviewed and approved by Institutional Review Board of the IRCCS Azienda Ospedaliero-Universitaria di Bologna, S. Orsola Hospital, University of Bologna, Italy (No.: 429/2021/Oss/AOUBo). The patients/participants provided their written informed consent to participate in this study.

Author contributions

Conceptualization: MA and PC; methodology: AAr, AR, DN, MF, AM, AT, and RP; software: AAl and AAr; validation: RP, AT, PC, and MG; formal analysis: DR, FF, and PS; investigation: AAl, DN, MF, CC, AT, and FF; resources: AAl, AR, MA, and MG; data curation: MA, AR, DR, CC, and AAl; writing-original draft preparation: MA, AR, DN, MF, and CC, writing-review and editing: MA, AAl, AR; visualization: MA, AR, DN, MF, AAr, AT, and AM; supervision: AM, RP, AM, PC, and RS; project administration: MA and PC. All authors contributed to the article and approved the submitted version.

Funding

The work reported in this publication was funded by the Italian Ministry of Health, RC-2022-n.2773472.

Conflict of interest

The authors declare that the research was conducted in the absence of any commercial or financial relationships that could be construed as a potential conflict of interest.

Publisher's note

Supplementary material

The Supplementary Material for this article can be found online at: https://www.frontiersin.org/articles/10.3389/fonc.2022.993629/full#supplementary-material

SUPPLEMENTARY FIGURE 1
Kaplan–Meier survival estimates of time to all-cause mortality, for prognostic group (stage, grade, age, BMI, stage, grade, LVSI, myometrial invasion, lymph node involvement, histotype, adjuvant treatment) and by 2 cm tumor diameter cut-off.

SUPPLEMENTARY FIGURE 2
Kaplan–Meier survival estimates of time to death from cancer, for prognostic group (stage, grade, age, BMI, stage, grade, LVSI, myometrial invasion, lymph node involvement, histotype, adjuvant treatment) and by 2 cm tumor diameter cut-off.

SUPPLEMENTARY FIGURE 3
Kaplan–Meier survival estimates of time to disease relapse, for prognostic group (stage, grade, age, BMI, stage, grade, LVSI, myometrial invasion, lymph node involvement, histotype, adjuvant treatment) and by 2 cm tumor diameter cut-off.

SUPPLEMENTARY FIGURE 4
Kaplan–Meier survival estimates of time to all-cause mortality, for prognostic group (stage, grade, age, BMI, stage, grade, LVSI, myometrial invasion, lymph node involvement, histotype, adjuvant treatment) and by 3 cm tumor diameter cut-off.

SUPPLEMENTARY FIGURE 5
Kaplan–Meier survival estimates of time to death from cancer, for prognostic group (stage, grade, age, BMI, stage, grade, LVSI, myometrial invasion, lymph node involvement, histotype, adjuvant treatment) and by 3 cm tumor diameter cut-off.

SUPPLEMENTARY FIGURE 6
Kaplan–Meier survival estimates of time to disease relapse, for prognostic group (stage, grade, age, BMI, stage, grade, LVSI, myometrial invasion, lymph node involvement, histotype, adjuvant treatment) and by 3 cm tumor diameter cut-off.

SUPPLEMENTARY FIGURE 7
Kaplan–Meier survival estimates of time to all-cause mortality, for prognostic group (stage, grade, age, BMI, stage, grade, LVSI, myometrial invasion, lymph node involvement, histotype, adjuvant treatment) and by 4 cm tumor diameter cut-off.

SUPPLEMENTARY FIGURE 8
Kaplan–Meier survival estimates of time to death from cancer, for prognostic group (stage, grade, age, BMI, stage, grade, LVSI, myometrial invasion, lymph node involvement, histotype, adjuvant treatment) and by 4 cm tumor diameter cut-off.

SUPPLEMENTARY FIGURE 9
Kaplan–Meier survival estimates of time to disease relapse, for prognostic group (stage, grade, age, BMI, stage, grade, LVSI, myometrial invasion, lymph node involvement, histotype, adjuvant treatment) and by 4 cm tumor diameter cut-off.

References

1. Raffone A, Travaglino A, Mascolo M, Carbone L, Guida M, Insabato L, et al. TCGA molecular groups of endometrial cancer: Pooled data about prognosis. *Gynecol Oncol* (2019) 155:374–83. doi: 10.1016/j.ygyno.2019.08.019

2. Raffone A, Travaglino A, Gabrielli O, Micheli M, Zuccalà V, Bitonti G, et al. Clinical features of ProMisE groups identify different phenotypes of patients with endometrial cancer. *Arch Gynecol Obs* (2021) 303:1393–400. doi: 10.1007/s00404-021-06028-4

3. Concin N, Matias-Guiu X, Vergote I, Cibula D, Mirza MR, Marnitz S, et al. ESGO/ESTRO/ESP guidelines for the management of patients with endometrial carcinoma. *Int J Gynecol Cancer* (2021) 31:12–39. doi: 10.1136/ijgc-2020-002230

4. Coyne GO, Takebe N, Chen AP. Defining precision: The precision medicine initiative trials NCI-MPACT and NCI-MATCH. *Curr Probl Cancer* (2017) 41:182–93. doi: 10.1016/j.currproblcancer.2017.02.001

5. Barroilhet L, Matulonis U. The NCI-MATCH trial and precision medicine in gynecologic cancers. *Gynecol Oncol* (2018) 148:585–90. doi: 10.1016/j.ygyno.2018.01.008

6. Coleman RL, Matulonis UA. Precision medicine. *Gynecol Oncol* (2016) 141:1. doi: 10.1016/j.ygyno.2016.03.017

7. Ball D, Mitchell A, Giroux D, Rami-Porta R, Institutions ISC. Participating effect of tumor size on prognosis in patients treated with radical radiotherapy or chemoradiotherapy for non-small cell lung cancer. An analysis of the staging project database of the international association for the study of lung cancer. *J Thorac Oncol* (2013) 8:315–21. doi: 10.1097/JTO.0b013e31827dc74d

8. Boussios S, Zarkavelis G, Seraj E, Zerdes I, Tatsi K, Pentheroudakis G. Non-epithelial ovarian cancer: Elucidating uncommon gynaecological malignancies. *Anticancer Res* (2016) 36:5031–42. doi: 10.21873/anticanres.11072

9. Boyraz G, Salman MC, Gultekin M, Basaran D, Cagan M, Ozgul N, et al. Incidence of lymph node metastasis in surgically staged FIGO IA G1/G2 endometrial cancer with a tumor size of more than 2 cm. *Int J Gynecol Cancer* (2017) 27:486–92. doi: 10.1097/IGC.0000000000000919

10. Berretta R, Patrelli TS, Migliavacca C, Rolla M, Franchi L, Monica M, et al. Assessment of tumor size as a useful marker for the surgical staging of endometrial cancer. *Oncol Rep* (2014) 31:2407–12. doi: 10.3892/or.2014.3108

11. Cox Bauer CM, Greer DM, Kram JJF, Kamelle SA. Tumor diameter as a predictor of lymphatic dissemination in endometrioid endometrial cancer. *Gynecol Oncol* (2016) 141:199–205. doi: 10.1016/j.ygyno.2016.02.017

12. Mariani A, Webb MJ, Keeney GL, Haddock MG, Calori G, Podratz KC. Low-risk corpus cancer: Is lymphadenectomy or radiotherapy necessary? *Am J Obs Gynecol* (2000) 182:1506–19. doi: 10.1067/mob.2000.107335

13. Schink JC, Lurain JR, Wallemark CB, Chmiel JS. Tumor size in endometrial cancer: a prognostic factor for lymph node metastasis. *Obs Gynecol* (1987) 70:216–9. doi: 10.1016/0090-8258(87)90055-2

14. Çakır C, Kılıç İ.Ç., Yüksel D, Karyal YA, Üreyen I, Boyraz G, et al. Does tumor size have prognostic value in patients undergoing lymphadenectomy in endometrioid-type endometrial cancer confined to the uterine corpus? *Turk J Med Sci* (2019) 49:1403–10. doi: 10.3906/sag-1902-224

15. Shah C, Johnson EB, Everett E, Tamimi H, Greer B, Swisher E, et al. Does size matter? Tumor size and morphology as predictors of nodal status and recurrence in endometrial cancer. *Gynecol Oncol* (2005) 99:564–70. doi: 10.1016/j.ygyno.2005.06.011

16. Kilts TP, Glaser GE, Langstraat CL, Kumar A, Weaver AL, Mc Gree ME, et al. Comparing risk stratification criteria for predicting lymphatic dissemination in endometrial cancer. *Gynecol Oncol* (2019) 155:21–6. doi: 10.1016/j.ygyno.2019.08.005

17. von Elm E, Altman DG, Egger M, Pocock SJ, Gøtzsche PC, Vandenbroucke JP, et al. The strengthening the reporting of observational studies in epidemiology (STROBE) statement: Guidelines for reporting observational studies. *Int J Surg* (2014) 12:1495–9. doi: 10.1016/j.ijsu.2014.07.013

18. Schink JC, Rademaker AW, Miller DS, Lurain JR. Tumor size in endometrial cancer. *Cancer* (1991) 67:2791–4. doi: 10.1002/1097-0142(19910601)67:11<2791::AID-CNCR2820671113>3.0.CO;2-S

19. Senol T, Polat M, Ozkaya E, Karateke A. Tumor diameter for prediction of recurrence, disease free and overall survival in endometrial cancer cases. *Asian Pac J Cancer Prev* (2015) 16:7463–6. doi: 10.7314/APJCP.2015.16.17.7463

20. Zhang S, Gong TT, Liu FH, Jiang YT, Sun H, Ma XX, et al. Global, regional, and national burden of endometrial cancer, 1990-2017: Results from the global burden of disease study, 2017. *Front Oncol* (2019) 9:1440. doi: 10.3389/fonc.2019.01440

21. Sopik V, Narod SA. The relationship between tumour size, nodal status and distant metastases: on the origins of breast cancer. *Breast Cancer Res Treat* (2018) 170:647–56. doi: 10.1007/s10549-018-4796-9

22. Laufer J, Scasso S, Papadia A, Sosa C, Cirillo F, Raspagliesi F. Association between tumor diameter and lymphovascular space invasion among women with early-stage endometrial cancer. *Int J Gynaecol Obs* (2013) 123:142–5. doi: 10.1016/j.ijgo.2013.05.012

23. Vargas R, Rauh-Hain JA, Clemmer J, Clark RM, Goodman A, Growdon WB, et al. Tumor size, depth of invasion, and histologic grade as prognostic factors of lymph node involvement in endometrial cancer: A SEER analysis. *Gynecol Oncol* (2014) 133:216–20. doi: 10.1016/j.ygyno.2014.02.011

24. Sozzi G, Uccella S, Berretta R, Petrillo M, Fanfani F, Monterossi G, et al. Tumor size, an additional risk factor of local recurrence in low-risk endometrial cancer: A Large multicentric retrospective study. *Int J Gynecol Cancer* (2018) 28:684–91. doi: 10.1097/IGC.0000000000001223

25. Chattopadhyay S, Cross P, Nayar A, Galaal K, Naik R. Tumor size: a better independent predictor of distant failure and death than depth of myometrial invasion in international federation of gynecology and obstetrics stage I endometrioid endometrial cancer. *Int J Gynecol Cancer* (2013) 23:690–7. doi: 10.1097/IGC.0b013e31828c85c6

26. Doll KM, Tseng J, Denslow SA, Fader AN, Gehrig PA. High-grade endometrial cancer: Revisiting the impact of tumor size and location on outcomes. *Gynecol Oncol* (2014) 132:44–9. doi: 10.1016/j.ygyno.2013.10.023

27. Coronado PJ, Santiago-López J, Santiago-García J, Méndez R, Fasero M, Herraiz MA. Tumoral volume measured preoperatively by magnetic resonance imaging is related to survival in endometrial cancer. *Radiol Oncol* (2021) 55:35–41. doi: 10.2478/raon-2020-0064

28. Ytre-Hauge S, Husby JA, Magnussen IJ, Werner HM, Salvesen Ø.O., Bjørge L, et al. Preoperative tumor size at MRI predicts deep myometrial invasion, lymph node metastases, and patient outcome in endometrial carcinomas. *Int J Gynecol Cancer* (2015) 25:459–66. doi: 10.1097/IGC.0000000000000367

29. Van Den Bosch T, Dueholm M, Leone FPG, Valentin L, Rasmussen CK, Votino A, et al. Terms, definitions and measurements to describe sonographic features of myometrium and uterine masses: A consensus opinion from the morphological uterus sonographic assessment (MUSA) group. *Ultrasound Obstet Gynecol* (2015) 46:284–98. doi: 10.1002/uog.14806

30. Faria SC, Devine CE, Rao B, Sagebiel T, Bhosale P. Imaging and staging of endometrial cancer. *Semin Ultrasound CT MR* (2019) 40:287–94. doi: 10.1053/j.sult.2019.04.001

31. Verbakel JY, Mascilini F, Wynants L, Fischerova D, Testa AC, Franchi D, et al. Validation of ultrasound strategies to assess tumor extension and to predict high-risk endometrial cancer in women from the prospective IETA (International endometrial tumor analysis)-4 cohort. *Ultrasound Obstet Gynecol* (2020) 55:115–24. doi: 10.1002/uog.20374

32. Travaglino A, Raffone A, Stradella C, Esposito R, Moretta P, Gallo C, et al. Impact of endometrial carcinoma histotype on the prognostic value of the TCGA molecular subgroups. *Arch Gynecol Obs* (2020) 301:1355–63. doi: 10.1007/s00404-020-05542-1

33. Travaglino A, Raffone A, Mollo A, Borrelli G, Alfano P, Zannoni GF, et al. TCGA molecular subgroups and FIGO grade in endometrial endometrioid carcinoma. *Arch Gynecol Obs* (2020) 301:1117–25. doi: 10.1007/s00404-020-05531-4

34. Raffone A, Travaglino A, Mascolo M, Carotenuto C, Guida M, Mollo A, et al. Histopathological characterization of ProMisE molecular groups of endometrial cancer. *Gynecol Oncol* (2020) 157:252–9. doi: 10.1016/j.ygyno.2020.01.008

35. Raffone A, Travaglino A, Raimondo D, Boccellino MP, Maletta M, Borghese G, et al. Tumor-infiltrating lymphocytes and POLE mutation in endometrial carcinoma. *Gynecol Oncol* (2021) 161:621–8. doi: 10.1016/j.ygyno.2021.02.030

36. Raffone A, Travaglino A, Raimondo D, Neola D, Renzulli F, Santoro A, et al. Prognostic value of myometrial invasion and TCGA groups of endometrial carcinoma. *Gynecol Oncol* (2021) 162:401–6. doi: 10.1016/j.ygyno.2021.05.029

frontiers | Frontiers in Oncology

TYPE Original Research
PUBLISHED 06 October 2022
DOI 10.3389/fonc.2022.1005191

OPEN ACCESS

EDITED BY
Alessio G. Morganti,
University of Bologna, Italy

REVIEWED BY
Komsun Suwannarurk,
Thammasat University, Thailand
Sung Bin Park,
Chung-Ang University Hospital,
South Korea

*CORRESPONDENCE
Kaiwu Lin
fjlkwu@163.com

SPECIALTY SECTION
This article was submitted to Gynecological Oncology, a section of the journal Frontiers in Oncology

RECEIVED 28 July 2022
ACCEPTED 26 September 2022
PUBLISHED 06 October 2022

CITATION
Wang C, Zheng X, Zhou Z, Shi Y, Wu Q and Lin K (2022) Differentiating cellular leiomyoma from uterine sarcoma and atypical leiomyoma using multi-parametric MRI. *Front. Oncol.* 12:1005191. doi: 10.3389/fonc.2022.1005191

Differentiating cellular leiomyoma from uterine sarcoma and atypical leiomyoma using multi-parametric MRI

Cong Wang, Xianying Zheng, Zuofu Zhou, Yuequan Shi, Qin Wu and Kaiwu Lin*

Department of Radiology, Fujian Maternity and Child Health Hospital, Fuzhou, Fujian, China

Objectives: To evaluate the diagnostic performance of conventional magnetic resonance imaging (cMRI) combined with diffusion-weighted MRI (DWI) in discrimination of cellular leiomyoma, uterine sarcoma, and atypical leiomyoma.

Methods: This retrospective study enrolled 106 patients with uterine masses, including 51 cellular leiomyomas (CLs), 32 uterine sarcomas (USs) and 23 degenerated leiomyomas (LMs) confirmed by histopathologic examination. Clinical data and imaging findings were assessed. Chi-squared test for qualitative variables and one way ANOVA analysis for quantitative variables were performed. Logistic regression analysis and the receiver operating characteristic (ROC) analysis were performed to determine the cut-off point and diagnostic performances for significant numeric values or multiple models.

Results: Morphology (Odds ratio [OR] = 6.36) and margin (OR = 13.84) derived from cMRI were independent indicators for differentiating CLs from USs, and T2WI signal (OR = 0.23) were an independent indicator for differentiating CLs from degenerated LMs (all $P < 0.05$). The cutoff value of apparent diffusion coefficient (ADC) derived from DWI for differentiating CLs from USs was 839 $\times 10^{-6}$ mm^2/sec and was 1239 $\times 10^{-6}$ mm^2/sec for differentiating CLs from degenerated LMs. Compared with the use of cMRI features and ADC value alone, combination of independent indicators and ADC value achieved higher AUCs for both differentiations (all $P < 0.05$).

Conclusions: cMRI is a reliable tool for differentiating CLs from USs and atypical leiomyoma, especially degenerated LMs. The combined use of cMRI and DWI can improve the differential diagnostic performance.

KEYWORDS

magnetic resonance imaging, uterine leiomyoma, uterine sarcoma, diffusion-weighted MRI, atypical leiomyoma

Introduction

Uterine leiomyomas (LMs) are the most common neoplasms in gynecologic system, occurring in approximately 20%-30% of women of reproductive age and up to 70% of premenopausal women (1, 2). More importantly, up to 65% of LMs are present with varied clinical symptoms and atypical imaging manifestations, including a variety degree of degeneration or cellular histologic subtype (3, 4). Although LMs are typically recognized as benign entities, some atypical LMs, particularly cellular leiomyomas (CLs), have now been defined as borderline tumors with a potential of malignant transformation and a high recurrence rate (5). Therefore, differentiation of CLs from other types of atypical LMs (especially degenerated LMs) and malignant tumors, is of great clinical relevance since their prognosis and therapeutic implications are completely different (1–7). In such condition, uterine sarcomas (USs) which are rare malignant uterine tumors should also be included into clinical differentiation because of their extremely aggressive biology behavior and poor prognosis (8, 9).

Magnetic resonance imaging (MRI) has been recognized as a highly useful modality in the diagnosis, localization, and management determination of this entity (10). Conventional MRI (cMRI) is capable of comprehensively evaluating the localization, morphology, boundary, vascularity, and internal components, especially when paramagnetic contrast is applied (10). Advanced MRI techniques, such as diffusion-weighted MRI (DWI), may supplement conventional imaging with respect to the physiological and functional information obtained (11). As previously reported, DWI holds a potential ability to differentiate uterine sarcomas from benign leiomyomas (11). In a very recent study, Abdel et al. (12) developed an algorithm based on DWI to differentiate benign atypical leiomyomas from malignant uterine sarcomas.

However, to the best of our knowledge, few studies have systematically elucidated the discriminative value of cMRI combined with DWI in distinguishing among atypical LMs, including degenerated LMs and CLs, and USs. Thus, the purpose of this study was to assess the benefit of adding DWI to the conventional MRI for the differential diagnosis of atypical LMs and leiomyosarcomas.

Materials and methods

Patients

This retrospective study was approved by our institutional review board, and the requirements for informed consent forms were waived. We retrospectively reviewed patients who underwent pelvic MRI examination with at least one uterine mass in our center between January 2014 and January 2022. Patients were selected according to the following condition (1): surgically and pathologically proved degenerated LMs, CL or USs (2); MRI features were different from typical leiomyomas. Patients were excluded according to the following condition (1): poor imaging quality or imaging data missing (2); metal or motion artifacts in the imaging (3); lesions were obviously located in endometrial. Finally, 106 patients were enrolled in the study, including 51 CLs, 32 USs and 23 degenerated LMs (Figure 1).

Imaging protocol

MRI examination was performed using a 1.5-T MRI scanner (GE Signa HD MRI system). The conventional nonenhanced MRI protocol consisted of the following sequence: axial gradient-echo T1-weighted sequence (T_1WI, TR/TE 450 msec/15 msec) with a matrix of 320 × 256; and fat-suppressed T2-weighted (fs-T_2WI, TR/TE 2800-4200 msec/74-82 msec) sequences in the axial, sagittal and coronal planes with a matrix of 320 × 256; axial DWI (b = 800 sec/mm^2) with a matrix of 128 × 28; axial T1-weighted three-dimensional (3D) gradient-recalled echo (LAVA) multiphase dynamic enhancement sequence (TR/TE 3.5 msec/1.6 msec) was obtained after a rapid intravenous injection of 0.1 mL/kg of gadopentetic acid (0.5 mmol/ml) at an injection rate of 3 mL/s.

Image analysis

The image assessment was performed by 2 radiologists with more than 10 years of radiographic experience in obstetrics and gynecology. Two radiologists independently evaluated the image manifestations, including (1): the number of the lesion (2); maximum diameter, margin and border (3); hemorrhage, necrosis and degeneration within the lesion; number of the lesion (4); T1WI and T2WI signal intensity of the lesion (5); DWI signal intensity and apparent diffusion coefficient (ADC) value (6); degree of enhancement (7); the thickness of endometrium. The morphology of lesions was described as round/oval and irregular. Maximum diameter measurement was taken in the axial plane. Compared with that of the iliopsoas, T1WI signal intensity, T2WI signal intensity and DWI signal intensity was graded as hypointense, isointense, and hyperintense; T2WI signal intensity was defined as hypointense, isointense, hyperintense. ADC value was assessed in the ADC map by using the circular region of interest (15-25 mm^2). Avoiding the degeneration, necrotic, and hemorrhage parts within the tumor, several circular regions of interest were placed in the solid area. Then the lowest value of mean ADC in these regions was recorded. Thickened endometrium was defined when the endometrium thickness was more than 10 mm.

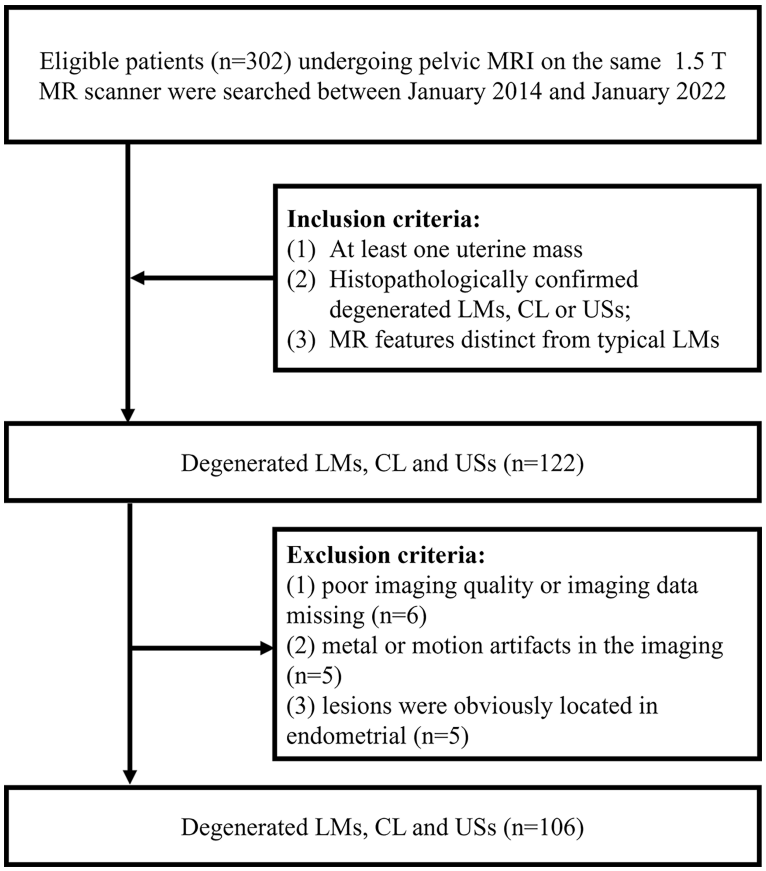

FIGURE 1
Flowchart showing the patient enrollment process.

Statistical analysis

All statistical analyses were performed with statistical software (GraphPad Prism, Version 8.1.0). We performed chi-squared test for qualitative variables and one way ANOVA analysis for quantitative variables. The variables that were significantly different among the three groups would be further evaluated with logistic regression analysis. The receiver operating characteristic (ROC) analyses and logistic regression analyses were performed at last to determine the cutoff point, sensitivity, specificity and area under the ROC curves (AUC) for significant numeric values or combined models. Statistical significance was considered when P value less than 0.05. Cohen kappa coefficient was used to analyze the interobserver reliability between observer 1 and observer 2: $\kappa < 0.40$, poor; 0.40-0.75, fair to good; >0.75, excellent (13).

Results

The κ values revealed excellent interobserver agreement (all $\kappa > 0.75$) for assessing all parameters. The conventional MR and DWI (ADC value) findings of all the lesions are summarized in Table 1 and representative images are shown in Figures 2–4. We found significant differences of morphology ($P < 0.0001$) and margin ($P < 0.0001$) among degenerated LMs, CLs and USs, in which LMs tended to display as round/oval and well-defined masses, whereas USs were more likely to be irregular and poorly defined. USs had a predilection for necrosis (18/32, 56.25%) and higher chance of hemorrhage (12/32, 37.5%). There were no significant differences in the probability of multiple lesion occurrences, thickness of endometrial, ascites, and T1WI signal among these three groups (all $P > 0.05$). Additionally, we found no USs were associated with degeneration, and a significant difference between benign and malignant lesions regarding the presence of degeneration ($P < 0.0001$). On T2WI images, the solid portions of both CLs and USs were present as hyperintense, whereas most of degenerated LMs showed hypointensity ($P < 0.0001$). Moreover, compared with degenerated LMs, solid portions of both CLs and USs showed higher DWI signal with lower ADC values ($P < 0.0001$).

As shown in Table 2, seven parameters, including patients' age, morphology, margin, hemorrhage, necrosis, degeneration

TABLE 1 Comparisons of clinical demographics, conventional MRI and DWI/ADC values among CLS, USs and degenerated LMs.

Characteristics	CLs	USs	Degenerated LMs	*P* value
Age	43.0 ± 9.6	48.2 ± 9.2	43.0 ± 9.4	0.046
Number				0.0789
Single	47	25	17	
Multiple	4	7	6	
Morphology				<0.0001
Round/oval	39	5	13	
Irregular	12	27	10	
Margin				<0.0001
Well defined	39	7	15	
Poorly defined	12	25	8	
Endometrial thickness				0.7018
≤1mm	41	28	19	
>1mm	10	4	4	
Hemorrhage				<0.0001
Yes	1	12	4	
No	50	20	19	
Necrosis				<0.0001
Yes	1	18	1	
No	50	14	22	
Degeneration				<0.0001
Yes	11	0	23	
No	40	32	0	
Ascites				0.2881
Yes	4	6	4	
No	47	26	19	
T1WI signal				0.9505
hypointense	1	1	1	
isointense	49	30	21	
hyperintense	1	1	1	
T2WI signal				<0.0001
hypointense	4	3	17	
isointense	2	2	0	
hyperintense	45	27	6	
DWI signal				<0.0001
hypointense	1	0	15	
hyperintense	50	32	8	
ADC value ($\times 10^{-6}$ mm^2/sec)	985.8 ± 188.1	838.4 ± 213.5	1451.2 ± 435.1	<0.0001

and T2WI signal, were further enrolled into the multivariate analysis with a forward manner for determining the independent predictors for differentiation of CLs from USs and degenerated LMs. Our multivariate analyses showed that morphology, margin and T2WI signal of the mass were independent predictors of CLs with odds ratios of 6.36, 13.84 and -1.47, respectively (P = 0.035, 0.006 and 0.019, respectively). The ROC curve analyses of ADC value for differentiating CLs from USs and degenerated LMs are shown in Table 3. The ROC analyses yielded a cutoff ADC value of 839 $\times 10^{-6}$ mm^2/sec, with a sensitivity of 59.38%, a specificity of 82.35% for differentiation of CLs from USs, and a cutoff ADC value of 1239 $\times 10^{-6}$ mm^2/sec, with a sensitivity of 78.26%, a specificity of 90.20 for differentiation of CLs from degenerated LMs (Figure 5).

To further improve the diagnostic performance, the independent predictors derived from cMRI were combined with ADC for distinguishing CLs from USs and degenerated LMs. As shown in Table 3 and Figure 5, the combination of cMRI parameters (morphology and margin) and ADC value significantly improved the diagnostic performance with an AUC of 0.915, a sensitivity of 90.62% and a specificity of 88.24% (ADC vs. cMRI+ADC: z statistic = 3.305, $P < 0.0001$;

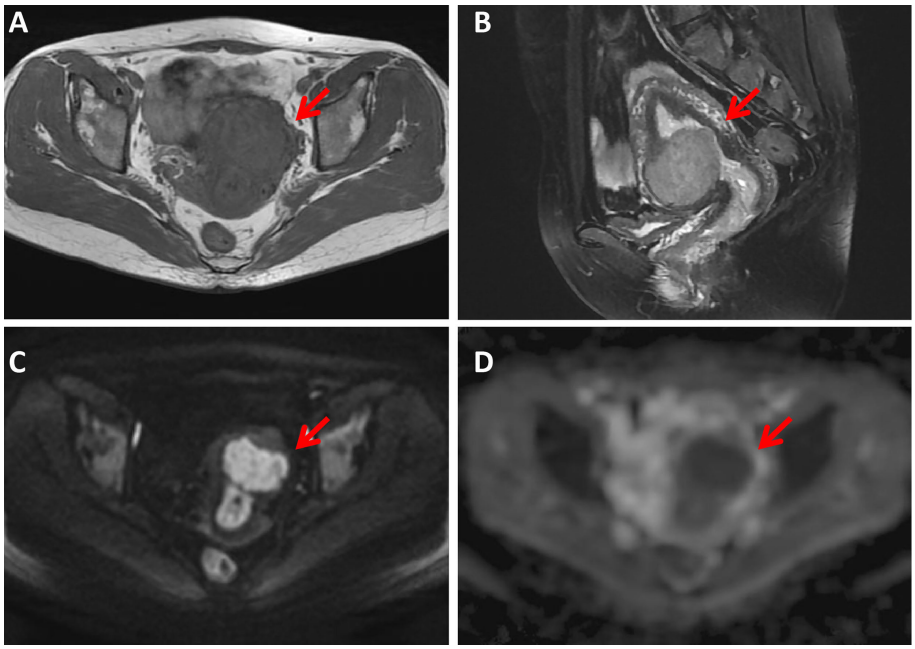

FIGURE 2
A 43-year-old woman with a cellular leiomyoma. A mass was located in the uterine anterior wall (arrow) with a clear margin, showing isointensity on T1WI **(A)** and hyperintensity on T2WI images **(B)**. This mass showed high signal intensity on diffusion-weighted MR image **(C)** with a low ADC value (ADC = 985 $\times 10^{-6}$ mm^2/sec) **(D)**.

TABLE 2 Logistic regression analysis of clinical demographics and conventional MRI for differentiating CLs from USs and degenerated LMs.

Variables	Coefficient	Odds ratio	95% CI	*P* value
Differentiation of CLs from USs				
Morphology	1.85	6.36	1.14-35.67	0.035
Margin	2.63	13.84	2.10-91.26	0.006
Differentiation of CLs from degenerated LMs				
T2WI signal	-1.47	0.23	0.067-0.790	0.019

TABLE 3 Measurements of the cut-off value, sensitivity, specificity, and AUC of ADC, conventional MRI parameters, and combination of ADC and cMRI parameters for differentiating CLs from USs and degenerated LMs.

	Cutoff value	Youden index	Sensitivity (%)	Specificity (%)	AUC
Differentiation of CLs from USs					
ADC ($\times 10^{-6}$ mm^2/sec)	839	0.417	59.38	82.35	0.710
cMRI	–	0.609	68.75	92.16	0.877
cMRI+ADC	–	0.789	90.62	88.24	0.915
Differentiation of CLs from degenerated LMs					
ADC ($\times 10^{-6}$ mm^2/sec)	1239	0.684	78.26	90.20	0.906
cMRI	–	0.578	69.57	88.24	0.780
cMRI+ADC	–	0.893	91.30	98.04	0.980

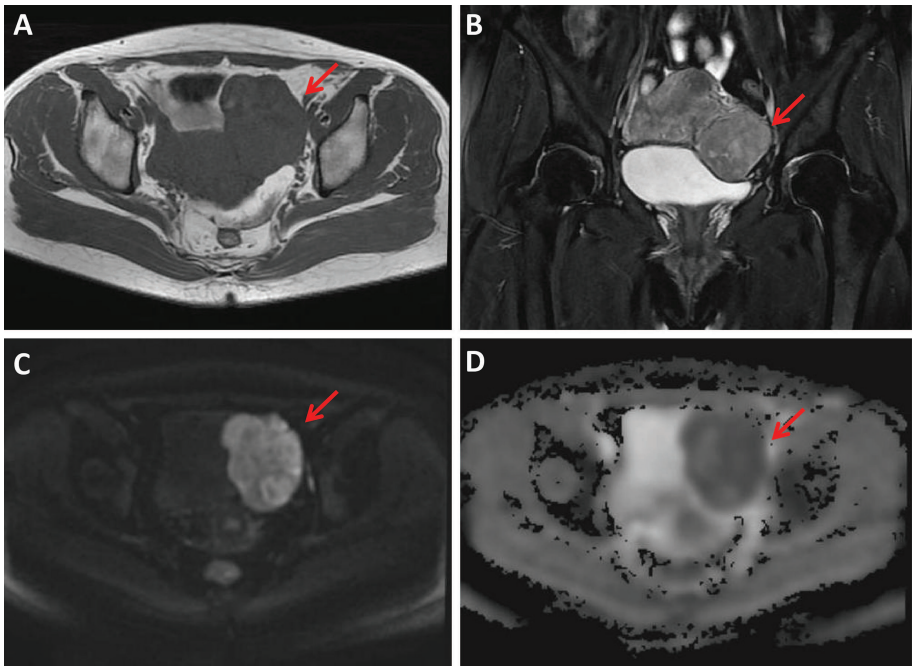

FIGURE 3
A 49-year-old woman with a uterine sarcoma. A mass was found in the uterine-side wall (arrow) with an unclear margin, showing heterogeneous iso-to-hyperintensity on T1WI **(A)** and heterogeneous hyperintensity on T2WI images **(B)**. The tumor showed high signal intensity on diffusion-weighted MR image **(C)** with a low ADC value (ADC = 736 × 10^{-6} mm^2/sec) **(D)**.

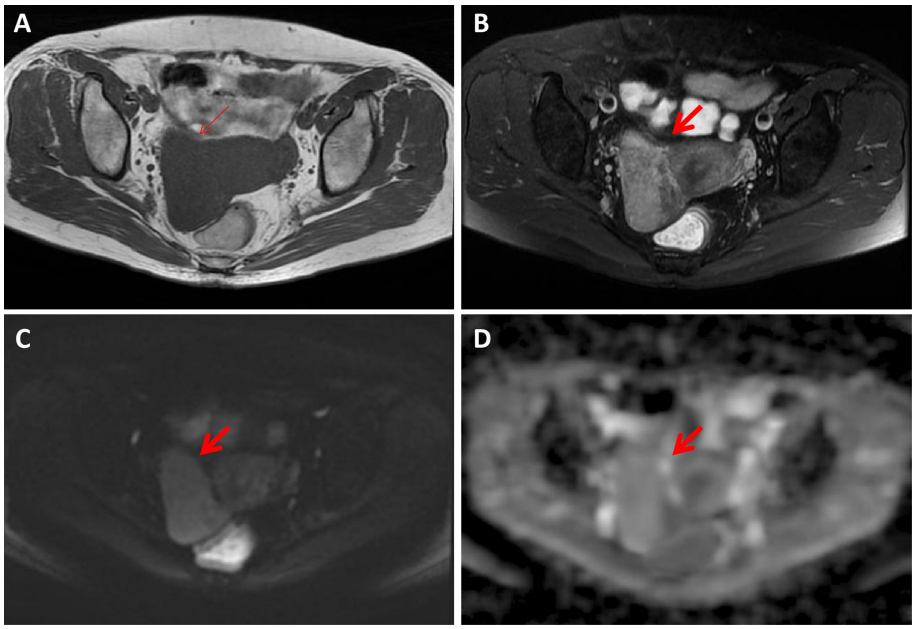

FIGURE 4
A 56-year-old woman with a hydropic degeneration leiomyoma. The mass was detected in the uterine right wall (arrow) with isointensity on T1WI **(A)** and heterogenous iso-to-hyperintensity on T2WI images **(B)**. The tumor showed high signal intensity on diffusion-weighted MR image **(C)** with a high ADC value (ADC = 1339 × 10^{-6} mm^2/sec) **(D)**.

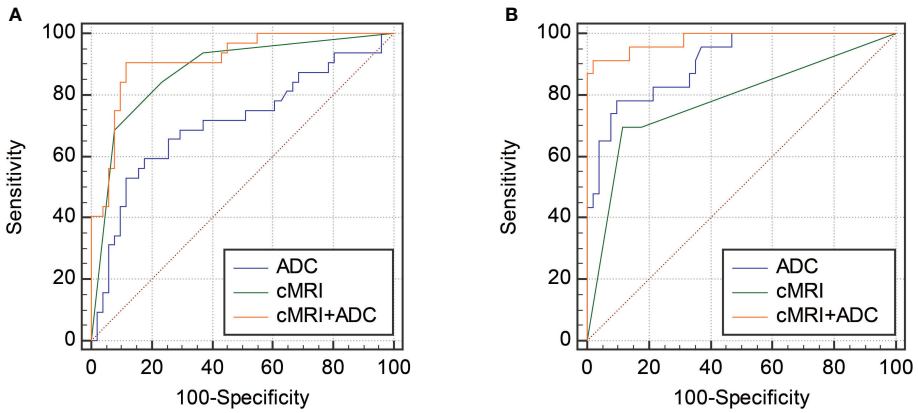

FIGURE 5
ROC curves showing the diagnostic performances of cMRI, ADC and the combination of cMRI and ADC in differentiating CLs from degenerated LMs **(A)** and USs **(B)**.

cMRI vs. cMRI+ADC: z statistic = 2.292, $P = 0.022$) for the differentiation of CLs from USs. The combination of T2WI signal from cMRI and ADC value also significantly improved the diagnostic performance for the discrimination of CLs from degenerated LMs with an AUC of 0.980, a sensitivity of 91.30% and a specificity of 98.04% (ADC vs. cMRI+ADC: z statistic = 2.083, $P = 0.037$; cMRI vs. cMRI+ADC: z statistic = 3.820, $P < 0.0001$).

Discussion

The incidence of CLs is low, and their signs and symptoms are non-specific, whereas the biological behavior of CLs is borderline, showing a potential of malignant transformation and a high recurrence rate (14). Hence, differentiation of CLs from other atypical CLs and USs is crucial for selecting optimal treatment strategies and improving prognosis of patients. In this current study, we systematically investigate the characteristics from cMRI and found that irregular morphology, ill-defined margin, and hyperintense signals on T2WI were most valuable features that could dramatically differentiate CLs from USs or degenerated LMs. With the combination of cMRI characteristics and ADC value derived from DWI, optimal sensitivity and specificity can be achieved in distinguishing these entities.

Uterine LMs are histologically composed of smooth muscle cells with little or no mitotic activity; on the other hand, CLs were defined as an atypical subset of uterine leiomyomas with higher cellularity than the adjacent myometrium. In clinic, diagnosis of typical LMs is not difficult when lesions in uterine have imaging characteristics, such as isointense T1 signal with regular morphology and well-defined margins (15). However, when LMs present atypical imaging manifestations, particularly with degeneration, the accurate differentiation will be very challenging (16, 17). In this study, we found both CLs and degenerated LMs can be associated with degeneration or cystic changes, inducing hyperintensity on T2WI images. However, for the solid portion of the uterine masses, we found CLs were more likely to show a global or focal hyperintensity on fs-T2WI images compared with degenerated LMs. Recent reviews have shown a significantly higher signal on T2-weighted images in hypercellular uterine tumors in comparison to benign leiomyomas, which generally demonstrate homogenously low signal on T2-weighted images (18, 19), which further helps in explaining in the findings present in this study, as CLs are increasingly recognized as a borderline tumor with hypercellularity. Additionally, CLs is composed of densely cellular fascicles of smooth muscle with little intervening collagen (20). Mitotic figures are few, and there is little or no cytologic atypia (20). Its hypercellular nature with little collagenous tissue may both contribute to signal increase on T2WI images. Moreover, an ADC value of 1239 $\times 10^{-6}$ mm^2/sec or less might indicate the diagnosis of CLs without manifestation of malignant tumor, which was consistent with a previous study (20). In that study, Takeuchi et al. (20) reported that the ADC value of CLs were significantly lower than that of degenerated LMs. Our finding indicated that the biological components of CLs are different from those of degenerated LMs. LMs with degeneration can still be considered as benign LMs which enriched in extracellular matrix with abundant collagen types I-III, whereas CLs are more hypercellular, resulting in higher prevalence of high signal intensity on T2WI images and lower ADC values (14). Of note, even though ADC can provider a slightly higher sensitivity and specificity, the diagnostic performance of ADC and cMRI is comparable. However, when we combined cMRI with ADC value from the solid portion of the mass, the diagnostic performance can be significantly improved with an AUC of 0.980.

Moreover, a recent case-control study showed that CLs had a distinct clinical phenotype from LMs and showed some characteristics shared with USs (5). Thus, CL may be recognized as a subgroup of leiomyoma variants where benign disease evolves to malignancy (5). Importantly, in this present study, we found both cMRI features, including morphology and margin, are independent indicators of USs. Specifically, when the uterine mass is associated irregular morphology and ill-defined margin, it highly suggests a possibility of US, which were in good line with previous studies (14, 16). Histopathologically, USs are aggressive malignant tumors which can easily invade the normal surrounding tissue, demonstrating the irregular and ill-defined margins. Additionally, compared with CLs, USs had a lower ADC value with a cutoff of 839×10^{-6} mm^2/sec. It was not surprising that CLs would be associated with higher ADC values compared with USs due to lower cellularity. However, promisingly, when ADC was added into the diagnostic flow of cMRI, the diagnostic performance of differentiating CLs from USs can be significantly improved with an AUC of 0.915.

Our study has several limitations. First, the number of patients with sarcomas was relatively small due to its extreme rarity. Second, this retrospective study was conducted without validation. Selection bias should be taken into consideration. An external and/or prospective validation with more numerous patients will be performed to translate our results into the clinic. Third, considering the rarity of uterine CLs, disease prevalence and a grade of suspicion would have influence on the results of the MRI systems.

In conclusion, we presented characteristic MRI features of among cellular leiomyomas, degenerated leiomyomas and uterine sarcomas. We also proved the ADC value of these lesions could assist the diagnosis and differentiate cellular leiomyoma from uterine sarcoma and atypical leiomyoma. The combination of cMRI and ADC value can be a reliable tool for distinguishing these entities, which is useful for optimization of treatment strategies for uterine tumor, avoiding inappropriate less invasive treatment options.

Data availability statement

The original contributions presented in the study are included in the article/Supplementary Material. Further inquiries can be directed to the corresponding author.

Ethics statement

The studies involving human participants were reviewed and approved by the ethical committee of Fujian Maternity and Child Health Hospital. Written informed consent for participation was not required for this study in accordance with the national legislation and the institutional requirements.

Author contributions

Study concept and design: CW and KL. Acquisition of data: CW, QW, and KL. Resources: CW, XZ, ZZ, YS, and KL. Analysis and interpretation of data: CW and KL. Drafting of the manuscript: CW. Critical revision of the manuscript for important intellectual content: CW and KL. Technical or material support: CW, XZ, ZZ, YS, and KL. Study supervision: KL. All authors read and approved the final manuscript.

Acknowledgments

The authors thank Dr. Zebin Xiao (MD, PhD), a principal investigator and professor at the University of Pennsylvania for kindly proofreading.

Conflict of interest

The authors declare that the research was conducted in the absence of any commercial or financial relationships that could be construed as a potential conflict of interest.

Publisher's note

References

1. Management of symptomatic uterine leiomyomas: ACOG practice bulletin, number 228. *Obstet Gynecol* (2021) 137(6):e100–e15. doi: 10.5603/GP.2016.0054

2. Sikora-Szczęśniak DL. Prevalence of cellular leiomyoma and partially cellular leiomyoma in postoperative samples - analysis of 384 cases. *Ginekol Pol* (2016) 87 (9):609–16. doi: 10.1148/radiographics.19.5.g99se131179

3. Murase E, Siegelman ES, Outwater EK, Perez-Jaffe LA, Tureck RW. Uterine leiomyomas: histopathologic features, MR imaging findings, differential diagnosis, and treatment. *Radiographics* (1999) 19(5):1179–97. doi: 10.1148/radiographics.19.suppl_1.g99oc04s131

4. Ueda H, Togashi K, Konishi I, Kataoka ML, Koyama T, Fujiwara T, et al. Unusual appearances of uterine leiomyomas: MR imaging findings and their histopathologic backgrounds. *Radiographics* (1999) 19:S131–45. doi: 10.1016/j.ajog.2010.03.018

5. Taran FA, Weaver AL, Gostout BS, Stewart EA. Understanding cellular leiomyomas: a case-control study. *Am J Obstet Gynecol* (2010) 203(2):109.e1–6. doi: 10.1016/j.ajog.2010.03.018

6. Guraslan H, Senturk MB, Helvacioglu C, Aktas AG, Yasar L. Recurrent cellular leiomyoma 10 years after total abdominal hysterectomy. *J Obstet Gynaecol* (2015) 35(8):854–5. doi: 10.3109/01443615.2015.1009421

7. Rothmund R, Kurth RR, Lukasinski NM, Huebner M, Hartkopf A, Wallwiener M, et al. Clinical and pathological characteristics, pathological reevaluation and recurrence patterns of cellular leiomyomas: A retrospective study in 76 patients. *Eur J Obstet Gynecol Reprod Biol* (2013) 171(2):358–61. doi: 10.1016/j.ejogrb.2013.10.004

8. Moinfar F, Azodi M, Tavassoli FA. Uterine sarcomas. *Pathology* (2007) 39 (1):55–71. doi: 10.1080/00313020601136146

9. Santos P, Cunha TM. Uterine sarcomas: Clinical presentation and MRI features. *Diagn Interv Radiol* (2015) 21(1):4–9. doi: 10.5152/dir.2014.14053

10. DeMulder D, Ascher SM. Uterine leiomyosarcoma: Can MRI differentiate leiomyosarcoma from benign leiomyoma before treatment? *AJR Am J Roentgenol* (2018) 211(6):1405–15. doi: 10.2214/AJR.17.19234

11. Sutter O, Soyer P, Shotar E, Dautry R, Guerrache Y, Placé V, et al. Diffusion-weighted MR imaging of uterine leiomyomas following uterine artery embolization. *Eur Radiol* (2016) 26(10):3558–70. doi: 10.1007/s00330-016-4210-0

12. Abdel Wahab C, Jannot AS, Bonaffini PA, Bourillon C, Cornou C, Lefrère-Belda MA, et al. Diagnostic algorithm to differentiate benign atypical leiomyomas from malignant uterine sarcomas with diffusion-weighted MRI. *Radiology* (2020) 297(2):361–71. doi: 10.1148/radiol.2020191658

13. Xiao Z, Zheng Y, Li J, Chen D, Liu F, Cao D. Four-dimensional CT angiography (4D-CTA) in the evaluation of juvenile nasopharyngeal angiofibromas: comparison with digital subtraction angiography (DSA) and surgical findings. *Dentomaxillofac Radiol* (2017) 46(8):20170171. doi: 10.1259/dmfr.20170171

14. Sun S, Bonaffini PA, Nougaret S, Fournier L, Dohan A, Chong J, et al. How to differentiate uterine leiomyosarcoma from leiomyoma with imaging. *Diagn Interv Imag* (2019) 100(10):619–34. doi: 10.1016/j.diii.2019.07.007

15. Malek M, Rahmani M, Seyyed Ebrahimi SM, Tabibian E, Alidoosti A, Rahimifar P, et al. Investigating the diagnostic value of quantitative parameters based on T2-weighted and contrast-enhanced MRI with psoas muscle and outer myometrium as internal references for differentiating uterine sarcomas from leiomyomas at 3T MRI. *Cancer Imag* (2019) 19(1):20. doi: 10.1186/s40644-019-0206-8

16. Barral M, Placé V, Dautry R, Bendavid S, Cornelis F, Foucher R, et al. Magnetic resonance imaging features of uterine sarcoma and mimickers. *Abdom Radiol (NY)* (2017) 42(6):1762–72. doi: 10.1007/s00261-017-1076-9

17. Deshmukh SP, Gonsalves CF, Guglielmo FF, Mitchell DG. Role of MR imaging of uterine leiomyomas before and after embolization. *Radiographics* (2012) 32(6):E251–81. doi: 10.1148/rg.326125517

18. Tanaka YO, Nishida M, Tsunoda H, Okamoto Y, Yoshikawa H. Smooth muscle tumors of uncertain malignant potential and leiomyosarcomas of the uterus: MR findings. *J Magn Reson Imag* (2004) 20(6):998–1007. doi: 10.1002/jmri.20207

19. Yamashita Y, Torashima M, Takahashi M, Tanaka N, Katabuchi H, Miyazaki K, et al. Hyperintense uterine leiomyoma at T2-weighted MR imaging: differentiation with dynamic enhanced MR imaging and clinical implications. *Radiology* (1993) 189(3):721–5. doi: 10.1148/radiology.189.3.8234695

20. Takeuchi M, Matsuzaki K, Nishitani H. Hyperintense uterine myometrial masses on T2-weighted magnetic resonance imaging: differentiation with diffusion-weighted magnetic resonance imaging. *J Comput Assist Tomogr* (2009) 33(6):834–7. doi: 10.1097/RCT.0b013e318197ec6f

frontiers | Frontiers in Oncology

TYPE Original Research
PUBLISHED 17 October 2022
DOI 10.3389/fonc.2022.958219

OPEN ACCESS

EDITED BY
Alessio G. Morganti,
University of Bologna, Italy

REVIEWED BY
Timothy Carroll,
The University of Chicago,
United States
Cristina Lavini,
Amsterdam University Medical Center,
Netherlands
Mira Liu,
University of Chicago Medicine,
United States

*CORRESPONDENCE
Zujun Hou
houzj@sibet.ac.cn

†These authors have contributed equally to this work and share first authorship

‡These authors have contributed equally to this work and share senior authorship

SPECIALTY SECTION
This article was submitted to Gynecological Oncology, a section of the journal Frontiers in Oncology

RECEIVED 31 May 2022
ACCEPTED 04 August 2022
PUBLISHED 17 October 2022

CITATION
Wang X, Li S, Lin X, Lu Y, Mao C, Ye Z, Li X, Koh T-S, Liu J, Liu J, Ma X, Cheng J, Ning G, Yan Z and Hou Z (2022) Evaluation of tracer kinetic parameters in cervical cancer using dynamic contrast-enhanced MRI as biomarkers in terms of biological relevance, diagnostic performance and inter-center variability. *Front. Oncol.* 12:958219. doi: 10.3389/fonc.2022.958219

Evaluation of tracer kinetic parameters in cervical cancer using dynamic contrast-enhanced MRI as biomarkers in terms of biological relevance, diagnostic performance and inter-center variability

Xue Wang[1†], Shujian Li[2†], Xianhui Lin[3], Yi Lu[1], Chuanwan Mao[1], Zhijun Ye[4], Xuesheng Li[4], Tong-San Koh[5,6], Jie Liu[2], Jingjing Liu[2], Xiaoyue Ma[2], Jingliang Cheng[2], Gang Ning[4], Zhihan Yan[1‡] and Zujun Hou[1,7*‡]

[1]Department of Radiology, The Second Affiliated Hospital and Yuying Children's Hospital of Wenzhou Medical University, Wenzhou, China, [2]Department of Magnetic Resonance Imaging (MRI), The First Affiliated Hospital of Zhengzhou University, Zhengzhou, China, [3]Department of Pathology, The Second Affiliated Hospital and Yuying Children's Hospital of Wenzhou Medical University, Wenzhou, China, [4]Department of Radiology, The Second Affiliated Hospital of Sichuan University, Chengdu, China, [5]Department of Oncologic Imaging, National Cancer Center, Singapore, Singapore, [6]The department of Jiangsu Key Laboratory of Medical Optics, Duke-National University of Singapore (NUS) Graduate Medical School, Singapore, Singapore, [7]Jiangsu Key Laboratory of Medical Optics, Suzhou Institute of Biomedical Engineering and Technology, Chinese Academy of Sciences, Suzhou, China

Objectives: This study assessed the clinical value of parameters derived from dynamic contrast-enhanced (DCE) MRI with respect to correlation with angiogenesis and proliferation of cervical cancer, performance of diagnosis and reproducibility of DCE-MRI parameters across MRI scanners.

Materials and Methods: A total of 113 patients with cervical carcinoma from two centers were included in this retrospective study. The DCE data were centralized and processed using five tracer kinetic models (TKMs) (Tofts, Ex-Tofts, ATH, SC, and DP), yielding the following parameters: volume transfer constant (Ktrans), extravascular extracellular volume (Ve), fractional volume of vascular space (Vp), blood flow (Fp), and permeability surface area product (PS). CD34 counts and Ki-67 PI (proliferation index) of cervical cancer and normal cervix tissue were obtained using immunohistochemical staining in Center 1.

Results: CD34 count and Ki-67 PI in cervical cancer were significantly higher than in normal cervix tissue ($p<0.05$). Parameter Ve from each TKM was significantly smaller in cervical cancer tissue than in normal cervix tissue ($p<0.05$), indicating the higher proliferation of cervical cancer cells. Ve of

each TKM attained the largest AUC to diagnose cervical cancer. The distributions of DCE parameters for both cervical cancer and normal cervix tissue were not significantly different between two centers (P>0.05).

Conclusion: Parameter Ve was similar to the expression of Ki-67 in revealing the proliferation of tissue cells, attained good performance in diagnosis of cervical cancer, and demonstrated consistent findings on measured values across centers.

KEYWORDS

imaging biomarker, dynamic contrast-enhanced imaging, reproducibility, multicenter study, cervix cancer

Introduction

Cervical cancer is one of the top three most common cancers in women under 45 years old worldwide. Approximately 570,000 new cases and 311,000 deaths from cervical cancer occurred in 2018 (1, 2). Studies have proved that intra-tumoral microvessel density (MVD) are related strongly to tumor aggressiveness (such as invasive growth, lymphatic metastasis, and disease-free survival) (3–5). However, tumor MVD and its proliferation is generally obtained by immunohistochemical staining, which could be expressed by CD34 and ki-67 proliferation index (PI) after biopsy or operation. It would be desirable to identify biomarkers that can be used to assess tumor biology and to monitor the effects of treatment *in vivo*.

Dynamic contrast-enhanced magnetic resonance imaging (DCE-MRI) is a potential tool for characterizing tumor microcirculation. A variety of tracer kinetic models (TKMs) have been employed to diagnose various tumors and to assess the effects of anti-angiogenic and anti-vascular drugs in clinical trials (6–11). The Tofts model and the Extended Tofts (Ex-Tofts) model are frequently used for analysis of DCE-MRI data in clinical research or in clinical trials. A variety of two-compartment (the compartment of intravascular space and the extravascular extracellular space) models (2CXM) were proposed, which separately describe the intravascular transport using parameters blood (plasma) flow (Fp) and the exchange between the intravascular and the extravascular space using vessel permeability (PS), including the standard two-compartment model (SC), the adiabatic approximation to tissue homogeneity (ATH) and the distributed parameter model (DP) (12–15). Five DCE parameters (Ktrans, Fp, Vp, Ve, and PS) from above TKMs were obtained to assess tissue microcirculation. Interested readers can refer to Koh et al. (14) for a review on tracer kinetic modeling and the relevant clinical applications.

In spite of the advancement of tracer kinetic modeling and the promising results in various clinical studies, it remains challenging in developing robust imaging biomarkers, which require that imaging measurements sensitively capture the tissue biology of interest in a reliable and standardized fashion. A good quantitative biomarker should have three properties (16): biological relevance to the disease process under study, sensitivity to the disease process, and reliability (i.e., good reproducibility). Relevance and sensitivity could be established in single-center studies. Reproducibility of measurements might be good at single centers where the initial studies were carried out (to establish the sensitivity). However, at multiple centers, this will have to be established again.

Very few studies have been conducted to assess the kinetic parameters derived using DCE-MRI TKMs from the view of rigorous definition of biomarker, which has limited the widespread use of DCE parameters in clinical practice. This study attempted to (1) examine the relationship between DCE parameters and immunohistochemical indicators (CD34 and ki-67) in cervical cancer, (2) investigate the diagnostic performance of DCE parameters in differentiating cervical cancer and normal cervix tissue, and (3) evaluate the reproducibility of measured DCE parameters from various TKMs in cervical cancer patients using different scanners in a multicenter clinical setting.

Materials and methods

Subjects of study

This retrospective study was approved by the local ethics review boards in two institutions of this study. A total of 166 consecutive female patients, who were diagnosed with cervical carcinoma by histology and underwent MRI examination were reviewed in this study in the period of April 2016 to May 2021 in two centers. The inclusion criteria were: (1) patients diagnosed

with cervical carcinoma by histology examination and (2) no history of chemoradiotherapy or surgery before MRI examination. Patients were excluded for the following reasons: (1) poor image quality of DCE-MRI such as significant motion artifacts or incomplete images (n=10), (2) patients with a history of targeted chemotherapy or radiation therapy before examination (n=16), (3) patients diagnosed with submucous myoma of uterus (n=5) and the endometrial carcinoma (n=4), and (4) no mass was identified for patients with stage Ia and Ib on DCE and other MRI sequences (n=18). Finally, 95 patients with cervix cancer and 18 cervical myoma were included in this retrospective study. ROIs (regions-of-interest) of normal tissue were obtained from cervical myoma and cervix cancer patients. ROIs for the tumor were obtained from cervix cancer patients.

Imaging protocol

All MRI examinations were performed using two scanners: a 3T GE scanner (Discovery 750, GE Healthcare, Waukesha, WI, USA) from Center 1 and a 3T Siemens scanner (Skyra, Siemens AG, Erlangen, Germany) from Center 2.

T1-, T2-weighted and diffusion weighted images were acquired before intravenous administration of a gadolinium-based extracellular contrast agent (0.2 mmol/kg). The injection rate was 2~3 ml/s, with a dose of 0.1 mmol/kg body weight, followed by a 20 ml normal saline flush. DCE images were acquired in the axial plane under quiet respiration. After that, a routine late contrast-enhanced T1-weighted scan was acquired in the sagittal plane. Parameter settings of DCE imaging protocols were implemented based on the recommendation of Quantitative Imaging Biomarkers Alliance (QIBA) (17) but with improvement on temporal resolution according to the Nyquist-Shannon sampling theorem as detailed in Table 1.

TABLE 1 Parameters of DCE MRI acquisition protocol.

	Center 1	Center 2
Vendor	GE	Siemens
Model	Discovery 750	Skyra
Field strength	3.0T	3.0T
Basic sequence	LAVA	VIBE
DCE protocol		
Pre-contrast FA	4°, 8°, 11°	3°, 5°, 8°
Post-contrast FA	11°	8°
TE (msec)	1.2	1.2
TR (msec)	3.3	2.4
FOV (mm2)	360×360	380×285
Matrix	256×256	224×134
Slice thickness (mm)	5	5
Number of slices	6	20
Pre-contrast phases	10	10
Post-contrast phases	180	180
Temporal resolution (sec)	2.0	2.0

LAVA, liver acquisition with volume acquisition.
VIBE, volumetric interpolated breath-hold examination.

Immunohistochemical assessment and histomorphometry of CD34 and Ki-67

Whether to perform the immunohistochemical analysis or not was according to the requirement of diagnosis in pathology or the treatment direction from clinician. Thus, immunohistochemical analysis with CD34 and Ki-67 may not be available for all the cervix cancer. In this study, the immunohistochemical analysis was performed in 14 cervix cancer and 12 cervix myoma. Some cervix masses were too large to accurately identify the normal cervix tissue in the visual field when reviewing the immunohistochemistry slides. Under 400 × magnification, we would exclude the CD34 count of the normal tissue if the number of CD34 of the normal tissue neighboring to the cervix mass was 0. Comparing with Ki-67, CD34 count of the normal tissue was evidently affected by the material limitation. Finally, the CD34 count and Ki-67 PI of cervix cancer mass were obtained from 14 cervix cancer patients. CD34 was obtained from 11 normal cervix tissue samples, including six cervix cancer and five cervix myoma. Ki-67 PI was obtained from 23 normal cervix tissue samples, including 13 cervix cancer and 10 cervix myoma.

The samples were fixed in 10% formalin and embedded in paraffin, according to standard procedures. A 3 μm thick sections were cut and mounted on glass slides. For each case, the routine hematoxylin and eosin staining, toluidine blue staining and immunohistochemical analysis with CD34 and Ki-67 were performed. Negative control was performed in immunohistochemical analysis. A gynecological pathologist with more than 6 years of experience reviewed the immunohistochemistry slides. The immunohistochemical analysis enabled calculation of two parameters:

(1) Microvessel density (MVD). CD34 of each tumor nuclei was labeled with CD34 monoclonal antibody (Maixin, Fuzhou, China). Single endothelial cell or clusters of endothelial cells positive for CD 34 was considered as a microvessel. The presence of blood cells or fibrin without any detectable endothelial cells is not sufficient to define a microvessel. Vessels with muscular walls were not counted. For each tumor, four hot spots (areas with the highest density of microvessels) were identified at low magnifications (×100). Subsequently, MVD was counted in each field (×400). The counts were expressed as the average of the four fields examined for each tumor.

(2) Ki-67 proliferation index (PI). Ki-67 of each tumor tissue was expressed as the percentage of tumor nuclei labeled with

anti-MIB-1 monoclonal antibody (Maixin, Fuzhou, China). Under 400 × magnification, 1000 tumor cells were counted in 10 high-power visual fields at random. The Ki-67 PI was then defined as the number of positive cells/total cell count.

Tracer kinetic models

DCE images were analyzed using a commercial software (MItalytics, FITPU Healthcare, Singapore). The following parameters were obtained: volume transfer constant (Ktrans, min−1) and extravascular extracellular volume (Ve, ml/100 ml) for Tofts; Ktrans, Ve, and fractional volume of vascular space (Vp, ml/100 ml) for Ex-Tofts; blood flow (Fp, ml/min/100 ml); permeability surface area product (PS, ml/min/100 ml), Vp, and Ve for ATH, SC, and DP. Details of the five tracer kinetic models (Tofts, Ex-Tofts, ATH, SC, and DP models) used in this study can be found in several review papers (13, 14, 18). For completeness, the operational equations of these models, which specify the dependence of tissue tracer concentration $C_{tiss}(t)$ (as a function of time t) on AIF and relevant physiological parameters were listed as follows:

Tofts model:

$$C_{tiss}(t) = AIF \otimes K^{trans}\exp\left(-\frac{K^{trans}}{v_e}t\right) \quad (1)$$

Ex-Tofts model:

$$C_{tiss}(t) = AIF\, v_p + AIF \otimes K^{trans}\exp\left(-\frac{K^{trans}}{v_e}t\right) \quad (2)$$

ATH model:

$$C_{tiss}(t) = AIF \otimes F_p\left\{\begin{array}{l} u(t) - u\left(t-\frac{v_p}{F_p}\right)+ \\ u\left(t-\frac{v_p}{F_p}\right)\left\{1-\exp\left(-\frac{PS}{F_p}\right)\left[1+\int_0^{t-\frac{v_p}{F_p}}\exp\left(-\frac{PS}{v_e}\tau\right)\sqrt{\frac{PS}{v_e}\frac{PS}{F_p}\frac{1}{\tau}}I_1\left(2\sqrt{\frac{PS}{v_e}\frac{PS}{F_p}\tau}\right)d\tau\right]\right\}\end{array}\right\} \quad (3)$$

SC model:

$$C_{tiss}(t) = AIF \otimes F_p[A\ \exp(\alpha t) + (1-A)\exp(\beta t)], \quad (4a)$$

where

$$\begin{pmatrix}\alpha\\ \beta\end{pmatrix} = \frac{1}{2}\left[-\left(\frac{PS}{v_p}+\frac{PS}{v_e}+\frac{F_p}{v_p}\right) \pm \sqrt{\left(\frac{PS}{v_p}+\frac{PS}{v_e}+\frac{F_p}{v_p}\right)^2 - 4\frac{PS}{v_e}\frac{F_p}{v_p}}\right], \quad (4b)$$

$$A = \frac{\alpha + \frac{PS}{v_p} + \frac{PS}{v_e}}{\alpha - \beta}, \quad (4c)$$

and

DP model:

$$C_{tiss}(t) = AIF \otimes F_p\left\{\begin{array}{l} u(t) - u\left(t-\frac{v_p}{F_p}\right)+ \\ u\left(t-\frac{v_p}{F_p}\right)\left\{1-\exp\left(-\frac{PS}{F_p}\right)\left[1+\int_0^{t-\frac{v_p}{F_p}}\exp\left(-\frac{PS}{v_e}\tau\right)\sqrt{\frac{PS}{v_e}\frac{PS}{F_p}\frac{1}{\tau}}I_1\left(2\sqrt{\frac{PS}{v_e}\frac{PS}{F_p}\tau}\right)d\tau\right]\right\}\end{array}\right\} \quad (5)$$

Image post-processing

For each patient, ROIs for the tumor and the normal tissue were manually delineated on the central slices of DCE images (to avoid possible effects of inflow and inhomogeneity near boundaries) by a radiologist with more than 10 years of experience in gynecological radiology. Routine T1-weighted, T2-weighted, and DW images were referenced to currently delineate ROIs. The size of ROI was no less than 10 voxels to ensure robustness of measurement. The normal ROIs were selected in the normal cervix tissue away from the lesions. The areas of necrotic, cystic, and hemorrhages were avoided when drawing the lesion ROIs. All ROIs were confirmed by a senior radiologist, and disagreements were resolved with consensus-based discussion. The arterial input function (AIF) was sampled from a voxel that clearly resided within the external iliac artery on one of the central slices. Desirable features for AIF selection included an early bolus arrival time, high peak value and signal-to-noise ratio. The sampled AIF and concentration-time curve of cervix cancer ROI and the normal tissue are showed in Figure 1. The concentration of normal tissue is higher than the tumor in each phase. In later phase, the enhanced pattern of normal tissue is “persist”, and the cancer is “wash out”.

Statistical analysis

The median parameter value of voxels in tumor ROIs on multiple slices for each patient was taken as a representative statistic of the parameter. Kolmogorov-Smirnov test was conducted to analyze the normality of CD34 counts, Ki-67 PI in Center 1, and DCE parameters in two centers. Independent sample t-test was used to compare the differences of CD34 counts between cervix cancer and the normal tissue in Center 1. Mann–Whitney U test was used to compare the differences of Ki-67 PI between cervical cancer and normal cervix tissue in Center 1. Pearson correlation coefficient r was used to explore possible relationship between immunohistochemical indicators (CD34 and Ki-67) and DCE kinetic parameters from the five models (Ex-Tofts, Tofts, ATH, SC, and DP) of cervix lesion and normal tissue in Center 1. A strong correlation was assumed for $0.8 < r \leq 1$, a moderate correlation for $0.5 < r \leq 0.8$, a weak correlation for $0.3 < r \leq 0.5$, and no correlation for $r \leq 0.3$ (19). Receiver operating

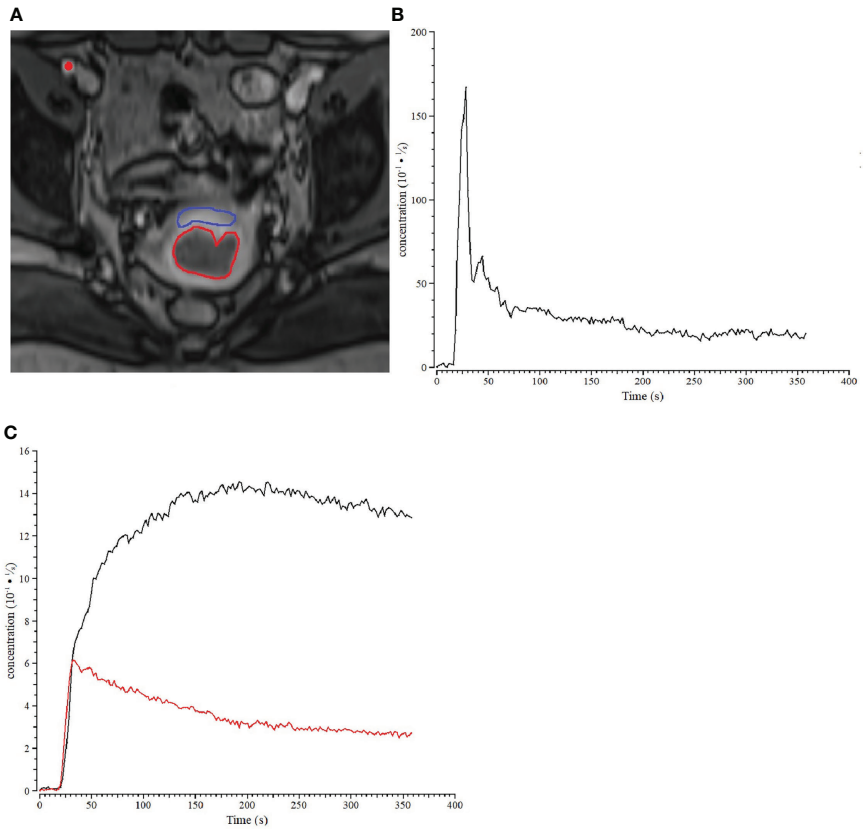

FIGURE 1
Example of a patient with stage IIb cervix cancer. **(A)** ROIs for cervix cancer (bred) and normal cervix tissue (blue) are shown for one slice of the DCE-MRI dataset, and the location within the iliac artery where the AIF was sampled was marked with a red dot. **(B)** Sample of AIF for the cervix cancer patient. **(C)** The concentration-time curve of cervix cancer (red) ROI and the normal tissue (black).

characteristic (ROC) analysis was performed to examine the ability of each parameter of the two centers in discriminating cervix tumor and normal tissue, and the discriminating power of each parameter was quantified using the area under ROC curve (AUC). Interpretation of AUC values is application-dependent, and in general, it is appropriate that values ≥0.9 would be "excellent", ≥0.8 "good", ≥0.7 "fair", and<0.7 "poor" (20). Mann–Whitney U test was used to compare the distribution differences of various parameters in two centers. $P<0.05$ indicated statistical significance. Analyses were performed using SPSS Statistics (version 21.0, IBM Corp., Armonk, NY, USA).

Results

Study population

Of the 166 cases, 113 cases met the criteria of inclusion and formed the final study cohort with age mean and range of 56 years (37–75 years) and 48.5 years (31–72 years) in Center 1 and Center 2, respectively (Figure 2). Characteristics for cervix cancer patients were summarized in Table 2.

Cervical cancer microenvironment characterization in center 1

CD34 counts in cervical cancer (20.35 ± 5.82) were significantly higher than in normal cervix tissue (5.98 ± 2.77) ($P<0.05$). Ki-67 PI in cervical cancer (65% ± 29%) was significantly higher than in normal cervix tissue (1%) ($P<0.05$) (Figure 3). Pearson correlation between immunohistochemical indicators (CD34 and Ki-67) and DCE kinetic parameters from the five models (Ex-Tofts, Tofts, ATH, SC, and DP) of cervix lesion and normal tissue in Center 1 were showed in Table 3. For Ex-Tofts and Tofts models, parameter Ktrans was negatively correlated with Ki-67 PI ($r>0.5$, $P<0.05$) for cervical cancer, and weak or little correlation was observed between parameters Vp

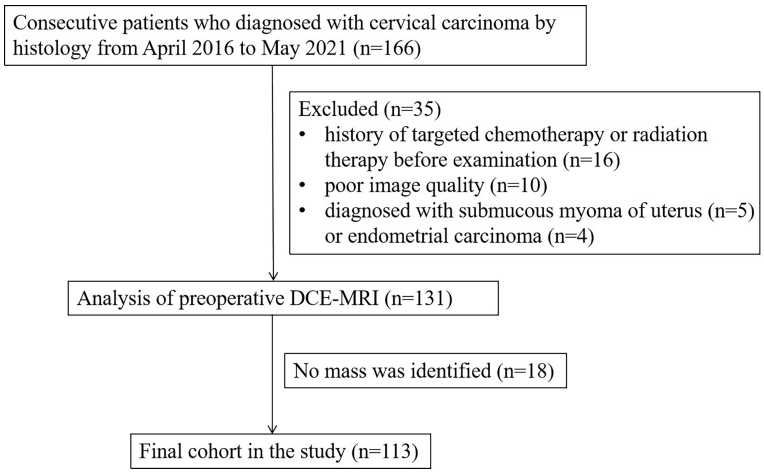

FIGURE 2
Flowchart of patient population.

or Ve and Ki-67 PI (r<0.4, *P* >0.05). For 2CXMs (ATH, SC, and DP), Vp was negatively correlated with Ki-67 PI (r>0.6, P<0.05) for cervical cancer. Weak or little correlation was observed in either cervical cancer or normal cervix tissue between Ve and Ki-67 PI (r<0.3, P>0.05). Inconsistent correlation across 2CXMs in cervical cancer was shown between PS and Ki-67 PI (r=-0.489, P=0.076 for ATH; r=0.218, P=0.454 for SC; and r=-0.143, P=0.627 for DP, respectively). Moderately, negative correlation was noted on Fp from SC and DP with Ki-67 PI in cervical cancer (r=-0.520, P=0.057 for SC; r=-0.537, P=0.047 for DP).

Correlations between DCE-MRI parameters and CD34 in cervical cancer or normal cervix tissue were largely weak or not correlated, except for Fp from ATH in normal cervix tissue (r=-0.622, P<0.05).

Diagnostic performance of DCE-MRI parameters in differentiating cervical cancer from normal cervix tissue

For Center 1, 47 ROIs for cervical cancer were obtained. A total of 63 ROIs for normal tissues were obtained from 16 cervix myoma and 47 cervical cancer patients. For Center 2, 48 ROIs for cervical cancer were obtained. A total of 50 ROIs for normal tissues were obtained from two cervix myoma and 48 cervical cancer patients.

AUC values of DCE kinetic parameters derived by five models (Ex-Tofts, Tofts, ATH, SC, and DP) in differentiating cervical carcinoma tissue from normal cervix tissue in two centers were listed in Table 4, where Ve attained the largest AUC in each TKM. Figure 4 showed the ROC of parameter Ve from the five models (Ex-Tofts, Tofts, ATH, SC, and DP) in Center 1 and Center 2, respectively. At least one parameter in each TKM attained good performance (AUC value > 0.8) to diagnose cervical cancer in both centers, except for parameter of SC model in Center 2 (the highest AUC value=0.761). Figure 5 showed the parameter (Ve) maps generated using the ATH model for cervix cancer and the normal tissue.

TABLE 2 Cervix cancer patient characteristics.

Characteristics	Center 1(n=47)	Center 2(n=48)
Age average (range)	56(37–75)	48.5(31–72)
Histologic type		
Squamous cell carcinoma (SCC)	45	39
Adenocarcinoma	2	6
Adenosquamous carcinoma	0	3
Grade		
G1	13	3
G2	17	4
G3	2	34
Not graded	15	7
Clinic stage		
Ia	6	3
Ib	17	33
IIa	12	7
IIb	7	3
IIIa	3	2
IIIc	1	0
IVa	1	0
IVb	0	0
Treatment before MR examination		
Chemoradiotherapy	0	0
Surgery	0	0
No Treatment	47	48

10.3389/fonc.2022.958219

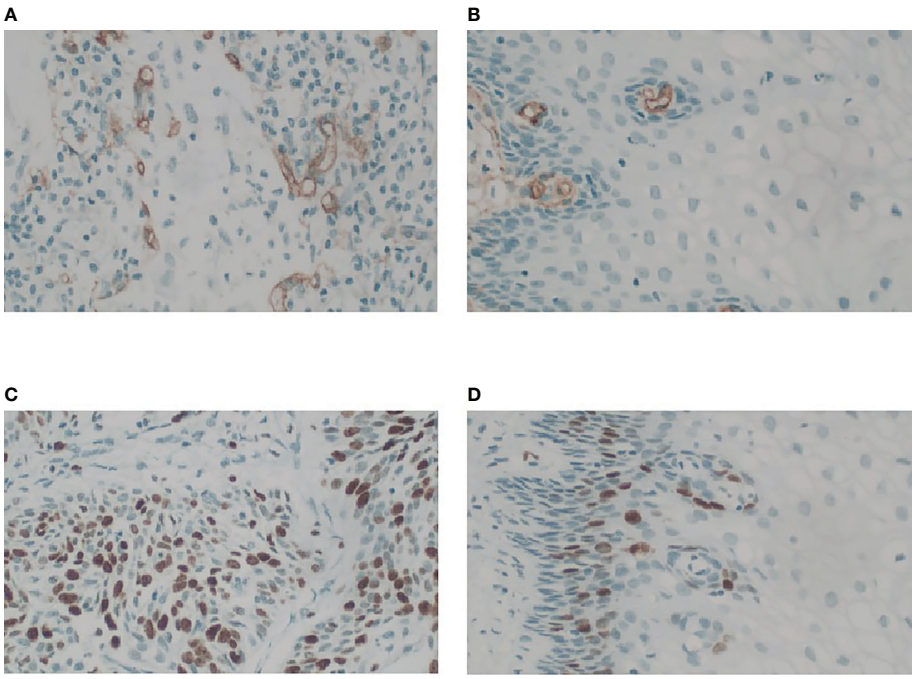

FIGURE 3
Microphotograph showing MVD and Ki-67 PI in cervix cancer mass and the normal tissue for stage IIb cervix cancer in Center 1 (GE 750). **(A)** Magnification (×40) of one of the hot spots in cervix cancer reveals a high histological microvessel density. **(B)** Magnification (×40) of one of the hot spots in normal cervix tissue reveals a low histological microvessel density. **(C)** Immunostain of a cervix cancer for Ki67 showing labelling of roughly 70% of nuclei, 40×. **(D)** Immunostain of the normal cervix tissue for Ki67 showing positive expression is located in the base, 40×.

TABLE 3 Results of Pearson correlation immunohistochemical indicators (CD34 and Ki-67) and DCE kinetic parameters (Ktrans, Fp,Vp, Ve, PS) from Tofts, Ex-Tofts, ATH, SC, and DP models of cervix lesion and normal tissue in Center 1, withcorrelation coefficients and p-values in the bracket.

	Ktrans (min^{-1})	Fp (ml/min/100 ml)	Vp (ml/100 ml)	Ve (ml/100 ml)	PS (ml/min/100 ml)
Tofts model					
Cervix lesion					
CD34	-0.024 (0.936)	–	–	0.09 (0.759)	–
Ki-67	-0.550 (0.041)	–	–	-0.216 (0.459)	–
Normal tissue					
CD34	-0.369 (0.264)	–	–	-0.473 (0.142)	–
Ex-Tofts model					
Cervix lesion					
CD34	-0.028 (0.924)	–	0.353 (0.215)	0.07 (0.813)	–
Ki-67	-0.554 (0.04)	–	-0.321 (0.263)	-0.252 (0.384)	–
Normal tissue					
CD34	-0.404 (0.218)	–	0.40 (0.223)	-0.491 (0.125)	–
ATH model					
Cervix lesion					
CD34	–	-0.046 (0.877)	0.068 (0.817)	0.065 (0.824)	-0.209 (0.473)

(Continued)

TABLE 3 Continued

	Ktrans (min^{-1})	Fp (ml/min/100 ml)	Vp (ml/100 ml)	Ve (ml/100 ml)	PS (ml/min/100 ml)
Ki-67	–	-0.057 (0.847)	-0.661 (0.01)	-0.198 (0.430)	-0.489 (0.076)
Normal tissue					
CD34	–	-0.622 (0.041)	0.357 (0.282)	-0.456 (0.158)	-0.493 (0.123)
CC model					
Cervix lesion					
CD34	–	0.08 (0.786)	-0.125 (0.669)	0.071 (0.808)	-0.389 (0.170)
Ki-67	–	-0.520 (0.057)	-0.747 (0.002)	-0.065 (0.824)	0.218 (0.454)
Normal tissue					
CD34	–	-0.146 (0.668)	-0.243 (0.471)	-0.245 (0.469)	-0.340 (0.307)
DP model					
Cervix lesion					
CD34	–	0.023 (0.938)	0.080 (0.787)	0.033 (0.911)	-0.329 (0.250)
Ki-67	–	-0.537 (0.047)	-0.673 (0.008)	-0.268 (0.355)	-0.143 (0.627)
Normal tissue					
CD34	–	-0.055 (0.872)	-0.198 (0.559)	-0.113 (0.742)	-0.41 (0.164)

Reproducibility of DCE-MRI parameters across centers

The distribution differences among various parameters of cervical cancer and normal tissue in different centers were assessed by Man–Whitney U test, and shown in Table 5 for the five models (Tofts, Ex-Tofts, ATH, SC, and DP). The distribution of parameters Ktrans, Ve from Tofts for both cervix cancer and normal tissue, showed similar in Center 1 and Center 2 (P>0.05). The distribution of parameters Fp, Vp, Ve, PS from ATH for cervix cancer showed similar in Center 1 and Center 2 (P>0.05). The distribution of at least three parameters from SC and DP models for cervix cancer showed similar between the two centers (P>0.05).

Discussion

In this study, we investigated the potential of DCE-MRI parameters as biomarkers with respect to correlation with

TABLE 4 AUC values of DCE kinetic parameters derived by various models in differentiating cervical carcinoma tissue from normal cervix tissue in the three centers.

DCE kinetic parameters	Center 1	Center 2
Tofts-Ktrans	0.503	0.517
Tofts-Ve (ml/100 ml)	0.894	0.847
Ex-Tofts–Ktrans	0.571	0.504
Ex-Tofts–Vp (ml/100 ml)	0.669	0.544
Ex-Tofts–Ve (ml/100 m)	0.891	0.864
ATH-Fp (ml/min/100 ml)	0.783	0.658
ATH-Vp (ml/100 ml)	0.693	0.508
ATH-Ve (ml/100 ml)	0.899	0.876
ATH-PS (ml/min/100 ml)	0.627	0.555
SC-Fp (ml/min/100 ml)	0.506	0.538
SC-Vp (ml/100 ml)	0.55	0.614
SC-Ve (ml/100 ml)	0.861	0.761
SC-PS (ml/min/100 ml)	0.782	0.668
DP-Fp (ml/min/100 ml)	0.505	0.504
DP-Vp (ml/100 ml)	0.504	0.612
DP-Ve (ml/100 ml)	0.915	0.884
DP-PS (ml/min/100 ml)	0.681	0.610

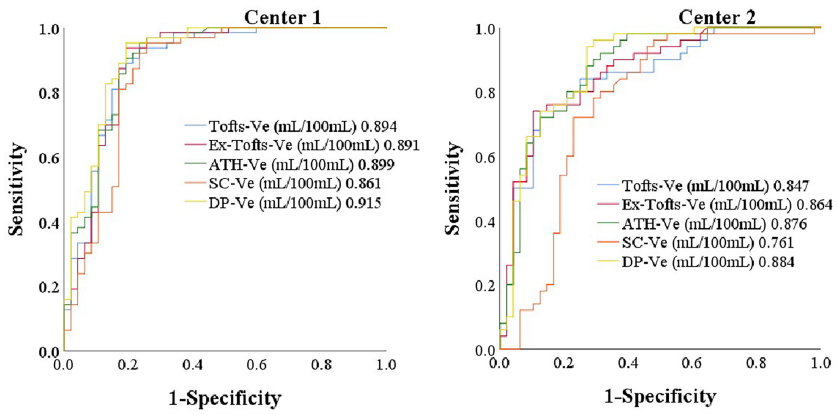

FIGURE 4
The ROC of parameter Ve from the five models (Ex-Tofts, Tofts, ATH, SC, and DP) in Center 1 and Center 2, respectively.

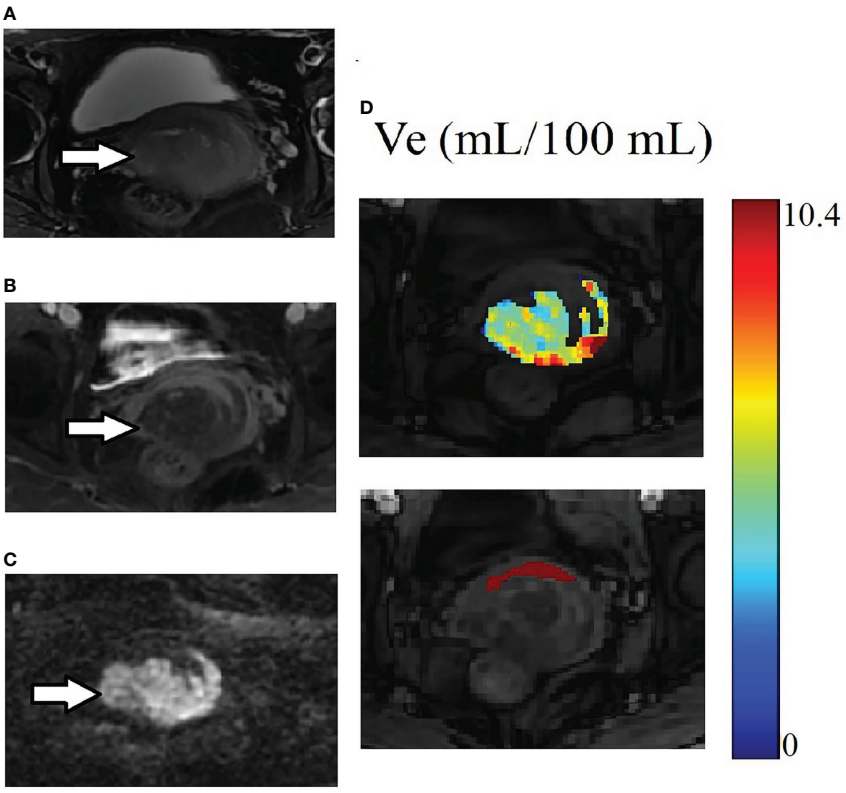

FIGURE 5
Example of MRI scans for the same patient in Figure 3. **(A)** Cervix cancer exhibits slightly high signal intensity on axial T2-weighted image. **(B)** The degree of enhancement for cervix cancer is lower than the normal cervix tissue on delayed contrast imaging. **(C)** Cervix cancer exhibits high signal intensity on DW image. **(D)** The parameter Ve maps generated using the ATH model for cancer and the normal tissue ROIs. The upper and lower images are for cancer and the normal tissue ROIs respectively. Parameter Ve value of cervix cancer is significantly smaller than that of normal cervix tissue.

TABLE 5 Measured values (median and inter-quantile range in the bracket) of DCE kinetic parameters (Ktrans, Fp,Vp, Ve, PS) derived from (Tofts, Ex-Tofts, ATH, SC, and DP models) in cervical cancer and normal cervix tissue, and the corresponding p-values of Mann−Whitney U test.

	Ktrans (min^{-1})	Fp (ml/min/100 ml)	Vp (ml/100 ml)	Ve (ml/100 ml)	PS (ml/min/100 ml)
Tofts model					
Cervix lesion					
Center 1	0.09 (0.08,0.13)	–	–	13.91 (11.32,17.30)	–
Center 2	0.13 (0.08,0.19)	–	–	13.97 (10.07,17.61)	–
Z value	-1.858	–	–	-0.074	–
P value	0.063	–	–	0.941	–
Normal tissue		–	–		–
Center 1	0.11 (0.07,0.14)	–	–	30.74 (22.40,42.62)	–
Center 2	0.12 (0.08,0.16)	–	–	28.46 (19.29,39.73)	–
Z value	-1.595			-1.350	
P value	0.111	–	–	0.177	–
Ex-Tofts model					
Cervix lesion					
Center 1	0.07 (0.05,0.10)	–	1.71 (1.21,2.34)	12.65 (10.05,17.30)	–
Center 2	0.10 (0.06,0.16)	–	1.45 (1.02,2.20)	14.04 (11.14,17.78)	–
Z value	-2.066	–	-1.042	-1.589	–
P value	0.039	–	0.297	0.112	–
Normal tissue		–			–
Center 1	0.09 (0.05,0.12)	–	1.08 (0.27,2.06)	33.75 (24.63,45.38)	–
Center 2	0.10 (0.07,0.13)	–	1.72 (0.93,2.80)	29.77 (19.93,41.44)	–
Z value	-1.333		-1.827	-2.220	
P value	0.182	–	0.068	0.026	–
ATH model					
Cervix lesion					
Center 1		21.88 (17.82,35.43)	2.43 (1.26,4.03)	11.16 (9.17,15.58)	7.10 (4.78,9.54)
Center 2		26.36 (18.03,36.74)	2.64 (1.64,3.97)	12.32 (8.62,17.35)	9.44 (5.61,13.21)
Z value		-.897	-.707	-.175	-1.924
P value		0.370	0.479	0.861	0.054
Normal tissue					
Center 1		39.25 (31.65,51.61)	1.00 (0.39,2.56)	33.89 (23.94,45.93)	9.57 (5.70,13.34)
Center 2		35.37 (24.98,46.73)	2.72 (1.43,6.29)	27.52 (18.14,38.91)	9.74 (6.43,14.76)
Z value		-1.908	-3.645	-2.197	-0.853
P value		*P*=0.056	*P*< 0.001	0.028	0.394
SC model					
Cervix lesion					
Center 1		15.26 (12.61,21.78)	6.12 (4.00,8.62)	8.74 (6.36,14.14)	4.76 (2.73,8.29)
Center 2		19.06 (15.40,30.82)	6.39 (5.01,8.27)	10.88 (6.68,19.83)	5.52 (3.13,10.82)
Z value		-2.791	-0.197	-0.867	-0.878
P value		0.005	0.844	0.386	0.380
Normal tissue					
Center 1		16.65 (12.15,20.51)	5.70 (2.99,9.91)	26.39 (19.25,39.25)	13.47 (6.61,22.14)
Center 2		22.14 (15.96,34.69)	8.49 (5.42,12.58)	31.11 (18.25,46.92)	9.39 (6.37,16.73)
Z value		-3.512	-2.321	-0.425	-1.734
P value		*P*< 0.001	0.02	0.671	0.083
DP model					
Cervix lesion					
Center 1		13.83 (11.64,17.00)	3.04 (2.08,5.37)	10.56 (8.63,14.83)	6.81 (4.92,9.33)
Center 2		14.81 (0.05,0.10)	4.04 (3.43,6.14)	10.48 (7.73,15.39)	8.31 (5.68,12.22)

(Continued)

TABLE 5 Continued

	Ktrans (min^{-1})	Fp (ml/min/100 ml)	Vp (ml/100 ml)	Ve (ml/100 ml)	PS (ml/min/100 ml)
Z value		-1.455	-2.099	-0.462	-1.012
P value		0.146	0.036	0.644	0.311
Normal tissue					
Center 1		13.93 (0.08,0.13)	3.77 (1.80,6.03)	29.82 (23.59,39.35)	11.63 (6.21,17.87)
Center 2		16.22 (11.27,22.54)	5.58 (4.09,8.80)	24.52 (17.35,35.95)	11.46 (7.30,14.95)
Z value		-2.017	-3.226	-2.208	-0.801
P value		.044	0.001	.027	.423

angiogenesis and proliferation of cervical cancer, performance of differential diagnosis, and reproducibility of DCM-MRI parameters across MRI scanners in different centers. It was turned out that Ktrans of Tofts or Ex-Tofts, Vp of three 2CXMs, Fp of ATH, and DP, showed moderately negative correlation with Ki-67 in cervical cancer tissue, and Fp of ATH showed moderately negative correlation with CD34 in normal cervix tissue. Ve of each TKM attained the largest AUC. No significant differences were observed on the distributions of most DCE-MRI parameters in either cervical cancer or normal cervix tissue between Center 1 and Center 2, indicating certain degree of reproducibility between these two scanners.

As a transmembrane glycoprotein expressed in capillary endothelial cells, CD34 is a useful angiogenesis marker reflecting the grade of microvascular modeling in cervical cancer (21). This study found that the expression of CD34 in cervical cancer tissue was significantly higher than that in normal cervix tissue, indicating that there is an increased neovascularization in cervical cancer tissue. In DCE tracer kinetic modeling, Vp reflects the fractional volume of intravascular space, with measurement corresponding to tissue MVD. However, measured Vp values in TKMs were smaller in cervical cancer than in normal cervix tissue, and showed little correlation with the expression of CD34. Hauge et al. (22) investigated the potential of DCE-MRI to assess MVD using patient-derived cervical cancer xenografts and found that none of the DCE-MRI parameters was related to MVD. The discrepancy could be explained as follows. As pointed out by Hylton (23), MVD, as measured using immunohistopathological method, gives a partial picture of the tissue microvasculature, but does not reflect the functional property of microvasculature, including permeability, which contributes to the DCE-MRI measurement. In addition, MVD is also a heterogeneous property of tumors. MVD measurement methods are limited by histopathologic sampling and are generally hotspot values, which are, by definition, localized. Accurate correlation necessitates precise comparison of anatomical MRI maps with whole-mount histological tumor specimens rather than with biopsy specimens that may only represent a small sample of the tumor, so that comparably sized and geometrically oriented regions of interest can be compared (24).

Instead of assessing direct association between global DCE-MRI parameter and local histopathologic sampling data, a more reasonable way could be relative comparison with self-reference. In the context of current study, study object is cervical cancer tissue and reference object is normal cervix tissue. Either DCE-MRI parameter or histopathologic indicator independently forms two sampled datasets in cervical cancer tissue and reference tissue, from which sample statistic can be estimated and inference between cervical cancer and reference tissue can be conducted. With this in mind, we can proceed to the interpretation of parameter Ve from the view point of biomarker.

Ve measures the fractional volume of extravascular extracellular space, which is inversely related to cellular density and could be linked to cell proliferation. Sustained proliferation of cells is one of the most important characteristics of cancer (25). Ki67, a nuclear antigen expressed in the nucleus of cells in active proliferation, is considered a valid nuclear marker of cell proliferation. Studies revealed that Ki67 is highly expressed in proliferative cells in many kinds of cancers, but rarely in normal cells (26, 27). As shown in the results, the expression of Ki-67 in cervical cancer tissue (65% ± 29%) was significantly higher than in normal cervix tissue (1%), indicating the higher proliferation of cervical cancer cells. On the other hand, measured values of Ve of each TKM were significantly smaller in cervical cancer tissue than in normal cervix tissue (Table 5), suggesting the higher density of cervical cancer cells, which was in accordance with the findings from Ki-67 expression. In addition, Ve almost attained the highest diagnostic performance in differentiating cervical cancer from normal cervix tissue by all TKMs, and the measured Ve values showed certain degree of reproducibility between Center 1 and Center 2.

The study had the following limitations. The experiment of immunohistopathologic staining was limited to a subset of cases in one center for patients for whom it was requested by the physician, which may have introduced bias. It would be desirable to conduct the experiment in a larger dataset across different

centers. The size of study cohort in each center was relatively small, and the differences of sample demographics and tumor grade distribution could be prone to sources of variations between the two centers. Next step, we will continue to explore the issue of parameter reproducibility in a larger cohort with the same grade cervix cancer among centers.

In conclusion, this study assessed the potential of DCE-MRI kinetic parameters as biomarkers in cervical cancer and found that, in each tracer kinetic model, parameter Ve was similar to the expression of Ki-67 in reflecting tissue cell proliferation, attained good performance in differential diagnosis of cervical cancer and normal cervix tissue, and demonstrated results on measured values across centers without significant difference between distributions. From this point of view, Ve measurements derived from primary tracer kinetic models were equally applicable as potential imaging biomarkers in cervical cancer diagnosis.

Data availability statement

The raw data supporting the conclusions of this article will be made available by the authors, without undue reservation.

Ethics statement

This study was reviewed and approved by Ethics Committee of the Second Affiliated Hospital and Yuying Children's Hospital of Wenzhou Medical University. The ethics committee waived the requirement of written informed consent for participation.

Author contributions

XW and SL co-first authors because they did data collection, compilation and postprocessing, literature study and manuscript drafting, and neither of them is a trainee. ZY and ZH were the senior author and corresponding author respectively, because they contributed the conception of the work, were responsible for the execution of the project in the respective institution, facilitated the progress of this multicenter study, revised the manuscript and approved the final manuscript for submission. Material preparation, data collection and analysis were performed by XiL, YL, ZJY, XuL, T-SK, JL, JJL, XM, JC, GN. All authors contributed to the article and approved the submitted version.

Funding

This study has received funding from Wenzhou Science and Technology Buteau in China (No.Y20220070) and Zhejiang Provincial Medical and Health Project (No.2023RC212).

Acknowledgments

The authors were grateful to Mr Liuyang Chen of Fitpu Healthcare for his assistance in software customization during data processing.

Conflict of interest

The authors declare that the research was conducted in the absence of any commercial or financial relationships that could be construed as a potential conflict of interest.

Publisher's note

References

1. Islami F, Chen W, Yu XQ, Lortet-Tieulent J, Zheng R, Flanders WD, et al. Cancer deaths and cases attributable to lifestyle factors and infections in China, 2013. *Ann Oncol* (2017) 28:2567–74. doi: 10.1093/annonc/mdx342

2. Arbyn M, Weiderpass E, Bruni L, de Sanjosé S, Saraiya M, Ferlay J, et al. Estimates of incidence and mortality of cervical cancer in 2018: A worldwide analysis. *Lancet Glob Health* (2020) 8(2):191–203. doi: 10.1016/S2214-109X(19)30482-6

3. Radzikowska J, Krzeski A, Czarnecka AM, Klepacka T, Rychlowska-Pruszynska M, Raciborska A, et al. Endoglin expression and microvessel density as prognostic factors in pediatric rhabdomyosarcoma. *J Clin Med* (2021). doi: 10.3390/jcm10030512

4. Marech I, Gadaleta CD, Ranieri G. Possible prognostic and therapeutic significance of c-kit expression, mast cell count and microvessel density in renal cell carcinoma. *Int J Mol Sci* (2014) 15:13060–76. doi: 10.3390/ijms150713060

5. O'connor JPB, Rose CJ, Waterton JC, Carano RA, Parker GJ, Jackson A. Imaging intratumor heterogeneity: Role in therapy response, resistance, and clinical outcome. *Clin Cancer Res* (2015) 21:249–57. doi: 10.1158/1078-0432.CCR-14-0990

6. Buckley DL, Shurrab AE, Cheung CM, Jones AP, Mamtora H, Kalra PA. Measurement of single kidney function using dynamic contrast-enhanced MRI: Comparison of two models in human subjects. *J Magnetic Resonance Imaging JMRI* (2006) 24:1117–23. doi: 10.1002/jmri.20699

7. Lu Y, Peng WW, Song J, Chen T, Wang X, Hou Z, et al. On the potential use of dynamic contrast-enhanced (DCE) MRI parameters as radiomics features of cervical cancer. *Med Phys* (2019) 46:5098–109. doi: 10.1002/mp.13821

8. Kiessling F, Lichy M, Grobholz R, Heilmann M, Farhan N, Michel MS, et al. Simple models improve the discrimination of prostate cancers from the peripheral

gland by T1-weighted dynamic MRI. *Eur Radiol* (2004) 14:1793–801. doi: 10.1007/s00330-004-2386-1

9. Thomas AL, Morgan B, Horsfield MA, Higginson A, Kay A, Lee L, et al. Phase I study of the safety, tolerability, pharmacokinetics, and pharmacodynamics of PTK787/ZK 222584 administered twice daily in patients with advanced cancer. *J Clin Oncol* (2005) 23:4162–71. doi: 10.1200/JCO.2005.09.034

10. Tofts PS, Brix G, Buckley DL, Evelhoch JL, Henderson E, Knopp MV, et al. Estimating kinetic parameters from dynamic contrast-enhanced T(1)-weighted MRI of a diffusable tracer: Standardized quantities and symbols. *J Magnetic Resonance Imaging JMRI* (1999) 10:223–32. doi: 10.1002/(SICI)1522-2586(199909)10:3<223::AID-JMRI2>3.0.CO;2-S

11. Wang X, Lin WX, Mao YT, Peng W, Song J, Lu Y, et al. A comparative study of two-compartment exchange models for dynamic contrast-enhanced MRI in characterizing uterine cervical carcinoma. *Contrast Media Mol Imaging* (2019). doi: 10.1155/2019/3168416

12. Thomassin-Naggara I, Balvay D, Cuenod CA, Darai E, Marsault C, Bazot M. Dynamic contrast-enhanced MR imaging to assess physiologic variations of myometrial perfusion. *Eur Radiol* (2010) 20:984–94. doi: 10.1007/s00330-009-1621-1

13. Khalifa F, Soliman A, El-Baz A, Abou El-Ghar M, El-Diasty T, Gimel'farb G, et al. Models and methods for analyzing DCE-MRI: Areview. *Med Phys* (2014) 41:124301. doi: 10.1118/1.4898202

14. Koh TS, Bisdas S, Koh DM, Thng CH. Fundamentals of tracer kinetics for dynamic contrast-enhanced MRI. *J Magnetic Resonance Imaging: JMRI* (2011) 34:1262–76. doi: 10.1002/jmri.22795

15. St Lawrence KS, Lee TY. An adiabatic approximation to the tissue homogeneity model for water exchange in the brain: I. theoretical derivation. *J Cereb Blood Flow Metab* (1998) 18:1365–77. doi: 10.1097/00004647-199812000-00011

16. Tofts PS, Collins DJ, Petersen J, Neuberger U, Bonekamp D. Multicentre imaging measurements for oncology and in the brain. *Br J Radiol* (2011) 84:213–26. doi: 10.1259/bjr/74316620

17. Shukla-Dave A, Obuchowski NA, Chenevert TL, Jambawalikar S, Schwartz LH, Malyarenko D, et al. Quantitative imaging biomarkers alliance (QIBA) recommendations for improved precision of DWI and DCE-MRI derived biomarkers in multicenter oncology trials. *J Magnetic Resonance Imaging JMRI* (2019) 49:101–21. doi: 10.1002/jmri.26518

18. Tofts PS, Brix G, Buckley DL, Evelhoch JL, Henderson E, Knopp MV, et al. Estimating kinetic parameters from dynamic contrast enhanced T(1)-weighted MRI of a diffusable tracer: Standardized quantities and symbols. *J Magnetic Resonance Imaging: JMRI* (1999) 10:223–32. doi: 10.1002/(SICI)1522-2586(199909)10:3<223::AID-JMRI2>3.0.CO;2-S

19. Zwick S, Brix G, Tofts PS, Strecker R, Kopp-Schneider A, Laue H, et al. Simulation-based comparison of two approaches frequently used for dynamic contrast-enhanced MRI. *Eur Radiol* (2010) 20:432–42. doi: 10.1007/s00330-009-1556-6

20. Youngstrom EA. A primer on receiver operating characteristic analysis and diagnostic efficiency statistics for pediatric psychology: We are ready to ROC. *J Pediatr Psychol* (2014) 39:204–21. doi: 10.1093/jpepsy/jst062

21. Aijaz M, Alam K, Maheshwari V, Hakim S, Kamal M. Clinicopathological study of role of CD34 expressions in the stroma of premalignant and malignant lesions of uterine cervix. *Ann Diagn Pathol* (2018) 38:87–92. doi: 10.1016/j.anndiagpath.2018.11.007

22. Hauge A, Wegner CS, Gaustad J-V, Simonsen TG, Andersen LMK, Rofstad EK. DCE-MRI of patient-derived xenograft models of uterine cervix carcinoma: Associations with parameters of the tumor microenvironment. *J Transl Med* (2017) 15:225. doi: 10.1186/s12967-017-1331-4

23. Hylton N. Dynamic contrast-enhanced magnetic resonance imaging as an imaging biomarker. *J Clin Oncol* (2006) 24:3293–8. doi: 10.1200/JCO.2006.06.8080

24. Mayr NA, Hawighorst H, Yuh WT, Essig M, Magnotta VA, Knopp MV. MR microcirculation assessment in cervical cancer: Correlations with histomorphological tumor markers and clinical outcome. *J Magnetic Resonance Imaging JMRI* (1999) 10:267–76. doi: 10.1002/(SICI)1522-2586(199909)10:3<267::AID-JMRI7>3.0.CO;2-Y

25. Hanahan D. Weinberg RA: Hallmarks of cancer: The next generation. *Cell* (2011) 144:646–74. doi: 10.1016/j.cell.2011.02.013

26. Kontzoglou K, Palla V, Karaolanis G, Karaiskos I, Alexiou I, Pateras I, et al. Correlation between Ki67 and breast cancer prognosis. *Oncology* (2013) 84:219–25. doi: 10.1159/000346475

27. Sun JZ, Chen C, Jiang G, Tian WQ, Li Y, Sun SR. Quantum dot-based immunofluorescent imaging of Ki67 and identification of prognostic value in HER2-positive (non-luminal) breast cancer. *Int J Nanomed* (2014) 9:1339–46. doi: 10.2147/IJN.S58881

frontiers | Frontiers in Oncology

TYPE Review
PUBLISHED 27 October 2022
DOI 10.3389/fonc.2022.1003930

OPEN ACCESS

EDITED BY
Alessio G. Morganti,
University of Bologna, Italy

REVIEWED BY
Roberto Grassi,
University of Campania Luigi Vanvitelli, Italy
Milly Buwenge,
University of Bologna, Italy

*CORRESPONDENCE
L. Manganaro
lucia.manganaro@uniroma1

†These authors share first authorship

SPECIALTY SECTION
This article was submitted to Gynecological Oncology, a section of the journal Frontiers in Oncology

RECEIVED 26 July 2022
ACCEPTED 26 September 2022
PUBLISHED 27 October 2022

CITATION
Ciulla S, Celli V, Aiello AA, Gigli S, Ninkova R, Miceli V, Ercolani G, Dolciami M, Ricci P, Palaia I, Catalano C and Manganaro L (2022) Post treatment imaging in patients with local advanced cervical carcinoma.
Front. Oncol. 12:1003930.
doi: 10.3389/fonc.2022.1003930

Post treatment imaging in patients with local advanced cervical carcinoma

S. Ciulla[1†], V. Celli[1†], A. A. Aiello[2], S. Gigli[1], R. Ninkova[1], V. Miceli[1], G. Ercolani[1], M. Dolciami[1], P. Ricci[1], I. Palaia[3], C. Catalano[1] and L. Manganaro[1*]

[1]Department of Radiological, Oncological and Pathological Sciences, Sapienza, University of Rome, Rome, Italy, [2]Department of Medical Sciences, University of Cagliari, Cagliari, Italy, [3]Department of Maternal and Child Health and Urological Sciences, Sapienza, University of Rome, Rome, Italy

Cervical cancer (CC) is the fourth leading cause of death in women worldwide and despite the introduction of screening programs about 30% of patients presents advanced disease at diagnosis and 30-50% of them relapse in the first 5-years after treatment. According to FIGO staging system 2018, stage IB3-IVA are classified as locally advanced cervical cancer (LACC); its correct therapeutic choice remains still controversial and includes neoadjuvant chemo-radiotherapy, external beam radiotherapy, brachytherapy, hysterectomy or a combination of these modalities. In this review we focus on the most appropriated therapeutic options for LACC and imaging protocols used for its correct follow-up. We explore the imaging findings after radiotherapy and surgery and discuss the role of imaging in evaluating the response rate to treatment, selecting patients for salvage surgery and evaluating recurrence of disease. We also introduce and evaluate the advances of the emerging imaging techniques mainly represented by spectroscopy, PET-MRI, and radiomics which have improved diagnostic accuracy and are approaching to future direction.

KEYWORDS

MRI, gynecologic malignancies, oncology, cervical cancer, gynecology

Abbreviations: CC, Cervical cancer; LACC, locally advanced cervical cancer; CCRT, Concurrent chemoradiation therapy; RT, Radiotherapy; SCC, Squamous cell carcinoma; LCR, Local Control Rate; OS, Overall Survival; DFS, Disease-Free Survival; NACT, Neoadjuvant chemotherapy; RS, Radical surgery; PFS, Progression-Free Survival; MRI, Magnetic Resonance Imaging; EBRT, External beam radiation therapy; T2WI, T2-weighted imaging; T1WI, T1-weighted imaging; FOV, Field of view; ESUR, European Society of Urogenital Radiology; DWI, Diffusion Weighted Images; FDG-PET, fluorodeoxyglucose-positron emission tomography; LN, Lymph node; NCCN, National Comprehensive Cancer Network; FIGO, International federation of gynecology and obstetrics; CT, Computed Tomography; SI, Signal intensity; ADC, Apparent diffusion coefficient; CRT, Chemoradiotherapy; DCE, Dynamic contrast-enhanced; IVIM, Intravoxel incoherent motion; 18F-FDG, 18F-fluorodeoxyglucose; SUV, Standardized Uptake Value; MRS, MR spectroscopy; CIN, Carcinoma in situ; NSCCs, Non-squamous cell carcinomas; LVSI, Lymphovascular space invasion; US, Ultrasound.

1 Introduction

Cervical cancer (CC) is the fourth leading cause of death in women worldwide, with an estimated global incidence of 470,000 new cases per-year (1).

Despite the introduction of screening programs about 30% of patients presents advanced disease at diagnosis and 30-50% of them relapse in the first 5-years after treatment (2).

Accurate staging is crucial to select a tailored treatment. According to the new International federation of gynecology and obstetrics (FIGO) staging system 2018, stage IA, IB1, IIa1 are classified as early stage of disease and can be treated with surgery, either fertility sparing trachelectomy or radical surgery while stages IB3-IVA are classified as locally advanced cervical cancer (LACC) (Supplementary Table I) (3). For this group of patients surgery remains still controversial, and options are neoadjuvant chemo-radiotherapy, external beam radiotherapy, brachytherapy, hysterectomy or a combination of these modalities (4–6).

Imaging plays a key role in therapeutic strategy allowing selection of responding and non-responding patients after treatment, early determination of additional surgical salvage if needed in presence of residual tumor after radiotherapy and detection of tumor recurrence during post treatment follow-up (7–9).

In this review we focus on the main therapeutic options in patients with LACC and on the wide spectrum of imaging findings after radiotherapy and surgery; moreover, we discuss the role of imaging in evaluating treatment response and selecting patients for salvage surgery in presence of residual tumor after radio-chemotherapy.

2 Research method

The literature search included articles published between 2002 and 2022 from MEDLINE, Embase, and the Cochrane Library. The following MeSH keywords were matched to guide the literature search on Pubmed: (LACC) AND (MRI) AND ((treatment) OR (follow-up)) 82; (LACC) AND (MRI) AND (recurrence) 16; (LACC) AND (MRI) AND (complication) 14; (cervical cancer) AND (MRI) AND (radiomics) 75; (cervical cancer) AND (MRI) AND (spectroscopy) 61; (cervical cancer) AND (MRI) OR (PET-MRI) 74. We included articles that provided detailed information on imaging modalities, treatment, follow-up, and recurrence of LACC, excluding those that did not properly fulfill the goal of our review. Next, case reports, case series, and articles providing views and opinions were excluded.

Our initial literature search included approximately 322 articles; 227 articles were excluded based on the previous criteria. 95 articles were selected for this review.

3 LACC treatment

Nowadays, the treatment of choice for LACC is concomitant chemoradiation therapy (CCRT). However, in case of disease persistence after CCRT, some authors suggest switching to salvage surgery although there is no shared consensus on this. In addition, some authors support the advantage of NACT plus RS as viable alternative treatment.

3.1 Concurrent chemoradiotherapy

Concurrent chemoradiation therapy (CCRT) which generally consists of cisplatin-based chemotherapy and external-beam radiotherapy followed by brachytherapy is the standard organ-preservation treatment for LACC and has become a cornerstone of treatment (4).

CCRT is the optimal choice for stages IB3, II, III and IVA of the disease improving local control and reducing the risk of local regional recurrence in comparison with radiation therapy alone. CCRT provides active systemic cytotoxic agents against CC with the potential to enhance tumor radiosensitivity and to eradicate micro-metastasis.

CCRT allows to decrease of 30% to 50% the risk of death compared to radiotherapy (RT) alone in accordance to the Meta-analysis Group of Medical Research Council Clinical Trials Unit of London which affirmed that chemoradiotherapy leads to a 6% improvement in 5-year survival (HR, 0.81; P<.001) (10). Datta et al. performed another meta-analysis in 2017 based on 2445 patients with > 95% squamous cell carcinoma (SCC) histology receiving either CCRT or RT only without surgery. The results confirmed that CCRT significantly improves outcomes, with increased of local control rate (LCR) and overall survival (OS) rates of 8.4% ($p < 0.001$) and 7.5% ($p < 0.001$), respectively (11).

3.1.1 CCRT followed by surgery

The role of completion surgery after CCRT is currently controversial, since surgery has a high postoperative morbidity (12, 13). The rate of residual disease after CCRT is 40%, and these patients generally have a poor prognosis because they show scarce response to cisplatin-based chemotherapy (14). In these cases, some authors propose radical hysterectomy as an adjunctive treatment, although no guidelines recommend it as a treatment for residual tumors.

Recent literature affirms different results regarding the role and benefit of surgery after CCRT.

Some authors supported the positive impact of adjuvant surgery after CCRT: Lèguevaque et al. argued that completion surgery could improve disease-free survival (DFS), in agreement with Yoshida et al. who also obtained more favorable survival results after adjuvant surgery (15, 16).

On the other hand, Fanfani et al. and Cochrane et al. observed no significant differences in DFS and OS (17, 18).According to Kim G. Van Kol, salvage surgery should be performed only if residual disease is histologically confirmed by biopsy in patients treated with CCRT, to avoid unnecessary surgery and complications (14). Surgery after CCRT undoubtedly leads to improved local control rates; however, distant recurrence often occurs in LACC (19). Further prospective randomized trials should be conducted to evaluate the survival benefit of this strategy.

3.2 NACT followed by RS

Neoadjuvant chemotherapy (NACT) followed by radical surgery (RS) is considered as a valid alternative for LACC and is currently used in many countries (20, 21). Several advantages have been suggested for NACT plus RS: tumor size reduction and possibility of surgical resection, systemic action and consequent loco-regional and distant disease control, sterilization of micrometastasis (22, 23).

According to Benedetti Panici, RS after NACT is a feasible option in LACC with an acceptable survival outcome and mild surgical complications with marginal impact on quality of life (24). Gupta et al. analyzed 635 patients with stages IB2, IIA and IIB and compared NACT followed by surgery with platinum-based CCRT. The authors found that 5-year DFS was lower (69.3% vs 76.7%; HR 1.38, 95% CI 1.02-1.87, p = 0.038) in the NACT group followed by surgery with no significant difference in 5-year OS (75.4% vs 74.7%; HR 1.02, 95% CI 0.75-1.40, p = 0.87) (25). More recently, Zhao et al., on 2158 patients, demonstrated no differences in terms of OS, Progression-Free Survival (PFS), local or distant recurrences (26) (Supplementary Table II).

4 Imaging algorithm and follow-up

In patients with LACC a pre-treatment MRI (Magnetic Resonance Imaging) is performed for loco-regional staging. Mid-treatment MRI (after 5 weeks of concurrent cisplatin chemotherapy with external beam radiation therapy (EBRT) and before intra-cavitary brachytherapy) allows brachytherapy dose-adjustment in proportion to the residual tumour volume (4). This increases local tumour control, reduces toxicity and improves survival. Choose proper sequences and correct plane angles is extremely important to avoid pitfall in local staging of CC. The central role in anatomic assessment of pelvic structures is assigned to T2-weighted imaging (T2WI); T2 sequences should be acquired with thin section (3-4 mm) and field of view (FOV) of 20-24 mm to provide high anatomic resolution and acquired on the cervical axis to provide better locoregional staging (27). In fact, for patients undergoing chemo-radiotherapy treatments, without hysterectomy, T2 sequences oriented on cervical axial and coronal planes are strongly recommended; these are acquired along planes perpendicular and parallel to the endocervical axis (para-axial and para-coronal plane). According to the European Society of Urogenital Radiology (ESUR) guidelines, at least one para-axial oriented plane is required for diffusion weighted images (DWI) (Supplementary Table III) (28).

Conversely, after complementary surgery no more angled planes are required and all the sequences are acquired on sagittal, coronal and axial pure plane. Axial/coronal T2WI or T1-weighted imaging (T1WI) from the renal hilum to the groin are suggested to assess the presence of hydronephrosis and bone and lymph node metastases. Moreover, fluorodeoxyglucose-positron emission tomography (FDG-PET) scanned during radiotherapy treatment may facilitate tailored radiation (e.g. adjustment of EBRT field in relation to the para-aortic lymph node (LN) status) and, if standardized, potentially predict outcome. According to National Comprehensive Cancer Network (NCCN) guidelines, CC follow-up/surveillance changes according to FIGO stage and MRI is considered the preferred imaging modality for assessing locoregional tumor extension while FDG-PET/Computed Tomography (CT) is indicated for nodal and distant staging (4).

Follow-up protocols for LACC include: for stage IB3 or patients who required post-operative adjuvant radiation or chemoradiation a whole body PET/TC FDG usually performed at 3-6 months after completion of CCRT; for stage II-IVa a whole body PET/CT (preferred) or chest/abdomen/pelvic CT with contrast within 3-6 months of completion of therapy, moreover a MRI with contrast is to be considered 3-6 months after the end of treatment. In all cases, the choice and addition of imaging techniques should be evaluated based on symptomatology or clinical concern for recurrence and PET/CT and MRI are considered the techniques of choice (4).

4.1 MRI

MRI is now widely accepted as the most effective modality for detection, staging, treatment planning and follow-up of CC; on MRI, the tumor presents an intermediate signal intensity (SI) on T2WI, a high signal intensity (SI) on DWI at high b-value and a low SI on the apparent diffusion coefficient (ADC) map (29).

Accurate evaluation of tumor regression after therapy can be used to optimize therapeutic strategy and surgical procedure; to this end MRI is the most reliable imaging modality for patients with LACC due to its high tissue resolution in the pelvis. Tumors treated with chemoradiotherapy (CRT) respond with a decrease in size and signal intensity on MRI. The response may be immediate (3–6 months) or, in larger tumors, delayed (6–9 months) (Figures 1–5).

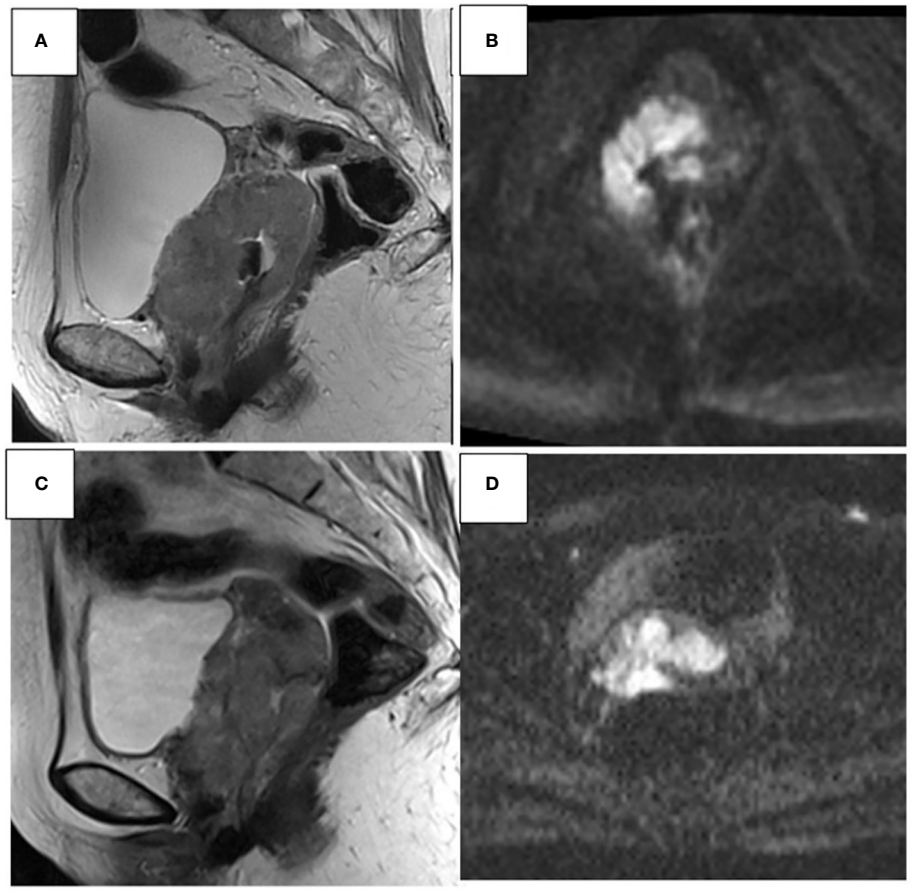

FIGURE 1
45- year-old woman. Sagittal T2W and axial DWI MR images show an invasive CC with parametrial invasion and extension of the upper 2/3 of the vagina **(A, B)**. Stable disease **(C, D)** after CCRT, CC is changed in morphology and size; however, infiltration of the vaginal fornix, upper 2/3 of the vagina, and both parameters remain.

4.1.1 T2W-images

Reconstitution of the normal signal hypointensity of stromal ring and homogeneous cervical low signal on T2-W images, is the most important sign of a complete macroscopic response to treatment (9).

Moreover, MRI has the advantages of a multiplanar evaluation of the surrounding structures, providing a clear assessment of the fornix and better definition of the vaginal wall. Normal vaginal vault has a strongly hypointense muscular wall in T2WI, with well-defined and regular contour.

In the first months after therapy, oedema and necrosis caused by CRT may persist for up to 6 months. For this reason the evaluation of the local response can be difficult since the endocervical canal may be enlarged and/or the cervical stroma may show hyperintensity in T2- WI, resulting in a high risk of false positives (30).

In their study Vincens et al. corelated end of treatment MRI results with histopathological findings in patients with CC and found a sensitivity and specificity of 80% and 55% respectively for the detection of residual disease (31).

4.1.2 Diffusion weighted sequences

The recent published ESUR guidelines (2021) for CC provide a central role of DWI sequences which are strictly recommended combined to T2-WI for a correct staging of CC and evaluation recurrence and response after therapy (28).

Traditionally, DWI sequence provides a qualitative evaluation of malignant tumors characterized by high cellular density which causes a restricts water diffusion in the interstitial space. Therefore, the residual disease appears as an area of high signal, especially to high b-value, associated with lower ADC values compared to normal cervical stroma. DWI allows to distinguish the residual tumor from fibrosis, especially in the patients treated with radiotherapy, which on the contrary, presents low signal intensity at high b values and low signal intensity in ADC maps.

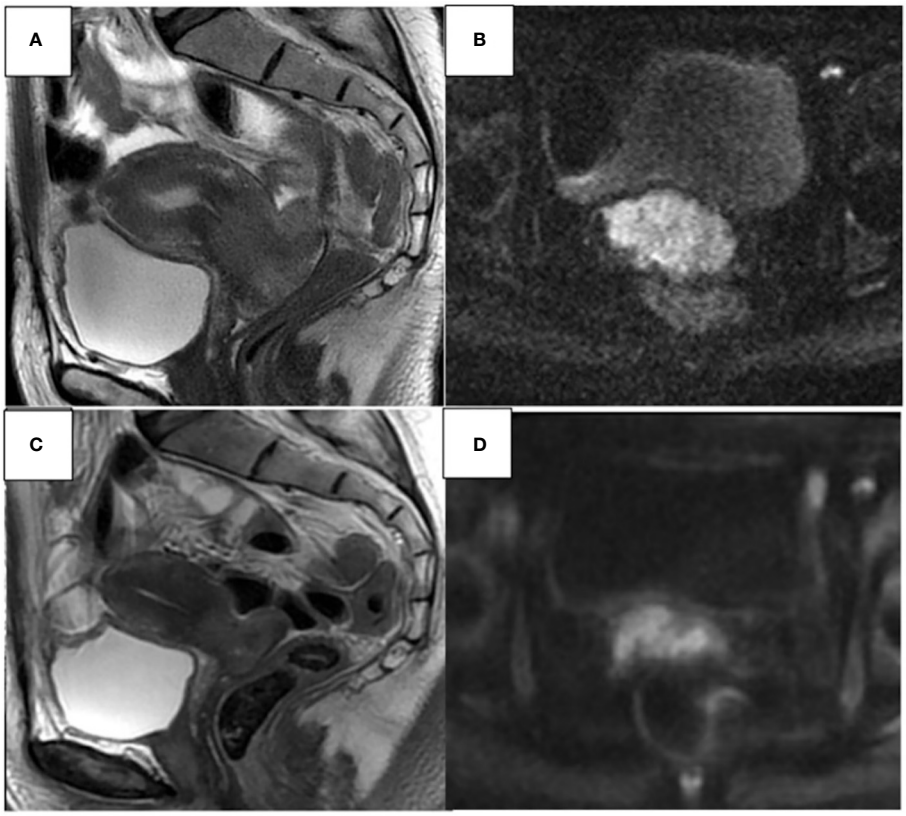

FIGURE 2
48- year-old woman. Sagittal T2W and axial DWI MR images show an invasive CC extending from the uterine isthmus to the external uterine orifice, laterally infiltrating both vaginal fornices, and extending beyond the stromal ring with extensive infiltration of the parameters. **(A, B)**. Partial response **(C, D)** approximately 30% reduction of cervical heteroplastic tissue.

A recent multicenter prospective study found that DWI significantly increases the specificity of MRI in detecting local residual tumor compared to T2W imaging alone when assessing cervical cancer response after radiotherapy. In fact, a previous study showed that T2-W sequence alone had a 50% false positive rate (31). Thomeer et al. highlighted that the combination of high intensity on T2-WI and high intensity on DWI was associated with high specificity in the detection of loco-regional residual disease (84%) (32).

Lucas et al. found that combination T2W/DWI had a positive predictive value of 100% and an accuracy of 92.1% for recurrence/residual disease detection, while T2W imaging alone and the combination T2W/DCE-MRI (Dynamic contrast-enhanced MRI) registered values of 93.3% and 80%, respectively (33).

Recently, some studies evaluated how DWI could also provide a quantitative data for CC. Specifically, quantitative analysis of ADC values obtained from a mono-exponential fit to DWI acquired using at least a value of b and b=0 s/mm2 may assume both a prognostic significance and a predictive value for treatment response and local recurrence (34–39).

In particular, *Fu C. et* all advocated that patients treated with neoadjuvant chemotherapy showed an early increased in ADC values before tumor size reduction after 4 weeks of therapy; this value correlates with a reduction in proliferating cell nuclear antigen and cell density suggestive for response to therapy (40).

Somoye et al. demonstrated that median ADC values at mid-treatment were higher in survivors (1.55 × 10-3 mm2/s) than in non-survivors (1.36 × 10-3 mm2/s) with a difference of 14% (41). Some studies, conducted in a large patient population, have pointed out that in cases of complete response the increase of ADC values in early assessment (≤ 2 weeks) is greater than in partial response and therefore the change of ADC value could be a potential biomarker in identifying tumor aggression and treatment-unresponsive disease (40).

4.1.2.1 Intravoxel incoherent motion

Further improvement have been achieved with the

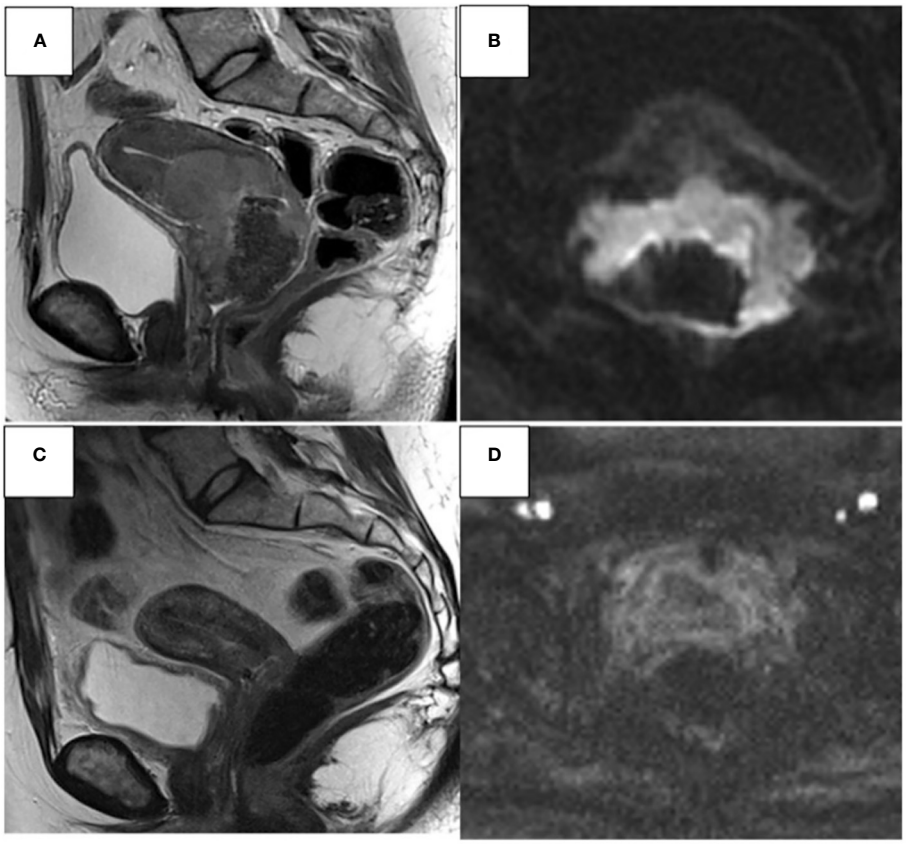

FIGURE 3
37- year-old woman. Sagittal T2W and axial DWI MR images show CC infiltrating both parameters, the upper 1/3 of the vaginal canal, the uterine body, and the left ureter **(A, B)**. Complete response **(C, D)** significant post-CHT reduction of heteroplastic tissue (around 90%).

introduction of intravoxel incoherent motion (IVIM) which uses a bi-exponential model to fit diffusion signal decay at different b-values (42, 43). IVIM allows to distinguishes the diffusion of water molecules in the extracellular space from capillary micro-perfusion through three quantitative parameters: diffusion "D" (diffusion of water in extracellular space); pseudo-diffusion "D*" (the movement of blood water molecules in the capillary network) and perfusion fraction "fp" (volume percentage of water flowing in the capillaries) (44). Different authors have highlighted correlations between this IVIM parameters and CC regarding: the detection of cervical cancer tissue, the presence of lymph node metastasis and treatment response (45–53). Moreover, recent studies suggested that a IVIM model may also predict the tumor aggressiveness and therapy response showing that D values were significantly higher in good responders patients (p = 0.001) and in moderate/high TILs (p = 0.018) and that fp showed significantly higher values in squamous cell tumors (p = 0.006) (54).

4.1.3 Dynamic contrast enhanced: DCE-MRI

According to the ESUR guidelines, DCE-MRI is not mandatory for local CC staging and its primary application is limited to research setting (55). There is not agreement on the most appropriate use of DCE-MRI and its application remains a challenge. However, some authors have evaluated that DCE may help to detect residual tumor and local recurrences (27, 56). DCE MRI is especially useful in post-treatment imaging because it improves the identification of complete or incomplete response distinguishing between the radiation-induced changes and residual disease (27). From the analysis of DCE time- signal intensity curves, Jalaguier et al. observed that intense enhancement of cervical tissue steeper than the myometrial time- intensity curves in the early stage (type B time- signal intensity curves) is significantly associated with the presence of residual tumor, tumor aggressiveness, incomplete response, worse prognosis, and early recurrence (55).

However, enhancement of the cervix is not specific and is

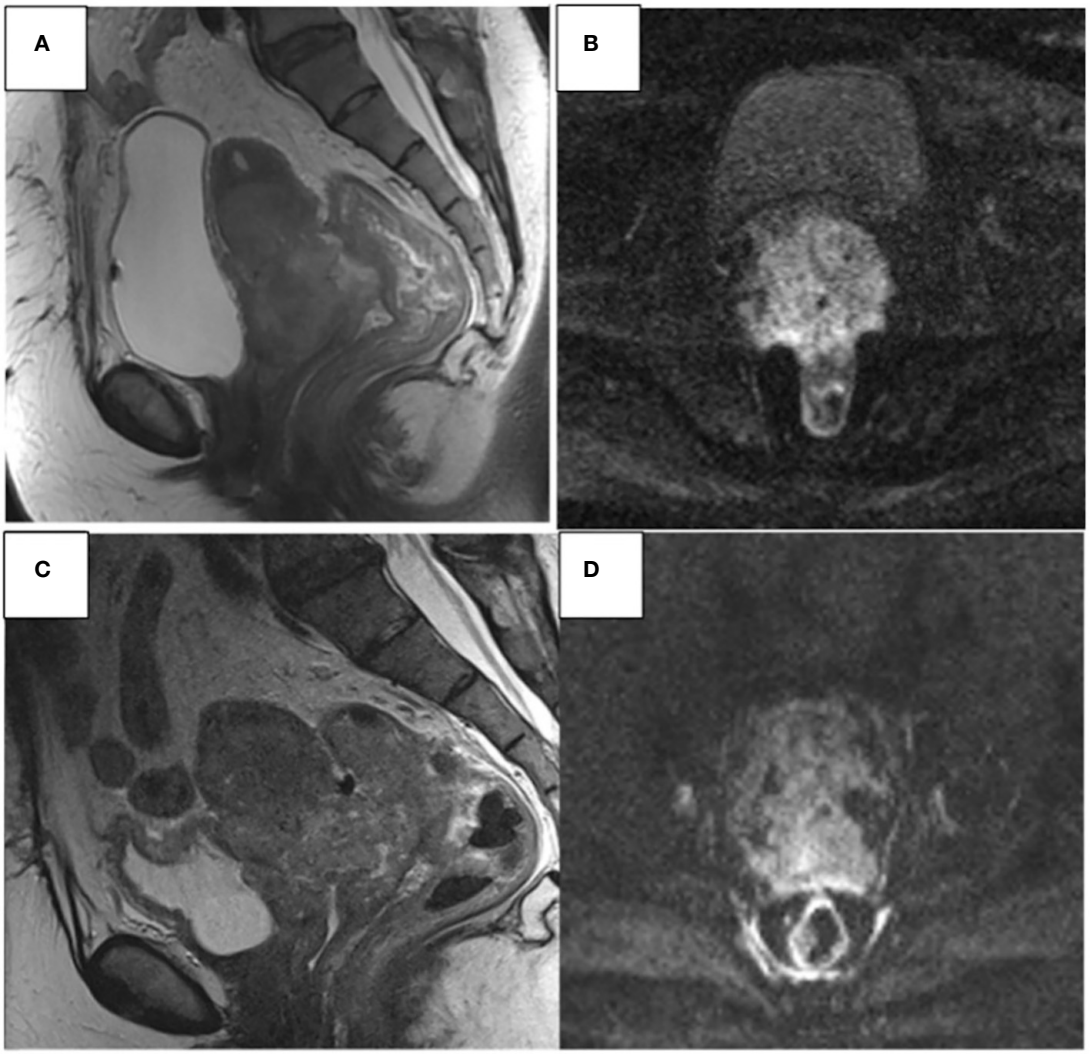

FIGURE 4
67- year-old woman. Sagittal T2W and axial DWI MR images show an invasive CC **(A, B)**. Progression disease **(C, D)** CC infiltrates the uterine body, lower 1/3 of the vaginal canal, mesorectum, anterior wall of the rectum, and posterior wall of the bladder.

also seen in post-radiotherapy fibrosis, inflammation and necrosis. DCE-MRI in combination with DWI improves the identification of residual/recurrent tumor compared to post-radiotherapy changes. In fact, tumor tissue shows early enhancement, hyperintensity at high b-values and low SI on the ADC map, while fibrosis shows no signal restriction in DWI, has no significant enhancement or shows enhancement in the late phase. Inflammatory changes may show intense enhancement and hyperintensity at high b-values, but have hypersignal in the ADC map (57).

Some studies have evaluated that DCE-MRI during CRT may also has prognostic value. High perfusion before and during CRT suggests increased vascularization and high oxygenation of the lesion and it is related to a better response to treatment and prognosis (56, 58–60) (Supplementary Table IV).

4.2 PET/CT

In recent years, the role of fluorine-18 fludeoxyglucose (^{18}F-FDG) positron emission tomography (PET)/CT in the staging and management of gynecological cancers has been increasing. It is a useful imaging method in the assessment of lymph node and distant metastases in patients with LACC and for assessing response to treatment and disease recurrence (61, 62). Most cervical tumors are 18F-fluorodeoxyglucose (FDG) avid, with

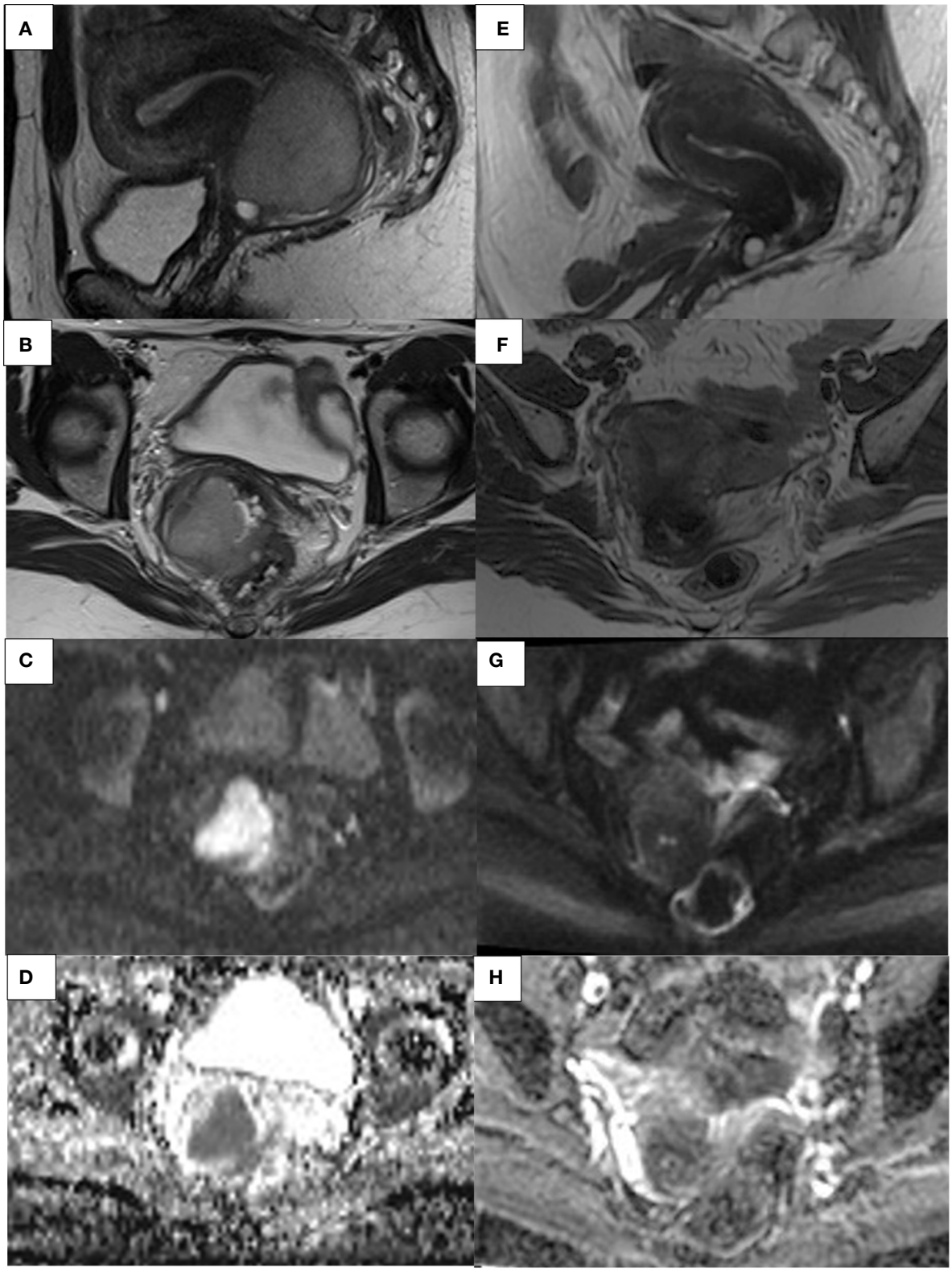

FIGURE 5
41- year-old woman. Sagittal and axial T2W **(A, B)** and axial DWI MR images with ADC map **(C, D)** show an invasive CC extending to the upper third of the vaginal canal and anterior rectal wall with focal parametrial infiltrations. Sagittal and axial T2W **(E, F)** and axial DWI MRI images with ADC map **(G, H)** shows a complete response after CCRT.

exception to adenocarcinomas, which may reveal low FDG uptake. The maximum standardized uptake value (SUV_{max}) is currently the most commonly used parameter in ^{18}F-FDG PET/CT.

In the context of primary tumor staging, PET/CT plays a valuable role in the evaluation of lymph node metastases. Nodal metastases are frequent in patients with advanced disease (i.e., FIGO stages IIB to IVB) and FDG-PET has been demonstrated to have a high specificity for the detection of nodes in this group of patients). Prospective studies have found sensitivities of 75–100% and specificities of 87–100% (63, 64).

In patients with advanced disease at presentation, PET or PET/CT has been found to alter management in a significant number of patients (65). Sistani et al. reported that the diagnostic sensitivity and specificity of PET/CT to detect residual tumor in patients with LACC were 86% and 95.5% respectively, while the diagnostic sensitivity and specificity to detect distant metastases were 97% and 99%, respectively (61, 62, 66).

Post-treatment FDG-PET/CT is usually performed at 3–6 months after completion of CCRT and it is a valid prognostic biomarker. No FDG uptake indicates a complete metabolic response and consequently a reduced risk of recurrence and excellent survival. Reduced FDG avidity indicates a partial metabolic response and thus a moderately high risk of recurrence and poor survival. Finally, unchanged or new areas of FDG uptake indicate persistent or progressive disease, which is associated with poor survival (33, 67, 68). Early detection of residual tumor is important to establish immediate curative salvage therapy, such as pelvic exenteration or concomitant CCRT (69, 70).

5 Complication

After chemoradiotherapy it is important to distinguish between expected changes after radiation therapy in pelvic organs and complications.

Post-radiotherapy complications can also be divided in to acute and chronic complications. The addition of chemotherapy potentiates the acute toxic effects of radiation and also possibly the chronic effects.

Acute toxic effects typically involve the bladder and bowel in the pelvis resulting in radiation cystitis and gastrointestinal symptoms such as colicky abdominal pain, nausea and diarrhea (71). Chronic complications tend to be due to the fibrotic changes in irradiated organs e.g. cervical stenosis, bowel and ureteric strictures. The parametrium soft tissues may also undergo fibrotic changes and appear hypointense. This post-radiation imaging appearance may mimic parametrial invasion thus becoming indistinguishable from the tumor. Vaginal adherents, stenosis, or atrophy are also usually determined. Fistulas are generally late complications of radiotherapy treatment and can also occur as a consequence of a disease recurrence affecting two adjacent organs. For the evaluation of fistulas, MRI is the imaging of choice, which in the sagittal plane are identifiable as hyperintense media in T2-fat suppression sequences and which show impregnation with paramagnetic contrast medium. Other common post-treatment changes are thickening of the bladder and rectal walls, usually associated with diffuse signal hyperintensity in T2-WI, thickening of the utero-sacral ligaments, expansion of the pre-sacral space and diffuse hyperintensity in images. Insufficiency fractures of the sacrum in the post-radiation therapy patient can mimic metastases (7).

6 Recurrence of cervical cancer

Recurrence of CC is defined as locoregional re-appearance of the tumor or development of lymph node or distant metastases at least six months after remission of the primary lesion (72). The most frequent locations of recurrence can be classified into central, regional and distant (lymph node or haematogenic metastases).

The central/local site represents the most frequent site of recurrence (30-45%) and includes the vaginal vault, cervix and uterus.

Regional recurrence can be distinguished into anterior (invasion of bladder, urethra), posterior (invasion of anal sphincter, rectum, sigma), lateral (invasion of lateral pelvic wall, iliac vessels, ureters, sciatic nerve, bone) or pelvic lymph nodes (external and internal iliac nodes, obturator nodes).

Distant recurrence includes lymphadenopathies, distinguished into infra-diaphragmatic (para-aortic nodes, inguinal nodes) or supra-diaphragmatic (hilar, mediastinal, axillary, supraclavicular nodes) and distant organ metastases (lungs, adrenal gland, liver, peritoneal carcinomatosis etc.).

The detection of metastatic lymph nodes by MRI and post-contrast CT is based on size and morphological criteria. Lymphadenopathy is characterized by a round shape, irregular margins, internal inhomogeneity and short axis diameter > 10 m; however, recent guidelines suggest short axis of 8 mm as pelvic lymph nodes cut-off (9).

18F-FDG PET/CT is better than the MRI or CT in identifying pathological lymph nodes (18F-FDG PET/CT: sensitivity 84%, specificity 90% and accuracy 87%; MRI: sensitivity 76%, specificity 80% and accuracy 78%; CT: sensitivity 68%, specificity 75% and accuracy 72% (73). 18F-FDG PET/CT also has a high sensitivity (85.7-100%) and specificity (86.7-100%) in the detection of abdominal and extra-abdominal disease (74).

Conversely, MRI is the best imaging technique to detect local recurrence after treatment showing sensitivity and specificity rates of 82-100% and 78-100%, respectively (9).

7 Emergent techniques

In the last few decades, ongoing scientific research and technological developments have significantly improved diagnostic accuracy and are approaching to future direction mainly represented by spectroscopy, PET-MRI and radiomics.

7.1 Spectroscopy

MR spectroscopy (MRS) is a very sensitive technique that reproduces tissue metabolism and can be used to increase the specificity of non-invasive tissue characterization and prognosis. A recent study analyzed the different lipid profiles in cervical carcinomas with 7 T MRS. It was observed that the 2.1 ppm/1.3 ppm fatty acid ratio could be associated with tumor grade in cervical cancer showing an increase in the amount of unsaturated fatty acids in poorly differentiated tumors. The medium chain of fatty acids becomes less saturated in poorly differentiated tumors (grade III) than in well-differentiated tumours (grade I) or in the normal cervix. Therefore, this ratio may have the potential to characterize tumor grade non-invasively and thus aid clinical diagnosis and management (75). Another recent study demonstrated the feasibility of MRS at 3 T in assessing the correlations between lipid changes in cervical carcinoma and low-prognosis HPV genotypes. MRS demonstrated a significantly elevated fat methyl resonance level at 0.9 ppm in HPV genotypes with a poor prognosis compared to those with a favorable prognosis. Prediction of HPV genotype by MRS may be a useful predictor of the effect of CCRT in patients with advanced cervical cancer, because CCRT is more successful in patients with the poorer prognostic genotype (HPV18- 58) Furthermore, methyl resonance at 0.9 ppm also showed potential in the prediction of persistent tumors after CCRT (76). In addition, methylene resonance at 1.3 ppm has been reported to be more frequently elevated in carcinoma *in situ* (CIN) than in the normal cervix with a sensitivity and specificity of 77% and 94% respectively in predicting the presence of cervical carcinoma (77, 78). MRS, together with morphological and functional MRI, may have the potential to become an integral part of routine MRI examination to add aspects of clinical phenotyping and thus to manage the treatment of cervical cancer patients.

7.2 PET/MRI

PET/MRI is an emerging hybrid technique which integrates the high diagnostic accuracy for metastasis and pathological lymph node of PET with the excellent soft tissue differentiation of MRI, strongly required in the local evaluation of gynecological tumors.

Therefore, PET/MRI technique integrates local and distant staging by combining morphological and metabolic information into a single examination that enables response monitoring, surveillance and assessment of recurrence.

Emerging data suggest that for local staging of primary cancer FDG-PET/MRI is equivalent to MRI and superior to FDG-PET/CT; while for lymph node staging it is comparable to FDG-PET/CT (79, 80). Moreover, FDG-PET/MRI is superior to MRI for detecting local recurrence and is highly accurate for identifying lymph nodes and distant metastases (81).

Other studies, highlighted that this hybrid technique has high diagnostic potential in evaluated the suspected recurrence of gynecologic pelvic cancer. Compared with MRI, PET/MRI has been shown superior results in identifying pelvic regional recurrence (82). For example, Sawicki et al. examined 71 women undergoing PET/MRI and MRI for pelvic cancer recurrence and found that PET/MRI correctly identified significantly more patients with cancer recurrence than MRI alone (100 vs. 83.6%) (83).

Therefore, through this new technique we could combine the advantages of two different investigations improving their diagnostic accuracy; moreover, it avoids the ionized radiation necessary for the common PET-CT examination. However, FDG-PET/MRI is poorly used in clinical practice due to limited availability and high cost.

7.3 Radiomics

In recent years, radiomics has been assuming a central role and increasing interest in research field; it consists essentially of a cross-disciplinary research area that correlates quantitative data extracted from imaging technique and anatomopathological/clinical information. The ultimate goal of these studies is to develop predictive models that may help identify the most appropriate therapeutic choice for the patient to improve outcome and reduce treatment invasiveness.

Multiple diagnostic techniques are used to stage and evaluate CC: ultrasound, CT, MR, [18F]- fludeoxyglucose (FDG) PET but the latter two are widely considered the most appropriate and therefore object of the main radiomics studies. The main topics of these studies evaluated the correlation with tumor prognostic factors risk facts (histology, parametric invasion and lymph node localizations), response to therapy and prediction of recurrence and distant metastasis.

In particular, in 2017, Tsujikawa et al. affirmed the second-order texture feature extracted by PET/CT imaging discriminating between squamous cell carcinomas (SCCs) and non-squamous cell carcinomas (NSCCs); others studies applied radiomic nomogram from features extracted by MRI and PET imaging to predict the histological grade, lymphovascular space invasion (LVSI) or parametrial invasion (84–86). In addition, other studies have

stated that the status of lymph nodes could be predicted by the radiomic pattern developed at first on PET-CT examinations, then on MRI, and ultimately also on ultrasound (US) and CT (87–92).

It is known that around 40% of LACCs undergo disease recurrence. Moreover, in these patients response to therapy is closely related to clinical pathologic prognostic factors but also to phenotypic and genomic features that cannot generally be identified by random sampling or biopsy. Many studies have tried to identify through radiomic analysis these different features to decide pre-operatively the correct therapeutic course. In this context, several studies conducted on both CT, MRI, and PET-CT examination have shown presence of highly predictive model to assess response to therapy (93–99). Similarly, correlations were found between radiomics features extracted from PET and MRI and regional or distant recurrence of disease on which predictive models of recurrence have been based (100). Recently, Lale Umutlu correlated texture features extracted from the innovative hybrid PET-MRI to the presence of N and M-stage resulting that a predictive model may by applying and M-stage prediction was superior compared to N-stage (101).

8 Conclusions

In the last decades, great progress has been made in the treatment of patients with LACC (FIGO 2018 stages IB3-IVA). The treatment of choice for LACC is concurrent chemo-radiotherapy, which generally consists of cisplatin-based chemotherapy and external beam radiotherapy followed by brachytherapy. However, the treatment strategy for LACC is still evolving, and there is no consensus on the role of surgery as adjuvant treatment. Imaging plays an important role in the initial and post-treatment evaluation, but also in the planning of radiotherapy allowing to detect residual disease from post-radiotherapy changes, allowing possible salvage therapies. Imaging in combination with chemotherapy and RT increased local disease control, also influencing DFS and OS. Future imaging techniques and scientific research may guide therapeutic management towards more tailored treatment.

Author contributions

CS and CV have given substantial contributions to manuscript draft; conceptualization, ML and PI; methodology, CS, CV, and ML; investigation, NR, MV and EG; resources, NR and MV; data curation, DM, EG, and GS; writing-original draft preparation, AA, CS, and CV; writing- review and editing, CS, CV, and GS; supervision, ML, PI, and CC; project administration, ML and RP; All authors have read and agreed to be published version of the manuscript.

Conflict of interest

The authors declare that the research was conducted in the absence of any commercial or financial relationships that could be construed as a potential conflict of interest.

Publisher's note

Supplementary material

The Supplementary Material for this article can be found online at: https://www.frontiersin.org/articles/10.3389/fonc.2022.1003930/full#supplementary-material

References

1. Zhao M, Wu Q, Hao Y, Hu J, Gao Y, Zhou S, et al. Global, regional, and national burden of cervical cancer for 195 countries and territories, 2007–2017: Findings from the global burden of disease study 2017. *BMC Womens Health* (2021) 21:419. doi: 10.1186/s12905-021-01571-3

2. Berek JS, Matsuo K, Grubbs BH, Gaffney DK, Lee SI, Kilcoyne A, et al. Multidisciplinary perspectives on newly revised 2018 FIGO staging of cancer of the cervix uteri. *J Gynecol Oncol* (2019) 30:e40. doi: 10.3802/jgo.2019.30.e40

3. Bhatla N, Aoki D, Sharma DN, Sankaranarayanan R. Cancer of the cervix uteri. *Int J Gynecol Obstet* (2018) 143:22–36. doi: 10.1002/ijgo.12611

4. Koh W-J, Abu-Rustum NR, Bean S, Bradley K, Campos SM, Cho KR, et al. Cervical cancer, version 3.2019, NCCN clinical practice guidelines in oncology. *J Natl Compr Canc Netw* (2019) 17:64–84. doi: 10.6004/jnccn.2019.0001

5. Marth C, Landoni F, Mahner S, McCormack M, Gonzalez-Martin A, Colombo N. Cervical cancer: ESMO clinical practice guidelines for diagnosis, treatment and follow-up. *Ann Oncol* (2017) 28:iv72–83. doi: 10.1093/annonc/mdx220

6. Gennigens C, De Cuypere M, Hermesse J, Kridelka F, Jerusalem G. Optimal treatment in locally advanced cervical cancer. *Expert Rev Anticancer Ther* (2021) 21:657–71. doi: 10.1080/14737140.2021.1879646

7. Papadopoulou I, Stewart V, Barwick TD, Park W-HE, Soneji N, Rockall AG, et al. Post–radiation therapy imaging appearances in cervical carcinoma. *RadioGraphics* (2016) 36:538–53. doi: 10.1148/rg.2016150117

8. Addley HC, Vargas HA, Moyle PL, Crawford R, Sala E. Pelvic imaging following chemotherapy and radiation therapy for gynecologic malignancies. *RadioGraphics* (2010) 30:1843–56. doi: 10.1148/rg.307105063

9. Miccò M, Lupinelli M, Mangialardi M, Gui B, Manfredi R. Patterns of recurrent disease in cervical cancer. *J Pers Med* (2022) 12:755. doi: 10.3390/jpm12050755

10. Vale C, Tierney JF, Stewart LA, Brady M, Dinshaw K, Jakobsen A. Reducing uncertainties about the effects of chemoradiotherapy for cervical cancer: A systematic review and meta-analysis of individual patient data from 18 randomized trials. *J Clin Oncol* (2008) 26:5802–12. doi: 10.1200/JCO.2008.16.4368

11. Datta NR, Stutz E, Liu M, Rogers S, Klingbiel D, Siebenhüner A, et al. Concurrent chemoradiotherapy vs . radiotherapy alone in locally advanced cervix cancer: A systematic review and meta-analysis. *Gynecol Oncol* (2017) 145:374–85. doi: 10.1016/j.ygyno.2017.01.033

12. Gosset M, Chargari C, Bentivegna E, Leary A, Genestie C, Maulard A, et al. Should we cease to perform salvage hysterectomy after chemoradiation and brachytherapy in locally advanced cervical cancer? *Anticancer Res* (2019) 39:2919–26. doi: 10.21873/anticanres.13421

13. Mazeron R, Gouy S, Chargari C, Rivin del Campo E, Dumas I, Mervoyer A, et al. Post radiation hysterectomy in locally advanced cervical cancer: Outcomes and dosimetric impact. *Radiother Oncol* (2016) 120:460–6. doi: 10.1016/j.radonc.2016.07.010

14. Kol KGG, Ebisch RMF, Piek JMJ, Zusterzeel PLM, Vergeldt TFM, Bekkers RLM. Salvage surgery for patients with residual disease after chemoradiation therapy for locally advanced cervical cancer: A systematic review on indication, complications, and survival. *Acta Obstet Gynecol Scand* (2021) 100:1176–85. doi: 10.1111/aogs.14093

15. Lèguevaque P, Motton S, Delannes M, Querleu D, Soulé-Tholy M, Tap G, et al. Completion surgery or not after concurrent chemoradiotherapy for locally advanced cervical cancer? *Eur J Obstet Gynecol Reprod Biol* (2011) 155:188–92. doi: 10.1016/j.ejogrb.2010.11.016

16. Yoshida K, Kajiyama H, Yoshihara M, Tamauchi S, Ikeda Y, Yoshikawa N, et al. The role of additional hysterectomy after concurrent chemoradiation for patients with locally advanced cervical cancer. *Int J Clin Oncol* (2020) 25:384–90. doi: 10.1007/s10147-019-01551-6

17. Fanfani F, Vizza E, Landoni F, de Iaco P, Ferrandina G, Corrado G, et al. Radical hysterectomy after chemoradiation in FIGO stage III cervical cancer patients versus chemoradiation and brachytherapy: Complications and 3-years survival. *Eur J Surg Oncol EJSO* (2016) 42:1519–25. doi: 10.1016/j.ejso.2016.05.011

18. Kokka F, Bryant A, Brockbank E, Powell M, Oram D. Hysterectomy with radiotherapy or chemotherapy or both for women with locally advanced cervical cancer. *Cochrane Database Syst Rev* (2015). doi: 10.1002/14651858.CD010260.pub2

19. Platt SL, Patel A, Humphrey PJ, Al-Booz H, Bailey J. Completion surgery after chemoradiotherapy for cervical cancer – is there a role? UK cancer centre experience of hysterectomy post chemo-radiotherapy treatment for cervical cancer. *J Obstet Gynaecol* (2019) 39:68–73. doi: 10.1080/01443615.2018.1463205

20. Rydzewska L, Tierney J, Vale CL, Symonds PR. Neoadjuvant chemotherapy plus surgery versus surgery for cervical cancer. *Cochrane Database Syst Rev* (2012) 12:12 doi: 10.1002/14651858.CD007406.pub3

21. Osman M. The role of neoadjuvant chemotherapy in the management of locally advanced cervix cancer: A systematic review. *Oncol Rev* (2014) 8(2):250 doi: 10.4081/oncol.2014.250

22. Angioli R, Plotti F, Montera R, Aloisi A, Luvero D, Capriglione S, et al. Neoadjuvant chemotherapy plus radical surgery followed by chemotherapy in locally advanced cervical cancer. *Gynecol Oncol* (2012) 127:290–6. doi: 10.1016/j.ygyno.2012.07.104

23. Plotti F, Sansone M, Di Donato V, Antonelli E, Altavilla T, Angioli R, et al. Quality of life and sexual function after type C2/Type III radical hysterectomy for locally advanced cervical cancer: A prospective study. *J Sex Med* (2011) 8:894–904. doi: 10.1111/j.1743-6109.2010.02133.x

24. Benedetti-Panici P, Greggi S, Colombo A, Amoroso M, Smaniotto D, Giannarelli D, et al. Neoadjuvant chemotherapy and radical surgery versus exclusive radiotherapy in locally advanced squamous cell cervical cancer: Results from the Italian multicenter randomized study. *J Clin Oncol* (2002) 20 (1):179–88. doi: 10.1200/JCO.2002.20.1.179

25. Gupta S, Maheshwari A, Parab P, Mahantshetty U, Hawaldar R, Sastri Chopra S, et al. Neoadjuvant chemotherapy followed by radical surgery versus concomitant chemotherapy and radiotherapy in patients with stage IB2, IIA, or IIB squamous cervical cancer: A randomized controlled trial. *J Clin Oncol* (2018) 36:1548–55. doi: 10.1200/JCO.2017.75.9985

26. Zhao H, He Y, Yang S-L, Zhao Q, Wu Y-M. Neoadjuvant chemotherapy with radical surgery vs radical surgery alone for cervical cancer: A systematic review and meta-analysis. *OncoTargets Ther* (2019) 12:1881–91. doi: 10.2147/OTT.S186451

27. Otero-García MM, Mesa-Álvarez A, Nikolic O, Blanco-Lobato P, Basta-Nikolic M, de Llano-Ortega RM, et al. Role of MRI in staging and follow-up of endometrial and cervical cancer: Pitfalls and mimickers. *Insights Imaging* (2019) 10:19. doi: 10.1186/s13244-019-0696-8

28. Manganaro L, Lakhman Y, Bharwani N, Gui B, Gigli S, Vinci V, et al. Staging, recurrence and follow-up of uterine cervical cancer using MRI: Updated guidelines of the European society of urogenital radiology after revised FIGO staging 2018. *Eur Radiol* (2021) 31:7802–16. doi: 10.1007/s00330-020-07632-9

29. Woo S, Suh CH, Kim SY, Cho JY, Kim SH. Magnetic resonance imaging for detection of parametrial invasion in cervical cancer: An updated systematic review and meta-analysis of the literature between 2012 and 2016. *Eur Radiol* (2018) 28:530–41. doi: 10.1007/s00330-017-4958-x

30. Gui B, Valentini AL, Miccò M, D'Agostino GR, Tagliaferri L, Zannoni GF, et al. Cervical cancer response to neoadjuvant chemoradiotherapy: MRI assessment compared with surgery. *Acta Radiol* (2016) 57:1123–31. doi: 10.1177/0284185115617346

31. Vincens E, Balleyguier C, Rey A, Uzan C, Zareski E, Gouy S, et al. Accuracy of magnetic resonance imaging in predicting residual disease in patients treated for stage IB2/II cervical carcinoma with chemoradiation therapy: Correlation of radiologic findings with surgicopathologic results. *Cancer* (2008) 113:2158–65. doi: 10.1002/cncr.23817

32. Thomeer MG, Vandecaveye V, Braun L, Mayer F, Franckena-Schouten M, de Boer P, et al. Evaluation of T2-W MR imaging and diffusion-weighted imaging for the early post-treatment local response assessment of patients treated conservatively for cervical cancer: A multicentre study. *Eur Radiol* (2019) 29:309–18. doi: 10.1007/s00330-018-5510-3

33. Lucas R, Dias JL, Cunha TM. Added value of diffusion-weighted MRI in detection of cervical cancer recurrence: Comparison with morphologic and dynamic contrast-enhanced MRI sequences. *Diagn Interv Radiol* (2015) 21:368–75. doi: 10.5152/dir.2015.14427

34. Liu Y, Ye Z, Sun H, Bai R. Grading of uterine cervical cancer by using the ADC difference value and its correlation with microvascular density and vascular endothelial growth factor. *Eur Radiol* (2013) 23:757–65. doi: 10.1007/s00330-012-2657-1

35. Yang W, Qiang JW, Tian HP, Chen B, Wang AJ, Zhao JG. Minimum apparent diffusion coefficient for predicting lymphovascular invasion in invasive cervical cancer: ADC for predicting lymphovascular invasion. *J Magn Reson Imaging* (2017) 45:1771–9. doi: 10.1002/jmri.25542

36. Song Q, Yu Y, Zhang X, Zhu Y, Luo Y, Yu T, et al. Value of MRI and diffusion weighted imaging in diagnosing normal-sized pelvic lymph nodes metastases in patients with cervical cancer. *Br J Radiol* (2020) 95 (1138):20200203. doi: 10.1259/bjr.20200203

37. Akkus Yildirim B, Onal C, Erbay G, Cem Guler O, Karadeli E, Reyhan M, et al. Prognostic values of ADC $_{mean}$ and SUV $_{max}$ of the primary tumour in cervical cancer patients treated with definitive chemoradiotherapy. *J Obstet Gynaecol* (2019) 39:224–30. doi: 10.1080/01443615.2018.1492528

38. Wang Y-T, Li Y-C, Yin L-L, Pu H. Can diffusion-weighted magnetic resonance imaging predict survival in patients with cervical cancer? a meta-analysis. *Eur J Radiol* (2016) 85:2174–81. doi: 10.1016/j.ejrad.2016.10.011

39. Gu K, Kim CK, Choi CH, Yoon YC, Park W. Prognostic value of ADC quantification for clinical outcome in uterine cervical cancer treated with concurrent chemoradiotherapy. *Eur Radiol* (2019) 29:6236–44. doi: 10.1007/s00330-019-06204-w

40. Fu C, Feng X, Bian D, Zhao Y, Fang X, Du W, et al. Simultaneous changes of magnetic resonance diffusion-weighted imaging and pathological microstructure in locally advanced cervical cancer caused by neoadjuvant chemotherapy: Correlation with ADC in NACT of LACC. *J Magn Reson Imaging* (2015) 42:427–35. doi: 10.1002/jmri.24779

41. Somoye G, Harry V, Semple S, Plataniotis G, Scott N, Gilbert FJ, et al. Early diffusion weighted magnetic resonance imaging can predict survival in women with locally advanced cancer of the cervix treated with combined chemo-radiation. *Eur Radiol* (2012) 22:2319–27. doi: 10.1007/s00330-012-2496-0

42. Capuani S, Guerreri M, Antonelli A, Bernardo S, Porpora MG, Giancotti A, et al. Diffusion and perfusion quantified by magnetic resonance imaging are markers of human placenta development in normal pregnancy. *Placenta* (2017) 58:33–9. doi: 10.1016/j.placenta.2017.08.003

43. Satta S, Dolciami M, Celli V, Di Stadio F, Perniola G, Palaia I, et al. Quantitative diffusion and perfusion MRI in the evaluation of endometrial cancer: Validation with histopathological parameters. *Br J Radiol* (2021) 94:20210054. doi: 10.1259/bjr.20210054

44. Iima M, Le Bihan D. Clinical intravoxel incoherent motion and diffusion MR imaging: Past, present, and future. *Radiology* (2016) 278:13–32. doi: 10.1148/radiol.2015150244

45. Lee EYP, Yu X, Chu MMY, Ngan HYS, Siu SWK, Soong IS, et al. Perfusion and diffusion characteristics of cervical cancer based on intraxovel incoherent motion MR imaging-a pilot study. *Eur Radiol* (2014) 24:1506–13. doi: 10.1007/s00330-014-3160-7

46. Wang X, Song J, Zhou S, Lu Y, Lin W, Koh TS, et al. Comparative study of methods for determining intravoxel incoherent motion parameters in cervix cancer. *Cancer Imaging* (2021) 21:12. doi: 10.1186/s40644-020-00377-0

47. Song J, Lu Y, Wang X, Peng W, Lin W, Hou Z, et al. Comparative study of four diffusion-weighted imaging models in the diagnosis of cervical cancer. *Acta Radiol* (2022) 63:536–44. doi: 10.1177/02841851211002017

48. Xu C, Li X, Shi Y, Wang B, Sun H. Combinative evaluation of primary tumor and lymph nodes to predict pelvic lymphatic metastasis in cervical cancer: An integrated PET-IVIM MRI study. *Cancer Imaging* (2020) 20:21. doi: 10.1186/s40644-020-00298-y

49. Xu C, Du S, Zhang S, Wang B, Dong C, Sun H. Value of integrated PET-IVIM MR in assessing metastases in hypermetabolic pelvic lymph nodes in cervical cancer: A multi-parameter study. *Eur Radiol* (2020) 30:2483–92. doi: 10.1007/s00330-019-06611-z

50. Perucho JAU, Chiu KWH, Wong EMF, Tse KY, Chu MMY, Chan LWC, et al. Diffusion-weighted magnetic resonance imaging of primary cervical cancer in the detection of Sub-centimetre metastatic lymph nodes. *Cancer Imaging* (2020) 20:27. doi: 10.1186/s40644-020-00303-4

51. Perucho JAU, Wang M, Vardhanabhuti V, Tse KY, Chan KKL, Lee EYP. Association between IVIM parameters and treatment response in locally advanced squamous cell cervical cancer treated by chemoradiotherapy. *Eur Radiol* (2021) 31:7845–54. doi: 10.1007/s00330-021-07817-w

52. Zheng X, Guo W, Dong J, Qian L. Prediction of early response to concurrent chemoradiotherapy in cervical cancer: Value of multi-parameter MRI combined with clinical prognostic factors. *Magn Reson Imaging* (2020) 72:159–66. doi: 10.1016/j.mri.2020.06.014

53. Zhang H, Zhou Y, Li J, Zhang P, Li Z, Guo J. The value of DWI in predicting the response to synchronous radiochemotherapy for advanced cervical carcinoma: Comparison among three mathematical models. *Cancer Imaging* (2020) 20:8. doi: 10.1186/s40644-019-0285-6

54. Dolciami M, Capuani S, Celli V, Maiuro A, Pernazza A, Palaia I, et al. Intravoxel incoherent motion (IVIM) MR quantification in locally advanced cervical cancer (LACC): Preliminary study on assessment of tumor aggressiveness and response to neoadjuvant chemotherapy. *J Pers Med* (2022) 12:638. doi: 10.3390/jpm12040638

55. Jalaguier-Coudray A, Villard-Mahjoub R, Delouche A, Delarbre B, Lambaudie E, Houvenaeghel G, et al. Value of dynamic contrast-enhanced and diffusion-weighted MR imaging in the detection of pathologic complete response in cervical cancer after neoadjuvant therapy: A retrospective observational study. *Radiology* (2017) 284:432–42. doi: 10.1148/radiol.2017161299

56. Donaldson SB, Buckley DL, O'Connor JP, Davidson SE, Carrington BM, Jones AP, et al. Enhancing fraction measured using dynamic contrast-enhanced MRI predicts disease-free survival in patients with carcinoma of the cervix. *Br J Cancer* (2010) 102:23–6. doi: 10.1038/sj.bjc.6605415

57. Park KJ, Braschi-Amirfarzan M, DiPiro PJ, Giardino AA, Jagannathan JP, Howard SA, et al. Multimodality imaging of locally recurrent and metastatic cervical cancer: Emphasis on histology, prognosis, and management. *Abdom Radiol* (2016) 41:2496–508. doi: 10.1007/s00261-016-0825-5

58. Andersen EKF, Hole KH, Lund KV, Sundfør K, Kristensen GB, Lyng H, et al. Dynamic contrast-enhanced MRI of cervical cancers: Temporal percentile screening of contrast enhancement identifies parameters for prediction of chemoradioresistance. *Int J Radiat Oncol* (2012) 82:e485–92. doi: 10.1016/j.ijrobp.2011.05.050

59. Andersen EKF, Hole KH, Lund KV, Sundfør K, Kristensen GB, Lyng H, et al. Pharmacokinetic parameters derived from dynamic contrast enhanced MRI of cervical cancers predict chemoradiotherapy outcome. *Radiother Oncol* (2013) 107:117–22. doi: 10.1016/j.radonc.2012.11.007

60. Zahra MA, Tan LT, Priest AN, Graves MJ, Arends M, Crawford RAF, et al. Semiquantitative and quantitative dynamic contrast-enhanced magnetic resonance imaging measurements predict radiation response in cervix cancer. *Int J Radiat Oncol* (2009) 74:766–73. doi: 10.1016/j.ijrobp.2008.08.023

61. Oh D, Lee JE, Huh SJ, Park W, Nam H, Choi JY, et al. Prognostic significance of tumor response as assessed by sequential 18F-Fluorodeoxyglucose-Positron emission Tomography/Computed tomography during concurrent chemoradiation therapy for cervical cancer. *Int J Radiat Oncol* (2013) 87:549–54. doi: 10.1016/j.ijrobp.2013.07.009

62. Valentini AL, Miccò M, Gui B, Giuliani M, Rodolfino E, Telesca AM, et al. The PRICE study: The role of conventional and diffusion-weighted magnetic resonance imaging in assessment of locally advanced cervical cancer patients administered by chemoradiation followed by radical surgery. *Eur Radiol* (2018) 28:2425–35. doi: 10.1007/s00330-017-5233-x

63. Cohen PA, Jhingran A, Oaknin A, Denny L. Cervical cancer. *Lancet* (2019) 393:169–82. doi: 10.1016/S0140-6736(18)32470-X

64. Devine C, Viswanathan C, Faria S, Marcal L, Sagebiel TL. Imaging and staging of cervical cancer. *Semin Ultrasound CT MRI* (2019) 40:280–6. doi: 10.1053/j.sult.2019.03.001

65. Wang D, Liu X, Wang W, Huo L, Pan Q, Ren X, et al. The role of the metabolic parameters of 18F-FDG PET/CT in patients with locally advanced cervical cancer. *Front Oncol* (2021) 11:698744. doi: 10.3389/fonc.2021.698744

66. Sanei Sistani S, Parooie F, Salarzaei M. Diagnostic accuracy of 18F-FDG-PET/CT and MRI in predicting the tumor response in locally advanced cervical carcinoma treated by chemoradiotherapy: A meta-analysis. *Contrast Media Mol Imaging* (2021) 2021:1–11. doi: 10.1155/2021/8874990

67. Hameeduddin A, Sahdev A. Diffusion-weighted imaging and dynamic contrast-enhanced MRI in assessing response and recurrent disease in gynaecological malignancies. *Cancer Imaging* (2015) 15:3. doi: 10.1186/s40644-015-0037-1

68. Beriwal S, Kannan N, Sukumvanich P, Richard SD, Kelley JL, Edwards RP, et al. Complete metabolic response after definitive radiation therapy for cervical cancer: Patterns and factors predicting for recurrence. *Gynecol Oncol* (2012) 127:303–6. doi: 10.1016/j.ygyno.2012.08.006

69. Friedlander M, Grogan M. Guidelines for the treatment of recurrent and metastatic cervical cancer. *Oncol* (2002) 7:342–7. doi: 10.1634/theoncologist.2002-0342

70. O'Shannassy SJ, Brown KGM, Steffens D, Solomon MJ. Referral patterns and outcomes of a highly specialised pelvic exenteration multidisciplinary team meeting: A retrospective cohort study. *Eur J Surg Oncol* (2020) 46:1138–43. doi: 10.1016/j.ejso.2020.02.031

71. Tan LT, Russell S, Burgess L. Acute toxicity of chemo-radiotherapy for cervical cancer: The addenbrooke's experience. *Clin Oncol* (2004) 16:255–60. doi: 10.1016/j.clon.2003.12.004

72. Antunes D. Recurrent cervical cancer: How can radiology be helpfull. *Omics J Radiol* (2013) 02. doi: 10.4172/2167-7964.1000138

73. Zhu Y, Shen B, Pei X, Liu H, Li GCT. MRI, And PET imaging features in cervical cancer staging and lymph node metastasis. *Am J Transl Res* (2021) 13:10536–44.PMCID: PMC8507065빵

74. Havrilesky LJ, Wong TZ, Secord AA, Berchuck A, Clarke-Pearson DL, Jones EL. The role of PET scanning in the detection of recurrent cervical cancer. *Gynecol Oncol* (2003) 90:186–90. doi: 10.1016/S0090-8258(03)00256-7

75. Arteaga de Castro CS, Hoogendam JP, van Kalleveen IML, Raaijmakers AJE, Zweemer RP, Verheijen RHM, et al. Proton MRS of cervical cancer at 7 T. *NMR Biomed* (2019) 32:e4015. doi: 10.1002/nbm.4015

76. Lin G, Lai C-H, Tsai S-Y, Lin Y-C, Huang Y-T, Wu R-C, et al. ^{1} h MR spectroscopy in cervical carcinoma using external phase array body coil at 3.0 Tesla: Prediction of poor prognostic human papillomavirus genotypes: HPV genotypes and cervical cancer MRS. *J Magn Reson Imaging* (2017) 45:899–907. doi: 10.1002/jmri.25386

77. Mahon MM, Cox IJ, Dina R, Soutter FRCOG WP, McIndoe MRCOG GA, Williams AD, et al. 1H magnetic resonance spectroscopy of preinvasive and invasive cervical cancer: In vivo-ex vivo profiles and effect of tumor load. *J Magn Reson Imaging* (2004) 19:356–64. doi: 10.1002/jmri.20012

78. Mahon MM, Williams AD, Soutter WP, Cox IJ, McIndoe GA, Coutts GA, et al. ^{1} h magnetic resonance spectroscopy of invasive cervical cancer: An in vivo study with ex vivo corroboration. *NMR Biomed* (2004) 17:1–9. doi: 10.1002/nbm.830. MRS OF CERVICAL CANCER.

79. Sarabhai T, Schaarschmidt BM, Wetter A, Kirchner J, Aktas B, Forsting M, et al. Comparison of 18F-FDG PET/MRI and MRI for pre-therapeutic tumor staging of patients with primary cancer of the uterine cervix. *Eur J Nucl Med Mol Imaging* (2018) 45:67–76. doi: 10.1007/s00259-017-3809-y

80. Nie J, Zhang J, Gao J, Guo L, Zhou H, Hu Y, et al. Diagnostic role of 18F-FDG PET/MRI in patients with gynecological malignancies of the pelvis: A systematic review and meta-analysis. *PloS One* (2017) 12:e0175401. doi: 10.1371/journal.pone.0175401

81. Zheng M, Xie D, Pan C, Xu Y, Yu W. Diagnostic value of 18F-FDG PET/MRI in recurrent pelvis malignancies of female patients: A systematic review and meta-analysis. *Nucl Med Commun* (2018) 39:479–85. doi: 10.1097/MNM.0000000000000839

82. Steiner A, Narva S, Rinta-Kiikka I, Hietanen S, Hynninen J, Virtanen J. Diagnostic efficiency of whole-body 18F-FDG PET/MRI, MRI alone, and SUV and ADC values in staging of primary uterine cervical cancer. *Cancer Imaging* (2021) 21:16. doi: 10.1186/s40644-020-00372-5

83. Sawicki LM, Kirchner J, Grueneisen J, Ruhlmann V, Aktas B, Schaarschmidt BM, et al. Comparison of 18F–FDG PET/MRI and MRI alone for whole-body staging and potential impact on therapeutic management of women with suspected recurrent pelvic cancer: A follow-up study. *Eur J Nucl Med Mol Imaging* (2018) 45:622–9. doi: 10.1007/s00259-017-3881-3

84. Tsujikawa T, Rahman T, Yamamoto M, Yamada S, Tsuyoshi H, Kiyono Y, et al. 18F-FDG PET radiomics approaches: Comparing and clustering features in cervical cancer. *Ann Nucl Med* (2017) 31:678–85. doi: 10.1007/s12149-017-1199-7

85. Shen W-C, Chen S-W, Liang J-A, Hsieh T-C, Yen K-Y, Kao C-H. [18] Fluorodeoxyglucose positron emission tomography for the textural features of cervical cancer associated with lymph node metastasis and histological type. *Eur J Nucl Med Mol Imaging* (2017) 44:1721–31. doi: 10.1007/s00259-017-3697-1

86. Becker AS, Ghafoor S, Marcon M, Perucho JA, Wurnig MC, Wagner MW, et al. MRI Texture features may predict differentiation and nodal stage of cervical cancer: A pilot study. *Acta Radiol Open* (2017) 6:205846011772957. doi: 10.1177/2058460117729574

87. Kan Y, Dong D, Zhang Y, Jiang W, Zhao N, Han L, et al. Radiomic signature as a predictive factor for lymph node metastasis in early-stage cervical cancer: Radiomic signature of LNM in cervical cancer. *J Magn Reson Imaging* (2019) 49:304–10. doi: 10.1002/jmri.26209

88. Wang T, Gao T, Yang J, Yan X, Wang Y, Zhou X, et al. Preoperative prediction of pelvic lymph nodes metastasis in early-stage cervical cancer using radiomics nomogram developed based on T2-weighted MRI and diffusion-weighted imaging. *Eur J Radiol* (2019) 114:128–35. doi: 10.1016/j.ejrad.2019.01.003

89. Wu Q, Wang S, Chen X, Wang Y, Dong L, Liu Z, et al. Radiomics analysis of magnetic resonance imaging improves diagnostic performance of lymph node metastasis in patients with cervical cancer. *Radiother Oncol* (2019) 138:141–8. doi: 10.1016/j.radonc.2019.04.035

90. Xiao M, Ma F, Li Y, Li Y, Li M, Zhang G, et al. Multiparametric MRI-based radiomics nomogram for predicting lymph node metastasis in early-stage cervical cancer. *J Magn Reson Imaging* (2020) 52:885–96. doi: 10.1002/jmri.27101

91. Jin X, Ai Y, Zhang J, Zhu H, Jin J, Teng Y, et al. Noninvasive prediction of lymph node status for patients with early-stage cervical cancer based on radiomics features from ultrasound images. *Eur Radiol* (2020) 30:4117–24. doi: 10.1007/s00330-020-06692-1

92. Chen J, He B, Dong D, Liu P, Duan H, Li W, et al. Noninvasive CT radiomic model for preoperative prediction of lymph node metastasis in early cervical carcinoma. *Br J Radiol* (2020) 93:20190558. doi: 10.1259/bjr.20190558

93. Ciolina M, Vinci V, Villani L, Gigli S, Saldari M, Panici PB, et al. Texture analysis versus conventional MRI prognostic factors in predicting tumor response to neoadjuvant chemotherapy in patients with locally advanced cancer of the uterine cervix. *Radiol Med (Torino)* (2019) 124:955–64. doi: 10.1007/s11547-019-01055-3

94. Sun C, Tian X, Liu Z, Li W, Li P, Chen J, et al. Radiomic analysis for pretreatment prediction of response to neoadjuvant chemotherapy in locally advanced cervical cancer: A multicentre study. *EBioMedicine* (2019) 46:160–9. doi: 10.1016/j.ebiom.2019.07.049

95. Fang M, Kan Y, Dong D, Yu T, Zhao N, Jiang W, et al. Multi-habitat based radiomics for the prediction of treatment response to concurrent chemotherapy and radiation therapy in locally advanced cervical cancer. *Front Oncol* (2020) 10:563. doi: 10.3389/fonc.2020.00563

96. Tian X, Sun C, Liu Z, Li W, Duan H, Wang L, et al. Prediction of response to preoperative neoadjuvant chemotherapy in locally advanced cervical cancer using multicenter CT-based radiomic analysis. *Front Oncol* (2020) 10:77. doi: 10.3389/fonc.2020.00077

97. Reuzé S, Orlhac F, Chargari C, Nioche C, Limkin E, Riet F, et al. Prediction of cervical cancer recurrence using textural features extracted from 18F-FDG PET images acquired with different scanners. *Oncotarget* (2017) 8:43169–79. doi: 10.18632/oncotarget.17856

98. Meng J, Zhu L, Zhu L, Xie L, Wang H, Liu S, et al. Whole-lesion ADC histogram and texture analysis in predicting recurrence of cervical cancer treated with CCRT. *Oncotarget* (2017) 8:92442–53. doi: 10.18632/oncotarget.21374

99. Meng J, Liu S, Zhu L, Zhu L, Wang H, Xie L, et al. Texture analysis as imaging biomarker for recurrence in advanced cervical cancer treated with CCRT. *Sci Rep* (2018) 8:11399. doi: 10.1038/s41598-018-29838-0

100. Lucia F, Visvikis D, Desseroit M-C, Miranda O, Malhaire J-P, Robin P, et al. Prediction of outcome using pretreatment 18F-FDG PET/CT and MRI radiomics in locally advanced cervical cancer treated with chemoradiotherapy. *Eur J Nucl Med Mol Imaging* (2018) 45:768–86. doi: 10.1007/s00259-017-3898-7

101. Umutlu L, Nensa F, Demircioglu A, Antoch G, Herrmann K, Forsting M, et al. Radiomics analysis of multiparametric PET/MRI for n- and m-staging in patients with primary cervical cancer. *RöFo - Fortschr Auf Dem Geb Röntgenstrahlen Bildgeb Verfahr* (2020) 192:754–63. doi: 10.1055/a-1100-0127

frontiers | Frontiers in Oncology

TYPE Systematic Review
PUBLISHED 02 November 2022
DOI 10.3389/fonc.2022.1057631

OPEN ACCESS

EDITED BY
Alessio G. Morganti,
University of Bologna, Italy

REVIEWED BY
Milly Buwenge,
University of Bologna, Italy
Federica Tomao,
European Institute of Oncology (IEO), Italy
Multinu Francesco,
European Institute of Oncology (IEO), Italy

*CORRESPONDENCE
Stefania Rizzo
stefania.rizzo@eoc.ch;
rizzos@usi.ch

SPECIALTY SECTION
This article was submitted to Gynecological Oncology, a section of the journal Frontiers in Oncology

RECEIVED 29 September 2022
ACCEPTED 21 October 2022
PUBLISHED 02 November 2022

CITATION
Rizzo S, Raia G, Del Grande M, Gasparri ML, Colombo I, Manganaro L, Papadia A and Del Grande F (2022) Body composition as a predictor of chemotherapy-related toxicity in ovarian cancer patients: A systematic review.
Front. Oncol. 12:1057631.
doi: 10.3389/fonc.2022.1057631

Body composition as a predictor of chemotherapy-related toxicity in ovarian cancer patients: A systematic review

Stefania Rizzo[1,2]*, Giorgio Raia[1], Maria Del Grande[3], Maria Luisa Gasparri[4], Ilaria Colombo[3], Lucia Manganaro[5], Andrea Papadia[2,4] and Filippo Del Grande[1,2]

[1]Istituto di Imaging della Svizzera Italiana (IIMSI), Ente Ospedaliero Cantonale (EOC), Lugano, Switzerland, [2]Facoltà di Scienze biomediche, Università della Svizzera Italiana, Lugano, Switzerland, [3]Istituto Oncologico della Svizzera Italiana (IOSI), Ente Ospedaliero Cantonale (EOC), Bellinzona, Switzerland, [4]Department of Gynecology and Obstetrics, Ente Ospedaliero Cantonale (EOC), Lugano, Switzerland, [5]Department of Radiological, Oncological and Pathological Sciences, University of Rome Sapienza, Rome, Italy

Objectives: The main objective of this systematic review was to examine the literature evaluating association of image-based body composition with chemotherapy-related toxicity in ovarian cancer patients. A secondary objective was to evaluate the different definitions of sarcopenia across studies.

Methods: This systematic review was conducted according to the PRISMA-DTA statement and the protocol was registered on Prospero. A comprehensive literature search of 3 electronic databases was performed by two authors. For each eligible article, information was collected concerning the clinical setting; basic study data; population characteristics; technical aspects; body composition features; chemotherapy drugs administered; association of body composition values and toxicities. The overall quality of the included studies was critically evaluated.

Results: After the initial retrieval of 812 articles, the systematic review included 6 articles (5/6 studies were retrospective; one was prospective). The number of patients ranged between 69 and 239; mean/median age ranged between 55 and 65 years; the percentage of sarcopenic patients ranged between 25% and 54%. The cut-off values to define sarcopenia and the vertebral levels for evaluation of body composition were different. Five studies included chemotherapy based on carboplatin and paclitaxel, 1 included chemotherapy based on pegylated liposomal doxorubicin. Among the studies including carboplatin and paclitaxel, 3/5 demonstrated an association with toxicity, whereas 2/5 did not. Altogether, 4/6 papers demonstrated an association between the body composition values and the development of chemotherapy-related toxicities.

Conclusions: There is a wide variability of results about the association of body composition and chemotherapy-related toxicity in ovarian cancer patients.

Therefore further studies, possibly including a comprehensive assessment of body compartments and where the definition of body composition cut-offs is constant, are warranted to better understand this association.

Systematic review registration: https://www.crd.york.ac.uk/prospero/display_record.php?ID=CRD42022337753, identifier (CRD42022337753).

KEYWORDS

ovarian cancer, chemotherapy, body composition, sarcopenia, toxicity

Introduction

Ovarian cancer (OC) is the second most frequent cancer among gynecological malignancies, with 19.880 estimated new cases in the US in 2022, and the most lethal, with 12.810 estimated deaths (1). The current standard treatment for OC is primary cytoreductive surgery with complete resection of all macroscopic disease, followed by adjuvant platinum-based chemotherapy with or without the antiangiogenic agent bevacizumab (2, 3). When the patient is considered not operable or the disease is deemed not completely resectable, interval debulking surgery after neoadjuvant chemotherapy (NACT) is usually considered (4). In stage III-IV high grade epithelial ovarian cancer, maintenance treatment with poly-ADP-ribose inhibitors (PARPi) has been also incorporate in first line (5–7).

In both scenarios (primary surgery followed by adjuvant chemotherapy, neoadjuvant chemotherapy followed by interval debulking surgery), chemotherapy is dosed aiming at a balance between optimal efficacy and acceptable toxicity. Indeed, if severe toxicity occurs during chemotherapy, the standard chemotherapeutic regimen might not be administered or the dose and schedule adjusted and this might potentially lead to suboptimal treatment and decreased survival. Factors potentially predisposing to toxicity are age, previous chemotherapy, genetic characteristics, including toxicity-related polymorphisms or BRCA mutational status (8, 9). Many authors have hypothesized that body composition, indicating the amount and distribution of muscle and fat compartments, is one of the factors that may predict interpatient variation in toxicity profiles, accounting for different metabolism of chemotherapeutic drugs (10–13). In fact, there is substantial evidence of the variability in body composition in cancer populations (14–16), as well as emerging evidence suggesting that the size of body composition compartments relate to prognosis in many cancer subtypes, including ovarian (17), lung (18), bladder (19) and pancreatic malignancies (20). As demonstrated by some authors, sarcopenic patients may be prone to get higher doses of chemotherapy agents for a rather small amount of muscle mass and they may therefore encounter higher toxicity (21, 22).

Since cancer patients routinely performs imaging examinations during their clinical management (23–25), imaging-based assessment of body composition might be added to the reading of imaging examinations (26, 27), so offering opportunistic clinical information that currently go unused. For instance, from Computed Tomography (CT) images it is possible to extract the areas of muscles at a pre-defined level, usually referred to as skeletal muscle area (SMA); psoas index (PI), indicating only the area of the psoas muscle; the area of visceral adipose tissue (VAT), indicating the fat within the abdomen outside the solid organs; the area of subcutaneous adipose tissue (SAT); the density of the skeletal muscle, as indirect sign of its adipose infiltration (SMD). Despite different definitions and a wide variability of cut-off values for the definition of sarcopenia, this is a condition that can be found in patients with OC and, although many studies have assessed its association with survival, only few studies have assessed the association with chemotherapy-related toxicity.

Therefore, the main objective of this systematic review was to collect and examine all the available literature evaluating association of image-based body composition with chemotherapy-related toxicity in patients with OC. A secondary objective was to evaluate the different definitions of sarcopenia across studies.

Methods

This systematic review was conducted according to the PRISMA-DTA (Preferred Reporting Items for Systematic Reviews and Meta-analysis for Diagnostic Test Accuracy) statement (28). The review protocol was registered on Prospero as CRD42022337753.

Search strategy

Two authors (SR and GR) performed a comprehensive literature search of the electronic databases PubMed, Cochrane and Web of Science to find primary publications evaluating association between body composition measures and chemotherapy-related toxicities in OC. No beginning date limit or language restrictions were used; the literature search was last updated on Aug 17th 2022; and the search was expanded by also screening the references of the retrieved articles for additional potentially eligible studies. The search terms consisted of ((ovarian cancer) OR (ovarian carcinoma)) AND ((sarcopenia) OR (body composition) OR (muscle) OR (fat) OR (adipose tissue)) AND ((complication) OR (complications) OR (chemotherapy-related) OR (adjuvant) OR (neo-adjuvant) OR (toxicity) OR (chemotoxicity) OR (chemo-toxicity)). Articles in which body composition assessment was based on CT were obtained in full for further independent evaluation by two authors (SR and GR). There was no exclusion for any type of toxicity and neither for the type or line of chemotherapy. Studies were excluded if they were case reports, conference abstracts, reviews or short communications because they do not provide sufficient information to assess the methodological quality. Uncertainties were resolved in consensus.

Data extraction

For each eligible article, information was collected by 3 authors (SR, GR, MDG) concerning the clinical setting (neo-adjuvant, adjuvant, further lines); basic study data (year of publication, country of origin, study design); population characteristics (number of patients, age, BMI, percentage of sarcopenic patients, cut-off values for sarcopenia used); technical aspects (axial level for evaluation of body composition); body composition features evaluated (SMA, SMI, VAT, SAT, SMD, PI, lean body mass (LBM), fat mass (FM)); chemotherapy drugs administered; association of body composition values and toxicities.

Quality assessment

The overall quality of the included studies was critically evaluated based on the revised "Quality Assessment of Diagnostic Accuracy Studies" tool (QUADAS-2) (29). This tool comprises four domains for evaluation of risk of bias (patient selection, index test, reference standard, and flow and timing) and three domains for applicability concerns (patient selection, index test, reference standard). Each domain was assessed and graphs were constructed appropriately.

Results

Literature search

The initial search yielded 812 articles, all in English. According to inclusion and exclusion criteria, 6 full-text articles were included in this systematic review (17, 30–34). Details about the literature search results are reported in Figure 1.

Given the small number of papers included, the clear heterogeneity of the methods and, as a consequence, of the results, it was not possible to perform a meta-analysis for pooled data.

Basic study data and population characteristics

As shown in Table 1, among the 6 studies included, three were from the US (30, 32, 34); the other were from different countries

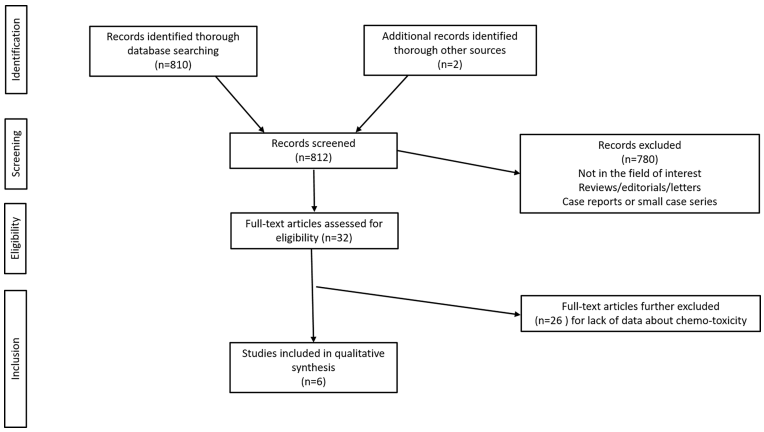

FIGURE 1
Study selection flowchart.

TABLE 1 Basic study and population characteristics.

Authors	Year	Country	Study design	N patients	Mean/median age (years)	BMI (mean)	Percentage of sarcopenic patients	Cut-off values for sarcopenia
Prado (29)	2014	US	Prospective	74	55	27.9	NA	NA
Yoshikawa (28)	2017	Japan	Retrospective	76	62	NA	50%	PI < 58.3 cm^2/m^2
Conrad (27)	2018	US	Retrospective	102	55	28	54%	PI<38.5 cm^2/m^2
Staley (25)	2020	US	Retrospective	201	64	26.9	27%	SMI<41 cm^2/m^2
Bruno (26)	2021	Brazil	Retrospective	239	56	NA	35%	SMI<38.9 cm^2/m^2
Del Grande (12)	2021	Switzerland	Retrospective	69	65	24.9	25%	SMI<41 cm^2/m^2

NA, not available; BMI, body mass index; SMI, skeletal muscle index; PI, psoas index.

(17, 31, 33). 5/6 studies were retrospective (17, 30–33); one was prospective (from a phase III clinical trial) (34). The number of patients included ranged between 69 (17) and 239 (31); mean/median age ranged between 55 (32, 34) and 65 years (17); the percentage of sarcopenic patients ranged between 25% (17) and 54% (32). The BMI ranged between 24.9 (17) and 28 (32). The cut-off values to define sarcopenia in different studies and the percentage of sarcopenic patients are summarized in Table 1.

Body composition evaluation details; chemotherapy administered and association of body composition to chemo-related toxicity

As shown in Table 2, 4/6 articles evaluated the body composition values at the level of the 3rd lumbar vertebra (L3) (17, 30, 31, 34); 1/6 at the level of the 4th lumbar vertebra (L4) (32); 1/6 at the level of the 5th lumbar vertebra (L5) (33). The main body composition parameters evaluated were: SMI (derived from SMA) in 3/6 studies (17, 30, 31); psoas index (PI) in 2/6 studies (32, 33); SAT in 3/6 studies (17, 31, 32); SMD in 3/6 (17, 31, 34). Five studies included chemotherapy based on carboplatin and paclitaxel (17, 30– 33), 1 included chemotherapy based on pegylated liposomal doxorubicina (34).

Two studies (12, 28) included both the neo-adjuvant and adjuvant settings; one declared only the first line setting (25); one included only patients treated with a further line treatment (29). Among the studies including carboplatin and paclitaxel, 3/5 demonstrated an association with toxicity (17, 31, 33), whereas 2/5 did not (30, 31). Altogether, 4/6 papers demonstrated an association between the body composition values and the development of chemotherapy-related toxicities (17, 31, 33, 35), with one showing association of VAT and SMD with chemotherapy cycle delays as well as of SMA and early discontinuation of chemotherapy (17); one showing an association of SAT and SMD with G3 adverse events and toxicity-induced modification of treatment (31); one showing association of the psoas index with neuropathy (33); one showing association of the FM/LBM ratio with toxicity only in overweight and obese patients (35).

TABLE 2 Body composition evaluation details; chemotherapy administered and association of body composition to chemo-related toxicity (if any).

Authors	Vertebra level for body composition assessment	Body composition features evaluated	Chemotherapy	Association of body composition and chemo-related toxicity
Prado (29)	L3	SMD; LBM; FM	Pegylated liposomal doxorubicina	FM/LBM ratio associated with toxicity only in overweight and obese patients
Yoshikawa (28)	L5	PI	Carboplatin and paclitaxel	PI associated with neuropathy
Conrad (27)	L4	PA; PI, VAT, SAT	Carboplatin and paclitaxel	No association
Staley (25)	L3	SMA, SMI	Carboplatin and paclitaxel	No association
Bruno (26)	L3	SMI, SAT, SMD	Carboplatin and paclitaxel	SAT and SMD associated with G3 adverse events and toxicity-induced modification of treatment
Del Grande (12)	L3	SMA, SMI, VAT, SAT, SMD	Carboplatin and paclitaxel	VAT and SMD associated with chemotherapy cycle delays; SMA with early discontinuation of chemotherapy

L3, 3rd lumbar vertebra; L4, 4th lumbar vertebra; L5, 5th lumbar vertebra; SMA, skeletal muscle area; SMI, skeletal muscle index; VAT, visceral adipose tissue; SAT, subcutaneous adipose tissue; SMD, skeletal muscle density; PA, psoas area; PI, psoas index; LBM, lean body mass; FM, fat mass; G3, grade 3.

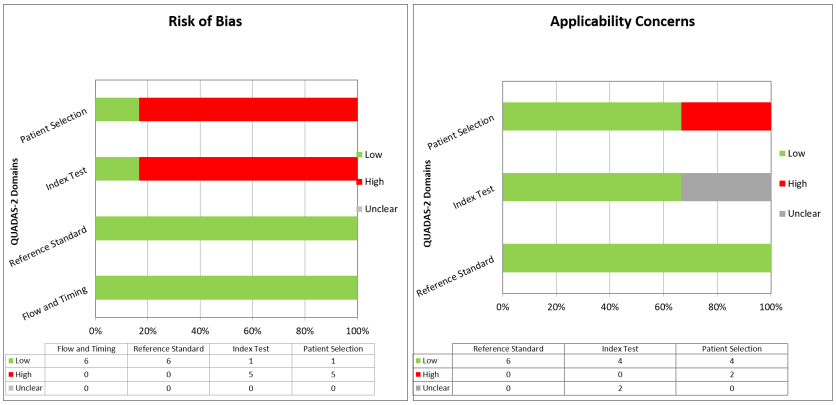

FIGURE 2
Overall quality assessment (risk of bias and applicability concerns) of the studies included in the Systematic Review, according to the QUADAS-2 Tool.

Quality assessment of the studies included

The overall quality assessment of the studies is reported in Figure 2.

Discussion

This systematic review demonstrates that the association between body composition and chemo-related toxicity in OC is still unclear. Indeed, 4/6 studies demonstrated the presence of a significant association, but 2/6 did not. Furthermore, the significant associations were not among the same covariates across studies.

Interestingly, the 2 studies showing no significant association of body composition and toxicity are from the same country (US) (30, 32), that is also known for its high percentage of overweight/obese patients. Indeed, the age-adjusted prevalence of obesity in the US in 2017–2018 was 42.4%, and the age-adjusted prevalence of severe obesity was as high as 9.2% among adults (>20 years), especially among women (35). This high prevalence of overweight/obese patients, confirmed by the high mean BMI in both studies, might have affected the results. Indeed, the low muscle mass may be underestimated in obese patients.

What emerges from the analysis of the results of the included studies, is that no study evaluated all the body compartments available, therefore some information is still missing. Indeed, for instance, Del Grande showed an association of SMA and early discontinuation of chemotherapy, but SMI was not significant (17). In the same study VAT and SMD were significantly associated with cycle delays, but SAT was not (17). Bruno et al. demonstrated the importance of SAT and SMD for G3 adverse events, but they did not evaluate the other compartments (31). Conrad and Yoshikawa analyzed only the PI, thus excluding all the other muscles in the same plane and even the other body compartments (32, 33).

Nevertheless, various methods are available for assessing body composition and they are based on an escalating level of complexity, from a two-compartment model (evaluating only fat mass and fat free mass), through a three-compartment model (including fat mass, lean tissue mass and bone mineral content), and a four-compartment model (including fat, mineral, total body water and proteins) to more complex multi-compartment models (including complex measurements of elements such as calcium, sodium, chloride, phosphorus, nitrogen, hydrogen, oxygen and carbon) (36). Therefore, other studies hypothesized that not only the quality and quantity of muscle are important in the metabolism of drugs, but also other compartments may contribute to the metabolism of chemotherapeutic agents (37). Indeed, the body proportions of lean and adipose tissues may be one of the phenotypic factors that affect the metabolism, clearance, and toxicity of antineoplastic agents (38). Accordingly, Schachar et al. analyzed a large number of body composition measures to assess predictors of toxicity in patients receiving chemotherapy for early stage breast cancer, and they demonstrated that body composition is extremely variable, demonstrating in their cohort that muscle metrics were clearly related to toxicity, whereas adipose metrics were not (39). Other studies tried to integrate the information of quality and quantity of muscle introducing a relatively new metric, a product of SMI and SMD (40), and demonstrated that this metric predicted G4 hematologic and G3/4 non-hematologic adverse event toxicity when eribulin was administered as a treatment in advanced soft tissue sarcoma (41).

As the technology advances, we may imagine that more comprehensive body composition quantifications will be possible as opportunistic assessments from imaging studies in patients with OC, including but not limited to assessment of bone mineral density, quantification of visceral and subcutaneous fat, assessment of muscle bulk and density, and quantification of liver fat (42).

This systematic review has some limitations. The first is the lack of a prospective cohort study evaluating the association of body

composition and chemotherapy-related composition as primary objective. However, this type of study is difficult to obtain and usually have prognosis as primary outcome. Secondly, we included studies where the body composition was based on CT images and we do not know if other studies, based on DEXA or other techniques may show different results. However, CT (along with magnetic resonance) is currently considered as gold standard for assessment of body composition, therefore we may affirm that the data collected are reliable among the included studies. Lastly, the variability of definition of sarcopenia among the included studies, and the lack of reasons for the authors to choose different cut-offs, makes difficult an appropriate comparison. Indeed, we cannot know if the use of the same cut-off value for sarcopenia, would have led to more consisting results.

In conclusion, this systematic review of the literature demonstrated that there is a wide variability of results about the association of body composition and chemotherapy-related toxicity in patients with OC. Therefore further studies, possibly including a comprehensive assessment of body compartments and a constant definition of body composition cut-offs, are warranted to better understand this association.

Data availability statement

The original contributions presented in the study are included in the article/supplementary material. Further inquiries can be directed to the corresponding author.

Author contributions

Conception and design: all authors. Data extraction from included studies: SR, GR, MDG, MLG. Analysis and interpretation of data: SR, GR, MDG, MLG. Manuscript writing: all authors. All authors contributed to the article and approved the submitted version.

Conflict of interest

The reviewer FT declared a shared affiliation with the author LM to the handling editor at the time of the review.

The remaining authors declare that the research was conducted in the absence of any commercial or financial relationships that could be construed as a potential conflict of interest.

Publisher's note

References

1. Siegel RL, Miller KD, Fuchs HE, Jemal A. Cancer statistics, 2022. *CA Cancer J Clin* (2022) 72(1):7–33. doi: 10.3322/caac.21708

2. Oza AM. Standard chemotherapy with or without bevacizumab for women with newly diagnosed ovarian cancer (ICON7): overall survival results of a phase 3 randomised trial. *Lancet Oncol* (2015) 16(8):928–36. doi: 10.1016/S1470-2045(15)00086-8

3. Tewari KS. Final overall survival of a randomized trial of bevacizumab for primary treatment of ovarian cancer. *J Clin Oncol* (2019) 37(26):2317–28. doi: 10.1200/JCO.19.01009

4. Colombo N, Sessa C, Bois AD, Ledermann J, McCluggage WG, McNeish I, et al. ESMO-ESGO consensus conference recommendations on ovarian cancer: pathology and molecular biology, early and advanced stages, borderline tumours and recurrent disease. *Ann Oncol* (2019) 30(5):672–705. doi: 10.1093/annonc/mdz062

5. DiSilvestro P, Banerjee S, Colombo N, Scambia G, Kim BG, Oaknin A, et al. Overall survival with maintenance olaparib at a 7-year follow-up in patients with newly diagnosed advanced ovarian cancer and a BRCA mutation: The SOLO1/GOG 3004 trial. *J Clin Oncol* (2022) JCO2201549. doi: 10.1200/JCO.22.01549

6. González-Martín A. PRIMA/ENGOT-OV26/GOG-3012 investigators. niraparib in patients with newly diagnosed advanced ovarian cancer. *N Engl J Med* (2019) 381(25):2391–402. doi: 10.1056/NEJMoa1910962

7. Ray-Coquard IPAOLA-1 Investigators. Olaparib plus bevacizumab as first-line maintenance in ovarian cancer. *N Engl J Med* (2019) 381(25):2416–28. doi: 10.1056/NEJMoa1911361

8. Ferracini AC, Lopes-Aguiar L, Lourenço GJ, Yoshida A, Lima CSP, Sarian LO, et al. GSTP1 and ABCB1 polymorphisms predicting toxicities and clinical management on carboplatin and paclitaxel-based chemotherapy in ovarian cancer. *Clin Transl Sci* (2021) 14(2):720–8. doi: 10.1111/cts.12937

9. Tomao F, Bardhi E, Di Pinto A, Sassu CM, Biagioli E, Petrella MC, et al. Parp inhibitors as maintenance treatment in platinum sensitive recurrent ovarian cancer: An updated meta-analysis of randomized clinical trials according to BRCA mutational status. *Cancer Treat Rev* (2019) 80:101909. doi: 10.1016/j.ctrv.2019.101909

10. Morgan DJ, Bray KM. Lean body mass as a predictor of drug dosage. implications for drug therapy. *Clin Pharmacokinet* (1994) 26(4):292–307. doi: 10.2165/00003088-199426040-00005

11. Aslani A, Smith RC, Allen BJ, Pavlakis N, Levi JA. The predictive value of body protein for chemotherapy-induced toxicity. *Cancer* (2000) 88(4):796–803. doi: 10.1002/(SICI)1097-0142(20000215)88:4<796::AID-CNCR10>3.0.CO;2-P

12. Prado CM, Baracos VE, McCargar LJ, Reiman T, Mourtzakis M, Tonkin K, et al. Sarcopenia as a determinant of chemotherapy toxicity and time to tumor progression in metastatic breast cancer patients receiving capecitabine treatment. *Clin Cancer Res* (2009) 15(8):2920–6. doi: 10.1158/1078-0432

13. Antoun S, Baracos VE, Birdsell L, Escudier B, Sawyer MB. Low body mass index and sarcopenia associated with dose-limiting toxicity of sorafenib in patients with renal cell carcinoma. *Ann Oncol* (2010) 21(8):1594–8. doi: 10.1093/annonc/mdp605

14. Prado CM, Lieffers JR, McCargar LJ, Reiman T, Sawyer MB, Martin L, et al. Prevalence and clinical implications of sarcopenic obesity in patients with solid tumours of the respiratory and gastrointestinal tracts: a population-based study. *Lancet Oncol* (2008) 9(7):629–35. doi: 10.1016/S1470-2045(08)70153-0

15. Baracos VE, Reiman T, Mourtzakis M, Gioulbasanis I, Antoun S. Body composition in patients with non-small cell lung cancer: a contemporary view of cancer cachexia with the use of computed tomography image analysis. *Am J Clin Nutr* (2010) 91(4):1133S–7S. doi: 10.3945/ajcn.2010.28608C

16. Martin L, Birdsell L, Macdonald N, Reiman T, Clandinin MT, McCargar LJ, et al. Cancer cachexia in the age of obesity: skeletal muscle depletion is a powerful prognostic factor, independent of body mass index. *J Clin Oncol* (2013) . 31 (12):1539–47. doi: 10.1200/JCO.2012.45.2722

17. Del Grande M, Rizzo S, Nicolino GM, Colombo I, Rossi L, Manganaro L, et al. Computed tomography-based body composition in patients with ovarian cancer: Association with chemotoxicity and prognosis. *Front Oncol* (2021) 11:718815. doi: 10.3389/fonc.2021.718815

18. Rizzo S, Petrella F, Bardoni C, Bramati L, Cara A, Mohamed S, et al. CT-derived body composition values and complications after pneumonectomy in lung cancer patients: Time for a sex-related analysis? *Front Oncol* (2022) 12:826058. doi: 10.3389/fonc.2022.826058

19. Sanchez A, Kissel S, Coletta A, Scott J, Furberg H. Impact of body size and body composition on bladder cancer outcomes: Risk stratification and opportunity for novel interventions. *Urol Oncol* (2020) 38(9):713–8. doi: 10.1016/j.urolonc.2020.03.017

20. Rizzo S, Scala I, Robayo AR, Cefalì M, De Dosso S, Cappio S, et al. Del grande f body composition as a predictor of chemotherapy-related toxicity in pancreatic cancer patients: A systematic review. *Front Oncol* (2022) 12:974116. doi: 10.3389/fonc.2022.974116

21. Sjøblom B, Grønberg BH, Benth JŠVerifytat, Baracos VE, Fløtten Ø, Hjermstad MJ, et al. Low muscle mass is associated with chemotherapy-induced haematological toxicity in advanced non-small cell lung cancer. *Lung Cancer* (2015) 90:85–91. doi: 10.1016/j.lungcan.2015.07.001

22. Tan BH, Birdsell LA, Martin L, Baracos VE, Fearon KC. Sarcopenia in an overweight or obese patient is an adverse prognostic factor in pancreatic cancer. *Clin Cancer Res* (2009) 15:6973–9. doi: 10.1158/1078-0432.CCR-09-1525

23. Bellomi M, Rizzo S, Travaini LL, Bazzi L, Trifirò G, Zampino MG, et al. Role of multidetector CT and FDG-PET/CT in the diagnosis of local and distant recurrence of resected rectal cancer. *Radiol Med* (2007) 112(5):681–90. doi: 10.1007/s11547-007-0172-2

24. Rietjens M, Villa G, Toesca A, Rizzo S, Raimondi S, Rossetto F, et al. Appropriate use of magnetic resonance imaging and ultrasound to detect early silicone gel breast implant rupture in postmastectomy reconstruction. *Plast Reconstr Surg* (2014) 134(1):13e–20e. doi: 10.1097/PRS.0000000000000291

25. Genovese E, Canì A, Rizzo S, Angeretti MG, Leonardi A, Fugazzola C. Comparison between MRI with spin-echo echo-planar diffusion-weighted sequence (DWI) and histology in the diagnosis of soft-tissue tumours. *Radiol Med* (2011) 116(4):644–56. doi: 10.1007/s11547-011-0666-9

26. Huber FA, Del Grande F, Rizzo S, Guglielmi G, Guggenberger R. MRI In the assessment of adipose tissues and muscle composition: how to use it. *Quant Imaging Med Surg* (2020) 10(8):1636–49. doi: 10.21037/qims.2020.02.06

27. Zaffina C, Wyttenbach R, Pagnamenta A, Grasso RF, Biroli M, Del Grande F, et al. Body composition assessment: comparison of quantitative values between magnetic resonance imaging and computed tomography. *Quant Imaging Med Surg* (2022) 12(2):1450–66. doi: 10.21037/qims-21-619

28. McInnes MDF, Moher D, Thombs BD, McGrath TA, Bossuyt PMPRISMA-DTA Group, et al. Preferred reporting items for a systematic review and meta-analysis of diagnostic test accu-racy studies: The PRISMA-DTA statement. *JAMA* (2018) 319(4):388–96. doi: 10.1001/jama.2017.19163

29. Whiting PF, Rutjes AW, Westwood ME, Mallett S, Deeks JJ, Reitsma JB, et al. QUADAS-2: a revised tool for the quality assessment of diagnostic accuracy studies. *Ann Intern Med* (2011) 155(8):529–36. doi: 10.7326/0003-4819-155-8-201110180-00009

30. Staley SA, Tucker K, Newton M, Ertel M, Oldan J, Doherty I, et al. Sarcopenia as a predictor of survival and chemotoxicity in patients with epithelial ovarian cancer receiving platinum and taxane-based chemotherapy. *Gynecol Oncol* (2020) 156(3):695–700. doi: 10.1016/j.ygyno.2020.01.003

31. Bruno KA, Sobreira da Silva MJ, Chaves GV. Association of body composition with toxicity to first-line chemotherapy and three-year survival in women with ovarian adenocarcinoma. *Acta Oncol* (2021) 60(12):1611–20. doi: 10.1080/0284186X.2021.1983210

32. Conrad LB, Awdeh H, Acosta-Torres S, Conrad SA, Bailey AA, Miller DS, et al. Pre-operative core muscle index in combination with hypoalbuminemia is associated with poor prognosis in advanced ovarian cancer. *J Surg Oncol* (2018) 117 (5):1020–8. doi: 10.1002/jso.24990

33. Yoshikawa T, Takano M, Miyamoto M, Yajima I, Shimizu Y, Aizawa Y, et al. Psoas muscle volume as a predictor of peripheral neurotoxicity induced by primary chemotherapy in ovarian cancers. *Cancer Chemother Pharmacol* (2017) 80(3):555–61. doi: 10.1007/s00280-017-3395-5

34. Prado CM, Baracos VE, Xiao J, Birdsell L, Stuyckens K, Park YC, et al. The association between body composition and toxicities from the combination of doxil and trabectedin in patients with advanced relapsed ovarian cancer. *Appl Physiol Nutr Metab* (2014) 39(6):693–8. doi: 10.1139/apnm-2013-0403

35. Hales CM, Carroll MD, Fryar CD, Ogden CL. *Prevalence of obesity and severe obesity among adults: United states, 2017–2018. NCHS data brief, no 360*. Hyattsville, MD: National Center for Health Statistics (2020).

36. Kuriyan R. Body composition techniques. *Indian J Med Res* (2018) 148 (5):648–58. doi: 10.4103/ijmr.IJMR_1777_18

37. Sandini M, Patino M, Ferrone CR, Alvarez-Pérez CA, Honselmann KC, Paiella S, et al. Association between changes in body composition and neoadjuvant treatment for pancreatic cancer. *JAMA Surg* (2018) 153(9):809–15. doi: 10.1001/jamasurg.2018.0979

38. Cushen SJ, Power DG, Teo MY, MacEneaney P, Maher MM, McDermott R, et al. Body composition by computed tomography as a predictor of toxicity in patients with renal cell carcinoma treated with sunitinib. *Am J Clin Oncol* (2017) 40 (1):47–52. doi: 10.1097/COC.0000000000000061

39. Shachar SS, Deal AM, Weinberg M, Williams GR, Nyrop KA, Popuri K, et al. Body composition as a predictor of toxicity in patients receiving anthracycline and taxane-based chemotherapy for early-stage breast cancer. *Clin Cancer Res* (2017) 23(14):3537–43. doi: 10.1158/1078-0432.CCR-16-2266

40. Weinberg MS, Shachar SS, Muss HB, Deal AM, Popuri K, Yu H, et al. Characterization of skeletal muscle and body mass indices in younger and older women with stage II and III breast cancer. *J Am Geriatr Soc* (2016) 24(3):278–284. doi: 10.1111/tbj.12952

41. Kobayashi H, Okuma T, Oka H, Okajima K, Ishibashi Y, Zhang L, et al. Body composition as a predictor of toxicity after treatment with eribulin for advanced soft tissue sarcoma. *Int J Clin Oncol* (2019) 24(4):437–44. doi: 10.1007/s10147-018-1370-8

42. Pickhardt PJ, Graffy PM, Perez AA, Lubner MG, Elton DC, Summers RM. Opportunistic screening at abdominal CT: Use of automated body composition biomarkers for added cardiometabolic value. *Radiographics* (2021) 41(2):524–42. doi: 10.1148/rg.2021200056

frontiers | Frontiers in Oncology

TYPE Opinion
PUBLISHED 09 November 2022
DOI 10.3389/fonc.2022.1020907

OPEN ACCESS

EDITED BY
Alessio G. Morganti,
University of Bologna, Italy

REVIEWED BY
Milly Buwenge,
University of Bologna, Italy

*CORRESPONDENCE
Nandita M. deSouza
nandita.desouza@icr.ac.uk

SPECIALTY SECTION
This article was submitted to Gynecological Oncology, a section of the journal Frontiers in Oncology

RECEIVED 16 August 2022
ACCEPTED 21 October 2022
PUBLISHED 09 November 2022

CITATION
deSouza NM, Choudhury A, Greaves M, O'Connor JPB and Hoskin PJ (2022) Imaging hypoxia in endometrial cancer: How and why should it be done?
Front. Oncol. 12:1020907.
doi: 10.3389/fonc.2022.1020907

Imaging hypoxia in endometrial cancer: How and why should it be done?

Nandita M. deSouza[1,2]*, Ananya Choudhury[3,4], Mel Greaves[5], James P. B. O'Connor[1,2,4] and Peter J. Hoskin[4,6]

[1]Division of Radiotherapy and Imaging, The Institute of Cancer Research, London, United Kingdom, [2]Department of Imaging, The Royal Marsden National Health Service (NHS) Foundation Trust, London, United Kingdom, [3]Radiation Oncology, The Christie National Health Service (NHS) Foundation Trust Manchester, Manchester, United Kingdom, [4]The Division of Cancer Sciences, University of Manchester, Manchester, United Kingdom, [5]Centre for Evolution and Cancer, The Institute of Cancer Research, London, United Kingdom, [6]Radiation Oncology, Mount Vernon Cancer Centre, Northwood, United Kingdom

KEYWORDS

hypoxia, endometrial cancer, magnetic resonance imaging (MRI), oxygen-enhanced MRI, molecular subtypes

Introduction

Tissues become hypoxic when their oxygen consumption exceeds their supply. In tumors, neoangiogenesis results in disordered vascular morphology and this leads to inadequate oxygen supply to rapidly growing cells (1). However, because vessels have variations in their vascular tone, hypoxic status is a dynamic rather than a static event; it may be transient and is often cyclical (2). Cyclical hypoxia with a median periodicity of 15 mins has been described in xenografts and head and neck cancers in patients (3). Hypoxia is important because it is well accepted as a poor prognostic factor in for patients with a range of cancer types (4–7) where it has been associated with disease that is progressive, resistant and metastatic (8).

Under hypoxic conditions, oxygen-sensitive transcription factors (hypoxia inducible factors [HIFs]) are upregulated. In the endometrium, HIF1α expression increases as the tissue undergoes changes from normality to being premalignant and then to become adenocarcinoma. This is paralleled by increased angiogenesis in the endometrium, suggesting that HIF1α and thus tissue hypoxia might be a key regulator in endometrial carcinogenesis (9). A poorer prognosis in patients with EC expressing HIF-1α has been demonstrated in a metaanalysis with a hazard ratio of 2.29 (10), and its link to tumor aggressiveness at other cancer sites is documented (11). Hypoxic status also has been associated with mutations of multiple genes in endometrial cancer (EC) (12). In other cancer types, driver mutations in p53, MYC and PTEN are enriched in hypoxic tumors (13) with an effect of hypoxia on mutational load (14). Therefore, as hypoxia is

likely to determine the evolutionary trajectories and as a result the management and outcomes of cancer, imaging tumor hypoxic status in EC may offer prognostic value and facilitate personalisation of treatment strategies (15).

Endometrial cancer: Diagnosis, staging and the changing molecular landscape

EC, (9,300 new cases per annum in the UK (16), 65,620 new cases in 2020 in USA (17) usually presents with post-menopausal bleeding and is detected at an early stage. Diagnostic confirmation on pipelle sampling of the endometrium or at hysteroscopy is followed by pelvic magnetic resonance imaging (MRI) for disease staging (18). Endometrioid and mucinous carcinomas are classified as type I and serous and clear cell carcinomas as type II. The former are usually low grade and low stage at presentation and the latter high grade and advanced stage. Disease outcome depends on tumor grade, stage, subtype, depth of myometrial invasion, lymphovascular space invasion and lymph node involvement (19). In fact, in type I endometrial adenocarcinoma, high expression of HIF-1 α showed a significant correlation with higher grade of the tumor, depth of myometrial invasion, adnexal invasion and clinical stage (20), which strengthens the argument for hypoxia driving tumor progression by favouring selection of adverse genetic clones.

Molecular classification is now used to define risk groups in EC, namely deoxyribose nucleic acid (DNA) polymerase ε ultramutated (POLEmut), mismatch repair-deficient (MMRd), p53 mutant (p53abn) and those EC lacking any of these alterations, referred to as NSMP (non-specific molecular profile) (21). Prognosis is extremely good in POLE and poor in p53 mutant cancers (22) with poor clinical outcomes in the latter group being independent of histology grade or stage (23–25); the other two categories fall between these two extremes. TP53 mutations are highly prevalent in the serous (Type II) subtype (88% of 42 serous ECs (26), and are also present in a subset of endometroid (Type I) carcinomas (15% of 186 endometroid ECs (26). Recent data show that a subset of p53mut EC is homologous recombination-deficient (HRD), and some of these EC can arise in the context of germline breast cancer (*BRCA)1/2* mutations (27–29). The exact prevalence of HRD in p53mut EC is currently unknown; in a small and selected set of cases it was 46% (28).

The biological and genetic mechanisms that causally link hypoxia with progression of disease are being unravelled. Hypoxia and associated acidosis activate the TP53 dependent stress response and apoptosis (30). This then provides selective evolutionary pressure for the emergence of mutants in the TP53 response (13). Such genetic variants then preferentially expand as a population. Their fitness benefit is however more than simple survival. They are intrinsically more resistant to many of the therapeutic modalities that operate *via* the TP53 apoptosis pathway. Their failure to undergo TP53 driven cell cycle arrest and DNA repair also leads to genetic instability (31). Additionally, as hypoxia mimics the mesenchymal stem cell niche (32), surviving TP53 mutants undergo Epithelial-Mesenchymal transition (EMT) to migratory, stem cell phenotypes. Hence the hypoxic microenvironment encourages the selection of cancer cell populations that have an expanded pool of stem cells (the critical units of selection in cancer progression) that are likely to be genetically unstable. These biological features fuel both disease progression and the likelihood of treatment resistance (33).

Methodology and challenges of imaging hypoxia

The prognostic relevance of hypoxia in EC has been determined largely by using the expression of HIF-1α (12) and the presence of tumor necrosis (34). Although the correlation of HIF-1α with imaging estimates of hypoxia is variable (35), an association has been demonstrated in EC (15). On imaging, hypoxia may be measured indirectly or directly. Traditionally, tumor vasculature has been imaged using ultrasound and computerized tomography (CT). Doppler ultrasound, based on the frequency shift of moving echo-generating components in flowing blood, has been used to classify endometrial pathologies (36). With contrast-enhanced CT, extracted metrics relate to blood flow, blood volume and vascular permeability (37). Although increased vascularity in tumors is highly disorganised and leaky, often indicating an increased hypoxic status (38), it is not a direct measurement.

Positron Emission Tomography (PET) uses hypoxia-specific tracers such as ^{18}F-labelled nitroimidazoles and copper (Cu)-labelled diacetyl-bis(N4-methylthiosemicarbazone) analogues (39). Under hypoxic conditions, free nitro radicals are retained within the cell. Though commonly used ^{18}F-fluoroimidazole (^{18}F-FMISO) (40) has relatively low uptake, slow kinetics and is influenced by non-hypoxic metabolism. ^{18}F-FAZA [1-(5-fluoro-5-deoxy-α-D-arabinofuranosyl)-2-nitroimidazole)] offers better resolution and signal-to-noise ratio (41). Cu complex agents with diacetyl-bis(N4-methylthiosemicarbazone) (ATSM) ligand under hypoxic conditions cannot be reversibly oxidised by the cell also making Cu-ATSM a possible means for evaluating hypoxia in the clinic (42–44). However, its specificity is debatable and validation with pimonidazole stained tissues has been variable and tumor type specific (45, 46)

A shift to non-invasive hypoxia imaging with MRI is advantageous (47). In blood oxygen level dependent (BOLD) MRI, also known as intrinsic susceptibility-weighted MRI,

paramagnetic deoxyhaemoglobin within red blood cells (in contrast to non-paramagnetic oxyhaemoglobin) increases the MR transverse relaxation rate (R2*, the inverse of the transverse relaxation time T2*), of water in blood and surrounding tissues. Variations in perfusion mean that the relationship between R2* and tissue pO_2 is non-linear and perfusion dependent. Nevertheless, BOLD-MRI is sensitive to changes in pO_2 within vessels and in tissues adjacent to perfused vessels (48, 49). R2* has been shown to correlate positively with tissue hypoxia score (HP5) and oxygen pressure (50) and with HIF-2α expression in colorectal cancer with different tumor stages (51, 52). Advantages of the BOLD-MRI technique for measurement of hypoxia are lack of need for externally administered contrast media, easy repeatability, near real-time visualisation of time-dependent changes and a measure independent of blood flow. Nevertheless, the variability of the measurement (53), means that measuring a change in R2* following an oxygen challenge may be preferable particularly as they have been shown to correlate strongly with pimonidazole staining in tumor models (54).

Oxygen in solution and deoxy Hb also affect the longitudinal relaxation rate of tissues (55) and are exploited in the technique of oxygen-enhanced (OE)- MRI, also known as tumor oxygen level dependent contrast (TOLD). Their effect on the rate of longitudinal proton relaxation (R1) can be enhanced by the inhalation of 100% O2 which results in an increase in the relaxation rate in normoxic tissues, primarily due to an increase in dissolved oxygen (56). A measurable signal change of up to 20% is achievable in normoxic tissues with 100% O_2 inhalation on clinical scanners (57) that can distinguish them from hypoxic tissue (58). OE-MRI has been validated in pre-clinical studies (59, 60) and had initial clinical translation (61, 62) with promising results. MRI measures of hypoxia can be implemented as an extension of the imaging staging examination but require standardisation of image acquisition and analysis methodology prior to clinical use.

Endometrial cancer– opportunities for adjusting management strategies to hypoxic status

Management of EC is primarily surgical as patients with uterus-confined low-risk disease are often cured by surgery. Prognostic factors that describe groups by their risk of recurrence (histological type and grade, age, tumor size, and lymphovascular space involvement (63) are used to determine need for adjuvant therapies. Several trials have compared external beam radiotherapy (EBRT) after surgery versus observation after surgery in intermediate and high-risk disease: the PORTEC 1 (64), ASTEC/EN5 (65) and Gynecologic Oncology Group (GOG) (66) trials all showed a reduced risk of vaginal and pelvic relapse though overall survival did not differ. PORTEC 2 then showed that equivalent locoregional control could be achieved with vaginal brachytherapy without the toxicity of EBRT, so that adjuvant brachytherapy is the standard-of-care in patients with intermediate-risk disease following surgery (67). More recently, the PORTEC-3 trial, concluded that molecular classification has strong prognostic value in high-risk EC, with significantly improved recurrence-free survival with adjuvant chemoradiotherapy compared to radiotherapy alone for p53abnormal tumors, regardless of histologic type (68).

Hypoxia imaging and its link to TP53 status offers potential to refine management strategies by selecting patients through prognostic stratification. Pre-operative hypoxia imaging could identify the women who would most benefit from adjuvant radiotherapy and select women who might benefit from EBRT rather than adjuvant brachytherapy alone. Also, in hypoxic tumors post-surgery, where there is residual disease, it may be possible to dose-escalate with either brachytherapy, external beam radiotherapy or the use of a radiosensitiser, or omit or dose de-escalation when tumor hypoxia is not demonstrated. In locally advanced endometrial cancer (stage III) treated primarily with chemoradiotherapy, hypoxia imaging may also indicate those who would benefit from hypoxia modification with a radiosensitiser. Drugs like carbogen and nicotinamide can be combined with radiation without increasing late toxicity but may improve survival outcomes as in muscle-invasive bladder cancer (69). The effect of hypoxia on the immune tumor microenvironment is complex, but it is likely to promote resistance to immune modulatory approaches (70).

Neoadjuvant chemotherapy (NAC) has primarily been trialled in patients with Stage 4 or metastatic disease at presentation with uterine papillary serous carcinomas (71) to facilitate optimal surgical cytoreduction. More recently this has been extended to endometrioid adenocarcinoma (72, 73) where the use of NAC to enable cytoreductive surgery resulted in an increased progression-free and overall survival (74). It may be possible to refine the use of NAC further if tumor hypoxic status along with tumor stage and volume were considered to select patients likely to respond. Finally, the association of hypoxia with genetic instability and DNA damage repair efficacy (supported by the prevalence of HRD in p53 mutated EC (28)), indicates that hypoxia imaging could be an important predictive selector for women who benefit from agents such as poly adenosine diphosphate ribose polymerase (PARP) inhibitors although their use in EC remains to be established.

As with EC in the primary setting, locally recurrent EC that shows a high degree of hypoxia may benefit from dose-escalation

or use of a radiosensitiser. Development of prognostic models based on hypoxic status and molecular profiling (75) may change approaches to maintenance therapies and surveillance. Poor prognostic tumors at risk of progressive disease thus identified may benefit from a more aggressive surveillance strategy adapted to their risk. It may also enable implementation of future maintenance therapy approaches in suitable patient cohorts.

Discussion and concluding remarks

The technical validation and demonstration of target monitoring with hypoxia imaging remains a major challenge. Continuous measurements indicate variable O_2 saturation, there is heterogeneity within each tumor and between tumor sites in the same patient (76) and thresholds for differentiating normoxic from hypoxic tissues in imaging studies are lacking. The impact of hypoxia on chemoresistance has been long established (77), but the range of hypoxia particularly across the different molecular subtypes needs to be understood. Recording hypoxia within tumors requires obsessive attention to imaging technique, adherence to imaging protocols such as those mandated by the Quantitative Imaging Biomarkers Alliance, and as with all biomarker studies, an establishment and understanding of the reproducibility of the measurement (78, 79). Despite these restrictions, when implemented according to protocol, hypoxia imaging with MRI can be a simple add-on to the staging examination of endometrial cancer. The additional imaging time of 10 mins for a BOLD evaluation and 10 mins for a TOLD evaluation is clinically achievable and can even be implemented in conjunction to increase the robustness of hypoxia evaluation. Methods such as MR fingerprinting may in future also allow simultaneous acquisition of both the T2* and T1 information (80) before,

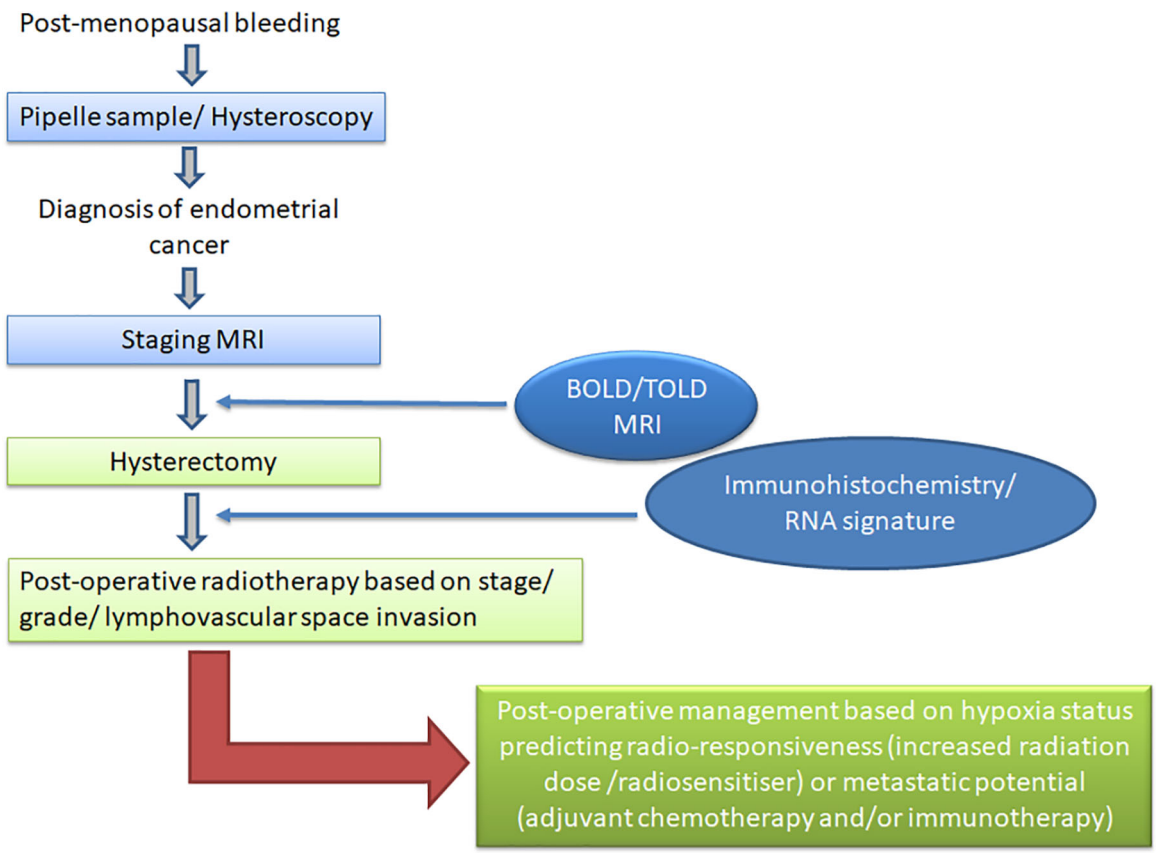

FIGURE 1
Diagnostic and management pathway for patients with endometrial cancer. Current diagnostic tests are shown in light blue and proposed hypoxia imaging in dark blue; current management options are shown in light green and alternative strategies based on hypoxia imaging and molecular stratification in dark green.

during and after the oxygen challenge, markedly reducing image acquisition time. The derived information is a useful adjunct to that already available and has the potential to substantially alter and enhance the management options offered to patients (Figure 1).

Author contributions

All authors contributed to the design, drafting, writing and editing of this opinion piece.

Funding

AC, JPBO'C and PJH are supported by the NIHR Manchester Biomedical Research Centre.

Conflict of interest

The authors declare that the research was conducted in the absence of any commercial or financial relationships that could be construed as a potential conflict of interest.

Publisher's note

References

1. Jain RK. Normalization of tumor vasculature: an emerging concept in antiangiogenic therapy. *Science* (2005) 307:58–62. doi: 10.1126/science.1104819

2. Singleton DC, Macann A, Wilson WR. Therapeutic targeting of the hypoxic tumour microenvironment. *Nat Rev Clin Oncol* (2021) 18:751–72. doi: 10.1038/s41571-021-00539-4

3. Panek R, Welsh L, Baker LCJ, Schmidt MA, Wong KH, Riddell AM, et al. Noninvasive imaging of cycling hypoxia in head and neck cancer using intrinsic susceptibility MRI. *Clin Cancer Res* (2017) 23:4233–41. doi: 10.1158/1078-0432.CCR-16-1209

4. Muz B, de la Puente P, Azab F, Azab AK. The role of hypoxia in cancer progression, angiogenesis, metastasis, and resistance to therapy. *Hypoxia (Auckl)* (2015) 3:83–92. doi: 10.2147/HP.S93413

5. Horsman MR, Vaupel P. Pathophysiological basis for the formation of the tumor microenvironment. *Front Oncol* (2016) 6:66. doi: 10.3389/fonc.2016.00066

6. Popper HH. Progression and metastasis of lung cancer. *Cancer Metastasis Rev* (2016) 35:75–91. doi: 10.1007/s10555-016-9618-0

7. Tafani M, Sansone L, Limana F, Arcangeli T, De Santis E, Polese M, et al. The interplay of reactive oxygen species, hypoxia, inflammation, and sirtuins in cancer initiation and progression. *Oxid Med Cell Longev* (2016) 2016:3907147. doi: 10.1155/2016/3907147

8. Unwith S, Zhao H, Hennah L, Ma D. The potential role of HIF on tumour progression and dissemination. *Int J Cancer* (2015) 136:2491–503. doi: 10.1002/ijc.28889

9. Horree N, van Diest PJ, van der Groep P, Sie-Go DM, Heintz AP. Hypoxia and angiogenesis in endometrioid endometrial carcinogenesis. *Cell Oncol* (2007) 29:219–27. doi: 10.1155/2007/434731

10. Zhu P, Shen L, Ren Q, Zeng Q, He X. Prognostic and clinicopathological significance of hypoxia-inducible factor-1alpha in endometrial cancer: A meta-analysis. *Front Oncol* (2020) 10:587420. doi: 10.3389/fonc.2020.587420

11. Daimiel I. Insights into hypoxia: Non-invasive assessment through imaging modalities and its application in breast cancer. *J Breast Cancer* (2019) 22:155–71. doi: 10.4048/jbc.2019.22.e26

12. Cai Y, Wang B, Xu W, Liu K, Gao Y, Guo C, et al. Endometrial cancer: Genetic, metabolic characteristics, therapeutic strategies and nanomedicine. *Curr Med Chem* (2021) 28:8755–81. doi: 10.2174/0929867328666210705144456

13. Bhandari V, Li CH, Bristow RG, Boutros PC, Consortium P. Divergent mutational processes distinguish hypoxic and normoxic tumours. *Nat Commun* (2020) 11:737. doi: 10.1038/s41467-019-14052-x

14. Hassan Venkatesh G, Bravo P, Shaaban Moustafa Elsayed W, Amirtharaj F, Wojtas B, Abou Khouzam R, et al. Hypoxia increases mutational load of breast cancer cells through frameshift mutations. *Oncoimmunology* (2020) 9:1750750. doi: 10.1080/2162402X.2020.1750750

15. Berg A, Fasmer KE, Mauland KK, Ytre-Hauge S, Hoivik EA, Husby JA, et al. Tissue and imaging biomarkers for hypoxia predict poor outcome in endometrial cancer. *Oncotarget* (2016) 7:69844–56. doi: 10.18632/oncotarget.12004

16. (2022). Available at: https://www.cancerresearchuk.org/health-professional/cancer-statistics/statistics-by-cancer-type/uterine-cancer/ (Accessed 8th August 2022).

17. Siegel RL, Miller KD, Jemal A. Cancer statistics, 2020. *CA Cancer J Clin* (2020) 70:7–30. doi: 10.3322/caac.21590

18. Koskas M, Amant F, Mirza MR, Creutzberg CL. Cancer of the corpus uteri: 2021 update. *Int J Gynaecol Obstet* (2021) 155 Suppl 1:45–60. doi: 10.1002/ijgo.13866

19. Prat J. Prognostic parameters of endometrial carcinoma. *Hum Pathol* (2004) 35:649–62. doi: 10.1016/j.humpath.2004.02.007

20. Pansare V, Munkarah AR, Schimp V, Haitham Arabi M, Saed GM, Morris RT, et al. Increased expression of hypoxia-inducible factor 1alpha in type I and type II endometrial carcinomas. *Mod Pathol* (2007) 20:35–43. doi: 10.1038/modpathol.3800718

21. Jamieson A, Thompson EF, Huvila J, Gilks CB, McAlpine JN. p53abn endometrial cancer: understanding the most aggressive endometrial cancers in the era of molecular classification. *Int J Gynecol Cancer* (2021) 31:907–13. doi: 10.1136/ijgc-2020-002256

22. Allo G, Bernardini MQ, Wu RC, Shih Ie M, Kalloger S, Pollett A, et al. ARID1A loss correlates with mismatch repair deficiency and intact p53 expression in high-grade endometrial carcinomas. *Mod Pathol* (2014) 27:255–61. doi: 10.1038/modpathol.2013.144

23. Stelloo E, Nout RA, Osse EM, Jurgenliemk-Schulz IJ, Jobsen JJ, Lutgens LC, et al. Improved risk assessment by integrating molecular and clinicopathological factors in early-stage endometrial cancer-combined analysis of the PORTEC cohorts. *Clin Cancer Res* (2016) 22:4215–24. doi: 10.1158/1078-0432.CCR-15-2878

24. Kommoss S, McConechy MK, Kommoss F, Leung S, Bunz A, Magrill J, et al. Final validation of the ProMisE molecular classifier for endometrial carcinoma in a large population-based case series. *Ann Oncol* (2018) 29:1180–8. doi: 10.1093/annonc/mdy058

25. Yano M, Ito K, Yabuno A, Ogane N, Katoh T, Miyazawa M, et al. Impact of TP53 immunohistochemistry on the histological grading system for endometrial endometrioid carcinoma. *Mod Pathol* (2019) 32:1023–31. doi: 10.1038/s41379-019-0220-1

26. Schultheis AM, Martelotto LG, De Filippo MR, Piscuglio S, Ng CK, Hussein YR, et al. TP53 mutational spectrum in endometrioid and serous endometrial cancers. *Int J Gynecol Pathol* (2016) 35:289–300. doi: 10.1097/PGP.0000000000000243

27. de Jonge MM, Ritterhouse LL, de Kroon CD, Vreeswijk MPG, Segal JP, Puranik R, et al. Germline BRCA-associated endometrial carcinoma is a distinct clinicopathologic entity. *Clin Cancer Res* (2019) 25:7517–26. doi: 10.1158/1078-0432.CCR-19-0848

28. de Jonge MM, Mooyaart AL, Vreeswijk MP, de Kroon CD, van Wezel T, van Asperen CJ, et al. Linking uterine serous carcinoma to BRCA1/2-associated cancer syndrome: A meta-analysis and case report. *Eur J Cancer* (2017) 72:215–25. doi: 10.1016/j.ejca.2016.11.028

29. de Jonge MM, Auguste A, van Wijk LM, Schouten PC, Meijers M, Ter Haar NT, et al. Frequent homologous recombination deficiency in high-grade endometrial carcinomas. *Clin Cancer Res* (2019) 25:1087–97. doi: 10.1158/1078-0432.CCR-18-1443

30. Pan Y, Oprysko PR, Asham AM, Koch CJ, Simon MC. p53 cannot be induced by hypoxia alone but responds to the hypoxic microenvironment. *Oncogene* (2004) 23:4975–83. doi: 10.1038/sj.onc.1207657

31. Luoto KR, Kumareswaran R, Bristow RG. Tumor hypoxia as a driving force in genetic instability. *Genome Integr* (2013) 4:5. doi: 10.1186/2041-9414-4-5

32. Mohyeldin A, Garzon-Muvdi T, Quinones-Hinojosa A. Oxygen in stem cell biology: a critical component of the stem cell niche. *Cell Stem Cell* (2010) 7:150–61. doi: 10.1016/j.stem.2010.07.007

33. Greaves M. Evolutionary determinants of cancer. *Cancer Discov* (2015) 5:806–20. doi: 10.1158/2159-8290.CD-15-0439

34. Bredholt G, Mannelqvist M, Stefansson IM, Birkeland E, Bo TH, Oyan AM, et al. Tumor necrosis is an important hallmark of aggressive endometrial cancer and associates with hypoxia, angiogenesis and inflammation responses. *Oncotarget* (2015) 6:39676–91. doi: 10.18632/oncotarget.5344

35. Thureau S, Piton N, Gouel P, Modzelewski R, Dujon A, Baste JM, et al. First comparison between [18f]-FMISO and [18f]-faza for preoperative pet imaging of hypoxia in lung cancer. *Cancers (Basel)* (2021) 13:1–12. doi: 10.3390/cancers13164101

36. Van Den Bosch T, Verbakel JY, Valentin L, Wynants L, De Cock B, Pascual MA, et al. Typical ultrasound features of various endometrial pathologies described using international endometrial tumor analysis (IETA) terminology in women with abnormal uterine bleeding. *Ultrasound Obstet Gynecol* (2021) 57:164–72. doi: 10.1002/uog.22109

37. Lin M, Zhang Q, Song Y, Yu X, Ouyang H, Xie L, et al. Differentiation of endometrial adenocarcinoma from adenocarcinoma of cervix using kinetic parameters derived from DCE-MRI. *Eur J Radiol* (2020) 130:109190. doi: 10.1016/j.ejrad.2020.109190

38. Ozbudak IH, Karaveli S, Simsek T, Erdogan G, Pestereli E. Neoangiogenesis and expression of hypoxia-inducible factor 1alpha, vascular endothelial growth factor, and glucose transporter-1 in endometrioid type endometrium adenocarcinomas. *Gynecol Oncol* (2008) 108:603–8. doi: 10.1016/j.ygyno.2007.11.028

39. Chia K, Fleming IN, Blower PJ. Hypoxia imaging with PET: which tracers and why? *Nucl Med Commun* (2012) 33:217–22. doi: 10.1097/MNM.0b013e32834eacb7

40. Krohn KA, Link JM, Mason RP. Molecular imaging of hypoxia. *J Nucl Med* (2008) 49 Suppl 2:129S–48S. doi: 10.2967/jnumed.107.045914

41. Postema EJ, McEwan AJ, Riauka TA, Kumar P, Richmond DA, Abrams DN, et al. Initial results of hypoxia imaging using 1-alpha-D: -(5-deoxy-5-[18F]-fluoroarabinofuranosyl)-2-nitroimidazole (18F-FAZA). *Eur J Nucl Med Mol Imaging* (2009) 36:1565–73. doi: 10.1007/s00259-009-1154-5

42. Dehdashti F, Grigsby PW, Lewis JS, Laforest R, Siegel BA, Welch MJ. Assessing tumor hypoxia in cervical cancer by PET with 60Cu-labeled diacetyl-bis (N4-methylthiosemicarbazone). *J Nucl Med* (2008) 49:201–5. doi: 10.2967/jnumed.107.048520

43. Piccardo A, Paparo F, Puntoni M, Righi S, Bottoni G, Bacigalupo L, et al. (64)CuCl2 PET/CT in prostate cancer relapse. *J Nucl Med* (2018) 59:444–51. doi: 10.2967/jnumed.117.195628

44. Minagawa Y, Shizukuishi K, Koike I, Horiuchi C, Watanuki K, Hata M, et al. Assessment of tumor hypoxia by 62Cu-ATSM PET/CT as a predictor of response in head and neck cancer: a pilot study. *Ann Nucl Med* (2011) 25:339–45. doi: 10.1007/s12149-011-0471-5

45. McCall KC, Humm JL, Bartlett R, Reese M, Carlin S. Copper-64-diacetyl-bis (N(4)-methylthiosemicarbazone) pharmacokinetics in FaDu xenograft tumors and correlation with microscopic markers of hypoxia. *Int J Radiat Oncol Biol Phys* (2012) 84:e393–399. doi: 10.1016/j.ijrobp.2012.05.005

46. Hansen AE, Kristensen AT, Jorgensen JT, McEvoy FJ, Busk M, van der Kogel AJ, et al. (64)Cu-ATSM and (18)FDG PET uptake and (64)Cu-ATSM autoradiography in spontaneous canine tumors: comparison with pimonidazole hypoxia immunohistochemistry. *Radiat Oncol* (2012) 7:89. doi: 10.1186/1748-717X-7-89

47. Dewhirst MW, Birer SR. Oxygen-enhanced MRI is a major advance in tumor hypoxia imaging. *Cancer Res* (2016) 76:769–72. doi: 10.1158/0008-5472.CAN-15-2818

48. Tatum JL, Kelloff GJ, Gillies RJ, Arbeit JM, Brown JM, Chao KS, et al. Hypoxia: importance in tumor biology, noninvasive measurement by imaging, and value of its measurement in the management of cancer therapy. *Int J Radiat Biol* (2006) 82:699–757. doi: 10.1080/09553000601002324

49. Howe FA, Robinson SP, McIntyre DJ, Stubbs M, Griffiths JR. Issues in flow and oxygenation dependent contrast (FLOOD) imaging of tumours. *NMR BioMed* (2001) 14:497–506. doi: 10.1002/nbm.716

50. Chopra S, Foltz WD, Milosevic MF, Toi A, Bristow RG, Menard C, et al. Comparing oxygen-sensitive MRI (BOLD R2*) with oxygen electrode measurements: a pilot study in men with prostate cancer. *Int J Radiat Biol* (2009) 85:805–13. doi: 10.1080/09553000903043059

51. Fan B, Wang XY, Yang XD, Zhong H, Wu CX, Jiang XX. Blood oxygen level-dependent MRI for the monitoring of neoadjuvant chemotherapy in breast carcinoma: initial experience. *Magn Reson Imaging* (2011) 29:153–9. doi: 10.1016/j.mri.2010.08.014

52. Ring J, Persigehl T, Remmele S, Heindel W, Dahnke H, Bremer C. Monitoring of bevacizumab-induced antiangiogenic treatment effects by "steady state" ultrasmall superparamagnetic iron oxide particles magnetic resonance imaging using robust multiecho DeltaR2* relaxometry. *Invest Radiol* (2011) 46:326–30. doi: 10.1097/RLI.0b013e3182045457

53. Leutritz T, Seif M, Helms G, Samson RS, Curt A, Freund P, et al. Multiparameter mapping of relaxation (R1, R2*), proton density and magnetization transfer saturation at 3 T: A multicenter dual-vendor reproducibility and repeatability study. *Hum Brain Mapp* (2020) 41:4232–47. doi: 10.1002/hbm.25122

54. Virani N, Kwon J, Zhou H, Mason R, Berbeco R, Protti A. *In vivo* hypoxia characterization using blood oxygen level dependent magnetic resonance imaging in a preclinical glioblastoma mouse model. *Magn Reson Imaging* (2021) 76:52–60. doi: 10.1016/j.mri.2020.11.003

55. Young IR, Clarke GJ, Bailes DR, Pennock JM, Doyle FH, Bydder GM. Enhancement of relaxation rate with paramagnetic contrast agents in NMR imaging. *J Comput Tomogr* (1981) 5:543–7. doi: 10.1016/0149-936X(81)90089-8

56. O'Connor JPB, Robinson SP, Waterton JC. Imaging tumour hypoxia with oxygen-enhanced MRI and BOLD MRI. *Br J Radiol* (2019) 92:20180642. doi: 10.1259/bjr.20180642

57. O'Connor JP, Jackson A, Buonaccorsi GA, Buckley DL, Roberts C, Watson Y, et al. Organ-specific effects of oxygen and carbogen gas inhalation on tissue longitudinal relaxation times. *Magn Reson Med* (2007) 58:490–6. doi: 10.1002/mrm.21357

58. Hammond EM, Asselin MC, Forster D, O'Connor JP, Senra JM, Williams KJ. The meaning, measurement and modification of hypoxia in the laboratory and the clinic. *Clin Oncol (R Coll Radiol)* (2014) 26:277–88. doi: 10.1016/j.clon.2014.02.002

59. O'Connor JP, Boult JK, Jamin Y, Babur M, Finegan KG, Williams KJ, et al. Oxygen-enhanced MRI accurately identifies, quantifies, and maps tumor hypoxia in preclinical cancer models. *Cancer Res* (2016) 76:787–95. doi: 10.1158/0008-5472.CAN-15-2062

60. Cao-Pham TT, Joudiou N, Van Hul M, Bouzin C, Cani PD, Gallez B, et al. Combined endogenous MR biomarkers to predict basal tumor oxygenation and response to hyperoxic challenge. *NMR BioMed* (2017) 30:1–12. doi: 10.1002/nbm.3836

61. Linnik IV, Scott ML, Holliday KF, Woodhouse N, Waterton JC, O'Connor JP, et al. Noninvasive tumor hypoxia measurement using magnetic resonance imaging in murine U87 glioma xenografts and in patients with glioblastoma. *Magn Reson Med* (2014) 71:1854–62. doi: 10.1002/mrm.24826

62. Salem A, Little RA, Latif A, Featherstone AK, Babur M, Peset I, et al. Oxygen-enhanced MRI is feasible, repeatable, and detects radiotherapy-induced change in hypoxia in xenograft models and in patients with non-small cell lung cancer. *Clin Cancer Res* (2019) 25:3818–29. doi: 10.1158/1078-0432.CCR-18-3932

63. Murali R, Soslow RA, Weigelt B. Classification of endometrial carcinoma: more than two types. *Lancet Oncol* (2014) 15:e268–278. doi: 10.1016/S1470-2045(13)70591-6

64. Creutzberg CL, van Putten WL, Koper PC, Lybeert ML, Jobsen JJ, Warlam-Rodenhuis CC, et al. Surgery and postoperative radiotherapy versus surgery alone for patients with stage-1 endometrial carcinoma: multicentre randomised trial. *PORTEC Study Group Post Operative Radiat Ther Endometrial Carcinoma. Lancet* (2000) 355:1404–11. doi: 10.1016/S0140-6736(00)02139-5

65. Group AES, Blake P, Swart AM, Orton J, Kitchener H, Whelan T, et al. Adjuvant external beam radiotherapy in the treatment of endometrial cancer (MRC ASTEC and NCIC CTG EN.5 randomised trials): pooled trial results, systematic review, and meta-analysis. *Lancet* (2009) 373:137–46. doi: 10.1016/S0140-6736(08)61767-5

66. Keys HM, Roberts JA, Brunetto VL, Zaino RJ, Spirtos NM, Bloss JD, et al. A phase III trial of surgery with or without adjunctive external pelvic radiation therapy in intermediate risk endometrial adenocarcinoma: a gynecologic oncology group study. *Gynecol Oncol* (2004) 92:744–51. doi: 10.1016/j.ygyno.2003.11.048

67. Nout RA, Smit VT, Putter H, Jurgenliemk-Schulz IM, Jobsen JJ, Lutgens LC, et al. Vaginal brachytherapy versus pelvic external beam radiotherapy for patients with endometrial cancer of high-intermediate risk (PORTEC-2): an open-label, non-

inferiority, randomised trial. *Lancet* (2010) 375:816–23. doi: 10.1016/S0140-6736(09)62163-2

68. Leon-Castillo A, de Boer SM, Powell ME, Mileshkin LR, Mackay HJ, Leary A, et al. Molecular classification of the PORTEC-3 trial for high-risk endometrial cancer: Impact on prognosis and benefit from adjuvant therapy. *J Clin Oncol* (2020) 38:3388–97. doi: 10.1200/JCO.20.00549

69. Song YP, Mistry H, Irlam J, Valentine H, Yang L, Lane B, et al. Long-term outcomes of radical radiation therapy with hypoxia modification with biomarker discovery for stratification: 10-year update of (Bladder carbogen nicotinamide) phase 3 randomized trial (ISRCTN45938399). *Int J Radiat Oncol Biol Phys* (2021) 110:1407–15. doi: 10.1016/j.ijrobp.2021.03.001

70. Noman MZ, Hasmim M, Messai Y, Terry S, Kieda C, Janji B, et al. Hypoxia: a key player in antitumor immune response. a review in the theme: Cellular responses to hypoxia. *Am J Physiol Cell Physiol* (2015) 309:C569–579. doi: 10.1152/ajpcell.00207.2015

71. Wilkinson-Ryan I, Frolova AI, Liu J, Stewart Massad L, Thaker PH, Powell MA, et al. Neoadjuvant chemotherapy versus primary cytoreductive surgery for stage IV uterine serous carcinoma. *Int J Gynecol Cancer* (2015) 25:63–8. doi: 10.1097/IGC.0000000000000321

72. de Lange NM, Ezendam NPM, Kwon JS, Vandenput I, Mirchandani D, Amant F, et al. Neoadjuvant chemotherapy followed by surgery for advanced-stage endometrial cancer. *Curr Oncol* (2019) 26:e226–32. doi: 10.3747/co.26.4655

73. Khouri OR, Frey MK, Musa F, Muggia F, Lee J, Boyd L, et al. Neoadjuvant chemotherapy in patients with advanced endometrial cancer. *Cancer Chemother Pharmacol* (2019) 84:281–5. doi: 10.1007/s00280-019-03838-x

74. Philp L, Kanbergs A, Laurent JS, Growdon WB, Feltmate C, Goodman A. The use of neoadjuvant chemotherapy in advanced endometrial cancer. *Gynecol Oncol Rep* (2021) 36:100725. doi: 10.1016/j.gore.2021.100725

75. Fjeldbo CS, Julin CH, Lando M, Forsberg MF, Aarnes EK, Alsner J, et al. Integrative analysis of DCE-MRI and gene expression profiles in construction of a gene classifier for assessment of hypoxia-related risk of chemoradiotherapy failure in cervical cancer. *Clin Cancer Res* (2016) 22:4067–76. doi: 10.1158/1078-0432.CCR-15-2322

76. Fleming IN, Manavaki R, Blower PJ, West C, Williams KJ, Harris AL, et al. Imaging tumour hypoxia with positron emission tomography. *Br J Cancer* (2015) 112:238–50. doi: 10.1038/bjc.2014.610

77. Vaupel P, Thews O, Hoeckel M. Treatment resistance of solid tumors: role of hypoxia and anemia. *Med Oncol* (2001) 18:243–59. doi: 10.1385/MO:18:4:243

78. Shukla-Dave A, Obuchowski NA, Chenevert TL, Jambawalikar S, Schwartz LH, Malyarenko D, et al. Quantitative imaging biomarkers alliance (QIBA) recommendations for improved precision of DWI and DCE-MRI derived biomarkers in multicenter oncology trials. *J Magn Reson Imaging* (2019) 49:e101–21. doi: 10.1002/jmri.26518

79. O'Connor JP, Aboagye EO, Adams JE, Aerts HJ, Barrington SF, Beer AJ, et al. Imaging biomarker roadmap for cancer studies. *Nat Rev Clin Oncol* (2017) 14:169–86. doi: 10.1038/nrclinonc.2016.162

80. Tippareddy C, Zhao W, Sunshine JL, Griswold M, Ma D, Badve C. Magnetic resonance fingerprinting: an overview. *Eur J Nucl Med Mol Imaging* (2021) 48:4189–200. doi: 10.1007/s00259-021-05384-2

frontiers | Frontiers in Oncology

TYPE Review
PUBLISHED 11 November 2022
DOI 10.3389/fonc.2022.1030967

OPEN ACCESS

EDITED BY
Alessio G. Morganti,
University of Bologna, Italy

REVIEWED BY
Fei Kuang,
Changhai Hospital of the Second Military Medical University, China
Maura Micco,
Agostino Gemelli University Polyclinic (IRCCS), Italy

*CORRESPONDENCE
Hirsch Matani
hirsch.matani@ahn.org

SPECIALTY SECTION
This article was submitted to Gynecological Oncology, a section of the journal Frontiers in Oncology

RECEIVED 29 August 2022
ACCEPTED 13 October 2022
PUBLISHED 11 November 2022

CITATION
Matani H, Patel AK, Horne ZD and Beriwal S (2022) Utilization of functional MRI in the diagnosis and management of cervical cancer. *Front. Oncol.* 12:1030967. doi: 10.3389/fonc.2022.1030967

Utilization of functional MRI in the diagnosis and management of cervical cancer

Hirsch Matani*, Ankur K. Patel, Zachary D. Horne and Sushil Beriwal

Division of Radiation Oncology, Allegheny Health Network Cancer Institute, Pittsburgh, PA, United States

Introduction: Imaging is integral part of cervical cancer management. Currently, MRI is used for staging, follow up and image guided adaptive brachytherapy. The ongoing IQ-EMBRACE sub-study is evaluating the use of MRI for functional imaging to aid in the assessment of hypoxia, metabolism, hemodynamics and tissue structure. This study reviews the current and potential future utilization of functional MRI imaging in diagnosis and management of cervical cancer.

Methods: We searched PubMed for articles characterizing the uses of functional MRI (fMRI) for cervical cancer. The current literature regarding these techniques in diagnosis and outcomes for cervical cancer were then reviewed.

Results: The most used fMRI techniques identified for use in cervical cancer include diffusion weighted imaging (DWI) and dynamic contrast enhancement (DCE). DCE-MRI indirectly reflects tumor perfusion and hypoxia. This has been utilized to either characterize a functional risk volume of tumor with low perfusion or to characterize at-risk tumor voxels by analyzing signal intensity both pre-treatment and during treatment. DCE imaging in these situations has been associated with local control and disease-free survival and may have predictive/prognostic significance, however this has not yet been clinically validated. DWI allows for creation of ADC maps, that assists with diagnosis of local malignancy or nodal disease with high sensitivity and specificity. DWI findings have also been correlated with local control and overall survival in patients with an incomplete response after definitive chemoradiotherapy and thus may assist with post-treatment follow up. Other imaging techniques used in some instances are MR-spectroscopy and perfusion weighted imaging. T2-weighted imaging remains the standard technique used for diagnosis and radiation treatment planning. In many instances, it is unclear what additional information functional-MRI techniques provide compared to standard MRI imaging.

Conclusions: Functional MRI provides potential for improved diagnosis, prediction of treatment response and prognostication in cervical cancer.

Specific sequences such as DCE, DWI and ADC need to be validated in a large prospective setting prior to widespread use. The ongoing IQ-EMBRACE study will provide important clinical information regarding these imaging modalities.

KEYWORDS

cervical cancer, MRI, functional imaging, DCE- MRI, DWI-MRI

Introduction

Among women, cervical carcinoma ranks fourth for both incidence and mortality worldwide. Within the United States in 2022, there are an estimated 14,100 cases and 4,280 deaths (1, 2). The most common histology is squamous cell carcinoma, accounting for 70-80% of all cervical cancers. Non-squamous histologies represent the minority of histologies, although are associated with worse prognosis (3). Prevalence of cervical cancer is strongly associated with socioeconomic status, in part due to differences in access to medical care and screening. Historically, staging based on the Federation of Gynecology and Obstetrics (FIGO) has been based upon clinical examination and limited imaging modalities including plain radiography, colposcopy, cystoscopy and proctoscopy, given the prevalence of these tumors within underdeveloped countries which often lack access to more advanced technologies. Without these technologies, defining the extent of primary tumor and the presence of pelvic and para-aortic lymph disease is difficult. Because of this, cross-sectional imaging is now included as an optional addition to assist with staging and prognostication, and assist with treatment (4). Imaging modalities commonly utilized in cervical cancer include magnetic resonance imaging (MRI) to assess the extent of local disease and define brachytherapy treatment volumes, and computed tomography (CT) or PET/CT to assess nodal status (5). Functional imaging is an even more novel approach being used to help define cervical cancer and its response to treatment, however its utility and implications on management have yet to be defined (6). This is a primary objective of the ongoing IQ-EMBRACE sub-study. In this study, MRI with T1, T2, diffusion and dynamic contrast-enhanced imaging will be obtained prior to treatment, along with diffusion-weighted and T2 imaging at the time of brachytherapy. Treatment will be delivered and patients will then be followed with this information to assess outcomes. As a novel imaging approach, we aim to review the current uses of functional imaging in the diagnosis and treatment cervical cancer.

MRI techniques

Standard MRI is performed on the foundation of nuclear magnetic resonance. The main component of this is the spin of nuclei which is related to the nuclear makeup (7). A magnetic field is applied to these atoms resulting in the synchronous precession of protons resulting in "bulk magnetization" which can be represented as a single vector precessing about the magnetic field. This precessing magnetization is detected as well as subsequent relaxation of these protons allowing for both T1 and T2 weighted sequences (8). With improvements in technology, there has been an increasing interest in functional MRI sequences such as Dynamic-Contrast Enhanced (DCE) MRI, diffusion-weighted MRI (DWI), and perfusion weighted imaging. During Dynamic Contrast Enhanced Imaging a bolus of contrast agent is administered to the patient prior to imaging. Due to their low molecular weights, these agents are able to move across vessel walls in tumor and distribute into the extracellular space prior to being washed out. On T1-weighted MRI imaging, signal intensity increases are seen and so rapid image acquisition is performed to assess movement of the contrast agent in tumor cells. As tumor vasculature exhibits a large amount of permeability, the uptake is perfusion limited and relies mainly upon blood flow and vascular density versus vessel permeability. DCE is not able to provide a direct measurement of tumor hypoxia, however with its characteristics, can indirectly provide this information through assessing tumor physiology with low-molecular weight contrast agents (9). DWI is a standard imaging tool for disease processes such as stroke, and relies upon apparent diffusion coefficient maps (ADC). Important parameters of DWI imaging include "b-value" relating to the strength of the motion probing gradient, and resulting signal-to-noise ratio. This underlying mechanism allows for diffusion changes that can be mapped. Increased cellularity is a characteristic of malignancies and as a result, diffusion is impeded at imaging. Therefore, signal intensity of malignancies is higher than that of normal parenchyma (10). Perfusion measurements with MRI can also be obtained utilizing injection of an exogenous endovascular tracer. Arterial spin

labeling is the idea of comparing the spin of inflowing blood water to stationary water in tissue. This tagging occurs looking at inversion of longitudinal magnetization. Images are obtained after a time delay to allow inflow after bolus reaches microvasculature and using signal differences, perfusion maps can be obtained (11). Lymphadenectomy is associated with high costs and so the addition of non-invasive methods for staging, specifically for detection of pelvic lymphadenopathy would be beneficial (12). The addition of MRI specifically for brachytherapy has also been associated with increased effectiveness of therapy and decreased costs by avoiding downstream cost of recurrence and management of toxicity from therapy (13). As a result, the costs of functional MRI techniques are expected to further provide information that can further improve diagnosis and therapies, and decrease costs. Along with costs, specific benefits of these MRI techniques are listed below.

Current use of magnetic resonance imaging for cervical cancer

Magnetic resonance imaging is an important component of staging for cervical cancer due to its superior soft tissue contrast resolution compared to CT. This characteristic makes MRI the preferred method for assessing the primary tumor and accurately assessing parametrial invasion and pelvic sidewall invasion with up to 95% accuracy or higher, ultimately allowing clinicians to determine the appropriate treatment modality (11, 14–17) (Figure 1). In addition, on the basis of the EMBRACE trials, MRI allows for image-guided adaptive brachytherapy (IGABT) with individualized target and organ at risk contouring, dose optimization and multiparametric dose prescription allowing for improved patient outcomes. In the Embrace cohort, 98% of patients could be treated with this method and overall local control was 92% across all stages, which was unprecendented (18). The mainstay of pelvic MRI to assess cervical tumors is T2 weighted imaging. Thin sections of 3-4mm are recommended and images should be acquired angled perpendicularly to the cervix (19).

Dynamic contrast enhanced MRI

Dynamic contrast enhanced (DCE) MRI is a widely accepted sequence of multi-parametric MRI for prostate and breast cancer imaging to assess suspicious findings on standard MRI and assist with treatment planning (20, 21). It is also the most studied

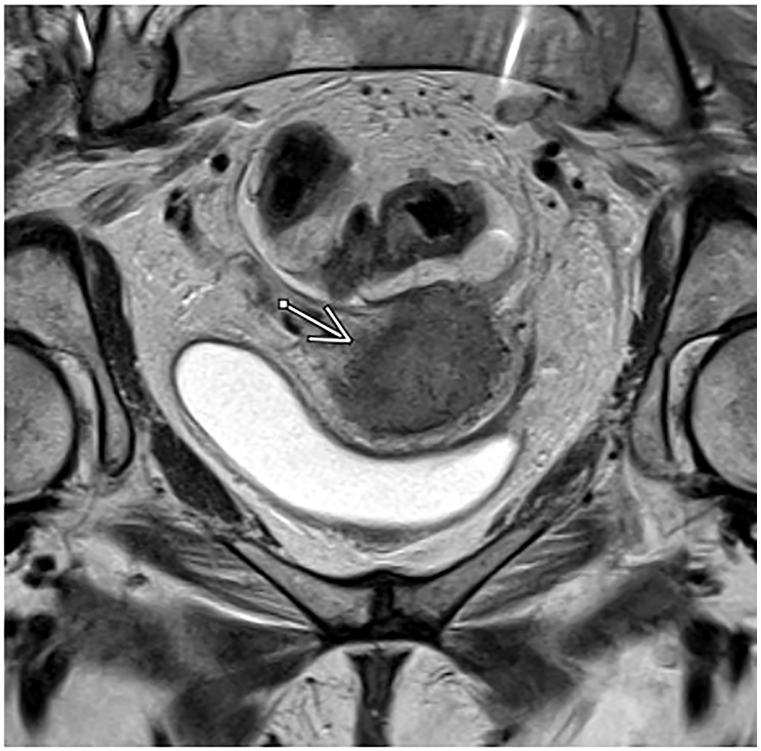

FIGURE 1
Axial T2-weighted MRI in a patient with FIGO IIIC1, pathologic T2 squamous cell carcinoma of the cervix.

functional imaging technique for locally advanced cervical cancer thus far and it is used to characterize tumor microvasculature, and therefore indirectly tumor perfusion status (22, 23). Hypoxia is a well-known feature of solid tumors and its presence is known to be associated with increased aggression of the tumor, increased risk of local invasion, metastasis and treatment failure. It is also known to influence the outcome of treatment with chemotherapy or radiotherapy, even in the case of microscopic tumor involvement (24). This is not surprising, as tumor hypoxia in cervical cancer specifically is an adverse risk factor and associated with poor outcomes, regardless of treatment modality (9). On this basis, DCE has been studied to predict for recurrence and survival outcomes in cervical cancer. (Figure 2) depicts tumor imaging on DCE. The largest study aimed to characterize a high risk "functional risk volume" of tumor voxels with low DCE signal intensity on MRI prior to and during radiation therapy. Those voxels included in the functional risk volume had a DCE signal intensity of <2.1 compared with pre-contrast imaging. At 6 years follow up, primary tumor control (p=0.003) and disease-specific survival ($p=1.9 \times 10^{-4}$) were significantly decreased in patients with a higher functional risk volume, and this parameter was superior to anatomic tumor volume as predictive and prognostic tool. The authors also found that high perfusion prior to treatment initiation or improved perfusion throughout treatment was associated with improved outcomes, which was hypothesized to reflect re-oxygenation and may have potential for monitoring response to therapy (25, 26). Validation of using DCE thresholds for characterizing voxels at risk for treatment failure has been performed, with findings similar to the prior study. Optimal signal intensity thresholds for differentiation of local recurrence and control ranged from 2.1-2.2 and for death and survival ranged from 1.8-2.2. A universal threshold based upon these values of 1.9 was identified for prediction of outcomes either prior to treatment or during treatment and this value remained significant for prediction of early treatment failures (27). The Mayr group has also published data regarding the use of DCE imaging at 2-2.5 weeks into radiation therapy to predict the risk of recurrence and death using a signal intensity cutoff of the lower 10^{th} percentile. Signal intensity was an independent predictor of recurrence and death and was significantly better than standard clinical prognostic factors in predicting outcomes (28). At least two studies, however have shown no correlation between DCE values and outcomes (29, 30). One study showed earlier onset of DCE enhancement to be associated with higher clinical stages, but not disease-free or overall survival. The other aimed to determine response to therapy by analyzing changes in tumor size and volume, for which pre-treatment DCE values did not correlate. One reason for this difference could be a lack of statistical power in the first study, which only had 12 patients evaluated and a short mean follow up of 11 years. Since DCE

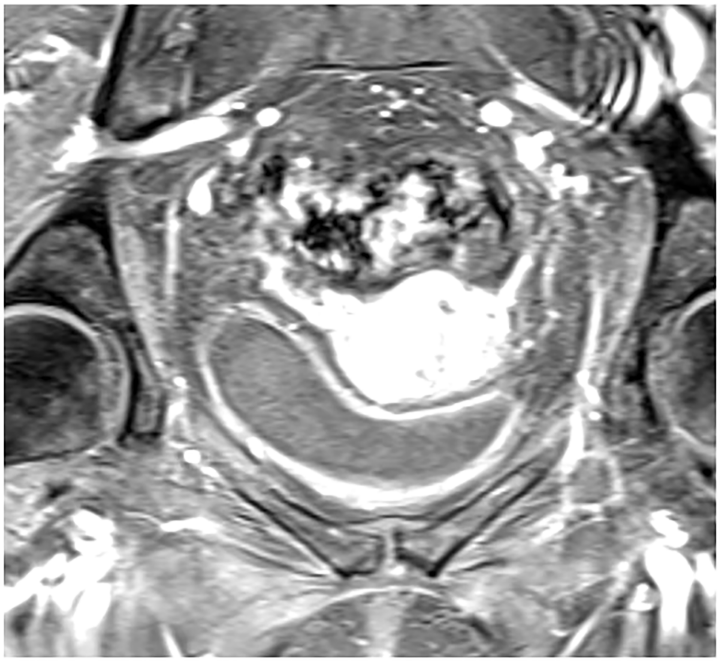

FIGURE 2
Post contrast dynamic contrast enhanced axial MRI showing increased signal intensity in a patient with FIGO IIIC1, pathologic T2 squamous cell carcinoma of the cervix.

values are indicative of the tumor microenvironment and vasculature, they may not directly correlate with anatomic tumor size or volume, which is a measure of the total number of cells within a tumor. There is a variety of different techniques that have been used to evaluate DCE, but given that the bulk of data is positive, DCE-MRI has potential to be used as an important predictive or prognostic factor in management of cervical cancer, and to help determine who may benefit from escalation of therapy.

Diffusion weighted imaging

Diffusion weighted imaging (DWI) is a method of signal contrast generation based upon differences in diffusion, also known as Brownian motion. Different tissues have a characteristic cellular architecture and pathologic processes can affect the water distribution within compartments, allowing for new anatomic information that can be gathered with conventional MRI sequences and is quantified by an apparent diffusion coefficient (ADC) map (31). Its current uses are mainly for diagnosis of central nervous system pathologies such as pediatric brain development, ischemic injury and white matter disease, although it has been used for diagnosis of malignancies throughout the body, as malignancies have a lower ADC compared with normal tissues (32). This feature is why diffusion-weighted MRI based imaging has been studied in the diagnosis of cervical and other gynecologic malignancies with some success, based on its ability to separate normal tissue from carcinomatous tissue (33). Particularly in the diagnosis of cervical cancer, a low ADC has been useful to help separate characterize the primary tumor as well as metastatic versus benign pelvic lymph nodes (34–37). Although the ADC values vary per study, using a value between 1.05 x 10^{-3} mm^2s and 1.14 x 10^{-3} mm^2/s as a cutoff yielded a sensitivity, specificity and accuracy as high as 95.83%, 94.55% and 94.94% (33). Another potential use of DWI is to characterize tumor histology. In one study, the ADC value was noted to be significantly lower for squamous cell carcinoma that for adenocarcinoma, however there was overlap between the two values and so currently it cannot be used to precisely separate the two (38). DWI has also been used to help characterize or predict treatment response. In one study out of Japan, for 9 patients ADC was correlated with response to chemotherapy and/or radiation therapy with an increase in mean ADC value of the lesion after treatment associated with adequate response (35). For squamous cell carcinoma specifically, the 90^{th} percentile of ADC values was lower in patients who responded to therapy compared to those who did not respond (39).

With all of these potential uses, DWI could play a significant role in the management of cervical malignancies through accurate diagnosis. This could help, particularly with patients who have equivocal post-treatment findings or lymph nodes after therapy. It is known that patients with adenocarcinoma have a worse prognosis with respect to progression free survival and local recurrence (40). If we are able to more accurately assess which patients with squamous cell carcinoma may be resistant to therapy or assist with histologic determination using DWI, we can potentially improve therapy to provide these patients with the best chance of controlling their disease.

A recent retrospective review of patients with medically inoperable stage I endometrial cancer treated with definitive radiation therapy found that the addition of DWI to standard post-contrast MRI to assess response to treatment increased reader confidence and the authors concluded that this sequence should be included as a standard addition (41). Another retrospective review out of MD Anderson Cancer Center analyzed patients with cervical cancer treated with definitive chemoradiation who had an MRI scan with DWI performed at baseline. They found that those with a higher mean pre-treatment ADC had improved disease-free survival with a trend toward improved overall survival and local recurrence. These outcomes remain similar to those from other institutions (42, 43).

For post-treatment follow up, the addition of DWI imaging has been shown to increase the early detection of patients who have a PET incomplete response after completion of definitive chemoradiotherapy, in a large retrospective review by Kalash et al. (Figure 3). Of 27 patients with a PET incomplete response who had DWI imaging, 11 were interpreted as DWI positive, with a median ADC of 0.973 x 10^{-3} mm^2/s. Of those 11 patients, 81.8% experienced a histologically confirmed local recurrence at mean interval of 4.1 months and of the 16 patients with negative response, only 12.5% experienced a local recurrence. In addition, a positive result on DWI was associated with significantly decreased local control at 2 years (92% vs. 20%, $p<0.005$) and decreased overall survival (83% vs. 36%, $p=0.049$). Overall the positive predictive value was 81.8% and negative predictive value was 87.5% (44).

Regarding its use for radiation treatment planning and contouring, only one prospective study performed in India has reported on the use of DWI in conjunction with T2 weighted MRI for target delineation for delivering MRI-guided adaptive brachytherapy and reported that per the GEC-ESTRO contouring guidelines, although the DWI based plan resulted in improved coverage of the high-risk CTV, doses to organs at risk were not significantly increased and DWI is recommended only as a supplement to standard T2-weighted imaging in the delivery of radiation therapy (45).

Perfusion-weighted imaging

Perfusion is defined as the steady-state delivery of blood to an element of tissue and specific MRI techniques have been developed to measure this non-invasively. The two major MRI

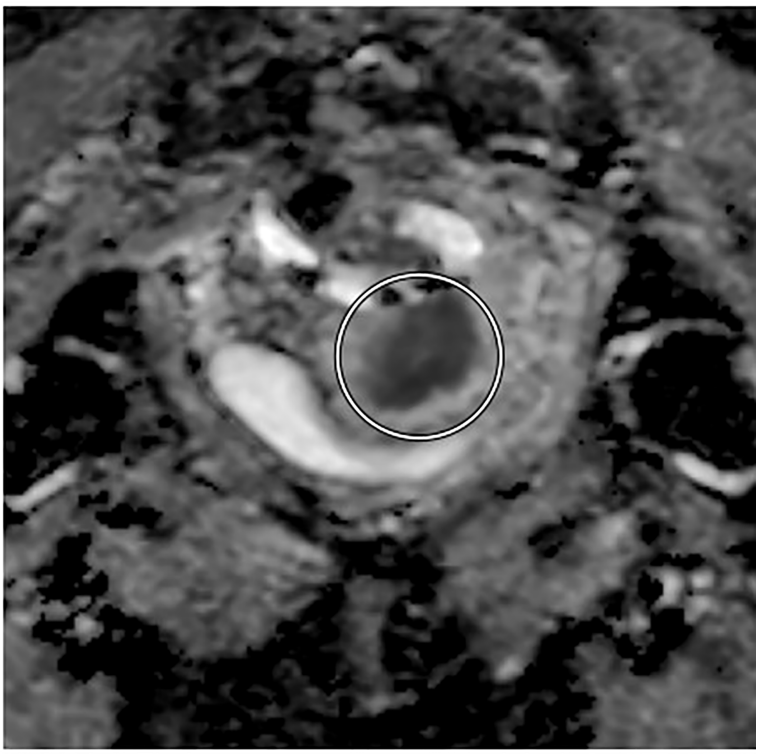

FIGURE 3
Axial diffusion-weighted MRI showing pre-treatment decreased tumor signal intensity in a patient with FIGO IIIC1, pathologic T2 squamous carcinoma of the cervix.

sequences to look at perfusion include use of DCE-MRI as briefly described above and dynamic susceptibility contrast-enhanced MRI. DCE MRI is obtained after injecting a contrast agent, often gadolinium-based and obtaining T1-weighted sequences to assess enhancement and other pharmacokinetic features. The most frequently used metric is ktrans which can reflect blood flow or vessel permeability depending on anatomic characteristics. Dynamic susceptibility contrast-enhanced (DSC) sequences also require injection of a contrast agent, but rely on T2-weighted sequences leading to MRI hypointensity. Cerebral blood volume and cerebral blood flow maps can then be derived from this information (46). Perfusion features of DCE have been described above, but briefly, DCE-MRI has been used as a predictive and prognostic tool. Low DCE-perfusion values are associated with poor response to therapy, local control and disease-free survival. They have also been shown in some small studies to predict response to therapy and early recurrences (25–27). Only one study has been recently published specifically looking at the role of DSC-MRI in management of cervical cancer. DSC-MRI values pre- and post-concurrent chemoradiation were examined and it was found that perfusion fraction of the tumor prior to concurrent chemoradiotherapy was higher in patients who had a partial response to therapy compared to those who had stable disease or progression (47).

MRI-spectroscopy

MRI-spectroscopy is a functional MRI technique that assesses the presence of small mobile molecules *in vivo* at the commonly used MRI strengths of 1.5T and 3T. In normal tissues, these molecules are choline, creatinine and N-acetyl-aspartate, whereas pathologic conditions including malignancies may increase the presence and detection of other molecules such as lactate or alanine (48). It is commonly used in the diagnosis of both benign and malignant central nervous system pathologies as well as malignancies throughout the body including prostate, colon, breast and cervical cancers (49, 50). Only a handful of published data is found regarding this technique in the diagnosis and management of cervical cancers. The most data, is regarding the analysis of lipid levels using *in-vivo* and ex-vivo samples to diagnose cervical cancer. Use of MR-spectroscopy to detect lipid levels, in particular in-phase triglyceride (CH)-2 *in vivo* and triglyceride (CH)-2 and (CH)-3 ex-vivo as able to predict the presence of cervical cancer compared to control subjects with an

in-vivo sensitivity and specificity of 77.4% and 93.8%. Ex-vivo sensitivity was 100% and specificity was 69%.55 Analysis of lipid levels for diagnosis has been corroborated by multiple groups (51–53). Using a 3T MRI to evaluate the presence of choline was unfortunately however not significantly different between different lesion types or in benign versus malignant disease (54).

To assess disease response, only a few studies have investigated variations in metabolite peaks during or after completion of treatment. Resolution of choline peak is correlated with tumor regression after radiation therapy, however its predictive value and clinical utility remain uncertain (55). This technique has also been used to identify increased choline signal along with T2-weighted imaging and ADC to guide adaptive radiotherapy, but outcomes thus far are unknown (56).

Future directions/conclusions

DCE and DWI are imaging techniques that have been useful to assist with diagnosis of cervical cancer as well as for its predictive/prognostic value. Future studies will be aimed at providing validation of their capabilities and identifying the specific clinical settings in which they provide the most additional utility. Currently, this appears to be their role in post-treatment follow up and management. Prospective data with larger sample sizes are needed and will be provided in the IQ-Embrace Cohort. MRI spectroscopy and other functional MRI sequences should be further investigated along with DCE and DWI to assess clinical uses and help improve care for cervical cancer patients.

Author contributions

HM contributed to the study design, data acquisition and writing the first draft of the manuscript. AP contributed to study design and data acquisition. ZH contributed to study design and data acquisition. SB contributed to conception of the study, study design and data acquisition. All authors contributed to manuscript revision, read and approved the submitted version.

Conflict of interest

The authors declare that the research was conducted in the absence of any commercial or financial relationships that could be construed as a potential conflict of interest.

Publisher's note

References

1. Bray F, Ferlay J, Soerjomataram I, Siegel RL, Torre LA, Jemal A, et al. Global cancer statistics 2018: GLOBOCAN estimates of incidence and mortality worldwide for 36 cancers in 185 countries. *CA: A Cancer J Clin* (2018) 68:394–424. doi: 10.3322/caac.21492

2. Surveillance, Epidemiology, and End Results (SEER) Program (www.seer.cancer.gov) SEER*Stat Database: Populations - Total U.S. (1969-2020) <Katrina/Rita Adjustment> - Linked To County Attributes - Total U.S., 1969-2020 Counties, National Cancer Institute, DCCPS, Surveillance Research Program, released January 2022.

3. Hu K, Wang W, Liu X, Meng Q, Zhang F. Comparison of treatment outcomes between squamous cell carcinoma and adenocarcinoma of cervix after definitive radiotherapy or concurrent chemoradiotherapy. *Radiat Oncol* (2018) 13:249. doi: 10.1186/s13014-018-1197-5

4. Salib MY, Russell JHB, Stewart VR, Sudderuddin SA, Barwick TD, Bockall AG, et al. FIGO staging classificiation for cervical cancer: Added benefits of imaging. *Radiographics* (2018) 40(6):1807–22. doi: 10.1148/rg.2020200013

5. Devine C, Viswanathan C, Faria S, Marcal L, Sagebiel TL. Imaging and staging of cervical cancer. *Semin Ultrasound CT MR* (2019) 40:280–6. doi: 10.1053/j.sult.2019.03.001

6. Kundu S, Chopra S, Verma A, Mahantshetty U, Engineer R, Shrivastava SK. Functional magnetic resonance imaging in cervical cancer: current evidence and future directions. *J Cancer Res Ther* (2012) 8(1):11–8. doi: 10.4103/0973-1482.95167

7. Rahman AU. *Nuclear magnetic resonance: basic principles*. New York: Springer (1986).

8. Plewes DB, Kucharczyk W. Physics of MRI: a primer. *J Magn Reson Imaging* (2012) 35(5):1038–54. doi: 10.1002/jmri.23642

9. Lyng H, Malinen E. Hypoxia in cervical cancer: from biology to imaging. *Clin Transl Imaging* (2017) 5(4):373–88. doi: 10.1007/s40336-017-0238-7

10. Higaki T, Nakamura Y, Tatsugami F, Kaichi Y, Akagi M, Akiyama Y, et al. Introduction to the technical aspects of computed diffusion-weighted imaging for radiologists. *Radiographics* (2018) 38(4):1131–44. doi: 10.1148/rg.2018170115

11. Dappa E, Elger T, Hasenburg A, Düber C, Battista MJ, Hötker AM. The value of advanced MRI techniques in the assessment of cervical cancer: a review. *Insights Imaging* (2017) 8:471–81. doi: 10.1007/s13244-017-0567-0

12. Shen G, Zhou H, Jia Z, Deng H. Diagnostic performance of diffusion-weighted MRI for detection of pelvic metastatic lymph nodes in patients with cervical cancer: a systematic review and meta-analysis. *Br J Radiol* (2015) 88 (1052):20150063. doi: 10.1259/bjr.20150063

13. Perdrizet J, D'Souza D, Skliarenko J, Ang M, Barbera L, Gutierrez E, et al. A cost-utility analysis of magnetic resonance (MR) guided brachytherapy versus two-dimensional and computed tomography (CT) guided brachytherapy for locally advanced cervical cancer. *Int J Radiat Oncol Biol Phys* (2020) 107(3):512–21. doi: 10.1016/j.ijrobp.2020.03.004

14. Sala E, Rockall AG, Freeman SJ, Mitchell DG, Reinhold C. The added role of MR imaging in treatment stratification of patients with gynecologic malignancies: what the radiologist needs to know. *Radiology* (2013) 266:717 740. doi: 10.1148/radiol.12120315

15. Patel-Lippmann K, Robbins J, Barroilhet L, Anderson B, Sadowski E, Boyum J. MR imaging of cervical cancer. *Magn Reson Imaging Clin N Am* (2017) 25(3):635–49. doi: 10.1016/j.mric.2017.03.007

16. Balleyguier C, Sala E, Da Cunha T, Bergman A, Brkljacic B, Danza F, et al. Staging of uterine cervical cancer with MRI: guidelines of the European society of

urogenital radiology. *Eur Radiol* (2011) 21:1102–10. doi: 10.1007/s00330-010-1998-x

17. Bhatla N, Aoki D, Sharma DN, Sankaranarayanan R. Cancer of the cervix uteri. FIGO cancer report 2018. *Int J Gynaecol Obstet* (2018) 143(Suppl. 2):22–36. doi: 10.1002/ijgo.12611

18. Pötter R, Tanderup K, Schmid MP, Jürgenliemk-Schulz I, Haie-Meder C, Fokdal LU, et al. MRI-Guided adaptive brachytherapy in locally advanced cervical cancer (EMBRACE-i): a multicentre prospective cohort study. *Lancet Oncol* (2021) 22(4):538–47. doi: 10.1016/S1470-2045(20)30753-1

19. Otero-García MM, Mesa-Álvarez A, Nikolic O, Blanco-Lobato P, Basta-Nikolic M, de Llano-Ortega RM, et al. Role of MRI in staging and follow-up of endometrial and cervical cancer: pitfalls and mimickers. *Insights Imaging* (2019) 10:19. doi: 10.1186/s13244-019-0696-8

20. Berman RM, Brown AM, Chang SD, Sankineni S, Kadakia M, Wood BJ, et al. DCE MRI of prostate cancer. *Abdom Radiol (NY)* (2016) 41(5):844–53. doi: 10.1007/s00261-015-0589-3

21. Xiao J, Rahbar H, Hippe DS, Rendi MH, Parker EU, Shekar N, et al. Dynamic contrast-enhanced breast MRI features correlate with invasive breast cancer angiogenesis. *NPJ Breast Cancer* (2021) 7:42. doi: 10.1038/s41523-021-00247-3

22. Brix G, Schreiber W, Hoffmann U, Guckel F, Hawighorst H, Knopp MV. Methodological approaches to quantitative evaluation of microcirculation in tissues with dynamic magnetic resonance tomography. *Radiologe* (1997) 37:470–80. doi: 10.1007/s001170050241

23. Neeman M, Dafni H. Structural, functional, and molecular MR imaging of the microvasculature. *Annu Rev BioMed Eng* (2003) 5:29–56. doi: 10.1146/annurev.bioeng.5.040202.121606

24. Rockwell S, Dobrucki IT, Kim EY, Marrison ST, Vu VT. Hypoxia and radiation therapy: past history, ongoing research, and future promise. *Curr Mol Med* (2009) 9(4):442–58. doi: 10.2174/156652409788167087

25. Mayr NA, Wang JZ, Zhang D, Grecula JC, Lo SS, Jaroura D, et al. Longitudinal changes in tumor perfusion pattern during the radiation therapy course and its clinical impact in cervical cancer. *Int J Radiat Oncol Biol Phys* (2010) 77(2):502–8. doi: 10.1016/j.ijrobp.2009.04.084

26. MayrNA, Huang Z, Wang JZ, Lo SS, Fan JM, et al. Characterizing tumor heterogeneity with functional imaging and quantifying high-risk tumor volume for early prediction of treatment outcome: Cervical cancer as a model. *Int J Radiat OncologyBiologyPhys* (2012) 83(3):972–9. doi: 10.1016/j.ijrobp.2011.08.011. ISSN 0360-3016.

27. Huang Z, Yuh KA, Lo SS, Grecula JC, Sammet S, Sammet CL, et al. Validation of optimal DCE-MRI perfusion threshold to classify at-risk tumor imaging voxels in heterogeneous cervical cancer for outcome prediction. *Magn Reson Imaging* (2014) 32(10):1198–205. doi: 10.1016/j.mri.2014.08.039

28. Mayr NA, Yuh WT, Jajoura D, Wang JZ, Lo SS, Montebello JF, et al. Ultra-early predictive assay for treatment failure using functional magnetic resonance imaging and clinical prognostic parameters in cervical cancer. *Cancer* (2010) 116 (4):903–12. doi: 10.1002/cncr.24822

29. Boss EA, Massuger LF, Pop LA, Verhoef LC, Huisman HJ, Boonstra H, et al. Post-radiotherapy contrast enhancement changes in fast dynamic MRI of cervical carcinoma. *J Magn Reson Imaging* (2001) 13(4):600–6. doi: 10.1002/jmri.1084

30. Kim JH, Kim CK, Park BK, Park SY, Huh SJ, Kim B, et al. Dynamic contrast-enhanced 3-T MR imaging in cervical cancer before and after concurrent chemoradiotherapy. *Eur Radiol* (2012) 22:2533–9. doi: 10.1007/s00330-012-2504-4

31. Baliyan V, Das CJ, Sharma R, Gupta AK. Diffusion weighted imaging: Technique and applications. *World J Radiol* (2016) 8(9):785–98. doi: 10.4329/wjr.v8.i9.785

32. Wilhelm T, Stieltjes B, Schlemmer HP. Whole-body-MR-diffusion weighted imaging in oncology. *Rofo* (2013) 184(10):950–8. doi: 10.1055/s-0033-1335428

33. Kilickesmez O, Bayramoglu S, Inci E, Cimilli T, Kayhan A. Quantitative diffusion-weighted magnetic resonance imaging of normal and diseased uterine zones. *Acta Radiol* (2009) 50(3):340–7. doi: 10.1080/02841850902735858

34. Chen YB, Hu CM, Chen GL, Hu D, Liao J. Staging of uterine cervical carcinoma: whole-body diffusion-weighted magnetic resonance imaging. *Abdom Imaging* (2011) 36(5):619–26. doi: 10.1007/s00261-010-9642-4

35. Naganawa S, Sato C, Kumada H, Ishigaki T, Miura S, Takizawa O. Apparent diffusion coefficient in cervical cancer of the uterus: comparison with the normal uterine cervix. *Eur Radiol* (2005) 15(1):71–8. doi: 10.1007/s00330-004-2529-4

36. Charles-Edwards EM, Messiou C, Morgan VA, De Silva SS, McWhinney NA , Katesmark M, et al. Diffusion-weighted imaging in cervical cancer with an endovaginal technique: potential value for improving tumor detection in stage ia and Ib1 disease. *RadiologyCharacterizing tumor heterogeneity with functional i* (2008) 249(2):541–50. doi: 10.1148/radiol.2491072165

37. Xue HD, Li S, Sun F, Sun HY, Jin ZY, Yang JX, et al. Clinical application of body diffusion weighted MR imaging in the diagnosis and preoperative n staging of cervical cancer. *Chin Med Sci J* (2008) 23(3):133–7. doi: 10.1016/s1001-9294(09)60027-4

38. Liu Y, Bai R, Sun H, Liu H, Wang D. Diffusion-weighted magnetic resonance imaging of uterine cervical cancer. *J Comput Assist Tomogr* (2009) 33 (6):858–62. doi: 10.1097/RCT.0b013e31819e93af

39. McVeigh PZ, Syed AM, Milosevic M, Fyles A, Haider MA. Diffusion-weighted MRI in cervical cancer. *Eur Radiol* (2008) 18(5):1058–64. doi: 10.1007/s00330-007-0843-3

40. Peters WA3rd, Liu PY, Barrett RJ2nd, Stock RJ, Monk BJ, Berek JS, et al. Concurrent chemotherapy and pelvic radiation therapy compared with pelvic radiation therapy alone as adjuvant therapy after radical surgery in high-risk early-stage cancer of the cervix. *J Clin Oncol* (2000) 18(8):1606–13. doi: 10.1200/JCO.2000.18.8.1606

41. Gebhardt BJ, Rangaswamy B, Thomas J, Kelley J, Sukumvanich P, Edwards R, et al. Magnetic resonance imaging response in patients treated with definitive radiation therapy for medically inoperable endometrial cancer-does it predict treatment response? *Brachytherapy*. (2019) 18(4):437–44. doi: 10.1016/j.brachy.2019.03.005

42. Ho JC, Allen PK, Bhosale PR, Rauch GM, Fuller CD, Mohamed AS, et al. Diffusion-weighted magnetic resonance imaging as a predictor of outcome in cervical cancer after chemoradiation. *Int J Radiat Oncol Biol Phys* (2017) 97 (3):546–53. doi: 10.1016/j.ijrobp.2016.11.015

43. Gladwish A, Milosevic M, Fyles A, Xie J, Halankar J, Metser U, et al. Association of apparent diffusion coefficient with disease recurrence in patients with locally advanced cervical cancer treated with radical chemotherapy and radiation therapy. *Radiology* (2016) 279(1):158–66. doi: 10.1148/radiol.2015150400

44. Kalash R, Glaser SM, Rangaswamy B, Horne ZD, Kim H, Houser C, et al. Use of functional magnetic resonance imaging in cervical cancer patients with incomplete response on positron emission Tomography/Computed tomography after image-based high-Dose-Rate brachytherapy. *Int J Radiat Oncol Biol Phys* (2018) 102(4):1008–13. doi: 10.1016/j.ijrobp.2018.01.092

45. Kumar R, Narayanan GS, Vishwanthan B, Narayanan S, Mandal S. A prospective comparative dosimetric study between diffusion weighted MRI (DWI) & T2-weighted MRI (T2W) for target delineation and planning in cervical cancer brachytherapy. *Rep Pract Oncol Radiother* (2020) 25(6):1011–6. doi: 10.1016/j.rpor.2020.08.008

46. Essig M, Shiroishi MS, Nguyen TB, Saake M, Provenzale JM, Enterline D, et al. Perfusion MRI: the five most frequently asked technical questions. *AJR Am J Roentgenol* (2013) 200(1):24–34. doi: 10.2214/AJR.12.9543

47. Perucho JAU, Wang M, Vardhanabhuti V, Tse KY, Chan KKL, Lee EYP. Association between IVIM parameters and treatment response in locally advanced squamous cell cervical cancer treated by chemoradiotherapy. *Eur Radiol* (2021) 31 (10):7845–54. doi: 10.1007/s00330-021-07817-w

48. Zhu H, Barker PB. MR spectroscopy and spectroscopic imaging of the brain. *Methods Mol Biol* (2011) 711:203–26. doi: 10.1007/978-1-61737-992-5_9

49. Shah N, Sattar A, Benanti M, Hollander S, Cheuck L. Magnetic resonance spectroscopy as an imaging tool for cancer: a review of the literature. *J Am Osteopath Assoc* (2006) 106(1):23–7. doi: 10.7556/jaoa.2006.106.1.23 19-56

50. Ratai EM, Gilberto González R. Clinical magnetic resonance spectroscopy of the central nervous system. *Handb Clin Neurol* (2016) 135:93–116. doi: 10.1016/B978-0-444-53485-9.00005-2

51. Delikatny EJ, Russell P, Hunter JC, Hancock R, Atkinson KH, van Haaften-Day C, et al. Proton MR and human cervical neoplasia: ex vivo spectroscopy allows distinction of invasive carcinoma of the cervix from carcinoma *in situ* and other preinvasive lesions. *Radiology* (1993) 188(3):791–6. doi: 10.1148/radiology.188.3.8351349

52. Mahon MM, Williams AD, Soutter WP, Cox IJ, McIndoe GA, Coutts GA, et al. 1H magnetic resonance spectroscopy of invasive cervical cancer: an *in vivo* study with ex vivo corroboration. *NMR Biomed* (2004) 17(1):1–9. doi: 10.1002/nbm.830

53. Lee JH, Cho KS, Kim YM, Kim ST, Mun CW, Na JH, et al. Localized *in vivo* 1H nuclear MR spectroscopy for evaluation of human uterine cervical carcinoma. *AJR Am J Roentgenol* (1998) 170(5):1279–82. doi: 10.2214/ajr.170.5.9574601

54. Booth SJ, Pickles MD, Turnbull LW. *In vivo* magnetic resonance spectroscopy of gynaecological tumours at 3.0 Tesla. *BJOG* (2009) 116(2):300–3. doi: 10.1111/j.1471-0528.2008.02007.x

55. Allen JR, Prost RW, Griffith OW, Erickson SJ, Erickson BA. *In vivo* proton (H1) magnetic resonance spectroscopy for cervical carcinoma. *Am J Clin Oncol* (2001) 24:522–9. doi: 10.1097/00000421-200110000-00021

56. Zhu J, Ma D, Lu D. MRI-Guided RT of cervical carcinoma: Applications with diffusion MRI & MR spectroscopy. *Int J Radiat Oncol Biol Phys* (2009) 75:3: S371. doi: 10.1016/J.IJROBP.2009.07.851

frontiers | Frontiers in Oncology

TYPE Original Research
PUBLISHED 02 December 2022
DOI 10.3389/fonc.2022.1046087

OPEN ACCESS

EDITED BY
Alessio G. Morganti,
University of Bologna, Italy

REVIEWED BY
Francesco Ricchetti,
Sacro Cuore Don Calabria Hospital (IRCCS), Italy
Beant S. Gill,
Independent Researcher, Waldorf, MD, United States

*CORRESPONDENCE
Anel Cordoba
a-cordoba@o-lambret.fr

SPECIALTY SECTION
This article was submitted to Gynecological Oncology, a section of the journal Frontiers in Oncology

RECEIVED 16 September 2022
ACCEPTED 02 November 2022
PUBLISHED 02 December 2022

CITATION
Cordoba A, Durand B, Escande A, Taieb S, Amor MBH, Le Deley MC, Michel A, Le Tinier F, Hudry D, Martinez C, Leblanc E, Becourt S, Abdedaim C, Bresson L, Lartigau E, Mirabel X and Narducci F (2022) Prognostic impact of tumor size reduction assessed by magnetic resonance imaging after radiochemotherapy in patients with locally advanced cervical cancer. *Front. Oncol.* 12:1046087. doi: 10.3389/fonc.2022.1046087

Prognostic impact of tumor size reduction assessed by magnetic resonance imaging after radiochemotherapy in patients with locally advanced cervical cancer

Abel Cordoba[1]*, Benedicte Durand[1], Alexandre Escande[1], Sophie Taieb[2], Mariem Ben Haj Amor[2], Marie Cecile Le Deley[3], Andree Michel[3], Florence Le Tinier[1], Delphine Hudry[4], Carlos Martinez[4], Eric Leblanc[4], Stephanie Becourt[5], Cyril Abdedaim[5], Lucie Bresson[6], Eric Lartigau[1], Xavier Mirabel[1] and Fabrice Narducci[4]

[1]Academic Radiotherapy Department, Oscar Lambret Center, Lille, France, [2]Radiology Department, Oscar Lambret Center, Lille, France, [3]Biostatistics Department, Oscar Lambret Center, Lille, France, [4]Medical Oncology Department, Oscar Lambret Center, Lille, France, [5]Surgical Oncology Department, Oscar Lambret Center, Lille, France, [6]Department of Surgical Oncology, Polyclinique Henin Beaumont, Henin, France

Objective: Pelvic magnetic resonance imaging (MRI) is a key exam used for the initial assessment of loco-regional involvement of cervical cancer. In patients with locally advanced cervical cancer, MRI is used to evaluate the early response to radiochemotherapy before image-guided brachytherapy, the prognostic impact of which we aimed to study.

Methods: Patients with locally advanced cervical cancer treated using concomitant radiochemotherapy followed by closure treatment between January 2010 and December 2015 were included in this study. Clinical, anatomopathological, radiological, therapeutic, and follow-up data were evaluated.

Results: After applying the inclusion and exclusion criteria to the initially chosen 310 patients, 232 were included for evaluation (median follow-up period, 5.3 years). The median age was 50 years (range, 25–83 years), and the median tumor size was 47.5 mm (range, 0–105 mm). Based on the International Federation of Gynaecology and Obstetrics classification system, 9 patients were in stage IB2; 20, IB3; 2, IIA; 63, IIB; 4, IIIA; 7, IIIB; and 127, IIIC1 or higher. The re-evaluation MRI was performed at the median dose of 55.5 Gy, and median reduction in tumor size was 55.2% (range, –20–100%). There was a difference between the disease-free and overall survival rates of the patients with a tumor response greater or lesser than 50%. The risk of recurrence or

death reduced by 39% in patients with a tumor size reduction >50%. The overall 5-year survival rate of patients with a response greater and lesser than 50% were 77.7% and 61.5%, respectively. The 5-year disease-free survival rate for these two groups of patients were 68.8% and 51.5%, respectively.

Conclusion: Our study confirms the prognostic impact of tumor size reduction using MRI data obtained after radiochemotherapy in patients with locally advanced cervical cancer.

KEYWORDS

locally advanced cervical cancer, tumor shrinkage, MRI, radiochemotherapy, brachytherapy

Introduction

Cervical cancer is the fourth cause of cancer incidence and mortality worldwide (1). Survival rates largely depend on the cancer stage at diagnosis (2). Since 2018, the International Federation of Gynecology and Obstetrics (FIGO) staging system has been revised thanks to the evolution of imaging modalities and use of additional procedures in everyday practice (3, 4). Locally advanced cervical cancer comprises bulky tumors in FIGO stages IB3–IVA. The standard treatment for such cervical cancers is pelvic (and paraaortic, if indicated) radiochemotherapy that includes radiation therapy and concurrent cisplatin chemotherapy, followed by image-guided brachytherapy (5). Many factors, such as age, FIGO stage, tumor width, uterine corpus involvement, lymph nodes, and concurrent chemotherapy, are known to negatively impact survival outcomes (6–8). While therapeutic strategies, such as neoadjuvant and adjuvant chemotherapies, may prevent systemic recurrence (9, 10), local or loco-regional recurrences may be prevented with radical surgery (11).

Magnetic resonance imaging (MRI) is important during several stages of cervical cancer treatment. Standard MRI protocols include T1- and T2-weighted imaging of the pelvis in different planes. After revision of the FIGO classification system, MRI data are being considered while assessing the tumor stage. This imaging method is superior to clinical examination alone to assess the extent of tumor infiltration (12) and is particularly useful in determining the requirement of adaptative radiotherapy for cervical cancer (13). The extent of tumor shrinkage is considered to adjust the volume and dose in adaptive radiotherapy and helps define the volume for image-guided brachytherapy. Furthermore, the changes observed on MRI, such as those in apparent diffusion coefficient and signal intensity, can help predict outcomes after chemoradiotherapy for cervical cancer (14–16).

Therefore, an easy, reproducible test, such as MRI, is best suited in daily clinical practice to obtain information that can help in early identification of patients at high risk of local and loco-regional recurrence so that adjuvant therapies may be administered. We performed this study to test our hypothesis that tumor response assessed by MRI after concomitant radiochemotherapy for locally advanced cervical cancer has a prognostic impact on recurrence.

Methods

Patients and treatment

In this single-center, observational study, we included consecutive patients with a histologically proven diagnosis of locally advanced cervical cancer (FIGO stages IB2– IVA) who were treated with radiochemotherapy at our institution from January 2010 to December 2015. The inclusion criteria were as follows: age ≥18 years, cervix carcinoma observed on biopsy, and availability of MRI data before and after radiochemotherapy on the institution's radiological picture archiving and communicating system at the time of the study. Patients who did not provide consent for the use of personal data according to the French national law regarding medical ethics in retrospective studies (Act no. 2012-300 of March 5, 2012) were excluded from the study. The treatment protocol that we implemented from 2010 to 2015 has been published previously (17, 18).

Data collection

We retrospectively evaluated the initial demographic and clinical data, tumor characteristics, therapeutic data (radiation therapy and chemotherapy protocol), closure treatments (image-guided brachytherapy with or without radical surgery), and follow-up data that we obtained from medical records.

Radiological data, including maximum tumor diameter at the time of diagnosis, before image-guided brachytherapy, and after concomitant radiochemotherapy, were collected by performing MRI. MRI 1.5 T with gadolinium were performed

at diagnosis and during the first week after completion of 45 Gy external beam radiotherapy prior to brachytherapy. Diffusion weighted imaging, and T1 and T2 weighted sequences with axial and sagittal planes acquired obliquely axed on the cervical canal were performed. Tumor size was defined as the largest tumor dimension measured on MRI T2 weighted sequences. All MRI examinations were evaluated by our radiologist specialized in female pelvic radiology.

Historically, in the gynecologic tumor committee of our center, MRI was performed the last week of radiochemotherapy in order to adapt the following treatment according to the response: Thus, for patients that tumor volume reduction was 50% or more, (estimated as maximum tumor diameter), treatment continued with uterovaginal brachytherapy and such patients were considered as good responders; on the other hand, those patients whose tumors had reduced in size by less than 50% were considered to be radioresistant and were offered surgical treatment 6-8 weeks after the end of radiochemotherapy.

Based in this argument, tumor size reduction rate of ≥50% was considered a satisfactory response and no tumor visualization was identified as a complete response.

Outcomes

The primary endpoint was disease-free survival that was defined as the time period between the first day of radiochemotherapy and any recurrence of the tumor (local, regional, loco-regional, or metastatic) or death due to any cause. Data were censored when there was no recurrence or death during the last time the patient data were evaluated. The secondary endpoint was overall survival defined as the time period between the first day of radiochemotherapy and death due to any cause. Data were censored when the patients were alive during the last time the patient data were evaluated. Times until local, loco-regional, and metastatic recurrence were calculated. Toxicities were assessed using the Common Terminology Criteria for Adverse Events, version 4.

Statistical analysis

Initial demographic and clinical data, treatment methods, survival and recurrence rates, and post-therapeutic complications were summarized using descriptive statistics. Missing data were specified. Initial categorical variables were expressed as numbers and percentages, while continuous variables were expressed as median (range) or mean (standard deviation). Disease-free and overall survival rates were assessed using the Kaplan–Meier method. The cumulative impact of local, regional or loco-regional, and metastatic recurrences was evaluated by the competing risks method described by Kalbfleisch and Prentice. To compare continuous and categorical variables, we used the Student's t-test or Mann–Whitney U test and Fisher's exact or chi-square test, respectively. The Fine and Gray model was used to compare the MRI data at the end of radiochemotherapy between responsive and non-responsive patients. The Cox regression analysis was used to test the association between various prognostic factors and disease-free survival. A p value <0.05 was considered statistically significant. All statistical analyses were performed using Stata Statistical Software, version 15 (StataCorp LP, College Station, TX, USA).

Results

The flowchart showing the selection criteria based on which 232 patients were included for evaluation is shown in Figure 1. The median follow-up period was 5.3 years.

Clinical and tumor characteristics

At diagnosis, the median age was 50 years (range, 27–83 years) with a performance status of 0 for 193 patients (82.5%) and ≥1 for 41 (17.5%). Active smoking was reported by 83 patients (35%), 81 (34.9%) never smoked, 20 (8.6%) stopped before diagnosis, and data were not reported for 48 (20.7%). The main clinical symptom was metrorrhagia that was reported by 180 patients (77.5%), 22 (9.4%) had other symptoms, and 30 (12.8%) displayed no symptoms.

The FIGO classification stage was IIIC1 or higher for 127 patients (54.7%), IB2 for 9 (3.8%), IB3 for 20 (8.6%), IIA for 2 (0.7%), IIB for 63 (26.9%), IIIA for 4 (1.7%), and IIIB for 7 (2.9%). Histological examination revealed tumor type as squamous carcinoma for 192 patients (82.8%), adenocarcinoma for 34 (14.5%), and other types for 6 (2.5%). The median tumor size at diagnosis was 47.5 mm (range, 0–105 mm) (Table 1).

Response and outcomes

All the patients received concomitant chemotherapy; 210 (90.5%) received cisplatin weekly; 21 (9.0%), carboplatin; and 1 (0.4%), cisplatin–5-fluorouracil. The median overall treatment time was 50 days (range, 37–225 days).

MRI was performed after radiochemotherapy (median radiation dose, 55.6 Gy). The median maximum tumor diameter before treatment was 47cm (0-105cm) and 21cm (0–53) after radiochemotherapy. The median tumor size reduction rate was 55.2% (−20–100%). Satisfactory response was observed in 139 patients (59.4%) and 29 (12.4%) demonstrated a complete response (Figure 2).

The risk of local recurrence after 1 and 5 years of follow-up since the beginning of treatment was 10% (95% confidence interval [CI]: 6.8%–14.7%) and 17% (95% CI: 12.5%–22.6%), respectively. In terms of recurrence-free survival, there were 78

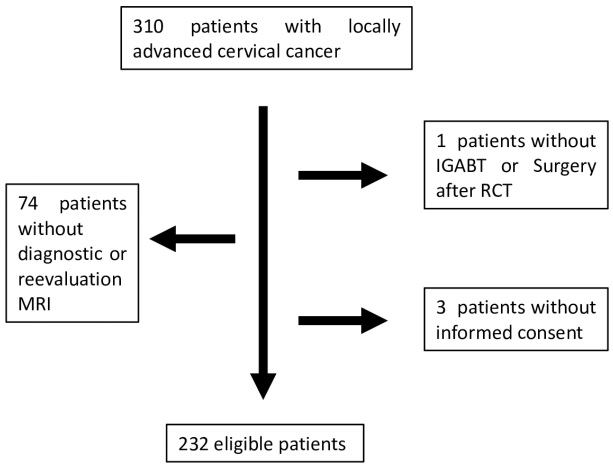

FIGURE 1
Flowchart showing patient selection.

events, namely, 67 recurrences followed by death, 11 recurrences without death, and 0 deaths without recurrences. The median time to recurrence-free survival was not achieved in this study after 11 years of follow-up since the start of treatment. The recurrence-free survival rates after 1, 3, and 5 years of follow-up since the start of treatment were 84.3% (95% CI: 78.9%–88.4%), 69.7% (95% CI: 63.2%–75.3%), and 66% (95%CI: 59.2%–72.0%), respectively. The overall survival rates after 1, 3, and 5 years of follow-up were 97.4% (95% CI: 94.3%–98.8%), 80.0% (95% CI: 73.9%–84.6%), and 70.7% (95% CI: 64.0%–76.5%), respectively.

Complete response was never obtained for 28 patients (12.1%) and 210 patients (89.7%) became disease free at one

TABLE 1 Histological characteristics at diagnosis.

Characteristics	N	%
FIGO stage		
IB1	1	0.00%
IB2	7	2.9%
IB3	21	8.9%
IIA	2	0.00%
IIB	63	26.9%
IIIA	4	1.7%
IIIB	7	2.9%
IIIC	59	25.2%
IVA	42	17.9%
IVB	20	8.5%
Clinical size of tumor at diagnosis (mm)		
median (min, max)	40	(0, 100)
Histological type		
Adenocarcinome	34	14.7%
Epidermoid	192	82.8%
Others	6	2.6%
Grade differentiation		
1	43	18.5%
2	54	23.3%
3	42	18.1%
Missing	93	40.1%

FIGO, Federation of Gynecology and Obstetrics.

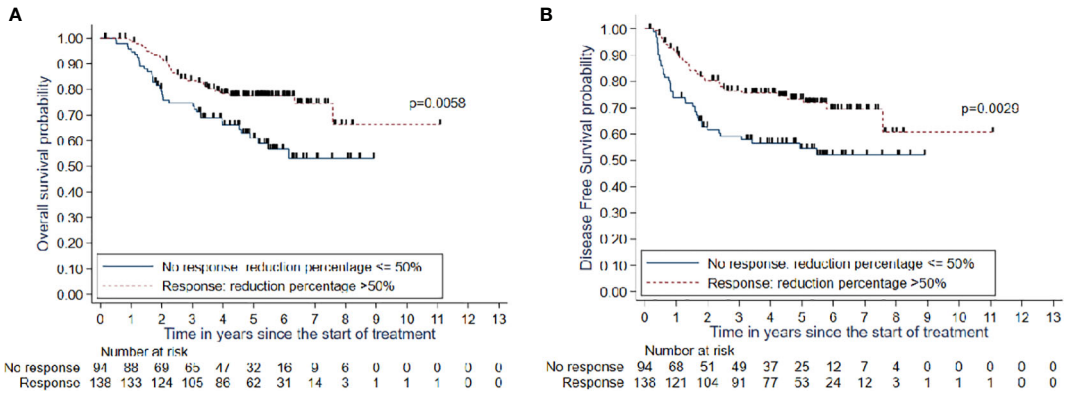

FIGURE 2
(A) OS and **(B)** DFS in patients with good response (>50%) or inadequate response (<=50%).

point. Recurrence was observed in 78 patients (33.3%) at a median time of 12.5 months (range, 3.2–69.5 months), i.e., 25 (32.1%) with local recurrences; 17 (21.8%), regional; 14 (17.9%), loco-regional; and 54 (69.2%), metastatic. While 67 patients (28.6%) died, 167 (71.4%) were alive at the end of the study.

There was a statistically significant difference in the 1- and 5-year overall survival rates between patients with a good tumor response and those with an inadequate tumor response (98.5% [95% CI: 94.2%–99.6%] and 77.5% [95% CI: 69.2%–83.8%] vs. 95.7% [95% CI: 88.8%–98.4%] and 61.0% [95% CI: 49.4%–70.7%]; p=0.005).

There was a statistically significant difference in the 1- and 5-year recurrence-free survival rates between patients with a good tumor response and those with a poor tumor response (91.1% [95% CI: 85%–94.9%) and 73.3% [95% CI: 64.6%–80. 2%] vs. (73.9% [95% CI: 63.7%– 81.7%) and 54.5% (95% CI: 43.2%–64.5%]; p=0.0029).

There was a significant rise in the 1- and 5-year risks of local recurrence in patients with an inadequate tumor response (18.5% [95% CI: 11.9%–28.0%] and 26.2% [95% CI: 18.1%–36. 9%]) than those of patients with a good tumor response (4.4% [95% CI: 2.0%–9.5%] and 10.7% (95% CI: 6.5%–17.6%]; p=0.007).

Prognostic factors

The characteristics that demonstrated a statistically significant association with disease-free survival in univariate analysis are shown in Table 2.

Histologically, there was a statistically significant difference between patients with squamous cell carcinoma and those with adenocarcinoma both in in response (p=0.038) and overall survival rates (p=0.02). The median overall survival rate was observed after 6 years of follow-up since the start of treatment in the adenocarcinoma group, whereas patients with squamous cell carcinoma did not achieve median survival even after 10 years of follow-up. The overall survival after 5 years of follow-up in patients with squamous cell carcinoma was 72.1% (95% CI: 64.5%–78.3%) compared with 60.9% (95% CI: 42.2%–75.1%) in patients with adenocarcinoma.

Multivariate analysis showed that the tumor response rate after chemoradiotherapy had a statistically significant association with disease-free survival after adjustment (p=0.008). Recurrence or death risk showed a statistically significant reduction by 46% in patients with a satisfactory response than the patients without a satisfactory response did (hazard ratio [HR]=0.54, 95% CI: 0.34–0.85).

The other prognostic factors associated with disease-free survival observed by multivariate analysis were performance status ≥1 (p<0.001), histologic type (p=0.005) and total time of treatment (p=0.003). Recurrence or death risk was three times higher in patients with a performance score ≥1 than in patients with a performance score of 0 (HR=3.49 [95% CI: 2.01–6.03], p<0.001). Furthermore, this risk was twice as high in patients with adenocarcinoma compared with that in patients with squamous cell carcinoma (HR=2.16 [95% CI: 1.25–3.72], p=0.005) (Figure 3). TTT superior to 50 days was associated in multivariate analysis to higher risk of relapse free survival (HR=2.26 [95% CI: 1.33–3.83], p=0.003)

Discussion

Summary of main results

In this study, we analyzed the MRI data of consecutive patients with locally advanced cervical cancer treated between 2010 and 2015. We found that the 1- and 5-years local control rates dropped significantly in patients with insufficient tumor response than those in patients with good. Furthermore, there was statistically significant reduction by 46% in recurrence or

10.3389/fonc.2022.1046087

TABLE 2 Prognostic value for disease-free survival using univariate and multivariate analyses.

Characteristics	N	Raw HR	95% CI	Raw p value	Adjusted HR	95% CI	Adjusted p value
Tumor response	**234**						
>50%	**139**	0.52	0.3– 0.81	0.004	0.54	0.34– 0.85	0.008*
<50%	**95**	1			1		
Age at diagnosis	**234**	1.08	0.98– 1.17	0.087	0.97	0.88– 1.07	0.549
OMS	**234**						
>1	41	2.94	1.83– 4.72	<0.001	3.49	2.01– 6.03	<0.001*
0	193	1			1		
FIGO stage	**234**			0.1274			0.067
IB1–IIA	31	0.52	0.24– 1.16		0.55	0.33– 0.93	
IIB–IIIB	75	0.69	0.42– 1.14		0.64	0.29– 1.43	
IIIC1 and higher	128	1			1		
Histological type	**228**			0.008			0.005*
Adenocarcinoma	34	2.04	1.20– 3.47		2.16	1.25– 3.72	
Squamous carcinoma	194	1			1		
Tobacco consumption	**186**			0.2355			
Yes	82	0.7	0.43– 1.14				
Ceased	20	0.59	0.25– 1.40				
No	84	1					
Clinical size of tumor at diagnosis	126	1.01	0.99– 1.03	0.292			

HR, hazard ratio; 95% CI, 95% confidence interval; OS: FIGO, Federation of Gynecology and Obstetrics.
*p <0.05 in multivariate analysis.

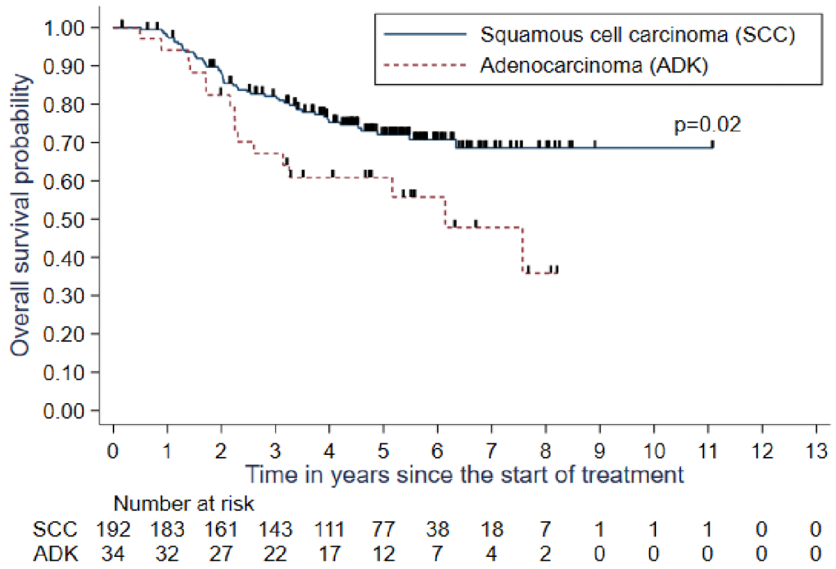

FIGURE 3
Overall survival (OS) depending histologic type.

death risk in the patients with satisfactory response compared with that in those without a satisfactory response.

Results in the context of published literature

MRI is the method of choice for local tumor staging at diagnosis and tumor response evaluation in cases of cervical cancer (19). Moreover, tumor size estimated by clinical palpation or using MRI measurements is an important prognostic factor in cervical cancer (20, 21). Recently, a European multi-institutional study has demonstrated that MRI-based image-guided brachytherapy is effective in providing local control and improving outcomes in patients with locally advanced cervical cancer (22). For selected elderly patients who cannot undergo uterovaginal brachytherapy, volumetric-modulated arc therapy with simultaneous integrated boost can be useful (23). Moreover, the dose to high-risk clinical target volume parameter and duration of treatment inferior to 50 days are correlated to local control (7).

Mazeron et al. found that a high-risk clinical target volume >30 cm^3 was an independent factor for local control with a relative local relapse risk ratio of 2.51 (p=0.048), and in such cases, a dose of 92 Gy was required to achieve a 90% probability of local control. However, a dose of 73.9 Gy was administered in cases of volumes <30 cm^3 (p =0.03) to achieve 90% local control (6). In a study by Potter et al., the 5-year local control rate was 92%; 5-year pelvic control rate, 87%; 5-year nodal control rate, 87%; 5-year overall survival rate, 74%; and 5-year disease-free survival rate, 68% (7). Dimopoulos et al. demonstrated a correlation between local control and dose to high-risk clinical target volume parameter depending on the residual tumor size after radiochemotherapy. The D90 for high-risk clinical target volume >87 Gy resulted in an LR incidence of 4% compared with 20% associated with D90 for high-risk clinical target volume <87 Gy (22).

Furthermore, MRI data have an important role in the revised cervical cancer FIGO classification system for local-regional tumor staging, evaluation of the response to treatment, and detection of tumor recurrence and possible complications (24) The recommendations of the Groupe Européen de Curiethérapie–European Society for Therapeutic Radiation and Oncology (GEC-ESTRO) group state that MRI is the main tool to identify the organs at risk and determine the target volume during uterovaginal image-guided brachytherapy in patients with locally advanced cervical cancer (25).

Similar to our findings, Schernberg et al. found that 247 patients with locally advanced cervical cancer treated with combined radiochemotherapy and image-guided brachytherapy demonstrated a reduction in gross tumor volume of at least 90%, which is correlated with reduced overall survival, progression-free survival, local control, and distant metastasis control (p<0.001). Reduction in gross tumor volume produces a survival impact that is greater than that by high-risk clinical target volume (26). EMBRACE group has also evaluated Local tumor regression evaluated by a T score, measured by MRI and clinical examination and they showed its local control predictive factor and also they demonstrated that it is useful to plan IGABT (27). This aspect is of utmost importance. Having the right information in terms of imaging with an MRI just before brachytherapy time will optimize the implant guided by a thorough clinical examination.

Angeles et al. evaluated the impact of tumor volume and regression after external beam radiotherapy measured by MRI on overall survival and relapse-free survival and found that tumor reduction rate ≥60% was significantly associated with a decreased risk of relapse and death (28). Nam et al. determined the impact of tumor regression measured by MRI at the beginning of radiotherapy or radiochemotherapy, mid-radiotherapy, and 1 month after completion of radiotherapy and found that patients with mid-radiotherapy regression ≥75% had 100% 5-year local control rates and better disease-free survival than those with mid-radiotherapy regression <75% (29). An important point to consider is whether tumor reduction should be assessed by regarding just the dimensions of the tumor or include volume measurements as well. In this study, we did not evaluate the tumor before treatment by diffusion-weighted MRI, which is known to be associated with local control and relapse-free survival of patients with locally advanced cervical cancer (14, 15, 30).

Concerning histologic type, adenocarcinomas have been historically described as radioresistant tumors compared with epidermoid carcinomas and are associated with poor clinical outcomes mostly due to incomplete tumor regression after radiochemotherapy (31). Our results showed an overall survival rate of 72.1% after 5 years of follow-up in patients with squamous cell carcinoma compared with 60.9% in patients with adenocarcinoma. However, a recent study based on the Surveillance, Epidemiology, and End Results database showed no difference in overall survival between patients with locally advanced cervical cancer having squamous carcinomas and adenocarcinomas (32).

Implications for practice and future research

A question arises regarding the action required in cases of non-responding patients and those with high-volume tumors observed while performing image-guided brachytherapy. The policy at our center before 2015 was to debate whether surgery was an option. In this study, among the 15 patients who underwent surgery after radiochemotherapy, tumors were not observed in 7 patients. Moreover, surgery is associated with a high risk of urinary disorders and bowel problems. Thus, the current policy at our institution is to treat all such patients, including those responding late to treatment, with radiochemotherapy and three-dimensional image-guided brachytherapy independent of the percentage of tumor regression observed on MRI.

Furthermore, concomitant/adjuvant strategies based on the addition of immunotherapy agents, such as atezolizumab (NCT03612791) or cisplatin agents (NCT04016142), are being evaluated in prospective studies. Overall, our study proves that MRI is a useful tool in the management of patients with locally advanced cervical cancer and the mandatory performance of MRI after radiochemotherapy before image-guided brachytherapy should be considered.

Strengths and weaknesses

The main strength of this study lies in the large, homogeneous study population and the long follow-up duration. Nevertheless, this study has a limitation, namely, the retrospective collection of data and emergence of late comorbidities. The current radiotherapy protocol has, therefore, been changed.

Conclusions

Our study highlights the importance of tumor shrinkage after radiochemotherapy measured by MRI in determining prognosis, which conforms to the findings of previous studies.

Data availability statement

The original contributions presented in the study are included in the article/supplementary material. Further inquiries can be directed to the corresponding author.

Author contributions

AC, BD, FT, EL, XM and AE contributed to conception and design of the study. BD and AC organized the database. MD and AM performed the statistical analysis. AC and BD wrote the first draft of the manuscript. AC, LB, EL, CM, DH and FN wrote sections of the manuscript. All authors contributed to manuscript revision, read, and approved the submitted version

Acknowledgments

We thank all the patients for giving us their consent.

Conflict of interest

The authors declare that the research was conducted in the absence of any commercial or financial relationships that could be construed as a potential conflict of interest.

Publisher's note

References

1. Bray F, Ferlay J, Soerjomataram I, Siegel RL, Torre LA, Jemal A. Global cancer statistics 2018: GLOBOCAN estimates of incidence and mortality worldwide for 36 cancers in 185 countries. *CA Cancer J Clin* (2018) 68(6):394–424. doi: 10.3322/caac.21492

2. Sant M, Chirlaque Lopez MD, Agresti R, Sánchez Pérez MJ, Holleczek B, Bielska-Lasota M, et al. Survival of women with cancers of breast and genital organs in Europe 1999-2007: Results of the EUROCARE-5 study. *Eur J Cancer Oxf Engl 1990* (2015) 51(15):2191–205. doi: 10.1016/j.ejca.2015.07.022

3. Bourgioti C, Chatoupis K, Moulopoulos LA. Current imaging strategies for the evaluation of uterine cervical cancer. *World J Radiol* (2016) 8(4):342–54. doi: 10.4329/wjr.v8.i4.342

4. Bhatla N, Aoki D, Sharma DN, Sankaranarayanan R. Cancer of the cervix uteri. *Int J Gynaecol Obstet Off Organ Int Fed Gynaecol Obstet* (2018) 143(Suppl 2):22–36. doi: 10.1002/ijgo.12611

5. Marth C, Landoni F, Mahner S, McCormack M, Gonzalez-Martin A, Colombo N, et al. Cervical cancer: ESMO clinical practice guidelines for diagnosis, treatment and follow-up. *Ann Oncol Off J Eur Soc Med Oncol* (2017) 28(suppl_4):iv72–83. doi: 10.1093/annonc/mdx220

6. Mazeron R, Castelnau-Marchand P, Dumas I, del Campo ER, Kom LK, Martinetti F, et al. Impact of treatment time and dose escalation on local control in locally advanced cervical cancer treated by chemoradiation and image-guided pulsed-dose rate adaptive brachytherapy. *Radiotherapy and Oncology* (2015) 114(2015):257–63.

7. Pötter R, Tanderup K, Schmid MP, Jürgenliemk-Schulz I, Haie-Meder C, Fokdal LU, et al. MRI-Guided adaptive brachytherapy in locally advanced cervical cancer (EMBRACE-i): a multicentre prospective cohort study. *Lancet Oncol* (2021) 22(4):538–47. doi: 10.1016/S1470-2045(20)30753-1

8. Sturdza AE, Pötter R, Kossmeier M, Kirchheiner K, Mahantshetty U, Haie-Meder C, et al. Nomogram predicting overall survival in patients with locally advanced cervical cancer treated with radiochemotherapy including image-guided brachytherapy: A retro-EMBRACE study. *Int J Radiat Oncol* (2021) 111(1):168–77. doi: 10.1016/j.ijrobp.2021.04.022

9. da Costa SCS, Bonadio RC, Gabrielli FCG, Aranha AS, Dias Genta MLN, Miranda VC, et al. Neoadjuvant chemotherapy with cisplatin and gemcitabine followed by chemoradiation versus chemoradiation for locally advanced cervical cancer: A randomized phase II trial. *J Clin Oncol Off J Am Soc Clin Oncol* (2019) 37(33):3124–31. doi: 10.1200/JCO.19.00674

10. Tangjitgamol S, Katanyoo K, Laopaiboon M, Lumbiganon P, Manusirivithaya S, Supawattanabodee B. Adjuvant chemotherapy after concurrent chemoradiation for locally advanced cervical cancer. *Cochrane Database Syst Rev* (2014) 12:CD010401. doi: 10.1002/14651858.CD010401.pub2

11. Platt SL, Patel A, Humphrey PJ, Al-Booz H, Bailey J. Completion surgery after chemoradiotherapy for cervical cancer - is there a role? UK cancer centre experience of hysterectomy post chemo-radiotherapy treatment for cervical cancer. *J Obstet Gynaecol J Inst Obstet Gynaecol* (2019) 39(1):68–73. doi: 10.1080/01443615.2018.1463205

12. Dhoot NM, Kumar V, Shinagare A, Kataki AC, Barmon D, Bhuyan U. Evaluation of carcinoma cervix using magnetic resonance imaging: Correlation with clinical FIGO staging and impact on management. *J Med Imaging Radiat Oncol* (2012) 56(1):58–65. doi: 10.1111/j.1754-9485.2011.02333.x

13. Tan LT, Tanderup K, Kirisits C, de Leeuw A, Nout R, Duke S, et al. Image-guided adaptive radiotherapy in cervical cancer. *Semin Radiat Oncol* (2019) 29 (3):284–98. doi: 10.1016/j.semradonc.2019.02.010

14. Ho JC, Fang P, Cardenas CE, Mohamed ASR, Fuller CD, Allen PK, et al. Volumetric assessment of apparent diffusion coefficient predicts outcome following chemoradiation for cervical cancer. *Radiother Oncol J Eur Soc Ther Radiol Oncol* (2019) 135:58–64. doi: 10.1016/j.radonc.2019.02.012

15. Liu B, Ma WL, Zhang GW, Sun Z, Zhong JM, Wei MQ, et al. Changes in magnetic resonance T2-weighted imaging signal intensity correlate with concurrent chemoradiotherapy response in cervical cancer. *J Contemp Brachytherapy* (2019) 11(1):41–7. doi: 10.5114/jcb.2019.83285

16. Minkoff D, Gill BS, Kang J, Beriwal S. Cervical cancer outcome prediction to high-dose rate brachytherapy using quantitative magnetic resonance imaging analysis of tumor response to external beam radiotherapy. *Radiother Oncol* 115 (1):78–83. doi: 10.1016/j.radonc.2015.03.007

17. Le Tinier F, Reynaert N, Castelain B, Lartigau E, Lacornerie T, Nickers P. Is adaptive intensity-modulated radiotherapy for uterine cervix carcinoma necessary? *Cancer Radiothérapie J Société Fr Radiothérapie Oncol* (2012) 16(8):681–7. doi: 10.1016/j.canrad.2012.06.007

18. Mouttet-Audouard R, Lacornerie T, Tresch E, Kramar A, Le Tinier F, Reynaert N, et al. What is the normal tissues morbidity following helical intensity modulated radiation treatment for cervical cancer? *Radiother Oncol* (2015) 115 (3):386–91. doi: 10.1016/j.radonc.2015.02.010

19. Merz J, Bossart M, Bamberg F, Eisenblaetter M. Revised FIGO staging for cervical cancer - a new role for MRI. *ROFO Fortschr Geb Rontgenstr Nuklearmed* (2020) 192(10):937–44. doi: 10.1055/a-1198-5729

20. Kovalic JJ, Perez CA, Grigsby PW, Lockett MA. The effect of volume of disease in patients with carcinoma of the uterine cervix. *Int J Radiat Oncol Biol Phys* (1991) 21(4):905–10. doi: 10.1016/0360-3016(91)90728-M

21. Lowrey GC, Mendenhall WM, Million RR. Stage IB or IIA-b carcinoma of the intact uterine cervix treated with irradiation: A multivariate analysis. *Int J Radiat Oncol Biol Phys* (1992) 24(2):205–10. doi: 10.1016/0360-3016(92)90672-5

22. Dimopoulos JCA, Pötter R, Lang S, Fidarova E, Georg P, Dörr W, et al. Dose–effect relationship for local control of cervical cancer by magnetic resonance image-guided brachytherapy. *Radiother Oncol* (2009) 93(2):311–5. doi: 10.1016/j.radonc.2009.07.001

23. Mazzola R, Ricchetti F, Fiorentino A, Levra NG, Fersino S, Di Paola G, et al. Weekly cisplatin and volumetric-modulated arc therapy with simultaneous integrated boost for radical treatment of advanced cervical cancer in elderly patients: Feasibility and clinical preliminary results. *Technol Cancer Res Treat* (2017) 16(3):310–5. doi: 10.1177/1533034616655055

24. Bhatla N, Berek JS, Cuello Fredes M, Denny LA, Grenman S, Karunaratne K, et al. Revised FIGO staging for carcinoma of the cervix uteri. *Int J Gynecol Obstet* (2019) 145(1):129–35. doi: 10.1002/ijgo.12749

25. Dimopoulos JCA, Petrow P, Tanderup K, Petric P, Berger D, Kirisits C, et al. Recommendations from gynaecological (GYN) GEC-ESTRO working group (IV): Basic principles and parameters for MR imaging within the frame of image based adaptive cervix cancer brachytherapy. *Radiother Oncol* (2012) 103(1):113–22. doi: 10.1016/S0167-8140(12)71974-6

26. Schernberg A, Bockel S, Annede P, Fumagalli I, Escande A, Mignot F, et al. Tumor shrinkage during chemoradiation in locally advanced cervical cancer patients: Prognostic significance, and impact for image-guided adaptive brachytherapy. *Int J Radiat Oncol* (2018) 102(2):362–72. doi: 10.1016/j.ijrobp.2018.06.014

27. Lindegaard JC, Petric P, Schmid MP, Nesvacil N, Haie-Meder C, Fokdal LU, et al. Prognostic implications of uterine cervical cancer regression during chemoradiation evaluated by the T-score in the multicenter EMBRACE I study. *Int J Radiat Oncol* (2022) 113(2):379–89. doi: 10.1016/j.ijrobp.2022.02.005

28. Angeles MA, Baissas P, Leblanc E, Lusque A, Ferron G, Ducassou A, et al. Magnetic resonance imaging after external beam radiotherapy and concurrent chemotherapy for locally advanced cervical cancer helps to identify patients at risk of recurrence. *Int J Gynecol Cancer* (2019) 29(3):480–6. doi: 10.1136/ijgc-2018-000168

29. Nam H, Park W, Huh S, Bae D, Kim B, Lee J, et al. The prognostic significance of tumor volume regression during radiotherapy and concurrent chemoradiotherapy for cervical cancer using MRI. *Gynecol Oncol* (2007) 107 (2):320–5. doi: 10.1016/j.ygyno.2007.06.022

30. Harry VN, Persad S, Bassaw B, Parkin D. Diffusion-weighted MRI to detect early response to chemoradiation in cervical cancer: A systematic review and meta-analysis. *Gynecol Oncol Rep* (2021) 38:100883. doi: 10.1016/j.gore.2021.100883

31. Huang YT, Wang CC, Tsai CS, Lai CH, Chang TC, Chou HH, et al. Long-term outcome and prognostic factors for Adenocarcinoma/Adenosquamous carcinoma of cervix after definitive radiotherapy. *Int J Radiat Oncol* (2011) 80 (2):429–36. doi: 10.1016/j.ijrobp.2010.02.009

32. Tian T, Gong X, Gao X, Li Y, Ju W, Ai Y. Comparison of survival outcomes of locally advanced cervical cancer by histopathological types in the surveillance, epidemiology, and end results (SEER) database: A propensity score matching study. *Infect Agent Cancer* (2020) 15:33. doi: 10.1186/s13027-020-00299-3

frontiers | Frontiers in Oncology

TYPE Original Research
PUBLISHED 08 December 2022
DOI 10.3389/fonc.2022.996516

OPEN ACCESS

EDITED BY
Alessio G. Morganti,
University of Bologna, Italy

REVIEWED BY
Komsun Suwannarurk,
Thammasat University, Thailand
Milly Buwenge,
University of Bologna, Italy

*CORRESPONDENCE
Byung Kwan Park
rapark@skku.edu
Jeong-Won Lee
garden.lee@samsung.com

SPECIALTY SECTION
This article was submitted to Gynecological Oncology, a section of the journal Frontiers in Oncology

RECEIVED 17 July 2022
ACCEPTED 21 November 2022
PUBLISHED 08 December 2022

CITATION
Jeon J, Park BK, Lee J-W, Choi CH, Lee Y-Y, Kim T-J and Kim B-G (2022) Invisible cervical cancers on MRI: Can the type of histology (SCC versus non-SCC) influence surgical planning? *Front. Oncol.* 12:996516. doi: 10.3389/fonc.2022.996516

Invisible cervical cancers on MRI: Can the type of histology (SCC versus non-SCC) influence surgical planning?

Jungeun Jeon[1], Byung Kwan Park[2*], Jeong-Won Lee[1*], Chel Hun Choi[1], Yoo-Young Lee[1], Tae-Joong Kim[1] and Byoungi-Gie Kim[1]

[1]Department of Obstetrics and Gynecology, Samsung Medical Center, Sungkyunkwan University School of Medicine, Seoul, Republic of Korea, [2]Department of Radiology, Samsung Medical Center, Sungkyunkwan University School of Medicine, Seoul, Republic of Korea

Background: Invisible cervical cancers on MRI can indicate less invasive surgery. Cervical cancers consist of squamous cell carcinoma (SCC) and non-SCC, each with different long-term outcomes. It is still unclear if surgical planning should be changed according to the histologic type of cervical cancer when it is not visible on MRI.

Purpose: The purpose of the study was to determine if surgical planning for cervical cancer that is not visible on MRI is influenced by the histologic type.

Materials and methods: Between January 2007 and December 2016, 155 women had Federation of Gynecology and Obstetrics (FIGO) stage 1B1 cervical cancer that was not visible on preoperative MRI. They underwent radical hysterectomies and pelvic lymph node dissections. Among them, 88 and 67 were histologically diagnosed with SCC and non-SCC, respectively. The size of the residual tumor, depth of stromal invasion, parametrial invasion, vaginal invasion, lymphovascular invasion, and lymph node metastasis were compared between these patients using the t-test, Mann–Whitney U test, Chi-squared test, or Fisher's exact test. The recurrence-free and overall 10-year survival rates were compared between the groups by Kaplan–Meier analysis.

Results: The mean sizes of residual tumors were 8.4 $\pm$ 10.4 mm in the SCC group and 12.5 $\pm$ 11.9 mm in the non-SCC group ($p = 0.024$). The mean depth of stromal invasion in the SCC group was 12.4 $\pm$ 21.2% (0%–100%), whereas that in the non-SCC group was 22.4 $\pm$ 24.4 (0%–93%) ($p = 0.016$). However, there was no difference in parametrial or vaginal invasion, lymphovascular invasion, or lymph node metastasis ($p = 0.504$–1.000). The recurrence-free and overall 10-year survival rates were 98.9% (87/88) and 95.5% (64/67) ($p = 0.246$), and 96.6% (85/88) and 95.5% (64/67) ($p = 0.872$), respectively.

Conclusions: The non-SCC group tends to have larger residual tumors and a greater depth of stromal invasion than the SCC group, even though neither is visible on MRI. Therefore, meticulous care is necessary for performing parametrectomy in patients with non-SCC cervical cancer.

KEYWORDS

uterus, cervical cancer, histology, MRI, FIGO staging

Introduction

Previously reported studies showed that postoperative outcomes were good when Federation of Gynecology and Obstetrics (FIGO) stage IB1 cervical cancer was not visible on preoperative magnetic resonance imaging (MRI) (1–3). This cancer has a much lower tumor burden than those visible on MRI. Accordingly, the former has a better prognosis than the latter. However, previous studies did not investigate whether postoperative outcomes differed according to histologic type. Patients with squamous cell carcinoma (SCC) frequently have better long-term outcomes than those without SCC.

Moreover, the tumor conspicuity of non-SCC is not as good as that of SCC, so it cannot be easily determined if non-SCC cervical cancer is visible on MRI (4–6). Minimizing parametrectomy is useful for avoiding postoperative complications (7–14). However, false-positive results for invisible tumors may lead to underestimating the extent of surgical resection needed. As a result, unnecessary additional treatments may follow a minimally invasive hysterectomy.

Thus, we hypothesized that the sizes of postoperative residual tumors differ according to the histologic types of FIGO stage IB1 cervical cancer, even though these are not visible on preoperative MRI. Rare studies have compared the postoperative outcomes of SCC and non-SCC patients. The purpose of this study was to determine if surgical planning for cervical cancer not visible on MRI is influenced by histologic type (SCC versus non-SCC).

Materials and methods

This study (File No.: 2022-04-030-001) was approved by the Institutional Review Board at Samsung Medical Center and the requirement for informed consent was waived due to the retrospective design.

Patients

Between January 2007 and December 2016, a total of 747 patients with FIGO IB1 cervical cancer underwent MRI prior to radical hysterectomy. Among them, 52 patients were excluded due to the poor image quality of the MRI examinations. Among the remaining 695 patients, 540 and 155 had visible cancer and invisible cancer, respectively, on preoperative MRI. Finally, 155 patients were included in the study population when they underwent 1.5 T or 3.0 T MRI. Of them, 88 patients were histologically confirmed to have squamous cell carcinoma (SCC) (SCC group). The remaining 67 patients were histologically confirmed to have other cervical cancers (non-SCC group). The medical records of the patients in the SCC group (48.5 ± 12.1 years; 20–81 years) and the non-SCC group (44.4 ± 8.5 years; 29–64 years) were reviewed. Colposcopic biopsy and conization were performed in 80.0% (124/155) and 60.0% (93/155), respectively.

Bimanual pelvic and rectovaginal examinations were done to determine the disease extent. Laboratory tests, chest radiography, cystoscopy, and sigmoidoscopy were routinely performed for clinical FIGO staging (15). The time interval between MRI and hysterectomy ranged from 1 to 47 days (median, 16 days) in the SCC group and from 0 to 39 days (median, 15 days) in the non-SCC group.

The MR images were preoperatively interpreted by one of two radiologists who had approximately five or more years of experience in gynecologic imaging. They were additionally reviewed by one radiologist who had approximately 19 years of experience in gynecologic imaging.

Radical hysterectomy, vaginectomy, and lymph node (LN) dissection were performed on all patients. Additional surgical procedures depend on the clinical stage and the surgeon's decision. When pelvic LNs were suspicious for metastasis at frozen sectioning, the para-aortic LNs were dissected.

Two pathologists examined the surgical specimens. They recorded the size of the residual tumor, histologic type, depth of stromal invasion, lymphovascular space (LVS) invasion, parametrial invasion, vaginal invasion, resection tumor margin, and LN metastasis.

After primary treatment, all patients received adequate follow-up procedures. During this period, patients underwent physical examinations, Pap smears, and tumor marker analysis every three months for the first two years and every six months for the next

three years. Imaging studies, such as abdominopelvic computed tomography (CT) or pelvic MRI, were conducted every 6 – 12 months for the first two years and then annually for the next three years.

MR imaging

Pelvic scans were conducted with a 1.5 (n = 27) MRI scanner (Signa, GE Medical System, Milwaukee, USA) or 3 T (n = 128) MRI scanner (Intera Achiva 3T; Philips Medical System, Best, The Netherlands). The upper abdomen was scanned by MRI or CT. The 1.5 T MRI sequences of the pelvis included T2-weighted images (T2WI), T1-weighted images, and dynamic contrast-enhanced (DCE) images. Diffusion-weighted imaging (DWI) was added to the 3 T MRI examination. However, DWI could not be scanned at the 1.5 T MRI because the MR software did not have the capability. T2WI were obtained in the axial, sagittal, and coronal planes. The other sequences were obtained in the axial plane. The upper abdomen was scanned from the lower lung to the aortic bifurcation. The same MR parameters as those used by Park et al. were used (1).

Data analysis

Invisible cancer was defined when the cervical tumor was invisible on T2W and DCE 1.5T MR images and when it was invisible on T2WI, DWI, and DCE 3T MR images (Figures 1, 2). When post-biopsy inflammation was differentiated from cervical cancer on T2W because both were hypertense, DWI or DCE images were reviewed; the former had no diffusion restriction or showed iso- or higher enhancement compared to neighboring cervical tissue, unlike the latter.

Patient age, biopsy type, histologic type, and SCC antigens or other tumor markers were compared between the SCC and non-SCC groups. The size of the residual tumor, depth of stromal invasion, LVS invasion, parametrial invasion, vaginal invasion, and LN metastasis were also compared between the groups.

Recurrent tumors were assessed on follow-up CT or MR images. Recurrence-free and overall 10-year survival rates were calculated and compared between the SCC and non-SCC groups.

Statistical analysis

Patient age, the size of the residual tumor, and the depth of stromal invasion were compared by the Mann–Whitney test because these data did not show a Gaussian distribution. SCC antigens were compared between two groups using the t-test.

The proportions of biopsy type, cancer histology, LVS invasion, parametrial invasion, vaginal invasion, LN metastasis, and recurrence rate were compared using the chi-square or Fisher's exact test.

Odds ratios (ORs) and 95% confidence intervals were calculated using the Woolf approximation. When the value was zero, 0.5 was added to each to make the calculation possible.

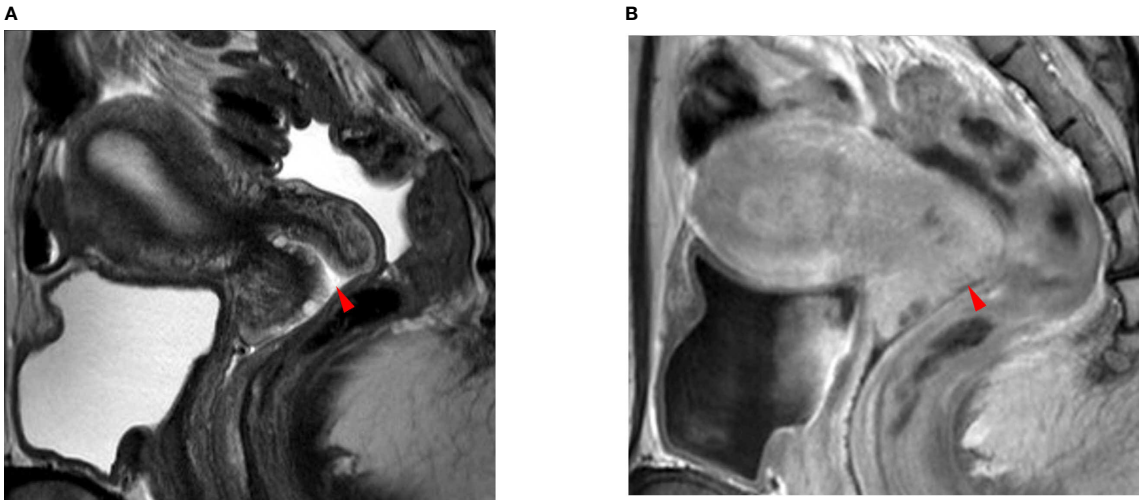

FIGURE 1
A 35-year-old woman with squamous cell carcinoma. **(A)** The T2-weighted sagittal MR image shows no focal lesion in the cervix. The red arrowhead indicates the external OS of the uterine cervix. **(B)** The delayed contrast-enhanced sagittal MR image shows no residual cancer in the cervix. The red arrowhead indicates the external OS of the uterine cervix. The pathologic report confirmed no residual cancer in the resected uterus. There was also no invasion of the lymphovascular space, vagina, parametrium, or lymph node metastasis.

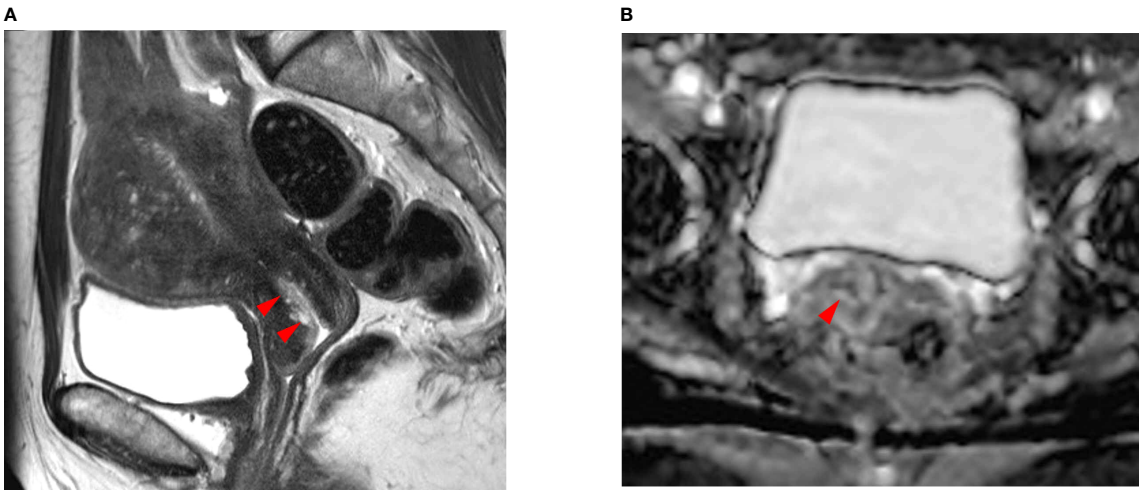

FIGURE 2
A 48-year-old woman with endocervical adenocarcinoma. **(A)** The T2-weighted sagittal MR image shows no tumor in the uterine cervix. The red arrows indicate a poorly demarcated cystic mass, which was preoperatively interpreted as normal endocervical glands. **(B)** The apparent diffusion coefficient (ADC) axial image shows no focal lesion with low ADC values in the cervical canal (red arrowhead). However, the pathologic report confirmed that there was a residual tumor in the endocervical canal. The tumor size was measured as 2.0 × 1.5 cm and the depth of stromal invasion was 0.4 cm in a 1.3-cm cervical wall. It was well-correlated with the endocervical lesion in **(A)**. Tumor invasion to the lymphovascular space, vagina, and parametrium and lymph node metastasis were all negative.

Recurrence-free and overall 10-year survival rates were compared using Kaplan–Meier survival curves.

Commercially available SPSS 24.0 software for Windows (SPSS Inc., Chicago, IL, USA) was used for the statistical analyses. A p-value of <0.05 was considered statistically significant.

Results

The median age of the patients in the SCC group was higher than that in the non-SCC group (p = 0.023) (Table 1). In the SCC group, 65.9% (58/88) underwent conization and 80.7% (71/88) had colposcopic biopsies, whereas in the non-SCC group, 52.2% (35/67) underwent conization and 79.1% (53/67) had colposcopic biopsies (p = 0.085 and p =0.808, respectively). The histologic diagnoses in the non-SCC group included adenocarcinoma in 89.6% (60/67) and adenosquamous carcinoma in 10.4% (7/67). There was no difference in tumor markers (p = 0.296–0.906) between the groups.

The median size of the residual tumor was 8.4 ± 10.4 mm (0–36 mm) in the SCC group and 12.5 ± 11.9 mm (0–55 mm) in the non-SCC group (p = 0.024) (Table 2) (Figures 1, 2). The median depth of stromal invasion was 12.4 ± 21.2% (0–100%) in the SCC group and 22.4 ± 24.4% (0–93%) in the non-SCC group (p = 0.016) (Figures 1, 2). Residual tumors in these groups were detected in 52.1% (50/88) and 68.7% (46/67) (p = 0.133), respectively. SCC group (n = 88) underwent conization in 58 (65.9%) who had residual cancer in 27 (46.6%). Non-SCC group (n = 67) underwent conization in 35 (52.2%) who had residual cancer in 16 (45.7%). There was no difference between SCC and non-SCC groups regarding the incidence of residual cancer following conization (p = 1.000).

Parametrial invasion in the SCC and non-SCC groups was detected at 0% (0/88) and 0% (0/67), respectively. LVS invasion was 9.1% (8/88) in the SCC group and 7.5% (5/67) in the non-SCC group, respectively (p = 0.701). LN metastasis was detected in 2.3% (2/88) and 0% (0/67) of the SCC and non-SCC groups, respectively (p = 0.504). Vaginal invasion was detected in 1.1% (1/88) and 0% (0/67) of the SCC and non-SCC groups, respectively (p = 1.000).

The tumor recurrence rate was 1.1% (1/88) in the SCC group and 4.5% (3/67) in the non-SCC group on follow-up CT or MR images (p = 0.316). The recurrence-free 10-year survival rate in the SCC and non-SCC groups was 98.9% (87/88) and 94.5% (64/67) (p = 0.246), respectively. The overall 10-year survival rate was 96.6% (85/88) and 95.5% (64/67) in the SCC and non-SCC groups, respectively (p = 0.872).

Recurrent tumors had the highest OR, at 4.078 in the SCC group versus the non-SCC group. The other ORs ranged from 0 to 1.665 for residual tumor, LN metastasis, LVS invasion, and vaginal invasion.

TABLE 1 Demographics in patients with IB1 SCC and non-SCC cervical cancers.

	FIGO stage IB1 cervical cancers		P values
	SCC (n=88)	Non-SCC (n=67)	
Age (years)	48.5± 12.1 (20–81)	44.4 ± 8.5 (29–64)	0.023
Conization	58 (65.9%)	35 (52.2%)	0.085
Colposcopic biopsy	71 (80.7%)	53 (79.1%)	0.808
SCC antigen (ng/ml)	1.3 ± 4.9 (0–46)	1.5 ± 2.8 (0–15)	0.869
CA-125	8.1 ± 5.7 (2–20)	13.3 ± 17.0 (0–107)	0.296
CA-19-9	5.9 ± 3.8 (2–10)	7.6 ± 6.1 (0–23)	0.906

SCC, squamous cell carcinoma.
Mann-Whitney test was used to compare age, CA-125.
T-test was used to compare SCC antigen.
Chi-square test was used to compare types of biopsy or histological types of cervical cancers.
Age and SCC antigen were shown as median ± standard deviation (range).

TABLE 2 Pathologic comparison of SCC and non-SCC groups.

	FIGO stage IB1 cervical cancers		P values
	SCC (n=88)	Non-SCC (n=67)	
Size of residual tumor (mm)	8.4 ± 10.4 (0–36)	12.5 ± 11.9 (0–55)	0.024
Depth of stromal invasion (%)	12.4 ± 21.2 (0–100)	22.4 ± 24.4 (0–93)	0.016
No residual tumor	38 (43.2%)	21 (31.3%)	0.133
Lymphovascular invasion	8 (9.2%)	5 (7.5%)	0.701
Parametrial invasion	0 (0.0%)	0 (0.0%)	–
Vaginal invasion	1 (1.1%)	0 (0.0%)	1.000
Lymph node metastasis	2 (2.3%)	0 (0.0%)	0.504

T-test was used to compare size of tumor and depth of stromal invasion.
Chi-square test was used to compare no residual tumor and lymphovascular invasion.
Fisher's exact test was used to compare vaginal invasion, and lymph node metastasis.
Size of tumor and SCC antigen were shown as median ± standard deviation (range).

Discussion

Our results showed that the residual tumor size in the SCC group was smaller than that in the non-SCC group, even though none of these tumors were visible on MRI. The depth of stromal invasion in the SCC group was also smaller than that in the non-SCC group.

Currently, MRI is more available for women with cervical cancer because it is more precise for measuring tumor size than a physical examination (16–18). These MR images can be scanned in the axial, sagittal, and coronal planes. Therefore, the greatest tumor diameter and tumor volume are measured more accurately by palpation. Gynecologists inspect the outer tumor surface alone, but not the inner margin, which is well-depicted on MRI. This imaging modality provides precise tumor staging, and thus, it is more sensitive to detecting parametrial invasion or endocervical cancer than visual assessment (16–18). MRI also has the potential to avoid intravenous urography, cystoscopy, and sigmoidoscopy if cervical cancer is in the early stages (19–22). Moreover, current FIGO staging requires metastatic work-up in iliac or paraaortic LNs, which are not palpable (22). T2WI is useful for detecting morphologic changes, such as increased size, round shape, and the obliterated fatty hilum of metastatic LNs (23, 24). DWI is sensitive to changes in the tissue cellularity of metastatic LNs (25, 26). These MRI findings are currently used to determine if there is LN metastasis.

Cervical cancer that is not visible on MRI strongly suggests a lower tumor volume compared to those that are visible on MRI (1–3). Therefore, tumor invasion of the parametrium or vagina is extremely rare in invisible cervical cancer. The likelihood of cervical stromal or lymphovascular space invasion is much lower in cervical cancer that is not visible on MRI. LN, or hematogenous metastasis, is also rare. As a result, the long-term survival of patients with invisible cancer is better than that of patients with cancer visible on MRI. Moreover, additional post-operative treatments, such as radiation therapy or chemotherapy, are rarely necessary for women with invisible cervical cancer. Tumor invisibility on MRI can be a strong indicator of minimally invasive surgery.

Huang et al. reported that DCEI improved the depiction of cervical cancer that was not visible on T2WI and DWI (27).

Quantitative analysis of DCEI parameters helps enhance the residual tumor after conization. Unfortunately, our study analyzed DCEI by visual assessment alone. Therefore, DCE-MRI quantitative parameters should be added to exclude the likelihood of residual cancer after conization. Hu et al. reported that radiomics had the potential to additionally detect cervical cancer that is not visible on conventional MRI (28). They demonstrated that analyzing radiomics improved diagnostic performance for detecting residual cancer after biopsy or conization. Xia et al. studied radiomics based on a nomogram to predict pelvic LN metastasis in women with early cervical cancer. They achieved high diagnostic accuracy for detecting preoperative pelvic LN metastasis (29).

Park et al. showed that many residual cancers were detected postoperatively even if the tumors were not visible on conventional MR images (1). They tried to identify useful MRI features to allow for minimally invasive surgery because radical hysterectomy with LN dissection results in serious postoperative morbidities. As such, invisible tumors on conventional MR images alone help gynecologists minimize parametrectomy procedures and reduce the extent of LN dissection.

We also agree with their point of view about the clinical significance of cancer-invisible MRI findings. In their research, almost half of the cases had a residual tumor, whose median size was 5 mm. Their 10-year recurrence-free survival rate was almost 100%. As a result, if small residual tumors are detected with new MRI techniques, the patients may undergo unnecessary radical surgery, which seems to be an excessive treatment. When cervical cancer is invisible on T2WI, DWI, and DCEI with visual assessment alone, these MRI findings can provide a clue for indicating minimally invasive surgery.

SCC cervical cancer tends to manifest as a solid tumor on MRI, and thus, the tumor size is easily measured (30). It is well correlated with the tumor size on the hysterectomy specimen. In contrast, the tumor margin of non-SCC cervical cancer is not easily demarcated on preoperative MRI because a cystic component is frequent (4–6). Therefore, if non-SCC is composed mainly of cysts, it is frequently difficult to differentiate from nabothian cysts. Besides, if a few cancer cells are just lining the surface of cysts, current MRI techniques make it difficult to determine if there is a residual tumor following a biopsy. For these reasons, the size of the residual tumor and the depth of stromal invasion in the non-SCC group could not be easily identified on preoperative MRI. These findings in the non-SCC group tend to be more frequent than in the SCC group, although neither are visible on MRI.

Radical hysterectomy is the standard treatment for FIGO stage IB1 cervical cancer and, subsequently, improves the long-term survival rate. This surgical technique consists of parametrectomy and LN dissection. Accordingly, patients have a higher risk of postoperative complications, such as voiding difficulty (7–9), anorectal dysfunction (10, 11), sexual dissatisfaction (10, 11), and lymphedema (12–14), if parametrectomy or LN dissection becomes aggressive. Therefore, greater attention is being paid to minimally invasive surgery to minimize these postoperative complications. The patients in our cases had a relatively younger median age (less than 50 years) and a higher overall survival rate. Because of the radical hysterectomy procedure, they have a high likelihood of postoperative morbidities for a long period. From this point of view, excessive surgical resection can be avoided in women who have cervical cancer that is not visible on MRI because local invasion or metastasis is histologically negative in almost all cases.

This study had several limitations. First, it was conducted retrospectively. Therefore, the likelihood of selection bias cannot be excluded. Second, the number of 1.5 T MRI examinations was relatively large. Unfortunately, our 1.5 T scanner could not provide DWI sequences because it was an old version. However, a 1.5 T scanner has a lower signal-to-noise ratio than a 3 T scanner. Third, the number of SCC cases was relatively small, and the proportion of SCC cases was relatively less than that of non-SCC. There was no difference in long-term survival rates, even though the recurrence rate of SCC was not the same as that of non-SCC.

Conclusion

The non-SCC group tends to have a larger size of residual tumor and a deeper depth of stromal invasion than the SCC group. Despite these histologic results, non-SCC cervical cancer is frequently invisible on preoperative MRI. Therefore, the extent of parametrectomy for non-SCC cervical cancer should be different from that for SCC cervical cancer, even though these tumors are not visible on preoperative MRI.

Data availability statement

The raw data supporting the conclusions of this article will be made available by the authors, without undue reservation.

Ethics statement

The studies involving human participants were reviewed and approved by Institutional Review Board of Samsung Medical Center. Written informed consent for participation was not required for this study in accordance with the national legislation and the institutional requirements.

Author contributions

Conceptualization, JJ, BP, and J-WL. Methodology, JJ, BP, and J-WL. Software, BP. Validation, BP and J-WL. Formal analysis, JJ and BP. Investigation, JJ and BP. Resources, BP. Data curation, JJ and BP. Writing-original draft preparation, JJ and BP. Writing-review and editing, all authors. Visualization, BP. Supervision, BP

and J-WL. Project administration, BP. All authors contributed to the article and approved the submitted version.

Conflict of interest

The authors declare that the research was conducted in the absence of any commercial or financial relationships that could be construed as a potential conflict of interest.

Publisher's note

References

1. Park JY, Lee JW, Park BK, Lee YY, Choi CH, Kim TJ, et al. Postoperative outcomes of MR-invisible stage IB1 cervical cancer. *Am J Obstet Gynecol* (2014) 211(2):168.e1–7. doi: 10.1016/j.ajog.2014.02.032

2. Park BK, Kim TJ. Useful MRI findings for minimally invasive surgery for early cervical cancer. *Cancers (Basel)* (2021) 13(16). doi: 10.3390/cancers13164078

3. Jeong SY, Park BK, Choi CH, Lee YY, Kim TJ, Lee JW, et al. Utility of 3T MRI in women with IB1 cervical cancer in determining the necessity of less invasive surgery. *Cancers (Basel)* (2022) 14(1). doi: 10.3390/cancers14010224

4. Kido A, Mikami Y, Koyama T, Kataoka M, Shitano F, Konishi I, et al. Magnetic resonance appearance of gastric-type adenocarcinoma of the uterine cervix in comparison with that of usual-type endocervical adenocarcinoma: a pitfall of newly described unusual subtype of endocervical adenocarcinoma. *Int J Gynecol Cancer* (2014) 24(8):1474–9. doi: 10.1097/igc.0000000000000229

5. Ando H, Miyamoto T, Kashima H, Takatsu A, Ishii K, Fujinaga Y, et al. Usefulness of a management protocol for patients with cervical multicystic lesions: A retrospective analysis of 94 cases and the significance of GNAS mutation. *J Obstet Gynaecol Res* (2016) 42(11):1588–98. doi: 10.1111/jog.13083

6. Saida T, Sakata A, Tanaka YO, Ochi H, Ishiguro T, Sakai M, et al. Clinical and MRI characteristics of uterine cervical adenocarcinoma: Its variants and mimics. *kjr* (2019) 20(3):364–77. doi: 10.3348/kjr.2018.0458

7. Panici PB, Angioli R, Palaia I, Muzii L, Zullo MA, Manci N, et al. Tailoring the parametrectomy in stages IA2–IB1 cervical carcinoma: is it feasible and safe? *Gynecol Oncol* (2005) 96(3):792–8. doi: 10.1016/j.ygyno.2004.11.018

8. Artman LE, Hoskins WJ, Bibro MC, Heller PB, Weiser EB, Barnhill DR, et al. Radical hysterectomy and pelvic lymphadenectomy for stage IB carcinoma of the cervix: 21 years experience. *Gynecol Oncol* (1987) 28(1):8–13. doi: 10.1016/S0090-8258(87)80002-1

9. Landoni F, Maneo A, Cormio G, Perego P, Milani R, Caruso O, et al. Class II versus class III radical hysterectomy in stage IB–IIA cervical cancer: A prospective randomized study. *Gynecol Oncol* (2001) 80(1):3–12. doi: 10.1006/gyno.2000.6010

10. Rob L, Halaska M, Robova H. Nerve-sparing and individually tailored surgery for cervical cancer. *Lancet Oncol* (2010) 11(3):292–301. doi: 10.1016/S1470-2045(09)70191-3

11. Bonneau C, Cortez A, Lis R, Mirshahi M, Fauconnier A, Ballester M, et al. Lymphatic and nerve distribution throughout the parametrium. *Gynecol Oncol* (2013) 131(3):708–13. doi: 10.1016/j.ygyno.2013.10.006

12. Rebegea LF, Stoleriu G, Manolache N, Serban C, Craescu M, Lupu MN, et al. Associated risk factors of lower limb lymphedema after treatment of cervical and endometrial cancer. *Exp Ther Med* (2020) 20(6):181. doi: 10.3892/etm.2020.9311

13. Togami S, Kawamura T, Fukuda M, Yanazume S, Kamio M, Kobayashi H. Risk factors for lymphatic complications following lymphadenectomy in patients with cervical cancer. *Japanese J Clin Oncol* (2018) 48(12):1036–40. doi: 10.1093/jjco/hyy151

14. Togami S, Kubo R, Kawamura T, Yanazume S, Kamio M, Kobayashi H. Comparison of lymphatic complications between sentinel node navigation surgery and pelvic lymphadenectomy in patients with cervical cancer. *Japanese J Clin Oncol* (2020) 50(5):543–7. doi: 10.1093/jjco/hyaa001

15. Pecorelli S. Revised FIGO staging for carcinoma of the vulva, cervix, and endometrium. *Int J Gynaecol Obstet* (2009) 105(2):103–4. doi: 10.1016/j.ijgo.2009.02.012

16. Steed H, Capstick V, Schepansky A, Honore L, Hiltz M, Faught W. Early cervical cancer and parametrial involvement: Is it significant? *Gynecol Oncol* (2006) 103(1):53–7. doi: 10.1016/j.ygyno.2006.01.027

17. Yamazaki H, Todo Y, Okamoto K, Yamashiro K, Kato H. Pretreatment risk factors for parametrial involvement in FIGO stage IB1 cervical cancer. *J Gynecol Oncol* (2015) 26(4):255–61. doi: 10.3802/jgo.2015.26.4.255

18. Kamimori T, Sakamoto K, Fujiwara K, Umayahara K, Sugiyama Y, Utsugi K, et al. Parametrial involvement in FIGO stage IB1 cervical carcinoma: Diagnostic impact of tumor diameter in preoperative magnetic resonance imaging. *Int J Gynecol Cancer* (2011) 21(2):349. doi: 10.1097/IGC.0b013e3182072eea

19. Rockall AG, Ghosh S, Alexander-Sefre F, Babar S, Younis MT, Naz S, et al. Can MRI rule out bladder and rectal invasion in cervical cancer to help select patients for limited EUA? *Gynecol Oncol* (2006) 101(2):244–9. doi: 10.1016/j.ygyno.2005.10.012

20. Pecorelli S, Zigliani L, Odicino F. Revised FIGO staging for carcinoma of the cervix. *Int J Gynaecol Obstet* (2009) 105(2):107–8. doi: 10.1016/j.ijgo.2009.02.009

21. Jeong BK, Huh SJ, Choi DH, Park W, Oh D, Kim T, et al. Indications for endoscopy according to the revised FIGO staging for cervical cancer after MRI and CT scanning. *J Gynecol Oncol* (2012) 23(2):80–5. doi: 10.3802/jgo.2012.23.2.80

22. Merz J, Bossart M, Bamberg F, Eisenblaetter M. Revised FIGO staging for cervical cancer - a new role for MRI. *Rofo* (2020) 192(10):937–44. doi: 10.1055/a-1198-5729

23. Kim SH, Kim SC, Choi BI, Han MC. Uterine cervical carcinoma: evaluation of pelvic lymph node metastasis with MR imaging. *Radiology* (1994) 190(3):807–11. doi: 10.1148/radiology.190.3.8115631

24. Bipat S, Glas AS, van der Velden J, Zwinderman AH, Bossuyt PM, Stoker J. Computed tomography and magnetic resonance imaging in staging of uterine cervical carcinoma: a systematic review. *Gynecol Oncol* (2003) 91(1):59–66. doi: 10.1016/s0090-8258(03)00409-8

25. Shen G, Zhou H, Jia Z, Deng H. Diagnostic performance of diffusion-weighted MRI for detection of pelvic metastatic lymph nodes in patients with cervical cancer: a systematic review and meta-analysis. *Br J Radiol* (2015) 88 (1052):20150063. doi: 10.1259/bjr.20150063

26. He XQ, Wei LN. Diagnostic value of lymph node metastasis by diffusion-weighted magnetic resonance imaging in cervical cancer. *J Cancer Res Ther* (2016) 12(1):77–83. doi: 10.4103/0973-1482.148726

27. Huang JW, Song JC, Chen T, Yang M, Ma ZL. Making the invisible visible: improving detectability of MRI-invisible residual cervical cancer after conisation by DCE-MRI. *Clin Radiol* (2019) 74(2):166.e15–.e21. doi: 10.1016/j.crad.2018.10.013

28. Hu Q, Shi J, Zhang A, Duan S, Song J, Chen T. Added value of radiomics analysis in MRI invisible early-stage cervical cancers. *Br J Radiol* (2022) 95 (1133):20210986. doi: 10.1259/bjr.20210986

29. Xia X, Li D, Du W, Wang Y, Nie S, Tan Q, et al. Radiomics based on nomogram predict pelvic lymphnode metastasis in early-stage cervical cancer. *Diagnostics* (2022) 12(10):2446. doi: 10.3390/diagnostics12102446

30. Salib MY, Russell JHB, Stewart VR, Sudderuddin SA, Barwick TD, Rockall AG, et al. 2018 FIGO staging classification for cervical cancer: Added benefits of imaging. *Radiographics* (2020) 40(6):1807–22. doi: 10.1148/rg.2020200013

frontiers | Frontiers in Oncology

TYPE Original Research
PUBLISHED 04 January 2023
DOI 10.3389/fonc.2022.1074173

OPEN ACCESS

EDITED BY
Alessio G. Morganti,
University of Bologna, Italy

REVIEWED BY
Abidin Kılınçer,
Selçuk University, Turkey
Sung Bin Park,
Chung-Ang University Hospital,
Republic of Korea

*CORRESPONDENCE
Guonan Zhang
zhanggn@hotmail.com

†These authors have contributed equally to this work and share first authorship

SPECIALTY SECTION
This article was submitted to Gynecological Oncology, a section of the journal Frontiers in Oncology

RECEIVED 19 October 2022
ACCEPTED 05 December 2022
PUBLISHED 04 January 2023

CITATION
Zhu Y, Tang Y, Zhang G, Zhang J, Li Y and Jiang Z (2023) Quantitative analysis of superb microvascular imaging for monitoring tumor response to chemoradiotherapy in locally advanced cervical cancer. *Front. Oncol.* 12:1074173. doi: 10.3389/fonc.2022.1074173

Quantitative analysis of superb microvascular imaging for monitoring tumor response to chemoradiotherapy in locally advanced cervical cancer

Yi Zhu[1†], Yixin Tang[1,2†], Guonan Zhang[3*], Jie Zhang[3], Yanjie Li[1,4] and Zhuolin Jiang[1,4]

[1]Outpatient Department (Ultrasound), The Affiliated Cancer Hospital, University of Electronic Science and Technology of China, Sichuan Cancer Hospital and Institute, Chengdu, China, [2]Department of Ultrasound, Suining Central Hospital, Suining, China, [3]Department Gynecological Oncology, The Affiliated Cancer Hospital, University of Electronic Science and Technology of China, Sichuan Cancer Hospital and Institute, Chengdu, China, [4]Graduate School, Chengdu Medical College, Chengdu, China

Objectives: As an ultrasound (US) image processing method, superb microvascular imaging (SMI) extracts and visualizes flow signals from vessels through advanced clutter suppression technology. We investigated the feasibility of SMI in monitoring treatment response in patients with locally advanced cervical cancer (LACC) undergoing chemoradiotherapy (CRT).

Methods: Forty-nine patients underwent CRT and received SMI examination at 3 time points: before therapy (baseline), 3 weeks during, and 1 month after CRT. The maximum tumor diameter (Dmax), vascularity index (VI), and their percentage changes (ΔDmax and ΔVI) were calculated. ΔDmax was compared with MRI results as the reference standard.

Results: Based on the MRI findings, 44 were classified as complete response (CR) group and 5 as partial response (PR) group. The Dmax and ΔDmax showed decrease in CR and PR groups at 3 weeks during CRT ($P< 0.05$), but no significant difference between the two groups ($P > 0.05$). Compared to the baseline, significant decrease in VI and ΔVI were observed at during and after treatment in the two groups ($P< 0.05$). Moreover, there were significant differences in VI and ΔVI at 3 weeks during CRT between the CR and PR groups ($P< 0.05$). ΔVI at 3 weeks during CRT showed a better predictive performance for responder prognosis than VI (AUC = 0.964, AUC = 0.950, respectively, $P = 0.001$), with a cut-off value of 41.6% yielding 100% sensitivity and 86.4% specificity.

Conclusions: The SMI parameters (VI and ΔVI) have potential for monitoring treatment response in LACC.

KEYWORDS

cervical cancer, chemoradiotherapy, ultrasound, superb microvascular imaging, vascularity index

Introduction

Cervical cancer, as the fourth most common malignancy, has become a global female health problem. Cervical cancer is estimated to cause 570,000 new cases and 311,000 deaths each year (1, 2). At the same time, the onset age of cervical cancer tends to be younger, from the original 40-50 years old to 35 years old, with an annual increase of 2%-3%. Especially in low- to middle-income countries (LMIC), where lack the screen and adequate treatment, approximately 90% of cervical cancer remains fatal (3). Locally advanced cervical cancer (LACC) (FIGO stage IB2-IVA) has the characteristics of large lesions (> 4 cm), easy distant metastasis, difficult to operate directly, and poor therapeutic effect. Concomitant chemotherapy and radiotherapy (CRT) consisting of cisplatin-based chemotherapy, external-beam radiotherapy (EBRT), and intracavitary brachytherapy (ICR) is considered the recommended standard treatment for LACC (4). Due to tumor heterogeneity, all cancers are unlikely to respond uniformly to a specific treatment regimen, resulting in tumor uncontrolled, locoregional recurrence, or distant metastases after treatment in some patients (5, 6). Thus, surveillance of changes in tumor burden associated with treatment will be helpful for adjusting treatment strategy to obtain a better outcome in LACC (7, 8).

Current conventional imaging techniques, such as magnetic resonance imaging (MRI), computed tomography (CT) and ultrasound (US), rely on identifying morphological changes to evaluate and monitor the effect of CRT or disease progression in LACC. In fact, changes at the molecular or cellular level that occur early in responders significantly precede changes in tumor volume or size (9). Microstructural and microcirculatory changes during anticancer therapy can be detected by functional imaging (18F-fluorodeoxyglucose positron emission tomography, dynamic contrast-enhanced MRI, diffusion-weighted MRI, et al.) (10–12). However, these new approaches have limitations such as increased radiation burden, potential reaction effects of contrast agents, high cost, or technical complexity, making them difficult to be used for monitoring in the clinical routine (9, 13). Therefore, based on efficacy, safety and health economics considerations, US remains the preferred method for tracking curative effect, especially in LMIC.

Increased vascularization plays a crucial for sustain tumor growth, invasion, and metastasis (14, 15). It is demonstrated that angiogenesis is an important factor affecting cervical cancer development and survival prognosis (16, 17). Some studies have reported that the degree of tumor vascularity decline is directly proportional to therapeutic response. Thus, the assessment of tumor vascularity could become a novel means of monitoring tumor response to CRT in LACC.

Color or power Doppler US plays an indispensable role in assessing tumor angiogenesis and predicting the efficacy of CRT in cervical cancer (18, 19). Unfortunately, color or power Doppler US is limited by a wall filter to truly distinguish between low-flow components and clutter motion artifacts, which makes the fine vessels of cervical lesions potentially undetectable. In addition, color or power Doppler US has demonstrated poor reproducibility (20). With the advent of intravenous US contrast agent, contrast-enhanced US (CEUS) significantly enhances the signal of slow and low-volume blood flow to improve the visualization of with microvascular (20 - 39 μm in diameter) (21). Cervical cancer has markedly different quantitative and qualitative filling patterns with CEUS. CEUS might be a valuable tool in predicting remaining tumor on treatment (22). However, CEUS is an invasive imaging and carries the risk of drug allergy. Superb microvascular imaging (SMI) is a unique ultrasonic Doppler technology. SMI extracts and visualizes flow signals from vessels through advanced clutter suppression technology, enabling clear visualization of low velocity small-volume blood vessels without the use of contrast agents. Under the qualitative guidance of SMI images, tumor angiogenesis was quantitatively evaluated by vascular index (VI) (23). Although some preliminary experience reports have demonstrated the benefits of SMI in the diagnosis of multiple tumors (23, 24), the potential of this new US technique for efficacy assessment in cervical cancer has not yet been fully evaluated.

We aimed to assess whether using SMI to evaluate tumor vascularity could provide a means for monitoring tumor response to CRT in a series of patients with LACC.

Materials and methods

Patients and treatment

Forty-nine patients with LACC (FIGO stage IIB to IVA) were enrolled from September 2020 and May 2022. The exclusion criteria were follows: (a) history of prior treatment; (b) dropping out during therapy; (c) incomplete US or MRI data (Figure 1). All patients received histopathological diagnosis through multiple punch biopsies and had complete medical records.

All patients underwent external beam radiotherapy (EBRT) with 15-MV photon beams at a daily dose of 1.8-2.0 Gy (5/w), with a median total dose of 50.4 Gy. Subsequently, high-dose-rate intracavitary brachytherapy (ICR) was performed twice a week with an iridium-192 source as 6 Gy per insertion in five fractions (a total dose of 30 Gy). Four to six cycles of platinum-based chemotherapy were supplemented at 3-week intervals. The formulation of chemotherapy cycle is generally determined by various factors such as FIGO stage, malignancy, and physical condition.

Treatment response evaluation

MRI is the best currently acceptable and reproducible method to assess objective response in cervical cancer. Whole-pelvic cavity and perineum MR data from patients with LACC were obtained from 3.0T MR scanner (Siemens Magnetom

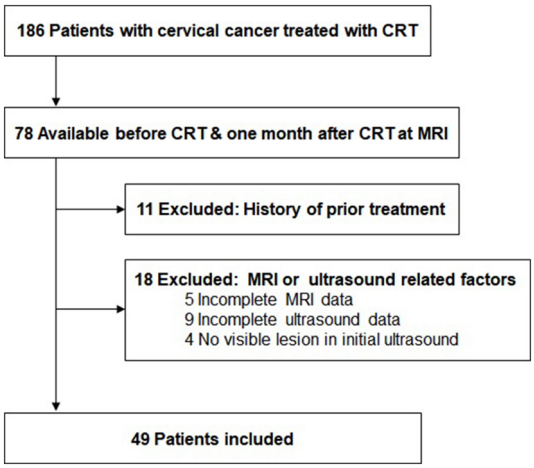

FIGURE 1
Flowchart of patient enrollment. CRT, chemoradiotherapy.

Skyra, Germany) within one week before treatment and 1 month after therapy completion. The longest tumor diameter was analyzed according to sagittal T2-weighted images and the percentage change in tumor size was calculated as follows:

$$Change \quad in \quad tumor \quad size\,\% = \frac{(pre-longest \quad diameter - post-longer \quad diameter)}{pre-longest \quad diameter} \times 100\,\%$$

The clinical efficacy was assessed by two radiologists with more than 5 years of experience in pelvic MRI diagnosis according to the Response Evaluation Criteria for Solid Tumors (RECIST) guidelines (version 1.1) (25). The radiologists reached consensus through discussion to resolve differences in image interpretation. All patients were divided into four groups: complete response (CR) as disappearance of all target lesions; partial response (PR) as a reduction in tumor diameter of more than 30%; progressive disease (PD) as an increase in tumor diameter of more than 20%; stable disease (SD) as neither sufficient regression to match PR nor sufficient enlargement to match PD (25).

Transvaginal ultrasound examination

All real-time transvaginal US (TVUS) examinations and the SMI analysis were performed by a group of three fellows with more than 8 years of experience in US of gynecological oncology, who were unaware of MRI findings and the treatment outcome. TVUS examination was performed at 3 time points: pre-therapy (baseline), 3 weeks during (mean, 18.4 days; range, 15 - 21 days), and 1 month after CRT (Figure 2), using an Aplio i800 US system (Canon Medical Systems, Tokyo, Japan) with a multifrequency linear 3 - 11 MHz endovaginal transducer. All SMI examination were acquired with the same settings throughout the study: 8.5 cm depth, 3.5 focal zone, 5.8 MHz Doppler frequency, 43 color gain, frame rate > 50 fps, to ensure quantitative US comparison. VI value was obtained by manually delineating the lesion (or cervix) boundary in a still SMI image with the maximum Doppler signals. One fellow performed real-time US including TVUS and measurement of the VI of SMI, followed by the other two fellows obtaining additional VI measurements for the lesion, then taking the average value. The change in VI was calculated based on the following formula:

$$Change \quad in \quad VI(\Delta VI) = \frac{(VIpre - VIpost)}{VIpre} \times 100\,\%$$

The change in the maximum long-axis diameter (Dmax) of the primary tumor was calculated to quantitatively evaluate the efficacy of CRT, according to the following formula:

$$Change \quad in \quad VI(\Delta Dmax) = \frac{(Dmaxpre - Dmaxpost)}{Dmaxpre} \times 100\,\%$$

Statistical analysis

Statistical analysis was put into action on SPSS software version 22.0 (SPSS Inc., Chicago, IL, USA). The difference in characteristics

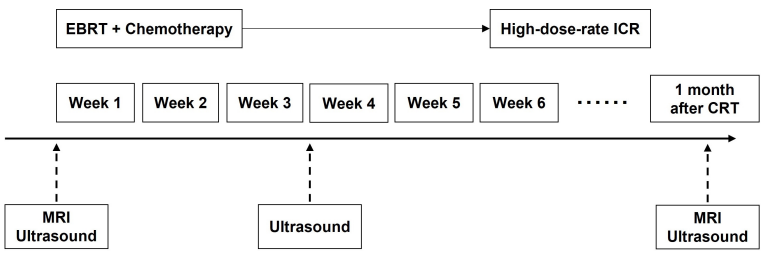

FIGURE 2
The schedule of MRI, TVUS examination and treatment. CRT, chemoradiotherapy; EBRT, external beam radiotherapy; ICR, intracavitary brachytherapy.

of the two groups was compared using Student's unpaired t-test or Mann-Whitney test. The multiple comparisons in VI, tumor Dmax and their changes between the two groups were assessed using repeated measures analysis of variance (ANOVA) and Student's unpaired t-test. Receiver operating characteristic (ROC) curve and area under curve (AUC) were applied to analyze the value of each index in predicting CRT. Intraclass correlation coefficients (ICCs) were calculated to estimate interobserver and intraobserver reproducibility. The ICC value was judged to provide excellent reliability (0.81 - 1.00), good reliability (0.61 - 0.80), moderate reliability (0.41 - 0.60), or poor reliability (0.00 - 0.20), fair reliability (0.21 - 0.40). Two-sided test was used for all tests, and $p< 0.05$ was considered statistically significant.

Results

Patient and tumor characteristics

The characteristics of the study patients are summarized in Table 1. The mean age of the 49 patients was 54 ± 10.7 years, ranging from 33 to 72 years. Based on the MRI findings, 44 were classified as CR group, 5 as PR group, and 0 in SD/PD groups. The mean age was 54.1 ± 11.0 years for the CR group and 52.8 ± 9.3 years for the PR group ($p = 0.636$). There was no significant difference between the CR and PR groups in the primary tumor Dmax ($p = 0.147$), FIGO stage ($p = 0.504$), histological type ($p = 0.554$) or histological grade ($p = 0.636$). Figure 3 illustrated the SMI images and corresponding axial T2-weighted MRI of a typical CR case throughout the treatment, while showed Figure 4 a representative PR case.

TABLE 1 Characteristics of the study group.

Characteristics	No. of patients (%)
Age (years)	
≤ 50	14 (28.6)
51 - 60	20 (40.8)
> 60	15 (30.6)
FIGO stage	
IIB	10 (20.4)
IIIA	15 (30.6)
IIIB	12 (24.5)
IIIC	8 (16.3)
IVA	4 (8.2)
Histologic type	
Squamous cell carcinoma	42 (85.7)
Adenocarcinoma	7 (14.3)
Histological grade	
G1 - G2	19 (38.8)
G3	30 (61.2)
Tumor diameter (primary)	
< 4 cm	8 (16.3)
≥ 4 cm	41 (83.7)
Treatment outcome	
Complete response	44 (89.8)
Partial response	5 (10.2)

G1, well differentiated; G2, moderately differentiated; G3, poorly differentiated; FIGO, the International Federation of Gynecology and Obstetrics.

Predictive values of tumor size and changes during CRT

At 3 weeks during CRT, Dmax of CR group was slightly lower than that of PR group ($p = 0.083$), and CR group had higher ΔDmax than PR group ($p = 0.435$), but there were no significant different between the two groups. After treatment, Dmax was significantly reduced in both CR and PR groups. Decrease in Dmax of CR group (ΔDmax = 100%) is obviously more than that of PR group (ΔDmax = 47.3 ± 6.8%) ($p< 0.001$) (Table 2). The results of ΔDmax of the two groups showed good agreement with MRI. The ROC analysis revealed no significant area-under-the-curve (AUC) values for Dmax (AUC = 0.745, $p = 0.087$) and ΔDmax (AUC = 0.536, $p = 0.792$) at 3 weeks during CRT (Figure S1).

Predictive values of VI and changes during CRT

Table 2 summarizes the mean VI and ΔVI of the tumors in the CR and PR groups at each time point. Before starting treatment, CR group and PR group demonstrated similar tumor angiogenesis, with mean VI of 0.400 ± 0.060 and 0.401 ± 0.032, respectively. VI decreased during CRT ($p< 0.001$) in patients with LACC. The VIs were significantly decreased from 3 weeks after treatment initiation to therapy completion in the CR group ($p< 0.001$), and the difference between CR and PR groups was found to be significant ($p = 0.004$ and $p< 0.001$). Compared to baseline at pre-therapy, VI of the PR group slightly decreased at 3 weeks during treatment ($p = 0.007$). However, no significant difference of VI was seen from 3 week after treatment initiation to therapy completion in PR group ($p = 0.078$). Similarly, ΔVI exhibited significant differences between the two groups at 3 weeks during treatment and after treatment (all $p< 0.001$). The VI as well as ΔVI at 3 weeks during CRT was able to predict the responder prognosis, with an AUC of 0.950 ($p = 0.001$) and 0.964 ($p = 0.001$), respectively. The optimal cut-off values for predicting responder prognosis were 0.264 for VI and 41.6% for ΔVI,

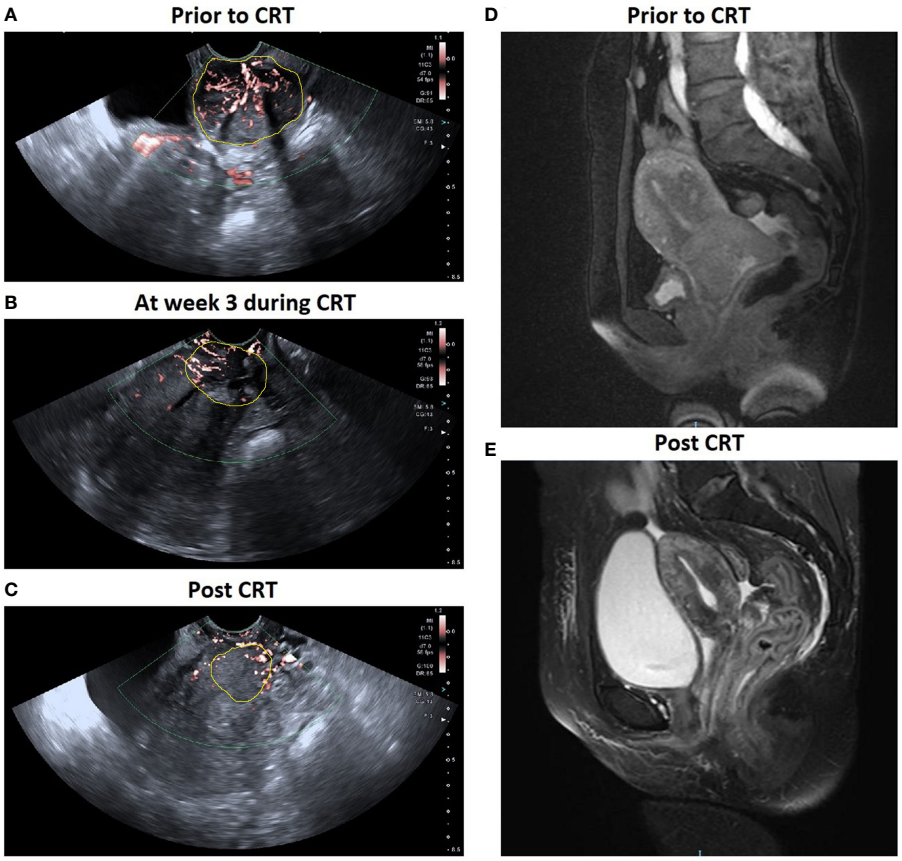

FIGURE 3
A patient with locally advanced cervical cancer (FIGO stage IIIB) experienced complete response to chemo-radiotherapy (CRT). SMI images show a significant decrease in VI in cervical cancer: **(A)** 0.367 prior to CRT; **(B)** 0.188 at week 3 during CRT; **(C)** 0.600 post CRT. Corresponding axial T2-weighted images exhibited a significant decrease in the maximal diameter of tumor: **(D)** 5.3 cm at pre-therapy e and **(E)** 0 cm post therapy.

respectively. Furthermore, ΔVI at 3 weeks during treatment showed a better predictive performance for responder prognosis than VI, with a 100% sensitivity and 86.4% specificity (Figure S1).

Reproducibility analysis

The ICCs of VI for interobserver and intraobserver variability of measurements were 0.911 (95% CI, 0.885 - 0.932; p< 0.001) and 0.925 (95% CI, 0.910 - 0.937; p = 0.001), respectively.

Discussion

CRT improves long-term survival and reduce local recurrence in patients, which is one of the most important methods of treatment for LACC (26). Due to cytotoxic effects, chemotherapeutic drugs (such as cisplatin and paclitaxel) act directly on microvascular and tumor cells to reduce tumor size, leading to tumor re-oxidation and cell cycle entry into a radiation-sensitive phase. Currently, imaging modalities are used to effectively evaluate tumor size change to intuitively reflect the treatment effect. We observed significant decreases in tumor size during and after CRT in patients with LACC, especially in the CR group. Although US is not recommended as a general tool in RECIST guideline (27), our study confirmed that tumor size reduction on US images were largely consistent with that on MRI images after CTR. However, there was no significant difference in tumor size between the CR and PR groups at 3 weeks during treatment, which did not appear to be useful in predicting tumor response at initial stage of treatment. However, reduction in tumor size may occur after several weeks, despite a positive functional response to therapy (28). Thus, an early and accurate predicting marker of effective therapy is needed to provide a basis for clinical optimization of treatment regimens, while also reducing unnecessary post-treatment toxicities and economic costs.

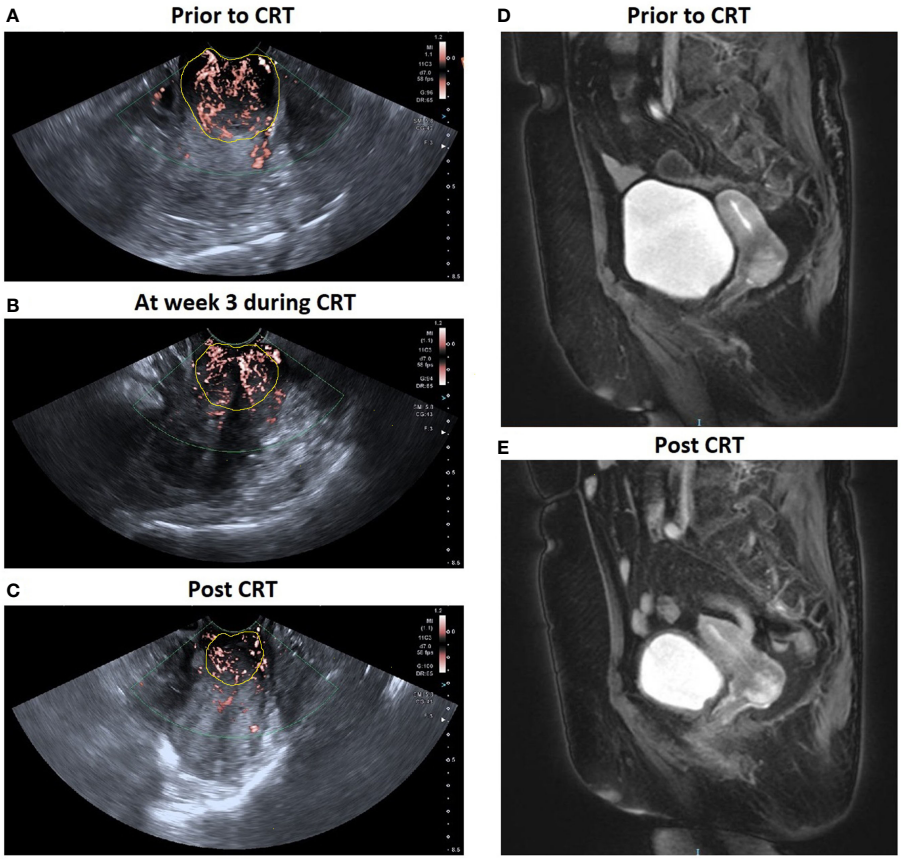

FIGURE 4
A patient with locally advanced cervical cancer (FIGO stage IIB) experienced complete response to CRT. SMI images show a significant decrease in VI in cervical cancer: **(A)** 0.398 prior to CRT; **(B)** 0.323 at week 3 during CRT; **(C)** 0.278 post CRT. Corresponding axial T2-weighted images exhibited a significant decrease in the maximal diameter of tumor: **(D)** 3.5 cm at pre-therapy e and **(E)** 1.8 cm post therapy.

Highly vascularized tumors are more aggressive and have a poorer prognosis than less vascularized tumors, indicating that highly vascularized tumors may be more resistant to chemotherapy and radiotherapy. With the gradual regression of vascularization during CRT, the tumor structure changed and size decreased step in step (29). Changes of vascularization are potential non-invasive markers for tumor response forecast to CRT in patients with cervical cancer (30). According to previous studies, using transvaginal color Doppler US (TVCD), 3-dimensional power Doppler angiography (3D-PDA) and CEUS to evaluate tumor vascularity correlates with some tumor features and could provide a means for predicting

TABLE 2 The mean Dmax and VI value of the tumor in the complete and partial responders at each time point.

Time-points	Dmax (cm)		*P*	VI		*P*	ΔDmax (%)		*P*	ΔVI (%)		*P*
	CR	PR		CR	PR		CR	PR		CR	PR	
Pre-therapy (Baseline)	5.1 ± 1.1	5.9 ± 1.4	0.147	0.400 ± 0.060	0.401 ± 0.032	0.970						
3 weeks during CRT	3.1 ± 0.9	3.8 ± 0.7	0.083	0.237 ± 0.045	0.320 ± 0.014	0.004	38.3 ± 14.6	32.8 ± 17.4	0.435	40.8 ± 6.7	19.6 ± 9.3	<0.001
1 month after CRT	0	3.1 ± 1.0	<0.001	0.072 ± 0.019	0.291 ± 0.023	<0.001	100	47.3 ± 6.8	<0.001	82.2 ± 3.5	26.6 ± 10.9	<0.001

Data are presented as mean ± standard deviation.
CR, complete responder; PR, partial responder; CRT, Concomitant chemotherapy and radiotherapy; Dmax, the maximum long-axis diameter; VI, vascularization index.

clinical response to CRT in patients with LACC (18, 19, 28, 31). Moreover, it is demonstrated that strain elastography was useful as an early predictor of respond and long-term outcomes after CCRT for patients with cervical cancer (13). But, there was no consensus on the effectiveness of SMI and strain elastography in the evaluation of tumors and treatment response (32, 33).

SMI can detect micro-vessels with diameter as small as 0.1 mm or low-velocity blood flow (≥ 0.8 cm/s), and is therefore considered a promising, low-cost, and safe method for imaging angiogenic changes in tumors. In several studies, SMI has significant advantages over color and power Doppler imaging in detecting ultra-low velocity blood flow in microvessels and blood microperfusion of tumor (34, 35). For evaluation tumors by assessing the microvasculature, the diagnostic performance of SMI appears to be comparable to that of CEUS (24). SMI quantitative analysis showed VI was in direct proportion to the vascularization. We found that the VI showed a significant downward trend compared with that before treatment. SMI is expected to be a reliable method for monitoring intratumor microvascular density changes after CRT. Our results showed changes in quantitative SMI parameters (VI) indirectly reflected the effectiveness of CRT, which were consistent with previous reports using TVCD and 3D-PDA technology.

Multiple studies have shown that CEUS revealed changes in tumor blood flow pattern during treatment precede anatomical changes detected by imaging (28, 36). However, CEUS is difficult to implement as a routine technique to track efficacy in daily clinical practice. Our study investigated whether VI discriminated between CR and PR groups at baseline and following CRT. We found that the VIs of CR decreased more significantly than that of PR group at 3 weeks during treatment in the condition that there were no significant changes in tumor size between the two groups. Our findings indicated that the significant size reduction usually occurs at a later stage of treatment, so the changes of tumor microvasculature can be detected by SMI quantitative analysis to reflect the early therapeutic effect.

The heterogeneity of tumor microvasculature distribution determines the efficacy of anticancer drugs in killing tumor cells by affecting the delivery of therapeutic drugs. Hypervascular tumors allow enough anticancer drugs to penetrate deeper into the tumor and be destroyed, whereas hypovascular tumors may be more likely to survive due to exposure to lower drug concentrations (37). Our study demonstrated that baseline VIs was slightly higher in the CR group than in the PR group before starting treatment, but no significant differences were obtained. Due to the varying sample size of each group, the statistical results may be biased. Although SMI quantitative analysis can reflect the blood supply of tumor tissue, we cannot conclude that the tumor response to CRT can be predicted by baseline VI. Thus, further investigation will be needed to verify whether baseline VI can guide the selection of pretreatment strategies for cervical cancer and be is a predictor of antiangiogenic therapy.

Our research has some limitations. First, this study was a single-center retrospective study with a small sample size, which may have limitations such as sample selection bias, short observation time. Second, due to the lack of long-term follow-up results of SMI in predicting clinical outcomes in LACC patients, further studies are needed. Finally, signal intensity of SMI is strongly dependent on depth and patient weight. We used the same US unit and setup for each patient, and as far as possible ensured that the tumor changes were evaluated with similar anatomical sections throughout the treatment, so the measurements at 3 time points were comparable.

Conclusion

SMI quantitative analysis can reflect changes in tumor microvasculature, which likely precede changes in tumor size following CRT. SMI is emerging as promising valuable vascular imaging technique for monitoring tumor response to CRT in LACC. Of course, multicenter, large-sample, controlled studies are needed to further investigate the role of SMI in monitoring clinic outcome in patients with LACC underwent CRT.

Data availability statement

The original contributions presented in the study are included in the article/Supplementary Material. Further inquiries can be directed to the corresponding author. A small sample of the study subjects has been used in previous reports at the 2021 RSNA (Yi Zhu. Superb Microvascular Imaging: Preliminary Results in Assessment the response to Chemoradiotherapy in Locally Advanced Cervical Cancer. 2020 RSNA. Abstract ID: 2021-SP-18091-RSNA). In this paper, we added more cases and enriched the analysis.

Ethics statement

Written informed consent was not obtained from the individual(s) for the publication of any potentially identifiable images or data included in this article.

Author contributions

YZ and GZ conceived, designed, or planned the study; YZ, YT, and JZ provided study patients, imaging and pathological data; YT and YL collected or assembled the data; YZ and YT performed or supervised analyses; YZ wrote sections of the initial draft; YZ and GZ provided substantive suggestions for revision or critically reviewed subsequent iterations of the manuscript; GZ provided administrative, technical, or logistic

support. YZ and YT contributed equally to this work. All authors reviewed and approved final version of the paper; are accountable for all aspects of the work in ensuring that questions related to the accuracy or integrity of any part of the work are appropriately investigated and resolved.

Funding

This work was supported by National Natural Science Foundation of China (grant numbers 81902670), Sichuan Key Research and Development Project from Sichuan Provincial Science and Technology Department (grant numbers 2019YFS0405, 2019YFS0424, and 2019YFS0036).

Conflict of interest

The authors declare that the research was conducted in the absence of any commercial or financial relationships that could be construed as a potential conflict of interest.

Publisher's note

Supplementary material

The Supplementary Material for this article can be found online at: https://www.frontiersin.org/articles/10.3389/fonc.2022.1074173/full#supplementary-material

SUPPLEMENTARY FIGURE 1
Receiver-operating characteristic (ROC) curve of morphological changes during the CRT. Maximum tumor diameter (Dmax, **A**) and their percentage changes (ΔDmax, **B**) cannot predict the long-term prognosis at 3 weeks during CRT. Vascularity index (VI, **C**) and ΔVI **(D)** can predict the long-term prognosis at 3 weeks during CRT.

References

1. Bhatla N, Aoki D, Sharma DN, Sankaranarayanan R. Cancer of the cervix uteri. *Int J Gynaecol Obstet* (2018) 143 Suppl 2:22–36. doi: 10.1002/ijgo.12611

2. Sung H, Ferlay J, Siegel RL, Laversanne M, Soerjomataram I, Jemal A, et al. Global cancer statistics 2020: GLOBOCAN estimates of incidence and mortality worldwide for 36 cancers in 185 countries. *CA Cancer J Clin* (2021) 0:1–41. doi: 10.3322/caac.21660

3. Simms KT, Steinberg J, Caruana M, Smith MA, Lew J, Soerjomataram I, et al. Impact of scaled up human papillomavirus vaccination and cervical screening and the potential for global elimination of cervical cancer in 181 countries, 2020-99: a modelling study. *Lancet Oncol* (2019) 20:394–407. doi: 10.1016/S1470-2045(18)30836-2

4. Marth C, Landoni F, Mahner S, McCormack M, Gonzalez-Martin A, Colombo N. Cervical cancer: ESMO clinical practice guidelines for diagnosis, treatment and follow-up. *Ann Oncol* (2017) 28:iv72–83. doi: 10.1093/annonc/mdx220

5. Friedlander M, Grogan MForce USPST. Guidelines for the treatment of recurrent and metastatic cervical cancer. *Oncologist* (2002) 7:342–7. doi: 10.1634/theoncologist.2002-0342

6. Rose PG, Bundy BN, Watkins EB, Thigpen JT, Deppe G, Maiman MA, et al. Concurrent cisplatin-based radiotherapy and chemotherapy for locally advanced cervical cancer. *N Engl J Med* (1999) 340:1144–53. doi: 10.1056/NEJM199904153401502

7. Gu KW, Kim CK, Choi CH, Yoon YC, Park W. Prognostic value of ADC quantification for clinical outcome in uterine cervical cancer treated with concurrent chemoradiotherapy. *Eur Radiol* (2019) 29:6236–44. doi: 10.1007/s00330-019-06204-w

8. Elit L, Fyles AW, Devries MC, Oliver TK, Fung-Kee-Fung MGynecology Cancer Disease Site G. Follow-up for women after treatment for cervical cancer: a systematic review. *Gynecol Oncol* (2009) 114:528–35. doi: 10.1016/j.ygyno.2009.06.001

9. Xu Y, Ru T, Zhu L, Liu B, Wang H, Zhu L, et al. Ultrasonic histogram assessment of early response to concurrent chemo-radiotherapy in patients with locally advanced cervical cancer: a feasibility study. *Clin Imaging* (2018) 49:144–9. doi: 10.1016/j.clinimag.2018.01.002

10. Li XS, Fan HX, Zhu HX, Song YL, Zhou CW. The value of perfusion CT in predicting the short-term response to synchronous radiochemotherapy for cervical squamous cancer. *Eur Radiol* (2012) 22:617–24. doi: 10.1007/s00330-011-2280-6

11. Choi J, Kim HJ, Jeong YH, Lee J, Cho A, Yun M, et al. The role of (18) f-FDG PET/CT in assessing therapy response in cervix cancer after concurrent chemoradiation therapy. *Nucl Med Mol Imaging* (2014) 48:130–6. doi: 10.1007/s13139-013-0248-y

12. Zhu L, Zhu L, Shi H, Wang H, Yan J, Liu B, et al. Evaluating early response of cervical cancer under concurrent chemo-radiotherapy by intravoxel incoherent motion MR imaging. *BMC Cancer* (2016) 16:79. doi: 10.1186/s12885-016-2116-5

13. Xu Y, Zhu L, Zhu L, Wang H, Ru T, Liu B, et al. Strain elastography as an early predictor of long-term prognosis in patients with locally advanced cervical cancers treated with concurrent chemoradiotherapy. *Eur Radiol* (2020) 30:471–81. doi: 10.1007/s00330-019-06345-y

14. Bremer GL, Tiebosch AT, van der Putten HW, Schouten HJ, de Haan J, Arends JW. Tumor angiogenesis: an independent prognostic parameter in cervical cancer. *Am J Obstet Gynecol* (1996) 174:126–31. doi: 10.1016/s0002-9378(96)70384-8

15. Schlenger K, Hockel M, Mitze M, Schäffer U, Weikel W, Knapstein PG, et al. Tumor vascularity–a novel prognostic factor in advanced cervical carcinoma. *Gynecol Oncol* (1995) 59:57–66. doi: 10.1006/gyno.1995.1268

16. Testa AC, Ferrandina G, Distefano M, Fruscella E, Mansueto D, Basso D, et al. Color Doppler velocimetry and three-dimensional color power angiography of cervical carcinoma. *Ultrasound Obstet Gynecol* (2004) 24:445–52. doi: 10.1002/uog.1703

17. Wiggins DL, Granai CO, Steinhoff MM, Calabresi P. Tumor angiogenesis as a prognostic factor in cervical carcinoma. *Gynecol Oncol* (1995) 56:353–6. doi: 10.1006/gyno.1995.1062

18. Alcázar JL, Jurado M, López-García G. Tumor vascularization in cervical cancer by 3-dimensional power Doppler angiography: correlation with tumor characteristics. *Int J Gynecol Cancer* (2010) 20:393–7. doi: 10.1111/IGC.0b013e3181d159f9

19. Tomalczyk A, Tomasik B, Fijuth J, Moszynska-Zielinska M, Gottwald L. Assessment of cervical vascularization density in patients with locally advanced squamous cell cervical carcinoma evaluated in colour Doppler and power Doppler functions. *Arch Gynecol Obstet* (2022) 305:955–61. doi: 10.1007/s00404-021-06161-0

20. Tekay A, Jouppila P. Controversies in assessment of ovarian tumors with transvaginal color Doppler ultrasound. *Acta Obstet Gynecol Scand* (1996) 75:316–29. doi: 10.3109/00016349609033324

21. Forsberg F, Kuruvilla B, Pascua MB, Chaudhari MH, Merton DA, Palazzo JP, et al. Comparing contrast-enhanced color flow imaging and pathological measures of breast lesion vascularity. *Ultrasound Med Biol* (2008) 34:1365–72. doi: 10.1016/j.ultrasmedbio.2008.02.010

22. Pálsdóttir K, Epstein E. OC14.05: *Contrast enhanced ultrasonography (CEUS) of cervical carcinoma: A pilot study on contrast distribution patterns and qualitative CEUS parameters in cervical cancer patients and in women with normal cervices. *Ultrasound Obstet Gynecol* (2017) 50:30–0. doi: 10.1002/uog.17645

23. Zhang XY, Zhang L, Li N, Zhu Q, Li J, Sun Q, et al. Vascular index measured by smart 3-d superb microvascular imaging can help to differentiate malignant and benign breast lesion. *Cancer Manag Res* (2019) 11:5481–7. doi: 10.2147/CMAR.S203376

24. Lee DH, Lee JY, Han JK. Superb microvascular imaging technology for ultrasound examinations: Initial experiences for hepatic tumors. *Eur J Radiol* (2016) 85:2090–5. doi: 10.1016/j.ejrad.2016.09.026

25. Eisenhauer EA, Therasse P, Bogaerts J, Schwartz LH, Sargent D, Ford R, et al. New response evaluation criteria in solid tumours: Revised RECIST guideline (version 1.1). *Eur J Cancer* (2009) 45:228–47. doi: 10.1016/j.ejca.2008.10.026

26. Green JA, Kirwan JM, Tierney JF, Symonds P, Fresco L, Collingwood M, et al. Survival and recurrence after concomitant chemotherapy and radiotherapy for cancer of the uterine cervix: A systematic review and meta-analysis. *Lancet* (2001) 358:781–6. doi: 10.1016/S0140-6736(01)05965-7

27. Fangberget A, Nilsen LB, Hole KH, Holmen MM, Engebraaten O, Naume B, et al. Neoadjuvant chemotherapy in breast cancer-response evaluation and prediction of response to treatment using dynamic contrast-enhanced and diffusion-weighted MR imaging. *Eur Radiol* (2011) 21:1188–99. doi: 10.1007/s00330-010-2020-3

28. Peng C, Liu LZ, Zheng W, Xie YJ, Xiong YH, Li AH, et al. Can quantitative contrast-enhanced ultrasonography predict cervical tumor response to neoadjuvant chemotherapy? *Eur J Radiol* (2016) 85:2111–8. doi: 10.1016/j.ejrad.2016.09.025

29. Min'ko BA, Ushakova GA, Mikhailova EA, Vinokurov VL, Evtushenko EV. [Ultrasound assessment of the effectiveness of chemoradiotherapy in cervical cancer]. *Vopr Onkol* (2009) 55:365–8.

30. Frühauf F, Dueckelmann A, Fischerova D, Zikan M, Pinkavova I, Duseket , et al. OP09.06: The association of changes in cervical cancerechogenicity and vascularization with treatment effect of neoadjuvant chemotherapy. *Ultrasound Obstet Gynecol* (2014) 44:83–4. doi: 10.1002/uog.13722

31. Alcazar JL, Castillo G, Martinez-Monge R, Jurado M. Transvaginal color Doppler sonography for predicting response to concurrent chemoradiotherapy for locally advanced cervical carcinoma. *J Clin Ultrasound* (2004) 32:267–72. doi: 10.1002/jcu.20033

32. Cebeci H, Öztürk M, Durmaz MS, Abidin K, Ömer E, Bahar Ç. Evaluation of benign parotid gland tumors with superb microvascular imaging and shear wave elastography. *J Ultrason* (2020) 20:185–90. doi: 10.15557/JoU.2020.0031

33. Uysal E, Öztürk M, Kilinçer A, Koplay M. Comparison of the effectiveness of shear wave elastography and superb microvascular imaging in the evaluation of breast masses. *Ultrasound Q* (2021) 37(2):191–7. doi: 10.1097/RUQ.0000000000000562

34. Park AY, Seo BK, Cha SH, Yeom SK, Lee SW, Chung HH. An innovative ultrasound technique for evaluation of tumor vascularity in breast cancers: Superb micro-vascular imaging. *J Breast Cancer* (2016) 19:210–3. doi: 10.4048/jbc.2016.19.2.210

35. Park AY, Seo BK. Up-to-date Doppler techniques for breast tumor vascularity: superb microvascular imaging and contrast-enhanced ultrasound. *Ultrasonography* (2018) 37:98–106. doi: 10.14366/usg.17043

36. Williams R, Hudson JM, Lloyd BA, Sureshkumar AR, Lueck G, Milot L, et al. Dynamic microbubble contrast-enhanced US to measure tumor response to targeted therapy: A proposed clinical protocol with results from renal cell carcinoma patients receiving antiangiogenic therapy. *Radiology* (2011) 260:581–90. doi: 10.1148/radiol.11101893

37. Galmarini FC, Galmarini CM, Sarchi MI, Abulafia J, Galmarini D. Heterogeneous distribution of tumor blood supply affects the response to chemotherapy in patients with head and neck cancer. *Microcirculation* (2000) 7:405–10. doi: 10.1111/j.1549-8719.2000.tb00138.x

frontiers | Frontiers in Oncology

TYPE Case Report
PUBLISHED 20 January 2023
DOI 10.3389/fonc.2022.1079716

OPEN ACCESS

EDITED BY
Alessio G. Morganti,
University of Bologna, Italy

REVIEWED BY
Maria Del Grande,
Ente Ospedaliero Cantonale (EOC), Switzerland
Alice Zamagni,
University of Bologna, Italy

*CORRESPONDENCE
Kazunori Nagasaka
nagasakak@med.teikyo-u.ac.jp

SPECIALTY SECTION
This article was submitted to Gynecological Oncology, a section of the journal Frontiers in Oncology

RECEIVED 25 October 2022
ACCEPTED 28 December 2022
PUBLISHED 20 January 2023

CITATION
Matsuura Y, Nishida H, Kosaka T, Shigekawa K, Takasaki K, Ichinose T, Hirano M, Hiraike H and Nagasaka K (2023) Case report: Posterior reversible encephalopathy syndrome, an adverse effect of lenvatinib and pembrolizumab combination therapy, in a patient with advanced endometrial cancer. *Front. Oncol.* 12:1079716. doi: 10.3389/fonc.2022.1079716

Case report: Posterior reversible encephalopathy syndrome, an adverse effect of lenvatinib and pembrolizumab combination therapy, in a patient with advanced endometrial cancer

Yuki Matsuura, Haruka Nishida, Takashi Kosaka, Kazuyuki Shigekawa, Kazuki Takasaki, Takayuki Ichinose, Mana Hirano, Haruko Hiraike and Kazunori Nagasaka*

Department of Obstetrics and Gynecology, Teikyo University School of Medicine, Tokyo, Japan

Background: Lenvatinib-pembrolizumab combination (LEAP) is an approved therapy in Japan for advanced endometrial cancer, based on the data from the KEYNOTE-775 clinical trial. We report a case of posterior reversible encephalopathy syndrome (PRES) in a patient who received LEAP therapy for advanced endometrial cancer.

Case presentation: A 53-year-old patient with stage IVB endometrial cancer having rectal metastases, after four cycles of paclitaxel-carboplatin therapy, was found to have increased rectal invasion, peritoneal dissemination, and multiple paraaortic lymph node metastases. She was treated with LEAP therapy and discharged on day 12 without adverse events, except for mild anemia on day 11 of treatment. She was carefully managed in the outpatient department, but on day 18, she was admitted to the emergency department with severely impaired consciousness and generalized seizures. Computed tomography of the head and lumbar tap showed no abnormal findings, and the seizures resolved with anticonvulsant medication alone. Based on a thorough physical examination and findings on magnetic resonance imaging (MRI), which showed high signal intensity in the left occipital lobe, encephalopathy, rather than encephalitis, was the likely diagnosis. Symptomatic improvement was observed, and pembrolizumab monotherapy was resumed.

Conclusions: If consciousness is impaired during LEAP treatment, it is necessary to differentiate between immunogenic encephalitis caused by pembrolizumab or encephalopathy caused by lenvatinib. MRI and lumbar tap can help in distinguishing between the two and diagnosing the responsible drug.

KEYWORDS

endometrial cancer, lenvatinib, pembrolizumab, posterior reversible encephalopathy syndrome, adverse effect

1 Introduction

Endometrial cancer is one of the most common gynecologic malignancies, and its incidence has increased rapidly. Adenomyosis, a condition in which ectopic endometrial glands and stroma develop in the myometrium, can increase the risk of endometrial cancer development, similar to leiomyomas or polycystic ovary syndrome (1). Adenomyosis and endometrial cancer have similar traits: a local microenvironment that promotes the growth of endometrial stromal cells and an isoechoic area to the endometrial tissue around altered junctional zone as an ultrasound characteristic. These traits indicate the similarity in the pathophysiology of these conditions (1, 2). Several novel biomarkers, such as relative telomere length in cell-free DNA (3) and glandular cells in preoperative cervical smear (4), have been reported for the early diagnosis and management of endometrial cancer.

The traditional first line of treatment for endometrial cancer is platinum-based chemotherapy (5). However, treatment for advanced or recurrent endometrial cancer after platinum-based chemotherapy is not standardized. In December 2021, a combination of lenvatinib and pembrolizumab (LEAP) was approved in Japan for advanced endometrial cancer, based on the result of the KEYNOTE-775 clinical trial (6) and could be considered standard therapy for platinum-resistant advanced endometrial cancer.

In contrast to the limited antitumor effects of each drug individually, the combination of lenvatinib and pembrolizumab is more effective in advanced or recurrent endometrial cancer, regardless of the tumor's genetic characteristics. Lenvatinib is a multiple tyrosine kinase inhibitor acting on vascular endothelial growth factor receptor (VEGFR), fibroblast growth factor receptor, platelet-derived growth factor receptor α, RET proto-oncogene, and KIT proto-oncogene. Lenvatinib has a limited efficacy against recurrent endometrial carcinoma when used as a single agent (7). Pembrolizumab is an inhibitor of programmed cell death 1, an immune checkpoint inhibitor. Antitumor effects of pembrolizumab have been reported in patients with microsatellite instability-high (MSI-H) or mismatch repair-deficient (dMMR) advanced endometrial carcinoma, while the effects are less significant in patients with microsatellite-stable or mismatch repair-proficient disease (8, 9).

A characteristic of this combination therapy, as opposed to traditional chemotherapy, is the variable adverse effects. The antitumor effects of traditional chemotherapy are mediated by cytotoxicity in malignant and benign cells. Contrarily, since molecularly targeted drugs are specifically toxic to malignant cells expressing the target protein, the adverse effects are also related to the target protein. Since immune checkpoint inhibitors mediate their antitumor effects by modulating the patient's immune system, the associated adverse effects include autoimmune diseases. Medical professionals should be more aware of these adverse effects because several such adverse effects may be asymptomatic.

Posterior reversible encephalopathy syndrome (PRES) is characterized by neurological symptoms such as disturbance of consciousness, seizures, headache, visual disturbances, focal neurological deficit, and status epilepticus (10). It is thought to occur due to impaired autoregulation caused by damaged vascular endothelial cells.

PRES is one of the various adverse effects of lenvatinib. Because autoimmune encephalitis is also an adverse effect of pembrolizumab, it is difficult to diagnose PRES in patients with advanced endometrial cancer receiving a combination of lenvatinib and pembrolizumab. The similar phenotypes make it difficult to differentiate between these two conditions.

Herein, we report a case of advanced endometrial cancer with neurological manifestations of PRES caused by lenvatinib. The patient provided informed consent for the publication of this case report, including images.

2 Case description

The patient was a 53-year-old woman with no relevant medical history. She experienced discomfort and pain in the anal region, and a colonoscopy detected a tumor in the colon. On the basis of imaging and endometrial sampling cytology with conventional biopsy findings, she was diagnosed with International Federation of Gynecology and Obstetrics stage IVB endometrial cancer (endometrioid adenocarcinoma Grade 1) with colon metastasis and lymphadenopathy in the bilateral obturator lymph nodes and sacrum. She received neoadjuvant chemotherapy (four cycles of paclitaxel 175 mg/m^2 and carboplatin area under curve 6). Two months later, Hartmann surgery was performed to prevent the tumor from occluding the colon. Pathological evaluation of the tumor specimen confirmed endometrial cancer, surgical stage IVB. MSI testing revealed the tumor was MSI-H.

After the surgery, computed tomography (CT) showed an enlarged recurrent tumor in the colon, with peritoneal dissemination and multiple metastases in the paraaortic lymph nodes. Hence, she was started on a combination of lenvatinib (20 mg, administered orally once daily) and pembrolizumab (200 mg, administered intravenously as a 30-minute infusion every 3 weeks). On day 11 after the LEAP therapy, she received 4 units of red blood cells due to a fall in her hemoglobin level to 7.3 g/dL. She was discharged on day 12. On day 15, she developed a gait disorder and tremors. Hypothyroidism (thyroid stimulating hormone [TSH] level: 5.350 ng/mL, free thyroxine 4 [FT4] level: 0.99 pg/mL, free thyroxine 3 [FT3] level: 2.08 pg/mL) was also detected on the same day on consultation with endocrinologists.

On day 18, she was referred to the emergency room for an altered sensorium. On arrival, her Glasgow Coma Scale score (Supplementary Figure 1) was E3V4M6. Her blood pressure showed a continued increase (Figure 1). There was no electrolyte imbalance or renal or liver failure (Table 1). An emergency CT scan found no brain metastasis or intracranial hemorrhage (Figure 2). Magnetic resonance imaging (MRI) showed a slightly high signal intensity in the left occipital lobe, with no apparent cerebral infarction (Figure 2). LEAP therapy was discontinued. Although there were no visual complaints or findings given the location of the MRI abnormalities and electroencephalogram was normal, her consciousness level gradually worsened, resulting in convulsions, which were suppressed by an intravenous injection of diazepam (5 mg). She was started on levetiracetam (200 mg) to prevent convulsions. For further investigation, additional blood tests and multiple lumbar taps were performed. While serum vitamin B1,

10.3389/fonc.2022.1079716

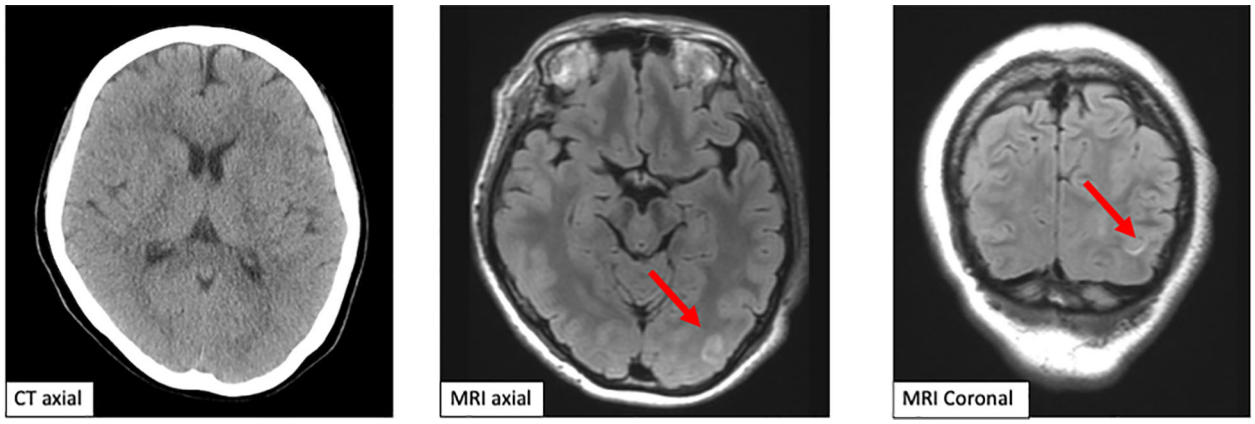

FIGURE 1
Computed tomography scan and magnetic resonance imaging of the brain. The emergent computed tomography scan of the brain shows no brain metastasis and intracranial hemorrhage. Magnetic resonance imaging shows a slightly high signal in the left occipital lobe axial and coronal.

TSH, FT4, and FT3 levels were normal, a slight increase was seen in the anti-thyroid peroxidase antibody levels (Table 1). The blood glucose level was 110 mg/dL. Analysis of the cerebrospinal fluid found cells (5/μL), protein (154 mg/dL), and glucose (50 mg/dL) (Table 1), suggesting that meningitis was unlikely. The disturbance in consciousness gradually improved with time, indicating the low probability of Hashimoto encephalopathy.

Previous clinical trials have revealed that the incidence of adverse effects of lenvatinib and pembrolizumab on the central nervous system was 0.4% (11) and less than 0.1% (12), respectively, and could have caused PRES and encephalitis, respectively. The absence of markers of inflammation in the cerebrospinal fluid and a high signal intensity in the left occipital lobe on MRI suggested PRES, rather than encephalitis. Therefore, it was concluded that these symptoms were caused by lenvatinib, not pembrolizumab. She was resumed on treatment with pembrolizumab. Although no long-term sequalae of PRES were observed, unfortunately, CT showed multiple lymph node metastases after four cycles of pembrolizumab monotherapy, indicative of further

TABLE 1 Laboratory results on day 18.

Laboratory results		
Blood test	γ-GTP 36U/L	Cort 9.5ug/dL
RBC 303 × 10^4/μL	**CK 215U/L**	**ACTH 6.3pg/mL**
Hb 9.3 g/dL	BUN 14.9mg/dL	TgAb 10.0IU/mL
Plt 7.8 × 10^4/μL	Cr 0.68mg/dL	
WBC 24 × 10^2/μL	**UA 5.8mg/dL**	**VBG**
PT% 100.0%	Na 144mEq/L	pH 7.403
INR 0.98	K 3.3 mEq/L	**PCO2 47.3mmHg**
APTT 31.6sec	Cl 104mEq/L	**PO2 48.4mmHg**
Fib 237mg/dL	Ca 9.2mg/dL	HCO3 28.8mEq/L
D-dimer 5.3 ug/mL	P 3.7mg/dL	**BE 3.5mEq/L**
TP 6.5g/dL	BS 78mg/dL	
Alb 3.1g/dL	NH3 22μg/dL	**CSF**
T-Bil 0.91mg/dL	**CRP 1.25mg/dL**	Cells 5/μL (Lym 5/μL)
D-Bil 0.15mg/dL	**TSH 7.970μIU/mL**	Protein 154mg/dL
AST 67U/L	FT4 0.96ng/dL	Glu 50mg/dL
ALT 44U/L	FT3 1.91 pg/mL	Cl 126Eq/L
LD 384U/L	VitB1 24ng/mL	ADA 3.6U/L
ALP 137U/L	HbA1c 5.5%	Viruses negative

Venous Blood Gas (VBG), Cerebrospinal Fluid (CSF). Laboratory test abnormalities are in bold.

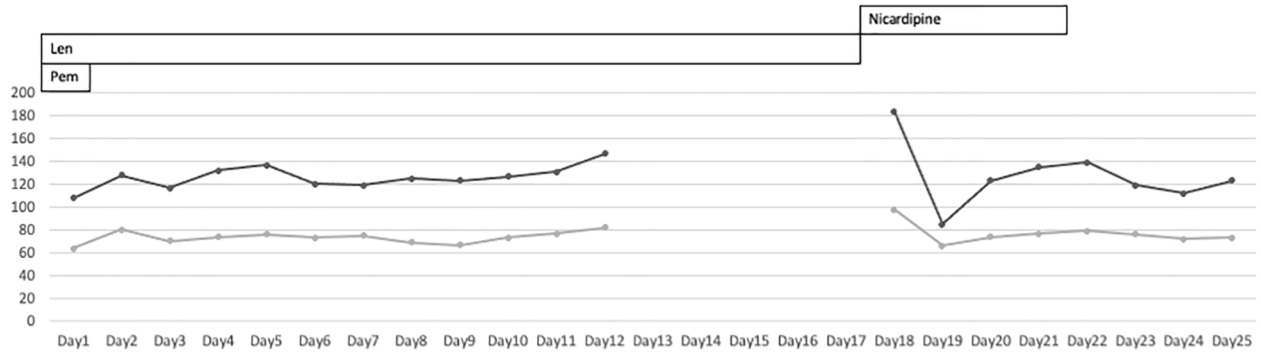

FIGURE 2
Patient's blood pressure during lenvatinib-pembrolizumab therapy. The patient's blood pressure was not monitored at home. It was abnormally high at the time of admission to the emergency room.

disease progression. Pembrolizumab was discontinued, and she is now enrolled in another clinical trial in Japan.

3 Discussion

Patients with advanced or recurrent endometrial cancer could experience neurological symptoms for many reasons. Lenvatinib and pembrolizumab adversely affect the central nervous system and may cause PRES and encephalitis, respectively. Cancer-related thrombophilia can cause cerebral infarction, and associated brain metastases may result in hyperten sive intracranial hemorrhage. Identifying the cause of neurological symptoms is crucial, especially when it is drug related. If lenvatinib causes PRES in MSI-H/dMMR patients, effective therapy with pembrolizumab alone can be restarted after cessation of lenvatinib.

The difference between encephalopathy and encephalitis is key to distinguishing between lenvatinib- and pembrolizumab-related adverse effects. Although both present with neurologic symptoms,

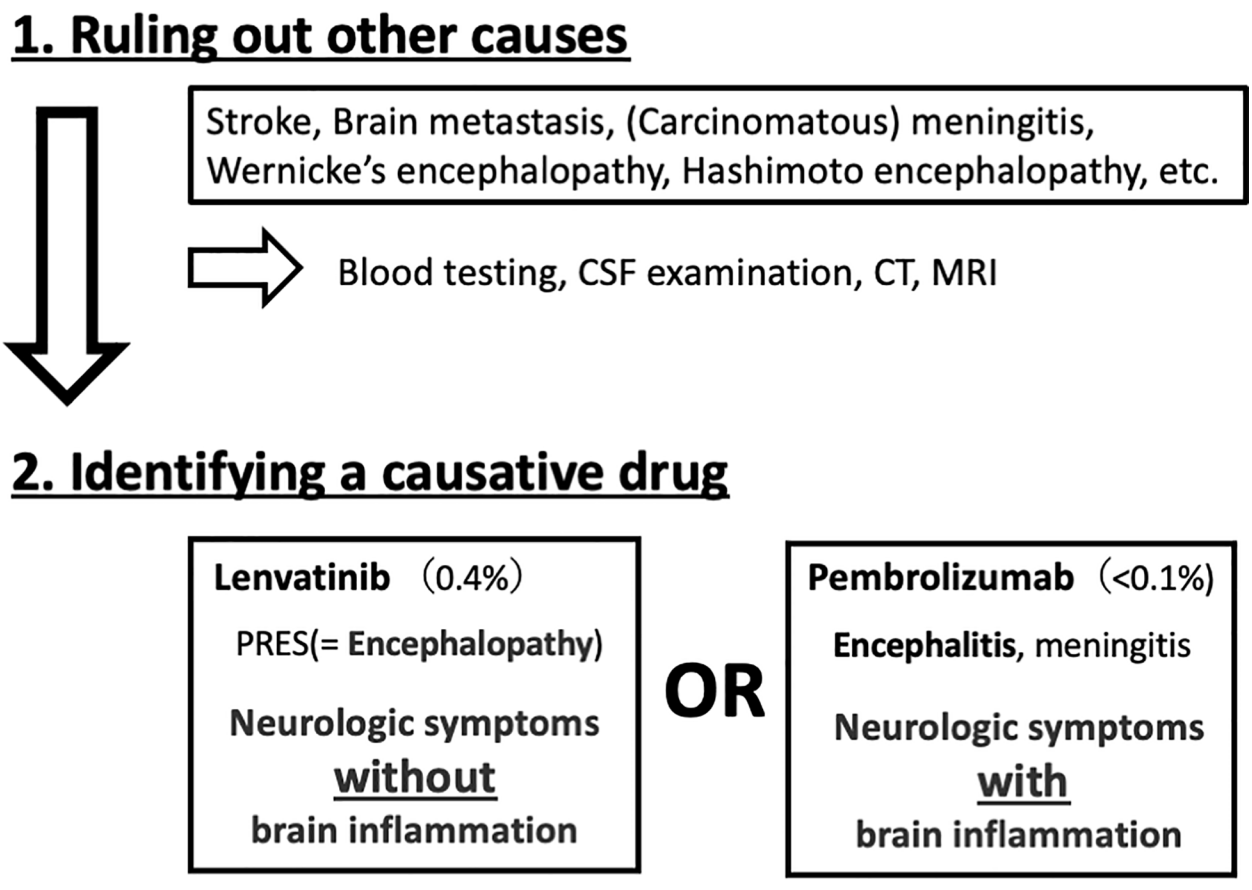

FIGURE 3
Steps to treat neurological adverse effects.

encephalitis is characterized by inflammation in the brain, while encephalopathy is non-inflammatory. A hyperimmune response due to high cytokine levels or cerebral edema due to vascular hyperpermeability can cause encephalopathy. A lumbar puncture is the best procedure to distinguish between these two conditions by confirming or ruling out brain inflammation (Figure 3).

PRES is characterized by interstitial edema caused by hyperperfusion resulting from a disruption in autoregulation due to damaged vascular endothelial cells. This damage is thought to be caused by hypertension, sepsis, pre-eclampsia, eclampsia, autoimmune disorders, and immunosuppressive or cytotoxic drugs (10). Cytokines, such as tumor necrosis factor-α, interleukin-1, and VEGF, increase vascular permeability. A common side effect of lenvatinib is hypertension. Lenvatinib-induced hypertension and VEGFR inhibition are closely associated with vascular endothelial cell damage. Pembrolizumab, when given in combination with lenvatinib, also acts as an immunomodulator and further increases vascular permeability. Hence, LEAP therapy increases the risk of PRES.

Brain imaging in PRES shows several distribution patterns, of which the holohemispheric watershed superior frontal sulcus and dominant parietal-occipital patterns are the most common. High signal intensity on T2-weighted/fluid-attenuated inversion recovery images and high apparent diffusion coefficient are seen, reflecting vasogenic edema. This patient showed a dominant parietal-occipital pattern (13).

Following the development of PRES, the LEAP therapy was suspended, and pembrolizumab monotherapy was instituted. The limitation of this case report is that the patient was fully informed about the side effects of the treatment on day 12 and was given discharge instructions, including home blood pressure monitoring. However, blood pressure control at home was inadequate, and the patient's physical condition was unknown until the emergency department visit on day 15. To the best of our knowledge, this is the first report of resuming chemotherapy after a differential diagnosis of urgent intervention-indicated encephalopathy. Our findings highlight that a thorough causal inference is critical for continuing effective therapy.

Data availability statement

The original contributions presented in the study are included in the article/Supplementary Material. Further inquiries can be directed to the corresponding author.

Ethics statement

Written informed consent was obtained from the patient to publish any potentially identifiable images or data included in this article. The study was approved by the ethics committee of the medical faculty at Teikyo University Hospital.

Author contributions

All authors contributed to the article and approved the submitted version. YM designed the report. YM and KN wrote the manuscript. YM and KN collected the patient's clinical data. YM, HN, TK, KS, KT, TI, MH, HH, and KN was responsible for the conception and revision of the manuscript. YM, HN, TK, KS, KT, TI, and KN carried out the patient management. All authors contributed to the article and approved the submitted version. This research received no external funding.

Conflict of interest

The authors declare that the research was conducted in the absence of any commercial or financial relationships that could be construed as a potential conflict of interest.

Publisher's note

Supplementary material

The Supplementary Material for this article can be found online at: https://www.frontiersin.org/articles/10.3389/fonc.2022.1079716/full#supplementary-material

References

1. Lagana AS, Scioscia M. Endometrial cancer in women with adenomyosis: an underestimated risk? *Int J Fertil Steril* (2020) 14:260–1. doi: 10.22074/ijfs.2020.44413

2. Scioscia M, Noventa M, Lagana AS. Abnormal uterine bleeding and the risk of endometrial cancer: Can subendometrial vascular ultrasound be of help to discriminate cancer from adenomyosis? *Am J Obstet Gynecol* (2020) 223:605–6. doi: 10.1016/j.ajog.2020.05.049

3. Benati M, Montagnana M, Danese E, Mazzon M, Paviati E, Garzon S, et al. Aberrant telomere length in circulating cell-free DNA as possible blood biomarker with high diagnostic performance in endometrial cancer. *Pathol Oncol Res* (2020) 26:2281–9. doi: 10.1007/s12253-020-00819-x

4. Casarin J, Bogani G, Serati M, Pinelli C, Lagana AS, Garzon S, et al. Presence of glandular cells at the preoperative cervical cytology and local recurrence in endometrial cancer. *Int J Gynecol Pathol* (2020) 39:522–8. doi: 10.1097/PGP.0000000000000642

5. Concin N, Matias-Guiu X, Vergote I, Cibula D, Mirza MR, Marnitz S, et al. ESGO/ESTRO/ESP guidelines for the management of patients with endometrial carcinoma. *Int J Gynecol Cancer* (2021) 31:12–39. doi: 10.1136/ijgc-2020-002230

6. Makker V, Colombo N, Casado Herráez A, Santin AD, Colomba E, Miller DS, et al. Lenvatinib plus pembrolizumab for advanced endometrial cancer. *N Engl J Med* (2022) 386:437–48. doi: 10.1056/NEJMoa2108330

7. Vergote I, Powell MA, Teneriello MG, Miller DS, Garcia AA, Mikheeva ON, et al. Second-line lenvatinib in patients with recurrent endometrial cancer. *Gynecol Oncol* (2020) 156:575–82. doi: 10.1016/j.ygyno.2019.12.039

8. Marabelle A, Le DT, Ascierto PA, Di Giacomo AM, Jesus-Acosta AD, Delord J-P, et al. Efficacy of pembrolizumab in patients with noncolorectal high microsatellite

instability/mismatch repair-deficient cancer: Results from the phase II KEYNOTE-158 study. *J Clin Oncol* (2020) 38:1–10. doi: 10.1200/JCO.19.02105

9. Ott PA, Bang YJ, Berton-Rigaud D, Elez E, Pishvaian MJ, Rugo HS, et al. Safety and antitumor activity of pembrolizumab in advanced programmed death ligand 1-positive endometrial cancer: Results from the KEYNOTE-028 study. *J Clin Oncol* (2017) 35:2535–41. doi: 10.1200/JCO.2017.72.5952

10. Fugate JE, Rabinstein AA. Posterior reversible encephalopathy syndrome: clinical and radiological manifestations, pathophysiology, and outstanding questions. *Lancet Neurol* (2015) 4:914–25. doi: 10.1016/S1474-4422(15)00111-8

11. Larkin J, Chmielowski B, Lao CD, Hodi FS, Sharfman W, Weber J, et al. Neurologic serious adverse events associated with nivolumab plus ipilimumab or nivolumab alone in advanced melanoma, including a case series of encephalitis. *Oncologist* (2017) 22:709–18. doi: 10.1634/theoncologist.2016-0487

12. Schlumberger M, Tahara M, Wirth LJ, Robinson B, Brose MS, Elisei R, et al. Lenvatinib versus placebo in radioiodine-refractory thyroid cancer. *N Engl J Med* (2015) 372:621–30. doi: 10.1056/NEJMoa1406470

13. Bartynski WS, Boardman JF. Distinct imaging patterns and lesion distribution in posterior reversible encephalopathy syndrome. *AJNR Am J Neuroradiol* (2007) 28:1320–7. doi: 10.3174/ajnr.A0549

frontiers | Frontiers in Oncology

TYPE Original Research
PUBLISHED 31 January 2023
DOI 10.3389/fonc.2023.1012491

OPEN ACCESS

EDITED BY
Alessio G. Morganti,
University of Bologna, Italy

REVIEWED BY
Martina Ferioli,
IRCCS Azienda Ospedaliero-Universitaria di Bologna, Italy
Milly Buwenge,
University of Bologna, Italy
Ankur Pruthi,
Manipal Hospital Delhi, India

*CORRESPONDENCE
Szu-Yuan Wu
szuyuanwu5399@gmail.com
Ben-Chang Shia
025674@mail.fju.edu.tw

†These authors have contributed equally to this work and share first authorship

SPECIALTY SECTION
This article was submitted to Gynecological Oncology, a section of the journal Frontiers in Oncology

RECEIVED 05 August 2022
ACCEPTED 16 January 2023
PUBLISHED 31 January 2023

CITATION
Su C-H, Chen W-M, Chen M, Shia B-C and Wu S-Y (2023) Survival effect of pre-RT PET-CT on cervical cancer: Image-guided intensity-modulated radiation therapy era. *Front. Oncol.* 13:1012491. doi: 10.3389/fonc.2023.1012491

Survival effect of pre-RT PET-CT on cervical cancer: Image-guided intensity-modulated radiation therapy era

Chih-Hsiung Su[1†], Wan-Ming Chen[2,3†], Mingchih Chen[2], Ben-Chang Shia[2,3*] and Szu-Yuan Wu[2,3,4,5,6,7,8,9,10*]

[1]Department of Accounting Information, Chihlee University of Technology, Taipei, Taiwan, [2]Graduate Institute of Business Administration, College of Management, Fu Jen Catholic University, Taipei, Taiwan, [3]Artificial Intelligence Development Center, Fu Jen Catholic University, Taipei, Taiwan, [4]Department of Food Nutrition and Health Biotechnology, College of Medical and Health Science, Asia University, Taichung, Taiwan, [5]Division of Radiation Oncology, Lo-Hsu Medical Foundation, Lotung Poh-Ai Hospital, Yilan, Taiwan, [6]Big Data Center, Lo-Hsu Medical Foundation, Lotung Poh-Ai Hospital, Yilan, Taiwan, [7]Department of Healthcare Administration, College of Medical and Health Science, Asia University, Taichung, Taiwan, [8]Cancer Center, Lo-Hsu Medical Foundation, Lotung Poh-Ai Hospital, Yilan, Taiwan, [9]Centers for Regional Anesthesia and Pain Medicine, Taipei Municipal Wan Fang Hospital, Taipei Medical University, Taipei, Taiwan, [10]Department of Management, College of Management, Fo Guang University, Yilan, Taiwan

Condensed abstract: No large-scale, well-designed randomized study with a long-term follow-up has evaluated the survival effect of pretreatment 18-fluorodeoxyglucose positron emission tomography–computed tomography (^{18}FDG-PET–CT) on patients with stage IB–IVA cervical cancer receiving image-guided intensity-modulated radiation therapy (IG-IMRT). This is the first head-to-head propensity score–matched, nationwide population-based cohort study evaluating this survival effect. The results revealed that pretreatment ^{18}FDG-PET–CT might be associated with longer survival in patients with stage IB–IVA cervical cancer receiving radiotherapy or concurrent chemoradiotherapy, especially in the IG-IMRT era.

Purpose: No large-scale, well-designed randomized study with a long-term follow-up has evaluated the survival effect of pretreatment 18-fluorodeoxyglucose positron emission tomography–computed tomography (^{18}FDG-PET–CT) on patients with stage IB–IVA cervical cancer receiving image-guided intensity-modulated radiation therapy (IG-IMRT). Therefore, in this propensity score–matched, population-based cohort study, we investigated these survival effects.

Patients and methods: We included 4167 patients with stage IB–IVA cervical cancer receiving radiotherapy (RT) or concurrent chemoradiotherapy (CCRT) through the IG-IMRT technique. The patients were categorized into two 1:2 propensity score–matched groups depending on whether they underwent pretreatment ^{18}FDG-PET–CT, and their outcomes were compared.

Results: We included 2778 and 1389 patients with cervical cancer in the nonpretreatment and pretreatment PET–CT groups, respectively. Univariable and multivariable analyses revealed an association between pretreatment PET–CT and improved survival in the patients (in the adjusted model, the adjusted

hazard ratio [aHR] was 0.88; 95% confidence interval [CI], 0.80–0.97: P = 0.010). Regardless of the cancer stage (early or advanced), pretreatment PET–CT was significantly superior to nonpretreatment PET–CT in terms of all-cause death (aHR, 0.78; 95% CI, 0.60–0.92; P = 0.013 and aHR, 0.90; 95% CI, 0.81–0.99; P = 0.039 for the early [IB–IIA] and advanced stages [IIB–IVA], respectively).

Conclusions: Pretreatment ^{18}FDG-PET–CT might be associated with longer survival in patients with stage IB–IVA cervical cancer receiving RT or CCRT, especially in the era of IG-IMRT.

KEYWORDS

IG-IMRT, ^{18}FDG-PET–CT, cervical carcinoma, survival, clinical stages

Introduction

Although cervical cancer is the fourth most common cancer in women globally, the number of cervical cancer cases has continuously declined in regions that have implemented screening programs (1). However, in resource-poor areas with no well-established screening programs, the incidence and mortality rates of cervical cancer remain disproportionately high. (1) Cervical cancer is the leading cause of cancer deaths in 42 countries, with the majority of cases being reported from sub-Saharan Africa and Southeast Asia (1). Compared with other gynecological cancers, cervical cancer more commonly affects younger women, with a mean age at diagnosis of 49 years.

Following the diagnosis of cervical cancer, a pretreatment staging evaluation is performed in all women to determine the treatment approach, which can then be stratified on the basis of whether the disease is early or locally advanced at presentation (2). Accurate cancer staging is the most vital for planning optimal treatments and thus for optimal survival (3). For patients with early-stage cervical cancer, surgery alone without adjuvant therapy or radiotherapy (RT) alone might be suitable based on the National Comprehensive Cancer Network (NCCN) guidelines. However, for patients with advanced-stage cervical cancer without metastasis, concurrent chemoradiotherapy (CCRT) might be necessary (2).

Prior to RT or CCRT, whole-body 18-fluorodeoxyglucose (^{18}FDG) positron emission tomography (PET)–computed tomography (CT) is conducted to evaluate the extent of the disease, with a particular focus on lymph node metastases, for obtaining information necessary to design RT fields (4). Compared with CT alone, PET–CT exhibits higher sensitivity for the detection of abdominal lymph node metastasis, a feature that affects the RT fields and estimates of patient prognosis (5, 6). However, no long-term follow-up study with an adequate sample size has evaluated the benefits of pretreatment PET–CT, which offers the most accurate imaging results for lymph node metastasis (7, 8), and its contribution to overall survival (OS) in patients with cervical cancer receiving RT or CCRT, especially in the era of image-guided intensity-modulated radiation therapy (IG-IMRT).

Patients and methods

Study design and patient data source

This retrospective study was conducted using data from the Health and Welfare Data Center (HWDC), established by Taiwan's Ministry of Health and Welfare. Data gathered by the Taiwanese government from various sources are consolidated by HWDC, deidentified, and made available for research purposes based on case-by-case approval. We particularly used data from the Taiwan Cancer Registry (TCR), which includes the detailed staging and treatment information of patients with cancer; the Cause of Death database, which lists all death certificates issued in Taiwan (9–11); and the National Health Insurance Research Database (NHIRD), which contains the claims data of all National Health Insurance (NHI)-reimbursed examinations, medications, and treatments. Absence of the evidence of death cannot be considered the evidence of life because all death certificates issued are government system–specific judgments. Without a death certificate, property inheritance, abandonment of inheritance to the court, burial, or cremation cannot be performed in Taiwan. The NHI program has been implemented since 1995 and covers more than 99% of Taiwan's population. Since July 2004, the NHI has been reimbursing ^{18}F-FDG-PET performed for the initial staging of cervical cancer when optimal

Abbreviations: PET–CT, positron emission tomography–computed tomography; ^{18}FDG-PET–CT, 18-fluorodeoxyglucose positron emission tomography–computed tomography; HR, hazard ratio; aHR, adjusted hazard ratio; CI, confidence interval; NCCN, National Comprehensive Cancer Network; RCT, randomized controlled trial; PSM, propensity score matching; HWDC, Health and Welfare Data Center; NHI, National Health Insurance; AJCC, American Joint Committee on Cancer; CCI, Charlson comorbidity index; OS, overall survival; *ICD-10-CM*, *International Classification of Diseases, Tenth Revision, Clinical Modification*; *ICD-9-CM*, *International Classification of Diseases, Ninth Revision, Clinical Modification*; RT, radiotherapy; CCRT, concurrent chemoradiotherapy; CT, computed tomography; MRI, magnetic resonance imaging; IMRT, intensity-modulated radiation therapy; IG-IMRT, image-guided intensity-modulated radiation therapy; NHIRD, National Health Insurance Research Database; ICBT, intracavity brachytherapy; EBRT, external beam radiotherapy.

staging was unachievable through conventional imaging modalities. All PET-CT scans were reviewed and reported by a professional nuclear medicine physician in the study. All HWDC databases are linked through a common but anonymized identifier to ensure privacy. The requirement for informed consent was waived because of the retrospective nature of the study and the use of deidentified data.

Inclusion and exclusion criteria

Patients were enrolled if they were diagnosed as having cervical cancer on the basis of pathological reports between January 1, 2008, and December 31, 2018, were aged ≥20 years, and had an American Joint Committee on Cancer (AJCC) clinical stage of IB–IVA based on the eighth edition. The diagnoses were confirmed using pathological data, and patients who were newly diagnosed as having cervical squamous cell carcinoma or adenocarcinoma were confirmed to have no other cancer. Patients with distant metastasis, cancer of unknown pathologic type, missing sex data, age <20 years, or unclear staging were excluded. In addition, patients were excluded if they did not receive RT within 3 months of diagnosis, RT involving contemporary IG-IMRT techniques, or a weekly platinum-based chemotherapy regimen during RT. Moreover, we excluded patients who received only sequential chemotherapy and RT. In this study, pelvic RT comprised external beam radiotherapy (EBRT) delivered once daily for 25–28 days for a total median dose of 50.4 Gy with IG-IMRT. Radiation oncologists in Taiwan prescribed total intracavity brachytherapy (ICBT) with a high-dose rate system, with a median dose of 25 Gy in five fractions when administered with or without concurrent chemotherapy. IMRT, a highly conformal EBRT technique, and its iteration—image-guided volumetric modulated arc therapy—were allowed in the study.

Covariates and outcome definition

Data regarding age, histology, AJCC clinical stages, treatments (RT alone or CCRT), tumor differentiation, EBRT cumulative dose, platinum cumulative dose, ICBT cumulative dose, Charlson comorbidity index (CCI) scores, diagnosis year, and hospital levels (medical or nonmedical center) at the last follow-up were extracted from the TCR. Age was considered a continuous variable. All patients with nonmetastatic cervical cancer underwent RT alone or definitive CCRT in accordance with NCCN guidelines. The date of RT initiation was the index date.

From the NHIRD, we identified patients who underwent ^{18}F-FDG PET–CT within 0–90 days before the index date. Only patients with a record of ^{18}F-FDG-PET–CT were considered to have undergone pretreatment PET–CT. All patients in the control group (nonpretreatment ^{18}FDG-PET–CT) received pelvic magnetic resonance imaging (MRI) with contrast to determine the local disease extent and chest/abdominal/pelvis CT for at least metastatic staging. The primary outcome of interest was all-cause death, which was calculated from the initial date to the date of death. Information on OS was obtained from the Cause of Death database. Patients with no death records were considered alive and censored on the last day of the database record (December 31, 2019).

Propensity score matching

After adjustment for confounders, we performed Cox proportional hazards regression to model time from the index date to all-cause death for patients with cervical cancer who underwent RT or CCRT. We used propensity score matching (PSM) to reduce confounding factors, thus controlling these factors and elucidating the directionality of the survival effect of pretreatment PET–CT. The following matching variables were employed: age, histology, differentiation, AJCC clinical stages, treatments, cumulative EBRT dose, cumulative platinum dose, cumulative ICBT dose, CCI scores, diagnosis year, and hospital levels. However, because a residual imbalance was noted in covariates, (12) multivariable Cox proportional regression models were used. For the CCI score calculation, comorbidities were determined according to the *International Classification of Diseases, Ninth or Tenth Revision, Clinical Modification (ICD-9-CM* or *ICD-10-CM*) codes in the main diagnosis of inpatient records or those in outpatient records if the number of outpatient visits was ≥2 within 1 year. Comorbidities with onset 12 months before the index date were recorded. We matched the cohorts at a ratio of 2:1 by using a greedy matching method, and covariates were matched with a propensity score within a caliper of 0.2. (13).

Statistical analysis

Continuous data are presented as the mean ± standard deviation or median (interquartile range), as applicable, and categorical data as the number and percentage. The distribution of patient characteristics was compared using the χ^2 test for categorical variables and the independent *t* test or Kruskal–Wallis test for continuous variables.

Survival curves were generated using the Kaplan–Meier and compared using the log-rank test. In addition, the Kaplan–Meier curves of overall survival (OS) for different stages of cervical cancer with or without pretreatment PET–CT were compared using the log-rank test. Cox proportional hazards models were used to estimate the hazard ratio (HR) and 95% confidence interval (CI) and to determine the effects of covariates on OS. Stratified analysis was performed to investigate the effect of pretreatment PET–CT on various AJCC clinical stages (IB–IIA and III–IVA) and on OS across various subgroups. All statistical analyses were performed using SAS (version 9.4; SAS Institute). A two-sided *P* value of <0.05 was considered significant.

Ethical approval

The study protocols were reviewed and approved by the Institutional Review Board of Tzu-Chi Medical Foundation (IRB109-015-B).

Results

Patient characteristics

A total of 4167 patients with cervical cancer met the inclusion criteria after PSM (Table 1). Of them, 2778 and 1389 patients who underwent RT or CCRT were included in the nonpretreatment and pretreatment PET–CT groups, respectively. All covariates were balanced between the groups after PSM (Table 1). The crude mean follow-up periods and crude mortality rates of the pretreatment and nonpretreatment PET–CT groups were 4.72 and 4.70 years and 45.64% and 51.08% ($P < 0.001$), respectively.

Predictors of survival

The findings of univariable and multivariable analyses revealed an association between pretreatment PET–CT and improved survival for the patients with cervical cancer (in the adjusted model, the adjusted hazard ratio [aHR] was 0.88; 95% CI, 0.80–0.97: $P = 0.010$; Table 2). Moreover, the results indicated that known prognostic factors, namely age > 60 years ($P = 0.014$); advanced clinical stages of IIA ($P = 0.026$), IIB ($P = 0.002$), III ($P < 0.001$), and IVA ($P < 0.001$); RT alone ($P < 0.001$); adenocarcinoma ($P < 0.001$); CCI score ≥ 1 ($P < 0.001$); and no ICBT ($P < 0.001$), were associated with poor OS (Table 2).

TABLE 1 Clinicodemographic characteristics of patients with cervical cancer with and without pretreatment PET–CT scan before RT or CCRT (after propensity score matching).

	Nonpretreatment PET–CT		Pretreatment PET–CT		*P* value	SMD
	N = 2778		N = 1389			
	N	%	N	%		
Age (mean ± SD)	61.81 ± 14.15		61.65 ± 13.95		0.224	0.051
Age, median (IQR), y	60.20 (51.00, 71.00)		60.00 (50.00, 70.00)		0.311	
Age					0.187	0.010
Age ≤ 40 y	612	22.03%	309	22.25%		
40 y < Age ≤ 50 y	833	29.99%	432	31.10%		
50 y < Age ≤ 60 y	667	24.01%	289	20.81%		
Age > 60 y	666	23.97%	359	25.85%		
Years of diagnosis					0.188	0.067
2008–2010	532	19.15%	241	17.35%		
2011–2014	1086	39.09%	531	38.23%		
2015–2018	1160	41.76%	617	44.42%		
CCI scores (mean ± SD)	0.41 ± 1.00		0.41 ± 0.88		0.709	0.017
CCI scores					0.371	0.016
0	2093	75%	1064	76.60%		
1	685	25%	325	23.40%		
AJCC stages	2778		1389		0.279	0.083
IB	437	15.73%	190	13.68%		
IIA	207	7.45%	90	6.48%		
IIB	891	32.07%	446	32.11%		
III	671	24.15%	346	24.91%		
IVA	566	20.37%	313	22.53%		
Missing	6	0.22%	4	0.29%		
Differentiation					0.220	0.072
I (well-differentiated)	84	3.02%	42	3.02%		
II (moderately differentiated)	1532	55.15%	814	58.60%		
III (poorly differentiated)	1089	39.20%	467	33.62%		

(Continued)

TABLE 1 Continued

	Nonpretreatment PET–CT		Pretreatment PET–CT		*P* value	SMD
	N = 2778		N = 1389			
	N	%	N	%		
IV (undifferentiated)	73	2.63%	66	2.38%		
Treatments					0.861	0.022
CCRT	2111	75.99%	1055	75.95%		
RT alone	667	24.01%	334	24.05%		
EBRT cumulative dose, Gy						
Mean (SD)	50.40 ± 18.70		50.40 ± 19.24		0.999	0.1000
Median (Q1–Q3)	50.40 (39.33, 60.00)		50.40 (46.00, 60.00)		0.999	
Chemotherapy, Platinum cumulative dose, mg						
Mean (SD)	632.33 ± 593.38		639.02 ± 577.10		0.753	0.011
Median (Q1–Q3)	500.00 (350.00, 600.0)		500.00 (350.00, 650.0)		0.224	
Brachytherapy dose, Gy						
Mean (SD)	24.68 ± 6.57		24.14 ± 6.55		0.717	0.014
Median (Q1–Q3)	25.00 (20.00, 30.00)		2500.00 (20.00, 30.00)		0.999	
Histological type					0.974	0.002
Adenocarcinoma	298	10.73%	150	10.80%		
Squamous cell carcinoma	2480	89.27%	1239	89.20%		
Medical centers					0.426	0.019
Nonmedical centers	1517	10.73%	745	53.64%		
Medical centers	1261	45.39%	644	46.36%		
Mean (SD) follow-up (y)	4.70 ± 2.83		4.72 ± 2.64		0.828	
Median (IQR) follow-up (y)	4.04 (1.27, 5.52)		4.07 (1.46, 5.54)		0.235	
All-cause death					<0.001	
No	1359	48.92%	755	54.36%		
Yes	1419	51.08%	634	45.64%		

PET–CT, positron emission tomography–computed tomography; AJCC, American Joint Committee on Cancer; CCI, Charlson comorbidity index; EBRT, external beam radiotherapy; RT, radiotherapy; CCRT, concurrent chemoradiotherapy; SD, standard deviation; IQR, interquartile range; y, years; SMD, standardized mean difference.

Stratified analysis of the effect of pretreatment PET–CT

To determine the effect of pretreatment PET–CT on various AJCC clinical stages, we stratified the stages (IB–IIA and III–IVA) by using a Cox regression model after adjustment for age, histology, tumor differentiation, AJCC clinical stages, treatments, cumulative EBRT dose, cumulative platinum dose, cumulative ICBT dose, CCI scores, diagnosis year, and hospital levels (Tables 3, 4). The prognostic factors were similar to those determined in the nonstage stratification analysis. Regardless of the cancer stage (early or advanced), pretreatment PET–CT was significantly superior to nonpretreatment PET–CT in terms of all-cause death (aHR, 0.78; 95% CI, 0.60–0.92; $P = 0.013$ and aHR, 0.90; 95% CI, 0.81–0.99; $P = 0.039$ for early and advanced stages, respectively). In the pretreatment and nonpretreatment groups, the 5-year OS was 54.56% and 50.11%, respectively, for all disease stages ($P < 0.001$); 71.87% and 64.92%, respectively, for stage IB–IIA disease ($P = 0.031$); and 50.73% and 46.832, respectively, for stage IIB–IVA disease ($P = 0.038$; Figures 1A–C). In both the groups, we noted the association of early- and advanced-stage cervical cancer treated with RT or CCRT with OS.

Discussion

Cervical cancer may metastasize to the pelvic or paraaortic lymph nodes as well as more distal nodes (14). Lymph node involvement is associated with poor prognosis and affects decisions regarding the design of RT fields (14). Whole-body FDG-PET–CT, in which both PET and CT are performed using an integrated PET–CT scanner, is the preferred imaging modality for detecting lymph node metastases (5, 6, 15). If the technology is not available, lymph nodes are evaluated

TABLE 2 Cox proportional hazard regression analysis of the risk of all-cause death in propensity score–matched patients with cervical cancer.

	Crude HR (95% CI)		*P* value	Adjusted HR (95% CI)		*P* value
Pretreatment PET–CT (ref. = No)						
Yes	0.88	(0.80, 0.96)	0.005	0.88	(0.80, 0.97)	0.010
Age (ref. Age ≤ 40 y)						
40 y < Age ≤ 50 y	1.02	(0.81, 1.15)	0.211	1.07	(0.76, 1.09)	0.233
50 y < Age ≤ 60 y	1.04	(0.81, 1.08)	0.376	1.08	(0.76, 1.12)	0.184
Age > 60 y	1.71	(1.51, 1.94)	<0.001	1.12	(1.07, 1.30)	0.014
CCI score (ref. = 0)						
≥1	1.65	(1.51, 1.82)	<0.001	1.37	(1.24, 1.52)	<0.001
Years of diagnosis (ref. = 2008–2010)						
2011–2014	0.96	(0.91, 1.24)	0.1157	0.99	(0.91, 1.18)	0.6025
2015–2018	0.97	(0.94, 1.21)	0.3046	0.98	(0.84, 1.12)	0.7025
AJCC stages (ref. = Stage IB)						
IIA	1.05	(1.01, 1.54)	0.030	1.39	(1.04, 1.86)	0.026
IIB	1.09	(1.04, 1.27)	0.046	1.38	(1.12, 1.70)	0.002
III	1.51	(1.25, 1.83)	<0.001	2.04	(1.68, 2.48)	<0.001
IVA	4.21	(3.50, 5.05)	<0.001	4.03	(3.32, 4.89)	<0.001
Treatment (ref. = CCRT)						
RT alone	2.51	(2.28, 2.77)	<0.001	1.91	(1.69, 2.16)	<0.001
Differentiation (ref. = Grade I)						
Grade II	1.01	(0.66, 1.28)	0.623	1.20	(0.85, 1.67)	0.297
Grade III	1.00	(0.72, 1.4)	0.986	1.12	(0.8, 1.57)	0.502
Grade IV	1.61	(0.91, 2.54)	0.343	1.38	(0.87, 2.21)	0.170
Histological type (ref. = Squamous cell carcinoma)						
Adenocarcinoma	1.77	(1.55, 2.01)	<0.001	1.75	(1.53, 2)	<0.001
Medical center (ref. = Nonmedical centers)						
Yes	0.89	(0.81, 1.97)	0.279	0.95	(0.86, 1.05)	0.3251
Brachytherapy (ref. = No brachytherapy)						
Yes	0.24	(0.22, 0.26)	<0.001	0.42	(0.38, 0.46)	<0.001

PET–CT, positron emission tomography–computed tomography; HR, hazards ratio; aHR, adjusted hazard ratio; CI, confidence interval; AJCC, American Joint Committee on Cancer; CCI, Charlson comorbidity index; RT, radiotherapy; CCRT, concurrent chemoradiotherapy; y, years.
*All covariates mentioned in Table 2 were adjusted.

through abdominopelvic CT with contrast (2). Pelvic MRI without or with contrast is another second-line alternative because its diagnostic performance is comparable to that of CT (2, 5, 6, 15). All women with cervical cancer should undergo a lymph node evaluation for appropriate staging and treatment (16, 17). For women with cervical cancer (stage IB–IVA) for whom primary RT or CCRT is planned, imaging prior to RT can be performed to evaluate the disease extent, with particular focus on lymph node metastases, to provide information necessary for designing RT fields (18, 19). A meta-analysis of 72 studies including 5042 patients with cervical cancer reported the following sensitivity and specificity values for the detection of lymph node metastasis: PET (75% and 98%), MRI (56% and 93%), and CT (58% and 92%), respectively (5). The more accurate detection of lymph nodes results in a more accurate RT field, thereby possibly contributing to OS benefits. However, studies have reported conflicting results regarding the association between OS and pretreatment PET in patients with cervical cancer (20–23). Only one short-term follow-up randomized controlled trial (RCT) including a small sample size and using conventional 2D-RT reported that pretreatment PET (instead of PET–CT) improved the detection of pelvic metastasis or paraaortic lymph nodes in patients with cervical cancer with pelvic lymph node positivity on pelvic MRI (AJCC stage III at least); however, the improved detection may not translate into a survival benefit (23). No study with an adequate sample size and a long-term follow-up and using a head-to-head PSM design mimicking the RCT has examined the survival benefit of

TABLE 3 Cox proportional hazard regression analysis of the risk of all-cause death in propensity score–matched patients with AJCC stage IB–IIA cervical cancer.

	Crude HR (95% CI)		*P* value	Adjusted HR (95% CI)		*P* value
Pretreatment PET–CT (ref. = No)						
Yes	0.74	(0.57, 0.95)	0.019	0.78	(0.60, 0.92)	0.013
Age (ref. Age ≤ 40 y)						
40 y < Age ≤ 50 y	1.04	(0.74, 1.48)	0.8091	1.05	(0.73, 1.49)	0.8064
50 y < Age ≤ 60 y	1.12	(0.77, 1.63)	0.5591	1.02	(0.69, 1.53)	0.9052
Age > 60 y	2.11	(1.54, 2.88)	<0.001	1.64	(1.12, 2.38)	0.0101
CCI score(ref. = 0)						
≥1	1.87	(1.48, 2.36)	<0.001	1.61	(1.26, 2.07)	<0.001
Years of diagnosis(ref. = 2008–2010)						
2011–2014	1.20	(0.86, 1.65)	0.281	1.16	(0.82, 1.65)	0.393
2015–2018	1.20	(0.85, 1.68)	0.301	1.02	(0.7, 1.50)	0.913
AJCC stage(ref. = Stage IB)						
IIA	1.16	(0.86, 1.56)	0.334	1.39	(1.01, 1.89)	0.040
Treatment(ref. = CCRT)						
RT alone	1.07	(0.56, 1.49)	0.373	1.04	(0.58, 1.11)	0.228
Differentiation(ref. = Grade I)						
Grade II	1.36	(0.50, 3.69)	0.543	2.81	(0.99, 7.97)	0.154
Grade III	1.37	(0.50, 3.76)	0.535	2.25	(0.79, 6.39)	0.129
Grade IV	2.07	(0.52, 8.29)	0.303	2.65	(0.64, 11.00)	0.179
Histological type(ref. = Squamous cell carcinoma)						
Adenocarcinoma	1.60	(1.17, 2.18)	0.0033	1.86	(1.34, 2.6)	0.0002
Medical center (ref. = No)						
Yes	0.76	(0.61, 1.15)	0.2182	0.77	(0.59, 1.19)	0.2439
Brachytherapy (ref. = No)						
Yes	0.22	(0.17, 0.27)	<0.001	0.31	(0.24, 0.4)	<0.001

PET–CT, positron emission tomography–computed tomography; HR, hazard ratio; aHR, adjusted hazard ratio; CI, confidence interval; AJCC, American Joint Committee on Cancer; CCI, Charlson comorbidity index; RT, radiotherapy; CCRT, concurrent chemoradiotherapy; y, years.
*All covariates mentioned in Table 2 were adjusted.

pretreatment PET–CT in patients with stage IB–IVA cervical cancer. In the current study including the largest sample size and a long-term follow-up and using modern RT techniques and PET facilities integrated with the CT scan, pretreatment PET–CT was significantly superior to nonpretreatment PET–CT in terms of all-cause death (aHR, 0.78; 95% CI, 0.60–0.92; $P = 0.013$ and aHR, 0.90; 95% CI, 0.81–0.99; $P = 0.039$ for early and advanced stages, respectively; Table 3).

This is the largest study using the head-to-head PSM design to balance potential confounding factors associated with mortality in patients with cervical cancer receiving IG-IMRT with or without pretreatment PET–CT. After PSM, all cofounding factors were balanced (Table 1). We believe that the selection bias would be minimal between the case and control groups. The results of multivariable Cox regression model analysis revealed that age > 60 years; advanced clinical stages of IIA, IIB, and IVA; RT alone; adenocarcinoma; CCI score ≥ 1; no ICBT; and nonpretreatment PET–CT were associated with poor OS. The poor prognostic factors are consistent with those reported by previous studies (24–27). Our study is the first to report poor prognostic factors for OS in patients with cervical cancer receiving the modern RT technique of IG-IMRT. Old age, advanced stages, RT alone, adenocarcinoma, CCI score ≥ 1, no IBCT, and nonpretreatment PET–CT were determined as poor prognostic factors for OS, even in the era of IG-IMRT. Moreover, although patients with cervical cancer were treated with the contemporary RT technique of IG-IMRT, ICBT was still necessary and IG-IMRT was insufficient as an alternative treatment to ICBT; this finding is consistent with that of a previous study (27).

Uncertainty regarding patient positioning requires clinicians to add extra margins to target volumes beyond those based on original tumor images (28–30). This uncertainty may be due to imprecision in patient positioning used on a daily basis, despite immobilization, or to

TABLE 4 Cox proportional hazard regression analysis of the risk of all-cause death in propensity score–matched patients with AJCC stage IIB–IVA cervical cancer.

	Crude HR (95% CI)		*P* value	Adjusted HR (95% CI)		*P* value
Pretreatment PET–CT (ref. = No)						
Yes	0.88	(0.80, 0.97)	0.014	0.90	(0.81, 0.99)	0.039
Age (ref. Age ≤ 40 y)						
40 y < Age ≤ 50 y	1.06	(0.75, 1.11)	0.054	1.03	(0.72, 1.06)	0.113
50 y < Age ≤ 60 y	0.88	(0.75, 1.03)	0.104	1.04	(0.72, 1.09)	0.135
Age > 60 y	1.65	(1.44, 1.89)	<0.001	1.04	(1.01, 1.22)	0.044
CCI score (ref. = 0)						
≥1	1.65	(1.49, 1.83)	<0.001	1.33	(1.19, 1.48)	<0.001
Years of Diagnosis (ref. = 2008–2010)						
2011–2014	1.12	(0.99, 1.27)	0.082	1.02	(0.89, 1.18)	0.747
2015–2018	1.08	(0.95, 1.23)	0.258	0.96	(0.82, 1.11)	0.562
AJCC stage (ref. = Stage IIB)						
III	1.16	(1.03, 2.93)	0.015	1.14	(1.09, 2.88)	0.036
IVA	2.67	(1.11, 6.43)	0.028	3.00	(1.24, 7.26)	0.014
Treatment (ref. = CCRT)						
RT alone	3.11	(2.79, 3.47)	<0.001	2.02	(1.76, 2.31)	<0.001
Differentiation (ref. = Grade I)						
Grade II	0.87	(0.61, 1.23)	0.432	1.10	(0.77, 1.57)	0.590
Grade III	0.93	(0.65, 1.32)	0.667	1.05	(0.73, 1.49)	0.809
Grade IV	1.55	(0.95, 2.52)	0.078	1.33	(0.81, 2.18)	0.265
Histological type (ref. = Squamous cell carcinoma)						
Adenocarcinoma	1.89	(1.64, 2.17)	<0.001	1.77	(1.52, 2.05)	<0.001
Medical center (ref. = Nonmedical centers)						
Medical centers	0.92	(0.84, 1.02)	0.109	0.99	(0.89, 1.11)	0.909
Brachytherapy (ref. = No)						
Yes	0.26	(0.24, 0.29)	<0.001	0.45	(0.4, 0.5)	<0.001

PET–CT, positron emission tomography–computed tomography; HR, hazard ratio; aHR, adjusted hazard ratio; CI, confidence interval; AJCC, American Joint Committee on Cancer; CCI, Charlson comorbidity index; RT, radiotherapy; CCRT, concurrent chemoradiotherapy; y, years.
*All covariates mentioned in Table 2 were adjusted.

inherent organ motion (28–30). During each treatment, the real-time imaging of the treatment target and normal organs allows for the minimization of such additional margins and the reduction of irradiated volumes, leading to a decreased risk of missing a target (28–30). This technology is collectively referred to as IGRT and employs various methods for real-time imaging and treatment adjustment. Refinements to 3D-CRT include IMRT and IGRT. Conformal therapy is generally used to reduce toxicity (28–30). The reduction in toxicity has enabled performing dose escalation trials for improving long-term tumor control or OS. Tsai et al. performed a RCT by including a small sample size and a short-term follow-up and demonstrated that pretreatment PET did not result in survival benefits but only enhanced the detection of extrapelvic metastasis, mainly paraaortic lymph nodes (23). These findings might be attributed to the use of old RT techniques (2D-RT) that resulted in more toxicity or insufficient irradiation doses to extrapelvic metastasis or paraaortic lymph nodes (23). However, compared with old RT techniques, such as 2D-RT, the dose escalation in IG-IMRT might result in less toxicity and more precision, leading to the accurate delineation of cervical cancer (31). Therefore, pretreatment PET–CT might be associated with longer OS compared with nonpretreatment PET–CT in the era of IG-IMRT.

In the future, a large and well-designed RCT may be necessary to confirm the survival benefit of pretreatment PET–CT for patients with stage IB–IVA cervical cancer receiving RT or CCRT in the era of IG-IMRT, although the inclusion of a control arm (nonpretreatment PET–CT) for patients with cervical cancer, especially for those with advanced stages, can be an ethical problem because of the accurate detection of extrapelvic metastasis or paraaortic lymph nodes (23). Owing to the difficulty in performing this type of RCT, a large

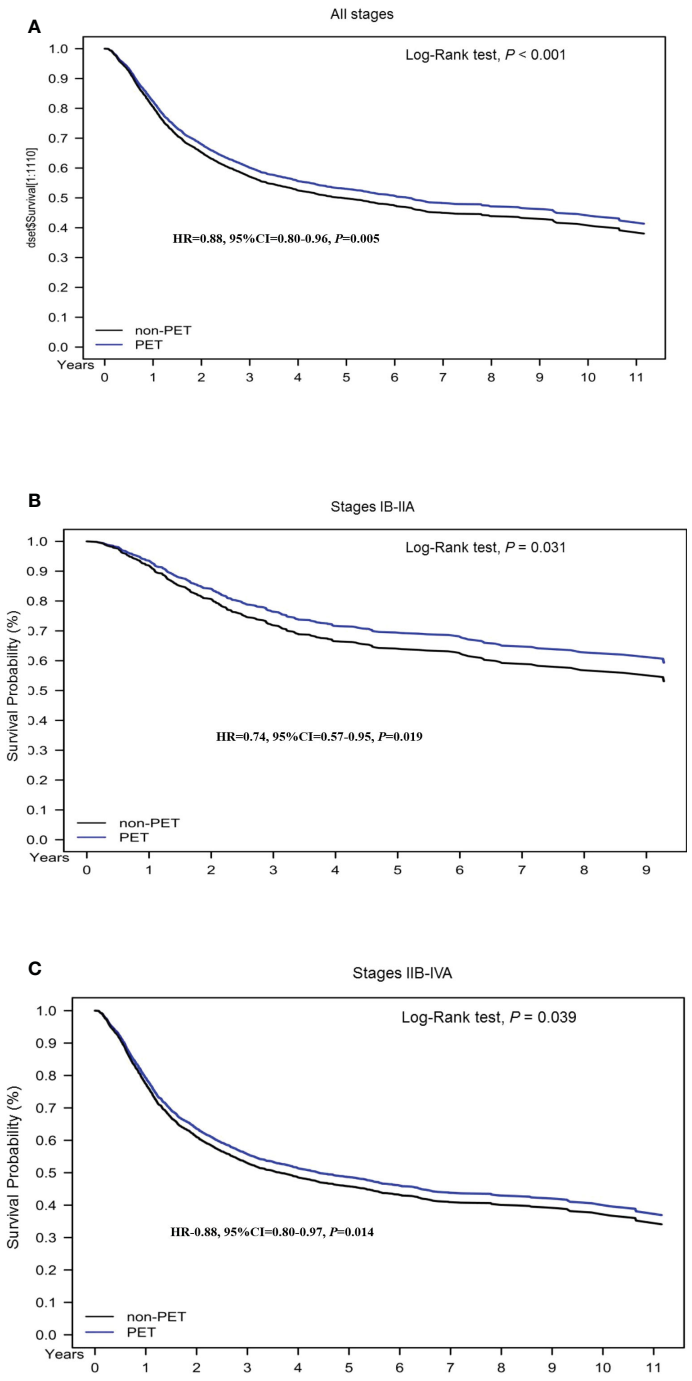

FIGURE 1
Kaplan–Meier overall survival curves for propensity score–matched patients with cervical cancer. **(A)** All stages; **(B)** stage IB–IIA; **(C)** stage IIB–IVA.

retrospective observational study might be necessary. However, in a large cohort, with in-depth postprocessing such as PSM, a retrospective study of an existing database without randomization cannot mimic a RCT, possibly resulting in a selection bias. Thus, a study with the PSM design can be performed to address the question regarding the use of available data and complement the lack of well-designed RCTs.

Our study strengths are as follows. This is the first, largest, long-term follow-up cohort study using a homogenous modality with integrated PET–CT to estimate the survival outcomes of pretreatment ^{18}This study investigated the effects of FDG-PET–CT or nonpretreatment PET–CT on patients with cervical cancer stratified by different clinical stages. Comparative reports for different clinical stages, sufficient sample sizes, long-term follow-up periods, homogenous ^{18}FDG-PET–CT modalities, and PSM design mimicking the RCT are lacking. In the present study, pretreatment ^{18}FDG-PET–CT was associated with survival benefits for the patients with stage IB–IVA cervical cancer. Our result suggests that

pretreatment ^{18}FDG-PET–CT is necessary for patients with cervical cancer receiving RT or CCRT, especially in the era of IG-IMRT. Our findings should be considered in future clinical practice and prospective clinical trials.

This study has some limitations. First, because all patients with cervical cancer were enrolled from the Asian population, the corresponding ethnic susceptibility compared with the non-Asian population remains unclear; hence, our results should be cautiously extrapolated to non-Asian populations. However, no evidence demonstrates differences in survival outcomes between Asian and non-Asian patients with cervical cancer receiving RT or CCRT. Second, although the main advantage of PSM is that it enables a more precise estimation of the intervention response, PSM cannot control for factors not accounted for in the model and is based on an explicit selection bias toward patients who could be matched (i.e., those who could not be matched are not part of the scope of inference). Third, we do not have data for young cervical cancer patients who may require fertility-sparing treatment, and this may limit the generalizability of our findings to this population. Fourth, the diagnoses of all comorbidities were based on *ICD-9-CM* or *ICD-10-CM* codes. However, the combination of the TCR and NHIRD appears to be a valid resource for population studies on comorbidities (32–34). Moreover, the TCR administration randomly reviews charts and interviews patients to verify the accuracy of diagnoses, and hospitals with outlier chargers or practices may be audited and subsequently heavily penalized if malpractice or discrepancies are identified. Despite these limitations, a major strength of the present study is the use of a nationwide population-based registry with detailed baseline and treatment information. Lifelong follow-up was possible through the linkage of the registry with the national Cause of Death database. Considering the magnitude and statistical significance of the observed effects in the current study, the limitations are unlikely to affect our conclusions.

Conclusion

Pretreatment ^{18}FDG-PET–CT might be associated with longer survival in patients with stage IB–IVA cervical cancer receiving RT or CCRT, especially in the era of IG-IMRT.

Data availability statement

The raw data supporting the conclusions of this article will be made available by the authors, without undue reservation.

Ethics statement

The study protocols were reviewed and approved by the Institutional Review Board of Tzu-Chi Medical Foundation (IRB109-015-B). Written informed consent for participation was not required for this study in accordance with the national legislation and the institutional requirements.

Author contributions

Conception and design, W-MC, MC, B-CS, and S-YW. Financial support, Lo-Hsu Medical Foundation, LotungPoh-Ai Hospital, supports S-YW's work (Funding Number: 11001, 11010, 11013 and 11103). Collection and assembly of data, W-MC, B-CS, and S-YW. Data analysis and interpretation, W-MC, B-CS, and S-YW. Administrative support, S-YW. Manuscript writing, W-MC. Final approval of manuscript, all authors. All authors contributed to the article and approved the submitted version.

Funding

Lo-Hsu Medical Foundation, LotungPoh-Ai Hospital, supports S-YW's work (Funding Number: 11001, 11010, 11013 and 11103).

Conflict of interest

The authors declare that the research was conducted in the absence of any commercial or financial relationships that could be construed as a potential conflict of interest.

Publisher's note

References

1. Sung H, Ferlay J, Siegel RL, Laversanne M, Soerjomataram I, Jemal A, et al. Global cancer statistics 2020: GLOBOCAN estimates of incidence and mortality worldwide for 36 cancers in 185 countries. *CA Cancer J Clin* (2021) 71:209–49. doi: 10.3322/caac.21660

2. Oncology N.C.P.G.I. *NCCN clinical practice guidelines in oncology: Cervical cancer* (2021). 94 N Woodhull Rd, Huntington, NY 11743: Harborside Press, LLC (Accessed 10/26/2021).

3. Narayanan P, Sahdev A. The role of (18)F-FDG PET CT in common gynaecological malignancies. *Br J Radiol* (2017) 90:20170283. doi: 10.1259/bjr.20170283

4. Gee MS, Atri M, Bandos AI, Mannel RS, Gold MA, Lee SI. Identification of distant metastatic disease in uterine cervical and endometrial cancers with FDG PET/CT: Analysis from the ACRIN 6671/GOG 0233 multicenter trial. *Radiology* (2018) 287:176–84. doi: 10.1148/radiol.2017170963

5. Selman TJ, Mann C, Zamora J, Appleyard TL, Khan K. Diagnostic accuracy of tests for lymph node status in primary cervical cancer: A systematic review and meta-analysis. *CMAJ* (2008) 178:855–62. doi: 10.1503/cmaj.071124

6. Atri M, Zhang Z, Dehdashti F, Lee SI, Ali S, Marques H, et al. Utility of PET-CT to evaluate retroperitoneal lymph node metastasis in advanced cervical cancer: Results of ACRIN6671/GOG0233 trial. *Gynecol Oncol* (2016) 142:413–9. doi: 10.1016/j.ygyno.2016.05.002

7. Leblanc E, Gauthier H, Querleu D, Ferron G, Zerdoud S, Morice P, et al. Accuracy of 18-fluoro-2-deoxy-D-glucose positron emission tomography in the pretherapeutic detection of occult para-aortic node involvement in patients with a locally advanced cervical carcinoma. *Ann Surg Oncol* (2011) 18:2302–9. doi: 10.1245/s10434-011-1583-9

8. Ramirez PT, Jhingran A, Macapinlac HA, Euscher ED, Munsell MF, Coleman RL, et al. Laparoscopic extraperitoneal para-aortic lymphadenectomy in locally advanced cervical cancer: A prospective correlation of surgical findings with positron emission tomography/computed tomography findings. *Cancer* (2011) 117:1928–34. doi: 10.1002/cncr.25739

9. Chang CL, Yuan KS, Wu SY. High-dose or low-dose cisplatin concurrent with radiotherapy in locally advanced head and neck squamous cell cancer. *Head Neck* (2017) 39:1364–70. doi: 10.1002/hed.24763

10. Lin KC, Chen TM, Yuan KS, Wu ATH, Wu SY. Assessment of predictive scoring system for 90-day mortality among patients with locally advanced head and neck squamous cell carcinoma who have completed concurrent chemoradiotherapy. *JAMA Netw Open* (2020) 3:e1920671. doi: 10.1001/jamanetworkopen.2019.20671

11. Liu WC, Liu HE, Kao YW, Qin L, Lin KC, Fang CY, et al. Definitive intensity-modulated radiotherapy or surgery for early oral cavity squamous cell carcinoma: Propensity-score-matched, nationwide, population-based cohort study. *Head Neck* (2020) 43:1142–52. doi: 10.1016/j.radonc.2020.08.016

12. Zhang Z, Kim HJ, Lonjon G, Zhu YWritten on Behalf Of, A.M.E.B.-D.C.T.C.GBalance diagnostics after propensity score matchingB*Ann Transl Med* (2019) 7:16. doi: 10.21037/atm.2018.12.10

13. Austin PC. Optimal caliper widths for propensity-score matching when estimating differences in means and differences in proportions in observational studies. *Pharm Stat* (2011) 10:150–61. doi: 10.1002/pst.433

14. Singh N, Arif S. Histopathologic parameters of prognosis in cervical cancer–a review. *Int J Gynecol Cancer* (2004) 14:741–50. doi: 10.1111/j.1048-891X.2004.014504.x

15. Sironi S, Buda A, Picchio M, Perego P, Moreni R, Pellegrino A, et al. Lymph node metastasis in patients with clinical early-stage cervical cancer: detection with integrated FDG PET/CT. *Radiology* (2006) 238:272–9. doi: 10.1148/radiol.2381041799

16. Bhatla N, Berek JS, Cuello Fredes M, Denny LA, Grenman S, Karunaratne K, et al. Revised FIGO staging for carcinoma of the cervix uteri. *Int J Gynaecol. Obstet.* (2019) 145:129–35. doi: 10.1002/ijgo.12749

17. Olawaiye AB, Baker TP, Washington MK, Mutch DG. The new (Version 9) American joint committee on cancer tumor, node, metastasis staging for cervical cancer. *CA Cancer J Clin* (2021) 71:287–98. doi: 10.3322/caac.21663

18. Varia MA, Bundy BN, Deppe G, Mannel R, Averette HE, Rose PG, et al. Cervical carcinoma metastatic to para-aortic nodes: extended field radiation therapy with concomitant 5-fluorouracil and cisplatin chemotherapy: A gynecologic oncology group study. *Int J Radiat Oncol Biol Phys* (1998) 42:1015–23. doi: 10.1016/S0360-3016(98)00267-3

19. Du XL, Sheng XG, Jiang T, Yu H, Yan YF, Gao R, et al. Intensity-modulated radiation therapy versus para-aortic field radiotherapy to treat para-aortic lymph node metastasis in cervical cancer: Prospective study. *Croat. Med J* (2010) 51:229–36. doi: 10.3325/cmj.2010.51.229

20. Grigsby PW, Siegel BA, Dehdashti F. Lymph node staging by positron emission tomography in patients with carcinoma of the cervix. *J Clin Oncol* (2001) 19:3745–9. doi: 10.1200/JCO.2001.19.17.3745

21. Kidd EA, Siegel BA, Dehdashti F, Grigsby PW. Pelvic lymph node f-18 fluorodeoxyglucose uptake as a prognostic biomarker in newly diagnosed patients with locally advanced cervical cancer. *Cancer* (2010) 116:1469–75. doi: 10.1002/cncr.24972

22. Kidd EA, Siegel BA, Dehdashti F, Rader JS, Mutch DG, Powell MA, et al. Lymph node staging by positron emission tomography in cervical cancer: relationship to prognosis. *J Clin Oncol* (2010) 28:2108–13. doi: 10.1200/JCO.2009.25.4151

23. Tsai CS, Lai CH, Chang TC, Yen TC, Ng KK, Hsueh S, et al. A prospective randomized trial to study the impact of pretreatment FDG-PET for cervical cancer patients with MRI-detected positive pelvic but negative para-aortic lymphadenopathy. *Int J Radiat Oncol Biol Phys* (2010) 76:477–84. doi: 10.1016/j.ijrobp.2009.02.020

24. Wu S-Y, Huang E-Y, Lin H. Optimal treatments for cervical adenocarcinoma. *Am J Cancer Res* (2019) 9:1224–34.

25. Zhang J, Qin L, Chen HM, Hsu HC, Chuang CC, Chen D, et al. Outcome patterns of cervical adenocarcinoma and squamous cell carcinoma following curative surgery: Before and after propensity score matching analysis of a cohort study. *Am J Cancer Res* (2020) 10:1793–807.

26. Zhang J, Qin L, Chen HM, Hsu HC, Chuang CC, Chen D, et al. Overall survival, locoregional recurrence, and distant metastasis of definitive concurrent chemoradiotherapy for cervical squamous cell carcinoma and adenocarcinoma: before and after propensity score matching analysis of a cohort study. *Am J Cancer Res* (2020) 10:1808–20.

27. Zhang J, Sun M, Li N, Miao M, Yang Y, Hsu HC, et al. Contemporary external beam radiotherapy boost or high dose-rate brachytherapy boost for cervical cancer: a propensity-score-matched, nationwide, population-based cohort study. *Am J Cancer Res* (2021) 11:1719–32.

28. Guerrero Urbano MT, Nutting CM. Clinical use of intensity-modulated radiotherapy: part I. *Br J Radiol* (2004) 77:88–96. doi: 10.1259/bjr/84246820

29. Pow EH, Kwong DL, Mcmillan AS, Wong MC, Sham JS, Leung LH, et al. Xerostomia and quality of life after intensity-modulated radiotherapy vs. conventional radiotherapy for early-stage nasopharyngeal carcinoma: initial report on a randomized controlled clinical trial. *Int J Radiat Oncol Biol Phys* (2006) 66:981–91. doi: 10.1016/j.ijrobp.2006.06.013

30. Garden AS, Morrison WH, Wong PF, Tung SS, Rosenthal DI, Dong L, et al. Disease-control rates following intensity-modulated radiation therapy for small primary oropharyngeal carcinoma. *Int J Radiat Oncol Biol Phys* (2007) 67:438–44. doi: 10.1016/j.ijrobp.2006.08.078

31. Chang CL, Tsai HC, Lin WC, Chang JH, Hsu HL, Chow JM, et al. Dose escalation intensity-modulated radiotherapy-based concurrent chemoradiotherapy is effective for advanced-stage thoracic esophageal squamous cell carcinoma. *Radiother Oncol* (2017) 125:73–9. doi: 10.1016/j.radonc.2017.08.025

32. Lin CC, Lai MS, Syu CY, Chang SC, Tseng FY. Accuracy of diabetes diagnosis in health insurance claims data in Taiwan. *J Formos. Med Assoc* (2005) 104:157–63. doi: 10.1002/pds.2087

33. Cheng CL, Kao YH, Lin SJ, Lee CH, Lai ML. Validation of the national health insurance research database with ischemic stroke cases in Taiwan. *Pharmacoepidemiol Drug Saf* (2011) 20:236–42. doi: 10.2188/jea.je20140076

34. *SEER cancer stat facts: Cervix uteri cancer* (2017). Available at: https://seer.cancer.gov/statfacts/html/cervix.html (Accessed February 11, 2017).

frontiers | Frontiers in Oncology

TYPE Original Research
PUBLISHED 16 February 2023
DOI 10.3389/fonc.2023.1100087

OPEN ACCESS

EDITED BY
Alessio G. Morganti,
University of Bologna, Italy

REVIEWED BY
Xin Cao,
Northwest University, China
Milly Buwenge,
University of Bologna, Italy

*CORRESPONDENCE
Yu Zhang
yuzhang@smu.edu.cn

†These authors have contributed equally to this work and share first authorship

SPECIALTY SECTION
This article was submitted to Gynecological Oncology, a section of the journal Frontiers in Oncology

RECEIVED 16 November 2022
ACCEPTED 01 February 2023
PUBLISHED 16 February 2023

CITATION
Wang J, Mao Y, Gao X and Zhang Y (2023) Recurrence risk stratification for locally advanced cervical cancer using multi-modality transformer network. *Front. Oncol.* 13:1100087. doi: 10.3389/fonc.2023.1100087

Recurrence risk stratification for locally advanced cervical cancer using multi-modality transformer network

Jian Wang[1,2†], Yixiao Mao[1,2†], Xinna Gao[3] and Yu Zhang[1,2*]

[1]School of Biomedical Engineering, Southern Medical University, Guangzhou, Guangdong, China, [2]Guangdong Provincial Key Laboratory of Medical Image Processing, Southern Medical University, Guangzhou, Guangdong, China, [3]Department of Radiation Oncology, Southern Medical University Nanfang Hospital, Guangzhou, Guangdong, China

Objectives: Recurrence risk evaluation is clinically significant for patients with locally advanced cervical cancer (LACC). We investigated the ability of transformer network in recurrence risk stratification of LACC based on computed tomography (CT) and magnetic resonance (MR) images.

Methods: A total of 104 patients with pathologically diagnosed LACC between July 2017 and December 2021 were enrolled in this study. All patients underwent CT and MR scanning, and their recurrence status was identified by the biopsy. We randomly divided patients into training cohort (48 cases, non-recurrence: recurrence = 37: 11), validation cohort (21 cases, non-recurrence: recurrence = 16: 5), and testing cohort (35 cases, non-recurrence: recurrence = 27: 8), upon which we extracted 1989, 882 and 315 patches for model's development, validation and evaluation, respectively. The transformer network consisted of three modality fusion modules to extract multi-modality and multi-scale information, and a fully-connected module to perform recurrence risk prediction. The model's prediction performance was assessed by six metrics, including the area under the receiver operating characteristic curve (AUC), accuracy, f1-score, sensitivity, specificity and precision. Univariate analysis with F-test and T-test were conducted for statistical analysis.

Results: The proposed transformer network is superior to conventional radiomics methods and other deep learning networks in both training, validation and testing cohorts. Particularly, in testing cohort, the transformer network achieved the highest AUC of 0.819 ± 0.038, while four conventional radiomics methods and two deep learning networks got the AUCs of 0.680 ± 0.050, 0.720 ± 0.068, 0.777 ± 0.048, 0.691 ± 0.103, 0.743 ± 0.022 and 0.733 ± 0.027, respectively.

Conclusions: The multi-modality transformer network showed promising performance in recurrence risk stratification of LACC and may be used as an effective tool to help clinicians make clinical decisions.

KEYWORDS

cervical cancer, recurrence risk stratification, multi-modality data, deep learning, transformer network

1 Introduction

Cervical cancer is one of the most common malignancies in females worldwide, which ranks as the 4th leading cause of death among cancers in women (1). Locally advanced cervical cancer (LACC), as the cervical cancer in IB2, IIA2 and IIB~IVA stages, is generally considered as a local mass with the size larger than 4cm or invades the surrounding tissues, in which distant metastasis does not occur (1). In clinical practices, the treatment for patients with LACC does not follow the same pattern (2). Most LACC patients are routinely treated with concurrent chemoradiation therapy, and the prognosis is heterogeneous (3). Despite neoadjuvant and adjuvant therapies are being tentatively introduced into the treatment regimen, the overall outcomes are not significantly improved (4, 5). The potential reason may be associated with the small-scale cohorts benefited from the neoadjuvant and adjuvant treatments, and all of these patients are from the high-risk recurrence group (6). Therefore, an interesting and crucial topic is to accurately predict recurrence risk so as to formulate the individualized therapeutic schedule for LACC patients.

With the rapid development of imaging techniques, imaging examinations has been considered as a routine for patients with cervical cancer. Currently, several studies have conducted recurrence and prognosis analysis for cervical cancer by extracting and evaluating high-throughput imaging features (7, 8). For example, some work has carried out texture analysis based on positron emission tomography (PET) or magnetic resonance (MR) images to predict the recurrence risk of cervical cancer (9, 10). In addition, the ultrasound (US) and computed tomography (CT) images were also used in recurrence-related tasks, such as lymph node metastasis prediction and survival assessment (11, 12). However, few studies have tried to focus on the recurrence risk stratification of LACC. Moreover, previous methods only utilized the information from mono-modality data and did not take multi-modality complementary information into consideration. Consequently, it is desirable to design an efficient model to make full use of multi-modality data (*i.e.*, CT and MR images) for accurately stratifying the recurrence status of LACC.

In recent years, deep learning has demonstrated its superiority over conventional radiomics methods based on hand-crafted features (13), and it avoids the complex hand-crafted feature extraction (14). Transformer, as one of the most popular deep learning architectures, has been successfully applied to various medical image analysis tasks and shows promising performance (15–17). In this study, we investigated the ability of transformer network in recurrence risk stratification of LACC by using non-contrast enhanced CT images and T1-Weighted MR images. Specifically, the transformer network consisted of three modality fusion modules to extract multi-modality and multi-scale information, and a fully-connected module to perform recurrence risk prediction. The performance of the model was assessed by six metrics. The results showed that our proposed model significantly outperformed the conventional radiomics methods.

Abbreviations: LACC, locally advanced cervical cancer; CT, computed tomography; MR, magnetic resonance; AUC, the area under the receiver operating characteristic curve; CI, confidence interval; PET, positron emission tomography; US, ultrasound; FIGO, International Federation of Gynecology and Obstetrics; VOI, volume of interest; BN, batch normalization; MLP, multi-layer perceptron; ViT, vision transformer; KNN, k-nearest neighbor; SVM, support vector machine; CPU, Central Processing Unit; GPU, Graphics Processing Unit; ROC, receiver operating characteristic; ESUR, European Society of Urogenital Radiology.

2 Materials and methods

2.1 Patients

This study was approved by the Institutional Review Board, and written informed consent requirement was waived. Totally, 104 patients with pathologically diagnosed LACC between July 2017 and December 2021 were retrospectively enrolled. For all participants, the inclusion criteria were as follows: (1) patients who pathologically confirmed LACC; (2) patients who underwent radiotherapy as the main treatment; (3) patients who underwent both CT and MR examinations within three weeks before radiotherapy. The exclusion criteria were as follows: (1) external irradiation treatment was interrupted for more than one month; (2) the radiation dose to tumor was less than 80Gy; (3) surgery was performed before radiotherapy. All enrolled participants with matched multi-modality data were randomly divided into training and testing cohorts at a ratio of 2: 1 to develop and assess the network, respectively.

Recurrent tumors were classified into local, regional, or distant progressive tumors after concurrent chemoradiotherapy was completed. Clinical follow-up exams of the patients were performed every 3 months until 36 months. Physical examination and tumor markers were checked. Imaging examination of pelvic MRI (CT for special patients) was performed when suspected of recurrence and the biopsy was performed for confirmation.

The clinicopathologic data of all enrolled patients, including age, tumor stage (FIGO 2009[1]), pathologic diagnosis, lymph node status and dose of radiotherapy, were obtained from medical records for statistical analysis and the recurrence status of all patients was also followed up.

2.2 CT and MR image acquisition

The CT images were collected from the CT scanner (Philips Healthcare, Best, The Netherlands). The scanning current and voltage were 300 mAs and 120 kV, respectively. Both slice thickness and slice distance were set to 3 mm, and the resolution was 512×512 pixels. The scanning range of CT was from the diaphragm to the proximal femur. The MR images were acquired from four MR scanners: an Achieva 3T MR scanner (Philips Medical Systems, Best, The Netherlands), with the repetition time of 431.5-697.4 msec, echo time of 10 msec, slice thickness of 5 mm, flip angle of 90°, percentage phase field of view of 100%, and matrix of 320×320 or 560×560; an Ingenia 3T MR scanner (Philips, Best, The Netherlands), with the repetition time of 431.5-

1 Since the data were collected from 2017, we uniformly used the FIGO 2009 staging system instead of the newly revised FIGO 2018.

697.4 msec, echo time of 10 msec, slice thickness of 5 mm, flip angle of 90°, percentage phase field of view of 100%, and matrix of 320×320 or 560×560; a Signa HDxt 1.5T MR scanner (GE Medical Systems, Milwaukee, Wis, USA), with the repetition time of 200-620 msec, echo time of 8.104 msec, slice thickness of 6 mm, flip angle of 90°, percentage phase field of view of 100%, and matrix of 512×512; an OPTIMA MR360 1.5T MR scanner (GE Healthcare, Milwaukee, Wis, USA), with the repetition time of 393-1179 msec, echo time of 12.36 msec, slice thickness of 5-7.5 mm, flip angle of 90°, percentage phase field of view of 100%, and matrix of 512×512. The scanning range of MR scanners was the whole pelvic area.

2.3 Imaging registration and VOI segmentation

In this study, we mainly focused on the imaging information of the primary tumor regions for recurrence risk stratification. The lymph node status was not included in the model. The specific reason is that the patients included in this study were all patients who had not undergone surgery, and there was no gold standard (pathological result) to verify the presence of lymph node metastasis. Previous studies (18, 19) have also shown that it is sufficient to use only the imaging information of primary lesions for cancer prognosis analysis, and the method selection of this study is generally in line with the previous research norms.

We chose non-contrast enhanced CT and T1-weighted MR images to carry out imaging analysis and used T1-weighted MR to contour the tumor. The main reason is that MR imaging has higher soft-tissue contrast resolution, so cervical cancer, which originates in the pelvis and is mixed with surrounding soft tissues, can be well identified. In order to ensure that the primary lesion area can be accurately located in CT images, we registered them with the MR images and then used the VOIs (*i.e.*, primary tumor regions) of MR images to extract lesion regions in both registered CT images and original MR images. Specifically, as shown in Figure 1, we first cropped CT images to focus on the pelvic area, and then aligned cropped CT images to the MR images via elastic registration (3D Slicer software 4.11). The VOIs were manually delineated on T1-weighted MR images by using ITK-SNAP 3.6 (ITK-SNAP 3.x Team, www.itksnap.org) by a radiologist with 10 years of experience.

2.4 Patch extraction

The lesion regions of all patients were resampled into a volume with the specified resolution of 86×86×12, and then zero-mean normalization was applied to each volume for image standardization so as to eliminate the bias introduced by inconsistent imaging parameters (20). Subsequently, each volume was split into nine patches with the size of 32×32×12, in which adjacent patches had 5-voxel overlap alone coronal and sagittal directions. Finally, paired multi-modality patches were taken as the input of transformer network for recurrence risk prediction.

2.5 Transformer network

The flow chart of transformer network is shown in Figure 1. The transformer network was composed of three modality fusion modules and a fully-connected module. The modality fusion module (as shown in Figure 2) consisted of two spatial pyramid units and a transformer unit. The former was used to extract the multi-scale image features effectively. The spatial pyramid features were obtained by utilizing three paralleled 3×3×3 convolutional layers with the dilation rates of 1, 3 and 5, respectively. Then, a pixel-wise summation operator and a 1×1×1 convolution layer were used to aggregate these features. In order to avoid gradient vanishing and accelerate convergence, a batch normalization (BN) layer and a Leaky ReLU nonlinearity operation were plugged after each convolutional layer. Subsequently, a

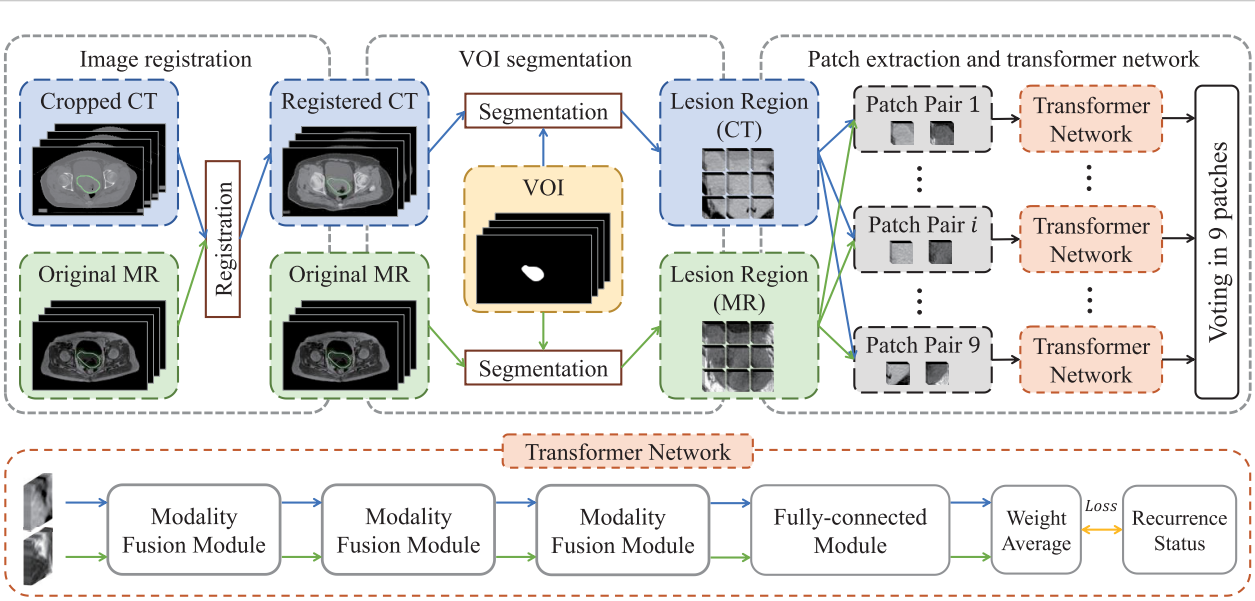

FIGURE 1
The flow chart of the proposed model for the recurrence risk stratification of LACC.

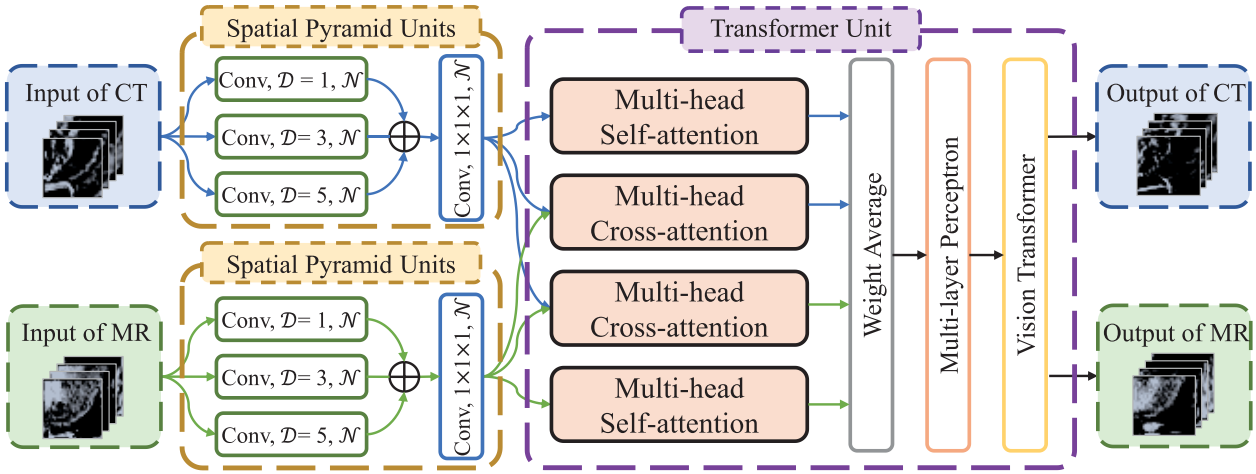

FIGURE 2
The architecture of modality fusion module. *D* is dilation rate in the convolutional layers and *N* is the number of convolutional kernels, which is set to 4, 8 and 16, respectively, in the three modality fusion modules.

transformer unit was utilized to capture semantic features between two modalities data (21). Specifically, we performed two multi-head self-attention operations for each modality to learn modality-specific information, and two multi-head cross-attention operations to extract complementary features from the other modality. Afterwards, weight average operator was adopted to aggregate all feature maps, and the weights of different features were learned automatically. A multi-layer perceptron (MLP) layer and a vision transformer (ViT) unit (17) were then applied to further extract semantic representations. Subsequently, CT and MR features were fed into the fully-connected module that contained a global average pooling layer, three stacked fully-connected layers (with the node number of 8, 4, 1, respectively) and a Sigmoid activation function to generate the patch-level predictions for CT and MR images, respectively. Another weight average operation was then used to aggregate the predicted probabilities of two modalities. Finally, we adopted the voting strategy to integrate the predicted probabilities of nine paired patches to obtain patient-level recurrence risk prediction.

2.6 Conventional radiomics methods and deep neural networks

To verify the effectiveness of our method, we compared the proposed method with some conventional radiomics methods and deep neural networks. For conventional radiomics methods, followed by (22), we extracted 4 non-texture features (including volume, size, solidity and eccentricity) and 10320 texture features from each modality for each patient. Subsequently, we utilized a filter-based feature selection method, namely Relief algorithm (23), to select the features with the best distinguishing power. The selected features were then used to construct the decision tree classifier (24), naive bayes classifier (25), k-nearest neighbor (KNN) classifier (26) and support vector machine (SVM) classifier (27), respectively, for recurrence risk prediction. For comparison with deep neural networks, we reproduced ResNet18 (28) and MobileNetV1 (29) networks. We employ the same data preprocessing strategy as the proposed method, and then utilized the input-level fusion strategy to fuse multi-modality images into deep networks by multi-channel.

2.7 Implementation details and statistical analysis

We conducted data augmentation strategy (*i.e.*, random affine transformation) to generate sufficient images to train the transformer network so as to alleviate the overfitting and data imbalance issues (30). Specifically, all VOIs were first scaled to the volume with the size of 560×560×20 and then underwent rotation (within π/18, π/18, π/4 in the coronal, sagittal and transverse sections, respectively) and zoom (between 0.75 and 1.25) operations, followed by patch extraction. For each method, we randomly divided the training and validation sets five times to verify the robustness of the method. In the training stage, we utilized binary cross entropy as the loss function and recurrence status as the label. And Kaiming initialization (31) and Adam optimizer (32) were adopted to initialize and optimize model's parameters. The model was complemented under the PyTorch (version 1.10.1) based on Python (version 3.8.0). All intensive calculations were offloaded to a workstation with Central Processing Unit (CPU) of Intel(R) Xeon(R) CPU E5-2623 v3 @ 3.00GHz, Graphics Processing Unit (GPU) of NVIDIA Pascal Titan X, and 125 GB RAM. The conventional radiomics model was carried out by MATLAB software (version 2020a).

Continuous variables were expressed as means (standard deviation), and categorical data were expressed as numbers (percentage). The model's prediction performance was assessed by six metrics, including the area under the receiver operating characteristic curve (AUC), accuracy, f1-score, sensitivity, specificity and precision. Univariate analysis with F-test was conducted to compare differences between clinical variables and recurrence status of LACC, while T-test for the difference comparison of AUCs, and significant difference was defined by $P < 0.05$. All statistical analyses were implemented using R software (version 4.0.2).

3 Results

3.1 Clinical characteristics

The clinical baseline characteristics of the enrolled participants are shown in Table 1. The inclusion and exclusion criteria are shown in Figure 3 (left). To develop and assess the proposed model, the enrolled patients were randomly divided into the training cohort and testing cohort with an approximate ratio of 2: 1. Then, in the training cohort, we further portioned two-thirds samples for training the network and the rest for validating the network, respectively. We performed three-fold augmentation for non-recurrence cases and ten-fold augmentation for recurrence cases in the training set to bridge the quantitative gap between two categories. Totally, 1989 (non-recurrence: recurrence = 999: 990), 882 (non-recurrence: recurrence = 432: 450) and 315 (non-recurrence: recurrence = 243: 72) patches were generated from training, validation and testing cohorts. The flow chart of the study is shown in Figure 3 (right). The all cohorts maintained the same class distribution.

3.2 Training process and prediction performance of transformer network

The training process of transformer network is shown in Figure 4, which suggests that the loss of model gradually converged and the accuracy gradually stabilized as iterations number increased. The

TABLE 1 Clinical characteristics of recurrence and non-recurrence cohorts.

	Total	Non-recurrence cohort	Recurrence cohort	P-value*
Number	N = 104	N = 80	N = 24	
Characteristics				
Age (year)	56.68 (8.88)	55.24 (7.89)	59.00 (10.12)	0.2023
FIGO[1] (2009 stage)				0.0008
IB2	5	5 (100%)	0 (0%)	
IIA1	3	3 (100%)	0 (0%)	
IIA2	9	8 (89%)	1 (11%)	
IIB	46	37 (80%)	9 (20%)	
IIIA	7	6 (86%)	1 (14%)	
IIIB	30	21 (70%)	9 (30%)	
IVA	2	0 (0%)	2 (100%)	
IVB	1	0 (0%)	1 (100%)	
Unknown	1	0 (0%)	1 (100%)	
Pathologic diagnosis				0.9002
Squamous cell carcinoma	96	74 (77%)	22 (23%)	
Adenocarcinoma	4	3 (75%)	1 (25%)	
Unknown	4	3 (75%)	1 (25%)	
Lymph node status				0.2674
Pelvic + Retroperitoneal	33	24 (73%)	9 (27%)	
Pelvic + groin	2	1 (50%)	1 (50%)	
Pelvic	15	11 (73%)	4 (27%)	
Retroperitoneal	3	2 (67%)	1 (33%)	
Unknown	51	42 (82%)	9 (18%)	
Dose of radiotherapy				0.8471
45Gy/25F	9	7 (78%)	2 (22%)	
45-60Gy/25F	6	6 (100%)	0 (0%)	
50.4Gy/28F	2	2 (100%)	0 (0%)	
50.4-60Gy/28F	46	31 (67%)	15 (33%)	
Unknown	41	34 (83%)	7 (17%)	

[1] FIGO, International Federation of Gynecology and Obstetrics.
* P-value is derived from the univariate analysis with F-test.

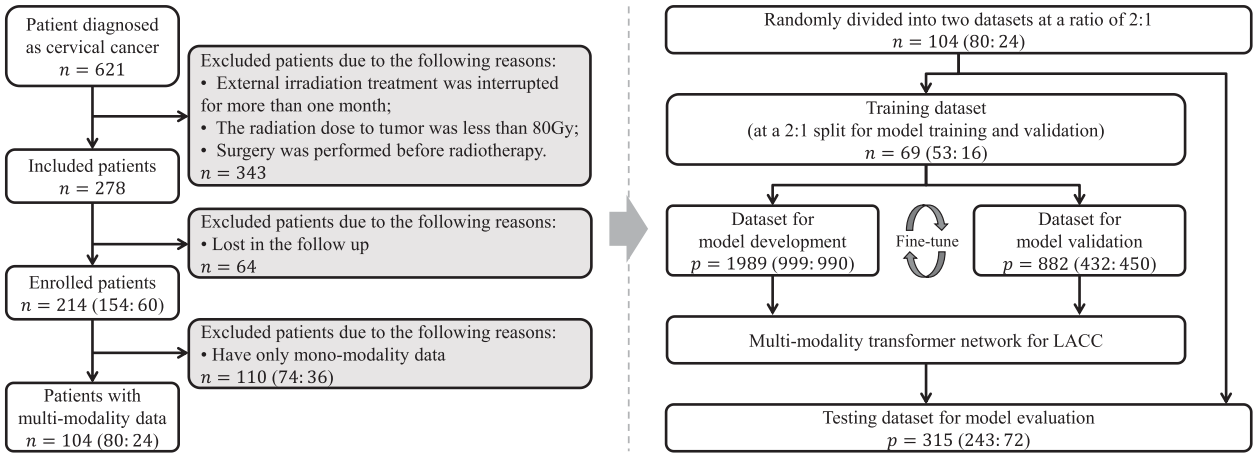

FIGURE 3
Patient inclusion and exclusion criteria, and the study flow chart.

prediction performance of transformer network on recurrence risk prediction of LACC is listed in Table 2. From Table 2, we can observe that the transformer network can accurately predict the recurrence status of all samples in the training cohort. Meanwhile, it achieved good performance with AUC of 0.819 ± 0.038, accuracy of 0.869 ± 0.023, f1-score of 0.914 ± 0.016, sensitivity of 0.911 ± 0.038, specificity of 0.725 ± 0.094 and precision of 0.919 ± 0.025 in the testing cohort.

3.3 Comparison with conventional radiomics methods and deep neural networks

We compared the proposed transformer network with conventional radiomics methods and deep neural networks. The results are shown in Table 2. We can find that the transformer network is generally superior to other methods in both training, validation and testing cohorts. Particularly, in testing cohort, the transformer network achieved the highest AUC of 0.819 ± 0.038, while conventional radiomics methods got the AUCs of 0.680 ± 0.050, 0.720 ± 0.068, 0.777 ± 0.048 and 0.691 ± 0.103, respectively. The AUCs of the ResNet18 and MobileNetV1 were 0.743 ± 0.022 and 0.733 ± 0.027, respectively, which did not show competitive performances. We analyzed that these two classical networks both used the input-level modality fusion strategy, which made it difficult to establish the intrinsic relationship between different modalities of the same patient, resulting in the degradation of the model performance (15). By contrast, we adopted the transformer structure, and used its unique attention mechanism to fully learn the complementary information between modalities and mined discriminative semantic features. Therefore, the proposed model was more accurate and robust. Figure 5 (left) plots the ROC curves of all competing methods in testing cohort.

3.4 Efficacy of multi-modality data

We compared the prediction performance of the proposed model on mono-modality data (*i.e.*, only trained with CT or MR images) and

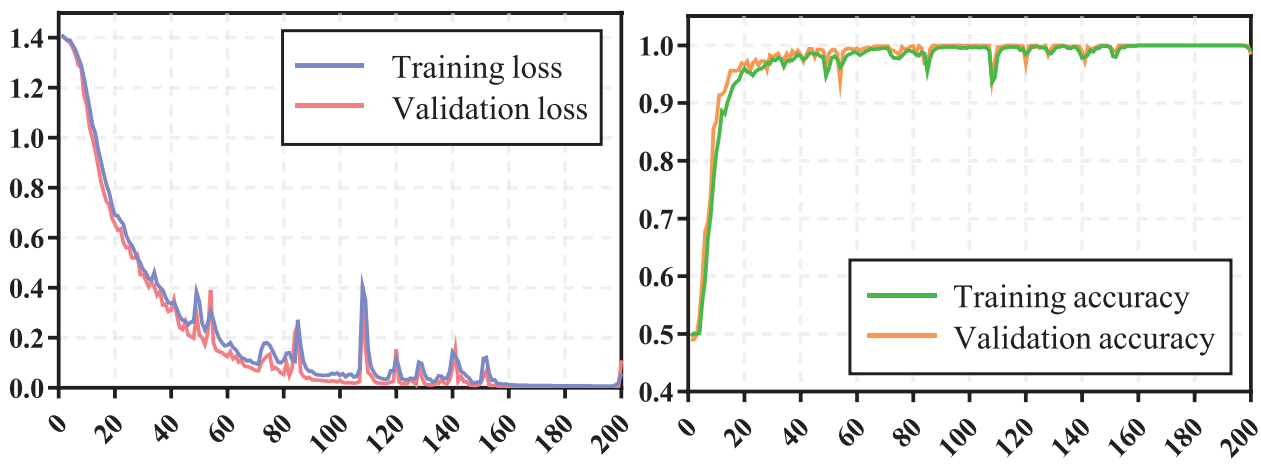

FIGURE 4
The training process of transformer network.

TABLE 2 Comparison results of the proposed method and other competing methods.

		AUC	Accuracy	F1-score	Sensitivity	Specificity	Precision	P-value*
Proposed	Training	0.987±0.025	0.986±0.029	0.984±0.031	0.971±0.058	1.000±0.000	1.000±0.000	
	Validation	0.989±0.021	0.988±0.024	0.987±0.027	0.975±0.050	1.000±0.000	1.000±0.000	
	Testing	0.819±0.038	0.869±0.023	0.914±0.016	0.911±0.038	0.725±0.094	0.919±0.025	
Decision Tree	Training	0.968±0.017	0.957±0.016	0.972±0.010	0.974±0.009	0.900±0.075	0.970±0.022	4.20e-05
	Validation	0.953±0.053	0.943±0.036	0.962±0.023	0.950±0.025	0.920±0.098	0.975±0.031	
	Testing	0.680±0.050	0.703±0.034	0.787±0.026	0.711±0.028	0.675±0.061	0.881±0.023	
Bayes Classifier	Training	0.867±0.020	0.878±0.015	0.924±0.009	0.970±0.015	0.575±0.047	0.883±0.011	7.54e-05
	Validation	0.903±0.066	0.867±0.019	0.915±0.013	0.950±0.025	0.600±0.000	0.884±0.003	
	Testing	0.720±0.068	0.691±0.042	0.777±0.030	0.696±0.028	0.675±0.100	0.879±0.037	
KNN	Training	0.925±0.031	0.843±0.023	0.905±0.014	0.966±0.014	0.437±0.068	0.851±0.016	1.40e-03
	Validation	0.929±0.067	0.838±0.023	0.904±0.012	1.000±0.000	0.320±0.098	0.825±0.021	
	Testing	0.777±0.048	0.731±0.053	0.807±0.047	0.741±0.084	0.700±0.100	0.895±0.030	
SVM	Training	0.989±0.013	0.980±0.012	0.987±0.007	0.996±0.008	0.925±0.047	0.978±0.014	7.39e-07
	Validation	0.975±0.038	0.952±0.030	0.969±0.020	0.987±0.025	0.840±0.080	0.952±0.024	
	Testing	0.691±0.103	0.646±0.023	0.737±0.020	0.644±0.030	0.650±0.050	0.862±0.017	
MobileNetV1	Training	0.979±0.031	0.977±0.033	0.976±0.035	0.961±0.054	0.994±0.012	0.993±0.014	7.70e-03
	Validation	0.975±0.040	0.973±0.044	0.971±0.048	0.954±0.073	0.992±0.016	0.990±0.020	
	Testing	0.743±0.022	0.811±0.023	0.875±0.020	0.859±0.054	0.650±0.094	0.894±0.020	
ResNet18	Training	0.968±0.053	0.966±0.055	0.964±0.060	0.948±0.082	0.984±0.029	0.981±0.034	7.60e-03
	Validation	0.977±0.040	0.971±0.052	0.967±0.062	0.946±0.108	0.996±0.008	0.996±0.008	
	Testing	0.733±0.027	0.800±0.031	0.863±0.026	0.822±0.049	0.725±0.050	0.910±0.011	

* P-value is calculated by T-test to measure significant differences from proposed model.

multi-modality data. The detailed experimental design can be found in Supplementary Materials. Table 3 shows the experimental results, and Figure S1 depicts the training process of transformer network on mono-modality data. We can see that the model with multi-modality data obtained the best results when compared with the models with only mono-modality data. Figure 5 (right) exhibits the corresponding ROC curves, further validating the above-mentioned contents. It is not surprising about the observation, in that multi-modality data can provide more complementary information for the recurrence risk stratification of LACC.

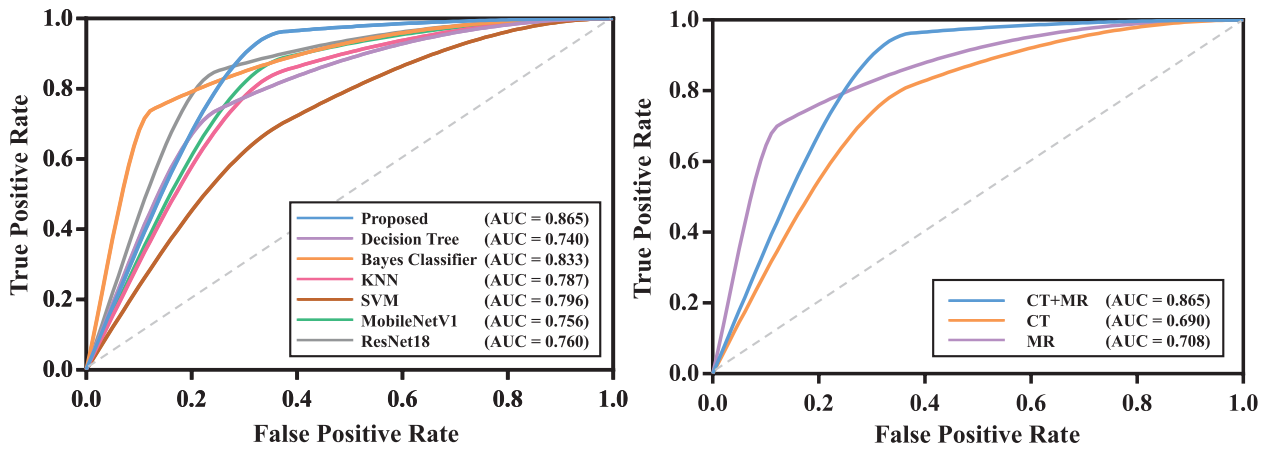

FIGURE 5
The ROC curves of models in testing cohort. The model with the best test result was shown. Left: ROC curves of all competing methods; Right: ROC curves of the proposed model with mono-modality and multi-modality data.

TABLE 3 Comparison results of the proposed method on mono-modality data and multi-modality data.

		AUC	Accuracy	F1-score	Sensitivity	Specificity	Precision	P-value*
CT+MR	Training	0.987±0.025	0.986±0.029	0.984±0.031	0.971±0.058	1.000±0.000	1.000±0.000	
	Validation	0.989±0.021	0.988±0.024	0.987±0.027	0.975±0.050	1.000±0.000	1.000±0.000	
	Testing	0.819±0.038	0.869±0.023	0.914±0.016	0.911±0.038	0.725±0.094	0.919±0.025	
CT	Training	0.998±0.005	0.997±0.005	0.997±0.005	0.995±0.010	1.000±0.000	1.000±0.000	5.75e-04
	Validation	0.996±0.008	0.996±0.008	0.996±0.009	0.992±0.017	1.000±0.000	1.000±0.000	
	Testing	0.677±0.021	0.737±0.042	0.813±0.039	0.748±0.068	0.700±0.061	0.895±0.013	
MR	Training	0.996±0.008	0.996±0.009	0.995±0.009	0.991±0.018	1.000±0.000	1.000±0.000	2.82e-03
	Validation	0.996±0.008	0.996±0.008	0.996±0.009	0.992±0.017	1.000±0.000	1.000±0.000	
	Testing	0.676±0.068	0.720±0.066	0.795±0.049	0.704±0.052	0.775±0.146	0.914±0.055	

* P-value is calculated by T-test to measure significant differences from proposed method on multi-modality data.

3.5 Efficacy of key modules in transformer network

We also validated the efficacy of key modules in transformer network. The detailed experimental design and results can be found in Supplementary Materials.

4 Discussion

In this study, we developed and evaluated a transformer network for the recurrence risk stratification of locally advanced cervical cancer (LACC) based on computed tomography (CT) and magnetic resonance (MR) images. The proposed method achieved excellent prediction performance, which could be potentially used as an effective tool for the decision-making support in a non-invasive way.

The individualized treatment of cervical cancer is guided by the FIGO staging (33, 34). For patients with LACC, the preferred treatment is concurrent chemoradiation rather than surgery (3). However, unlike surgery treatment that can evaluate recurrence risk based on the resected tumor, the concurrent chemoradiation lacks of the conditions for adequate pathological evaluation after local biopsy. Hysteretic risk assessment and intervention would lead to cancer recurrence for partial patients. Therefore, it is desirable to accurately predict the recurrence risk of LACC so as to determine appropriate adjuvant treatment strategies.

Under the current advocacy of precision medicine (35) powered by patient data (36), personalized treatment is the inevitable trend of current medical technology development. The FIGO 2018 staging system has acknowledged the value of imaging for optimal risk stratification and treatment planning (37, 38) and European Society of Urogenital Radiology (ESUR) guidelines also affirmed the important role of MR images in the risk assessment of cervical cancer recurrence (39). Additionally, medical imaging acquisition and storage techniques enable the non-invasive analysis for various diseases, which efficiently assists clinicians in disease diagnosis, treatment and prognosis (40, 41). Typically, radiomics signatures have been widely used and show promising value (42, 43). With the widespread promotion of deep learning technology, the threshold for mastering such high-precision models has been completely lowered. Compared to conventional radiomics methods, deep learning simplifies the multi-step pipeline by automatically learning useful features from images, and exhibits better predictive performance (44). As one of the challenges of deep learning, large-scale data are needed for model training. However, the low incidence of LACC might lead to insufficient training data. To this end, in our work, we employed the patch-based strategy to extract a large amount of image patches from each patient and additionally performed data augmentation to scale up training data and prevent overfitting. Furthermore, we designed a relatively simple network, which embedded three modality fusion modules and a fully-connected module, and the satisfactory results demonstrated its ability of recurrence risk stratification.

Computed tomography (CT) and magnetic resonance (MR) have been considered as the routine examinations of cervical cancer patients. Previous studies have suggested that CT and MR images help identify metastatic lymph nodes and distant metastases for patients with cervical cancer (45) and MR images can also evaluate the extent of tumors in the cervix and in the pelvis (46). Additionally, CT and MR images can provide information of tumors, such as lesion size and invasion degree, which is crucial for preliminary clinical staging and prognosis evaluation (47–51). Therefore, many models based on CT or MR images have been proposed for the subtype identification (52), staging analysis (53, 54), lymph node metastasis prediction (54, 55) and prognosis analysis (12, 56, 57) of cervical cancer. Compared to the above methods, the main contributions of this paper lie in the following aspects: (I) We first investigated the feasibility of deep learning method in accurately predicting recurrence risk so as to help formulate the individualized therapeutic schedule for LACC patients. (II) With matched CT and MR images, we proposed a multi-modality model to fully extract modality-specific and modality-sharable features for improving model's performance. (III) We developed a transformer network which can utilize multi-scale and multi-modality discriminative information and experimental results demonstrated its efficacy.

Our study had some limitations. First, our model was constructed only based on imaging (*i.e.*, CT and MR) features, and more integrable factors (e.g., tumor size and tumor marker level) can be collected for further analysis. Second, the VOI segmentation was still a manual process, which was time-consuming and experience-

dependent. Last but not the least, this work was a retrospective and single-site study, and a prospective and multi-site cohort is required to further evaluate the model's performance. Nevertheless, to the best of our knowledge, this is the first work to predict the recurrence risk of LACC patients via the deep learning technique, which might supply a valuable reference for the application of deep learning in LACC.

In conclusion, we investigated the ability of transformer network in recurrence risk stratification of LACC based on CT and MR images. The promising results demonstrated that the proposed models might help clinicians make clinical decisions for patients with LACC.

Data availability statement

The raw data supporting the conclusions of this article will be made available by the authors, without undue reservation.

Ethics statement

The studies involving human participants were reviewed and approved by the institutional review board of NanFang Hospital, Guangzhou, Guangdong, 510515, PR China. Written informed consent for participation was not required for this study in accordance with the national legislation and the institutional requirements.

Author contributions

JW: Conceptualization, resources, data curation. YM: Writing - original draft, methodology, visualization. XG: Investigation, resources. YZ: Supervision, funding acquisition, writing - review & editing, conceptualization. All authors contributed to the article and approved the submitted version. We would like to express our sincere gratitude towards Zhenyuan Ning for his treasured and generous support.

Funding

This work was supported in part by the National Natural Science Foundation of China under Grant 61971213 and Grant 61671230, in part by the Basic and Applied Basic Research Foundation of Guangdong Province under Grant 2019A1515010417, and in part by the Guangdong Provincial Key Laboratory of Medical Image Processing under Grant No. 2020B1212060039.

Conflict of interest

The authors declare that the research was conducted in the absence of any commercial or financial relationships that could be construed as a potential conflict of interest.

Publisher's note

All claims expressed in this article are solely those of the authors and do not necessarily represent those of their affiliated organizations, or those of the publisher, the editors and the reviewers. Any product that may be evaluated in this article, or claim that may be made by its manufacturer, is not guaranteed or endorsed by the publisher.

Supplementary material

The Supplementary Material for this article can be found online at: https://www.frontiersin.org/articles/10.3389/fonc.2023.1100087/full#supplementary-material

References

1. Sung H, Ferlay J, Siegel RL, Laversanne M, Soerjomataram I, Jemal A, et al. Global cancer statistics 2020: GLOBOCAN estimates of incidence and mortality worldwide for 36 cancers in 185 countries. *CA Cancer J Clin* (2021) 71:209–49. doi: 10.3322/caac.21660

2. Loizzi V, Cormio G, Vicino M, Selvaggi L. Neoadjuvant chemotherapy: An alternative option of treatment for locally advanced cervical cancer. *Gynecol Obstet Invest* (2008) 65:96–103. doi: 10.1159/000108600

3. Cho O, Chun M. Management for locally advanced cervical cancer: New trends and controversial issues. *Radiat Oncol J* (2018) 36:254–64. doi: 10.3857/roj.2018.00500

4. Horeweg N, Mittal P, Gradowska PL, Boere I, Nout RA, Chopra S. A systematic review and meta-analysis of adjuvant chemotherapy after chemoradiation for locally advanced cervical cancer. *Crit Rev Oncol Hematol* (2022) 172:103638. doi: 10.1016/j.critrevonc.2022.103638

5. Nguyen VT, Winterman S, Playe M, Benbara A, Zelek L, Pamoukdjian F, et al. Dose-intense cisplatin-based neoadjuvant chemotherapy increases survival in advanced cervical cancer: An up-to-Date meta-analysis. *Cancers (Basel)* (2022) 14:842. doi: 10.3390/cancers14030842

6. Kokka F, Bryant A, Brockbank E, Powell M, Oram D. Hysterectomy with radiotherapy or chemotherapy or both for women with locally advanced cervical cancer. *Cochrane Database Syst Rev* (2015) 4:CD10260. doi: 10.1002/14651858.CD010260.pub2

7. Kumar V, Gu Y, Basu S, Berglund A, Eschrich SA, Schabath MB, et al. Radiomics: The process and the challenges. *Magn Reson Imaging* (2012) 30:1234–48. doi: 10.1016/j.mri.2012.06.010

8. Ai Y, Zhu H, Xie C, Jin X. Radiomics in cervical cancer: Current applications and future potential. *Crit Rev Oncol Hematol* (2020) 152:102985. doi: 10.1016/j.critrevonc.2020.102985

9. Reuz ES, Orlhac F, Chargari C, Nioche C, Limkin E, Riet F, et al. Prediction of cervical cancer recurrence using textural features extracted from 18F-FDG PET images acquired with different scanners. *Oncotarget* (2017) 8:43169. doi: 10.18632/oncotarget.17856

10. Gao S, Du S, Lu Z, Xin J, Gao S, Sun H. Multiparametric PET/MR (PET and MR-IVIM) for the evaluation of early treatment response and prediction of tumor recurrence in patients with locally advanced cervical cancer. *Eur Radiol* (2020) 30:1191–201. doi: 10.1007/s00330-019-06428-w

11. Jin X, Ai Y, Zhang J, Zhu H, Jin J, Teng Y, et al. Noninvasive prediction of lymph node status for patients with early-stage cervical cancer based on radiomics features from ultrasound images. *Eur Radiol* (2020) 30:4117–24. doi: 10.1007/s00330-020-06692-1

12. Yusufaly TI, Zou J, Nelson TJ, Williamson CW, Simon A, Singhal M, et al. Improved prognosis of treatment failure in cervical cancer with nontumor PET/CT radiomics. *J Nucl Med* (2022) 63:1087–109. doi: 10.2967/jnumed.121.262618

13. Szegedy C, Vanhoucke V, Ioffe S, Shlens J, Wojna Z. Rethinking the inception architecture for computer vision. *Proceedings of the IEEE conference on computer vision and pattern recognition* (2016) 2818-26.

14. Chartrand G, Cheng PM, Vorontsov E, Drozdzal M, Turcotte S, Pal CJ, et al. Deep learning: A primer for radiologists. *Radiographics* (2017) 37:2113–31. doi: 10.1148/rg.2017170077

15. Dai Y, Gao Y, Liu F. Transmed: Transformers advance multi-modal medical image classification. *Diagnostics* (2021) 11:1384. doi: 10.3390/diagnostics11081384

16. He K, Gan C, Li Z, Rekik I, Yin Z, Ji W, et al. Transformers in medical image analysis: A review. *Intelligent Medicine* (2022).

17. Dosovitskiy A, Beyer L, Kolesnikov A, Weissenborn D, Zhai X, Unterthiner T, et al. *An image is worth 16×16 words: Transformers for image recognition at scale*. arXiv preprint arXiv (2020). p. 2010.11929.

18. Liu S, Li R, Liu Q, Sun D, Yang H, Pan H, et al. Radiomics model of 18F-FDG PET/CT imaging for predicting disease-free survival of early-stage uterine cervical squamous cancer. *Cancer Biomarkers: Section A Dis Markers* (2022) 33(2):249–59. doi: 10.3233/CBM-210201

19. Beukinga RJ, Hulshoff JB, Mul VEM, Noordzij W, Kats-Ugurlu G, Slart R, et al. Prediction of response to neoadjuvant chemotherapy and radiation therapy with baseline and restaging (18)F-FDG PET imaging biomarkers in patients with esophageal cancer. *Radiology* (2018) 287(3):983-992. doi: 10.1148/radiol.2018172229

20. Onofrey JA, Casetti-Dinescu DI, Lauritzen AD, Sarkar S, Venkataraman R, Fan RE, et al. Generalizable multi-site training and testing of deep neural networks using image normalization. *Proc IEEE Int Symp BioMed Imaging* (2019) 2019:348–51. doi: 10.1109/ISBI.2019.8759295

21. Petit O, Thome N, Rambour C, Themyr L, Collins T, Soler L. U-Net transformer: Self and cross attention for medical image segmentation. In *International Workshop on Machine Learning in Medical Imaging* (2021) Springer 267–76.

22. Ning Z, Luo J, Li Y, Han S, Feng Q, Xu Y, et al. Pattern classification for gastrointestinal stromal tumors by integration of radiomics and deep convolutional features. *IEEE J BioMed Health Inform* (2018) 23:1181–91. doi: 10.1109/JBHI.2018.2841992

23. Kira K, Rendell LA. The feature selection problem: Traditional methods and a new algorithm. *AAAI'92* (1992) 2(1992a):129–34. doi: 10.5555/1867135.1867155

24. Safavian SR, Landgrebe D. A survey of decision tree classifier methodology[J]. *IEEE Trans Syst Man Cybern B Cybern* (1991) 21(3):660–74. doi: 10.1109/21.97458

25. Rish I. An empirical study of the naive bayes classifier[C]. In: *IJCAI 2001 workshop on empirical methods in artificial intelligence* (2001) 3(22):41-46.

26. Peterson LE. K-Nearest neighbor[J]. *Scholarpedia* (2009) 4(2):1883. doi: 10.4249/scholarpedia.1883

27. Cortes C, Vapnik V. Support vector machine. *Mach Learn* (1995) 20:273–97. doi: 10.1007/BF00994018

28. He K, Zhang X, Ren S, Sun J. (2016). Deep residual learning for image recognition[C], in: *Proceedings of the IEEE conference on computer vision and pattern recognition*, . pp. 770–8.

29. Howard AG, Zhu M, Chen B, Kalenichenko D, Wang W, Weyand T, et al. *Mobilenets: Efficient convolutional neural networks for mobile vision applications[J]*. arXiv preprint arXiv (2017).

30. Perez L, Wang J. The effectiveness of data augmentation in image classification using deep learning. *Convolutional Neural Networks Vis. Recognit*(2017) 11(2017):1-8.

31. He K, Zhang X, Ren S, Sun J. Delving deep into rectifiers: Surpassing human-level performance on ImageNet classification. *Biochem Biophys Res Commun* (2015) 498:254–61. doi: 10.1109/ICCV.2015.123

32. Kingma DP, Ba J. *Adam: A method for stochastic optimization*. arXiv preprint arXiv (2014). p. 1412.6980.

33. Koh W, Abu-Rustum NR, Bean S, Bradley K, Campos SM, Cho KR, et al. Cervical cancer, version 3.2019, NCCN clinical practice guidelines in oncology. *J Natl Compr Canc Netw* (2019) 17:64–84. doi: 10.6004/jnccn.2019.0001

34. Bhatla N, Berek JS, Cuello Fredes M, Denny LA, Grenman S, Karunaratne K, et al. Revised FIGO staging for carcinoma of the cervix uteri. *Int J Gynaecol Obstet* (2019) 145(1):129–35. doi: 10.1002/ijgo.12749

35. Collins FS, Varmus H. A new initiative on precision medicine[J]. *N Engl J Med* (2015) 372(9):793–5. doi: 10.1056/NEJMp1500523

36. Hodson R. Precision medicine[J]. *Nature* (2016) 537(7619):S49–9. doi: 10.1038/537S49a

37. Wright JD, Matsuo K, Huang Y, Tergas AI, Hou JY, Khoury-Collado F, et al. Prognostic performance of the 2018 international federation of gynecology and obstetrics cervical cancer staging guidelines[J]. *Obstetrics Gynecol* (2019) 134(1):49. doi: 10.1097/AOG.0000000000003311

38. Manganaro L, Lakhman Y, Bharwani N, Gui B, Gigli S, Vinci V, et al. Staging, recurrence and follow-up of uterine cervical cancer using MRI: Updated guidelines of the European society of urogenital radiology after revised FIGO staging 2018[J]. *Eur Radiol* (2021) 31(10):7802–16. doi: 10.1007/s00330-020-07632-9

39. Kubik-Huch RA, Weston M, Nougaret S, Leonhardt H, Thomassin-Naggara I, Horta M, et al. European Society of urogenital radiology (ESUR) guidelines: MR imaging of leiomyomas[J]. *Eur Radiol* (2018) 28(8):3125–37. doi: 10.1007/s00330-017-5157-5

40. Xie C, Pang C, Chan B, Wong EY, Dou Q, Vardhanabhuti V. Machine learning and radiomics applications in esophageal cancers using non-invasive imaging methods–a critical review of literature. *Cancers* (2021) 13:2469. doi: 10.3390/cancers13102469

41. Huang G, Cui Y, Wang P, Ren J, Wang L, Ma Y, et al. Multi-parametric magnetic resonance imaging-based radiomics analysis of cervical cancer for preoperative prediction of lymphovascular space invasion. *Front Oncol* (2021) 11:663370. doi: 10.3389/fonc.2021.663370

42. Liu D, Zhang X, Zheng T, Shi Q, Cui Y, Wang Y, et al. Optimisation and evaluation of the random forest model in the efficacy prediction of chemoradiotherapy for advanced cervical cancer based on radiomics signature from high-resolution T2 weighted images. *Arch Gynecol Obstet* (2021) 303:811–20. doi: 10.1007/s00404-020-05908-5

43. Jia CL, Cao Y, Song Q, Zhang WB, Li JJ, Wu XX, et al. Radiomics nomogram of MR: A prediction of cervical lymph node metastasis in laryngeal cancer. *Zhonghua Er Bi Yan Hou Tou Jing Wai Ke Za Zhi* (2020) 55:1154–61. doi: 10.3760/cma.j.cn115330-20200719-00604

44. Borowiec ML, Dikow RB, Frandsen PB, McKeeken A, Valentini G, White AE. Deep learning as a tool for ecology and evolution. *Methods Ecol Evol* (2021) 13(8):1640–60. doi: 10.1111/2041-210X.13901

45. Haldorsen IS, Lura NAL, Blaak Ae RJ, Fischerova D, Werner HM. What is the role of imaging at primary diagnostic work-up in uterine cervical cancer? *Curr Oncol Rep* (2019) 21:1–15. doi: 10.1007/s11912-019-0824-0

46. Devine C, Viswanathan C, Faria S, Marcal L, Sagebiel TL. Imaging and staging of cervical cancer. *Semin Ultrasound CT MR* (2019) 40:280–6. doi: 10.1053/j.sult.2019.03.001

47. Yu K, Zhang C, Berry GJ, Altman RB, Re C, Rubin DL, et al. Predicting non-small cell lung cancer prognosis by fully automated microscopic pathology image features. *Nat Commun* (2016) 7:1–10. doi: 10.1038/ncomms12474

48. Cozzi L, Dinapoli N, Fogliata A, Hsu WC, Reggiori G, Lobefalo F, et al. Radiomics based analysis to predict local control and survival in hepatocellular carcinoma patients treated with volumetric modulated arc therapy. *BMC Cancer* (2017) 17:1–10. doi: 10.1186/s12885-017-3847-7

49. van Timmeren JE, Leijenaar RT, van Elmpt W, Reymen B, Oberije C, Monshouwer R, et al. Survival prediction of non-small cell lung cancer patients using radiomics analyses of cone-beam CT images. *Radiother Oncol* (2017) 123:363–9. doi: 10.1016/j.radonc.2017.04.016

50. Ning Z, Luo J, Xiao Q, Cai L, Chen Y, Yu X, et al. Multi-modal magnetic resonance imaging-based grading analysis for gliomas by integrating radiomics and deep features. *Ann Transl Med* (2021) 9:298. doi: 10.21037/atm-20-4076

51. Chen T, Ning Z, Xu L, Feng X, Han S, Roth HR, et al. Radiomics nomogram for predicting the malignant potential of gastrointestinal stromal tumours preoperatively. *Eur Radiol* (2019) 29:1074–82. doi: 10.1007/s00330-018-5629-2

52. Tsujikawa T, Rahman T, Yamamoto M, Yamada S, Tsuyoshi H, Kiyono Y, et al. 18F-FDG PET radiomics approaches: Comparing and clustering features in cervical cancer. *Ann Nucl Med* (2017) 31:678–85. doi: 10.1007/s12149-017-1199-7

53. Mu W, Chen Z, Liang Y, Shen W, Yang F, Dai R, et al. Staging of cervical cancer based on tumor heterogeneity characterized by texture features on 18F-FDG PET images. *Phys Med Biol* (2015) 60:5123. doi: 10.1088/0031-9155/60/13/5123

54. Song J, Hu Q, Ma Z, Zhao M, Chen T, Shi H. Feasibility of T2WI-MRI-based radiomics nomogram for predicting normal-sized pelvic lymph node metastasis in cervical cancer patients. *Eur Radiol* (2021) 31:6938–48. doi: 10.1007/s00330-021-07735-x

55. Dong T, Yang C, Cui B, Zhang T, Sun X, Song K, et al. Development and validation of a deep learning radiomics model predicting lymph node status in operable cervical cancer. *Front Oncol* (2020) 10:464. doi: 10.3389/fonc.2020.00464

56. Liu S, Li R, Liu Q, Sun D, Yang H, Pan H, et al. Radiomics model of 18F-FDG PET/CT imaging for predicting disease-free survival of early-stage uterine cervical squamous cancer. *Cancer biomark* (2022) 33:249–59. doi: 10.3233/CBM-210201

57. Autorino R, Gui B, Panza G, Boldrini L, Cusumano D, Russo L, et al. Radiomics-based prediction of two-year clinical outcome in locally advanced cervical cancer patients undergoing neoadjuvant chemoradiotherapy. *Radiol Med* (2022) 127:498–506. doi: 10.1007/s11547-022-01482-9

frontiers | Frontiers in Oncology

TYPE Original Research
PUBLISHED 14 April 2023
DOI 10.3389/fonc.2023.1109495

OPEN ACCESS

EDITED BY
Alessio G. Morganti,
University of Bologna, Italy

REVIEWED BY
Heidi Espedal,
University of Bergen, Norway
Hong Huang, Chongqing University, China

*CORRESPONDENCE
Bojana Scepanovic
drbojanascepanovic@gmail.com
Nikola Andjelic
nikola.andjelic@mf.uns.ac.rs

SPECIALTY SECTION
This article was submitted to Gynecological Oncology, a section of the journal Frontiers in Oncology

RECEIVED 27 November 2022
ACCEPTED 27 March 2023
PUBLISHED 14 April 2023

CITATION
Scepanovic B, Andjelic N, Mladenovic-Segedi L, Kozic D, Vuleta D, Molnar U and Nikolic O (2023) Diagnostic value of the apparent diffusion coefficient in differentiating malignant from benign endometrial lesions.
Front. Oncol. 13:1109495.
doi: 10.3389/fonc.2023.1109495

Diagnostic value of the apparent diffusion coefficient in differentiating malignant from benign endometrial lesions

Bojana Scepanovic[1]*, Nikola Andjelic[1,2]*, Ljiljana Mladenovic-Segedi[3,4], Dusko Kozic[1,2], Dusan Vuleta[4], Una Molnar[5,6] and Olivera Nikolic[2,6]

[1]Department of Radiological Diagnostics, Oncology Institute of Vojvodina, Sremska Kamenica, Serbia, [2]Department of Radiology, Faculty of Medicine, University of Novi Sad, Novi Sad, Serbia, [3]Department of Gynecology and Obstetrics, Faculty of Medicine, University of Novi Sad, Novi Sad, Serbia, [4]Department of Gynecology and Obstetrics, Clinical Center of Vojvodina, Novi Sad, Serbia, [5]Faculty of Sciences, University of Novi Sad, Novi Sad, Serbia, [6]Center for Radiology, Clinical Center of Vojvodina, Novi Sad, Serbia

Introduction: Magnetic resonance imaging (MRI) with its innovative techniques, such as diffusion-weighted imaging (DWI) and apparent diffusion coefficient (ADC), increases the diagnostic accuracy in distinguishing between malignant and benign lesions of the endometrium. The aim of the study was MRI differentiation between malignant and benign endometrial lesions and correlation with histopathological findings with a special emphasis on quantitative analysis. An additional aim was to correlate the ADC values and histological tumor grades.

Methods: The prospective study included 119 female patients with or without vaginal bleeding and pathological values of endometrial thickness, who underwent MRI examinations. According to MRI reports the patients were divided into 45 suspicious malignant and 74 suspicious benign endometrial lesions. The radiological diagnosis was compared to the histopathological evaluation, which confirmed 37 malignant lesions while the rest were benign.

Results: The mean ADC value for malignant lesions was $0.761 \pm 0.13\times10^{-3}$ mm^2/s and for benign lesions was $1.318 \pm 0.20\times10^{-3}$ mm^2/s. The ADC values for malignant lesions were expectedly lower than those of benign lesions ($p<0.001$). The ADC cut-off value was 1.007×10^{-3} mm^2/s with a sensitivity of 100%, specificity of 92.7%, a positive predictive value of 60.3%, and a negative predictive value of 100%. In comparison with the histopathological findings, the sensitivity of MRI was 100%, specificity 90.2%, positive predictive value was 82.2%, and negative predictive value was 100%. Observing the histological grades 1, 2, and 3 of endometrial carcinoma, no statistically significant differences of mean ADC values were found. The mean ADC values for histological tumor grades 1,2 and 3 were $0.803 \pm 0.13\times10^{-3}$ mm^2/s, $0.754 \pm 0.12\times10^{-3}$ mm^2/s and $0.728 \pm 0.13\times10^{-3}$ mm^2/s, respectively.

Conclusion: DWI and ADC values represent clinically useful tools for the differentiation between malignant and benign endometrial lesions with high sensitivity and good specificity, but the results failed to demonstrate their usefulness in differentiating histological grades of endometrial cancer.

KEYWORDS

diffusion magnetic resonance imaging, endometrium, endometrial cancer, gynecology, pathology

1 Introduction

Endometrial cancer (EC) is ranged as the most common gynecological cancer in developed countries with an incidence of 15-25 per 100.000 women annually (1). Although EC is predominantly revealed in postmenopausal women, it is also estimated in 10-15% of premenopausal or perimenopausal women, with 2-5% of them being younger than 40 years (2, 3). The most common symptom of EC is vaginal bleeding which can often lead to early diagnosis, but in 5-10% of postmenopausal women it is asymptomatic (4–6). In these patients, EC is the cause of vaginal bleeding in about 1-14% of cases (7).

EC is divided into type I and type II. Type I is the most common and includes endometrioid adenocarcinoma accounting to 75-80% of all endometrial cancers according to literature data, while type II is more aggressive and shows a tendency to greater infiltration of the myometrium (8). The most common histological subtypes of type II are serous, clear-cell and undifferentiated EC.

In addition to EC, benign endometrial lesions are often diagnosed as causes of abnormal uterine bleeding and, among them, endometrial hyperplasia and endometrial polyps are most common (4). Both can undergo a malignant transformation in EC. Endometrial lesions are a diagnostic challenge for both gynecologists and radiologists (9). It is considered that magnetic resonance imaging (MRI) can replace the limitations of the ultrasound examination in the assessment of the nature of endometrial lesions and that, its innovative techniques, the diffusion-weighted imaging (DWI) and the apparent diffusion coefficient (ADC), can increase the diagnostic accuracy in distinguishing between malignant and benign lesions of the endometrium (10). DWI is used to display tissue characteristics based on the Brownian diffusion motion of water molecules and is useful in assessing the extension and stage of the EC, detection of metastatic lymph nodes and the assessment of the response of the EC to therapy (8, 11). ADC is joined to DWI and represents quantitative information about the diffusion of water molecules between tissue cells. In previous research ADC is considered as a reliable auxiliary parameter in differentiating between malignant and benign lesions of the endometrium and normal tissue.

In this research we focused on MRI differentiation between malignant and benign endometrial lesions in correlation with histopathological findings. A special emphasis was on the use of quantitative MRI analysis, DWI and ADC techniques, which are irreplaceable in radiological oncology. In some cases, biopsy and histopathological analysis may be limited due to the localization and size of the observed endometrial lesion, the size of the uterine cavum, congenital malformations in younger women, cervical stenosis, and the size of the obtained sample which may be insufficient for histopathological analysis. High accuracy of DWI and ADC in assessing the existence of malignant and benign lesions would contribute to the affirmation of MRI as a non-invasive method for evaluation of endometrial pathology. Another aim of the study was to correlate the ADC values and histological grade of the tumor.

Abbreviations: EC, Endometrial cancer; MRI, Magnetic resonance imaging; DWI, Diffusion-weighted imaging; ADC, Apparent diffusion coefficient; TVUS, Transvaginal ultrasound; T2W FR FSE, T2-weighted fast relaxation fast spin-echo sequence; T1W FSE, T1-weighted fast spin-echo; T1W FSE FS, T1-weighted fast spin-echo with fat suppression; T2W FR FSE, T2-weighted fast relaxation fast spin-echo; LAVA, Liver Acquisition with Volume Acquisition; TR, Repetition time; TE, Echo time; FOV, Field of view; ROI, Region of interest; WHO, The World Health Organization; FIGO, International Federation of Gynecology and Obstetrics; PPV, Positive predictive value; NPV, Negative predictive value.

2 Materials and methods

2.1 Patients

The prospective study was conducted in the period from September 2017 to June 2022 on a total sample of 143 female patients who were examined by a gynecologist due to vaginal bleeding or as a routine control and were reported to have a pathological endometrial thickness on transvaginal ultrasound (TVUS) examination. Subsequently, all patients were examined on MRI with DWI. Twenty-four patients were excluded from the study based on the exclusion criteria and the total number of patients was 119. According to the MRI results, patients were divided into two groups. The first group consisted of 45 patients with reported suspected malignant endometrial lesions, and the second group of 74 patients with reported suspected benign endometrial lesions on MRI. After MRI examination the final diagnosis was established according to histopathological evaluation, and the results were compared to MRI reports. The study was approved by the institutional ethical committee. All patients gave written informed consent to take part in this study. Inclusion criteria were: postmenopausal patients with bleeding and TVUS measured endometrial thickness greater than 5 mm, asymptomatic postmenopausal patients with TVUS measured

endometrial thickness greater than 11 mm, premenopausal or perimenopausal women with abnormal uterine bleeding and TVUS measured endometrial thickness greater than 16 mm, no contraindications for MRI examination, indication set by the gynecologist to perform exploratory curettage or hysteroscopy and some of the patients were indicated for operation.

The main exclusion criteria were patients with contraindications for MRI examination, large submucosal myoma of the uterus that protruded into the lumen of the uterine cavum limiting the evaluation, endometrial changes that were unclearly displayed on the DWI and ADC map making their evaluation impossible, and the absence of subsequent histological finding.

The following flowchart presents methodological steps from patients' selection phase to MRI examination and analysis (ADC measurements), histopathological evaluation and comparation between MRI and histopathology data (Figure 1).

2.2 MRI protocol

MR examination of the pelvis in all patients was performed using a 1.5 Tesla MR unit (Signa HDxt, General Electric Healthcare, Boston, MA, USA). Images were acquired with an 8-channel body array coil using the lower configuration in the supine position. The following sequences were used: T2-weighted fast relaxation fast spin-echo sequence (T2W FR FSE) sagittal, coronal and axial plane, T1-weighted fast spin-echo (T1W FSE) axial plane, T1-weighted fast spin-echo with fat suppression (T1W FSE FS) axial plane, T2-weighted fast relaxation fast spin-echo sequence (T2W FR FSE) axial oblique (perpendicular) to the uterine cavity, diffusion-weighted imaging (DWI) in the axial plane, Liver Acquisition with Volume Acquisition (LAVA) sequence in the axial plane before and after contrast administration. Apparent diffusion coefficient (ADC) maps were generated with the manufacturer's

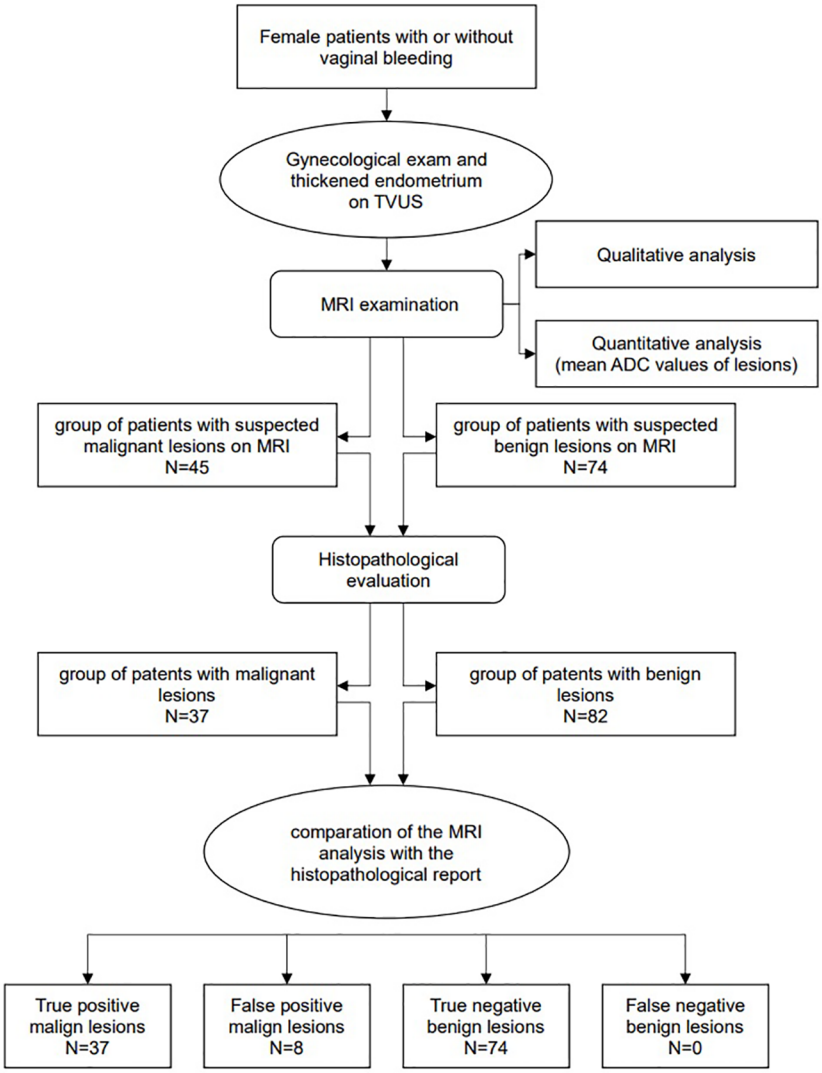

FIGURE 1
The general flowchart shows the methodological steps of the study.

TABLE 1 Parameters of MRI sequences for pelvis examination.

Sequence	T2W FR FSE	T2W FR FSE	T2W FR FSE	T1W FSE	T1W FSE fs	T2W FR FSE	DWI	LAVA before and after contrast administration
Imaging plane	Sagittal	Axial	Corona	Axial	Axial	Perpendicular to the uterus	Axial	Axial
TR/TE (ms) (Repetition time/ Echo time)	2760/10	2220/102	7240/102	460/min full (13.9 -37.1)	440/min full (13.1-35.0)	5560/102	10760/ 78.7	3.1/1.3-11.0
Matrix size	384x256	320x224	416x224	352x224	320x224	256x224	82x128	160x160
FOV (cm) (Field of view)	33x33	30x30	34x34	30x30	30x30	24x24	30x30	40x40
Slice thickness/ Gap (mm)	5/1	5/1	4/1	5/1	5/1	4/1	5/1	2/-
Number of slices	30	39	34	39	39	25	39	140-248
Bandwidth (Hz)	41.67	25.00	31.25	31.25	31.25	25.00	–	62.50
NEX (Number of excitations)	2.00	3.00	2.00	2.00	2.00	6.00	–	–
b values (s/mm^2)	–	–	–	–	–	–	0; 1200	–
Scan time (min: s)	3:30	4:54	3:59	3:49	6:23	6:13	4:40	0:33

software. The parameters of the MRI sequences are presented in Table 1. To prepare for the examination, patients fasted between 3 and 6 hours (except those with diabetes). Patients received an intramuscular injection of antiperistaltic agent hyoscine butylbromide (Buscopan ampoule 20 mg) to decrease artifacts due to peristaltic movements, except in cases it was contraindicated.

2.3 Image analysis

Image analysis and measurements were done on a clinical picture archiving and communication system workstation monitor and post-processed using the General Electric Functool software package (Advantage 4.7; GE Medical Systems/Healthcare, Waukesha, WI, USA). Quantitative and qualitative analyses of the images were performed by two experienced radiologists independently, who then came to a joint conclusion. First, an evaluation of conventional and post-contrast sequences was made, which were then correlated with DWI sequence and corresponding ADC map, including both qualitative and quantitative analysis. The ADC map itself poorly shows anatomical details, so it is necessary to perform the analysis together with other MR images, which, besides DWI sequence, include high-resolution anatomical images and post-contrast images. On T2W sequence, morphological characteristics of the uterus were observed, i.e., its appearance, size, shape, as well as zonal anatomy. The corpus and cervix of the uterus were particularly observed. Then an evaluation of the appearance of the uterine cavity and the presence of any content was checked. Special emphasis was placed on the evaluation of the endometrium and its lesions as the subject of this study. The thickness of the endometrium was measured, with careful observation of its signal-morphological characteristics. On T1W sequence, the appearance of the uterus was observed, i.e., external contours, the presence of any hematometra or hemorrhagic content, the appearance of the endometrium, and lymph nodes. On T2W sequences, DWI, and post-contrast images, we evaluated the tumor invasion of the myometrium.

The characteristics of endometrial lesions were observed with an emphasis on DWI images. Lesions and areas that were suspected of malignancy showed high signal intensity on DWI images with the b value of 1200 mm^2/s and corresponding low signal intensity on ADC maps which indicated signs of diffusion restriction. In other cases, when hyperintensity on DWI corresponded to a high signal intensity on ADC maps, lesions were suspected to be benign. The ADC values of both suspected malign and suspected benign endometrial lesions were measured manually using a circular region of interest (ROI). The ROI was manually drawn and placed on a representative region as large as possible to include only the solid parts of the endometrial lesion. We cautiously avoided areas of normal myometrium and junctional zone, cystic or necrotic areas and hemorrhagic content. To do so, the conventional and postcontrast MRI sequences were evaluated and correlated with DWI and ADC maps. The size of ROI in each case depended on the size of the endometrial lesion. The ROI was set on the T2-weighted image and was manually copied to the corresponding ADC map, whereupon ADC values were automatically calculated. Three individual ROIs were drawn at different sections of each lesion, based on which the average ADC value for each patient was calculated.

2.4 Histopathological evaluation

Definitive diagnoses were set based on histopathological evaluation and reports after fractionated exploratory curettage, hysteroscopy and/or surgical operation. They were made by two pathologists experienced in gynecological pathology and were in compliance with the WHO (The World Health Organization) Classification of Tumors and FIGO (International Federation of Gynecology and Obstetrics) grading of endometrial carcinoma.

2.5 Statistical analysis

Statistical analysis was performed using the Statistical Package for Social Science – IBM SPSS Statistics 21. Numerical variables were presented through mean values (arithmetic mean) and measures of variability (value range, standard deviation), and attributive variables were presented using frequencies and percentages. We checked a normal distribution using the Kolmogorov-Smirnov test, and appropriate tests were used in relation to that. The comparison of numerical values between two groups was performed using the Student's t-test and Mann-Whitney test, while one-way analysis of variance (ANOVA) was used to compare values between three and more groups of data. Testing the difference in frequencies of attributive variables was performed using the χ^2 test. ROC analysis was used to define the cut-off value of the test that gives the best ratio of specificity and sensitivity. Values of significance level $p<0.05$ are considered statistically significant. The results are presented in tables and figures.

3 Results

In our study the mean age of female patients was 63.28 ± 8.02 (range 44-82 years) and among them 112 were in postmenopausal and 7 in perimenopausal period. Mean endometrial thickness measured at TVUS examination was 15.51 ± 6.05 mm (range 7-35 mm). Vaginal bleeding was noted in 80 patients, while in 39 cases it was asymptomatic. Endometrial thickness values in patients with benign lesions were statistically significantly lower than in those with malignant lesions (t=3,850; p<0,001). Significantly more patients with malignant lesions had vaginal bleeding compared to those with benign lesions (χ^2 = 14,826; p<0,001).

Based on the MRI analysis, in 74 cases endometrial changes were reported as probably benign, with the mean ADC value of $1.361 \pm 0.161\times10^{-3}$ mm^2/s (range $1.044\text{-}1.858\times10^{-3}$ mm^2/s) and in 45 cases they were reported as probably malign, with the mean ADC value $0.790 \pm 0.14\times10^{-3}$ mm^2/s (range $0.542\text{-}1.059\times10^{-3}$ mm^2/s).

Figures 2, 3 show the MRI appearance of the malignant and benign lesions of the endometrium from the samples of our patients.

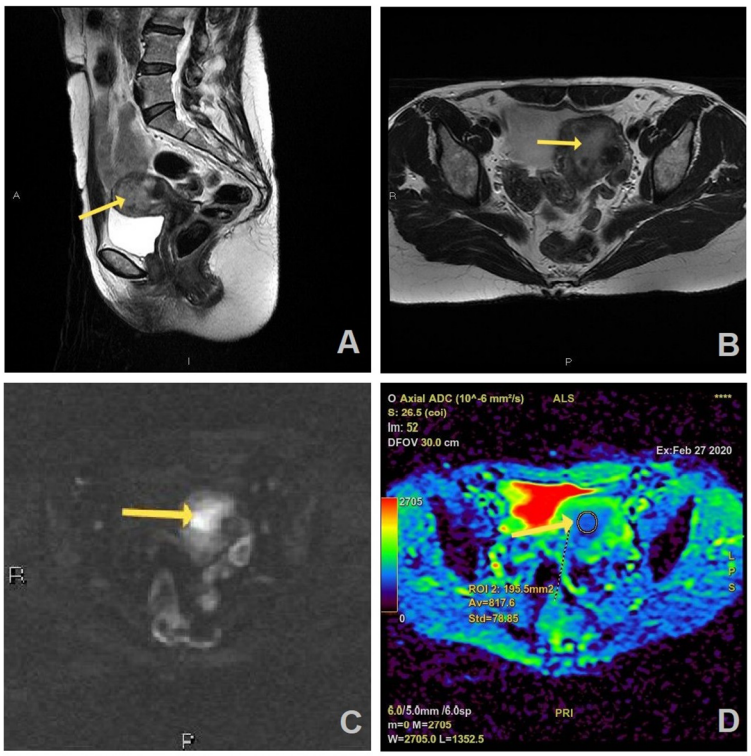

FIGURE 2
MR images of a 55-year old woman with a history of vaginal bleeding, high suspicious EC on MRI, and histopathologically proven endometrial endometrioid carcinoma, HG2 (FIGO stage II): **(A)** sagittal and **(B)** axial T2W FR FSE image shows endometrial mass (arrow) in uterine cavity which is hyperintense on axial DWI (b=1200 s/mm^2) **(C)** and has correlation on ADC map with the measured ADC value of 0.817×10^{-3} mm^2/s **(D)**.

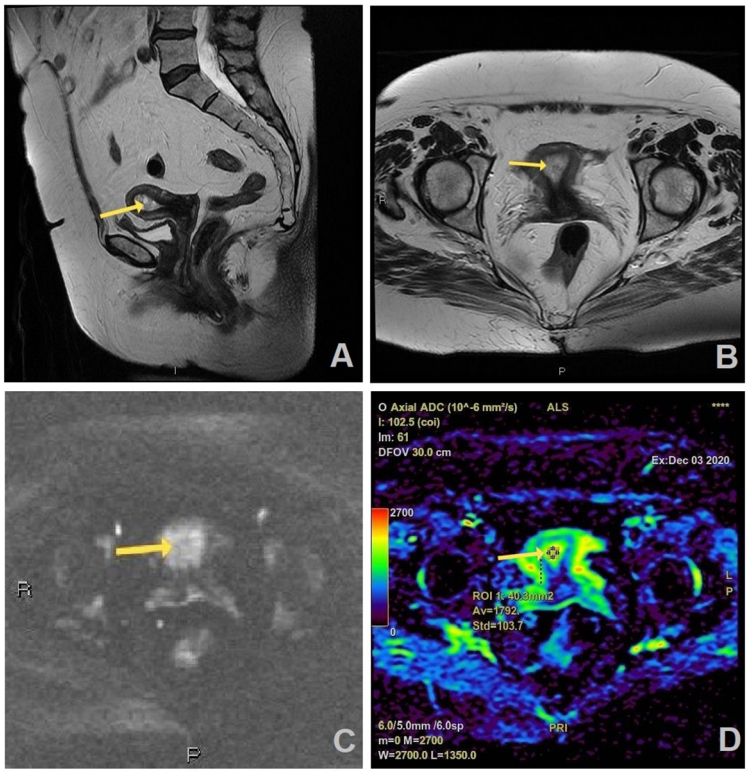

FIGURE 3
MR images of a 66-year old woman with a history of vaginal bleeding, suspicious benign lesion on MRI, and histopathologically proven endometrial hyperplasia: **(A)** sagittal and **(B)** axial T2W FR FSE image shows thickened endometrium in uterine cavity (arrow) which is slightly hyperintense on axial DWI (b=1200 s/mm^2) **(C)** and has no correlation on ADC map with the measured ADC value of 1.792 × 10^{-3} mm^2/s **(D)**.

According to histopathological reports, malignancy was confirmed in 37 out of 45 cases reported as malignant on MRI, and the rest of 82 cases were proved to be benign. The mean ADC value of confirmed malignant lesion was 0.761 ± 0.13×10^{-3} mm^2/s (range 0.542-1.007×10^{-3} mm^2/s), whereas the mean ADC value of benign lesions was 1.318 ± 0.20×10^{-3} mm^2/s (range 0.756-1.858×10^{-3} mm^2/s). The histopathological findings are summarized in Table 2.

The box-and-whisker plots presented in Figure 4 show the distribution of ADC values between the group of benign and malignant endometrial lesions. According to the pathological findings, the mean ADC values of malignant lesions were

TABLE 2 Histopathological diagnoses of benign and malignant endometrial lesions.

Pathohistological findings							
	Benign lesions		Malignant lesions		Total		Mean ADC (x10^{-3} mm^2/s) ± SD
	N	%	N	%	N	%	
Endometrial endometrioid carcinoma	0	0.0	29	78.4	29	24.4	0.758 ± 0.13
Serous carcinoma	0	0.0	5	13.5	5	4.2	0.778 ± 0.09
Clear cell adenocarcinoma	0	0.0	2	5.4	2	1.7	0.660 ± 0.11
Undifferentiated carcinoma	0	0.0	1	2.7	1	0.8	0.954
Endometrial polyp	44	53.7	0	0.0	44	37.0	1.311 ± 0.20
Simple endometrial hyperplasia without atypia	30	36.6	0	0.0	30	25.2	1.344 ± 0.19
Endometrial polyp with simple endometrial hyperplasia without atypia	6	7.3	0	0.0	6	5.0	1.249 ± 0.28
Adenomyoma	2	2.4	0	0.0	2	1.7	1.292 ± 0.08
Total	82	100	37	100	119	100	

10.3389/fonc.2023.1109495

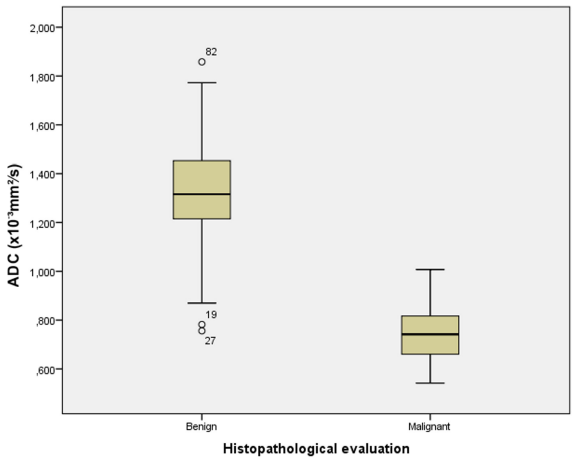

FIGURE 4
The box-and-whisker plots show the ADC values of benign and malignant endometrial lesions according to histopathological analysis.

statistically significantly lower than those of benign lesions (t=15.289; p<0.001). In the group of patients with benign lesions were some outlier values represented by circles. Two values were more than 1.5 x interquartile range below the first quartile which were the mild outliers. In our data set this were case numbers 19 and 27 with the ADC values of 0.782 x 10^{-3} mm^2/s and 0.756 x 10^{-3} mm^2/s, respectively. The case number 82 with the ADC value of 1.858 x 10^{-3} mm^2/s was an extreme outlier. This value is more than 3.0 x interquartile range above the third quartile.

The results of ROC curve analysis presenting sensitivity and specificity of ADC values in differentiation between malignant and benign endometrial lesions are shown in Figure 5. Based on the area under the curve (AUC=0.985; CI (confidence interval) 0.968-1.000), we can see that lower ADC values predict malignant lesions with 98.5% accuracy. The ADC cut-off value was 1.007 x 10^{-3} mm^2/s. Using this value, the sensitivity for distinguishing malignant from benign lesions was 100%, specificity was 92.7%, positive predictive value (PPV) was 60.3%, and negative predictive value (NPV) was 100%.

Figure 6 shows a comparison of the two ROC curves. Explanation for ROC curve analysis (marked blue) that represents sensitivity and specificity of ADC values in differentiation between malignant and benign endometrial lesions is given in previous paragraph. The second ROC curve analysis (marked green) represents sensitivity and specificity of endometrial thickness measured by TVUS in differentiation between malignant and benign endometrial lesions. Based on the area under this curve (AUC=0.676; CI 0.566-0.787), we can see that prediction for malignant lesions is 67.6% compared to benign lesions in patients with thickened endometrium. The cut-off value for endometrial thickness was 14.85mm. Using this value, the sensitivity for distinguishing malignant from benign lesions was 70.3%, specificity was 61%, PPV was 16.69%, and NPV was 94.87%. By comparing the areas under these curves, our results showed that ADC values are a statistically significantly better predictor of malignancy than TVUS-measured endometrial thickness.

By comparing the MRI findings with the findings obtained after the histopathological analysis, the sensitivity of MRI in relation to histopathological findings was 100%, specificity was 90.2%, PPV 82.2% and NPV was 100%.

In the group of proved malignant lesions, the mean ADC value for histological grade 1 tumors (n=11) was 0.803 ± 0.13×10^{-3} mm^2/s (range 0.620-1.007×10^{-3} mm^2/s), for grade 2 (n=15) 0.754 ± 0.12×10^{-3} mm^2/s (range 0.542-0.953×10^{-3} mm^2/s) and for grade 3 (n=11) was 0.728 ± 0.13×10^{-3} mm^2/s (range 0.579-0.954×10^{-3} mm^2/s). There was no statistically significant difference (F=1.018; p=0.372) in the mean ADC values depending on the histological grade of the malignant lesions, as demonstrated in Figure 7.

In cases where EC was confirmed, FIGO stage was determined. According to MRI analysis and histopathological reports, the stages IA, IB, II, IIIA and IV were present (Table 3). Based on MRI

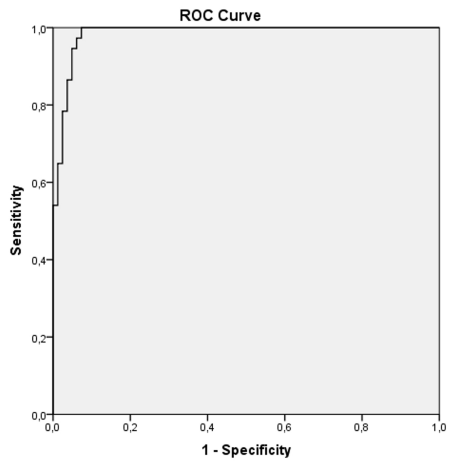

FIGURE 5
ROC curve analysis of ADC values in differentiation between malignant and benign endometrial lesions.

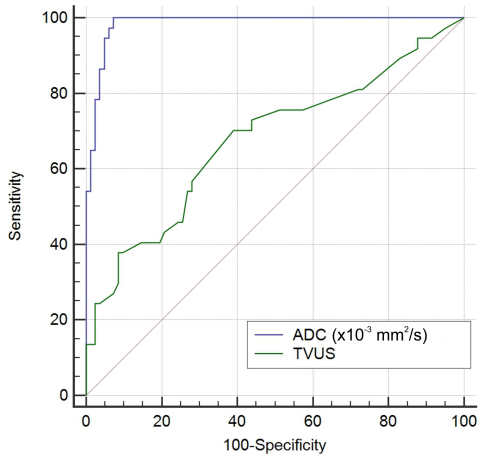

FIGURE 6
Comparison of the ROC curves of ADC values (blue curve) and endometrial thickness measured by TVUS (green curve) in differentiation between malignant and benign endometrial lesions.

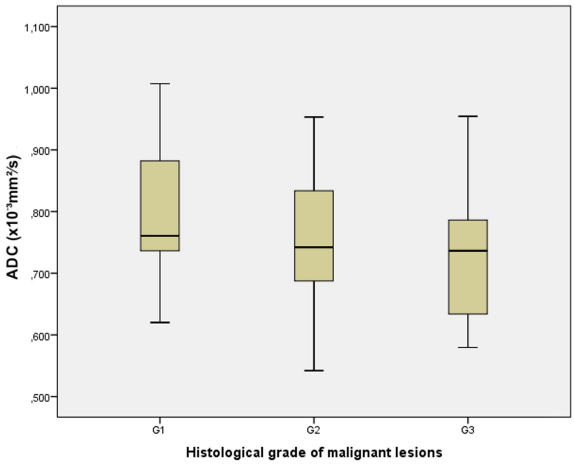

FIGURE 7
The box-and-whisker plots show the ADC values in different histological grades (G1, G2, and G3) of malignant lesions.

analysis in the current study, FIGO stage IA was present in 20 patients (54.1%), IB in eight (21.6%), II in two (5.4%), III also in two patients (5.4%) and stage IV in five patients (13.5%). Referring to histopathological reports, stage IA was present in 16 patients (43.3%), IB in seven (18.9%), II in four (10.8%), III in five (13.5%) and IV stage also in five patients (13.5%). The largest number of patients had confirmed stage IA with the mean ADC value of 0.811 ± 0.13 ×10^{-3} mm^2/s and stage IB with the mean ADC value of 0.696 ± 0.12×10^{-3} mm^2/s. We noticed that the stages IA and IB were most represented and there was no statistically significant difference in the mean ADC values between the mentioned stages (U=29,000; p=0.071).

4 Discussion

In oncological imaging the functional DWI technique is recognized as an imaging biomarker due to its ability to detect microscopic changes in the tumor structure (12, 13). As the lack of universal, standardized range and cut-off values of the ADC for different tissue is indicated in the literature, it would be useful for each radiological center to establish specific ADC values for different tissues. In current research this has been done for EC and benign endometrial lesions based on the measurements obtained for a certain number of examined female patients (14).

Invasive diagnostic methods for obtaining tissues for histopathological analysis of the endometrium have limitations. In 2-28% of cases they cannot provide a diagnosis due to possible errors in collecting a tissue sample or obtaining an insufficient sample (10). In such cases MRI with its DWI, ADC map and ADC values may have a significant role in reaching a diagnosis. Moreover, when EC is present, they can also contribute to determining the stage of the disease and thus serve as one of the prognostic factors.

Histopathological verification of the accuracy of the DWI and ADC in the differentiation of malignant and benign changes of the endometrium would contribute to verifying the reliability of radiological MRI findings and to the affirmation of MRI as a non-invasive and preferred method in diagnostics. At the same time, the number of invasive diagnostic procedures, exploratory curettage and hysteroscopy could be reduced. It is predicted that MRI with DWI and ADC may become a method for monitoring women with risk factors for development of EC and with an initially benign endometrial lesion, which is primarily important for the early detection of EC.

In previous research the most attention has been devoted to examining the role of DWI and ADC in the differentiation of EC from various benign endometrial lesions in a more precise diagnosis of EC, as well as to the possibility of determining its histological grade (10, 15–17).

In our study the results show that there is a statistically significant difference in the ADC values for malignant versus benign endometrial lesions. The mean ADC value for malignant lesions was 0.761± 0.13×10^{-3} mm^2/s and for benign lesions 1.318 ± 0.20×10^{-3} mm^2/s, where the cut-off ADC value was 1.007×10^{-3} mm^2/s. The results of most studies confirm that there is a statistically significant difference in the mean ADC value of EC in relation to benign endometrial lesions (16, 18–23). Bakir et al. and Ahmed et al. agreed that quantitative analysis with ADC map is fundamental for endometrial lesion characterization (24, 25).

Kececi et al. also evaluated the quantitative values of diffusion and showed that the ADC values of EC were significantly lower than the values of benign lesions, which was also confirmed by our results (22). Kececi and associates reported that the mean ADC value for EC was 0.94 ± 0.18×10^{-3} mm^2/s, while our values were lower (0.761 ± 0.13×10^{-3} mm^2/s), but there was a correlation with

TABLE 3 FIGO stages of EC based on MRI analysis and histopathological reports.

FIGO stage	MR analysis			Histopathological reports		
	N	%	Mean ADC (x$10^{-3}$$mm^2$/s) ± SD	N	%	Mean ADC (x$10^{-3}$$mm^2$/s) ± SD
IA	20	54.1	0.797 ± 0.13	16	43.3	0.811 ± 0.13
IB	8	21.6	0.688 ± 0.11	7	18.9	0.696 ± 0.12
II	2	5.4	0.667 ± 0.10	4	10.8	0.748 ± 0.15
IIIA	2	5.4	0.689 ± 0.04	5	13.5	0.657 ± 0.05
IV	5	13.5	0.805 ± 0.07	5	13.5	0.804 ± 0.07

the cut-off value of 1.007×10^{-3} mm^2/s (22). It should be noted that the detection of small endometrial changes and their evaluation is not always possible, and this was not the focus of our research.

Çavuşoğlu et al. conducted MRI examination also using 1.5 Tesla and made evaluation on DWI obtained with the b value of 0 and 1000 s/mm^2. In our study DWI sequence was obtained using b values 0 and 1200 s/mm^2. The authors also reported that the mean ADC values of EC were significantly lower ($0.88 \pm 0.10\times10^{-3}$ mm^2/s) than those of benign lesions with the calculated cut-off value of 1.18×10^{-3} mm^2/s (26). The mean ADC value for benign lesion according to their results was $1.78 \pm 0.27\times10^{-3}$ mm^2/s, which is higher compared with our mean ADC values.

Based on the calculated ADC cut-off value of 1.007×10^{-3} mm^2/s on MRI examination, 45 cases in our research were diagnosed as probably malignant endometrial lesions, while 74 cases were identified as benign endometrial lesions. The sensitivity was 100%, specificity 92.7%, PPV 60.3% and NPV was 100%. Based on histopathological findings, malignant endometrial lesions were confirmed in 37 cases, while the rest were benign. MRI analysis had a sensitivity of 100%, specificity 90.2%, PPV 82.2% and NPV was 100% in relation to histopathological findings.

In the work of Moharamzad et al. where the results of eleven studies were summarized, the sensitivity ranged from 80 to 100% and the specificity was between 75 and 100%, while the cut-off values were in the range from 0.90 to 1.20×10^{-3} mm^2/s. The highest sensitivity (100%) and specificity (97%) were observed in two studies at cut-off ADC values of 0.90 and 0.98×10^{-3} mm^2/s (27).

Elsammak et al. also showed that the mean ADC values of malignant lesions were statistically significantly lower than the values of benign lesions ($p<0.001$), where the mean ADC values for malignant and benign lesions were $0.82 \pm 1.09\times10^{-3}$ mm^2/s and $1.44 \pm 0.15\times10^{-3}$ mm^2/s, respectively (21). In their protocol authors used three different b values to obtain DWI: 0, 800 and 1000 s/mm^2. Based on the calculated ADC cut-off value of 1.19×10^{-3} mm^2/s, 16 patients were diagnosed to have malignant lesions and 26 benign lesions (21). Based on histopathological diagnosis, malignancy was present in 18 cases and benign changes in 24 cases. At the cut-off value of 1.19×10^{-3} mm^2/s for distinguishing malignant from benign lesions, sensitivity was 88.9%, specificity 100%, PPV 100% and NPV 92% (21). In our work, the sensitivity was 100%, and the specificity was lower.

A study by Shen et al. showed that on a sample of 24 EC and 7 benign lesions of the endometrium, based on DWI analysis (b=1000 s/mm^2) and ADC value measurements, the mean ADC values for carcinoma were $0.864 \pm 0.31\times10^{-3}$ mm^2/s and $1.277 \pm 0.22\times10^{-3}$ mm^2/s for benign lesions with a statistically significant difference (28).

On the basis of histopathological findings of the current study, in a total of 31.1% of cases of EC, the most common subtype was endometrial endometrioid carcinoma with the mean ADC value of $0.758 \pm 0.13\times10^{-3}$ mm^2/s. Yan et al. also reported that the endometrial endometrioid carcinoma was most common, with the mean ADC value of $0.936 \pm 0.223\times10^{-3}$ mm^2/s, which is higher than our recorded value. In the study by Çavuşoğlu et al. all malignant lesions were endometrioid adenocarcinomas with the mean ADC value of $0.88 \pm 0.10\times10^{-3}$ mm^2/s (26, 29).

In the current study, benign lesions were present in 68.9% of female patients, with endometrial polyp and simple endometrial hyperplasia being the most common, as in the study of Elsammak et al. and Gharibvand et al. (17, 21). Literature data point to a risk of progression of endometrial hyperplasia to EC up to 5% for endometrial hyperplasia without cell atypia and even 30% in the case of hyperplasia with atypia (30). In women diagnosed with atypical hyperplasia of the endometrium after explorative curettage, EC may also coexist, which is diagnosed later based on postoperative histopathological findings (31). In the examined sample, two patients had altered endometrium suspicious for EC, based on MRI findings, and endometrial hyperplasia with atypia was diagnosed on the histopathological reports after explorative curettage. The post-operative histopathological reports definitively confirmed the diagnosis of EC. In their study Natarajan et al. have shown that MRI has a potential diagnostic value for identifying a concurrent malignancy or malignant transformation in patients with endometrial hyperplasia with atypia (32).

Important prognostic factors for EC are the histological subtype of tumor, histological grade, stage, the depth of myometrial invasion and the presence of lymphovascular invasion, among which the stage and histological grade correlate with the risk of lymph node metastasis and the patient's prognosis (33–35). EC with a low histological grade has a lower cell density and greater movement of water molecules in the matrix and therefore tends to have higher ADC values. Conversely, EC with a higher histological grade has a higher cell density and therefore is expected to have lower ADC values (11). In previous publications on the possibility of ADC in determining the histological grade of a tumor, the results are inconsistent. Some studies have shown that there is no statistically significant correlation between the ADC value and a certain histological grade of the tumor, which is in line with our results (15, 18, 20, 24, 26, 28, 36–38). In the present study, we did not obtain a statistically significant difference in ADC values between three different histological grades of tumors that would enable their differentiation. Some authors, such as Tamai et al. showed that the ADC values of the histological grade 3 were significantly lower compared to the grade 1 (15, 39–41). There were also overlaps in ADC values between individual histological grades, as was the case with our results. The mean ADC values overlapped and were similar between the grades 2 and 3, $0.754 \pm 0.12\times10^{-3}$ mm^2/s and $0.728 \pm 0.13\times10^{-3}$ mm^2/s, respectively. The mean ADC value for grade 1 was $0.803 \pm 0.13\times10^{-3}$ mm^2/s.

Yan et al. reported a statistically significant difference in the mean ADC values between grade 1 ($0.921 \pm 0.133\times10^{-3}$ mm^2/s) and grade 2 ($0.968 \pm 0.240\times10^{-3}$ mm^2/s) in relation to the value in grade 3 ($0.917 \pm 0.184\times10^{-3}$ mm^2/s) (29).

Kakkar et al. reported that the mean ADC values of endometrial cancer for histologic grades 1, 2 and 3 were $0.72 \pm 0.13\times10^{-3}$ mm^2/s, $0.76 \pm 0.17\times10^{-3}$ mm^2/s and $0.74 \pm 0.12\times10^{-3}$ mm^2/s, respectively (42). There were statistically significant differences between grade 1 and grade 2. Ozturk et al. found that high-grade EC had significantly lower ADC values compared to low-grade EC (43).

DWI can be used with great diagnostic accuracy to determine the depth of tumor invasion in the myometrium of the uterus, which strongly correlates with the presence of metastases in the

lymph nodes (3% with superficial myometrial invasion and 46% with deep myometrial invasion) (33, 44). This is why it is clinically important to differentiate between superficial and deep invasion of the myometrium to plan a further therapeutic approach (33, 44). In our study the largest number of patients had confirmed stage IA with the mean ADC value of 0.811 ± 0.13 $\times 10^{-3}$ mm^2/s and stage IB with the mean ADC value of 0.696 ± 0.12$\times 10^{-3}$ mm^2/s. As for our results, no statistically significant difference in the mean ADC values was obtained between the mentioned stages, and this corroborates with the results of several earlier studies (15, 26, 45). In contrast, Husby et al. have shown that there was a statistically significant difference in the mean ADC values of ECs with deep myometrial invasion (0.75×10^{-3} mm^2/s), which were significantly lower than the mean ADC values of tumors with superficial invasion (0.85×10^{-3} mm^2/s) (46).

Recent articles that have attracted the interest of prestigious medical scientific journals are about the application of artificial intelligence, specifically its subfield of deep learning-based methods. The literature indicates that weakly-supervised learning-based deep learning methods using convolutional neural networks have shown significant results in image pattern recognition (47). Published articles about deep learning-based methods in MRI diagnostics of EC include staging early EC on MR, predicting myometrial invasion in patients with stage I EC, determining the depth of myometrial invasion, and identifying lesions on MR images (48–53). In a retrospective study, Urushibara et al. examined the effectiveness of a deep learning model based on using convolutional neural networks in the diagnosis of EC on MRI images, compared to the evaluation made by three radiologists (47). The research included both histopathologically confirmed EC and benign lesions. According to their results, this model showed significantly better results based on a single image of the ADC map and axial contrast-enhanced T1-weighted image in differentiating the presence of EC compared to the radiologist's evaluation (47). Adding other types of images with different sequences improved the diagnostic value in some cases, but without a significant difference (47). The authors pointed out several limitations in their study, including the evaluation of only one selected image. In contrast, our study evaluated all sequences to accurately place the ROI in the lesion and measure the ADC value.

In our country and other developing countries, such models of deep learning methods are currently unavailable. Our method has the advantage of being widely available and simple to apply, with the possibility of implementation in routine clinical practice in the evaluation of MR images, without requiring better computer equipment. Deep learning methods are trained to perform a specific task, and they require verification, as they may have some shortcomings depending on the input data and how they were trained (54). Based on the input data, the model can learn certain characteristic parameters of the uterus region (48). In our sample of female patients, we had one case with a bicornuate uterus where we measured ADC values in the corpus with endometrial thickening, while the endometrium in the other corpus was thin. The question is whether the deep learning method can adequately recognize and evaluate certain cases, such as those with a different shape or position of the uterus or the presence of additional lesions in or around the uterus that would require additional control by a radiologist.

5 Conclusion

According to the results obtained in our study DWI with ADC map and measurements of ADC values represents a clinically useful tool in differentiation between malignant and benign endometrial lesions. Determination of the cut-off ADC value increases the diagnostic accuracy. The mean ADC values of malignant lesions are significantly lower than those of benign lesions and our results are in line with most of previous studies. In correlation to histopathological reports, MRI had a high sensitivity (100%) and good specificity of 90.2%. In our study population, there was no statistically significant difference in ADC values between different histological grades of tumors, and therefore grade prediction was impossible. The limitation may be due to the small number of patients with EC in the total sample. Future research on a larger sample of patients with EC could contribute to the determination of the histological grade of the tumor as an important prognostic factor. In determining FIGO stage, the most common were stages IA and IB, and there was no significant difference in the mean ADC values.

Data availability statement

The raw data supporting the conclusions of this article will be made available by the authors, without undue reservation.

Ethics statement

The studies involving human participants were reviewed and approved by Clinical Center of Vojvodina, Novi Sad, Serbia. The patients/participants provided their written informed consent to participate in this study. Written informed consent was obtained from the individual(s) for the publication of any potentially identifiable images or data included in this article.

Author contributions

The authors confirm their contribution to the paper as follows: study conception and design: ON and LM-S; data collection: BS, LM-S, and DV; analysis and interpretation of results: BS, ON, NA, and UM; draft manuscript preparation: BS, NA, and DK. All authors contributed to the article and approved the submitted version.

Conflict of interest

The authors declare that the research was conducted in the absence of any commercial or financial relationships that could be construed as a potential conflict of interest.

Publisher's note

References

1. Ravegnini G, Gorini F, De Crescenzo E, De Leo A, De Biase D, Di Stanislao M, et al. Can miRNAs be useful biomarkers in improving prognostic stratification in endometrial cancer patients? an update review. *Int J Cancer* (2022) 150(7):1077–90. doi: 10.1002/ijc.33857

2. Colombo N, Creutzberg C, Amant F, Bosse T, González-Martín A, Ledermann J, et al. ESMO-ESGO-ESTRO consensus conference on endometrial cancer: diagnosis, treatment and follow-up. *Ann Oncol* (2016) 27(1):16–41. doi: 10.1093/annonc/mdv484

3. Iram S, Musonda P, Ewies A. Premenopausal bleeding: When should the endometrium be investigated? - a retrospective non-comparative study of 3006 women. *Eur J Obstet Gynecol Reprod Biol* (2010) 148(1):86–9. doi: 10.1016/j.ejogrb.2009.09.023

4. Renaud MC, Le T. Epidemiology and investigations for suspected endometrial cancer. *J Obstet Gynaecol Can* (2013) 35(4):380–3. doi: 10.1016/S1701-2163(15)30970-1

5. Van den Bosch T, Coosemans A, Morina M, Timmerman D, Amant F. Screening for uterine tumours. *Best Pract Res Clin Obstet Gynaecol* (2012) 26(2):257–66. doi: 10.1016/j.bpobgyn.2011.08.002

6. Wolfman W, Leyland N, Heywood M, Singh SS, Rittenberg DA, Soucy R, et al. Asymptomatic endometrial thickening. *J Obstet Gynaecol Can* (2010) 32(10):990–9. doi: 10.1016/s1701-2163(16)34690-4

7. ACOG committee opinion no. 734: The role of transvaginal ultrasonography in evaluating the endometrium of women with postmenopausal bleeding. *Obstet Gynecol* (2018) 131(5):e124–9. doi: 10.1097/AOG.0000000000002631

8. Dokter E, Anderson L, Cho SM, Cohen–Hallaleh V, Lam KM, Saidi SA, et al. Radiology–pathology correlation of endometrial carcinoma assessment on magnetic resonance imaging. *Insights Imaging* (2022) 13(1):80. doi: 10.1186/s13244-022-01218-3

9. Nakamura J, Yoshikawa T, Maeda E, Akai X, Ohtsu H, Hayashi N, et al. Evaluation of endometrial thickness in postmenopausal women by using 3.0-T MRI. *S Afr J Rad* (2014) 18(1):1–4. doi: 10.4102/sajr.v18i1.603

10. Bakir B, Sanli S, Bakir VL, Ayas S, Yildiz SO, Iyibozkurt AC, et al. Role of diffusion weighted MRI in the differential diagnosis of endometrial cancer, polyp, hyperplasia, and physiological thickening. *Clin Imaging* (2017) 41:86–94. doi: 10.1016/j.clinimag.2016.10.016

11. Chilla GS, Tan CH, Xu C, Poh CL. Diffusion weighted magnetic resonance imaging and its recent trend-a survey. *Quant Imaging Med Surg* (2015) 5(3):407–22. doi: 10.3978/j.issn.2223-4292.2015.03.01

12. Kido A, Fujimoto K, Okada T, Togashi K. Advanced MRI in malignant neoplasms of the uterus. *J Magn Reson Imaging* (2013) 37(2):249–64. doi: 10.1002/jmri.23716

13. Winfield JM, Payne GS, deSousa NM. Functional MRI and CT biomarkers in oncology. *Eur J Nucl Med Mol Imaging* (2015) 42(4):562–78. doi: 10.1007/s00259-014-2979-0

14. Dhanda S, Thakur M, Kerkar R, Jagmohan P. Diffusion-weighted imaging of gynecologic tumors: diagnostic pearls and potential pitfalls. *Radiographics* (2014) 34 (5):1393–416. doi: 10.1148/rg.345130131

15. Rechichi G, Galimberti S, Signorelli M, Franzesi CT, Perego P, Valsecchi MG, et al. Endometrial cancer: correlation of apparent diffusion coefficient with tumour grade, depth of myometrial invasion, and presence of lymph node metastases. *AJR Am J Roentgenol* (2011) 197(1):256–62. doi: 10.2214/AJR.10.5584

16. Fujii S, Matsusue E, Kigawa J, Sato S, Kanasaki Y, Nakanishi J, et al. Diagnostic accuracy of the apparent diffusion coefficient in differentiating benign from malignant uterine endometrial cavity lesions: initial results. *Eur Radiol* (2008) 18(2):384–9. doi: 10.1007/s00330-007-0769-9

17. Gharibvand MM, Ahmadzadeh A, Asadi F, Fazelinejad Z. The diagnostic precision of apparent diffusion coefficient (ADC) in grading of malignant endometrial lesions compared with histopathological findings. *J Family Med Prim Care* (2019) 8(10):3372–8. doi: 10.4103/jfmpc.jfmpc_142_19

18. Cao K, Gao M, Sun YS, Li YL, Sun Y, Gao YN, et al. Apparent diffusion coefficient of diffusion weighted MRI in endometrial carcinoma-relationship with local invasiveness. *Eur J Radiol* (2012) 81(8):1926–30. doi: 10.1016/j.ejrad.2011.04.019

19. Mainenti PP, Pizzuti LM, Segreto S, Comerci M, Fronzo S, Romano F, et al. Diffusion volume (DV) measurement in endometrial and cervical cancer: A new MRI parameter in the evaluation of the tumor grading and the risk classification. *Eur J Radiol* (2016) 85(1):113–24. doi: 10.1016/j.ejrad.2015.10.014

20. Haldorsen IS, Salvesen HB. What is the best preoperative imaging for endometrial cancer? *Curr Oncol Rep* (2016) 18(4):25. doi: 10.1007/s11912-016-0506-0

21. Elsammak A, Shehata S, Abulezz M, Gouha G. Efficiency of diffusion weighted magnetic resonance in differentiation between benign and malignant endometrial lesions. *Egypt J Radiol Nucl Med* (2017) 48(3):751–9. doi: 10.1016/j.ejrnm.2017.02.008

22. Kececi IS, Nural MS, Aslan K, Danaci M, Kefeli M, Tosun M. Efficacy of diffusion-weighted magnetic resonance imaging in the diagnosis and staging of endometrial tumors. *Diagn Interv Imaging* (2016) 97(2):177–86. doi: 10.1016/j.diii.2015.06.013

23. Heo SH, Shin SS, Kim JW, Lim HS, Jeong YY, Kang WD, et al. Pre-treatment diffusion-weighted MR imaging for predicting tumor recurrence in uterine cervical cancer treated with concurrent chemoradiation: value of histogram analysis of apparent diffusion coefficients. *Korean J Radiol* (2013) 14(4):616–25. doi: 10.3348/kjr.2013.14.4.616

24. Bakir VL, Bakir B, Sanli S, Yildiz SO, Iyibozkurt AC, Kartal MG, et al. Role of diffusion-weighted MRI in the differential diagnosis of endometrioid and non-endometrioid cancer of the uterus. *Acta Radiol* (2017) 58(6):758–67. doi: 10.1177/0284185116669873

25. Ahmed SA, El Taieb HA, Abotaleb H. Diagnostic performance of sonohysterography and MRI diffusion in benign endometrial lesion characterization. *Egypt J Radiol Nucl Med* (2018) 49(2):579–89. doi: 10.1016/j.ejrnm.2018.02.010

26. Çavuşoğlu M, Sözmen Ciliz D, Ozsoy A, Duran S, Elverici E, Atalay CR, et al. Diffusion-weighted MRI of postmenopausal women with vaginal bleeding and endometrial thickening: Differentiation of benign and malignant lesions. *J Belg Soc Radiol* (2016) 100(1):70. doi: 10.5334/jbr-btr.1118

27. Moharamzad Y, Davarpanah AH, Yaghobi Joybari A, Shahbazi F, Toosi L, Kooshkiforooshani M, et al. Diagnostic performance of apparent diffusion coefficient (ADC) for differentiating endometrial carcinoma from benign lesions: a systematic review and meta-analysis. *Abdom Radiol* (2021) 46(3):1115–28. doi: 10.1007/s00261-020-02734-w

28. Shen SH, Chiou YY, Wang JH, Yen MS, Lee RC, Lai CR, et al. Diffusion-weighted single-shot echo-planar imaging with parallel technique in assessment of endometrial cancer. *AJR Am J Roentgenol* (2008) 190(2):481–8. doi: 10.2214/AJR.07.2155

29. Yan B, Zhao T, Liang X, Niu C, Ding C. Can the apparent diffusion coefficient differentiate the grade of endometrioid adenocarcinoma and the histological subtype of endometrial cancer? *Acta Radiol* (2018) 59(3):363–70. doi: 10.1177/0284185117716198

30. Abu Hashim H, Zayed A, Ghayaty E, El Rakhawy M. LNG-IUS treatment of non-atypical endometrial hyperplasia in perimenopausal women: a randomized controlled trial. *J Gynecol Oncol* (2013) 24(2):128–34. doi: 10.3802/jgo.2013.24.2.128

31. Djordjevic B, Stanojevic Z, Zivkovic V, Lalosevic D, Gligorijevic J, Krstic M. Preoperative and postoperative histopathological findings in patients with endometrial hyperplasia. *Med Pregl* (2007) 60(7-8):372–6. doi: 10.2298/MPNS0708372D

32. Natarajan P, Vinturache A, Hutson R, Nugent D, Broadhead T. The value of MRI in management of endometrial hyperplasia with atypia. *World J Surg Oncol* (2020) 18(1):34. doi: 10.1186/s12957-020-1811-5

33. Takeuchi M, Matsuzaki K, Nishitani H. Diffusion-weighted magnetic resonance imaging of endometrial cancer: differentiation from benign endometrial lesions and preoperative assessment of myometrial invasion. *Acta Radiol* (2009) 50(8):947–53. doi: 10.1080/02841850903099981

34. Yamada I, Miyasaka N, Kobayashi D, Wakana K, Oshima N, Wakabayashi A, et al. Endometrial carcinoma: Texture analysis of apparent diffusion coefficient maps and its correlation with histopathologic findings and prognosis. *Radiol Imaging Cancer* (2019) 1(2):e190054. doi: 10.1148/rycan.2019190054

35. Chryssou EG, Manikis GC, Ioannidis GS, Chaniotis V, Vrekoussis T, Maris TG, et al. Diffusion weighted imaging in the assessment of tumor grade in endometrial cancer based on intravoxel incoherent motion MRI. *Diagnostics (Basel)* (2022) 12 (3):692. doi: 10.3390/diagnostics12030692

36. Parameswaran BK, Lau E, Ferris NJ. Recognising pitfalls in assessment of tumours by diffusion-weighted MRI: a pictorial essay. *J Med Imaging Radiat Oncol* (2015) 59(2):188–94. doi: 10.1111/1754-9485.12278

37. Bharwani N, Miquel ME, Sahdev A, Narayanan P, Malietzis G, Reznek RH, et al. Diffusion-weighted imaging in the assessment of tumour grade in endometrial cancer. *Br J Radiol* (2011) 84(1007):997–1004. doi: 10.1259/bjr/14980811

38. Kishimoto K, Tajima S, Maeda I, Takagi M, Ueno T, Suzuki N, et al. Endometrial cancer: correlation of apparent diffusion coefficient (ADC) with tumor cellularity and tumor grade. *Acta Radiol* (2016) 57(8):1021–8. doi: 10.1177/0284185115612249

39. Tamai K, Koyama T, Saga T, Umeoka S, Mikami Y, Fujii S, et al. Diffusion-weighted MR imaging of uterine endometrial cancer. *J Magn Reson Imaging* (2007) 26 (3):682–7. doi: 10.1002/jmri.20997

40. Tanaka T, Terai Y, Fujiwara S, Tanaka Y, Sasaki H, Tsunetoh S, et al. Preoperative diffusion-weighted magnetic resonance imaging and intraoperative frozen sections for predicting the tumor grade in endometrioid endometrial cancer. *Oncotarget* (2018) 9(93):36575–84. doi: 10.18632/oncotarget.26366

41. Inoue C, Fujii S, Kaneda S, Fukunaga T, Kaminou T, Kigawa J, et al. Correlation of apparent diffusion coefficient value with prognostic parameters of endometrioid carcinoma. *J Magn Reson Imaging* (2015) 41(1):213–9. doi: 10.1002/jmri.24534

42. Kakkar C, Gupta K, Jain K, Narang V, Singh A, Saggar K, et al. Diagnostic accuracy of calculated tumor volumes and apparent diffusion coefficient values in predicting endometrial cancer grade. *Int J Appl Basic Med Res* (2022) 12(1):37–42. doi: 10.4103/ijabmr.ijabmr_553_21

43. Ozturk M, Kalkan C, Danaci M, Kefeli M. Diffusion-weighted MRI at 3T in endometrial cancer: Correlation of apparent diffusion coefficient with histopathological prognostic parameters. *J Coll Physicians Surg Pak* (2021) 31(12):1399–405. doi: 10.29271/jcpsp.2021.12.1399

44. Das SK, Niu XK, Wang JL, Zeng LC, Wang WX, Bhetuwal A, et al. Usefulness of DWI in preoperative assessment of deep myometrial invasion in patients with endometrial carcinoma: a systematic review and meta-analysis. *Cancer Imaging* (2014) 14(1):32. doi: 10.1186/s40644-014-0032-y

45. Lin G, Ng KK, Chang CJ, Wang JJ, Ho KC, Yen TC, et al. Myometrial invasion in endometrial cancer: diagnostic accuracy of diffusion-weighted 3.0-T MR imaging–initial experience. *Radiology* (2009) 250(3):784–92. doi: 10.1148/radiol.2503080874

46. Husby JA, Salvesen ØO, Magnussen IJ, Trovik J, Bjørge L, Salvesen HB, et al. Tumour apparent diffusion coefficient is associated with depth of myometrial invasion and is negatively correlated to tumour volume in endometrial carcinomas. *Clin Radiol* (2015) 70(5):487–94. doi: 10.1016/j.crad.2014.12.016

47. Urushibara A, Saida T, Mori K, Ishiguro T, Inoue K, Masumoto T, et al. The efficacy of deep learning models in the diagnosis of endometrial cancer using MRI: a comparison with radiologists. *BMC Med Imaging* (2022) 22(1):80. doi: 10.1186/s12880-022-00808-3

48. Mao W, Chen C, Gao H, Xiong L, Lin Y. A deep learning-based automatic staging method for early endometrial cancer on MRI images. *Front Physiol* (2022) 13:974245. doi: 10.3389/fphys.2022.974245

49. Hodneland E, Dybvik JA, Wagner-Larsen KS, Šoltészová V, Munthe-Kaas AZ, Fasmer KE, et al. Automated segmentation of endometrial cancer on MR images using deep learning. *Sci Rep* (2021) 11(1):179. doi: 10.1038/s41598-020-80068-9

50. Pelikan HM, Trum JW, Bakers FC, Beets-Tan RG, Smits LJ, Kruitwagen RF. Diagnostic accuracy of preoperative tests for lymph node status in endometrial cancer: a systematic review. *Cancer Imaging* (2013) 13(3):314–22. doi: 10.1102/1470-7330.2013.0032

51. Qin L, Lai L, Wang H, Zhang Y, Qian X, He D. Machine learning-based Gray-level Co-occurrence matrix (GLCM) models for predicting the depth of myometrial invasion in patients with stage I endometrial cancer. *Cancer Manag Res* (2022) 14:2143–54. doi: 10.2147/CMAR.S370477

52. Chen X, Wang Y, Shen M, Yang B, Zhou Q, Yi Y, et al. Deep learning for the determination of myometrial invasion depth and automatic lesion identification in endometrial cancer MR imaging: a preliminary study in a single institution. *Eur Radiol* (2020) 30(9):4985–94. doi: 10.1007/s00330-020-06870-1

53. Rodríguez-Ortega A, Alegre A, Lago V, Carot-Sierra JM, Ten-Esteve A, Montoliu G, et al. Machine learning-based integration of prognostic magnetic resonance imaging biomarkers for myometrial invasion stratification in endometrial cancer. *J Magn Reson Imaging* (2021) 54(3):987–95. doi: 10.1002/jmri.27625

54. Li C, Li W, Liu C, Zheng H, Cai J, Wang S. Artificial intelligence in multiparametric magnetic resonance imaging: A review. *Med Phys* (2022) 49(10): e1024–54. doi: 10.1002/mp.15936

frontiers | Frontiers in Oncology

TYPE Original Research
PUBLISHED 24 April 2023
DOI 10.3389/fonc.2023.1101297

OPEN ACCESS

EDITED BY
Alessio G. Morganti,
University of Bologna, Italy

REVIEWED BY
Angelo Finelli,
ULSS2 Marca Trevigiana, Italy
Sung Bin Park,
Chung-Ang University Hospital, Republic of Korea

*CORRESPONDENCE
Furong Lv
lfr918@sina.com
Hongmei Dong
dhmqq@yeah.net

SPECIALTY SECTION
This article was submitted to Gynecological Oncology, a section of the journal Frontiers in Oncology

RECEIVED 17 November 2022
ACCEPTED 03 April 2023
PUBLISHED 24 April 2023

CITATION
Hu Y, Chen B, Dong H, Sheng B, Xiao Z, Li J, Tian W and Lv F (2023) Comparison of ultrasound–based ADNEX model with magnetic resonance imaging for discriminating adnexal masses: a multi-center study.
Front. Oncol. 13:1101297.
doi: 10.3389/fonc.2023.1101297

Comparison of ultrasound –based ADNEX model with magnetic resonance imaging for discriminating adnexal masses: a multi-center study

Yanli Hu[1,2,3], Bo Chen[4], Hongmei Dong[1,2]*, Bo Sheng[3], Zhibo Xiao[3], Jia Li[3], Wei Tian[5,6] and Furong Lv[3]*

[1]Department of Ultrasonography, Chongqing Health Center for Women and Children, Chongqing, China, [2]Department of Ultrasonography, Women and Children's Hospital of Chongqing Medical University, Chongqing, China, [3]Department of Radiology, The First Affiliated Hospital of Chongqing Medical University, Chongqing, China, [4]Department of Ultrasonography, The First Affiliated Hospital of Chongqing Medical University, Chongqing, China, [5]Department of Radiology, Women and Children's Hospital of Chongqing Medical University, Chongqing, China, [6]Department of Radiology, Chongqing Health Center for Women and Children, Chongqing, China

Objectives: The ADNEX model offered a good diagnostic performance for discriminating adnexal tumors, but research comparing the abilities of the ADNEX model and MRI for characterizing adnexal tumors has not been reported to our knowledge. The aim of this study was to evaluate the diagnostic accuracy of the ultrasound-based ADNEX (Assessment of Different NEoplasias in the adneXa) model in comparison with that of magnetic resonance imaging (MRI) for differentiating benign, borderline and malignant adnexal masses.

Methods: This prospective study included 529 women with adnexal masses who underwent assessment *via* the ADNEX model and subjective MRI analysis before surgical treatment between October 2019 and April 2022 at two hospitals. Postoperative histological diagnosis was considered the gold standard.

Results: Among the 529 women, 92 (17.4%) masses were diagnosed histologically as malignant tumors, 67 (12.7%) as borderline tumors, and 370 (69.9%) as benign tumors. For the diagnosis of malignancy, including borderline tumors, overall agreement between the ADNEX model and MRI pre-operation was 84.9%. The sensitivity of the ADNEX model of 0.91 (95% confidence interval [CI]: 0.85–0.95) was similar to that of MRI (0.89, 95% CI: 0.84–0.94; P=0.717). However, the ADNEX model had a higher specificity (0.90, 95% CI: 0.87–0.93) than MRI (0.81, 95% CI: 0.77–0.85; P=0.001). The greatest sensitivity (0.96, 95% CI: 0.92–0.99) and specificity (0.94, 95% CI: 0.91–0.96) were achieved by combining the ADNEX model and subjective MRI assessment. While the total diagnostic accuracy did not differ significantly between the two methods (P=0.059), the ADNEX model showed greater diagnostic accuracy for borderline tumors (P<0.001).

Conclusion: The ultrasound-based ADNEX model demonstrated excellent diagnostic performance for adnexal tumors, especially borderline tumors, compared with MRI. Accordingly, we recommend that the ADNEX model, alone or with subjective MRI assessment, should be used for pre-operative assessment of adnexal masses.

KEYWORDS

adnexal mass, ovarian cancer, magnetic resonance imaging, adnex, ultrasound

Introduction

Adnexal malignancy is an uncommon, life-threatening gynecological tumor with a high recurrence rate and low survival rate (1). It is usually detected at an advanced stage, contributing to the low 5-year survival rate. However, when detected in the early stage, the 5-year overall survival rate is more than 90% (2), such as borderline ovarian tumors (BOTs) survival is 95% at 5 years (3). Therefore, accurate early diagnosis of adnexal tumors is not only crucial for improving patient survival by applying appropriate treatments, which differ according to the status of tumor (4–6), but also important for the young female patients who want to preserve their fertility potential (7). Benign masses can be observed *via* follow-up or locally excised *via* laparoscopic surgery and BOTs could even adopt a strategy of fertility-sparing surgery because of its excellent reproductive outcome and long-term survival (7), whereas malignant masses must to properly stage and debulking surgery performed by a gynecological oncologist (8).

Imaging techniques, including transvaginal ultrasound and magnetic resonance imaging (MRI), are important tools for the preoperative evaluation of adnexal tumors (5, 6, 8). Although transvaginal ultrasound is a preferred method for the detection of adnexal masses, the value of this method for the diagnosis of adnexal masses is strongly dependent on the ultrasound operator's experience (9). To increase the diagnostic accuracy and repeatability of ultrasonic assessment for adnexal tumors, the International Ovarian Tumor Analysis (IOTA) group created a new ultrasound-based ADNEX (Assessment of Different NEoplasias in the adneXa) model that offers better performance for identifying malignant tumors among adnexal tumors (10). This model can predict the probability of malignancy based on three clinical and six ultrasonic characteristics. Multiple studies have confirmed that the ADNEX model offers better diagnostic performance than previous IOTA models (11–13), with a higher sensitivity (0.98, 95% confidence interval [CI]: 0.93–1.00). However, its specificity was lowest among all models (0.62, 95% CI: 0.55–0.68) (14).

MRI is a helpful tool for distinguishing benign and malignant adnexal tumors. However, the cost and operative time of MRI limit its routine use in the screening of adnexal tumors. According to the European Society of Urogenital Radiology (ESUR) guidelines, MRI is recommended only for masses that cannot be discriminated by ultrasound (15). Previous studies have indicated that the IOTA LR2 model and MRI give comparable results (16–18). However, a multi-center research comparing the abilities of the ADNEX model and MRI for characterizing adnexal tumors has not been reported to our knowledge. The aim of this multi-center study was to compare the diagnostic performances of the ultrasound-based ADNEX model and subjective MRI evaluation for distinguishing benign and malignant adnexal masses. Furthermore, we aimed to assess the diagnostic performance of the combination of the ADNEX model and subjective MRI assessment.

Material and methods

Study design and patients

This multi-center, prospective cohort study was carried out at gynecological oncology center of the First Affiliated Hospital of Chongqing Medical University and the Women and Children's Hospital of Chongqing Medical University (Figure 1). A total of 529 women treated at these two hospitals were enrolled consecutively between October 2019 and April 2022, and their adnexal masses were assessed using both ultrasound and MRI. This study was approved by the institutional ethics committees of the two hospitals, and all patients voluntarily provided informed consent.

The inclusion criteria were as follows: (a) at least one adnexal mass that had been evaluated by ultrasound and MRI examination at either of the two hospitals. The most complicated or largest mass was chosen for the final analysis if bilateral adnexal masses were detected; and (b) planned surgical excision of the mass, as recommended by a gynecological oncologist. The exclusion criteria were as follows: (a) history of ovarian tumor; (b) pregnancy; (c) refusal to undergo ultrasound or MRI examination; and (d) lack of surgical excision of the mass within 120 days after the imaging examinations (16).

All the patients underwent ultrasound and MRI examinations, and the results of the evaluations were recorded simultaneously. The results for serum CA125 were unknown at the time of the ultrasound and MRI examinations.

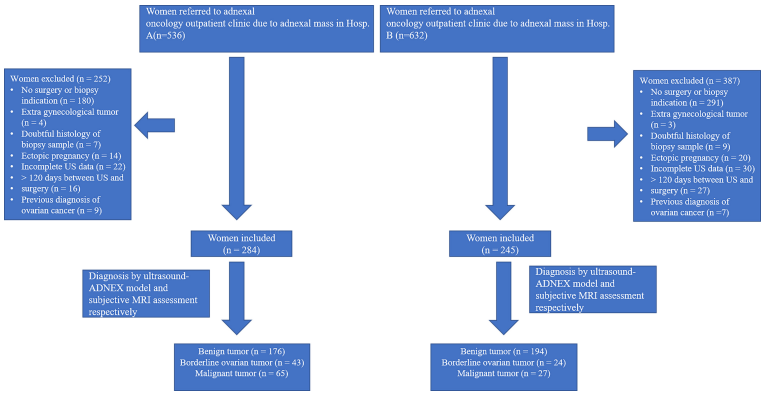

FIGURE 1
Flowchart of enrollment in study cohort of women diagnosed with adnexal mass in two hospitals.

Ultrasound acquisition and analysis

All the adnexal masses were assessed by an ultrasound doctor using the IOTA ADNEX model before MRI examination. For all masses, transvaginal ultrasound was performed with a Voluson S6® or Voluson E8® ultrasound system with probe frequencies ranging between 5 and 9 MHz (GE Healthcare Ultrasound, Milwaukee, WI, USA). Transabdominal ultrasound was performed if the masses were so large so that their complete shape could not be seen using transvaginal probes.

The eight variables factored into the calculation were as follows: (a) patient's age (year); (b) maximum diameter of the lesion (mm); (c) maximum diameter of the largest solid part (mm); (d) > 10 locules in the tumor (yes = 1, no = 0); (e) presence of acoustic shadows (yes = 1, no = 0); (f) number of papillary projections; and (g) presence of ascites (yes = 1, no = 0); (h) Gynecological oncology center (yes=1, no=0). In the IOTA ADNEX assessment for patients, we set 0.15 as the cut-off value of probability of malignancy (POM), and masses were considered malignant if POM >0.15 (19).

MRI acquisition and analysis

MRI data were preoperatively analyzed subjectively by a radiologist who was blinded to the results of the ADNEX model. MRI examinations were conducted using a 1.5-T MR scanner (Ingenia Ambition; Philips Healthcare, Erlangen, Germany or Signa HD Excite, GE Healthcare, Milwaukee, WI, USA) with a phase-array body coil. The MRI protocol was as follows: axial and sagittal T2-weighted fast spin-echo sequences followed by axial T1-weighted gradient recall echo and diffusion weighted image (DWI: b = 0, 1,000 mm^2/s) sequences. Then dynamic contrast-enhanced MR images were acquired *via* axial fat-saturated T1-weighted imaging after intravenous injection of a bolus of 0.2 ml/kg gadodiamide as the contrast agent (GE Healthcare).

According to the ESUR guideline (20), the radiologist judged whether the mass was possibly malignant, borderline or benign *via* subjective assessments. MRI data were analyzed by two experienced radiologists. The final MRI results were decided through discussion if the two radiologists originally had conflicting findings for a case.

Reference standard

After surgery, all excised specimens were examined histologically at one of the two hospitals in the study, and the masses were classified according to the guidelines of the World Health Organization for the classification of tumors (21). For each case, the histopathological diagnosis was considered as the reference standard.

Statistical analysis

All statistical analyses were using SPSS 25.0 software (IBM, Armonk, NY, USA). The descriptive statistics included mean ± standard deviation for continuous variables and number (percentage) for categorical variables (ultrasound-ADNEX results). The sensitivity, specificity, negative predictive value (NPV), positive predictive value (PPV), and 95% Wilson score confidence intervals were calculated for evaluation of the diagnostic performance of the ultrasound-based ADNEX model and MRI evaluation. Analyses of agreement (percent total agreement) was used to compare the ability of the two methods to detect malignancy. McNemar's exact χ^2 test was applied to analyze the differences in discriminatory ability between the two strategies or the two hospitals. We also analyzed the diagnostic efficacy of combining the ADNEX model and subjective MRI assessment. If the two methods produced different results for a case, the mass was then considered a malignant tumor. For analysis of the six variables of the ultrasound-based ADNEX model, one-way analysis of variance (ANOVA) or Mann–Whitney U test (if appropriate) was used to compare variables among benign, borderline, and malignant tumors. Statistical significance was assumed at a level of $P<0.05$ for all comparisons.

Results

Diagnoses of patients with adnexal masses

The histologically confirmed diagnoses of 529 patients with at least one adnexal mass are shown in Table 1. Overall, 370 (69.9%) masses were benign tumors, and 159 (30.1%) masses were malignant tumors (including 67 borderline and 92 malignant tumors). Malignant tumors were seen in 23.4% (65/278) of patients treated at the First Affiliated Hospital of Chongqing Medical University and in 11% (27/245) treated at the Women and Children's Hospital of Chongqing Medical University. No statistically significant difference in the diagnostic accuracy rate was detected between the two centers (P=0.563, Table 2). Although the characteristics of patients treated at the two hospitals were acquired by different researchers, the ultrasound-based ADNEX model and MRI assessments conducted at the two hospitals showed similar diagnostic performance, suggesting the results of this study are generalizable (Tables 2, 3).

Validation of the IOTA ultrasound-based ADNEX model

The clinical and sonographic features considered in the ADNEX model are presented in Table 4. The patients with malignant tumors were older than those with benign and borderline tumors (both P<0.001), and the patients with borderline tumors were older than those with benign tumors (P<0.001). Several variables were closely related to the properties of the adnexal masses. For example, the maximum diameter of the lesion and largest solid part of the lesion were greater in cases with malignant tumors than in cases with benign and borderline tumors (all P<0.001). However, the maximum diameter of the lesion and largest solid part of the lesion did not differ significantly between benign tumors and borderline tumors (P=0.786 and P=0.187, respectively). The risk of malignancy was closely related to the presence of ascites (odds ratio [OR]=12.88, 95% confidential interval [CI): 6.45–25.74, P<0.001]. However, acoustic shadows were significantly related with benign tumors (OR=7.576, 95% CI:

TABLE 1 Histological subtypes of adnexal tumors in patients treated in two institutions.

Histology	All(n=529)	By center	
		Hosp. A (n=284)	Hosp. B(n=245)
Benign	**370(69.9%)**	**176 (62.0%)**	**194 (79.2%)**
Teratoma	110(29.7%)	46 (26.1%)	64(33.0%)
Serous cystadenoma	84(22.7%)	50 (28.4 %)	34(17.5%)
Mucinous cystadenoma	49(13.2%)	18(10.2%)	31(16…)
Cystadenofibroma	2(0.5%)	2(1.1%)	0(0)
Fibroma	6(1.6%)	2(1.1%)	4(2.1%)
Brenner tumor	4(1.1%)	3(1.7%)	1(0.5%)
Ovarian torsion	31(8.4%)	20(11.4%)	11(5.7%)
Functional cyst	76(20.5%)	29(16.5%)	47(24.2%)
Other benign lesion	8(2.2%)	6(3.4%)	2(1.0%)
Borderline	**67(12.7%)**	**43(15.1%)**	**24(9.8%)**
Serous borderline tumor	41(61.2%)	29(67.4%)	12(50%)
Mucinous borderline tumor	22(32.8%)	13(30.2%)	9(37.5%)
Other borderline tumor	4(6.0%)	1(2.3%)	3(12.5%)
Malignancy	**92(17.4%)**	**65(22.9%)**	**27(11.0%)**
Serous adenocarcinoma	48(52.2%)	32(49.2%)	16(59.3%)
Clear cell carcinoma	20(21.7%)	14(21.5%)	6(22.2%)
Granulosa cell tumor	7(7.6%)	6(9.2%)	1(3.7%)
Mucinous adenocarcinoma	6(6.5%)	3(4.6%)	3(11.1%)
Sertoli leydig	2(2.2%)	2(3.1%)	0(0.0%)
Ovarian metastasis	9(9.8%%)	8(12.3%)	1(3.7%)

Hosp A: The First Affiliated Hospital of Chongqing Medical University; Hosp B: Women and Children's Hospital of Chongqing Medical University.

TABLE 2 Comparison of the diagnostic performances of the methods at the two institutions.

Imaging method	US-based IOTA ADNEX model		*P*	MRI subjective assessment		*P*	Combination of ADNEX and MRI[a]		*P*
	Hosp. A	Hosp. B		Hosp. A	Hosp. B		Hosp. A	Hosp. B	
Correctly classified	253	222	0.563	237	205	0.945	270	232	0.844
Incorrectly classified	31	23		47	40		14	13	

[a]Cases of disagreement were classified as malignant. Hosp A: The First Affiliated Hospital of Chongqing Medical University; Hosp B: Women and Children's Hospital of Chongqing Medical University.

2.32–24.69, *P*<0.001). The feature of >10 locules was statistically different only between benign and malignant tumors (*P*=0.001). The ADNEX model had a sensitivity of 0.91 (95% CI: 0.85-0.95), specificity of 0.90 (95% CI: 0.87–0.93), PPV of 0.79 (95% CI: 0.73–0.85), and NPV of 0.95 (95% CI: 0.93–0.98; Table 3). Among the 529 women, the ADNEX model classified only 54 (10.2%) adnexal tumors incorrectly, including 16 benign tumors as malignant and 38 malignant tumors (including borderline tumors) as benign. Figures 2 showed representative case.

Subjective MRI assessment results

For distinguishing malignant tumors, including borderline tumors, from benign adnexal tumors, MRI had a sensitivity of 0.89 (95% CI: 0.84–0.94), specificity of 0.81 (95% CI: 0.77–0.85), PPV of 0.67 (95% CI: 0.61–0.74), and NPV of 0.94 (95% CI: 0.92–0.97; Table 3). Among the 529 cases, MRI classified 87 (16.4%) adnexal tumors incorrectly, including 18 malignant tumors (including borderline tumors) as benign and 69 benign tumors as malignant. Figures 2 showed representative case.

Comparison of the diagnostic performances of the ADNEX model and subjective MRI assessment

The results for the preoperative diagnostic accuracy and agreement of the two methods are shown in Table 5. Good total agreement (84.9%) between the ADNEX model and subjective MRI assessment was observed, but poor agreement between the ADNEX model and MRI was observed for borderline tumors (67.2%). From the comparison of diagnostic performance, the sensitivity of the ADNEX model (0.91; 95% CI: 0.85-0.95) for detecting malignant tumors, including borderline tumors, was similar to that of MRI (0.89; 95% CI: 0.84–0.94; *P*=0.717; Table 4). However, the specificity of the ADNEX model (0.90; 95% CI: 0.87–0.93) was higher than of MRI (0.81; 95% CI: 0.77–0.85; *P*=0.001; Table 4). The accuracy of the ADNEX model (0.90; 95% CI: 0.87–0.92) did not differ significantly from that of MRI assessment (0.84; 95% CI: 0.80-0.87, *P*=0.059, Table 5). However, when we compared the agreement rate between the ADNEX model and MRI for borderline tumors, the ADNEX model showed superior accuracy compared with MRI (*P*<0.001, Table 5). No statistically significant differences were detected between the two methods for benign and malignant tumors (*P*=0.721 and *P*=0.246 respectively, Table 5). When we combined the ADNEX model with subjective MRI assessment, the sensitivity increased to 0.97 (95% CI: 0.94–1.00) and the specificity increased to 0.94 (95% CI: 0.91–0.96), and these values were significantly higher than those for either the ADNEX model (*P*=0.013 and *P*=0.001, respectively) or MRI (*P*=0.005 and *P*<0.001) alone.

Discussion

The IOTA ultrasound-based ADNEX model performed well in distinguishing malignant and benign adnexal masses using data obtained in two hospitals in China, especially for borderline tumors, even though CA125 level data were not included in this study. Although

TABLE 3 Comparison of the diagnostic performances of the ADNEX model and subjective MRI assessment.

Imaging method	Correctly classified		Incorrectly classified		Sensitivity (95% CI)	Specificity (95% CI)	PPV (95% CI)	NPV (95% CI)	Accuracy (95% CI)
	Malignant	benign	Malignant as benign	Benign as malignant					
US-based IOTA ADNEX model									
All	143	332	16	38	0.91 (0.85-0.95)	0.90 (0.87-0.93)	0.79 (0.73-0.85)	0.95 (0.93-0.98)	0.90 (0.87-0.92)
Hosp A	98	155	10	21	0.92 (0.85-0.96)	0.88 (0.83-0.93)	0.88 (0.75-0.89)	0.97 (0.90-0.98)	0.89 (0.85-0.93)

(Continued)

TABLE 3 Continued

Imaging method	Correctly classified		Incorrectly classified		Sensitivity (95% CI)	Specificity (95% CI)	PPV (95% CI)	NPV (95% CI)	Accuracy (95% CI)
	Malignant	benign	Malignant as benign	Benign as malignant					
Hosp B	45	177	6	17	0.92 (0.79-0.97)	0.91 (0.87-0.95)	0.80 (0.61-0.84)	0.97 (0.94-0.99)	0.91 (0.87-0.94)
MRI subjective assessment									
All	141	301	18	69	0.89 (0.84-0.94)	0.81 (0.77-0.85)	0.67 (0.61-0.74)	0.94 (0.92-0.97)	0.84 (0.80-0.87)
Hosp A	96	141	12	35	0.89 (0.83-0.95)	0.80 (0.74-0.86)	0.73 (0.66-0.81)	0.92 (0.88-0.97)	0.83 (0.79-0.88)
Hosp B	45	160	6	34	0.88 (0.79-0.97)	0.82 (0.77-0.88)	0.57 (0.46-0.68)	0.96 (0.94-0.99)	0.84 (0.79-0.88)
Combination of ADNEX and MRI[a]									
All	154	346	5	24	0.97 (0.94-1.00)	0.94 (0.91-0.96)	0.87 (0.82-0.92)	0.99 (0.97-1.00)	0.95 (0.93-0.97)
Hosp A	105	165	3	11	0.97 (0.94-1.00)	0.93 (0.90-0.97)	0.91 (0.85-0.96)	0.98 (0.96-1.00)	0.95 (0.93-0.98)
Hosp B	49	183	2	11	0.96 (0.91-1.00)	0.94 (0.91-0.98)	0.82 (0.71-0.92)	0.99 (0.97-1.00)	0.95 (0.92-0.97)

[a]Cases of disagreement were classified as malignancy. Hosp A: The First Affiliated Hospital of Chongqing Medical University; Hosp B: Women and Children's Hospital of Chongqing Medical University.
Malignant tumor included the borderline tumor. Malignant include borderline tumor.

CA125 is one of the clinical variables (www.iotagroup.org/adnexmodel/), the applications allow risk calculation even without information on serum CA-125 level despite the decrease in performance and it is important for good discrimination between stage II-IV cancer and stage I and secondary metastatic cancer in the ultrasound-based ADNEX model (10). Besides, previous studies also demonstrated that the CA125 level had no significant impact on the diagnostic accuracy of the ADNEX model (22–24). This is because CA125 is not a specific

TABLE 4 Sonographic features of adnexal masses in 529 women treated in two institutions.

Variables included in IOTA ADNEX model	Benign	borderline	Malignant	*P*
Age (years)	47.4±13.4	51.0±13.6	56.5±11.3	<0.001
Ascites	11(3.0)	2(3.0)	43(46.7)	<0.001
Maximal diameter of the lesion (mm)	118.1±58.8	122.2±46.6	157.4±73.4	<0.001
Maximal diameter of the largest solid part (mm)	34.3±29.2	55.6±28.0	93.0±48.9	<0.001
>10 locules	52(14.1)	11(16.4)	28(30.4)	0.001
Number of papillary projections				NA
0	346(93.5)	45(67.2)	75(81.5)	
1	10(2.7)	12(17.9)	7(7.6)	
2	4(1.1)	3(4.5)	0(0)	
3	6(1.6)	0(0)	3(3.3)	
>3	4(1.1)	7(10.4)	7(7.6)	
Acoustic shadows	89(24.1)	2(3.0)	1(1.1)	<0.001

Data are given as mean ± SD or n (%). Groups compared using McNemar's exact $\chi 2$, one-way analysis of variance or Kruskal–Wallis test, if appropriate. Max, maximum; NA, not applicable.

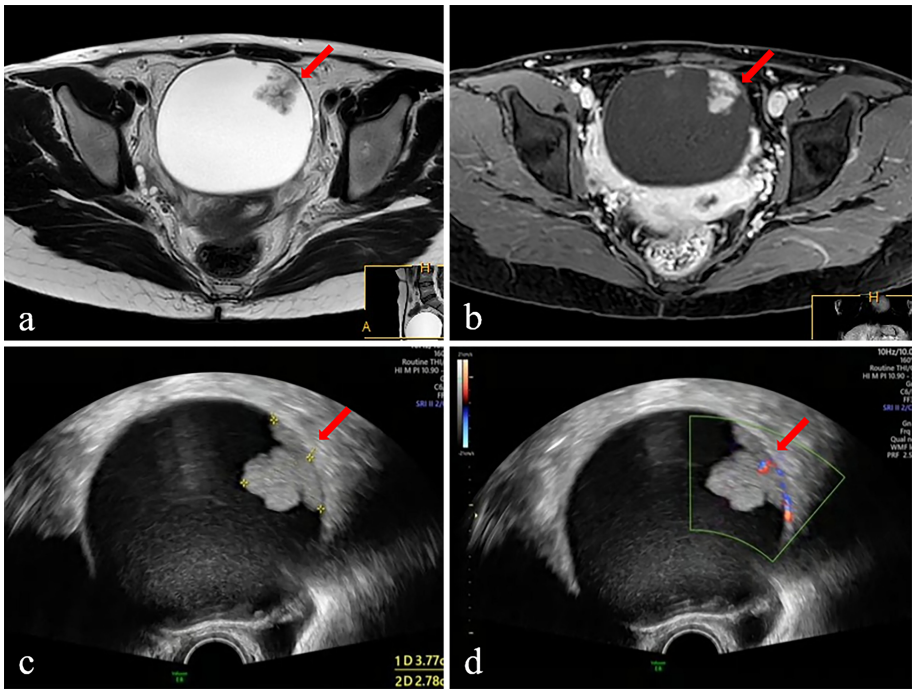

FIGURE 2
The ultrasound and MR images of a 28-year-old female patient with adnexal mass. The mass was diagnosed borderline tumor preoperatively by ADNEX-US and subjective MRI assessment. **(A)** Axial T 2 WI displays intermediate SI of the solid component (arrow) and high SI of cystic component. **(B)** Postcontrast axial T1-fat-suppressed image shows obvious persistent enhancement of the solid component (arrow) and walls of the cystic component. **(C)** Ultrasound images (Gray scale) displayed an anechoic mass with equal echo of the solid component (arrow). **(D)** Ultrasound images (color Doppler) displayed the solid component of mass has dotted blood flow signal. Surgery was performed, and the diagnosis was confirmed on histopathology as the borderline tumor.

marker for ovarian cancer, and it can be increased in cases with benign lesions, such as endometriosis and uterine fibroids (25, 26). Human epididymal protein-4 (HE-4) has been identified as a new tumor marker for ovarian cancer (27), and research has verified that HE-4 is more valuable than CA125 for ovarian cancer (28). As a result, the ADNEX model may be further optimized for the diagnosis of adnexal masses in the future.

In the present study, the diagnostic performance of the two methods showed no statistically significant difference between the two hospitals, suggesting good repeatability of these methods in two institutions. In addition, the diagnostic performance for the ADNEX model was similar to that of the expert US examiners' subjective assessment in the analysis of 3511 adnexal masses (29). These observations indicate that the IOTA ultrasound-based ADNEX model is a widely applicable tool in different populations and institutions to assist sonographers, gynecologists, and even non-professional doctors with various training backgrounds and levels of experience in the diagnosis of adnexal tumors. However, the sensitivity and specificity of the ADNEX model in our study was lower than that calculated in by Valentin et al. (29), whereas the specificity in our study was higher than that in other studies (11, 14). This may be related to differences in the study samples, but another reason could be use of the cut-off value of 0.15 for the ADNEX model results. Because Huang X et al. have found that the cut-off value of 0.15 for the ADNEX model had high diagnostic accuracy in identifying ovarian malignant tumor (19).

We noted obvious differences in the maximum diameter of lesions and the largest solid component of tumors in the present study, but these findings differed from those in a previous study (11). Moreover, in our study, the ultrasound feature of acoustic shadowing was applied as a predictive criterion for benign adnexal tumors and the risk of malignancy was closed related with the presence of ascites, findings which were similar to those of the previous study (11). These results indicate the importance of the features of acoustic shadowing and ascites.

The present study showed good agreement between the ADNEX model and MRI assessment. Additionally, the sensitivity of the ADNEX model was similar to that of MRI. However, the ADNEX model had a higher specificity, suggesting that the ADNEX model provided fewer false-positive cases compared with MRI. Among the benign, borderline and malignant tumors, the agreement rate between the ADNEX model and MRI was lowest for borderline tumors (only 67.2%), suggesting that the diagnostic accuracy of the ADNEX model for borderline tumors was superior to that of MRI. Although previous studies have reported characteristics of borderline tumors, few parameters can reliably differentiate borderline tumors from benign tumors on MRI (30, 31). Perhaps this was a reason that the specificity of the ADNEX model was higher than that of MRI. As a result, the ADNEX model may play an additional important role in determining the appropriate surgical management before operation and can be helpful to promote optimal patient management in the future due to its good diagnostic accuracy rate.

10.3389/fonc.2023.1101297

TABLE 5 Diagnostic agreement and comparison of agreement rates between the ADNEX model and MRI with adnexal tumor histology as reference standard.

Histology	n	Discriminating between different types of tumors				p	Agreement analysis				Agreement (%)
		US-ADNEX model		MRI subjective assessment			US-ADNEX correct		US-ADNEX incorrect		
		Correctly classified	Incorrectly classified	Correctly classified	Incorrectly classified		MRI correct	MRI incorrect	MRI correct	MRI incorrect	
All	529	475	54	455	74	0.059	425	50	30	24	84.9%
Benign	370	332	38	329	41	0.721	308	24	21	17	87.8%
Borderline	67	64	3	42	25	<0.001	42	22	0	3	67.2%
Malignant	92	79	13	84	8	0.246	75	4	9	4	85.9%

In the current study, the ADNEX model classified 54 (10%) adnexal tumors incorrectly. A collaborative analysis of IOTA studies reported that only a small portion (approximately 7%) of adnexal masses cannot be accurately classified preoperatively, even when subjective ultrasound assessment is performed by an experienced sonographer (29). However, this collaborative analysis aimed to discriminate between benign and malignant tumors using a logistic regression (LR) model only for masses that were deemed unclassifiable by the sonographer. This is likely the reason that the rate of inaccurate classification was higher in our study than in the previous analysis.

The combination of the ADNEX model and MRI provided improved accuracy for the preoperative diagnosis of adnexal tumors than either method alone, likely because subjective MRI assessment underestimated the risk of malignancy. In the present study, the greatest sensitivity and specificity also were obtained by combining the ADNEX model and subjective MRI assessment. Therefore, to decrease the risk of misclassification, combination of both imaging strategies should be recommended for preoperative assessment of adnexal masses.

This study has some limitations to consider. First, the numbers of enrolled patients and institutions were small for a multi-center study. Although the ADNEX model demonstrated greater specificity than MRI in the present study, these limitations likely affected the diagnostic performance of both methods. Second, all MRI examinations were performed on a 1.5T MR system, and we did not compare differences between results obtained with a 3.0T MRI system and the ADNEX model. Third, the ADNEX model was not used for clinical management, and therefore, the influence of this model on patient management is unknown. Fourth, because the ADNEX model is still not commonly used, it remains unfamiliar to many clinicians. Moreover, it is still under modification in China, especially for use in primary hospitals.

In conclusion, the IOTA ultrasound-based ADNEX model is as sensitive as subjective MRI assessment for distinguishing adnexal tumors, but has a higher specificity compared with MRI and a higher accuracy rate for borderline tumors compared with benign and malignant tumors. These findings reveal that the ADNEX model is a reliable points-scoring system for the preoperative diagnosis of adnexal mass. We recommend the addition of the ADNEX model, either alone or in combination with MRI, for preoperative assessment of adnexal masses.

Data availability statement

The original contributions presented in the study are included in the article/supplementary material. Further inquiries can be directed to the corresponding author.

Ethics statement

The studies involving human participants were reviewed and approved by Ethics Committee of the First Affiliated Hospital of Chongqing Medical University and Women and Children's Hospital of Chongqing Medical University. Written informed consent to participate

in this study was provided by the participants' legal guardian/next of kin. Written informed consent was obtained from the individual(s), and minor(s)' legal guardian/next of kin, for the publication of any potentially identifiable images or data included in this article.

Author contributions

Conception and design: YH, BC, HD, BS, ZX, JL, WT, FL. Analysis and interpretation: YH, BC. Data collection: HD, BS, ZX, JL, WT. Writing the article: YH, FL. Critical revision of the article: YH, BC, HD, BS, ZX, JL, WT, FL. Final approval of the article: YH, BC, HD, BS, ZX, JL, WT, FL. Statistical analysis: YH, BC Obtained funding: FL. Overall responsibility: FL. All authors contributed to the article and approved the submitted version.

Funding

This work was supported by Chongqing Natural Science Foundation of China (cstc2020jcyj-msxmX0423) and Chongqing Science and Technology Commission (cstc2018jscx-mszdX0042).

Acknowledgments

We thank Medjaden Inc. for scientific editing of this manuscript.

Conflict of interest

The authors declare that the research was conducted in the absence of any commercial or financial relationships that could be construed as a potential conflict of interest.

Publisher's note

References

1. Torre LA, Trabert B, DeSantis CE, Miller KD, Samimi G, Runowicz CD, et al. Ovarian cancer statistics, 2018. *CA Cancer J Clin* (2018) 68(4):284–96. doi: 10.3322/caac.21456

2. Siegel RL, Miller KD, Jemal A. Cancer statistics, 2019. *CA Cancer J Clin* (2019) 69 (1):7–34. doi: 10.3322/caac.21551

3. Huchon C, Bourdel N, Abdel Wahab C, Azaïs H, Bendifallah S, Bolze PA, et al. Borderline ovarian tumors: French guidelines from the CNGOF. part 1. epidemiology, biopathology, imaging and biomarkers. *J Gynecol Obstet Hum Reprod* (2021) 50 (1):101965. doi: 10.1016/j.jogoh.2020.101965

4. Cho KR, Shih Ie M. Ovarian cancer. *Annu Rev Pathol* (2009) 4:287–313. doi: 10.1146/annurev.pathol.4.110807.092246

5. Wahab CA, Rousset P, Bolze PA, Thomassin-Naggara I. Tumeurs frontières de l'ovaire. recommandations pour la pratique clinique du CNGOF – imagerie [borderline ovarian tumours: CNGOF guidelines for clinical practice - imaging]. *Gynecol Obstet Fertil Senol* (2020) 48(3):260–76. doi: 10.1016/j.gofs.2020.01.014

6. Marko J, Marko KI, Pachigolla SL, Crothers BA, Mattu R, Wolfman DJ. Mucinous neoplasms of the ovary: Radiologic-pathologic correlation. *Radiographics* (2019) 39(4):982–97. doi: 10.1148/rg.2019180221

7. Della Corte L, Mercorio A, Serafino P, Viciglione F, Palumbo M, De Angelis MC, et al. The challenging management of borderline ovarian tumors (BOTs) in women of childbearing age. *Front Surg* (2022) 23(9):973034. doi: 10.3389/fsurg.2022.973034

8. Kaijser J, Vandecaveye V, Deroose CM, Rockall A, Thomassin-Naggara I, Bourne T, et al. Imaging techniques for the pre-surgical diagnosis of adnexal tumours. *Best Pract Res Clin Obstet Gynaecol* (2014) 28(5):683–95. doi: 10.1016/j.bpobgyn.2014.03.013

9. Timmerman D, Schwarzler P, Collins WP, Claerhout F, Coenen M, Amant F, et al. Subjective assessment of adnexal masses with the use of ultrasonography: An analysis of interobserver variability and experience. *Ultrasound Obstet Gynecol* (1999) 13(1):11–6. doi: 10.1046/j.1469-0705.1999.13010011.x

10. Van Calster B, Van Hoorde K, Valentin L, Testa AC, Fischerova D, Van Holsbeke C, et al. Evaluating the risk of ovarian cancer before surgery using the ADNEX model to differentiate between benign, borderline, early and advanced stage invasive, and secondary metastatic tumours: Prospective multicentre diagnostic study. *BMJ* (2014) 349:g5920. doi: 10.1136/bmj.g5920

11. Araujo KG, Jales RM, Pereira PN, Yoshida A, de Angelo Andrade L, Sarian LO, et al. Performance of the IOTA ADNEX model in preoperative discrimination of adnexal masses in a gynecological oncology center. *Ultrasound Obstet Gynecol* (2017) 49(6):778–83. doi: 10.1002/uog.15963

12. Epstein E, Van Calster B, Timmerman D, Nikman S. Subjective ultrasound assessment, the ADNEX model and ultrasound-guided tru-cut biopsy to differentiate disseminated primary ovarian cancer from metastatic non-ovarian cancer. *Ultrasound Obstet Gynecol* (2016) 47(1):110–6. doi: 10.1002/uog.14892

13. Sayasneh A, Ferrara L, De Cock B, Saso S, Al-Memar M, Johnson S, et al. Evaluating the risk of ovarian cancer before surgery using the ADNEX model: A multicentre external validation study. *Br J Cancer* (2016) 115(5):542–8. doi: 10.1038/bjc.2016.227

14. Meys EMJ, Jeelof LS, Achten NMJ, Slangen BFM, Lambrechts S, Kruitwagen R, et al. Estimating risk of malignancy in adnexal masses: external validation of the ADNEX model and comparison with other frequently used ultrasound methods. *Ultrasound Obstet Gynecol* (2017) 49(6):784–92. doi: 10.1002/uog.17225

15. Spencer JA, Forstner R, Cunha TM, Kinkel K, Sub-Committee EFI. ESUR guidelines for MR imaging of the sonographically indeterminate adnexal mass: An algorithmic approach. *Eur Radiol* (2010) 20(1):25–35. doi: 10.1007/s00330-009-1584-2

16. Shimada K, Matsumoto K, Mimura T, Ishikawa T, Munechika J, Ohgiya Y, et al. Ultrasound-based logistic regression model LR2 versus magnetic resonance imaging for discriminating between benign and malignant adnexal masses: A prospective study. *Int J Clin Oncol* (2018) 23(3):514–21. doi: 10.3389/fsurg.2022.973034

17. Medeiros LR, Freitas LB, Rosa DD, Silva FR, Silva LS, Birtencourt LT, et al. Accuracy of magnetic resonance imaging in ovarian tumor: A systematic quantitative review. *Am J Obstet Gynecol* (2011) 204(1):67.e1–10. doi: 10.1016/j.ajog.2010.08.031

18. Meys EM, Kaijser J, Kruitwagen RF, Slangen BF, Van Calster B, Aertgeerts B, et al. Subjective assessment versus ultrasound models to diagnose ovarian cancer: A systematic review and meta-analysis. *Eur J Cancer* (2016) 58:17–29. doi: 10.1016/j.ejca.2016.01.007

19. Huang X, Wang Z, Zhang M, Luo H. Diagnostic accuracy of the ADNEX model for ovarian cancer at the 15% cut-off value: A systematic review and meta-analysis. *Front Oncol* (2021) 11:684257. doi: 10.3389/fonc.2021.684257

20. Forstner R, Thomassin-Naggara I, Cunha TM, Kinkel K, Masselli G, Kubik-Huch R, et al. ESUR recommendations for MR imaging of the sonographically indeterminate adnexal mass: an update. *Eur Radiol* (2017) 27(6):2248–57. doi: 10.1007/s00330-016-4600-3

21. Meinhold-Heerlein I, Fotopoulou C, Harter P, Kurzeder C, Mustea A, Wimberger P, et al. The new WHO classification of ovarian, fallopian tube, and primary peritoneal cancer and its clinical implications. *Arch Gynecol Obstet* (2016) 293:695–700. doi: 10.1007/s00404-016-4035-8

22. Poonyakanok V, Tanmahasamut P, Jaishuen A, Wongwananuruk T, Asumpinwong C, Panichyawat N, et al. Preoperative evaluation of the ADNEX model for the prediction of the ovarian cancer risk of adnexal masses at siriraj hospital. *Gynecol Obstet Invest* (2021) 86(1-2):132–8. doi: 10.1159/000513517

23. Peng XS, Ma Y, Wang LL, Li HX, Zheng XL, Liu Y. Evaluation of the diagnostic value of the ultrasound ADNEX model for benign and malignant ovarian tumors. *Int J Gen Med* (2021) 14:5665–73. doi: 10.2147/IJGM.S328010

24. Chen H, Qian L, Jiang M, Du Q, Yuan F, Feng W. Performance of IOTA ADNEX model in evaluating adnexal masses in a gynecological oncology center in China. *Ultrasound Obstet Gynecol* (2019) 54(6):815–22. doi: 10.1002/uog.20363

25. Stukan M, Badocha M, Ratajczak K. Development and validation of a model that includes two ultrasound parameters and the plasma d-dimer level for predicting malignancy in adnexal masses: An observational study. *BMC Cancer* (2019) 19 (1):564. doi: 10.1186/s12885-019-5629-x

26. Drapkin R, von Horsten HH, Lin Y, Mok SC, Crum CP, Welch WR, et al. Human epididymis protein 4 (HE4) is a secreted glycoprotein that is overexpressed by serous and endometrioid ovarian carcinomas. *Cancer Res* (2005) 65(6):2162–9. doi: 10.1158/0008-5472.CAN-04-3924

27. Yanaranop M, Tiyayon J, Nakrangsee S, Thinkhamrop B. Diagnostic accuracy and optimal cutoff value of serum HE4 to predict ovarian cancer in Thai women with pelvic masses. *J Med Assoc Thai* (2016) 99(12):1263–71.

28. Holcomb K, Vucetic Z, Miller MC, Knapp RC. Human epididymis protein 4 offers superior specificity in the differentiation of benign and malignant adnexal masses in premenopausal women. *Am J Obstet Gynecol* (2011) 205(4):358 e1–6. doi: 10.1016/j.ajog.2011.05.017

29. Valentin L, Ameye L, Savelli L, Fruscio R, Leone FP, Czekierdowski A, et al. Adnexal masses difficult to classify as benign or malignant using subjective assessment of gray-scale and Doppler ultrasound findings: Logistic regression models do not help. *Ultrasound Obstet Gynecol* (2011) 38(4):456–65. doi: 10.1002/uog.9030

30. Okamoto Y, Tanaka YO, Tsunoda H, Yoshikawa H, Minami M. Malignant or borderline mucinous cystic neoplasms have a larger number of loculi than mucinous cystadenoma: A retrospective study with MR. *J Magn Reson Imaging* (2007) 26(1):94–9. doi: 10.1002/jmri.20948

31. Zhao SH, Qiang JW, Zhang GF, Wang SJ, Qiu HY, Wang L. MRI In differentiating ovarian borderline from benign mucinous cystadenoma: Pathological correlation. *J Magn Reson Imaging* (2014) 39(1):162–6. doi: 10.1002/jmri.24083

Frontiers in Oncology

Advances knowledge of carcinogenesis and tumor progression for better treatment and management

The third most-cited oncology journal, which highlights research in carcinogenesis and tumor progression, bridging the gap between basic research and applications to imrpove diagnosis, therapeutics and management strategies.

Discover the latest Research Topics

See more →

Frontiers

Avenue du Tribunal-Fédéral 34
1005 Lausanne, Switzerland
frontiersin.org

Contact us

+41 (0)21 510 17 00
frontiersin.org/about/contact